

**Structure, Petrology and Geochemistry of the Coastal  
Dyke Swarm in Goa: Tectono-magmatic Evolution of the  
Western Indian Continental Margin**

A THESIS SUBMITTED TO

**GOA UNIVERSITY**

FOR THE AWARD OF THE DEGREE OF

**DOCTOR OF PHILOSOPHY**

IN

**GEOLOGY**

By

**RAGHAV RAJARAM GADGIL**

Under the supervision of

**Dr ANTHONY A. A. A. VIEGAS**

School of Earth, Ocean and Atmospheric Science

Goa University

Taleigao Plateau-403206, Goa, India

July 2020

## **CERTIFICATE**

This is to certify that the thesis entitled “**Structure, Petrology and Geochemistry of the Coastal Dyke Swarm in Goa: Tectono-magmatic Evolution of the Western Indian Continental Margin**” submitted to the Goa University, by **Raghav R. Gadgil** for the award of the degree of **Doctor of Philosophy in Geology** is a record of original and independent work carried out by him during the period of May 2014 – July 2020 under my supervision and the same has not been previously submitted for the award of any diploma, degree, associateship or fellowship or any other similar title.

Goa University

July 2020

**DR ANTHONY A. A. A. VIEGAS**

(Research Guide)

## **DECLARATION**

I hereby declare that the matter embodied in this thesis entitled “**Structure, Petrology and Geochemistry of the Coastal Dyke Swarm in Goa: Tectono-magmatic Evolution of the Western Indian Continental Margin**” submitted to the Goa University, for the award of the degree of **Doctor of Philosophy in Geology** is a record of original and independent work carried out by me during the period of May 2014 – June 2020 under the supervision of Dr. Anthony A. A. Viegas, Associate Professor, School of Earth, Ocean and Atmospheric Sciences, Goa University and that it has not been previously formed the basis for award of any diploma, degree, associateship or fellowship or any other similar title.

Goa University

July 2020

**RAGHAV R GADGIL**

(Research Scholar)

## ACKNOWLEDGEMENTS

*I take this opportunity to thank everyone who has made this possible.*

*Firstly, I extend my immense gratitude to my research guide Dr. Anthony Viegas for his constant encouragement, guidance and help at all times. I greatly appreciate the liberty he granted me to work in my own way during this research. His timely financial help for carrying out the geochemical analysis will never be forgotten. He was always a sanguine, jovial and lighthearted mentor. I will always cherish these years of working with him.*

*I also thank the Vice Chancellor's nominee, Dr. Sridhar D. Iyer for his regular evaluation and his constructive criticism of my work. His constant emphasis on learning and understanding the research problem, greatly improved the quality of my work. He inspired me to be thorough and earnest throughout.*

*I am grateful to Prof. Hetu C. Sheth, Department of Earth Sciences, Indian Institute of Technology, Bombay for his keen appreciation of the field data gathered and inspiring me to systematically compile the same. I acknowledge his constant suggestions in during the writing of this thesis and for pushing me beyond my limits. The paper published from this research work wouldn't have been possible without his invaluable and selfless help.*

*My sincere thanks to Dr. T. A. Viswanath, former Associate Professor, Department of Earth Science, Goa University for his assistance in mineral identifications, petrographic descriptions, and his valuable comments on several parts of thesis. I am grateful to him for providing his collection of USGS Standards that were used in this thesis to cross-check the analyzed data.*

*Several lengthy discussions via emails with Prof. Agust Gudmundsson (Royal Holloway, University of London, UK), Dr Vivek Kale (Advanced Center for Water Resources Development and Management, Pune), Dr Elena Druguet (Autonomous University of Barcelona, Spain), Prof. Tapas Kumar Biswal (IIT-Bombay), Dr. Aditya Joshi (MSU, Gujarat) are acknowledged and thanked. I especially thank Dr. Surendra Pal Verma (Universidad Nacional Autónoma de México) for helping in the CIPW Norm calculations to assign rock names using the IgRoCs software. I also thank Prof. M. G. Kale (University of Pune) for providing me important and inaccessible reference on the turbidite sequence in North Goa.*

*I am grateful to Prof. H. B. Menon, Dean, School of Earth, Ocean and Atmospheric Sciences, Goa University and the former Heads of Department of Earth Science, Prof. A. G. Chachadi and Prof. Kotha Mahender for kindly allowing me to access facilities of the Department.*

*My heartfelt thanks go to Dr. John Kurian and Dr. Thamban Meloth of the National Centre for Polar and Oceanic Research (NCPOR), Goa for their kind permission and assistance to conduct analysis in their laboratories. I am also grateful to Ms. Lathika, Dr Parijat Roy, Ms. Vinita Mahale, Mr. Deepak Agraval, and Mr. Chandrakant Rathore of NCPOR for their help in carrying out the geochemical analysis.*

*I thank Ms. Ankeeta Amonkar and Mr. Dafilgo Fernandes for lending me the required books from the library of the National Institute of Oceanography, Dona Paula, Goa. I am thankful to Dr Sohini Ganguly, DST-INSPIRE Faculty at the School of Earth, Ocean and Atmospheric Sciences, Goa University for her various valuable suggestions at various stages in this research work. I thank Mr. Purushottam Verlekar, my friend and colleague, for his constant encouragement and for being with me in thick and thin of the PhD life. He inspired me to develop my love towards the Konkani language.*

*I am indebted to Dr. Loïc Vanderkluyzen from Drexel University, Philadelphia, USA for analyzing my samples at his University and providing me with high quality trace element data of the dykes.*

*I would like to thank the Directorate of Higher Education, Government of Goa for promptly granting me the required Study Leave necessary to complete my thesis writing.*

*I am grateful to my teachers Mr. A. G. Agshikar, Mr. D. S. Parab, Dr. M. M. Ibrampurkar, Ms. M. A. Miranda and my colleagues Ms. Delia Cardozo and Ms. Vinita Mayenkar of the Department of Geology, Dhempe College of Arts and Science, Miramar - Goa for encouraging me to carry out this work. I also thank my Principal Dr. Vrinda Borker for her support.*

*I am thankful to the non-teaching staff of Goa University: Mr. Premakant Gauns, Mr. Devidas Gawas, Ms. Sangeeta Tilve, Ms. Tulsi Gaonkar, Ms. Heena Kaushal, Mr. Dnyaneshwar Padekar and of Dhempe College: Mr. Vijay Kurundwad, Mr. Yogesh Dhuri and Mr. Sarvesh Paidarkar for assisting me in my work.*

*I appreciate the efforts taken by Adv. Albertina Almeida for patiently and critically proofreading the thesis chapters.*

*Many thanks go to my students: Mr. Akshay Tari, who accompanied me several times in the field, Ms. Sneha Chougule, for the Kyanite sample, Mr. Anmol Naik for the unending discussions on several topics in geology and Karuna, Manjusha, Heston, Nestor, Pradeep, Supriya, Neil, Blessy, Sanish, Alina, Palash, Ananya, Naveen, Anmol, Noel, Floyd for their inputs in fieldwork and data compilation.*

*I wish to express my profound gratitude to my parents, Baba and Aaie, and my in-laws, Mr. Moreshwar Ranade and Mrs. Sneha Ranade for their immense support. I thank my wife Shweta for her faith, love, support, devotion in keeping the family embers burning, reassuring and strengthening my morale and applauding my efforts. My son Shreyas who always inquired whether my diagrams are completed, grew up too fast in too less time!*

*Raghav Gadgil*

# Contents

<b>List of Figures</b>	11
<b>List of Tables</b>	17

## CHAPTER 1

### Introduction

1.1 Dykes and dyke swarms in the Large Igneous Province (LIP)	20
1.2 Importance of the dyke swarms	23
1.3 Emplacement mechanisms and structural analysis of the dykes	27
1.4 Earliest works on dykes in India	29
1.5 The west coast dyke swarm of the Deccan LIP	30
1.6 Greywackes	31
1.7 The Problem	32
1.8 Objectives	33
1.9 Workflow	33
1.10 Study area	34
<i>1.10.1 Location</i>	34
<i>1.10.2 Accessibility</i>	34

## CHAPTER 2

### Geological Framework

2.1 Geology of the Dharwar craton	36
2.2 Geology of Goa	40
<i>2.2.1 Anmod Ghat trondhjemite gneiss</i>	41
<i>2.2.2 Chandranath granite gneiss</i>	41
<i>2.2.3 Dudhsagar granite</i>	42
<i>2.2.4 Canacona granite</i>	43
<i>2.2.5 Bondla mafic-ultramafic layered complex</i>	43
<i>2.2.6 Barcem Group</i>	44
<i>2.2.7 Ponda Group</i>	45
<i>2.2.7.1 Sanvordem Formation</i>	45
<i>2.2.7.2 Bicholim Formation</i>	45
<i>2.2.7.2 Vagheri Formation</i>	46
<i>2.2.8 Mafic intrusives</i>	46
<i>2.2.9 Deccan Traps</i>	47
<i>2.2.10 Laterite</i>	49
<i>2.2.11 Structural aspects of the rocks of Goa</i>	49
2.3 Basic dyke swarms	50
<i>2.3.1 Proterozoic dyke swarms in the western Dharwar</i>	50
<i>2.3.2 Deccan lavas and associated dyke swarms</i>	53

## CHAPTER 3

### Field characters of country rocks and dykes

3.1 Country rocks	66
3.1.1 Aguada Headland	66
3.1.2 Baga Headland	72
3.1.3 Vagator-Chapora Headland	76
3.1.4 Arambol-Keri Headland	78
3.1.5 Structural features	81
3.1.5.1 Fracture patterns	81
3.1.5.2 Trend of fractures	81
3.1.5.3 Types of fractures	83
3.1.5.4 Mineral veins, gash veins and grooves	86
3.1.5.5 Shear zones	91
3.2 Dykes: Field observations	96
3.2.1 Structural attributes and internal features of dykes	101
3.2.1.1 Strike and dip	102
3.2.1.2 Length and thickness	102
3.2.1.3 Horns	103
3.2.1.4 Dykes along pre-existing anisotropies	104
3.2.1.5 Rock bridges	106
3.2.1.6 Contact relations and vesicles	108
3.2.1.7 Columnar jointing	110
3.2.2 Tectonic aspects of Goa dykes	111
3.2.2.1 Crustal dilation	111
3.2.2.2 Magmatic overpressures and source depths	113
3.3 Discussion	115
3.3.1 Interpretations of field structures of country rocks	115
3.3.1.1 The sequence of deposition of sediments	115
3.3.1.2 Soft-sediment deformation structures (SSDs)	116
3.3.1.3 Breccia	117
3.3.1.4 Mineral veins	118
3.3.2 Interpretations of field structures of dykes	119
3.3.2.1 Thermal erosion	119
3.3.2.2 Dyke trends and paleostresses	119
3.3.2.3 Inclined dykes	122
3.3.2.4 Nature of vesicles	122
3.3.2.5 Feeder or non-feeder dykes?	123

## CHAPTER 4

### Petrography of country rocks and dykes

4.1 Country rocks	127
4.1.1 Metagreywackes and Argillites	127
4.1.2 Breccia	130
4.1.3 Calcareous rocks	132

4.2 Petrography and nomenclature of dykes	132
4.2.1 <i>Tholeiitic basalts and dolerites</i>	132
4.2.2 <i>Tholeiitic hypersthene dolerites</i>	141
4.2.3 <i>Tholeiitic picrite basalts</i>	142
4.2.4 <i>Alteration patches</i>	144
4.3 Discussion	148

## CHAPTER 5

### **Geochemistry of country rocks and dykes**

5.1 Introduction	154
5.2 Analytical techniques and Sample preparation	156
5.2.1 <i>X-Ray Fluorescence</i>	157
5.2.2 <i>Inductively Coupled Plasma-Mass Spectroscopy</i>	160
5.3 Geochemistry of country rocks	163
5.3.1 <i>Major elements</i>	163
5.3.2 <i>Trace elements</i>	169
5.4 Geochemistry of dykes	172
5.4.1 <i>Major elements</i>	172
5.4.2 <i>Trace elements</i>	185

## CHAPTER 6

### **Petrogenesis of country rocks and dykes**

6.1 Country rocks	194
6.1.1 <i>Comparison to other greywackes</i>	194
6.1.2 <i>Tectonic setting and provenance</i>	197
6.2 Dykes	204
6.2.1 <i>Crystallization Process</i>	204
6.2.2 <i>Mantle source characteristics and Tectonic implications</i>	215
6.2.3 <i>Mantle melting conditions</i>	230
6.2.4 <i>Crustal contamination</i>	234
6.3 The need for geochemical correlations	238
6.3.1 <i>Comparison of multi-element patterns for Group 1 dykes</i>	239
6.3.2 <i>Group 1 dykes as feeders to Bushe Formation of the Deccan Traps?</i>	241
6.3.3 <i>Binary geochemical diagrams for Group 2 dykes</i>	245
6.3.4 <i>Comparison of multi-element patterns for Group 2 dykes</i>	248
6.3.5 <i>Affinities of Group 2 dykes to Deccan Traps</i>	253
6.3.6 <i>Stratigraphic implications</i>	256

## CHAPTER 7

### **Tectono-magmatic evolution of the western Indian continental margin**

7.1 Introduction	259
7.2 Stages in the development of western Indian continental margin	261

7.2.1 Stage 1: felsic magmatism (93 Ma), mafic magmatism (88 Ma), the origin of the western ghats of India	261
7.2.2 Stage 2: India's interaction with the Reunion hotspot leading to Deccan volcanism (mafic) (~70-65 Ma)	262
7.2.3 Stage 3: India-Seychelles micro-continent rifting	263
7.2.4 Stage 4: Formation of the Panvel flexure	264
7.2.5 Stage 5: Isostatic subsidence/thermal collapse relating to the loading/eruption of Deccan basalts	265
7.2.6 Stage 6: Subsidence of Bombay offshore region due to reactivation of SONATA rift	267
7.2.7 Stage 7: Buckling of south India	267
7.2.8 Stage 8: Separation of Laccadive-Chagos ridge from the southern part of the Mascarene plateau because of shifting of the Central Indian Ridge (40 Ma)	268
7.2.9 Stage 9: Tilting of the Peninsula northward due to collision and subduction	268
7.3 Tectono-magmatic evolution of the western Indian continental margin	269

## CHAPTER 8

<b>Conclusions</b>	269
<b>References</b>	277
<b>Research publications</b>	326

## List of Figures

	Page No.
<b>CHAPTER 1</b>	
<b>Figure 1.1:</b> Radiating dyke swarms and their mantle plume centers. (Modified from Ernst et al., 2001) ( <a href="http://www.largeigneousprovinces.org/19jul">http://www.largeigneousprovinces.org/19jul</a> )	22
<b>Figure 1.2:</b> Types of regional-scale dyke swarms. (From Ernst and Buchan, 2001). ( <a href="http://www.largeigneousprovinces.org/19jul">http://www.largeigneousprovinces.org/19jul</a> )	23
<b>Figure 1.3:</b> Global distribution of giant circumferential dyke swarms. ( <a href="http://www.largeigneousprovinces.org/19jul">http://www.largeigneousprovinces.org/19jul</a> )	25
<b>Figure 1.4:</b> Giant circumferential Lake Victoria dyke swarm. (From Buchan and Ernst, 2019). ( <a href="http://www.largeigneousprovinces.org/19jul">http://www.largeigneousprovinces.org/19jul</a> )	26
<b>Figure 1.5:</b> (a) Map of western India showing extent of Deccan Traps and major dyke swarms marked (Modified after Vijayan et al., 2016). (b) Geological map of North Goa showing study areas.	35
<b>CHAPTER 2</b>	
<b>Figure 2.1:</b> Geology of Dharwar craton and adjoining terranes (Modified after Valdiya, 2016)	37
<b>Figure 2.2:</b> Proterozoic mafic dykes on the geological map for Dharwar craton. (Modified from French and Heaman, 2010).	39
<b>Figure 2.3:</b> Geological map of Goa (Modified after Dessai, 2011).	42
<b>CHAPTER 3</b>	
<b>Figure 3.1:</b> Dyke maps for the study areas (a) Aguada Headland	68
<b>Figure 3.1:</b> (b) Baga Headland	69
<b>Figure 3.1:</b> (c) Vagator-Chapora Headland	70
<b>Figure 3.1:</b> (d) Arambol-Keri Headland	71
<b>Figure 3.2:</b> Field photographs of Aguada Headland	74
<b>Figure 3.3:</b> Field photographs of sedimentary structures at Aguada and Baga	75

Headland.

<b>Figure 3.4:</b> Field photographs of sedimentary structures at Aguada and Baga Headland.	76
<b>Figure 3.5:</b> Field photographs of sedimentary structures in argillites	77
<b>Figure 3.6:</b> Field photographs of sedimentary structures at Arambol-Keri Headland	79
<b>Figure 3.7:</b> Field photographs of Soft Sediment Deformation (SSD) structures	80
<b>Figure 3.8:</b> Oblique aerial views of part of Baga and Aguada Headland showing joint patterns.	82
<b>Figure 3.9:</b> Field photograph of dyke AG-23 and country rocks showing joints	83
<b>Figure 3.10:</b> Outcrop-scale extension fractures at Aguada Headland	84
<b>Figure 3.11:</b> Different types of fractures in country rocks	85
<b>Figure 3.12:</b> Different types of fractures in country rocks	86
<b>Figure 3.13:</b> Types of veins in country rocks	88
<b>Figure 3.14:</b> Quartz vein passing on to a bedding plane	89
<b>Figure 3.15:</b> Sigmoidal tension gash veins in country rocks	90
<b>Figure 3.16:</b> Flexural-slip folds and quartz grooves in country rocks	91
<b>Figure 3.17:</b> Field photographs of hydrofractures and shear zone	93
<b>Figure 3.18:</b> Field photographs of breccia at Vagator-Chapora Headland	94
<b>Figure 3.19:</b> Planar view of hydrofracture in Vagator-Chapora Headland	95
<b>Figure 3.20:</b> Type of weathering on country rock and dyke and a discontinuous dyke outcrop	96
<b>Figure 3.21:</b> Field photographs of intersecting dykes, margins of dykes, multiple-injection dykes	100
<b>Figure 3.22:</b> Plots of the number of dykes versus (a) dyke strike (b) dyke dip (c) dyke length (d) dyke thickness.	102

<b>Figure 3.23:</b> Field photograph of dyke AG-22 showing ‘horn’ feature	104
<b>Figure 3.24:</b> Field photographs showing control of pre-existing joints on the dyke emplacement	105
<b>Figure 3.25:</b> Field photographs showing control of pre-existing joints on the dyke emplacement	106
<b>Figure 3.26:</b> Field photographs of dykes showing ‘rock bridge’ feature	107
<b>Figure 3.27:</b> Field photographs of chilled margins, vesicles, dyke contacts and heating effects on country-rocks	109
<b>Figure 3.28:</b> Central concentration of vesicles in dyke AG-24	110
<b>Figure 3.29:</b> Columnar joints in dyke AR-4	111

#### **CHAPTER 4**

<b>Figure 4.1:</b> Thin-section photographs of metagreywackes	129
<b>Figure 4.2:</b> Thin-section photographs of metagreywackes	130
<b>Figure 4.3:</b> Thin-section photographs of breccia	131
<b>Figure 4.4:</b> Thin-section photographs of dykes	134
<b>Figure 4.5:</b> Thin-section photographs of textures in dykes	135
<b>Figure 4.6:</b> Thin-section photographs of olivine and iddingsite	136
<b>Figure 4.7:</b> Thin-section photographs of plagioclase inclusions	137
<b>Figure 4.8:</b> Thin-section photographs of ophitic and sub-ophitic texture	139
<b>Figure 4.9:</b> Thin-section photographs of ‘swallow-tail’ plagioclase, palagonite and skeletal opaques	140
<b>Figure 4.10:</b> Thin-section photographs of reddish rimmed plagioclase and orthopyroxenes	142
<b>Figure 4.11:</b> Thin-section photographs of tholeiitic picrite basalts	143
<b>Figure 4.12:</b> Thin-section photographs of alteration patches	145

## CHAPTER 5

<b>Figure 5.1:</b> Photograph of ball-mill	156
<b>Figure 5.2:</b> Photographs of sample preparation	157
<b>Figure 5.3:</b> Binary plot of (a) $K_2O/Na_2O$ vs $SiO_2/Al_2O_3$ (after Wimmenauer, 1984) (b) $\log(SiO_2/Al_2O_3)$ vs $\log(Na_2O/K_2O)$ (after Pettijohn et al., 1972) (c) $\log(SiO_2/Al_2O_3)$ vs $\log(Fe_2O_3/K_2O)$ (after Pettijohn et al., 1972)	168
<b>Figure 5.4:</b> Total-Alkali Silica diagram (after Le Maitre et al. 1989) for metagreywackes	169
<b>Figure 5.5:</b> Total-Alkali Silica diagram (after Le Maitre et al. 1989) for Group 1 and Group 2 dykes	182
<b>Figure 5.6:</b> (a) $(Na_2O+K_2O)-FeO^T-MgO$ (AFM) diagram (after Irvine and Baragar, 1971) (b) $TiO_2-Al_2O_3-MgO$ diagram (after Jensen, 1976). Both the diagrams for Group 1 and Group 2 dykes.	184

## CHAPTER 6

<b>Figure 6.1:</b> Variation diagram of major oxides vs $SiO_2$ for metagreywackes	195
<b>Figure 6.2:</b> Variation of (a) Cr and (b) Ni vs MgO (wt. %) (c) Rb vs K (d) U vs Th. All plots for metagreywackes	196
<b>Figure 6.3:</b> Tectonic setting discrimination diagrams for metagreywackes (a) $Al_2O_3/SiO_2$ (b) $TiO_2$ (c) $K_2O/Na_2O$ (d) $Al_2O_3/(CaO+Na_2O)$ plots (after Bhatia, 1983; Banerjee and Bhattacharya, 1994).	199
<b>Figure 6.4:</b> Plot of Th vs La (after Bhatia and Crook, 1986) for metagreywackes	200
<b>Figure 6.5:</b> Chondrite normalised REE patterns for the metagreywackes	203
<b>Figure 6.6:</b> CaO- $Na_2O$ - $K_2O$ triangular plot for the metagreywackes	204
<b>Figure 6.7:</b> (a) Co vs Ni (ppm) (b) $CaO/Al_2O_3$ vs Cr/Ni. Plots for both groups of dykes.	206
<b>Figure 6.8:</b> $TiO_2$ versus $CaO/Al_2O_3$ variation diagram (after Dungan and Rhodes, 1978) for both groups of dykes	207
<b>Figure 6.9:</b> (a) to (g) Variation of major elements with respect to MgO in both	209

the Groups of dykes. (h) Variation of MgO vs CaO/Al<sub>2</sub>O<sub>3</sub>

**Figure 6.10:** (a) to (w) Variations of trace elements and the REE's with respect to MgO for both the Groups of dykes 212-214

**Figure 6.11:** Variations of (a) Ba, (b) Sr and (c) Hf with respect to Zr. (d) Variation of Sc/Y vs MgO. The plots are for both the groups of dykes 215

**Figure 6.12:** Plot of Zr (ppm) vs Zr/Y (after Pearce and Norry, 1979) for both the groups of dykes 217

**Figure 6.13:** Primitive mantle normalized multi-element diagram for (a) Group 1 dykes and (b) Group 2 dykes. Normalization factors after (Lyubetskaya and Korenaga (2007) 218-219

**Figure 6.14:** Chondrite normalized multi-element diagram for (a) Group 1 dykes (b) Group 2 dykes. Normalizing values are from Sun and McDonough (1989) 221

**Figure 6.15:** Plot of (a) Zr/Y-Nb/Y and (b) Nb/Th-Zr/Nb (after Condie, 2003) for both the groups of dykes. 223

**Figure 6.16:** Plot of Nb/Yb vs. Th/Yb diagram (after Pearce, 2008) for both the groups of dykes 230

**Figure 6.17:** Plot of La/Yb vs Dy/Yb (Jung et al., 2006) for both the groups of dykes 232

**Figure 6.18:** Plot of (Ce/Sm)<sub>N</sub> vs (Yb/Sm)<sub>N</sub> (Storey et al., 1997) normalized (N) to PM values (Lyubetskaya and Korenaga, 2007) for both the groups of dykes 234

**Figure 6.19:** PM-normalised multi-element pattern for Group 1 dykes compared with the country-rock metagreywackes. Normalization factors after (Lyubetskaya and Korenaga (2007) 238

**Figure 6.20:** Comparison of PM-normalized multi-element patterns of the Group 1 dykes with that of (a) Dandeli dyke (French and Heaman, 2010) (b) Kalyadi dyke (Chandrasekharam, 2008) (c) Goa-Dharwar Sector dykes (Devaraju et al., 2008) (d) Bushe Formation of Deccan Traps (Vanderkluyzen et al., 2011) 240-241

**Figure 6.21:** (a) Schematic diagram of the distribution of Deccan Traps (Modified after Vijayan et al., 2016) and simplified stratigraphic column compiled from Beane et al. (1986), Devey and Lightfoot (1986), Mitchell and Widdowson (1991), Mahoney et al. (2000), Vanderkluyzen et al. (2011), Schoene et al. (2015). (b) Schematic cross-sections along A-A' (from 244

Vanderkluyesen et al., 2011) and E-W (from Mitchell and Widdowson, 1991).

**Figure 6.22:** Variation diagrams of (a) Ba/Y vs Nb/Zr, (b) Zr/Nb vs Ti/Y, (c) Zr (ppm) vs Th (ppm) for the Group 2 dykes. Fields for several southwestern Deccan formations are from Devey and Lightfoot (1986), Lightfoot et al. (1990), Sheth et al. (2004, 2019) and Mitchell and Widdowson (1991) 247

**Figure 6.23:** Comparison of PM-normalized multi-element patterns of the Group 2 dykes with those of Desur Formation average (Hegde et al., 2014) 250

**Figure 6.24:** Comparison of PM-normalized multi-element patterns of the Group 2 dykes with those of Ambenali Formation averages (Vanderkluyesen et al., 2011) 251

**Figure 6.25:** Comparison of PM-normalized multi-element patterns of the Group 2 dyke with those of Poladpur Formation averages (Vanderkluyesen et al., 2011) 252

**Figure 6.26:** Comparison of PM-normalized multi-element patterns of the Group 2 dykes with those of MMD13 (Sheth et al., 2014) 252-253

## CHAPTER 7

**Figure 7.1:** Schematic diagrams adapted from Pande et al. (2017) depicting the major stages of India-Seychelles-Madagascar breakup and early opening of the Arabian Sea. 266

## List of Tables

	<b>Page No</b>
<b>CHAPTER 2</b>	
<b>Table 2.1:</b> Lithostratigraphic sequence of Goa Group (Modified after Dessai, 2011, 2018)	44
<b>Table 2.2:</b> Stratigraphy of the Deccan Traps in the Western Ghats region. Based on Subbarao and Hooper (1988), Peng et al. (1994), Schoene et al. (2019).	48
<b>CHAPTER 3</b>	
<b>Table 3.1:</b> Field data on the Goa dykes exposed in the four study areas (Gadgil et al., 2019)	98-99
<b>Table 3.2:</b> Details of the dilation profiles, traverse lengths, dykes encountered and calculated dilation (Gadgil et al. 2019)	113
<b>CHAPTER 4</b>	
<b>Table 4.1:</b> Table showing modal mineralogy of the dyke rocks	145
<b>CHAPTER 5</b>	
<b>Table 5.1:</b> Major element compositions obtained from XRF for USGS standard rocks	159
<b>Table 5.2:</b> Trace and REE compositions for certified reference standards obtained from ICP-MS	162
<b>Table 5.3:</b> Representative major (in wt. %) and trace element (in ppm) data for country-rock greywackes	166
<b>Table 5.4:</b> Average major oxides (in wt. %) of the greywackes under study as compared with other examples	167
<b>Table 5.5:</b> Average trace element concentrations (in ppm) and ratios of the greywackes under study as compared with other examples	171
<b>Table 5.6:</b> Representative major element oxide and CIPW data of the Group 1 dykes in Goa	173

<b>Table 5.7:</b> Representative major element oxide and CIPW data of the Group 2 dykes in Goa	174- 176
<b>Table 5.8:</b> (a) Representative trace element data of the Group 1 dykes in Goa (b) Trace element ratios of Group 1 dykes in Goa	186- 187
<b>Table 5.9:</b> (a) Representative trace element data of the Group 2 dykes in Goa (b) Trace element ratios of Group 2 dykes in Goa	188- 189

## CHAPTER 6

<b>Table 6.1:</b> Plate tectonic classification of continental margins and oceanic basins (adopted from Bhatia and crook, 1986)	200
<b>Table 6.2:</b> Comparison of trace element characteristics of metagreywackes from the study area to other tectonic settings (adapted from Bhatia and Crook (1986), Table 5)	201
<b>Table 6.3:</b> Incompatible trace element ratios in the major chemical reservoirs and their comparison with Group 1 and 2 dykes (Weaver, 1991)	228
<b>Table 6.4:</b> Geochemical criteria used to distinguish the younger stratigraphic units, WG (Sheth et al., 2014)	255

# **CHAPTER 1**

## **Introduction**

## 1.1 Dykes and dyke swarms in the Large Igneous Province (LIP)

The term Large Igneous Provinces (LIPs) was coined and used by Coffin and Elholm (1992; 1993; 1994). These provinces involve pulsative magmatic fluxes where voluminous outpourings of mantle-borne mafic magmas spread over extensive areas of continents and oceans within a relatively short time span (Coffin and Eldholm, 1994; 2005; Mahoney and Coffin, 1997). Ernst (2014) defined LIP as “A *LIP* is mainly mafic (+ultramafic) magmatic province with areal extent  $> 0.1$  million  $\text{km}^2$  and igneous volume  $> 0.1$  million  $\text{km}^3$ , that has intraplate characteristics, and is emplaced in a short duration pulse or multiple pulses (less than 1-5 Ma) with a maximum duration of  $< c. 50$  Ma. Silicic magmatism (including that of LIP scale, termed Silicic LIPs (SLIPs)) and also carbonatites and kimberlites may be associated”.

LIPs have a plumbing system that comprises of dykes, sills, differentiated intrusions of layered mafic to ultramafic magmatism and magmatic underplating (Ernst, 2014). This system facilitates the movement of magma from underlying mantle sources, and its distribution throughout the lithospheric mantle and crust and onto the surface of the Earth. Rocks, either ejected at the Earth’s surface as lavas or those solidified within the crust as giant sill-complexes are often expressed at the surface as swarms of dykes, also known as lava pile dyke-swarm couple (White et al., 1987). Dykes serve as major conduits for magma transfer from the mantle to the upper crust and constitute a common expression of crustal extension. Emplacement of dyke swarms also takes place due to short-lived mantle-generated magmatic events. Such events are common during rifting and the continental breakup of crust (White et al., 1987). When the thermal anomalies beneath the continents cause stretching of the crust (White and McKenzie, 1989), massive outbursts of igneous activity sometimes accompany the rifting of the continents, as they break to form new ocean basins. Much of this evidence remains deeply buried on continental margins under

thick piles of sediment that lies hidden underwater. Mafic dyke swarms are a part of such an important igneous litho-association and are often exposed as spectacular vast, linear or radial swarms, in all the continental areas ranging in age from Archaean to the Tertiary (Windley, 1984). They are reliable indicators of the episodicity of magmatism and classic indicators of nature and type of magmatic activity. The unfolding of the plate tectonics theory is made easy by studying the dyke swarms as they enlighten on extensional processes occurring both in the continental as well as oceanic lithosphere.

Before I dwell on the types of dyke swarms, there is a need to define the components of the plumbing system. A dyke is defined as “*a tabular igneous intrusion that cuts across the bedding or foliation of the country-rock*” (Neuendorf et al., 2011) and a sill as “*a tabular igneous intrusion that parallels the bedding or foliation of the sedimentary or metamorphic country rock, respectively*” (Neuendorf et al., 2011). However, Ernst and Buchan (2004) resorted to the usage of the orientation of the dykes or sills *at the time of emplacement* regardless of the relationship with the bedding or foliation (c.f. Hall, 1996). Accordingly, a dyke is defined as “*a tabular igneous body that was sub-vertical at the time of emplacement. A dyke swarm is a set of coeval dykes which typically display a linear, radiating or arcuate geometry*” (Ernst and Buchan, 2004; Ernst, 2014) and a sill is correspondingly defined as an originally sub-horizontal tabular body. The primary advantage of considering the latter types of definitions for dykes and sills is that it can be directly related to the prevalent stress conditions at the time of emplacement.

Mafic dykes usually occur together in large groups known as “swarms”. Such large dyke swarms are very prominent in most of the basement terrains, whose dimensions are at least 300 km long and can be more than 2000 km long (Ernst et al., 1995) and cover extensive areas (Ernst, 2014) (*Fig. 1.1*). Individual dykes could have widths of 10 to 40 m (Parker et al., 1990; Ernst et al., 1995). There are six types of regional-scale dyke swarms

described, based on their characteristic geometric pattern (*Fig. 1.2*). These are classified as having continuous fanning pattern (Type I), fanning pattern divided into separate subswarms (Type II), subswarms of parallel dykes that radiate from a common point (Type III), subparallel dykes over a broad area (Type IV), subparallel dykes over a narrow zone (Type V) and an arcuate pattern (type VI) (Ernst and Buchan, 2001; Ernst, 2014). Recent research has revealed the existence of giant circumferential swarms (Type VI), initially recognized in Ernst and Buchan (1998) but fully characterized in Buchan and Ernst (2018, 2019). Earlier these types of dyke swarms were recognized around individual volcanoes (Chadwick and Howard, 1991). These newly recognized dyke swarms have a quasi-circular or quasi elliptical geometry with outer diameters ranging from ~450 to ~2500 km (*Fig. 1.3 & 1.4*). All circumferential dyke swarms currently known are of mafic composition.

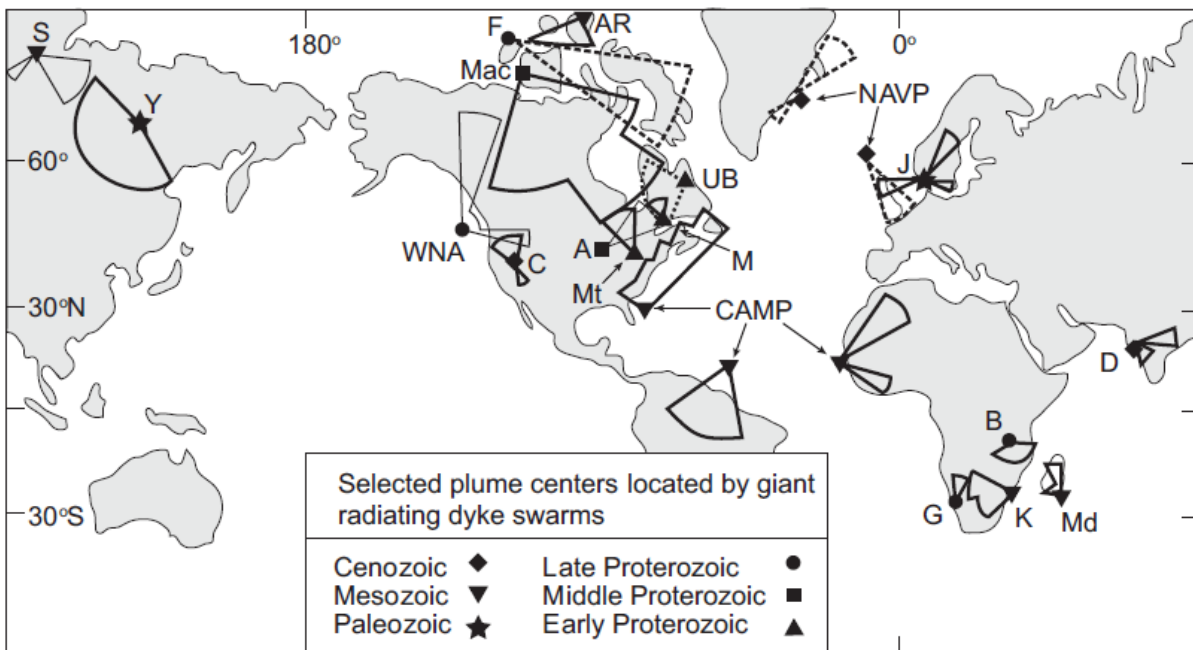


*Fig. 1.1. Radiating dyke swarms and their mantle plume centres. Selected examples: Columbia River (C), North Atlantic Volcanic Province (NAVP), Deccan (D), Madagascar (Md), Alpha Ridge (AR), Karoo–Ferrar (K), Central Atlantic Magmatic Province (CAMP), Jutland (J), Yakutsk (Y), Gannakouriep (G), Franklin (F), Western North America (WNA), Bukoban (B), Abitibi (A), Mackenzie (Mac), Ungava Bay (UB), Matachewan (Mt), Mistassini (M), and Siberian Trap (S). Adopted from Ernst (2014)*

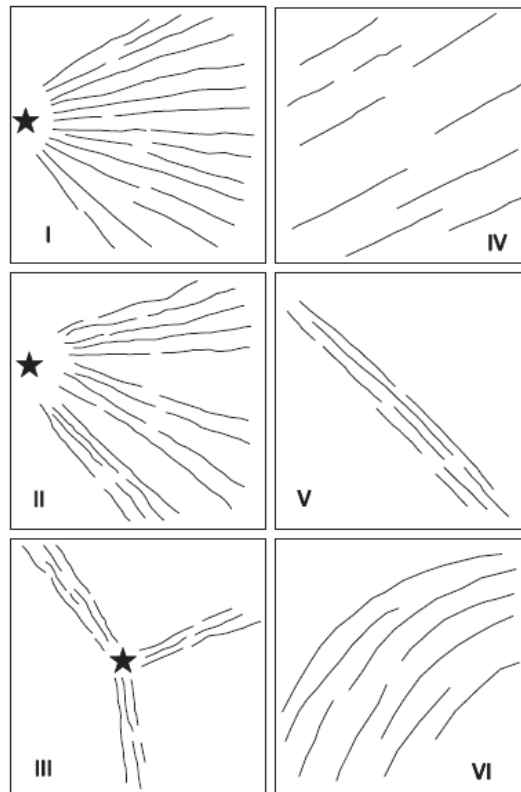


Fig 1.2 Types of regional-scale dyke swarms. Six characteristic geometries of giant radiating dyke swarms: I, continuous fanning pattern; II, fanning pattern divided into separate subswarms; III, subswarms of subparallel dykes that radiate from a common point; IV, subparallel dykes over a broad area; V, subparallel dykes in a narrow zone; VI, arcuate pattern. Stars locate probable mantle plume centres defined by the convergence of radiating patterns of dykes. While types IV and V could be subsets of types I–III, they can also have distinct origins as discussed in the text. (<http://www.largeigneousprovinces.org/19jul>)

## 1.2 Importance of the dyke swarms

The salient features of the dyke swarms are:

- 1) The trend of each dyke matters: It has been generally assumed that the crosscutting trends of regional-scale dykes in a single region have the same age. However, studies have revealed that each dyke swarm (same age) characteristically has a consistent linear trend or regional radiating pattern (Halls, 1982; Fahrig et al., 1986; Buchan and Ernst, 2004). Also, a single dyke trend can also include more than one swarm. Another significant observation is that the regional dyke trends are more

indicative of regional stresses rather than weaknesses in the host rock (except in their local manifestation).

- 2) Emplacement of the dykes takes place normal to minimum compressive stress ( $\sigma_3$ ): Regional dyke sets intersecting at acute angles were earlier believed to be coeval and intruded along conjugate shear sets (Hanmer et al., 1997), but it is now proved that each dyke swarm is independent and unrelated to another (Ernst and Bleeker, 2010). The regional dyke swarms are typically emplaced normal to the  $\sigma_3$ . Hence each dyke in a cross-cutting relationship, was emplaced during two phases separated by time periods ranging from a few days (Gundmundsson, 1984) to a few million years (Hooper et al., 2010).
- 3) Horizontal emplacement of the dykes: It is typically assumed that dykes are fed vertically from underlying source areas. With increased research based on magnetic fabric studies, modelling based on textural indicators of flow direction and comparison with lateral dyke injections in Hawaii and Iceland, it is revealed that dyke swarms can be emplaced laterally for long distances into cratonic interiors (up to >2000 km) (Halls, 1982; Fahrig, 1987; Lister and Kerr, 1991; Ernst and Baragar, 1992; Baragar et al., 1996; Ray et al., 2007; Hastie et al., 2014). Vertical emplacement of the dykes usually takes place above a mantle plume head, whereas the lateral flow takes place away from the plume head.
- 4) Every dyke is a distinct (magma injection) event: It is increasingly evident from studies that each dyke in a single swarm represents a distinct emplacement event. This is exemplified by a pair of dykes (~200 km long) separated by a narrow gap of 10-20 km, in which each had a distinct composition and paleomagnetic direction (Halls, 1986; Buchan et al., 1993).

5) Radiating regional dykes are the norm: It has been increasingly seen that Paleoproterozoic dyke swarms in the basement rocks of cratons radiate into the cratonic interior from points along its margins. Such large dyke swarms generated due to plumes are present as broken entities on the cratons that were once amalgamated (Ernst and Srivastava, 2008; French and Heaman, 2010). Hence such dyke swarms aid in reconstructing the palaeogeography.

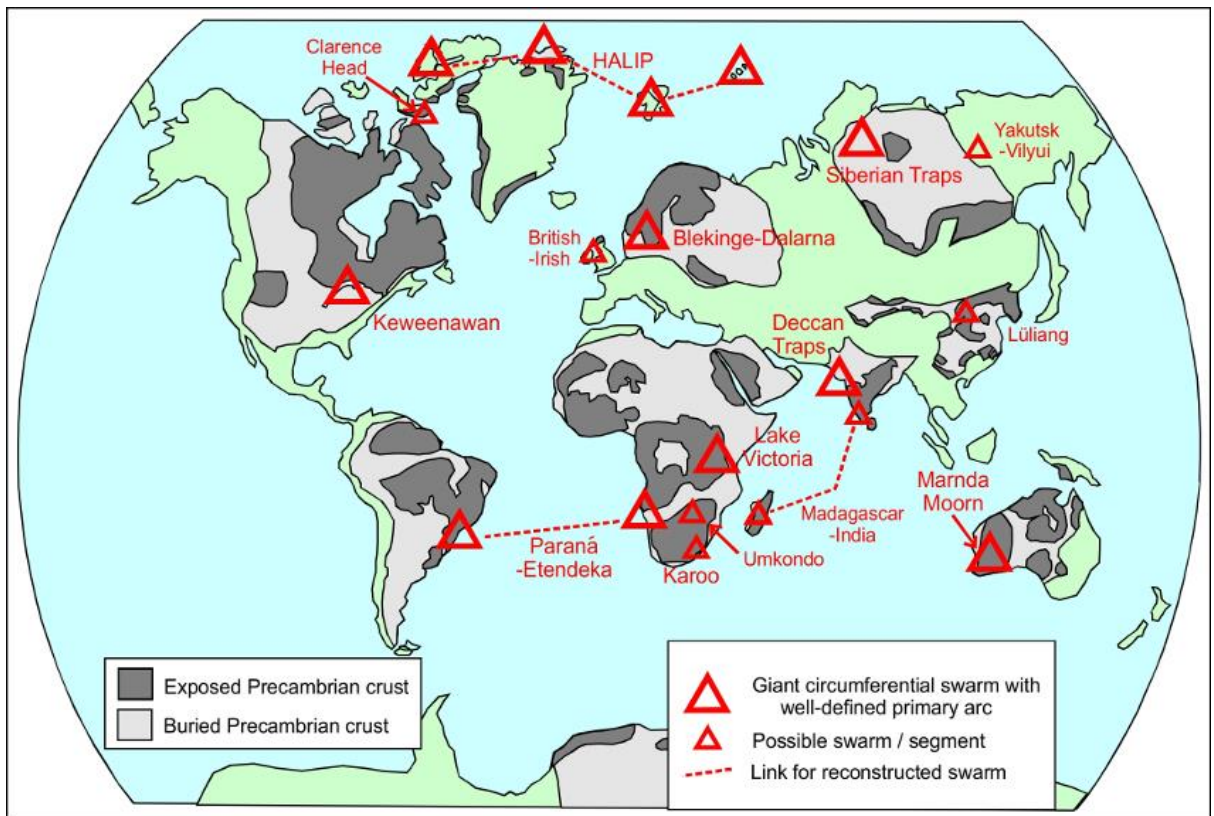


Fig. 1.3 Global distribution of giant circumferential dyke swarms and their possible segments. (<http://www.largeigneousprovinces.org/19jul>)

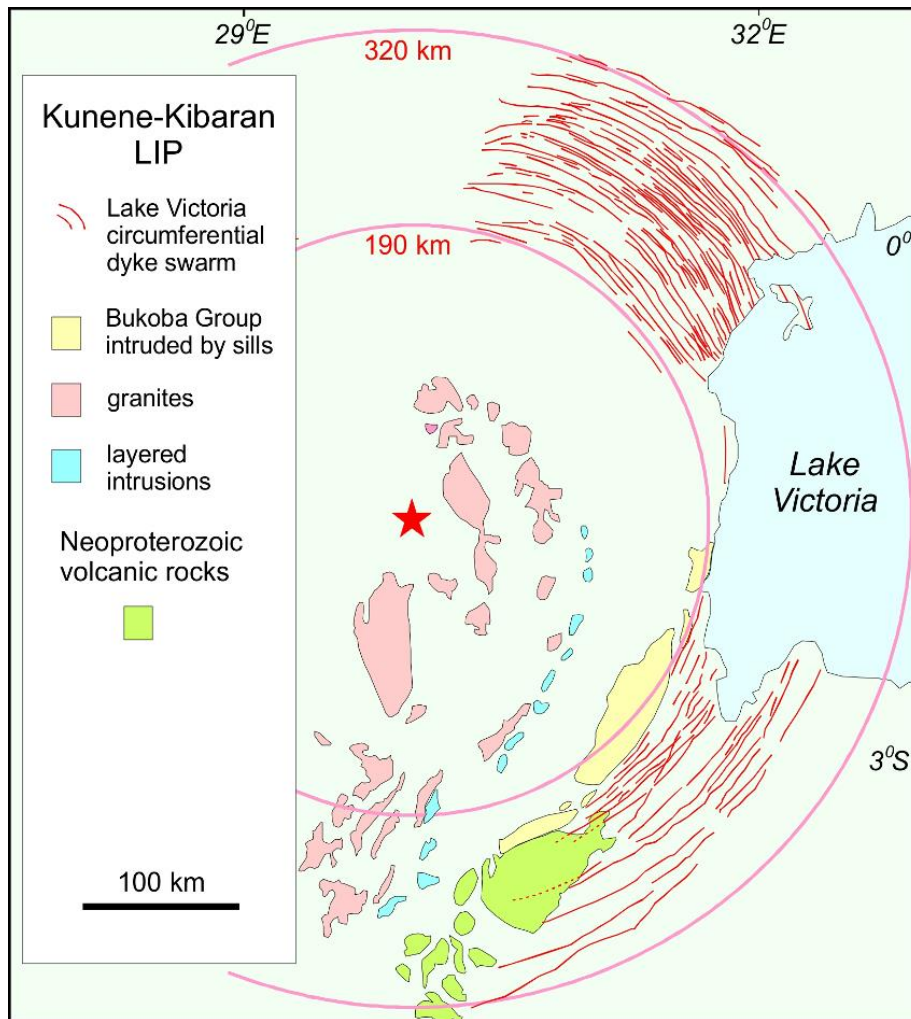


Fig. 1.4 Giant circumferential Lake Victoria dyke swarm (~1370 Ma) related to the Kunene-Kibaran LIP of eastern Africa, traced mainly from aeromagnetic data. Two pink circles indicate the approximate outer and inner dimensions of the swarm. The red star is the centre of the swarm. (<http://www.largeigneousprovinces.org/19jul>)

Understanding the evolution of the crust and getting an insight into the crustal growth processes has been the prime objective of the geological fraternity the world over. The apparent concentrations of large dyke swarms in North America, Scandinavia and Africa resulted in a more extensive study of dykes in these regions, commensurate with their occurrences. Hence the study of dyke swarms is essential to understand the process of crustal growth. The exchange between the ascending magmas and the pre-existing crust is linked to the development of compositional heterogeneities within the crust. Understanding

the kinematics of these differentiation processes, therefore, provide insight into the dynamics of crustal growth.

### **1.3 Emplacement mechanisms and Structural analysis of the dykes:**

The emplacement process is said to culminate of the formation of igneous intrusions. Changes in the propagation path constitute the beginning of the emplacement process and as the emplacement progresses, fractures lose their propagation capacity due to decrease in fluid pressure within the magmatic system (Watanabe et al., 2002). Emplacement can also be ceased due to “stoppers” present in the way of magma in the form of heterogeneities or discontinuities in the rock (Clemens and Mawer, 1992; Hogan et al., 1998). Classical work on mechanics of dyke intrusion by Anderson (1951), lead to several researchers dwelling on the problem (Weertman, 1971; Pollard, 1973; Pollard et al., 1975; Delaney and Pollard, 1981; Gudmundsson, 1984; Gudmundsson and Marinoni, 2002; Gudmundsson and Loetveit, 2005; Galindo and Gudmundsson, 2012). Though a relationship exists between the mechanics of dyke intrusion and the formation of the volcanic edifice, Gudmundsson (1984) cautions that there is a need to distinguish between a dyke that acts as a feeder to flow and a dyke whose movement is arrested at the crustal levels. Emplacement as a process involves interaction between magma and the host rock (Martinez Poza et al., 2014). This process comprises of two opposing mechanisms (Pitcher, 1979; Lister and Kerr, 1991; Hutton, 1982; Rubin, 1993): the first one is a forceful emplacement (hydro fracturing) when the dyke tip causes stress perturbation that fractures the host rock where magma material can migrate (Pollard et al., 1984; Ray et al., 2007), the second mechanism is the passive emplacement along pre-existing cracks and fractures (Paterson and Fowler, 1993; Vijayan et al., 2016).

On a general note, the magmatic pressure is high enough to generate hydrofractures in the crust and migrate upwards (Rivalta et al., 2015). The presence of pre-existing fracture networks is not necessary for a magmatic intrusion, but if present, the magma may exploit preferential areas of weaknesses (Delaney et al., 1986; Ziv et al., 2000). It has been significantly seen that only those fractures whose orientations are in consonance with regional stress field will be filled with magma, while others will be left unfilled except for local examples (Valentine and Krogh, 2006; Ray et al., 2007; Hooper et al., 2010; Gadgil et al., 2019). Owing to the low-negligible tensile strength of pre-existing structures (Mege and Korme, 2004), and in addition, as the rocks naturally possess pre-existing structures or fabrics, therefore the magmatic intrusions are of mixed-mode.

The morphologies of the dykes in their occurrence are a result of emplacement and deformation processes. The arrangement of dyke segments in an *en echelon* array (Pollard et al. 1982) is typical. The formation of horns or branching structures results due to the change in the stress field at the interaction point between two dyke segments (Hoek, 1991; Ramsay and Lisle, 2000). Various dyke swarm patterns provide clues to paleo-stress, crustal kinematics and geotectonic regimes (Martinez Poza et al., 2014). Structural analysis is an essential aspect of dyke studies (e.g., Babiker and Gudmundsson, 2004; Baer and Beyth, 1990; Delaney and Pollard, 1981; Gudmundsson, 1983, 1984, 1990, 1995, 2002, 2004, 2006; Chatterjee and Deshmukh, 1996; Mandal et al., 2006; Mége and Korme, 2004; Walker et al., 1995).

The emplacement mechanisms of Deccan dykes have been discussed earlier by Chatterjee and Deshmukh (1996), and also in more general studies such as the studies by Sant and Karanth (1990), Bhattacharji et al. (1996) and Sheth (2000). A critical aspect of current work is the new structural data and the use of magmatic overpressures to infer emplacement of the dykes. Gudmundsson (1983) used dyke aspect ratios to calculate

magmatic overpressures and thereby the depths of dyke origin in eastern Iceland. Babiker and Gudmundsson (2004) used aspect ratios of mafic dykes in Sudan to calculate magmatic overpressures. The study by Ray et al. (2007) used the length, trend and thickness distributions of the Nandurbar-Dhule dykes to calculate the magmatic overpressures. Source depths of some of the dykes are also calculated in the current study. This data are used to construct a tectonic model for the emplacement of the dykes.

#### **1.4 Earliest works on dykes in India**

All cratons of the Indian shield host numerous dykes and dyke swarms. A lesser number are found in the Purana (Proterozoic) basins (Srivastava et al., 2008). The dykes have been polymetamorphosed along the mobile belts (e.g. Eastern Ghats Mobile belt, Central Indian tectonic zone) due to recurrent deformation and such dykes can be distinguished from flows and sills. One of the earliest studies dates back to mid-nineteenth century when Clark (1869) reported preliminary data on the basaltic dykes from the Mainland of India opposite the islands of Bombay and Salcette. Blanford (1869) and Bose (1884) studied the dyke swarms from the lower Narmada valley. Deccan Traps have been the special attraction owing to their extreme diversity in differentiates and associated intrusives from Saurashtra and Kathiawar (e.g. Fermor, 1938; West, 1958).

Proterozoic magmatism in the Singhbhum craton comprises of a system of reticulate dolerite dykes termed as “Newer Dolerites” intrusive into the Singhbhum granite pluton (Dunn, 1929). Vredenburg (1906) reported diamondiferous sills and dykes intruding the Bijawars and Coulson (1933) reported similar dykes intruding the Lower Cuddapahs. Auden (1949) and Pascoe (1950) described the dykes from the Deccan area. Heron (1953) reported dykes intruding the upper amphibolite to granulite facies rocks of Banded Gneissic Complex in parts of Aravalli craton. Saha et al. (1973), Naqvi et al. (1974) initiated

geochemical studies on these dykes. Athavale and Verma (1970), Hasnain and Qureshy (1971) and Anjanappa (1972) are some of the earliest studies of paleomagnetism of Indian dykes. Crawford and Compston (1970), Balasubrahmanian (1975) and Ikramuddin and Stueber (1976) carried out geochronological studies on Indian dykes.

### **1.5 The west coast dyke swarm of the Deccan LIP**

The west coast dyke-swarm with a strike of NNW-SSE is a regional feature that is often exposed along the rocky stretch of beaches along almost the entire west coast of India (Deshmukh and Sehgal, 1988; Hooper, 1990; Dessai and Viegas; 1995; Vanderkluyesen et al., 2011). Systematic studies are, however, localized to select areas around Mumbai and in the vicinity of Trivandrum. Clark (1869) was among the first to describe the dykes along western India, with Auden (1949) presenting detail field features. Murthy (1987; 1995), Deshmukh and Sehgal (1988), Devaraju (1995) have provided more information on the dyke-swarms of western peninsular India. Most of the work carried out on the dykes pertains to the Deccan Traps covered areas (i.e. western part of Maharashtra) to the north of Goa.

In the north, at Mumbai, the dyke swarm is essentially parallel to the axis of the Panvel Flexure (best exposed between Mumbai and Panvel) and can be traced up to Ratnagiri in the south. The average inferred crustal dilation at Murud-Janjira south of Mumbai is about 30 % (Dessai et al., 1990). Dessai and Viegas (1995) suggest the crustal extension of 10-25 % at Borlai-Korlai north of Murud-Janjira. By contrast to the north Deccan, the SW Deccan region has fewer dykes studied except for a Poladpur-type feeder dyke identified near Chiplun (Devey, 1986).

The dykes in the coastal tract of southwestern peninsular India belong to Proterozoic and Phanerozoic ages. The latter dykes mostly are of Cretaceous age, but

belong to two distinct episodes separated by a narrow age gap of 10-15 Ma (Radhakrishna, 2007): The long en-echelon leucogabbro in central and north Kerala, a few isolated dykes in Agali-Coimbatore area and the St Mary's Island volcanism constitute the 90-85 Ma igneous episode. Two dykes from Hariyalurdurg area, about 80 km southwest of Bangalore in Karnataka have also obtained equivalent plateau ages (Kumar et al., 2001). The dominant NW-SE dolerites of central Kerala, NNW-NW/NNE-NE dolerites of north Kerala, and some dykes from Goa constitute the 70-65 Ma dyke activity coeval with Deccan continental flood basalt volcanism, to the south of Deccan Traps (Widdowson et al., 2000). In terms of their incompatible and immobile element chemistry, these 90-85 Ma dykes compare well with the east coast tholeiites of Madagascar (Storey et al., 1997). In contrast, the 70-65 Ma dolerite magmas resemble well the upper stratigraphic formations, particularly the Ambenalli Formation, of the Deccan lavas. The igneous episodes related to these two dyke intrusions are related to events of the Reunion plume and rifting of the Seychelles-Indian subcontinent and the Marion plume and rifting of Seychelles-India and Madagascar.

## **1.6 Greywackes**

Greywackes are one of the most abundant lithologies in the Dharwar craton, specifically in the Shimoga Supracrustal Belt occupying about 30,000 Km<sup>2</sup>. They are a major part of the Goa-Dharwar Sector (Devaraju et al., 2010) and also constitute a major part of the Sanvordem and Vagheri Formation of the Goa Group of rocks (Soman, 1993; Dessai, 2018). Few papers that pertain to greywackes are Gokul et al. (1985), Hegde and Chavadi (2009), Widdowson (2009), Devaraju et al. (2010), Fernandes et al. (2016), Dessai (2011, 2018).

Geochemical studies of fine grained clastic sedimentary rocks have proven useful to study the average composition of the upper crust (Hegde and Chavadi, 2009). Greywackes are the most abundant products of the Archean sedimentation process. Greywackes preserve a variety of trace elements due to the diverse framework mineralogy and matrix characteristics and hence have especially been used to understand provenance and evolution of the Archaean crust (Taylor and McLennan, 1985; Naqvi et al., 1988; Feng and Kerrich, 1990; Absar and Sreenivas, 2015, Ugarkar et al., 2017).

A study of sedimentary structures yields information about the depositional environment and can prove useful not only to understand the depositional environment but also post-depositional processes and basin evolution (Fernandes et al., 2016).

### **1.7 The Problem**

Iyer et al. (1990), Widdowson et al. (2000), Patil and Rao (2002), Fernandes and Widdowson (2009), Dessai (2018) have studied the dykes from the state of Goa, which provide relevant information on the various aspects of lineaments in Goa, dyke magmatism and crustal evolutionary processes. However, all these studies are either relating the dykes to the paleomagnetic history or their stratigraphical status in the Geology of Goa. Detailed discussion on the geochemistry of these dykes lacks in literature. Though there are reports of Proterozoic as well as Phanerozoic age dykes in Goa, there is a presumption in the international fraternity that all dykes of Goa belong to the Deccan phase.

In this thesis, I fill this gap, and provide hitherto unavailable data on the structural attributes and internal features of the Goa dykes, dilation profiles as well as detailed geological maps that give ground truth. I also discuss these dykes based on their petrological and geochemical characters. These combined approaches attempt to answer the question of the feeder or non-feeder nature of the Goa dykes to the Deccan Traps. I also

present the study of country rocks to assess their role as a contaminant, if present, in the dykes.

### **1.8 Objectives**

To fill the gap in the existing knowledge, in this present study, the following objectives are set:

- i. Establish the Spatio-temporal distribution of dykes by identifying sub-populations of dykes.
- ii. To have a better understanding of the spatial and temporal variation in dyke orientation and their attitude, which will provide a measure of paleo-tectonics.
- iii. To study the mutual relationship amongst the dykes vis-à-vis compositional variability
- iv. Petrogenesis of the dykes as well as of the country rocks
- v. Tectono-magmatic evolution of the western Indian continental margin

### **1.9 Workflow**

- i. Study of the satellite data complemented with aerial photographs so as to understand the orientation of the lineaments in the area.
- ii. Field check and reconnaissance mapping on a small scale map. Sectors showing a large population of dykes to be subjected to detail mapping on 1:5000 and 1:1000 scales to bring out the interrelationship of the dykes.
- iii. Study of the attitude of rocks and their mutual relationship with each other. Preparation of geological maps of selected areas.
- iv. Sampling for petrographic and geochemical investigations.
- v. Chemical analysis of rocks.

- vi. Computation and presentation of analytical data. Analysis and synthesis of data with reference to relevant literature.

## **1.10 Study area**

### ***1.10.1 Location***

The northern coast of Goa is situated along the western coastal margin of India. It is located ~150 km south of the southernmost exposures of the Deccan Traps (*Fig. 1.5a*). My study area is located along the coastline of Goa, north of the capital city of Panjim (*Fig. 1.5b*). It is included in the Survey of India toposheets 48E/10 and 48E/15. It comprises essentially of two *talukas*: Bardez and Pernem. Extensive exposures of country rocks (argillites, metagreywackes and quartzites) belonging to the Sanvordem Formation of the Goa Group (Gokul, 1985; Fernandes, 2009; Dessai, 2018; Gadgil et al., 2019) are traversed by the intrusives.

### ***1.10.2 Accessibility***

All the study areas are well connected by road network. They are accessible from the capital city of Panjim and towns of Pernem and Mapusa. As the exposures are present along the rocky coast, the intrusives and country rocks have to be approached on foot.

The next chapter will highlight the geological framework in which the study area lies.

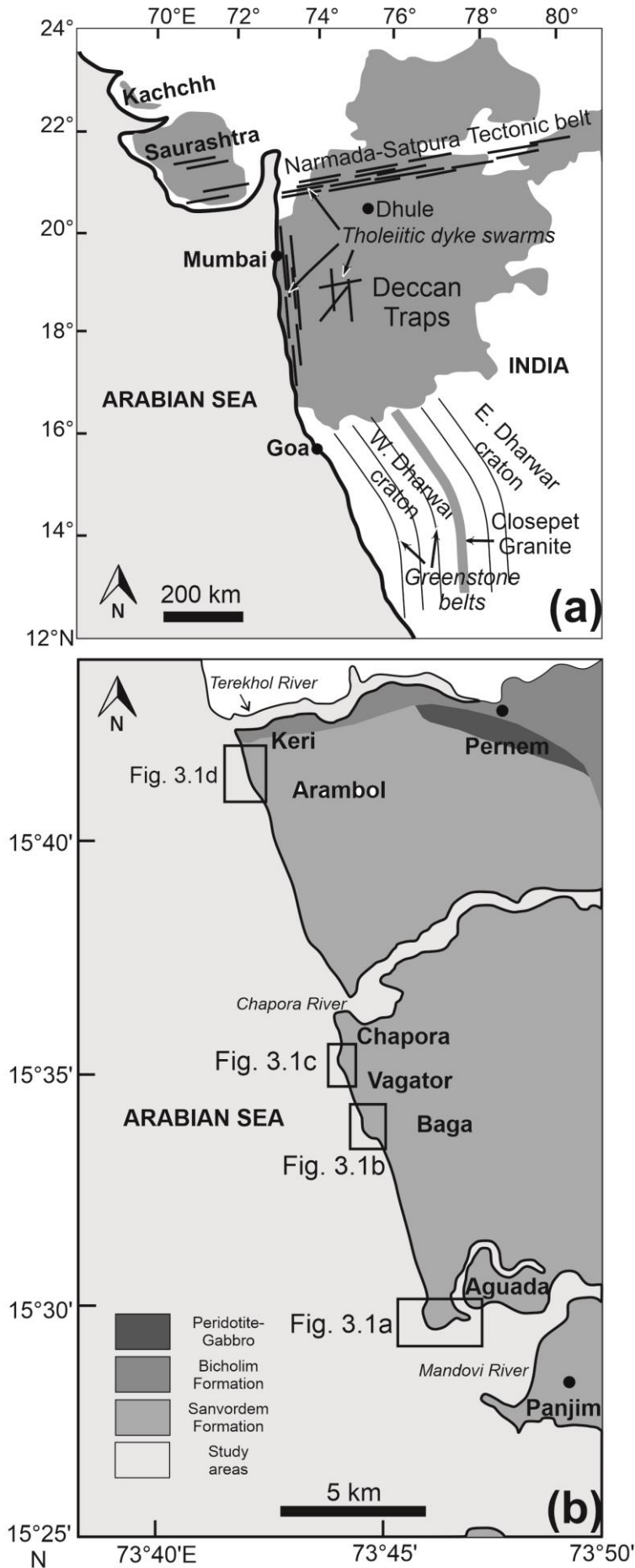


Fig. 1.5 (a) Map of western India showing the present-day extent of Deccan Traps with some major features and localities mentioned in the text marked. The three major dyke swarms of the province (Satpura-Tapi, ENE-WSW; Coastal, NNW-SSE along the continental margin; and Nasik-Pune, inland) are shown. Modified from Vijayan et al. (2016). (b) Geological map of the part of northern Goa (north of the capital Panjim), showing the locations of the four individual study areas (rectangles). Modified from Dessai (2011) and Gadgil et al. (2019).

## **CHAPTER 2**

# **Geological Framework**



## 2.1 Geology of the Dharwar craton

The Indian shield is a mosaic of Archaean cratons with the dominant ones being Dharwar, Bastar, Singhbhum, Bundelkhand and Aravalli. Three Proterozoic mobile belts constrain them. They are the Eastern Ghats Mobile Belt fringing the Dharwar, Bastar and Singhbhum cratons, the Pandyan Mobile Belt skirting the Dharwar craton and the Satpura mobile belt fringing the Bastar, Singhbhum, Bundelkhand and the Aravalli cratons and extending into Shillong Plateau (Ramakrishnan and Vaidyanadhan, 2010). The Dharwar craton of Archean age is a ~500 km N–S by ~700 km E–W crustal domain which is bounded by the ~65 Ma Deccan Flood Basalt Province to the North, washed by the waters of the Arabian sea to the West, and the Godavari rift as well as Eastern Ghats Belt to the east, and the transition to a granulite terrain in the South (Rogers, 1986; Naqvi and Rogers, 1987). This craton exposes a large oblique section of continental crust from lower crustal level (in the South) to upper crust (in the North) (Chardon et al., 2008, 2011). It comprises of three rock suites: TTG regionally known as Peninsular Gneisses, greenstone sequences of two generations and at least three generations of potassic to calc-alkaline granitoid intrusions (Bhaskar Rao et al., 1992; Nutman et al., 1992, 1996; Chadwick et al., 2000; Jayananda et al., 2000, 2006, 2008, 2013; Peucat et al., 1993, 1995, 2013).

The Dharwar craton is divided into the Western and Eastern Dharwar cratons (WDC and EDC). Closepet granite (2518 Ma) divides Dharwar craton into western (WDC) and eastern (EDC) sectors (Naqvi and Rogers, 1987; Jayananda et al., 2000; Moyen et al., 2003; Ramakrishnan and Vaidyanadhan, 2010). The WDC includes a basement of >3.0 Ga Tonalite–Trondhjemite–Granodiorite (TTG) gneisses, interlayered with Sargur Group rocks unconformably overlain by 2.9–2.6 Ga Dharwar Supergroup greenstone sequences that include basalts, komatiites, dacites, andesites, rhyolites, banded iron formation (BIF), conglomerates and sandstones (Ramakrishnan and Vaidyanadhan, 2010). The EDC consists

primarily of greenstone belts with pillowed basalts, pyroclastics and BIF with subordinate quartzite, marble, pelite and manganese formations (Ramakrishnan and Vaidyanadhan 2010).

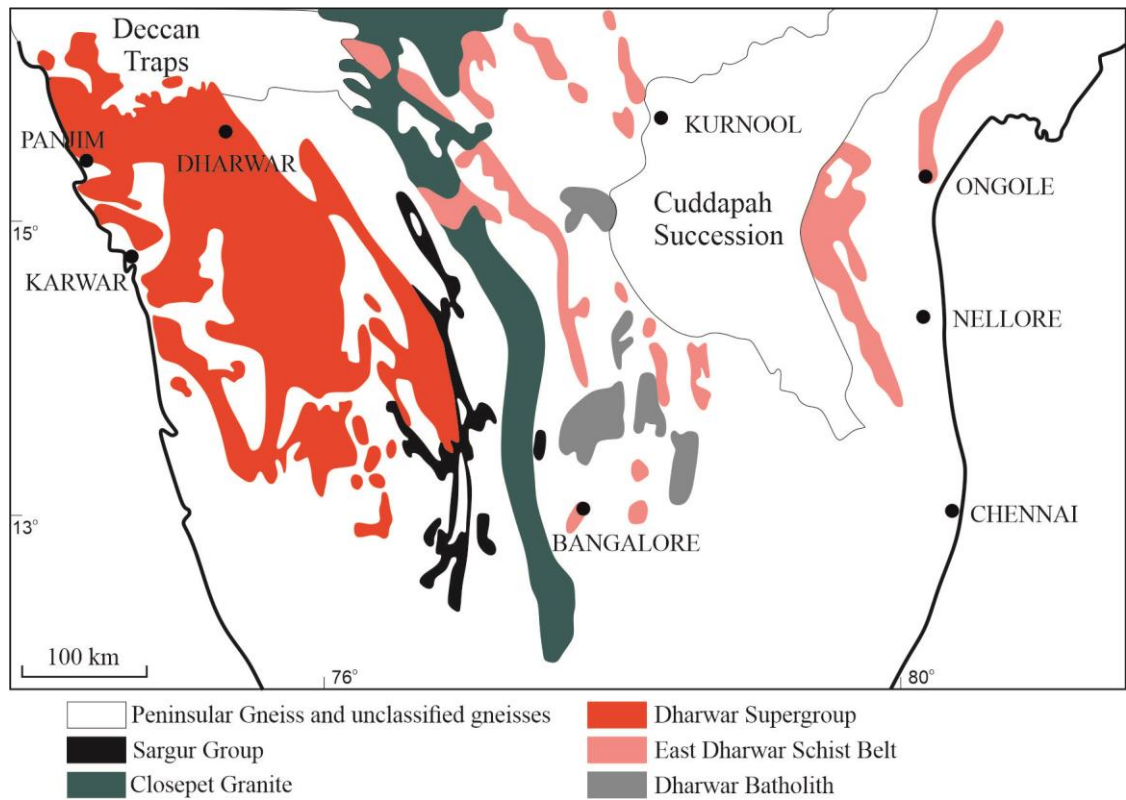


Fig 2.1 Figure showing the geology of the Dharwar craton and adjoining terranes (after Valdiya 2016)

The Dharwar Supergroup is further sub-divided into the lower Bababudan Group and the upper Chitradurga Group (Swaminath and Ramakrishnan, 1981). The lower Bababudan Group comprises of oligomictic conglomerate, phyllite, quartzite, mafic–felsic volcanics, tuffs and thick BIFs. The Chitradurga Group consists of polymictic conglomerate, greywackes, argillites and limestones with intercalations of mafic to felsic volcanic rock and BIFs (Seshadri et al., 1981; Viswanatha and Ramakrishnan, 1981; Ramakrishnan and Vaidyanadhan, 2010). Mafic volcanics from Bababudan yielded an Sm-Nd isochron age of  $3.03 \pm 0.23$  Ga (Drury, 1983) and Rb-Sr isochron age of  $2.58 \pm 0.27$  Ga (Bhaskar Rao et al. 1992). Nutman et al. (1996) obtained a SHRIMP U-Pb date of zircon from acid volcanic rocks from the lower Chitradurga Group, to be  $\sim 2.61$  Ga. Metamorphism in the WDC varies from low-temperature

greenschist to amphibolite facies, whereas the EDC exhibits high-temperature greenschist to amphibolite facies (Chadwick et al. 1997).

The Dharwar craton of the Indian shield exposes some of the tholeiitic dykes that are a part of the Proterozoic mafic dyke swarm (Ikramuddin and Stueber, 1976; Murthy, 1987; French and Heaman, 2010) (*Fig. 2.2*).

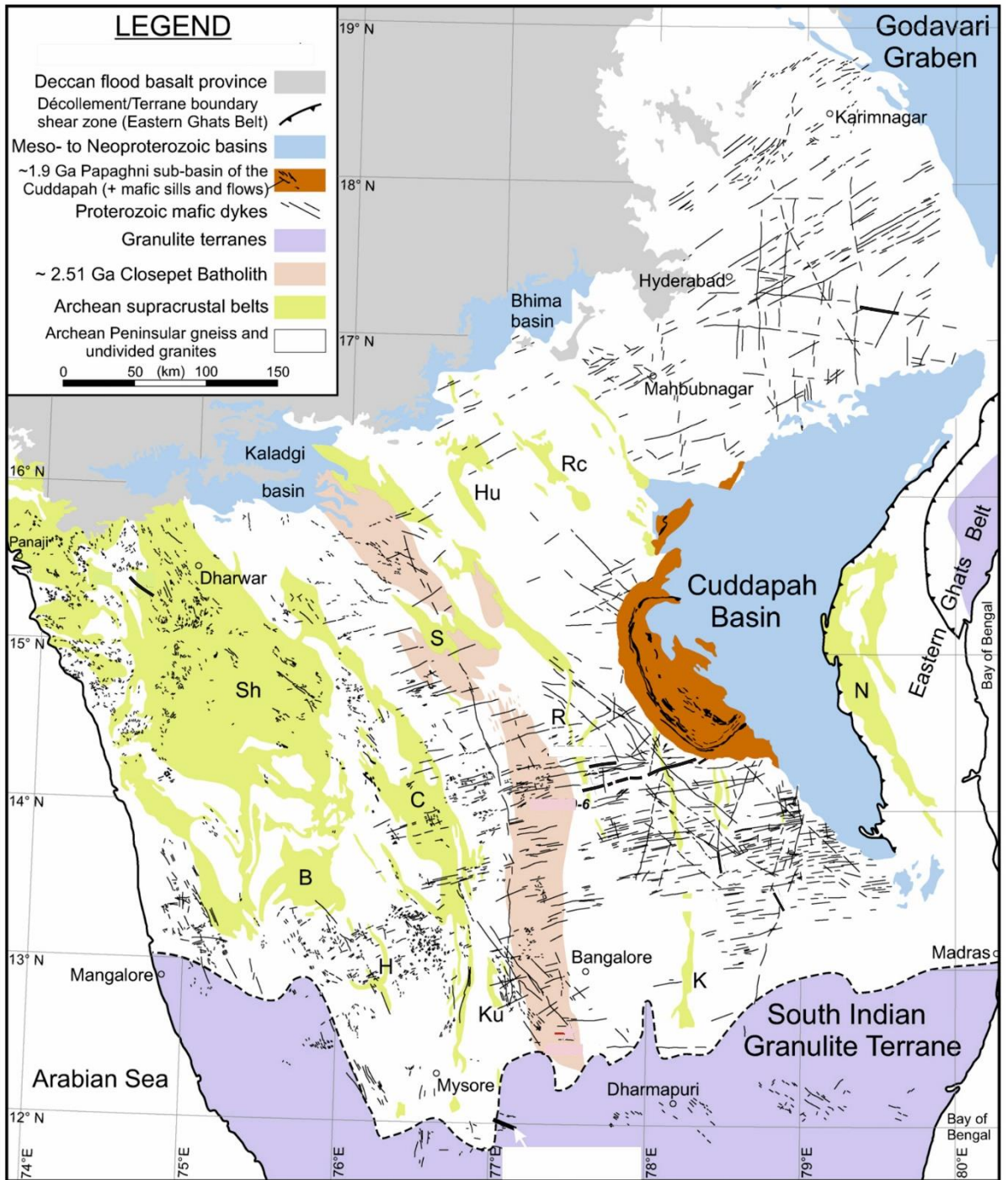


Fig. 2.2. Proterozoic mafic dykes on the Geological map for Dharwar craton. Greenstone belts: B, Bababudan; C, Chitradurga; H, Holenarsipur; Hu, Hutti; K, Kolar; Ku, Kunigal; N, Nellore; R, Ramgiri; Rc, Raichur; S, Sandur; Sh, Shimoga. Modified from French and Heaman (2010).

## 2.2 Geology of Goa

The state of Goa lies on the western coast of India with an area of 3702 sq. Km. The state is situated between latitudes 14°53' N and 15° 47' E and between longitudes 73° 40' N and 74° 20' E. It is bounded by Maharashtra towards the North and North-East, by Karnataka in the South and East and by the Arabian Sea towards the West. Western Ghats border Goa towards the east. *Fig. 2.3* depicts the geological map of Goa (modified after Dessai, 2011) that also shows the study area.

The regional stratigraphy and lithological associations of Goa, as well as their age, have been discussed by several researchers (Gokul et al., 1985; Dessai, 2011; Rekha et al., 2013a, 2013b; Ishwar-Kumar et al., 2013, 2016; Fernandes et al., 2016, 2018; Armistead et al., 2018; Gadgil et al., 2018; 2019). The state of Goa geologically represents the northwesterly extension of the granitoid-greenstone terrain of the western Dharwar Craton in Karnataka. It forms a part of the NNW-SSE trending Shimoga-Goa supracrustal belt comprising of characteristic litho-assemblages of Archean cratons, i.e. (i) Tonalite-Trondhjemite-Granodiorite (TTG) gneisses (ii) volcano-sedimentary sequences of greenstone belts and (iii) granitoid plutons. Here, Dessai (2011) divided the Goa Group of rocks into Barcem Group and Ponda Group with further subdivisions into the Barcem Formation, Sanvordem Formation, Bicholim Formation and Vageri Formation in the ascending order of superposition (*Table 2.1*). Granitoids, ultramafic rocks and mafic dykes intrude the Goa Group (Dessai 2011). The rocks of Goa Group are referred to as Goa schist belt and correlated with the Chitradurga Group (WDC) and the Mananara Group in the Antongil-Masora Block, NE Madagascar (Rekha et al., 2013b). I describe the salient aspects of petrology and geochronology of these lithologies in the following paragraphs.

### **2.2.1 Anmod Ghat trondhjemite gneiss**

It is amongst the oldest gneisses from India that temporally correlate with the Gorur Gneiss from Hassan district of Karnataka (Beckinsale et al. 1980). The Anmod Ghat Trondhjemite gneiss varies in composition from trondhjemite, tonalite to granodiorite (TTG). The foliation trends N-S and dips steeply at 60-70° due west. The gneiss has yielded an Rb/Sr whole-rock age of  $3400 \pm 140$  Ma (Dhondial et al. 1987) and recent Sm-Nd, and U-Pb work has provided ages of about 3300 Ma (Devaraju et al. 2007).

### **2.2.2 Chandranath granite gneiss**

It is classified as granite-monzogranite (Devaraju et al., 2007) with foliation trending in NE-SW and dipping 50° due east (Dessai, 2011). EPMA U-Pb monazite spot ages (*Quepem* granitoids of Rekha et al., 2013a) of  $2500 \pm 37$  to  $2619 \pm 37$  Ma differ with earlier Rb-Sr whole-rock age of  $2650 \pm 100$  Ma (Dhondial et al., 1987). This age is in contrast with the Sm-Nd isotope age of 2900 Ma (Devaraju et al., 2007). This granite gneiss formed as a response to the deformation-metamorphism marking the closing of the Neoproterozoic Goa basin (Rekha et al., 2013b). This granitoid temporally correlates with the Londa Granite in Karnataka (Dessai, 2018) and Masoala Suite in the Antongil-Masora Block, NE Madagascar (Rekha et al., 2013b).

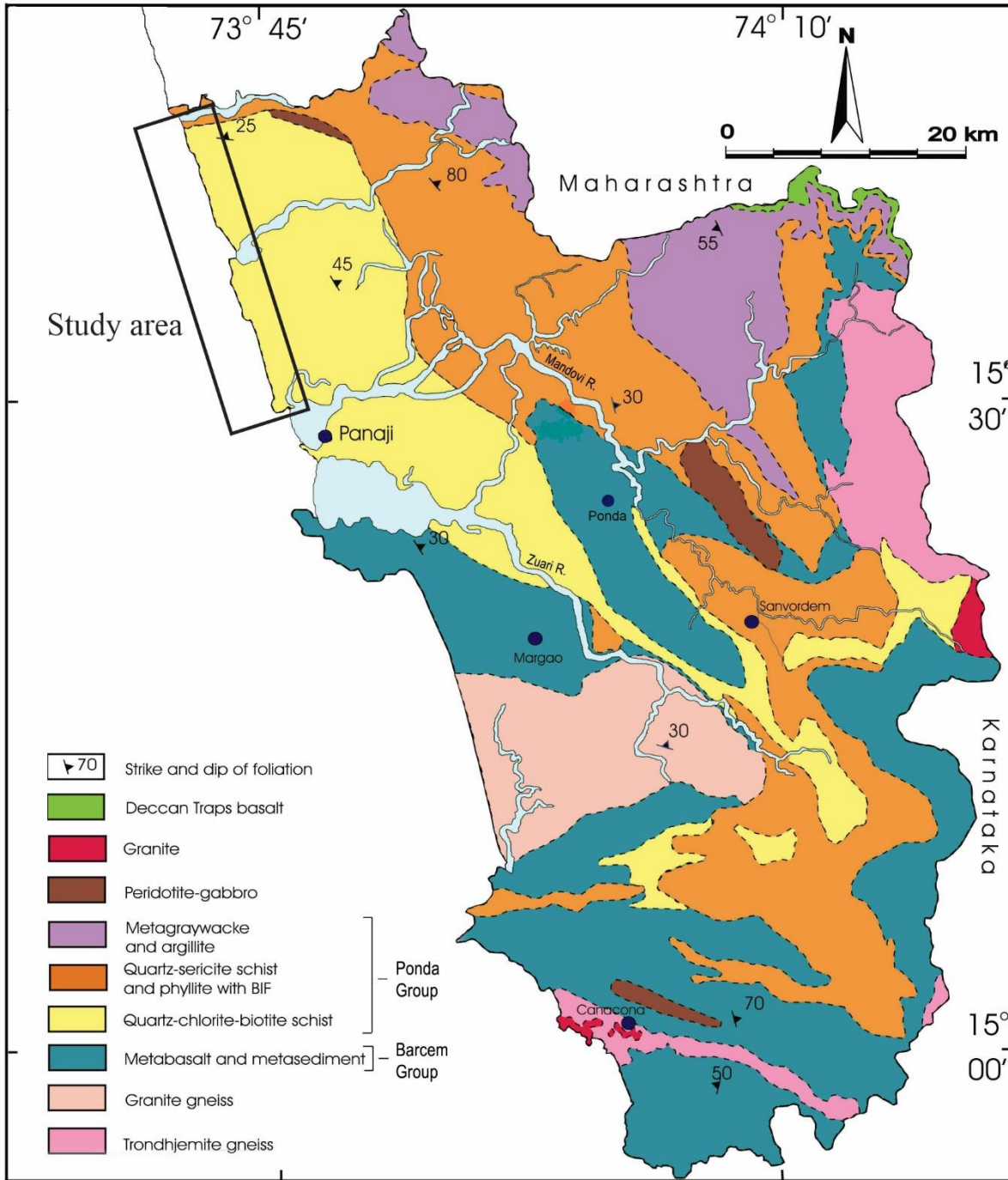


Fig 2.3 Geological map of Goa showing the study area (modified after Dessai, 2011)

### 2.2.3 Dudhsagar granite

Dudhsagar Granite is a coarse-grained rock showing weak to moderate foliation and preferred orientation of feldspar megacrysts parallel to foliation. It is either synkinematically

intrusive (Gokul et al. 1985) into the metavolcanics and metasediments or late to post-tectonic intrusion (Dhondial et al. 1987). Rb-Sr whole-rock isotopic data for this granitoid suggests an age of  $2565 \pm 95$  (Dhondial et al., 1987) while the recent Sm-Nd isotope systematics indicate an age of 2.85 to 2.96 Ga (Devaraju et al., 2007). The recent age overlaps with that of Canacona Granite.

The WNW-ESE gneiss-granite belt is flanked by the greenstones of the Barcem Formation, that rests on a basement of the trondhjemite gneiss (Dhondial et al. 1987).

#### **2.2.4 Canacona granite**

The granite here is unfoliated, blastoporphyratic, coarse-grained, preserves the euhedral/subhedral magmatic shape and it exhibits a discordant relationship with the WNW-ESE foliation of the older TTG/migmatite (Dessai, 2011; Rekha et al., 2013a, b). EPMA U-Pb monazite spot ages yield an age of  $2924 \pm 50$  Ma (Rekha et al., 2013b). This age determination proves that it is much older than previously thought ( $2395 \pm 390$  Ma; Dhondial et al., 1987).

#### **2.2.5 Bondla mafic-ultramafic layered complex**

The NW/SE-trending, ophiolitic, layered Bondla ultramafic-mafic complex consists of gabbro, troctolite, wehrlite, dunite, peridotite, pyroxenite, and chromitite, as well as serpentinite with chromite (Jena, 1980, 1985; Sreeramachandra Rao et al., 1996; Dessai et al., 2009, Ishwar-Kumar et al., 2016). Dessai and Peshwa (1982) have shown that the complex occupies a major shear zone that runs NW-SE. Its origin could be due to the result of modification of sub-alkaline tholeiitic magma by periodic injection with a more primitive chrome-rich magma in two interconnected sub-chambers concomitant with fractional crystallization (Dessai et al., 2009). Recent research attributed its possible origin in a

subduction-related setting (Ishwar-Kumar et al., 2016). This complex has been dated by the K-Ar method on biotite separates in gabbro at 1644 to 1536 Ma (Ishwar-Kumar et al., 2013).

**Table 2.1:** Lithostratigraphic sequence of Goa Group (Modified after Dessai, 2011, 2018).

Rocks	Age/Formation	Lithology
Newer Intrusives	$62.8 \pm 0.2 \text{ Ma}^1$	Dolerite
Older Intrusives	Proterozoic	Metadolerite
Mafic-ultramafic layered complex	1644-1536 Ma <sup>2</sup>	Dunite-peridotite-gabbro complex and equivalents
Ponda Group	Vagheri Formation	Metabasalt, argillite and metagreywacke
	Bicholim Formation	Banded ferruginous quartzite, Manganiferous chert breccia, Limestone, Ferruginous phyllite, Quartz-chlorite-amphibolite schist
	Sanvordem Formation (2458 to 2566 Ma <sup>3</sup> ) (2424 to 2462 Ma <sup>5</sup> )	Metagreywacke, Argillite, Quartzite, Para-conglomerate
~~~~~ Unconformity ~~~~~		
Barcem Group	Barcem Formation	Metagabbro, Peridotite, talc-chlorite schist, Quartzite, Phyllite, Quartz Porphyry, Massive, schistose and vesicular metabasalt
~~~~~ Unconformity ~~~~~		
Chandranath Granite Gneiss	$2500 \pm 37$ to $2619 \pm 37 \text{ Ma}^3$	Granodiorite
Canacona Granite	$2924 \pm 35 \text{ Ma}^3$	Porphyritic potassic granite
Anmod Ghat trondhjemite gneiss	$3138 \pm 35 \text{ Ma}^3$ $3300 \text{ Ma}^4$	Basement : trondhjemite-tonalite-granodiorite

<sup>1</sup>Widdowson et al., 2000; <sup>2</sup>Ishwar-Kumar et al., 2013; <sup>3</sup>Rekha et al., 2013b; <sup>4</sup>Devaraju et al., 2007; <sup>5</sup>Armistead et al. 2018.

### 2.2.6 Barcem Group

Dessai (2011) elevated the status of Barcem Formation to a 'Group' and co-related to the lower part of Kalaspura Formation of Bababudan Group. With the quartz-pebble conglomerate as the basal horizon, the litho-units consist of metavolcanics (quartz sericite-schists and quartz porphyry) with intercalations of quartzites and pelites. Mafic and felsic lavas represent the volcanics along with agglomerates and tuffs.

### 2.2.7 Ponda Group

The Ponda Group comprises three formations which in ascending order are the Sanvordem Formation, Bicholim Formation and the Vagheri Formation.

#### 2.2.7.1 Sanvordem Formation

It rests on the Chandranath granite gneiss with a polymict metaconglomerate at the base and comprises of metagreywacke, and argillites with a thickness of over 1.2 km (Dessai, 2011). However, Gokul et al. (1985) did not assign any stratigraphic significance to this conglomerate owing to its occurrence as small lensoidal bodies within the widely distributed metagreywacke. They regarded it as a turbidite deposit based on its matrix-supported fabric. The metagreywacke consists of sub-angular quartz, plagioclase and lithic fragments in a matrix of sericite, chlorite and quartz. The argillites consist of quartz in a sericite-chlorite matrix with opaques. Detailed petrography of this metaconglomerate is available in Devaraju et al. (2010), Rekha et al. (2013a), and Gadgil et al. (2018). Zircon U-Pb geochronology of three greywacke samples along the northern coast of Goa yielded an age distribution of  $2424 \pm 27$  to  $2462 \pm 30$  Ma (Armistead et al., 2018). EPMA Th-U-Pb monazite dating of tonalite clasts in metaconglomerate yielded an age of  $3128 \pm 60$  Ma and the chlorite-biotite-muscovite-calcite matrix is dated by the same method to  $2566 \pm 53$  to  $2458 \pm 34$  Ma (Rekha et al., 2013b).

#### 2.2.7.2 Bicholim Formation

It consists of amphibole schists, ferruginous and manganiferous phyllites, limestones and Banded Haematite Quartzites (BHQ) that occur as intercalations within the phyllites with an average thickness of about 1.4 km (Gokul et al., 1985). These BHQ's serves as the protores for the iron ore deposits in Goa. Limestone exposures are rare and occur in the northeast part of Goa.

### 2.2.7.3 Vagheri Formation

It is the youngest formation of the Ponda Group. It comprises metagreywacke-argillite with intercalated metabasalts. The metagreywackes consist of angular to sub-angular mono- and lithic-fragments in a fine-grained mesostasis made up of quartz, feldspar and chlorite. The rocks are immature with poorly sorted angular and subangular clasts of andesitic tuffs (Devaraju et al., 2010). The metabasalts consists of chlorite, tremolite/actinolite, plagioclase, epidote, zoisite, opaques and quartz which may be secondary.

### 2.2.8 Mafic intrusives

Igneous mafic intrusives are a common feature and cross-cut the entire sequence of Goa Group of rocks. Coastal tracts expose these dykes very well due to prevalent marine erosion. Geochemical, geochronological and paleomagnetic studies are carried out on selected areas of Goa (Widdowson et al., 2000; Patil and Rao, 2002; Fernandes and Widdowson, 2009).

Selected dykes from the coastal part of North Goa are geochemically akin to Deccan type magmatic products and specifically to transitional Ambenali-Mahabaleshwar magma type (Widdowson et al. 2000). These same dykes were dated using the  $^{40}\text{Ar}/^{39}\text{Ar}$  technique to  $62.8 \pm 0.2$  Ma (Widdowson et al., 2000), an age that is significantly younger than the current estimates for the age range of Deccan Traps volcanism (~65-69 Ma) (Sprain et al., 2019). The ages are looked upon with caution owing to the absence of any plateau ages (Baksi, 2014).

Few dykes in south Goa (Canacona region) reveal geochemical similarity to normal MORB (mid-oceanic ridge basalts) and IAT (island arc tholeiites) and have K, Rb, Ba and Zr contents significantly lower than average diabase and Deccan Trap basalts (Fernandes and Widdowson, 2009). These dykes are dated using  $^{40}\text{Ar}/^{39}\text{Ar}$  laser ablation technique which generates data for individual crystals in the samples. Spot dates yielded variable ages from 2.7

– 4 Ga with the majority of the feldspar ages occurring within the 2.7 – 3.4 Ga range (Fernandes and Widdowson, 2009). However, these authors claim that this age is by no means as robust as experiments on younger, fresh, sub-aerial lavas and the readers are advised to observe caution while referring to these ages.

A rather brief description and insights on the petrogenesis of the dyke swarm at Aguada considers dykes belonging to two age groups (Dessai 2018). Petrological description classifies these dykes into tholeiites and oceanites. Lineament studies revealed that the dyke emplacement is facilitated by the rejuvenation of the basement trends along a system of NNW-SSE to NW-SE trending fault/fracture system related to the “Panvel Flexure” (Dessai and Bertrand, 1995; Dessai and Viegas, 1995; Dessai, 2018). These dykes are believed to be synchronous with the late intrusive phase associated with the Deccan Traps and were not considered as ‘feeders’ for the Deccan Trap lavas (Dessai, 2018).

A detailed study using alternating field (AF) and thermal demagnetisation techniques on selected dykes located at Aguada Headland and in central Goa (Madgaon) has revealed that 6 dykes (from Madgaon) have reverse magnetic polarity direction and 3 dykes (from Aguada) exhibit normal polarity (Patil and Rao, 2002). A paleomagnetic pole thus calculated lies close to the Deccan super pole suggesting that the some of the dykes in Goa are indeed related to Deccan basalt eruptions.

### **2.2.9 Deccan Traps:**

The Deccan Traps flood basalt province covers an area of 500,000 km<sup>2</sup> of Indian states viz. Maharashtra and adjoining regions in Gujarat, Madhya Pradesh, Andhra Pradesh, Karnataka and the northeastern strip of Goa (Krishnan, 1960; Agashe and Gupte, 1971; Raja Rao et al., 1978). Offshore drilling in the western Indian continental coast has revealed its sub-

surface extension is sometimes lying 1500 m below the mean sea level (Valdiya, 2016). With original lava volumes above  $(1-3) \times 10^6 \text{ km}^3$  (Wadia, 1975; Sen, 2001), they are mostly composed of laterally extensive flat-lying tholeiite flows (West 1959; Raja Rao et al. 1978). The basalt flows are of two types, “compound” and “simple” (Bondre et al., 2004a,b).

Based on studies in Mahabaleshwar-Nasik region, a standard stratigraphy has been established (Najafi et al., 1981; Beane et al., 1986; Cox and Hawkesworth, 1984, 1985; Lightfoot et al., 1990; Peng et al., 1994). Based on measured sections, paleomagnetism, geochemistry and isotopes, the Deccan Traps have been divided into three subgroups comprising eleven formations (Table 2.2).

**Table 2.2:** Stratigraphy of the Deccan Traps in the Western Ghats region. Based on Subbarao and Hooper (1988), Peng et al. (1994), Schoene et al. (2019). N = Normal magnetic polarity, R = Reverse magnetic polarity.

Group	Sub-group	Formation	Magnetic polarity
		Desur (~100 m)	N
		Panhala (>175 m)	N
	Wai	Mahabaleshwar (280 m)	N
		Ambenali (550 m)	R
		Poladpur (375 m)	R
Deccan Basalt Supergroup	Lonavala	Bushe (325 m)	R
		Khandala (140 m)	R
	Kalsubai	Bhimashankar (140 m)	R
		Thakurvadi (650 m)	R
		Neral (100 m)	R
		Jawhar-Igatpuri (>700 m)	R

Several methods have been used to estimate the age of the Deccan Traps that include stratigraphical, paleontological, paleomagnetic and radiometric methods (Baksi, 1994; Jaeger et al., 1989; Vandamme et al., 1991; Venkatesan et al., 1993; Venkatesan and Pande, 1996; Hofmann et al., 2000; Pande, 2002; Schoene et al. 2015; 2019; Sprain et al., 2019). There are estimates of a very rapid eruption of the basalts over perhaps a million years at  $67.5 \pm 0.3 \text{ Ma}$  (Courtilot et al., 1986, 1988; Duncan and Pyle 1988; Allègre et al., 1995; Hofmann et al., 2000). However, contrary to the suggestions of Pande (2002) and Schoene et al. (2019)

suggestions of the episodic nature of Deccan volcanism, Sprain et al. (2019) suggest that >80 % of volcanism took place within 1 million years.

#### **2.2.10 Laterite**

Goa is covered by a layer of laterite ranging in thickness from a few meters to 25 meters. It is generally pisolitic (Gokul et al., 1985). Apart from granite exposures in Goa, laterite has developed almost overall lithologies especially over metabasalts of the Barcem Group and metagraywacke and argillite of the Sanvordem Formation which underlie many of the coastal plateaux areas (Widdowson, 2009). A detailed account on the laterite profile of the Mercedes quarry, Panjim is available (Widdowson, 2009 and the references therein).

#### **2.2.11 Structural aspects of the rocks of Goa**

The rocks of the Goa Group exhibit essentially three cycles of folding. The first fold movement resulted in a general E-W trending round hinged upright normal folds. The relict axial traces of this fold are preserved in the southern part of Goa. Associated with this fold movement, the syntectonic Chandranath granite gneiss has been emplaced along the axial zone of a major anticlinal fold (Gokul, 1985; Rekha et al., 2013b).

The second cycle of folding, which was the most prolific movement was responsible for the development of the NW-SE trending folds, overturned towards SW and plunging towards NW and SE. The folding movement imparted the NW-SE Dharwar trend to these rocks. The feldspathic gneiss and the hornblende granite exposed along the Western Ghats are syntectonic and related to the second fold movement (Gokul, 1985).

The third fold movement whose manifestation is noticed only in the northeast part of Goa has resulted in a northwest-plunging broad open synclinal fold with its axis running in the N30°W direction west of Valpoi. Compared to the earlier two, the third fold movement is the feeblest. All the three cycles of folding have resulted in greenschist facies of metamorphic

rocks. Only at the contact of various intrusive granite rocks, the grade of metamorphism has locally risen to upper amphibolite facies (Gokul, 1985).

As opposed to the view of Gokul (1985), Rekha et al. (2013b) observed two tectonic fabrics in the youngest dated Goan metamorphic rocks in the WDC. Rekha et al. (2013b) made structural and lithologic correlation speculating the possible connection of the rocks in Goa with that of Antongil-Masora Block of the northeastern coast of Madagascar. The authors termed the metamorphic rocks belonging to the Goa Group as the “Goa Schist Belt (GSB)” and correlated them to the Mananara Group and Amodiriana Formation of Madagascar. The authors also claimed, “Chandranath Granite Gneiss” called as “Quepem Granitoid” connects well with the felsic plutonic Masoala Suite in Madagascar.

### **2.3 Basic dyke swarms**

I have attempted to provide a summary of relevant literature published to date. This summary is extensive but not exhaustive.

#### **2.3.1 Proterozoic dyke swarms in the western Dharwar**

These dykes are important because Dharwar craton was a principal part of ancient super-continents (Rogers, 1996; Heaman, 2008; Srivastava et al., 2008) and help in paleocontinental reconstructions.

Murthy (1995) noted that the dominant trends of mafic dykes in Southern Peninsular India are E-W, NW-SE and NE-SW. He divided the dyke swarms into 5 groups for easy understanding. Swarm 1 veers in strike between ENE to ESE and forms near Cuddapah basin. Swarm 2 lies on the NW margin of Cuddapah basin forming two clusters. One cluster contains discontinuous outcrops traced towards Hutti schist belt and other group lies to the north-

trending NE-SW and N-S dykes. Swarm 3 lies east of Hyderabad having ENE-WSW and WNW-ESE trends traversed by widespread NNE-SSW to N-S dykes. Swarm 4 consists of several small, dense and widely separated clusters spread in Karnataka in gneisses and greenstone belts. The west coast in Kerala has a NNW and NW trending swarms. He also mentions that smaller swarms (e.g. swarm in Madgao-Goa) occupy the dilations in the domal upwarps in the Peninsular gneiss basement between the major greenstone belts downwarps. Swarm 1 is dated and consists of age groups of 2420-2068 Ma, 1938-1700 Ma, 1470-1250 Ma and 650 Ma. Swarm 2 and 3 is 2270-2065 Ma old. Swarm 4 is 2193-1900 Ma, 1600-1400 Ma and, 1535-1018 Ma. Swarm 5 has two age clusters, 2200-1660 Ma and 476-75 Ma.

Halls et al. (2007) provided an age of  $2367 \pm 0.1$  Ma for a diabase dyke in the E-W dyke swarm and suggested the presence of a major early Proterozoic dyke swarm that cuts across the Dharwar Craton. The swarm was estimated to be at least 300 km x 300 km with a fan angle of  $30^\circ$  converging to the West. It was thought that this swarm together with Widgiemooltha dykes of Australia, must have been a part of a plume event active from 2418 to 2367 Ma.

Chandrasekharam et al. (2008) studied the picritic basalts and basaltic andesite dykes at Kalyadi (E-W) showing at least two different petrogenetic affinities. These picite basalts and basaltic andesite dykes do not have signatures of plume-related melts but are instead a product of passive melting of asthenospheric mantle without interacting with the crustal parts of the lithosphere.

Devaraju et al. (2008) studied Paleoproterozoic (>2000 – 1650 Ma), Mesoproterozoic (~1100 Ma) and rare Eocene (62-63 Ma) mafic dyke intrusions in a zone 225 km long and 40 km wide in northern Western Dharwar Craton. The dykes usually strike E-NE, unmetamorphosed, undeformed, showing chilled margins, fracture-controlled and are of sub-

alkaline tholeiite type. Based on geochemistry, they inferred that they bear affinity to the ocean floor, volcanic arc and N-MORB emplaced along destructive plate margin. Owing to a close association of these dykes it is believed that they are related to the same magma chamber and have intruded in several batches with the considerable time gap in successive intrusions.

French and Heaman (2010) provided seven ages for the mafic dykes that defined new dyking events at 2221-2209 (Kandlamadugu and Somala dyke) and 2181-2177 Ma (Dandeli and Bandepalem dykes) and confirmed a third at 2369-2365 Ma (Bangalore). Three E-W trending dykes from Bangalore dyke swarm indicate rapid emplacement in less than five million years thus qualifying for a newly recognised pulse of mafic magmatism at 2369-2365 Ma. Using the similarity in timings of emplacement of Paleoproterozoic mafic dyke swarm in Dharwar and Slave Cratons, they constrained the configuration of the ~2.2 Ga supercraton Sclavia.

Piispa et al. (2011) made a study on paleomagnetism and geochemistry of the Proterozoic dykes in the Dharwar. They suggested that the Bastar and the Dharwar cratons amalgamated before ~2370 Ma. Their study also indicated the presence of two distinct ~E-W trending dyke swarms, at ~2370 Ma and ~1890 Ma respectively, in the Dharwar craton, both possibly extending till Bastar craton.

Kumar et al. (2012) provide new geochronology, geochemistry and paleomagnetic data for a 2.367 Ga Dharwar giant dyke swarm. The geochronology constrains the emplacement of this dyke swarm in a period of ~5 Ma. With a fanning angle of 40°, the converging focal point lies 300 km west of the present-day Dharwar craton boundary. The authors state that there is uniformity in their geochemical characteristics despite being spread over an extensive area and attribute mantle plume for its origin. Rameshbabu et al. (2018) gathered new paleomagnetic results for this swarm and constructed paleogeography from coeval dyke events

linking Dharwar craton, Yilgarn craton (Australia), Kola-Karelia craton (Baltica shield) and Zimbabwe craton (Africa) and suggest these cratons to be spatially linked during ~2.3 to ~2.4 Ga.

Belica et al. (2014) present paleomagnetic and geochronologic results of a radiating dyke swarm within Peninsular India at 1.88 Ga and the paleocontinental reconstruction at this time conflicts with the archetypal Columbia model. The authors also thrust on two separate paleomagnetic directions for ~2.2 Ga dykes and attribute this to the two magma pulses highlighted by French and Heaman (2010). Paleomagnetic results from 2.37 Ga dykes place India at polar latitudes. They also attribute Paleoproterozoic Apparent Polar Wander Path for the Dharwar Craton and comment on its paleogeographic relations for the 2.37-1.88 Ga time interval.

Silpa and Satish-Kumar (2018) emphasized on the shortage of studies carried out on mafic dyke swarms in the Western Dharwar Craton which was the reason to carry out studies on the Tiptur dykes (South Karnataka) and compare them with the Eastern Dharwar Craton. The NW-SE trending dykes are dolerites whereas NE-SW trending ones are metadolerites. Petrography and geochemistry studies suggested that they may not be cogenetic. Since there are no reports of metadolerites from EDC, the authors believe that the Tiptur metadolerites could be a part of an earlier event restricted only in WDC before the amalgamation of the WDC and EDC.

### **2.3.2 Deccan lavas and associated dyke swarms**

Blanford (1869), Clark (1869), Bose (1884), Crookshank (1936), Fermor (1938) and West (1958) were amongst the workers on dyke swarms of the Deccan Traps. Auden (1949) provided a comprehensive account of the field features and their interpretations. He believed

that not all dykes have acted as feeders to the Deccan Traps and some of them are post-Trap injections.

Agashe and Gupte (1971) attempted to answer the question of mode of eruption of Deccan Trap basalts. Their field studies revealed that vast swathes of the Deccan Trap area remained devoid of dykes, however, they found volcanic vents at a number of widely separated localities. This led them to suggest that many of the lava flows were the products of central type of volcanicity.

Cox (1980) reviewed the paradox of the nature of CFB magmas; whether they are primary or derived from picritic parent magmas, he advocated the presence of the latter process.

Cox and Hawkesworth (1984) divided the basalts in the Mahabaleshwar area into three formations: the Poladpur, Ambenali and Mahabaleshwar Formations. They interpreted Poladpur Formation as having developed by Ambenali magma type contaminated with ancient granitic crust, with simultaneous fractionation of a gabbroic mineral assemblage. The Ambenali magma is essentially an uncontaminated one. The Mahabaleshwar Formation is contaminated by enriched mantle or lower continental crust. Peng et al. (1994) studied lower formations of the western Deccan Traps and hinted at the contamination of lavas by Indian Archean basic amphibolite into Ambenali type primitive magma.

Cox and Hawkesworth (1985) described Bushe, Lower Poladpur, Upper Poladpur, Ambenali and Mahabaleshwar Formations in detail. They note that substantial crustal contamination in lower formations decreases up the sequence. They strongly advocate the RTF (replenished, tapped, fractionated) magma chamber model and the idea of periodic replenishment by picritic magmas.

Beane et al. (1986) studied vast swathes of Deccan Traps in the Western Ghats with the intention of establishing flow stratigraphy. They divided the Deccan basalt into three subgroups and ten formations. They described geochemistry and isotopes and, in detail, seven principal formations and most prominent individual flows. They provided evidence of persistent southerly dip and gentle southerly plunging anticlinal form of the flows, the lensoid shape of many formations and randomly oriented feeder-dyke system and advocated for the formation of central volcanic edifice as the Indian plate migrated over the mantle plume/hotspot.

Deshmukh and Sehgal (1988) provided detailed maps of Deccan mafic dykes located in the West coast, and Narmada-Tapti lineament zones. They regarded these dykes to be post-Trap hypabyssal injections. The dominant trend was N-S to NNE-SSW on the west coast whereas E-W to ENE and ESE in the Narmada-Tapti zone. The pre-existing lineaments controlled these dykes in these areas.

Lightfoot et al. (1990) studied stratigraphy between Mahabaleshwar Ghat and Belgaum and described the Desur Unit of the Panhala Formation. They found that the magma generation for flows older than Ambenali is either attributed to gabbro fractionation or to crustal interaction with the hotter magma. They concluded that there was an apparent switch from crustal lithospheric contributions to mantle lithospheric contributions through the stratigraphy.

Hooper (1990) tried to tackle the problem of the initiating factor for the extension and rifting of the crust to be either mantle plume or the rifting. Based on his flow-by-flow mapping of Columbia River Basalt Group and Deccan Basalt Group he concluded that the eruption of the main tholeiitic phase was preceded by significant extension and thinning of the crust.

Hence, mantle upwelling initiated the crustal extension with the help of rifting and decompression.

Peng and Mahoney (1995) studied picritic and basaltic lavas from three drillholes in the northwestern Deccan Traps. They provide isotope evidence on the composition of the mantle source. The first trend reflects mixing between a mantle end-member very similar to that of modern Reunion Island and broadly like a lithospheric end-member in the Madagascar province. The second trend reflects mixing between the similar continental lithospheric material and a mantle end-member resembling that of the thick Ambenali Formation of the southwestern Deccan.

Dessai and Viegas (1995) studied the multigeneration mafic dyke swarm intrusive into Deccan basalts that straddle the “Panvel Flexure” (Auden, 1949) containing four generations of dykes: the first one trending E-W (2.5 to 40 m wide) gradational contact with the lavas, second one N-S oriented pre-flexure dykes with steep dips of 60-80° due east, a third one was post-flexure *en echelon* in character (NNW to NNE trending and vertical) while the fourth generation comprised of felsic dykes and plugs that showed evidence of magma mixing. Due to the foundering and stretching of the crust at the “Panvel Flexure”, rifting of India from Seychelles resulted in an intense magmatic discharge into these rifts.

Bhattacharji et al. (1996) carried out integrated geophysical, tectonic, geochemical and geochronologic studies of the mafic dykes and associated Deccan flows along the Narmada-Tapti rift and western continental margin rift and showed that the basalt eruptions spanned between 67 and 64 Ma (with peak activity at ~65 Ma). Geophysical data suggested the presence of discontinuous mafic bodies between 5-6 km deep along Narmada-Tapti rift and elongated anomalous mantle body along continental margin rift. They also established the comagmatic nature of these dykes and basal flows, in fact, many of them being primary

feeders. Evidence of crustal contamination is shown by the dykes and basal flows that diminishes from lower to upper flows. Also, the basal flows and dykes of Narmada-Tapti region along with basal flows of Gujarat region were older than the Igatpuri flows in the Western Margin region.

Pande (2002) reviewed the then available radiometric and paleomagnetic data from the Deccan Flood Basalt Province and suggested that the volcanism was episodic and continued from 69 Ma to 63 Ma (Between 31R and 28N). The intense pulse of volcanism was at  $66.9 \pm 0.2$  Ma. Pande (2002) also expressed the possibility that the lava flows constituting reverse polarity sequence must have erupted in more than one reversed magnetic chron due to incomplete magnetostratigraphic record.

Bondre et al. (2006) carried out detailed study of the mafic dykes in the Sangamner area in the Western Deccan Volcanic Province with respect to their field, geochemical and isotopic characteristics. It was found that all of the dykes were similar in composition to Khandala and Poladpur Formations, except one having an affinity towards the Ambenali Formation. Another dyke had a unique composition amongst the other dykes in the study area, but many similarities with the Bushe and Khandala formations were seen. Owing to their distinctly different isotopic compositions in relation to many of the known values for specific flows/members within certain formations, it was proposed that either the range for isotopic compositions is broader than previously thought for those members or that the magmas with different isotopic compositions underwent broadly similar petrogenetic evolution leading to similarities in elemental composition. It could also be that some of the dykes along this system were late-stage intrusions of magmas representing the younger formations.

Ray et al. (2007) provided the first account of the discussions of field relationships on the Nandurbar-Dhule mafic dyke swarm. They studied a total of 210 dykes having >1 km

length, vertical with a mean trend of N88°. Using aspect ratios of dykes, calculated depths of dykes conform well with the earlier models. They proposed that both vertical and lateral injection of magma played a role in their formation.

Misra (2008) believed that decompression melting along major tectonic structures and in the localised areas was mainly responsible for the emplacement of the two major dyke swarms. He disbelieved the existence of any mantle plume. He agreed with Auden (1949) that the dykes are a post-volcanic hypabyssal phase. The reasoning for the absence of downward continuation of the dykes within the basement was suggested to be a squeeze up of the underlying molten flows along fractures in the upper layers.

Dessai and Viegas (2010) discussed the petrogenesis of late-stage Deccan type tholeiitic and alkaline intrusions and Dessai et al. (2008) presented data on crustal xenoliths in these dykes. Alkaline dykes were diverse in petrology due to fractional crystallization and mixing between evolved and primitive melts under different P-T conditions. Sodic and potassic lamprophyres comprise the most primitive, with nephelinites being responsible for the formation of tephriphonolites. Microdiorites represent hybrid rocks produced due to mixing of tholeiitic and trachytic magmas. Mafic and felsic granulites represent xenoliths with the former being peraluminous, LREE enriched with high Ba/Nb and very low Sm/Nd and Rb/Sr ratios. The latter being meta igneous quartz-normative rocks with low Ba and Sr. Lithologies of the dykes consisted of tholeiites and picrites that have undergone fractional crystallization and mixing between evolved and primitive tholeiitic melts, coupled with the assimilation of lower crustal felsic granulites.

Sheth et al. (2009) studied tholeiitic dyke-sill intrusives around Panchmarhi, central India. They found out that the Panchmarhi intrusions are more evolved than the Deccan basalts

and appear to be products of mixing between Deccan basalt magmas and partial melts of Precambrian amphibolites.

Hooper et al. (2010) presented results of detailed mapping of dykes along the Mumbai coast coupled with  $^{40}\text{Ar}/^{39}\text{Ar}$  dating. They classified the dykes into group I (oldest), group II and group III (youngest). The critical conclusions were: the E-W separation of India and Seychelles must have begun only during that final phases of basalt eruptions, the timing of the Panvel flexure was around 64-65 Ma and, the extension and thinning of the lithosphere due to separation tectonics led to the eruption of spilites, tuffs, trachytes and rhyolites of Mumbai volcanics (between 65-60 Ma).

Vanderkluysen et al. (2011) emphasized on the presence of three dyke systems in the Deccan Traps: the N-S trending west coast swarm, the E-W trending Narmada-Tapi swarm and the unoriented Nasik-Pune swarm. They provided comprehensive data of the dyke affinities utilising geochemistry and isotope data. It was inferred that the Poladpur, Ambenali and Mahabaleshwar Formations (upper parts of lava pile) had probable feeder dykes represented in Nasik-Pune and coastal swarms. Oriented dykes of Narmada-Tapi and coastal regions, intruded under a system of N-S and E-W extensional tectonics respectively, are found to have affinities to the Jawhar, Igatpuri, Thakurwadi and Bushe Formations (lower parts of lava pile). In sharp contrast, it is noted that the magma supply for the upper formations was independent of regional extension. The authors also verified the validity of the Poladpur Formation affiliation to two dykes in Goa and found it to be correct.

Ju et al. (2013) proposed a numerical model “rifts-plume or hot spot-drift” for the emplacement of the Narmada-Tapi dyke swarm, the Nasik-Pune dyke swarm and the West Coast dyke swarm. The finite element method in three stages was utilised using the dyke swarms. It was found that the horizontal maximum principal compressive stress ( $\sigma_1$ ) was

~ENE-WSW for Narmada-Tapi swarm in stage I, for stage II the  $\sigma_1$  was weak along NW-SE and E-W (Nasik-Pune swarm), and for stage III the  $\sigma_1$  was ~N-S (West Coast swarm).

Sheth et al. (2014) obtained precise Ar/Ar age for Dongri rhyolite of  $62.6 \pm 0.6$  Ma and  $62.9 \pm 0.2$  Ma and reported a sedimentary deposit under this rhyolite. They also reported that shale fragments from this sedimentary deposit are found in Uttan-Dongri area tuffs. They opined that the total duration of the Deccan magmatism is at least 8-9 million years. They discredited the hypothesis that the Panvel flexure could have formed at 65-64 Ma and instead argued an age of 63-62 Ma for its formation. Later, Pande et al. (2017) reported ~62 Ma age for the formation of Panvel flexure.

Baksi (2014) critically assessed the  $^{40}\text{Ar}/^{39}\text{Ar}$  methods employed based on the statistical reliability of plateau/isochron sections and the relative freshness of the material dated for the Deccan Traps. It was found that only six reliable ages were found from the Composite Western Ghats Section, whereas the alkaline rocks from Anjar, Kutch, give three reliable ages that suggested hiatus in lava extrusion around Cretaceous-Paleogene boundary (KPgB). From the analysed data it was realised that the most volumes in the ghat section extruded essentially around KPgB. He is also of the opinion that there is a close temporal relationship between the Chixculub Crater and the voluminous extrusion relating both with the faunal extinction at the KPgB.

Srivastava et al. (2014) have identified two distinct sets of Cretaceous mafic dykes (NNE to ENE and NW to NNW respectively) within the Chhotanagpur Gneissic Complex which have been classified as high-Ti and low-Ti dolerites derived from two distinct mantle melts. Available field, paleomagnetic and limited geochronological data attributed their origin to the Rajmahal Traps (110-115 Ma) though their relation to the Deccan Traps cannot be ruled out completely.

Peng et al. (2014) found that central Deccan Trap sections are very similar to those in the southwestern Deccan and hence sharing similar petrogenesis. These central Deccan lavas can be grouped into Thakurwadi, Bhimashankar, Khandala and Poladpur-types present in the Western Ghats. Their results indicate that the Khandala and Poladpur formations extend over west-east distances of >300 km and some individual members (like Dhak Dongar) may extend over as much as 500 km. The authors also found that the regional southward dip observed in the southwestern Deccan is similar to that observed in the central Deccan. They conclude by hinting that large volumes of basaltic lavas derived from eruptive centers in the western Deccan may have covered both the central and southwestern Deccan areas.

Cucciniello et al. (2015) have studied dykes from the Central Saurashtra mafic dyke swarm with obtained ages as  $65.6 \pm 0.2$ ,  $66.6 \pm 0.3$  and  $62.4 \pm 0.3$  Ma indicating that the swarm was emplaced over several million years. Fractional crystallization and crystal accumulation were the important processes in magma genesis with very limited crustal contamination. This study establishes the length of the Sardhar multiple-injection dyke to at least 62 km, based on identical Sr-Nd compositions along its length. Most of the dykes have distinct parental magmas and the authors propose that these dykes may not be feeders to lava-flow sequences in Saurashtra owing to their distinct Sr-Nd isotopic compositions.

Richards et al. (2015) argued that the events of Cretaceous-Paleogene boundary (KPG) mass extinction, the Chicxulub impact in Mexico and, the voluminous yet brief eruptive pulse at the end of the “main stage” eruptions of DFB in India occurred within less than about a hundred thousand years of each other. Geochronologic and magnetic-polarity data pointed towards an ongoing Deccan volcanism when there was meteorite impact at Chicxulub. But the historical data and seismic modelling of Chicxulub impact suggested to release energy sufficient to cause volcanic eruptions. Hence the authors hypothesized that this impact could have triggered the sudden spurt of magmatism for the most voluminous Wai Subgroup

supported by the fact that at approximately Chicxulub/Cretaceous-Paleogene time, a huge pulse of mantle plume-derived uncontaminated magma erupted on the surface.

Misra and Mukherjee (2017) made detailed field descriptions of the thin dykes that occur on the subhorizontal outcrops at Murud, Nandgaon, Kashid, Barashiv, Borlai and Korlai areas of Dessai and Viegas (1995) and Hooper et al. (2010). They found that group I dykes (of Hooper et al., 2010) pre-date the deformation related to the separation of Seychelles-India rifting whereas group II and III dykes (of Hooper et al., 2010) post-date this event. Though group I dykes lacked a preferred trend, group II and III dykes were dominantly the N-S, NW-SE and NE-SW ones that intruded brittle shears/fault planes. They also emphasize on syndeformation intrusion in the group II and III dykes that also match the trends of brittle sinistral shears. They proposed that the direction of Seychelles-India rifting should be deduced from studying brittle shears/fault planes rather than doing it only based on N-S trending dykes and erroneously interpreting it as near E-W extension.

Shrivastava et al. (2017) have presented the  $^{40}\text{Ar}/^{39}\text{Ar}$  plagioclase crystallization ages from the dykes in the Satpura Mountain range near Betul-Jabalpur-Panchmarhi area. A dyke near Mohpani yielded  $66.56 \pm 0.42$  Ma and is interpreted to be older or contemporaneous with the Mandla lava flows. The second dyke near Olini village yielded  $56.95 \pm 1.08$  Ma which the authors believe to be correlating well with the uppermost Poladpur, Ambenali and Mahabaleshwar Formations of the Deccan Traps and may be representing the terminal stage of dyke activity.

Pande et al. (2017) reported the  $^{40}\text{Ar}/^{39}\text{Ar}$  ages of  $62.4 \pm 0.7$  and  $62.4 \pm 0.3$  Ma on two flows and  $62.2 \pm 0.3$ ,  $62.8 \pm 0.3$  and  $61.8 \pm 0.2$  Ma on three dykes exposed in Ghatkopar-Powai area (Sheth et al., 2014) thus pointing towards its younger nature as compared to the intense 66-65 Ma Deccan sequence in the Western Ghats. They showed the instantaneous formation

of the Panvel flexure owing to mutually indistinguishable ages of pre-flexure flows and post-flexure dykes. These ages have overlapped with the Dongri rhyolite flow (Sheth and Pande, 2014) and the Saki Naka trachyte (Sheth et al. 2001) indicating an intense extrusive and intrusive phase at 62.5 Ma throughout Mumbai.

Basavaiah et al. (2018) provided new paleomagnetic data on twenty-nine Deccan age dykes that cut across the basement of lava flows along east and South of Mumbai. They showed that twenty dykes exhibited N-polarity and the remaining nine dykes exhibited R-polarity. These dykes were divided into two groups (Group I and II); each group containing both N- and R-polarity dykes. Group II had a contemporaneous time of emplacement with the basement lava flows. The difference in the paleolatitudes of both groups is found to be  $\sim 4.4^\circ$ . These magnetizations and their comparisons with the existing data indicate the possible existence of two more additional reversals older than the well-established three-Chron magnetostratigraphy.

Sheth et al. (2019) have studied ENE-WSW trending Nandurbar-Dhule mafic dyke swarm and obtained  $^{40}\text{Ar}/^{39}\text{Ar}$  ages of  $67.06 \pm 0.6$ ,  $67.49 \pm 0.89$  and  $63.43 \pm 0.48$  pointing towards the temporal spread of  $\geq 2.5$  million years for the swarm emplacement. Based on isotopic data, they have identified multiple injections in some dykes and also probable feeder dykes to lower Western Ghats sequence and in Saurashtra. Majority of the dykes have distinct chemical signatures of the Kolhapur unit of the southernmost Western Ghats, and reportedly have a unique combination of isotopic and chemical characteristics resembling cross-combination features of different eruptive units in the Wai subgroup. The dyke-sills in Panchmarhi, Rewa-Shahdol areas and Deccan dykes cross-cutting Rajmahal Traps have close similarities to the “Nandurbar-type” geochemical flavour, but this signature is not found in the Western Ghats. Hence it is concluded that the stratigraphic development of the N and NE

Deccan regions is largely independent of the Western Ghats. Such geochemical possibilities were also hinted at previously (Melluso et al., 1999).

Kumar and Chaubey (2019) carried out a detailed study of the North-Western Continental Margin of India (NWCMI), drilled wells results and published seaward dipping reflectors using P-wave velocity in the flood basalt as a proxy, and found that flood basalt lie below sediment and carpets the ocean from NWCMI up to the Laxmi-Laccadive ridges. The depth to which the flood basalt occurs ranges from 800 to 7400 m with a maximum thickness of ~3900 m in the eastern part of Laxmi basin.

Cucciniello et al. (2019) studied the silicic complexes belonging to the Deccan Traps forming hills in Barda (granophyre) and Alech (rhyolite) in Saurashtra. Though earlier studies report that such silicic complexes post date the Deccan Traps, this study indicates that Barda granophyre significantly pre-date the intense 66-65 Ma basalt phase by 3-4 Ma (actual age of 69.5-68.5 Ma). There being a minimum involvement of ancient Precambrian basement crust, they authors concluded that the Barda-Alech silicic rocks must have formed by advanced (70-75 %) nearly closed system fractional crystallization of basaltic magmas in crustal magma chambers.

Sprain et al. (2019) contradict the hypothesis of the eruption of Deccan Traps (DT) caused (KPB) ecosystem crises. They performed Ar-Ar dating of the ash beds and constrained the location of KPB within the Deccan Traps. These dates were supplemented with the data from Renne et al. (2015). They also discredit the claim that the DT erupted in three discrete pulses and instead opine >90% of DT volume erupted in <1 million years with ~75% emplaced post-KPB. They suggest that either the release of climate-modifying gases is not directly related to eruptive volume or that DT volcanism was not the source of Late Cretaceous climate change.

Schoene et al. (2019) have used U-Pb zircon geochronology to resolve four high-volume eruptive period, with the view being contrary to Sprain et al. (2019). Schoene et al. (2019) found that maximum eruption rates occurred before and after KPB extinction and particularly, one pulse initiated tens of thousands of years before both the Chicxulub bolide impact (Richards et al., 2015) and extinction. Hence they concluded that such catastrophic events drove both, the environmental deterioration associated with KPG extinction and its aftermath.

Patel et al. (2020) studied 66-65 Ma sequence of lava flows and dykes exposed at the Elephanta Island near Mumbai, India. Geochemical correlations with Khandala and Ambenali Formations match here. These tholeiites have undergone crystal fractionation and accumulation of olivine, with minor crustal contamination. They also put forth an argument that majority of the dykes presently belonging to Coastal dyke swarm have acted as feeders to the Ambenali Formation urging reconsideration of current view about unorganized crustal extension. A normal fault with a downthrow of 220 m is also reported on the island. They also hinted at the presence of the ~62 Ma ankaramite dyke feeder to the Powai ankaramite flow in the 62.5 Ma Mumbai sequence 20 km away from the Elephanta Island.

I discuss the field characters of country rocks and dykes in the next chapter.

## **CHAPTER 3**

# **Field Characters of country rocks and dykes**

This chapter describes the field characteristics of country rocks and dykes in the study areas<sup>1</sup>

### 3.1 Country Rocks

For the ease of description, I have divided the study area into four parts, namely Aguada headland, Baga headland, Vagator-Chapora headland and Arambol-Keri headland. *Fig. 3.1a-d* shows geological maps of these sub-areas. In this chapter, I describe the geological features from the southern tip of the study area towards its northern extremity. This description comprises the lithological characteristics as well as structures within the sedimentary rocks. The country rocks have northward dips, thereby exposing progressively younger beds from Aguada through Baga, Vagator-Chapora towards Arambol-Keri headland. The entire lithology on the coast belongs to the Sanvordem Formation of the Goa Group of rocks (Gokul et al., 1985; Soman, 1993; Dessai, 2018). These rocks belong to lower greenschist facies, similar to Ranibennur metagreywackes studied by Hegde and Chavadi (2009). The entire sequence of rocks is exposed intermittently in the littoral zone. I describe it as follows.

#### 3.1.1 Aguada Headland

The rock exposed on this headland is an association of argillite and metagreywacke belonging to Sanvordem Formation of Goa Group. Sandstones are intercalated with them. Mafic dykes intrude both these lithologies at various places.

The Aguada headland (the southern part of the study area) is primarily covered by argillites overlain by medium-grained metagreywackes as one approaches Baga to the North. At places, the argillites also contain intercalations of metagreywackes. Both these rock types stand out as headlands (*Fig. 3.2a*).

---

<sup>1</sup> A part of this chapter is published as: Gadgil, R.; Viegas, A.; Iyer, S.D. (2019) Structure and emplacement of the Coastal Deccan tholeiitic dyke swarm in Goa, on the western Indian rifted margin. *Bulletin of Volcanology*, 81, 35, doi: 10.1007/s00445-019-1297-6.

The vicinity of Aguada Jail (*Fig. 3.1a*), is covered by light grey to deep grey argillites displaying fine laminations (*Fig.3.2b*). The argillites trend<sup>2</sup> 20-30°/10-30° towards 290-310°. These beds vary in thickness from 0.15 - 0.30 m. They typically form rhomboidal to box-shaped blocks as a result of intersecting sets of near-orthogonal fractures (*Fig. 3.2c*). This part has also well-developed wave-cut platforms and cliffs (*Fig. 3.2d*).

In the Siquerim section of Aguada headland (*Fig. 3.1a*), argillite gives way to more indurated and weakly metamorphosed metagreywacke. However, it does contain argillitic intercalations and, the beds are much thicker here (*Fig. 3.2e*). This occurrence is similar to the Ranibennur metagreywackes from the western Dharwar craton (Hegde and Chavadi, 2009). I have observed depositional features like ripple marks of the symmetrical type with rounded crests (*Fig. 3.3a*). Their measured ripple height is 1-2 cm with a wavelength of 4-5 cm, indicating that the rock surface was shallow enough to experience the circular orbital motion (Boggs, 2009) of rippled water.

The Soft-sediment deformation (SSD) structures are rare in Precambrian successions across the world (Owen, 1995; Sarkar et al., 1995; Bose et al., 1997; Bhattacharya and Bandopadhaya, 1998; Zhang et al., 2007; Mazumder et al., 2009; Ghosh et al., 2012; Fernandes, 2018). I have observed SSD structures frequently in these rocks though the studied country rocks are Precambrian in age (Armistead et al., 2018). These structures are abundant along the metagreywacke-argillite interfaces that I believe are a part of a distal turbidite deposited by low-density currents. The SSD structures are however absent in those horizons dominated by single grain size.

---

<sup>2</sup> This should be read as strike/amount of dip towards dip direction, henceforth in this chapter and subsequent ones.

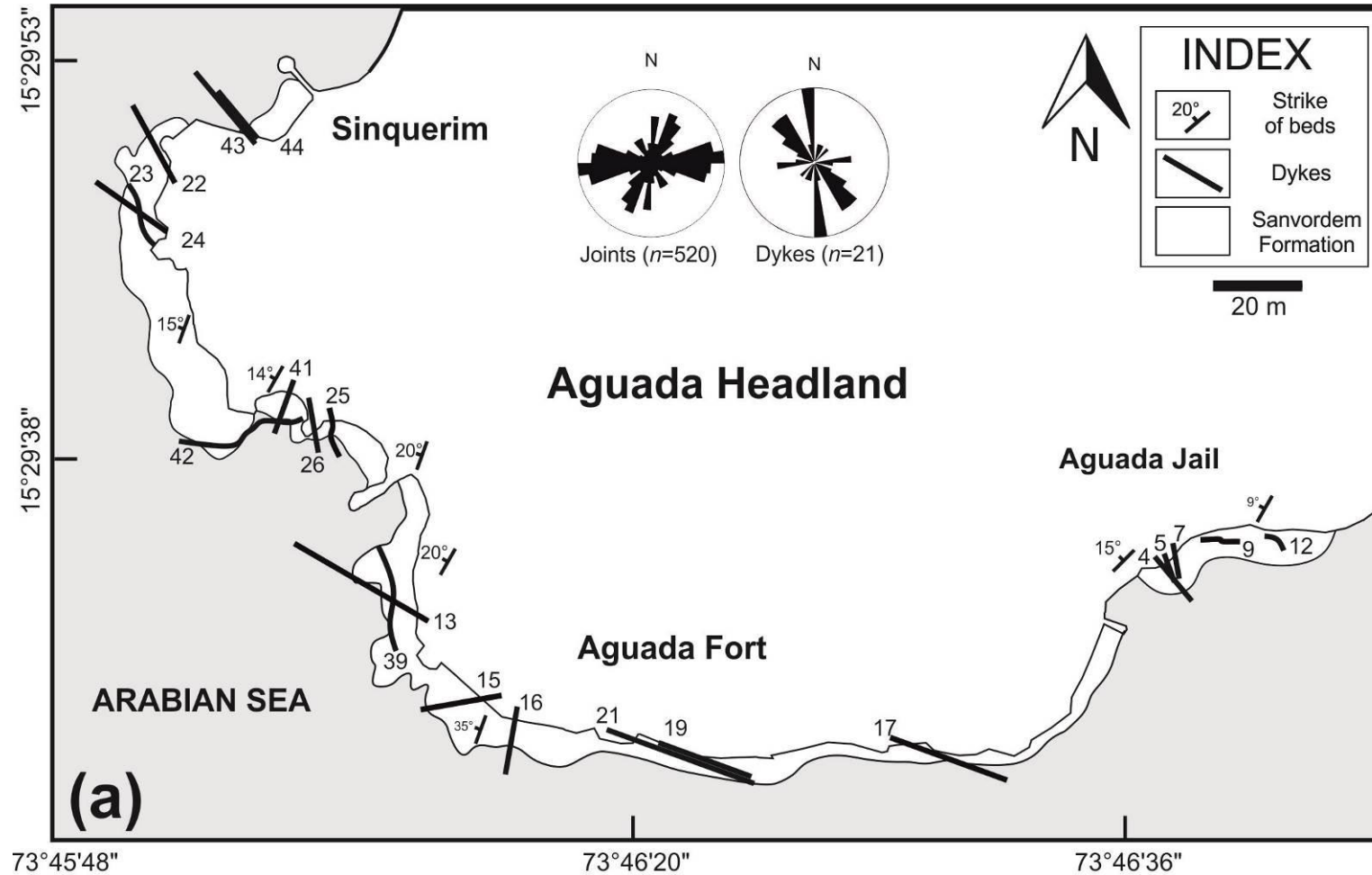


Fig. 3.1. Dyke maps for the study areas. (a) Aguada Headland. The dyke numbers are without the prefixes “AG”, “BG”, “VG” and “AR” (abbreviations for Aguada, Baga, Vagator-Chapora and Arambol-Keri, respectively) to avoid cluttering. These prefixes are the same as in Table 1. Each map has rose diagrams for host rock joints and dykes;  $n$  is the number of measurements taken for the rose diagrams. The white patch delineated by a black line along the coastline shows a beach or rocky stretch.

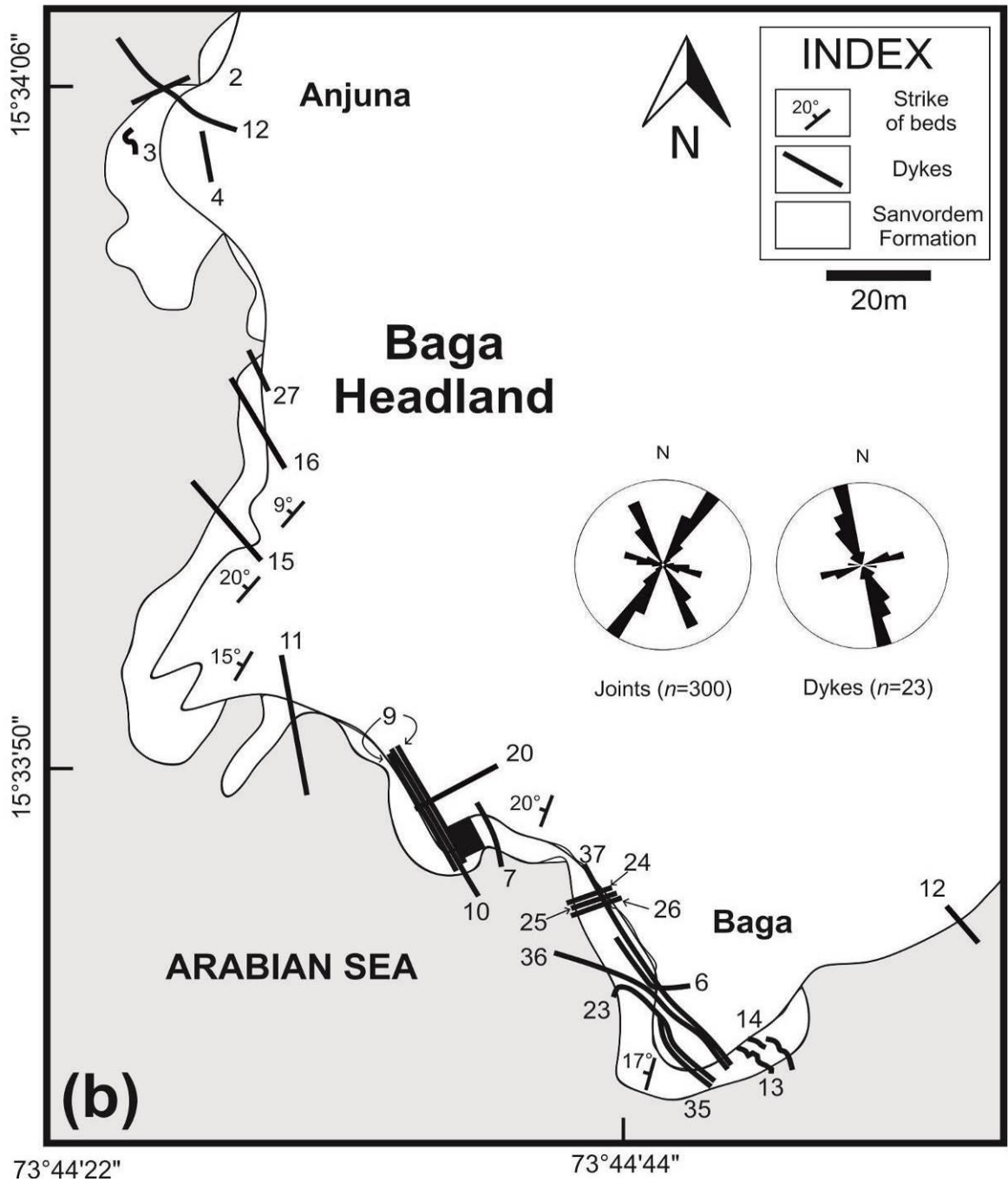


Fig. 3.1. (b) Baga Headland.

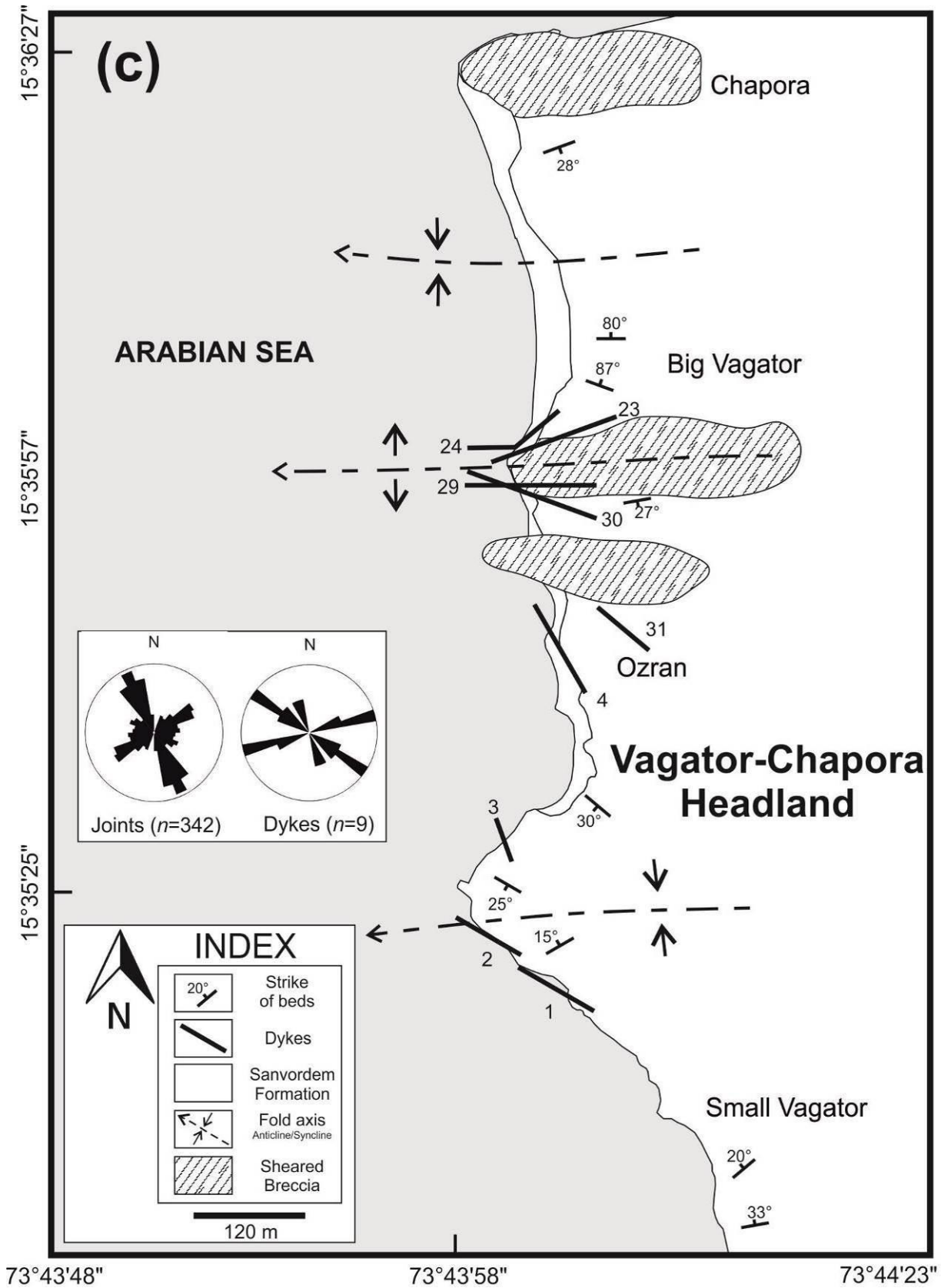


Fig. 3.1. (c) Vagator-Chapora Headland.

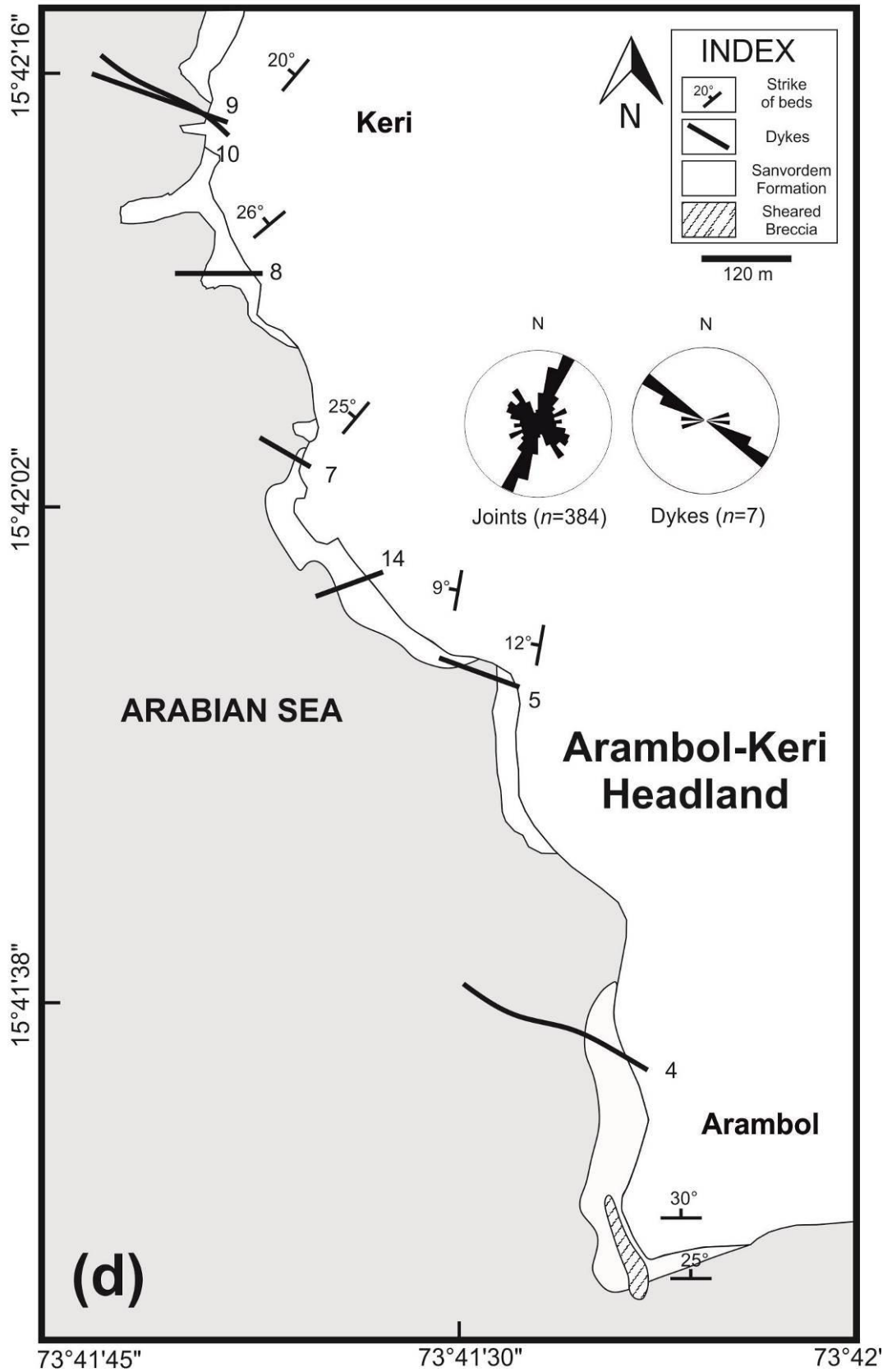


Fig. 3.1. (d) Arambol-Keri Headland.

In the beds which are stratigraphically younger than the rippled argillites, a sub-horizontal outcrop exposes SSD structures that shows isoclinal folds with inclined to horizontal fold axis (*Fig.3.3b*). Undeformed beds overlie and underlie such structures; leading to the conclusion that they are “synsedimentary”. A cliff on the headland, further North, mimics “monocline”-like deformation (*Fig. 3.3c*). However, I do not ascribe causal effect to “tectonic” because the deformation dies out in the upper reaches of the vertical face scarp. Some of the thicker beds of metagreywacke (also called mega beds) are also cross-bedded (*Fig. 3.3d*).

### **3.1.2 Baga Headland**

There is no direct clue to the type of lithology between Aguada and Baga headlands (~7 km long stretch) since beach sands perennially cover the area. I assume this intervening area has the same lithology as that of Aguada and Baga on account of similar rock exposures and, most importantly, consistent trends on both the headlands (Aguada and Baga).

At the southern tip of the Baga headland (*Fig. 3.1b*), the lithology is again overwhelmingly argillite-rich. As one proceeds towards North, noticeable enrichment in quartz and rock fragments coupled with low-grade metamorphism qualifies it to be a metagreywacke. These rocks display similar strike and dip as the rock strata in Aguada. Metagreywackes are grey coloured, mega beds up to 1 m thick and display cross-bedding. The grains dominantly are made up of quartz, while the matrix is siliceous with micas and clayey matter. Argillites occur interlayered with metagreywackes as finely laminated beds (*Fig.3.3e*). These argillites show polygonal, irregular ridges possibly formed due to a syneresis process (*Fig.3.3f*) active due to water escape (Tucker, 2011). I have observed these polygonal structures only on a single bedding plane that gently dips into the cliff.

‘Water-escape’ structures (*Fig. 3.4a*), could be interpreted as channel deposit. These mega beds, some of them ferruginous, have slump folds (*Fig.3.4b*).

On the Baga headland at Anjuna (*Fig. 3.1b*), the greywacke is more quartz-rich, giving a granular texture to the rocks that also show synsedimentary reverse faults (*Fig. 3.4c*). This part of the rock displays cross-beds that are honeycomb weathered (*Fig. 3.4d*). The trends of the beds vary from  $40^{\circ}/15-30^{\circ}$  due  $300^{\circ}$ ,  $50^{\circ}/9-40^{\circ}$  due  $310^{\circ}$ , and  $35^{\circ}/15-17^{\circ}$  due  $295^{\circ}$ .



Fig 3.2. (a) A panoramic view over Aguada headland (b) Finely laminated argillites exposed at Aguada Jail area (Refer to geological map for location). (c) A plan-view of rhomboidal to box type blocks formed as a result of near-orthogonal fractures (Aguada Jail area). (d) Wave-cut platform and wave-cut cliff at Aguada Jail locality. The person is 1.6 m tall. (e) An oblique-view of gently dipping beds with thickness more than 1 m exposed at Sinquerim. The person is 1.6 m tall.

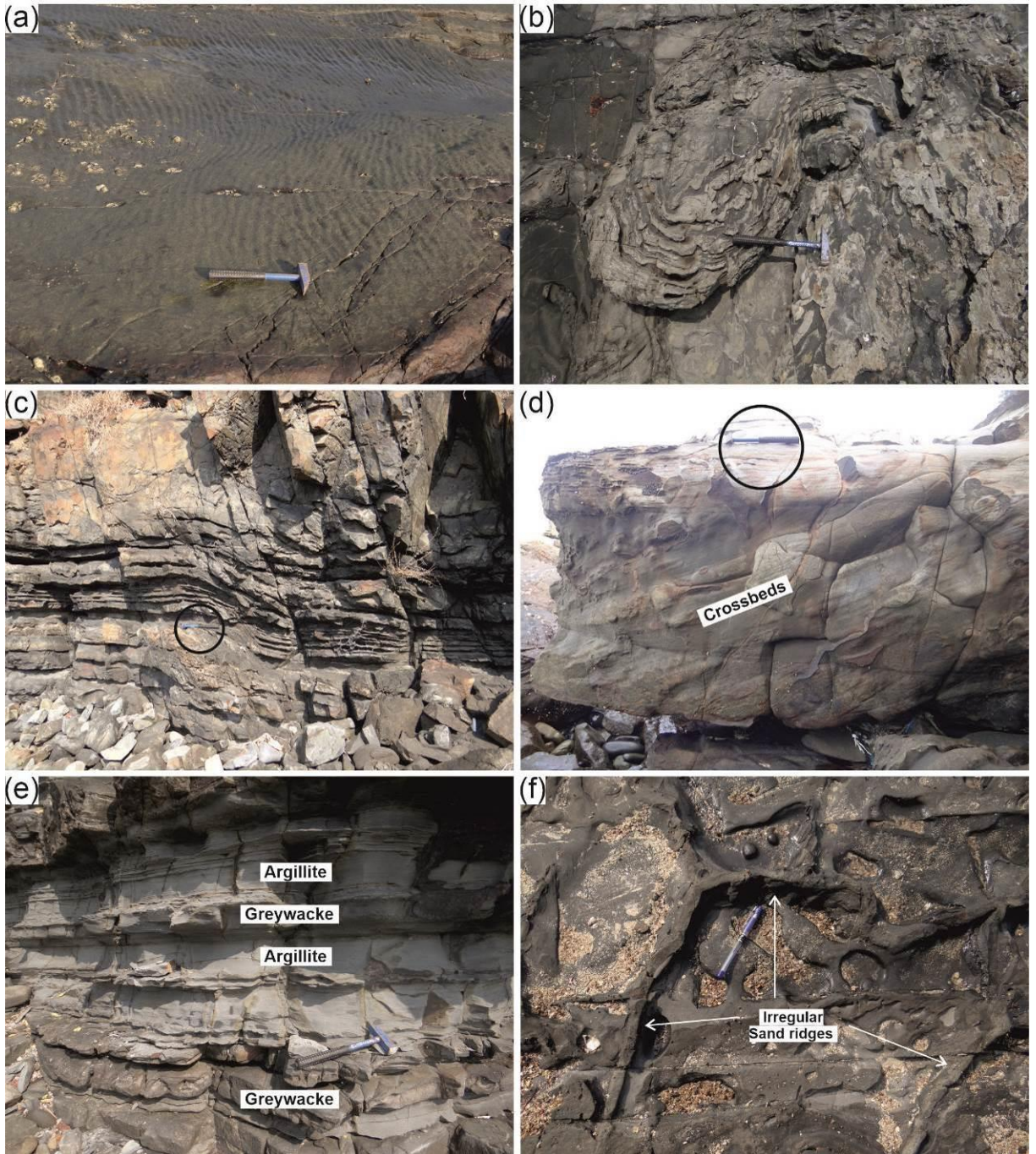


Fig 3.3. (a) An oblique-view of ripples formed at the bedding plane exposed on the surface at Aguada headland. (b) An oblique-view of soft-sediment deformation (SSD) structures with inclined to horizontal fold axis at Aguada. (c) SSD on a vertical cliff on Aguada headland in which the beds mimic 'monocline', but here this deformation dies upward in the sequence. The black circle encloses a hammer (0.35m) for scale. (d) Cross-beds exposed at Aguada. The black circle encloses a hammer for size (0.35m). (e) The systematic alternating sequence of argillite and greywacke at Baga. (f) A plan-view of SSD in the form of sand ridges that form polygonal shape jutting out of argillite beds on a subhorizontal outcrop at Baga. Pen for scale (13cm).

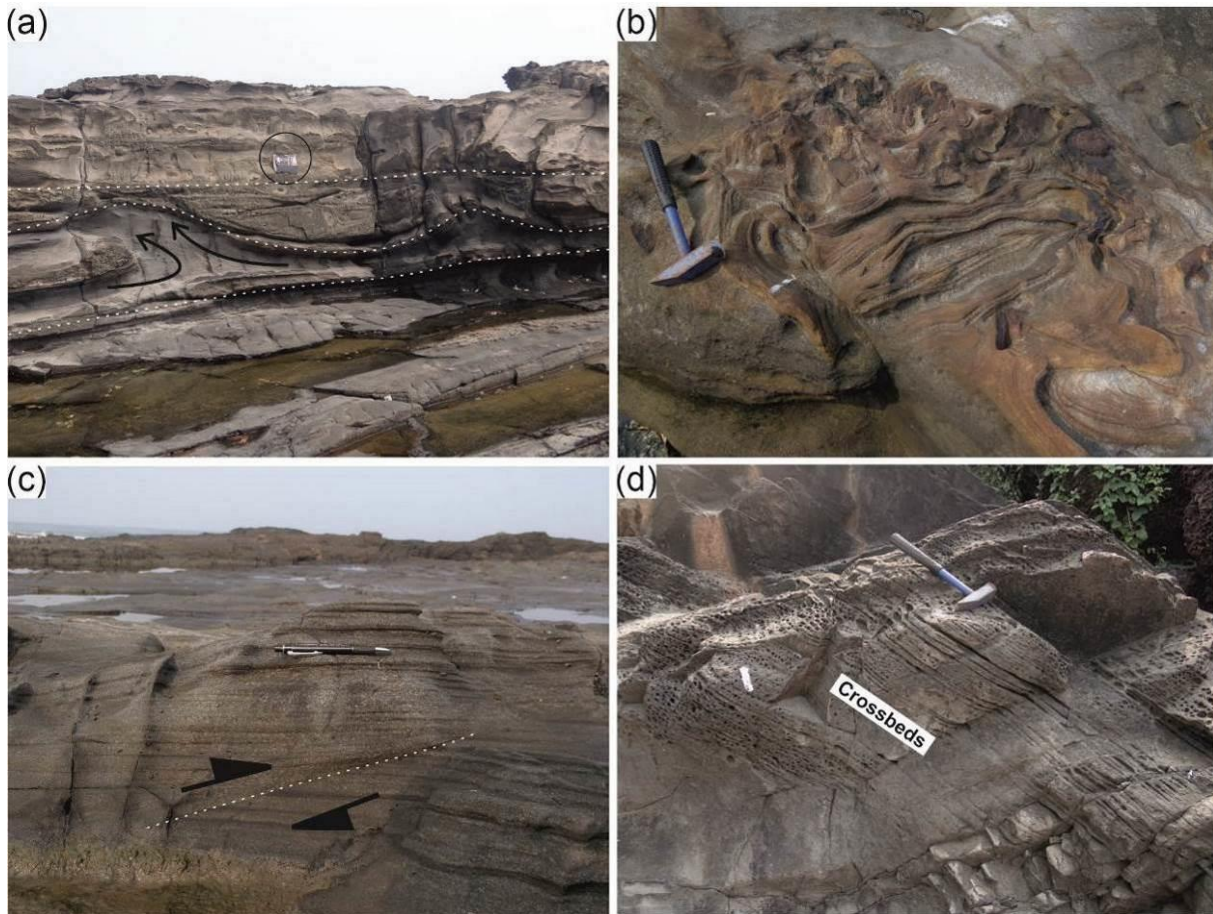


Fig 3.4. (a) “Water-escape” structures (black arrows) where the argillite (fine-grained) moves upwards into metagreywacke-quartzite (medium-grained). Note the un-bent layers at the top (marked in dotted white line). Field note book is kept for sale and is encircled in black. (b) A plan-view of SSD in the form of iron-rich convolute beds on a sub-horizontal outcrop. (c) A vertical-section of quartzitic lamination planes displaying syn-sedimentary reverse fault (marked in dotted white line). Note that it dies out in the bottom-left corner of the photograph. The pen is for scale. (d) A vertical-section of ‘Honey-comb’ weathering seen in thickly cross-bedded rocks. All photos from Baga headland.

### 3.1.3 Vagator-Chapora Headland

Here, I describe the area that comprises of the famous Ozran beach to the south, Vagator in the central part and Chapora to North (Fig. 3.1c). The country rocks here are again argillites-metagreywackes and quartzites that have developed in sequence from South to North of this sub-area. The rocks here display typical sedimentary features with some structural deformation.

Around Ozran beach, the argillites are laminated having trends  $50-80^{\circ}/20-33^{\circ}$  due  $330-350^{\circ}$ . They are very fine-grained, have biotite-rich layers, are soft and friable (Fig.

3.5a). In the stratigraphically younger intervals within the argillites, syndimentary deformation structures are observed represented by stacked up layers bound by faults (Fig.3.5b), disrupted laminations (Fig.3.5c) and argillites exposed in Vagator display ball and pillow structure.

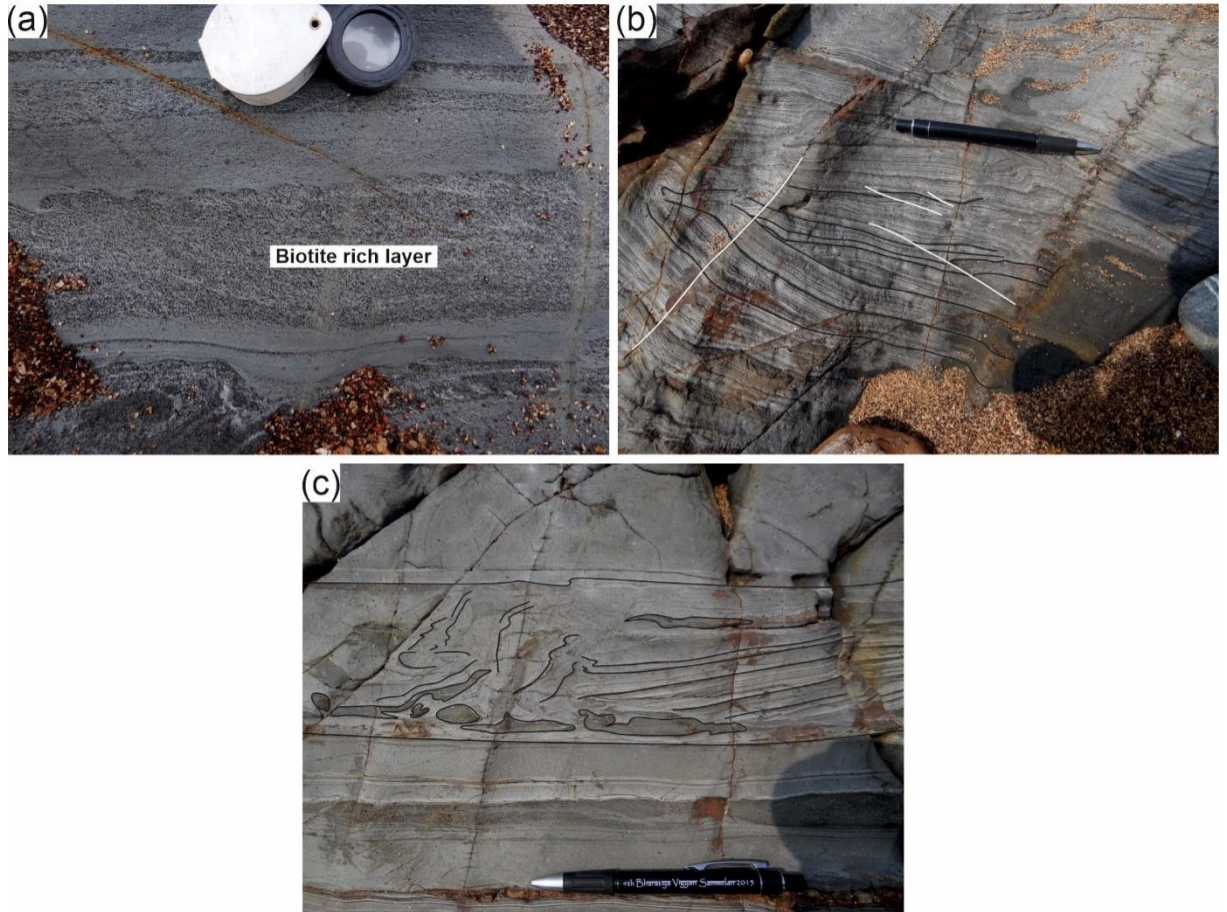


Fig 3.5. (a) Argillites have biotite-rich layers in them. Handlens for scale. (b) SSD is showing stacked up layers with normal and reverse faulting. Black lines are laminations, and white lines are the faults. Pen for scale (14cm). (c) Disrupted laminations SSD in argillite with pillow-like structures. Pen for size (14cm). All photos from Vagator-Chapora headland.

In the area south of Vagator (central part of the study area), the argillite indicate a trend swerve from  $300^{\circ}/25^{\circ}$  due  $210^{\circ}$  and to E-W/ $46^{\circ}$  due south (From previous dip directions of  $\sim$ NNW changing to SW/S) resulting in the formation of a syncline (Fig. 3.1c). On the northern side of the syncline, the argillites grade into metagreywackes, while retaining the laminated character intact. These folds have gentle dips on either of their

limbs, with shorter amplitude and longer wavelengths. At Vagator, white to buff coloured quartzites occur as lenses within the metagreywackes. The quartzites occur in the synclinal portions of the folds exposed on either side of the Vagator headland, thus pointing towards their stratigraphically younger nature than the argillite-metagreywacke lithology (*Fig. 3.1c*). The structural data define broad open E-W trending folds in the area corresponding to the first phase of folding  $F_1$  (Gokul, 1985). However, Gokul (1985) in his paper, notes that manifestations of  $F_1$  folding phase to be present only in South Goa.

#### **3.1.4 Arambol-Keri Headland**

The lithotypes here (*Fig. 3.1d*) are calcareous sediments interlaminated with argillites in the southern part (Arambol) that grade to quartzites in the northern part (Keri).

The rocks exposed at the southern end of the headland are indurated calcareous sediments interlayered with shale. These rocks are greyish, fine-grained, give effervescence when treated with HCl, and form pinnacles. Three prominent sets of joints are present in them. The general trend of these rocks is NE-SW to E-W/ $5^\circ$ - $30^\circ$  due NW to N. This is also the trend of the bedding joint; the other joint trends are  $210^\circ/45^\circ$  due  $120^\circ$  and  $160^\circ/64^\circ$  due  $250^\circ$  (*Fig. 3.6a*). The rocks have criss-cross veins of muscovite-quartz that sometimes contain kyanite, the veins ranging in width from 2 to 4 cm (*Fig. 3.6b-d*). Argillites occur interlayered with this lithology.

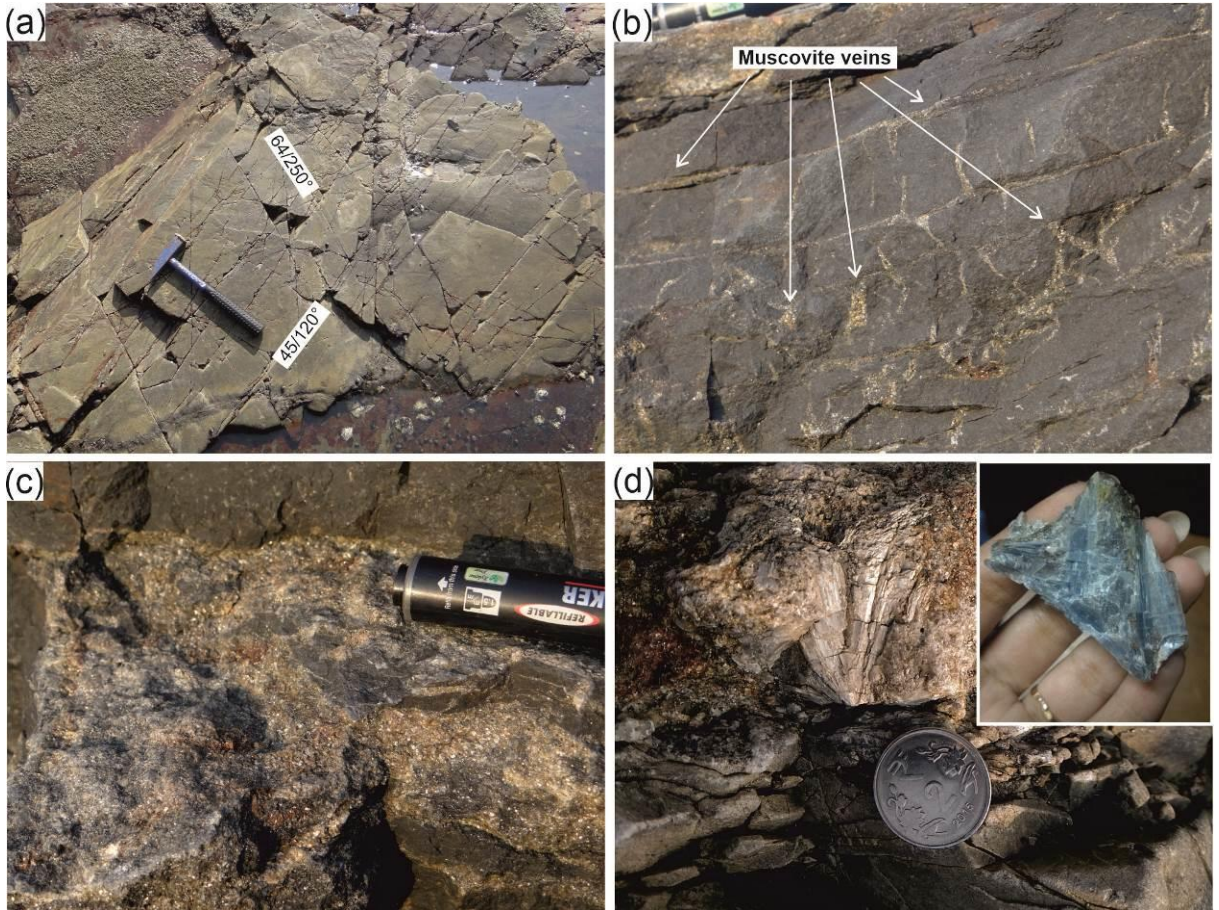


Fig 3.6. (a) An oblique-view of calcareous sediment outcrop with three sets of fractures (Read the numbers as the amount of dip/dip direction of the fractures). (b) A vertical-section of the muscovite veins and (c) Close-up of muscovite veins in calcareous sediments. (d) Field photograph of kyanite vein and in the inset is kyanite hand specimen (Sample courtesy: Sneha Chougule). All photos are from Arambol headland.

These calcareous rocks interlayered with argillites have SSD structures manifest by folds (recumbent, tight and isoclinal), with the N-S axis plunging by an amount of 20-35° due 350-10° (Fig. 3.7a-e) (cf. Fernandes, 2018). The fold axis in this area is consistently N-S directed. Since these deformation features are within a zone that is underlain and overlain by undeformed sediments, their origin is unequivocally attributed to synsedimentary processes and specifically to slump folding of sediments. Some of the fold axes are vertical (Fig. 3.7e). Few folds have transverse faults to their limbs (Fig. 3.7f). These folded beds abut against dyke AR-4 beyond which the country rocks are either gently dipping (wherever exposed) or concealed under beach deposits.



Fig 3.7. (a) Un-interpreted and (b) interpreted reverse faulting on an inclined fold limb resulted due to SSD in alternating layers of calcareous sediments and argillites. The hammer is close to the fold axial plane marked in white dotted line. (c) Folds with vertical axial planes formed due to SSD. The person is 1.5 m tall. Close up photos of a fold with horizontal axis in (d) and vertical fold axis in (e). (f) The limbs of a fold disrupted by faults (layers marked in black lines). All photos are from Arambol headland.

The lithology is made up of quartzite with intercalations of clay and greywacke in the North up to Keri headland. It begins as a white to buff coloured massive quartzite and then grades to quartzite with clayey material. This layered rock, at Keri, has been profusely traversed with veins of quartz.

### **3.1.5 Structural features:**

#### *3.1.5.1 Fracture patterns*

A rock fracture is a mechanical break or discontinuity that separates a rock body into two or more parts. An extension fracture forms by normal stress or fluid pressure and opens in a direction parallel with the maximum tensile (minimum compressive) principal stress (Fossen, 2010). There are two main types: one is a tension fracture, which forms when the stress perpendicular to the fracture is negative; the other is a hydrofracture, which is driven open by internal fluid pressure, while a joint is a fracture with a slight fracture-normal displacement (opening) but no visible fracture-parallel movement. Hence it is an extension fracture (Gudmundsson, 2011). Armed with this available information, I have compiled the various structural data associated with the fractures within the country rocks. This data assesses the type of relationships between fracture formation and emplacement of dykes.

I measured structural attributes such as strike, amount of true dip and the dip direction with the help of a Brunton compass. I have used statistical methods to highlight the salient features in them. I also attempted to classify the fractures into their types and their chronology of their formation.

#### *3.1.5.2 Trend of fractures*

I collected more than 1500 trend readings from the field and plotted them to generate a rose diagrams using the software GeoRose (Yong Technology Inc, 2014). The

sub-vertical joint pattern consists of two systematic orthogonal sets, namely ~NW-SE and ~NE-SW, with subordinate joint sets being WNW-ESE, E-W, N-S and ENE-WSW (Fig. 3.8a-b). These variably oriented, mutual cross-cutting joints render a blocky appearance to the host rock, and the erosion of these rock blocks have resulted in rounded knobs. Sometimes, the host rock fractures are seamless within the dyke, thus proving that some dykes had intruded earlier to the fracturing event (Fig. 3.9).



Fig 3.8. (a) Oblique aerial view of a part of Baga Headland, showing criss-cross joints on a subhorizontal outcrop. Numbers indicate the orientation of the major joint sets (Whole Circle Reading). Person (encircled) is 1.7 m tall. (b) Oblique view of the platform at Aguada Jail locality. Set of conjugate fractures (white lines) as well as some later fractures (marked in black) that displace the conjugate sets are exposed. Backpack width 30cm for scale.

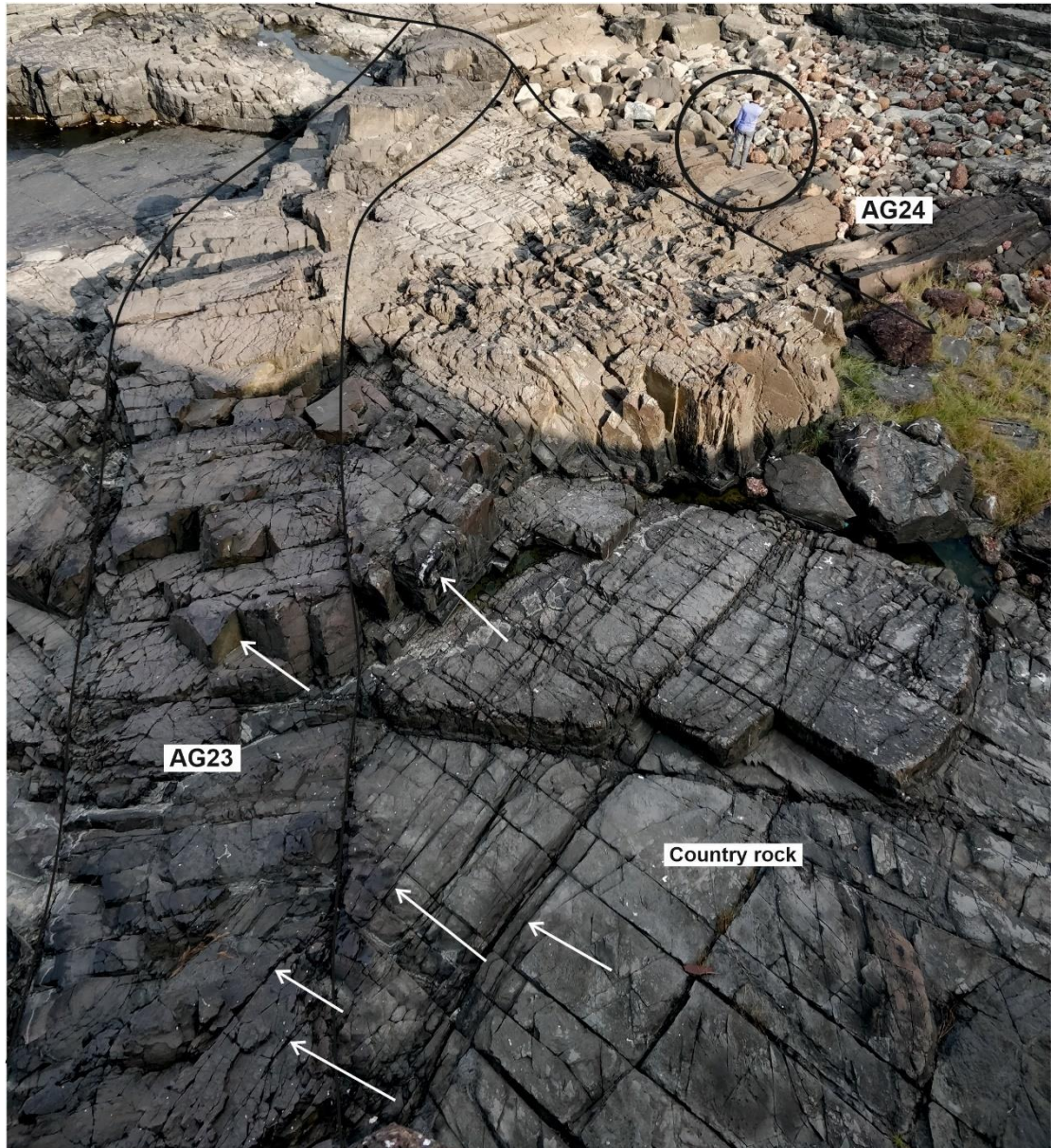


*Fig 3.9. Dyke AG-23 intrudes the country rocks at Siquerim area of Aguada headland. Note that the prominent fractures in the host rock also traverse in the adjacent dyke (marked by white arrows). The person (circled in black) is 1.6m tall.*

### 3.1.5.3 Types of fractures

I examined the varieties of fractures occurring in the area in the horizontal as well as in well exposed vertical sections. Many pronounced vertical sections, displaying bedding fractures and the fractures cutting across it, could be viewed even from a distance. Varieties

of shapes developed due to the intersection of joint sets and their corresponding angular relationships were of great help in the determination of various kinds of fractures.

The majority of fractures in this area are consistent along their strikes, and frequently they have been the avenues where erosion has formed deep furrows. These are termed as master fractures or more appropriately as ‘master joints’ (Fig.3.2e).

Close examination of fracture surfaces reveals their jagged and rough nature. There is a visible gap between the fractures that are exposed for long lengths, and hence I termed them as ‘extension fractures’ (Fig. 3.10a-b).

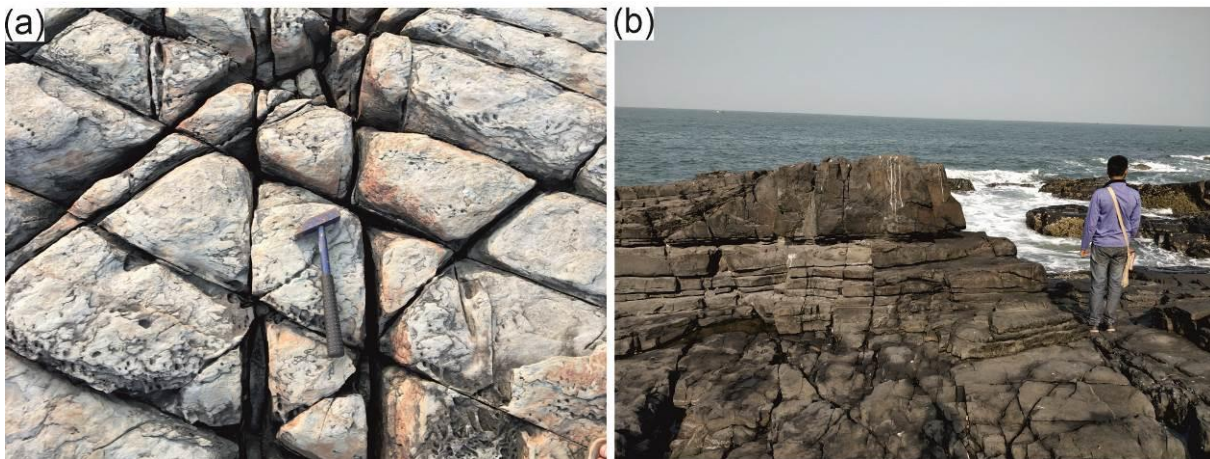


Fig 3.10. (a) and (b) are outcrop-scale extension fractures in Aguada area. The person is 1.6 m tall.

These rocks also exhibit extension along the prominent bedding planes, thus forming ‘bedding fractures’ (Fig.3.11a). Conjugate joints are those fractures that make an angle of  $60^\circ$  with each other. I have observed such joints at multiple places in the study area (Fig. 3.11b-c). Box fractures: The two fracture sets trend  $20^\circ$  and  $110^\circ$  subtend at an angle of  $90^\circ$  (Fig. 3.2c). Polygonal fractures: These fractures have a geometry resembling columnar joints (Fig.3.12a). Checkered fractures: Unusual type of fractures seen very locally (Fig.3.12b). En echelon: These fractures form as tension cracks along potential planes of shear in response to a stress field in a brittle-ductile regime (Mandal, 1995)

(Fig.3.12c). They have a step-like geometry of closely-spaced similar length veins or seams (Seyum and Pollard, 2016).

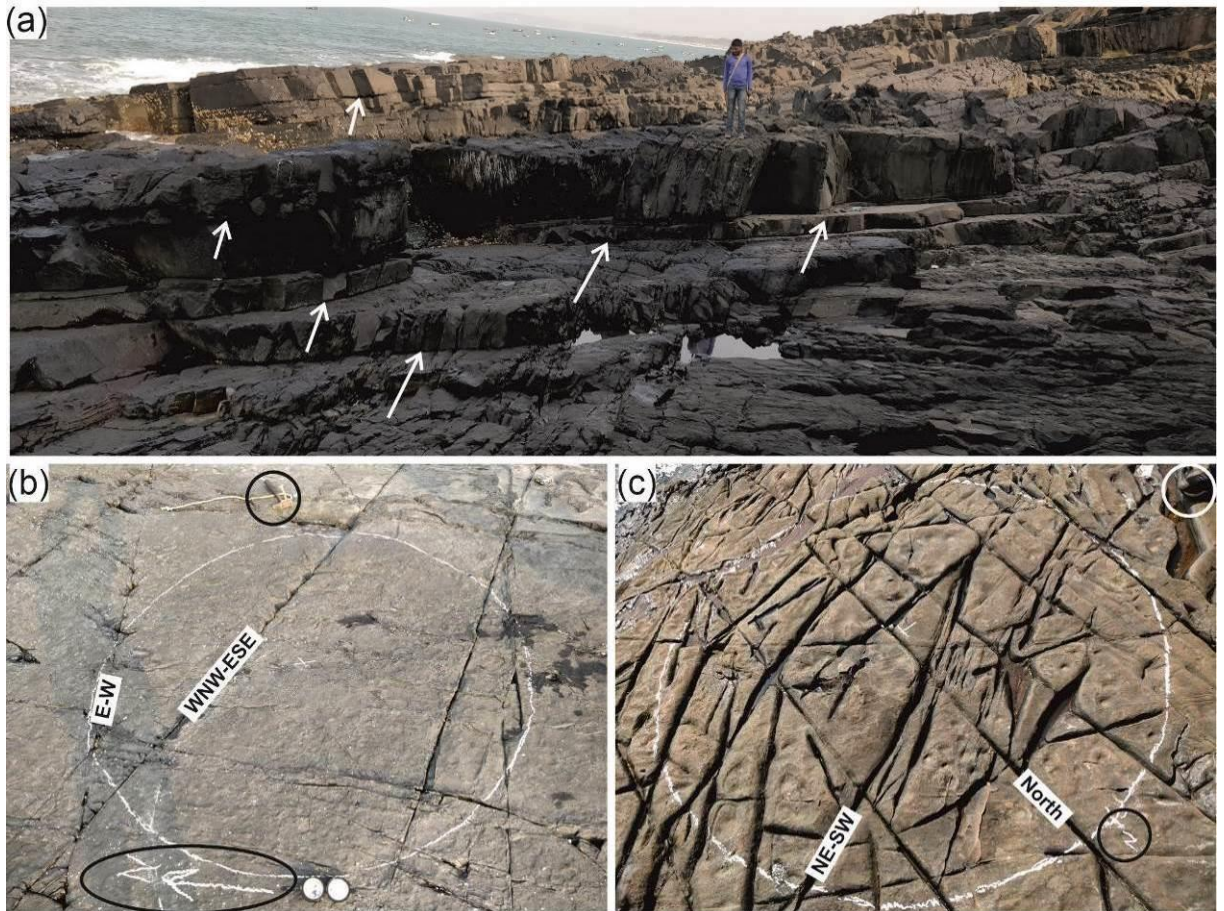


Fig 3.11. (a) Bedding fractures (marked with white arrows) that are also extension fractures. The person standing is 1.6m tall. Photo from Aguada headland. (b) and (c) Conjugate sets of fractures as seen on sub-horizontal outcrops on the Baga headland. The black colour ellipse shows North and black circle denotes a hammer for scale. The black circle in (c) shows North, and a shoe is circled in white in the top right corner for scale.

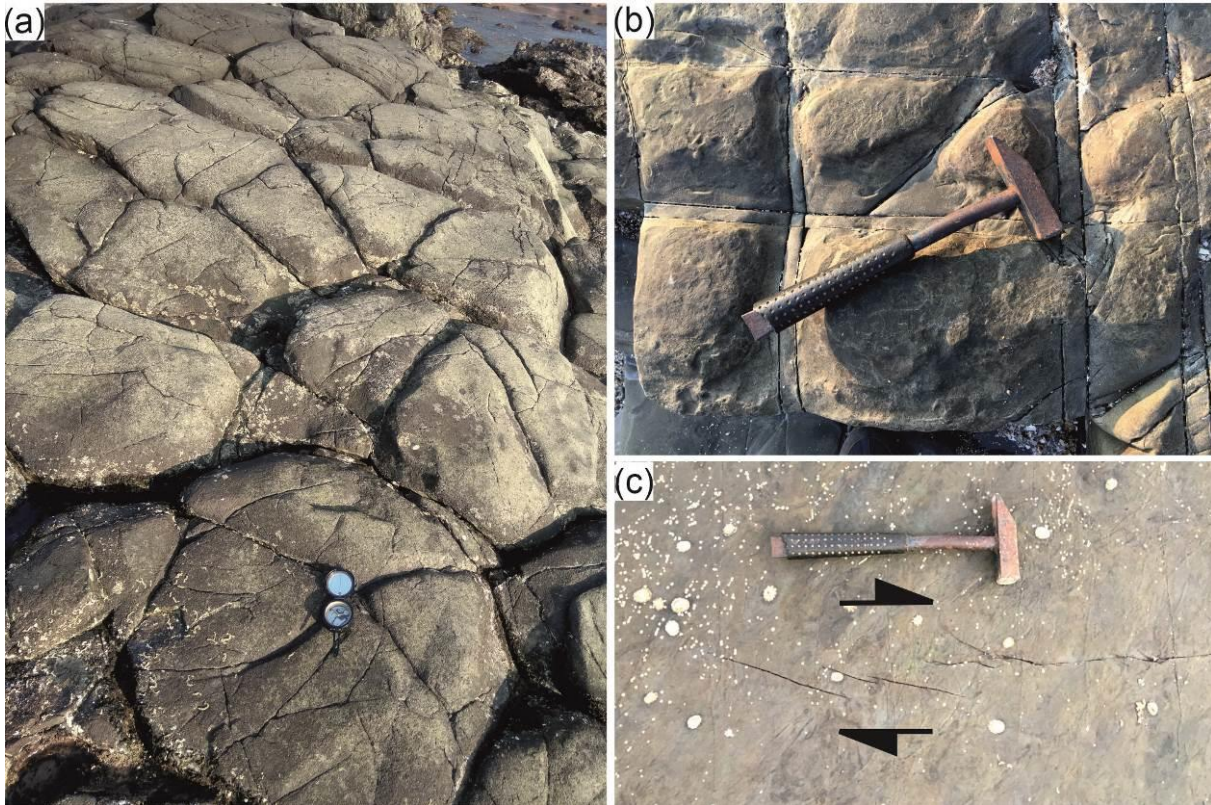


Fig 3.12. (a) Polygonal fractures. (b) “checked” fractures (c) en echelon fractures with a dextral sense of shear. All photos are from Baga headland.

#### 3.1.5.4 Mineral veins, gash veins and grooves

Mineral veins are prevalent in my study area; quartz is the dominant mineral, followed by calcite and an association of quartz-muscovite-kyanite. The joints in the host rock have varied orientations, but I noted filled mineral veins only along N 0-30°, and N 255-290° trending ones (Fig. 12b in Gadgil et al., 2019). Some of them show a vug structure (Fig. 3.13a). These veins are offset by ~NW-SE-striking joints that do not display any infillings (Fig. 3.13b). The ~N-S trending veins frequently show an *en echelon* pattern. The quartz veins cross-cut by dykes, have been “blackened” due to the heating effects of hot magma (Fig. 3.13c). Very thick quartz veins (>15 cm thick) occur in Vagator headland, where they also abut against the dykes signifying they are relatively older than dykes (Fig. 3.13d). These veins show rafts of host rocks due to the coalescence of the vein (Fig. 3.13d). I have also observed the continuous passage of quartz vein from a discordant to a

concordant relationship with the host rock. Here it passes along the bedding planes (*Fig. 3.14*). I believe that such quartz veins (usually discordant), now unexposed, must be the feeders to the extensive grooved quartz found on the bedding planes of this area (now concordant) (*Fig. 3.14*). These mineral veins resist erosion or weathering and stand out tall within the host rocks.

A distinct sigmoidal vein (*tension gash*) with negative dilatation (Ramsay and Huber, 1987) is also seen (*Fig. 3.15a-b*). Sub-horizontal outcrop of metagreywacke exposes this gash vein. The ends of the tension fissures are reoriented at an angle of about  $43^\circ$  to the walls of the deformed zone, but the central sectors of many of the larger veins make a higher angle with the walls, giving the individual veins a sigmoidal form. Small veins making angles of  $45^\circ$  to the walls of the shear zone are also found in the central parts of the deformed zone (veins marked in red) and appear to have been formed during the last increments of deformation to accommodate additional strain (Durney and Ramsay, 1973). The sense of movement is sinistral.

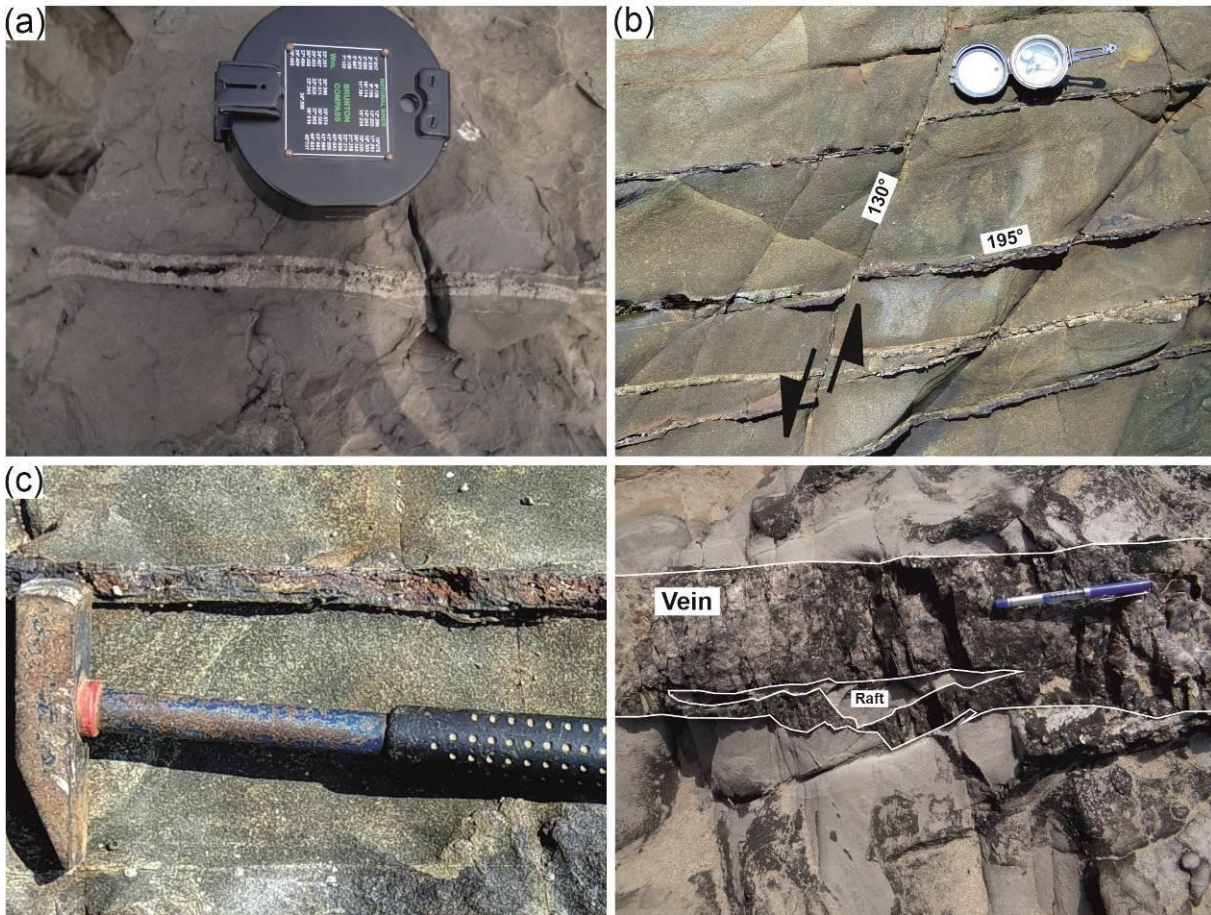


Fig 3.13. (a) Vug structure in a quartz vein in a plan view. (b) Country rock joints in plan view at Quartz-mineralized older joints ( $195^\circ$ ) and non-mineralised later joints ( $130^\circ$ ) are observed. There are also a few younger, ~N-S joints that are unmineralized (upper part of the photo). (c) A plan view of 'Blackened' or 'roasted' quartz vein due to the intrusion of a mafic dyke in close vicinity. (a) (b) and (c) photos are from Baga headland. (d) A thick quartz vein with a country-rock 'raft' exposed on a sub-horizontal outcrop in Vagator. The fingers of the vein follow fractures in host rock.



*Fig 3.14. Quartz vein exposed on an inclined outcrop at the Vagator headland is seen passing on to a bedding plane (marked in black ellipse and circle) where this quartz forms grooves due to slippage along bedding planes.*

Another similar tension gash is exposed on a sub-vertical face of argillite at Aguada (Fig. 3.15c) and shows top to the left sinistral sense of shear towards  $320^\circ$  (Towards NW) (It is next to AG-22). A gash vein filled with quartz (Fig.3.15d) exposes itself on a gently dipping bedding plane surface of greywacke below the “Big Vagator” headland (close to VG29 and VG30). It shows a dextral shear towards  $125^\circ$ .

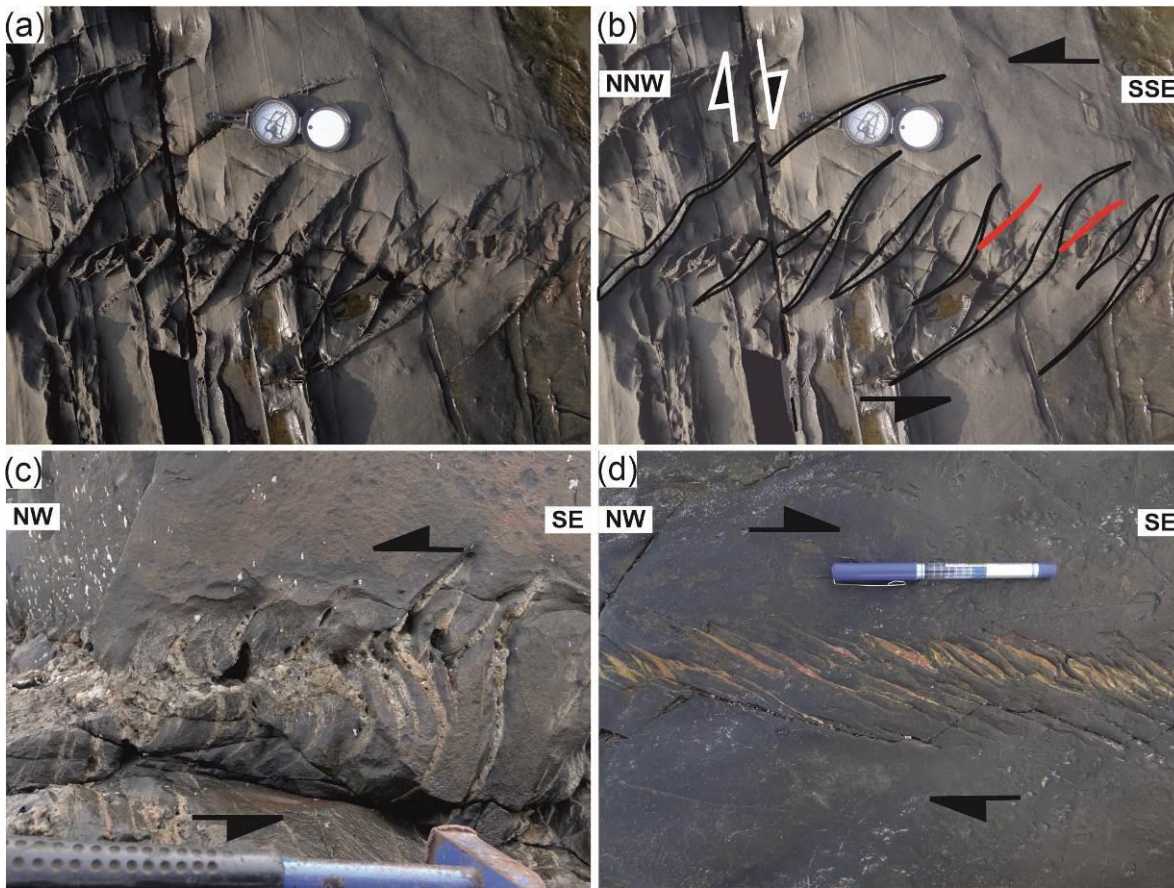


Fig 3.15 (a) Uninterpreted and interpreted (b) planar view field photographs of sigmoidal tension gash veins (black lines) and some newly formed veins (red lines) having a dextral sense of shear, from Baga headland. These are, in turn, faulted along the ENE-WSW trend. (c) Sigmoidal gash veins filled with vuggy quartz with a greater curvature than in (a) exposed on a vertical face near dyke AG-22 in Siquerim headland. Sinistral sense of shear. (d) Tension gash filled with quartz on a sub-horizontal outcrop at Vagator near dyke VG-29 and VG-30 showing a dextral sense of shear.

I have observed quartz grooves on the surfaces of the bedding planes at various places in the study area, it is common at Vagator. These grooves are present on successive bedding planes in any particular area (Aguada or Baga or Vagator). The limb of the fold in southern Vagator consists of repeating closely spaced bedding planes marked with the grooves of quartz mineralization (Fig. 3.16a-c). This type of occurrence is very similar to the ‘flexural slip’ folds (Fossen, 2010). These type of folds develop in a layered medium in the upper crustal brittle regime. Here the bedding surfaces act like fault planes. They preserve lineations, evidenced by grooves trending due N-S (Fig. 3.16c). Here the bedding

planes trend  $300^\circ$  with a dip of  $22^\circ$  due  $210^\circ$ . The average rake measured at these grooves is  $49^\circ$ . Baga and Aguada areas too display grooves (Fig. 3.16d).

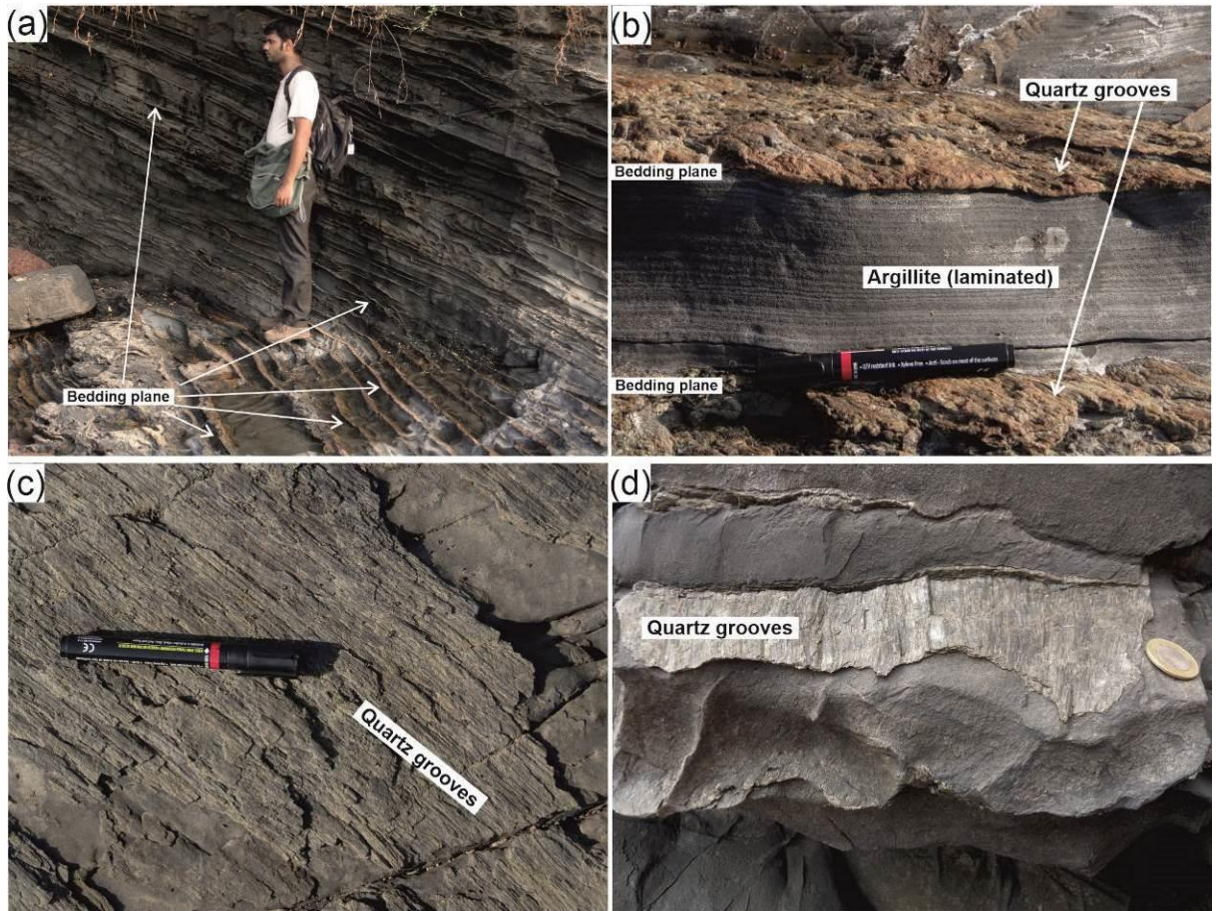


Fig 3.16. (a) ‘Flexural slip’ folds are formed at Vagator where there are quartz grooves on the slipped bedding planes. The person is 1.6m tall. (b) The occurrence of the quartz grooves above and below the laminated argillite bed at Vagator. The bed within itself is undeformed. Pen of length 15 cm is for scale. (c) Quartz grooves exposed on an inclined bedding surface. The pen trends in  $300^\circ$  whereas the rake of the grooves is  $49^\circ$ . Pen of length 15 cm is for scale. (d) Fault grooves as seen on an inclined bedding plane at Baga next to dyke AG25. Coin is 2.7cm in diameter for scale.

### 3.1.5.5 Shear zones

“A shear zone is a tabular zone in which the strain is notably higher than the surrounding rocks” (Fossen, 2010). There are of two types: ductile and non-ductile. While the ductile shear zones require formation depths over 10-15 km, the non-ductile shear zones are restricted to the upper crustal regimes (Davies et al., 2012). At least six shear zones

traverse the country rocks. Two of them are zones of an intense close-spaced network of quartz veins (Aguada), and the rest four are breccias (Vagator and Arambol).

Two shear zones trending ~NW-SE are in the Siquerim headland (*Fig. 3.1a*) with an exposed width of about ~50 m. They have close-spaced fractures, and joints filled with secondary quartz. The rocks in the central part of Aguada Headland (*Fig. 3.1a*) exhibit effects of hydrofracturing in the form of a criss-cross network of white quartz veins intervening the argillites (*Fig. 3.17a-c*). The argillite has haphazardly oriented angular fragments. I have also noted normal micro-faults (*Fig. 3.17d*).

The shear zone exposed on Arambol-Keri headlands (*Fig. 3.1c*) trends  $320^{\circ}$  (~NNW). This zone is ~2 m wide and extends for a length of ~35 m, concealed on either side under sand deposits (*Fig. 3.17e-f*). Its western margin has sharp contact with the country-rock, while its northern end abuts against SSD folds (*Fig. 3.7*), and its southern end disappears under seawater. The relative direction of movement along this shear zone is not apparent due to the absence of complementary sharp contact of the shear zone with the country-rock.

Three E-W trending brittle shear zones with an average width of 70 m traverse the country rocks in Vagator-Chapora (*Fig. 3.1c*). The southern margin of the shear zone is distinctly with respect to the country-rock (*Fig. 3.18a*) while its northern margin is found to be gradational. This breccia primarily has fragmented argillite (>80%), along with fragments of dolerite and black quartzite. The argillite fragments vary in size from being submicroscopic to as much as several meters across (*Fig. 3.18b-c*). The clasts range in shape from being sub-angular to ones with rugged outlines. Fragmented dolerite and black quartzite have rounded to angular shape and vary in size from ~15 to ~35 cm. (*Fig. 3.18d-e*). The rocks are traversed by joints that criss-cross each other resulting in blocks that resemble rhombs. Quartz veins in the shear zones have formed silicified breccia. This

brecciated zones closely resemble fluidized hydrothermal breccias formed due to excess fluid pressure (Branquet et al., 1999).

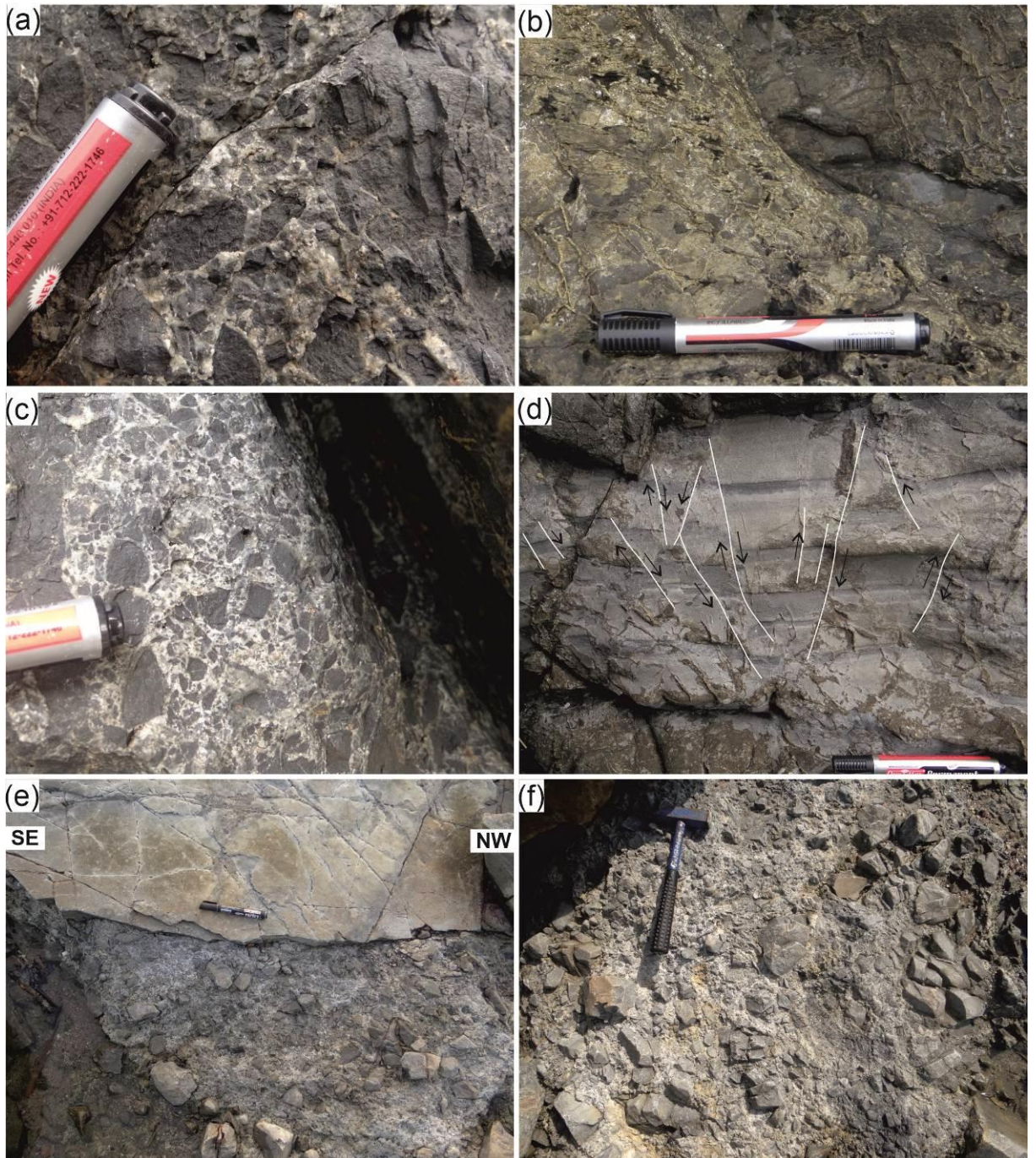


Fig 3.17. (a), (b) and (c) Hydrofracturing of the argillites by silica-rich fluids. (d) Normal micro faults in argillites at Aguada. (e) and (f) Planar view of NW-SE trending shear zones at Arambol. Note in (e) that the western margin of the shear zone shares a razor sharp boundary with the host rock. The marker used in Fig a-e is 15 cm long, and the hammer used in f is 35 cm long.

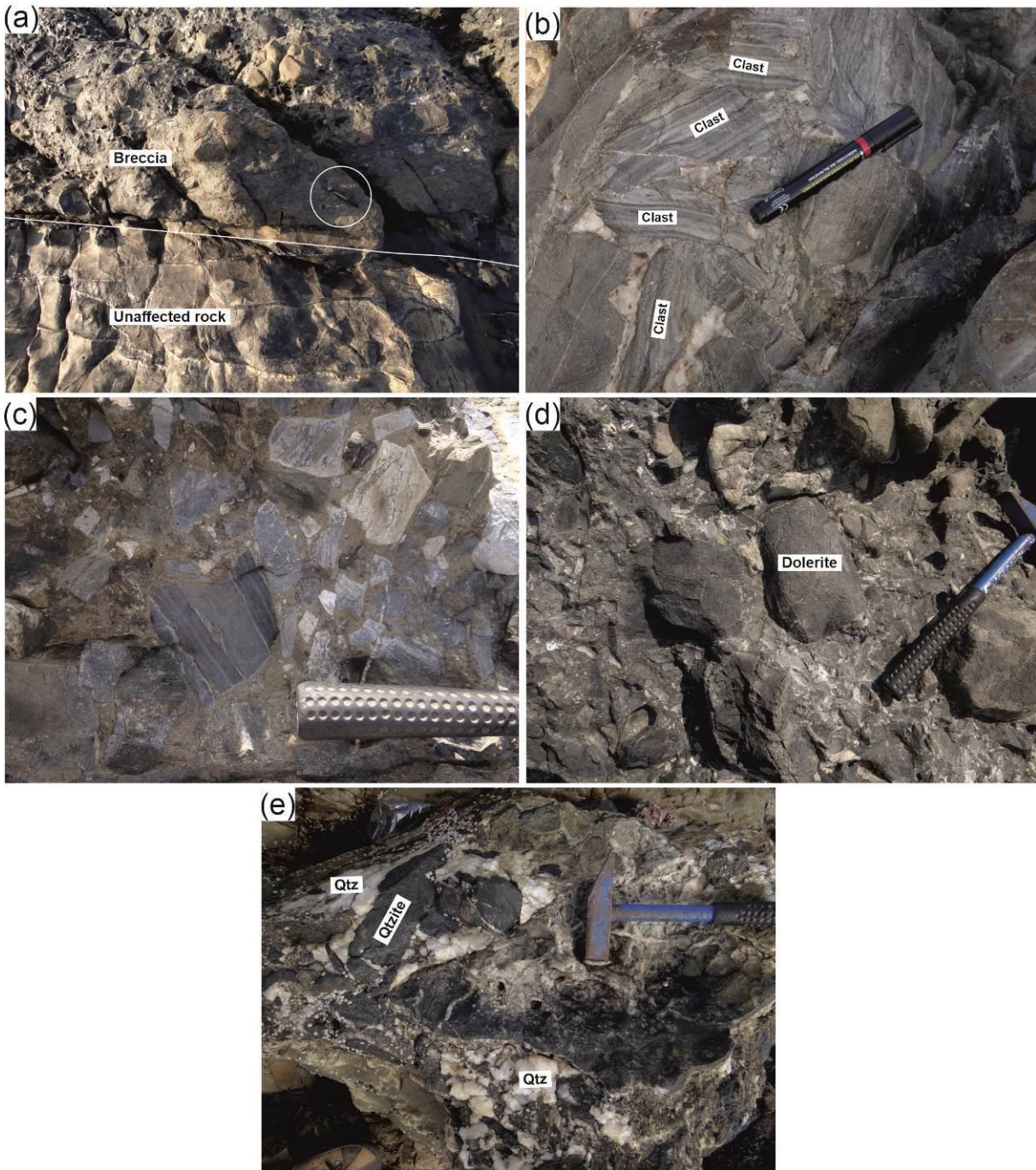
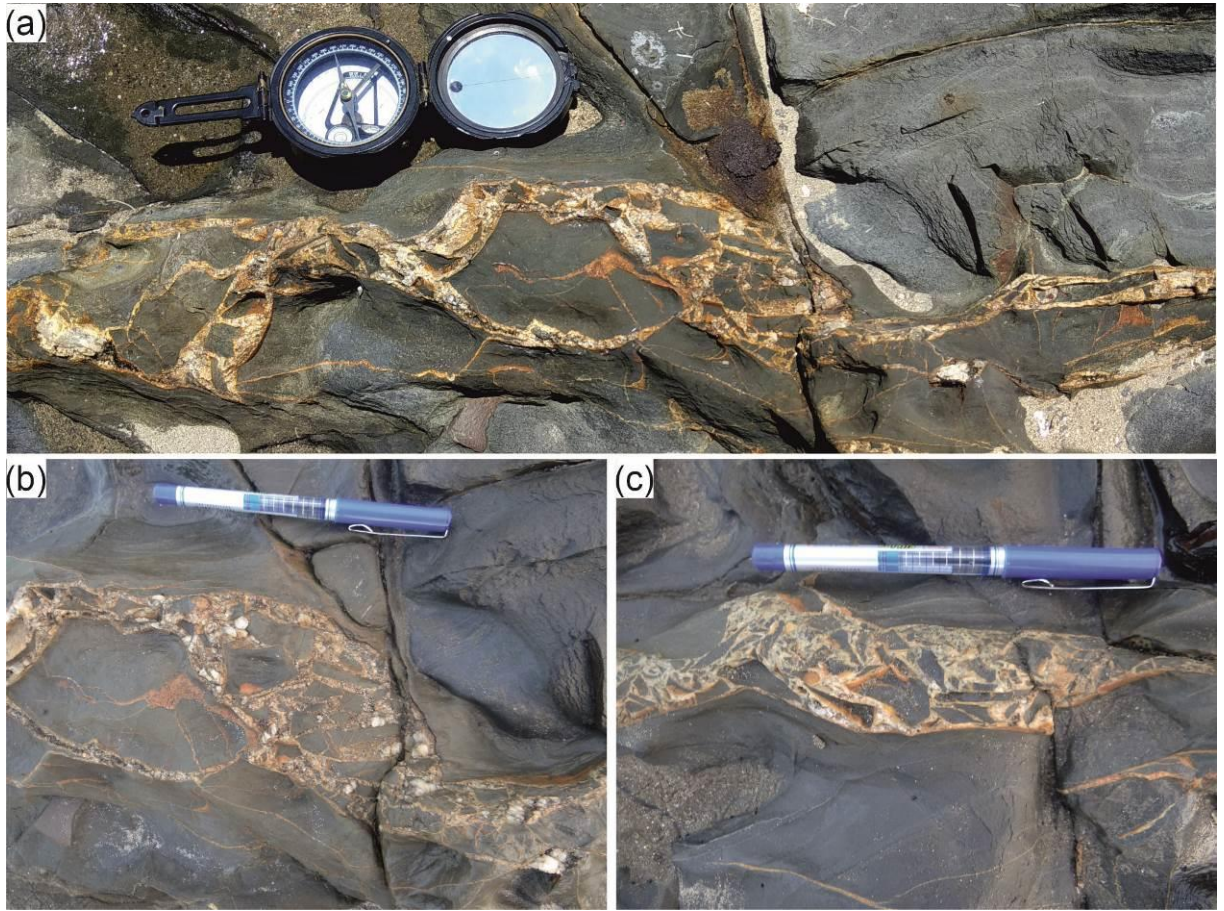


Fig 3.18. (a) The sharp boundary between sheared (breccia) and non-sheared (unaffected rock) host rock. (b) A chaotic mixture of argillite clasts cemented by milky white quartz. (c) Breccia containing fragments of argillite in a fine-grained matrix. (d) Dyke fragment (dolerite) in the breccia. (e) Black quartzite (qtzite) fragments cemented by milky white quartz (qtz). All photos are from Vagator headland. The black marker used as the scale is 15cm long, and the hammer is 0.35m long.

In the same tract of Vagator (Fig. 3.1c) are exposed few E-W trending veins displaying brecciated angular fragments of country rock dispersed in white quartz (Fig. 3.19a-c). I believe it might have formed by excess SiO<sub>2</sub> fluid pressure over the prevailing

lithostatic pressure. They resemble implosion breccias with jigsaw puzzle features (Sibson, 1986).



*Fig 3.19. (a) A planar view of a hydro fracture in the host rock. (b) And (c) These close-ups of the crack in (a). Here the fragments of the host rock are seen disoriented in a matrix of milky white quartz. Clear boundaries mark these small breccia zones. The Brunton compass used is 25cm long and the pen is 15cm long.*

The nature of the fragmentation of the country-rock mineralization in the form of massive smoky quartz, implosion breccia veins, and the occurrence of dolerite, all point that they owe their origin to fluidized excess pressures that were later than the intrusive phases of rocks.

### 3.2 Dykes: Field observations

The gently dipping sedimentary strata of the study area are traversed by several dykes, the study of which is significant for understanding the extensional tectonic regimes as well as mantle dynamics. The dykes are exposed along the rugged headlands punctuated by cliffs and bays. Their field characters like black colour (as against greyish colour of host rocks), linear outcrop pattern, and frequently high relief relative to host rock (on account of resistance to weathering), and differing types of weathering pattern (*Fig. 3.20a*) make them distinctly noticeable. Few of the dykes, I saw, are in the form of pockets of boulders occurring in a linear manner (*Fig. 3.20b*). Farther into the mainland, a thick cover of laterite obscures their observation. In total, sixty mafic dykes that constitute the Goa dyke swarm, are exposed in this area (Gadgil et al., 2019). Out of the total dykes, twenty-one dykes are in Aguada; twenty-three are in Baga, nine are seen in Vagator and seven stand out in Arambol (*Fig. 3.1a-d*).

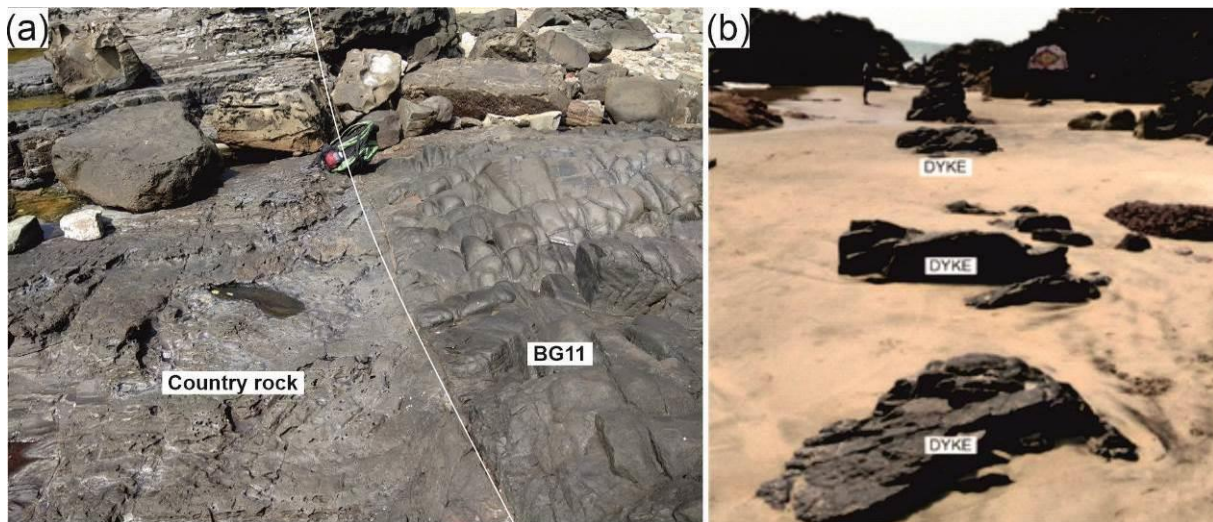


*Fig 3.20. (a) Differing weathering effect on the dyke BG-11 and country-rock (white line separates the two) Backpack for scale is on the contact. (b) Dyke AR-5 exposed as linear discontinuous outcrops. A person standing in the background serves the scale.*

I obtained the strike and dip of the dykes with a Brunton compass, and the length and thickness were measured using a metre tape (*Table 3.1*). A majority of the dykes have evident outcrops allowing their critical study of the field characters concerning their geometric forms, contact relationships, and within-dyke features such as columnar jointing and vesicular zones. Many of the dykes, viz. AG-39, BG-24, BG-25, BG-26 were exposed only during the lowest tide levels, while VG-31 concealed under beach sand, was revealed after an initial spell of rain washed off the sand veneer over it.

I ascertained the relative emplacement ages of the dykes by observing their cross-cutting relationships (*Fig. 3.21a*). Individual dykes that are adjacent to each other show strikingly different jointing patterns (*Fig. 3.21b*). The margins of the dyke with that of country-rock range from straight (*Fig. 3.21a*) to wavy (*Fig. 3.21c*). A majority of the dykes are vertical, with a few being steeply dipping. Several dykes form pairs sharing a common chilled margin, e.g. dykes AG-19 and AG-21, and AG-43 and AG-44, at Aguada (*Fig. 3.1a*), and dykes BG-09 and BG-10 at Baga (*Fig. 3.1b; 3.21b*). This is akin to the observation made by Bondre et al. (2006) for the Sangamner dykes, part of the Nasik-Pune dyke swarm in Maharashtra, India. Here, however, a few meters wide screen of country-rock separates the two dykes of a pair.

**Table 3.1** Field data on the Goa dykes exposed in the four study areas (Gadgil et al., 2019)<sup>3</sup>

<u>Sr. no.</u>	<u>Location</u>	<u>Dyke no.</u>	<u>Trend</u>	<u>Thickness (m)</u>	<u>Latitude (N)</u>	<u>Longitude (E)</u>	<u>Length (m)</u>	<u>Aspect ratio (Length/Thickness)</u>
1	Aguada	AG4	140°	2.00	15 29 30.0	73 46 38.6	20.8	10.4
2	Aguada	AG5	160°	5.80	15 29 33.6	73 46 39.0	24.4	4.21
3	Aguada	AG7	170°	0.50	15 29 34.1	73 46 40.1	14.0	28.0
4	Aguada	AG9	90°/85°→180°	0.50	15 29 34.5	73 46 41.7	45.8	91.6
5	Aguada	AG12	140°/75°→230°	3.50	15 29 34.3	73 46 45.7	23.3	6.66
6	Aguada	AG13	120°	17.8	15 29 32.9	73 46 03.8	106	5.96
7	Aguada	AG15	80°	10.1	15 29 27.0	73 46 07.0	100	9.90
8	Aguada	AG16	10°	3.00	15 29 27.7	73 46 07.6	72.0	24.0
9	Aguada	AG17	110°	12.4	15 29 25.6	73 46 26.2	98.3	7.93
10	Aguada	AG19	130°	11.4	15 29 25.2	73 46 19.5	92.0	8.07
11	Aguada	AG21	130°	5.00	15 29 25.2	73 46 19.5	103	20.6
12	Aguada	AG22	170°	16.0	15 29 50.2	73 45 53.8	82.0	5.13
13	Aguada	AG23	170°/60°→80°	2.60	15 29 47.1	73 45 53.2	61.3	23.6
14	Aguada	AG24	125°	5.00	15 29 47.3	73 45 53.4	58.0	11.6
15	Aguada	AG25	170°	1.50	15 29 39.5	73 46 01.3	20.3	13.6
16	Aguada	AG26	170°	2.20	15 29 39.5	73 46 00.0	29.7	13.5
17	Aguada	AG39	35° & 165°	3.50	15 29 33.8	73 46 03.8	72.0	20.6
18	Aguada	AG41	40°	18.0	15 29 40.4	73 45 59.9	34.4	1.91
19	Aguada	AG42	80°/74°→350°	0.70	15 29 45.8	73 45 53.1	68.7	98.1
20	Aguada	AG43	240°/75°→230°	3.50	15 29 52.5	73 45 55.1	53.0	15.1
21	Aguada	AG44	130°/75°→230°	7.10	15 29 51.9	73 45 56.5	57.0	8.03
22	Baga	BG2	65°	1.20	15 34 6.60	73 44 29.8	58.0	48.3
23	Baga	BG3	~N-S	0.03	15 34 5.20	73 44 28.7	23.0	767
24	Baga	BG4	160°	12.0	15 34 2.70	73 44 31.4	36.1	3.01
25	Baga	BG6	170°	3.80	15 33 40.0	73 44 44.0	37.2	9.79
26	Baga	BG7	155°	3.50	15 33 48.0	73 44 37.8	36.8	10.5
27	Baga	BG9	150°	19.0	15 33 46.9	73 44 36.5	96.0	5.05
28	Baga	BG10	150°	15.5	15 33 47.2	73 44 36.8	96.0	6.19
29	Baga	BG11	160°	3.00	15 33 51.3	73 44 31.5	32.0	10.7
30	Baga	BG12	140°	1.30	15 33 44.4	73 44 51.4	21.7	16.7
31	Baga	BG13	90°	0.50	15 33 41.0	73 44 45.0	32.0	64.0

<sup>3</sup> The geographic coordinates are in degrees, minutes and seconds (dms). The trend should be read as strike°/amount of true dip°→dip direction°.

Chapter 3 – Field Characters of country rocks and dykes

32	Baga	BG14	140°	1.50	15 33 40.9	73 44 45.5	37.6	25.1
33	Baga	BG15	140°	13.0	15 33 55.5	73 44 30.6	40.6	3.12
34	Baga	BG16	120°	20.3	15 33 57.2	73 44 31.2	35.0	1.72
35	Baga	BG20	60°	0.20	15 33 48.0	73 44 39.0	17.7	88.5
36	Baga	BG22	130°	5.10	15 34 07.4	73 44 29.0	187	36.7
37	Baga	BG23	160°	0.80	15 33 41.9	73 44 42.6	98.0	122
38	Baga	BG24	70°	0.62	15 33 44.0	73 44 41.6	38.0	61.2
39	Baga	BG25	70°	0.30	16 33 44.0	74 44 41.6	40.0	133
40	Baga	BG26	70°	0.49	17 33 44.0	75 44 41.6	35.0	71.4
41	Baga	BG27	155°	0.25	15 33 56.5	73 44 31.7	15.0	60.0
42	Baga	BG35	165°	19.5	15 33 40.0	73 44 43.0	105	5.38
43	Baga	BG36	160°	3.50	15 33 40.1	73 44 44.7	190	54.3
44	Baga	BG37	160°	2.50	15 33 41.0	73 44 44.0	222	88.8
45	Vagator	VG1	120°	8.00	15 35 19.9	73 44 00.0	57.0	7.13
46	Vagator	VG2	120°	1.90	15 35 22.8	73 43 56.4	59.0	31.1
47	Vagator	VG3	160°	7.00	15 35 30.4	73 43 58.5	56.3	8.04
48	Vagator	VG4	150°	5.10	15 35 45.2	73 44 1.70	64.4	12.6
49	Vagator	VG30	70°/75°→340°	0.40	15 35 53.3	73 44 00.0	72.0	180
50	Vagator	VG31	130°	1.60	15 35 47.9	73 44 1.80	52.0	32.5
51	Vagator	VG23	70°	0.60	15 35 59.0	73 43 59.6	32.2	53.7
52	Vagator	VG24	60°	7.90	15 35 59.9	73 43 59.0	100	12.7
53	Vagator	VG29	110°	0.30	15 35 53.8	73 43 59.9	71.6	239
54	Arambol	AR4	120°/50°→30°	13.0	15 41 38.1	73 41 53.5	153	11.8
55	Arambol	AR5	110°	5.40	15 41 59.0	73 41 45.8	66.2	12.3
56	Arambol	AR7	70°	7.00	15 42 00.0	73 41 43.6	62.0	8.86
57	Arambol	AR8	120°	3.00	15 42 14.3	73 41 38.1	50.0	16.7
58	Arambol	AR9	110°	3.40	15 42 16.5	73 41 38.3	58.7	17.3
59	Arambol	AR10	120°	7.20	15 42 15.8	73 41 37.6	60.0	8.33
60	Arambol	AR14	90°	4.00	15 42 11.3	73 41 38.9	42.0	10.5

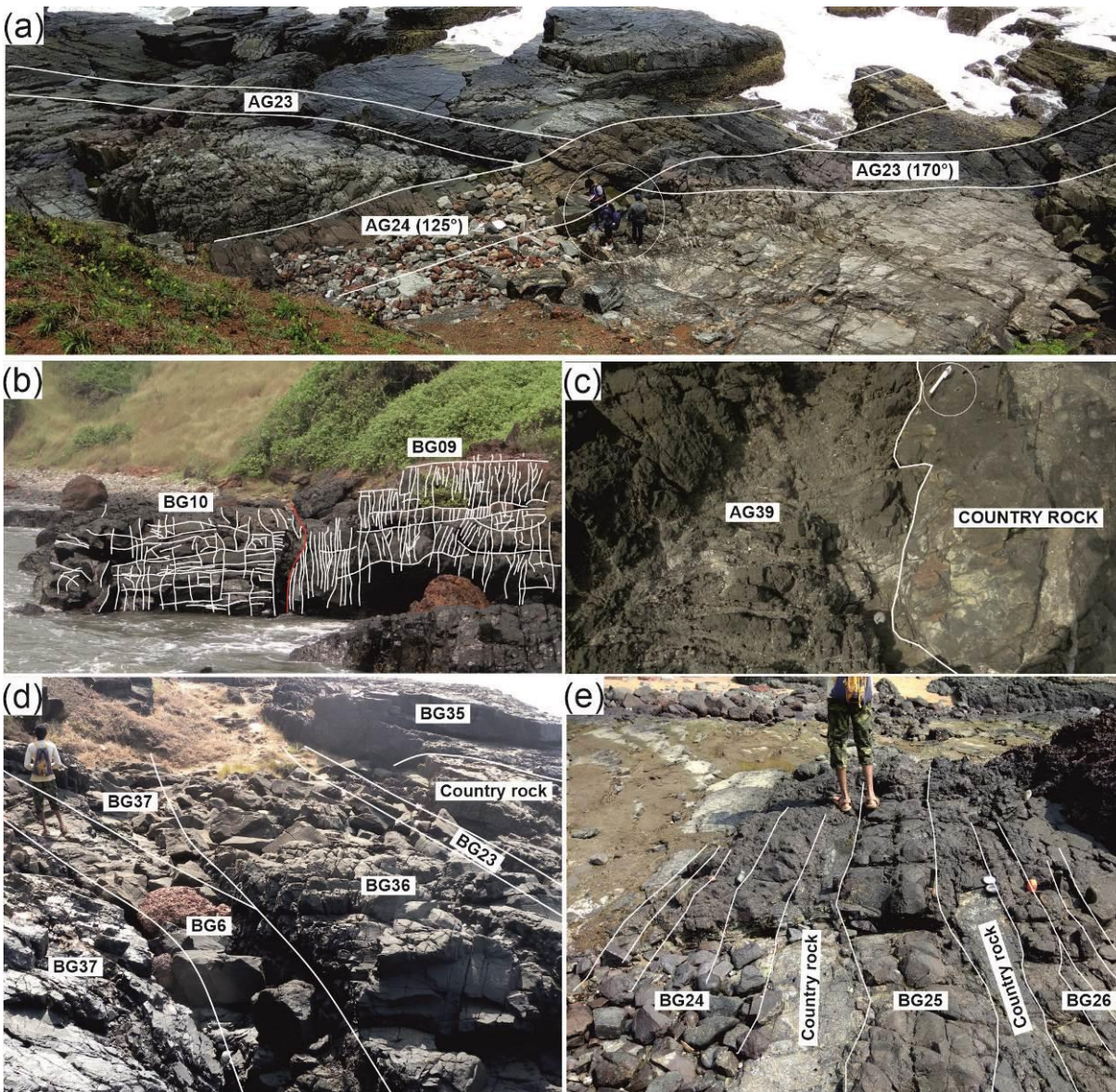


Fig 3.21. (a) Intersecting dykes AG-24 and AG-23 at Aguada, where the former cuts the latter. People (white circle) at the intersection of the dykes provide a scale. (b) Two dykes (BG-10 and BG-09) at Baga showing a joint pattern different from each other. BG-10 is 15.5 m thick. (c) Irregular contact between dyke AG-39 and country rock at Aguada. Here, the contact relations are controlled by host rock joints. White pen (encircled) is 9 cm long. (d) A multiple-injection dyke at Baga, with each injection named separately (BG-23, BG-36, BG-37 and BG-6). The person for scale is 1.7 m tall. (e) Dykes BG-24 and -26 are multiple injection dykes with an intervening single injection dyke BG-25. The person is 1.7 m tall.

One or more magma injections can lead to the formation of individual dykes or a swarm of dykes. The single magma injection dykes are characterized by columnar jointing which is margin-perpendicular of the individual dyke, whereas multiple magma injection dykes are identified by multiple rows of transverse columnar jointing (Gudmundsson 1995;

Sheth and Cañón-Tapia 2015). All of the multiple-injection dykes are restricted to Baga Headland (Gadgil et al., 2019). I have mapped the constituting dykes BG-6, BG-23, BG-36 and BG-37, all trending ~NW-SE, and named separately (*Fig. 3.1b; 3.21d*). The first three of these show common chilled margins, central vesicular zones and strike-perpendicular joints. There were some more dykes slightly north of the previously described outcrop (*Fig. 3.21d*). These are ENE-WSW-trending dykes, namely, BG-24 (with four magma injections) and BG-26 (with three magma injections) (*Fig. 3.1b, 3.21e*). The multiple-injection dykes BG-24 and BG-26 are separated by, a relatively thick (30 cm), single-injection dyke BG-25 (*Fig. 3.1b, 3.21e*). A thin screen of the country-rock is present on either side of BG-25. The individual injections in BG-26 and BG-24 have a thickness between 8 and 26 cm. Bondre et al. (2006) describe a similar situation for the Sangamner dykes, at Maharashtra - India.

The dykes BG-10 and BG-09 with the same trend, which appears to form a pair (*Fig. 3.1b, 3.21b*), may be considered to be a case of double injection. The southern end of the dyke BG-10 branches into thin finger-like dykelets and also shows chilled margins throughout its length in contact with BG-09. Again, dykes BG-09 and BG-10 are separated from dyke BG-07 by a 5 m wide screen of country rock (*Fig. 3.1b; Gadgil et al., 2019; cf. Bondre et al. 2006*).

### **3.2.1 Structural attributes and internal features of the dykes**

In the usual case, each multiple-injection dyke is treated as a single dyke (Ray et al., 2007) in any given study area for statistical treatment. However, in this study, all individual magma injections within a multiple-injection dyke are treated as several dykes. Hence, all the dykes in the study area include each of the single-injection dykes and all constituent parts of multiple-injection dykes. Thus, the double-injection dykes (BG-10 and BG-09), are counted as two dykes.

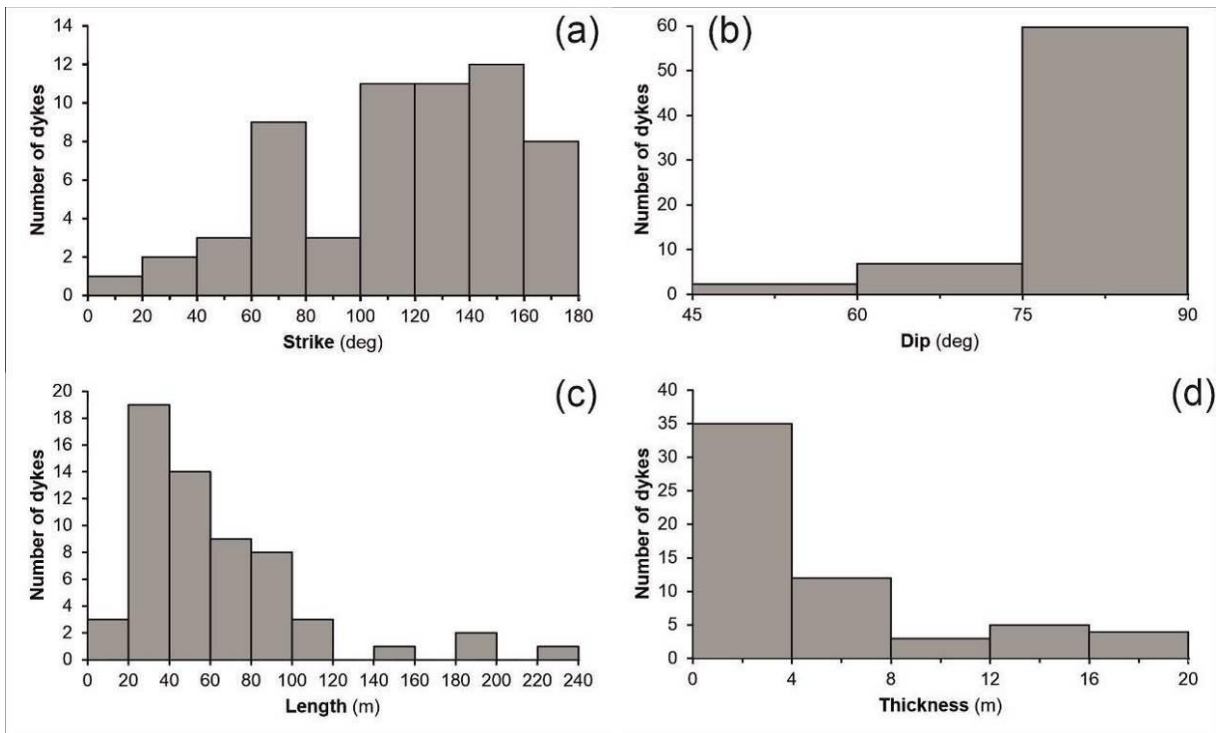


Fig 3.22. Plots of the number of dykes versus (a) dyke strike, (b) dyke dip, (c) dyke length, and (d) dyke thickness.

### 3.2.1.1 Strike and dip

The statistical treatment of strike values revealed that 42 of 60 dykes (i.e. 70%) have a trend restricted within  $N100^{\circ}$  and  $N180^{\circ}$  (~E-W to N-S) (Fig. 3.22a). The mean and median strike directions are  $N123^{\circ}$  and  $N130^{\circ}$ , respectively, and the mode is  $N160^{\circ}$  (NNW-SSE). The statistical treatment of dip values revealed that 52 dykes out of 60 (87%) are sub-vertical with the remaining eight dipping at various angles that vary from  $50^{\circ}$  to  $85^{\circ}$ ; with an average dip of  $71^{\circ}$  (Fig. 3.22b). Six of these dykes dip due NNW-NNE, one dips due east and one due south.

### 3.2.1.2 Length and thickness

The dykes along the coast are generally of shorter length. A majority of the exposed dykes are  $<100$  m in length with the most extended length being 222 m (Gadgil et al., 2019) (Fig. 3.22c). The cliff along the coast is constraining the lengths of the dykes and they are not comparable with those in Iceland (Paquet et al., 2007; Gudmundsson, 1984), Deccan

(Ray et al., 2007) or in Dharwar craton (Murthy, 1995) where the dykes run for a metre to many kilometres. The thickness of the study area dykes ranges from 3 cm to as much as 20 m with an average thickness of ~6 m (*Fig. 3.22d*). Only 13 of the 60 dykes (22%) are >10 m thick. As a result of their short lengths, I found their aspect ratios (length/thickness) to be very small which tend to yield unrealistic source depths, compared to others in the Deccan (e.g. Nandurbar-Dhule swarm where aspect ratios reach as high as 11630; Ray et al. 2007). For the dykes in the study area, the low aspect ratios may be in part due to incomplete along-strike exposure, implying that all reported lengths are minimum lengths.

### 3.2.1.3 Horns

Horns are defined as short branches of dykes located at dyke tips and also along the edges of dykes with variable thickness (Hoek 1991; Martínez-Poza et al. 2014). The thicker dykes in the study area possess planar contacts which do not necessarily follow joint planes in the country-rock. I noted the ‘horn’ structure in two dykes, namely AG-22 in Aguada (*Fig. 3.23*) and BG-6 in Baga.

The dyke AG-22 is oriented along the NW-SE joint set with its horn following a WNW-ESE joint locally (Gadgil et al., 2019) (*Fig. 3.23*). Likewise, BG-6 has its horn occupying a joint set within the dyke BG-35. The mechanisms for the formation of horns include (i) stress perturbations at the dyke tip or (ii) by magma moving along pre-existing host rock fractures along dyke margins (Martínez-Poza et al. 2014). I ascribe the latter process to be responsible for the formation of horns observed in the dykes of the study area.

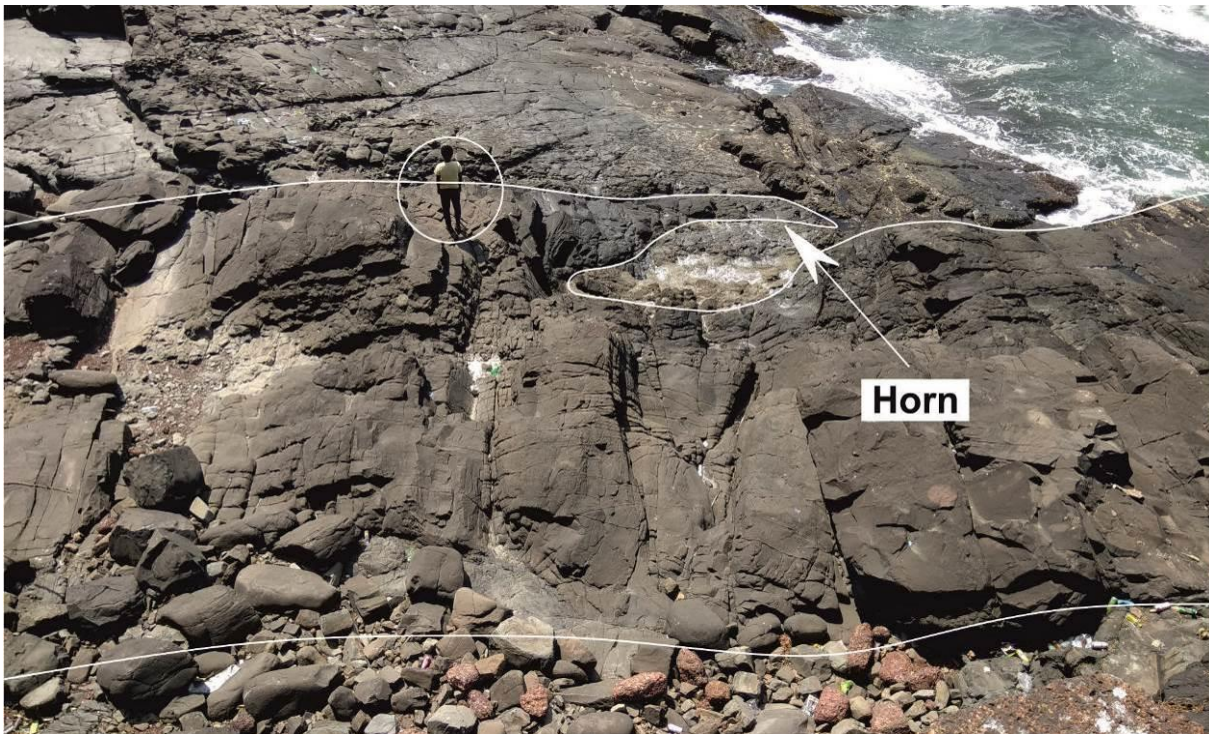


Fig. 3.23. Dyke AG22 (16m thick trending  $170^\circ$ ) at Aguada, with its “horn” following country-rock joints. The upper half of the photo shows prominent joints. The picture is clicked obliquely by standing on the Aguada Fort wall. Person (encircled) is 1.6 m tall.

#### 3.2.1.4 Dykes along pre-existing anisotropies

Thin dykes (<20 cm) are strongly controlled by the anisotropies within either the host rock greywacke (Fig. 3.24a) or another dyke (Fig. 3.24b). A similar situation exists in the Chimei complex of eastern Taiwan, where thin diabase dykes abruptly change direction, apparently controlled by fractures in the altered andesite host (Fig. 3.24c). In Fig. 3.24a, it appears that two orthogonal joint sets (NW-SE and NE-SW) were utilized by the magma to cause dilation. A slightly thicker dyke (AG-42, 50 cm) at Aguada occupies a pre-existing joint set that trends  $\sim N90^\circ$  (Fig. 3.25a), and the one at Baga (BG-13) is 30 cm thick (Fig. 3.25b). Occasionally, offshoots from thicker dykes occupy joints in the country rocks (Fig. 3.25c).

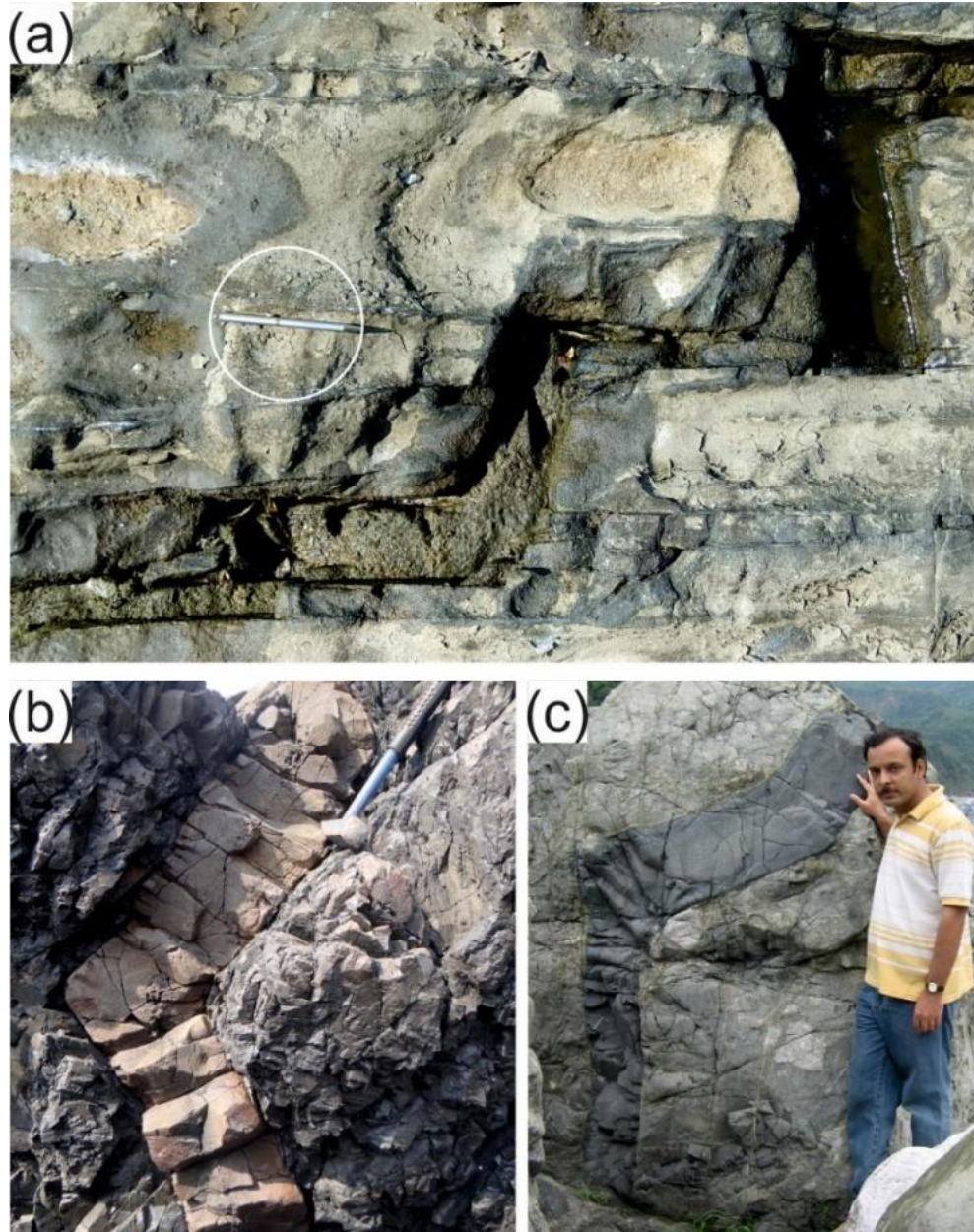


Fig. 3.24. (a) Control of pre-existing country-rock joints on the emplacement of dyke BG3 at Baga. Pen (encircled) is 15 cm long. (b) Vertical section showing dyke BG20 at Baga occupying pre-existing weak planes within the dyke BG09. BG20 also shows a concentration of vesicles along its middle. (c) Vertical section showing a deflected diabase dyke cutting altered andesite, Chimei complex, eastern Taiwan. Note well-developed fractures in the andesite near and exactly parallel to the vertical and inclined segments of the dyke, suggesting that the dyke occupies a pre-existing fracture network. **Person standing is Dr Ayaz Alam. Photograph courtesy: Prof Hetu Sheth.**

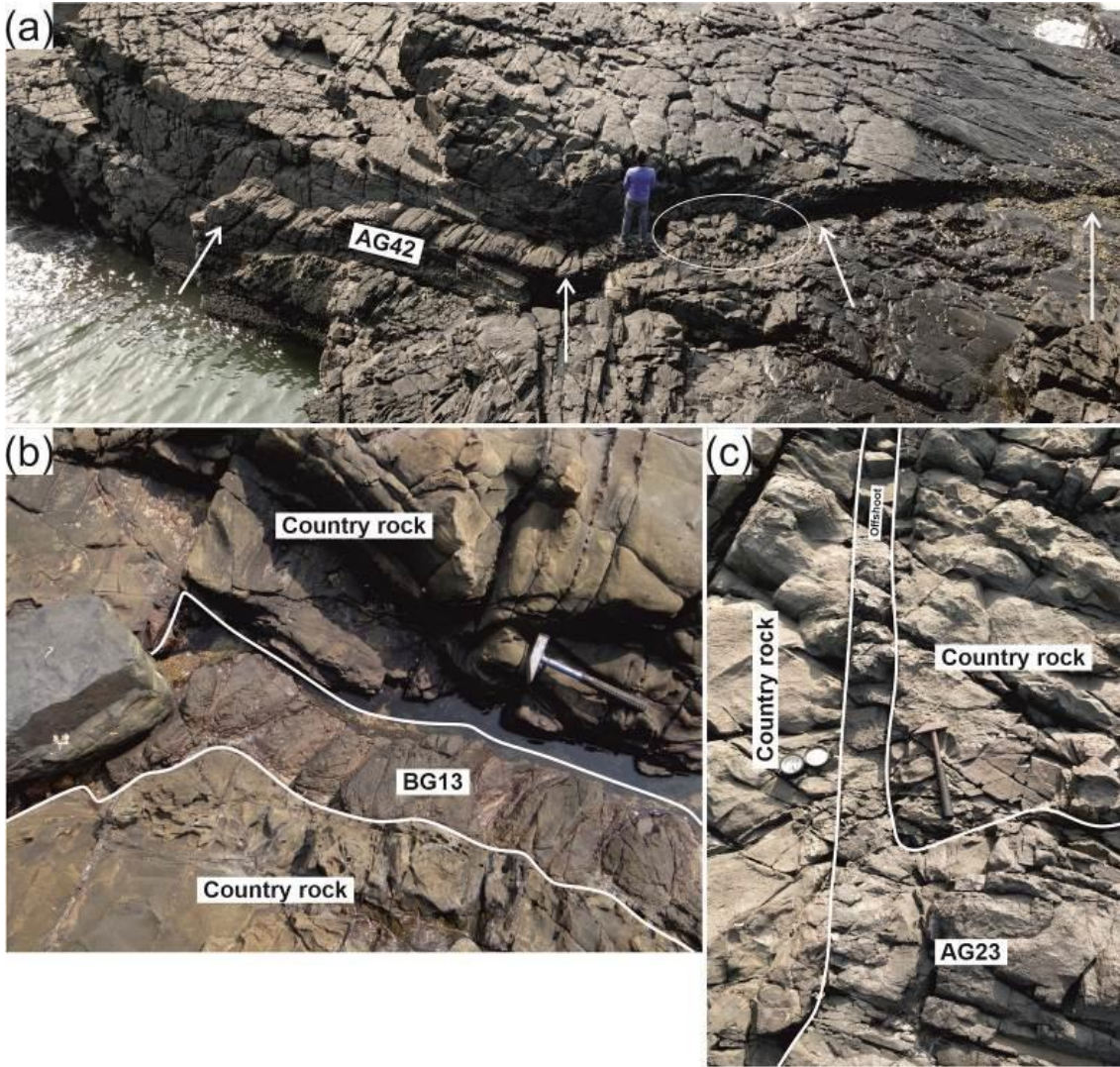


Fig. 3.25. (a) Dyke AG-42 (width = 50 cm) following host rock joints (marked with white arrows). The person is 1.6m tall for scale. (b) Host rock joints strongly control dyke BG-13. Hammer for scale. (c) An offshoot of dyke AG-23 follows the country-rock joints. It dies out after ~3 m away from dyke margins — Hammer for scale.

### 3.2.1.5 Rock bridges:

A rock bridge is a block of host rock bounded by two *en echelon* segments of a single dyke located at an offset of the dyke-fracture system (Hoek 1991). In sub-horizontal outcrops, both dyke segments become thinner where there are rock bridges (Babiker and Gudmundsson 2004). Though the segments seem disconnected at the present exposure level, they must be connected at a deeper level for the magma to be transported. There have been many studies of the occurrence and origin of rock bridges (Currie and Ferguson 1970; Pollard 1973; Pollard et al. 1982; Hoek 1991; Daniels et al. 2012). Sometimes, rotation and

deformation of rock bridges occur during an ongoing dilation event along en echelon dyke segments having either straight or curved propagation paths (Nicholson and Pollard 1985). Rock bridges indicate coeval tectonics and magmatism (Martínez-Poza et al. 2014).

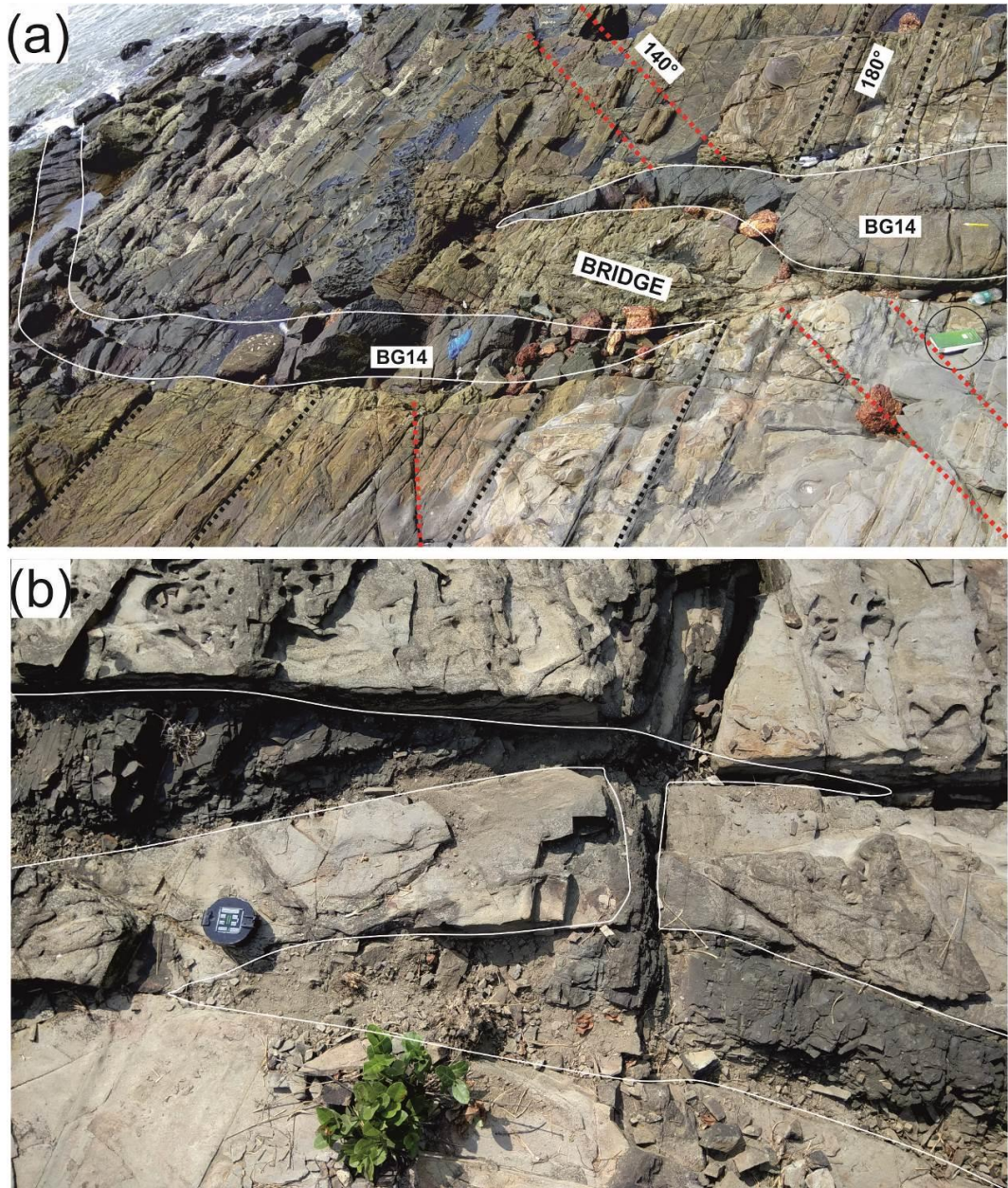


Fig 3.26. (a) View of the dyke BG-14 in a flat outcrop on the wave-cut platform at Baga, taken in an oblique and inclined manner from a cliff to show all features of interest in the same photo. Note the overlapping dyke tips around a host rock “bridge”. The far end of the left segment of the dyke occupies a joint that trends 140°. Field notebook (encircled, with the long dimension of 25 cm) near the right edge of the photo, provides a scale and is horizontal. (b) Plan view of the offshoot of the dyke BG-16. It shows two overlapping segments with right-stepping geometry and a mutual connection.

I observed two instances of such rock bridges at Baga. A highly fractured greywacke bridge separates two overlapping segments of dyke BG-14 (Fig. 3.26a), and

magma has entered the fractures. In this outcrop, the remote part of the left segment of the dyke (*Fig. 3.26a*) follows an NW-SE (N140°) joint set that is not followed by the right segment of the same dyke. I have not come across any literature on the Deccan that shows such rock bridges in dykes of comparable width. In the other instance at Baga, an offshoot of dyke BG16 runs parallel to the main dyke and has two overlapping segments with a right-stepping geometry (*Fig. 3.26b*, note also the connection between the two segments).

#### 3.2.1.6 Contact relations and vesicles:

Intrusive bodies form chilled margins because of a significant difference in the heat flux of the country-rock and the intrusive body (Huppert and Sparks, 1989). This margin can either remain or get eroded due to flow in the dyke. Though not in all dykes, some of them exposed in the study area show chilled margins (*Fig. 3.27a*). These margins have glassy selvages that are usually <1 cm thick (up to 9 cm thick). Several dykes (e.g. AG-23), are characterized by finer grain size. These dykes, mainly, are also fine-grained throughout. This could happen if the country rock is also at appreciably high temperatures at the time of intrusion. Typical close-spaced transverse joints are present at such margins that gradually become wider spaced in the centre of the dyke. The central portions of many dykes (Eg. AG-24, AG-21, AG-22, BG-36, VG-4, AR-4 etc.) are transformed into large rounded coarse-grained boulders due to spheroidal weathering around cross joints (Gadgil et al., 2019). The joints in the country-rock immediately at the contact of the dykes have been sometimes filled with magma (*Fig. 3.27b*). At several locations in the study area, are seen heating effects of the magma in the form of hardening of the country-rock (though without mineralogical changes), that has resulted into brittle fractures and formation of sharp-edged blocks (*Fig. 3.27d*).

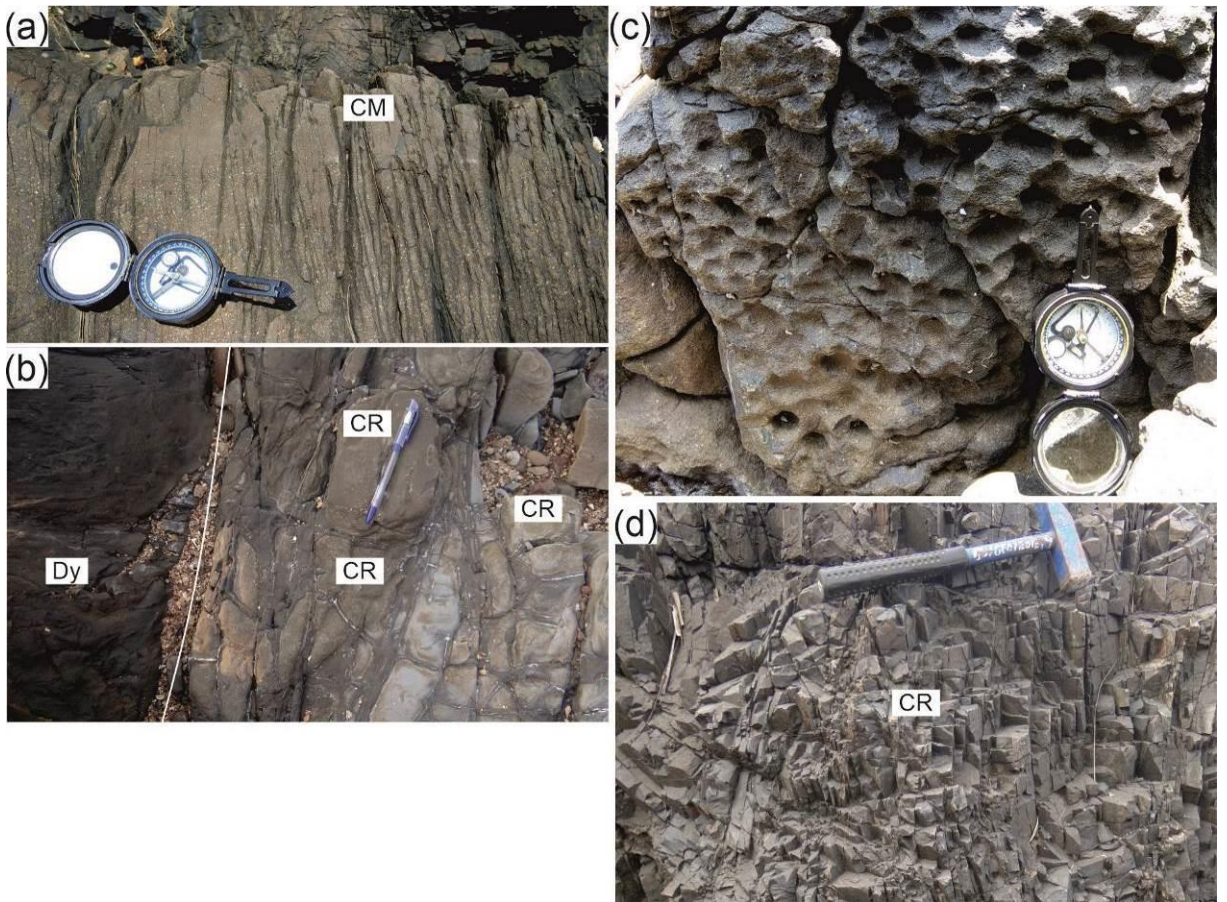


*Fig 3.27. (a) Chilled margin (CM) of dyke BG-36 at Baga, showing very fine grain size. Brunton compass provides a scale. (b) The contact of dyke VG-3 with country-rock at Vagator. Dyke magma fills roughly orthogonal fractures, and the magmatic heat has hardened the host rock. Dy=dyke, CR=Country Rock (c) Closeup of the central cross-section along the length of dyke BG-23 shows the spherical shape of vesicles. (d) Hardened country-rock (CR) due to magmatic heat next to dyke BG-12 is brittle and broken to angular fragments.*

Vesicles are a common feature in feeder dykes, with various shapes (elliptical or even teardrop) that suggest the movement of gas bubbles, helping to infer magma flow directions from their orientations (Varga et al. 1998; Noguera et al. 2009; Galindo and Gudmundsson, 2012). In the Goa dykes, I noticed that the vesicles are a common feature that concentrates along their central portions (*Fig. 3.27c, 3.28*). All of the studied vesicles are circular (and spherical) with a primary diameter of few millimetres (secondary diameter is the one formed by weathering along with these vesicles and can be centimetres across; *Fig. 3.27c*). The vesicle bands are entirely in the centre of the dykes irrespective of their thicknesses. These bands are usually 2-40 cm wide and are susceptible to weathering,

sometimes forming a deep central furrow (Fig. 3.28). Such divided dykes give false impressions of multiple intrusions.



Fig 3.28. Dyke AG24 at Aguada shows the concentration of vesicles in a 1.6 m wide zone along its central part. The vesicular zone is eroded more than the vesicle-free zones on either side. The hammer is 0.36 m long.

### 3.2.1.7 Columnar jointing:

Columnar jointing is a feature that occurs in a variety of rocks (Spry 1962). Igneous intrusions usually form well developed transverse (cooling) joints that are free from country-rock jointing effects. Such nicely developed columnar joints were seen only in one dyke (AR-4) (Fig. 3.29). These columns are characterised by four- to six-sided polygons that stretch throughout the dyke thickness. Other jointing patterns developed include curving columns of irregular width across the dyke thickness. Cooling cracks in the magma slowly developing into columnar joints result from tensional stress due to decrease in volume, cracks propagate inward and perpendicular to the isotherms which are parallel to the margins (DeGraff and Aydin 1987; Budkewitsch and Robin 1994; Grossenbacher and McDuffie 1995). Weak or irregular development of columns in these dykes could be due to the encounter of the magma with the water-table that usually causes distortions in the isotherms, as it occurs in lava flows (e.g., Long and Wood, 1986; Lyle, 2000; Sheth et al., 2015; Sheth, 2019).



Fig 3.29. Cross-section of joint columns, four to six-sided, in the Arambol dyke AR4. The view is perpendicular to the dyke walls. Hammer is 0.35 m long.

### 3.2.2 Tectonic Aspects of the Goa dykes

#### 3.2.2.1 Crustal dilation

Dykes are magma-driven extension fractures (mode I crack, akin to hydraulic fractures) that form in a direction perpendicular to the minimum principal compressive stress, and dyke swarms produce significant crustal extension during emplacement (e.g., Gudmundsson 1995; Marinoni 2001; Ray et al. 2007). In regional-scale mafic dyke swarms such as those in Iceland or the Deccan Traps, most dykes are steeply-dipping and subparallel since the regional stress field controls the major attitudes of dykes (e.g., Gudmundsson 1983; Ernst et al. 1995; Ray et al. 2007). However, there can be local deviations in the overall stress field, arising from factors such as shallow-level magma chambers or rock layers with anomalously high or low mechanical strength (Gudmundsson 1995, 2011). Marinoni (2001) presents methods for computing the crustal dilation

associated with dyke swarm emplacement. Given the nature of the terrain in my study area (rocky headlands and bays along the coastline, as well as beach deposits), there is no single straight traverse that would cut across all the exposed dykes. Two sizeable coastal stretches with either beach deposits or an intervening estuary (~7 km between Aguada and Baga headlands, and ~10 km between Vagator and Arambol headlands), provide no rock exposures, and were therefore not included in the calculations. I also avoided selecting traverses where the dykes would be parallel to the traverse (e.g., Baga). With these inherent limitations, I took four *local* traverses, suitably oriented to cut across a maximum number of dykes. The thickness of the dykes was measured perpendicular to the dyke strike. I calculated the cumulative thickness of the dykes (T) and determined the traverse length (L), and calculated the dilation using the equation (Marinoni 2001):

$$\% \text{ dilation} = (\text{aggregate dyke thickness}) / (\text{length of the traverse} - \text{aggregate dyke thickness}) \quad (1)$$

The traverses taken were from dyke AG-15 to AG-17 in the Jail tract at Aguada (*Fig. 3.1a*), dyke AG-42 to AG-43 in the Siquerim tract at Aguada (*Fig. 3.1a*), dyke VG-3 to VG-24 in the Vagator tract (*Fig. 3.1c*), and dyke AR-5 to AR-10 in the Arambol tract (*Fig. 3.1d*). I did not extend the Arambol traverse to dyke AR-4 as there is a 600 m long beach with no outcrops from AR-4 to AR-5. The dilation values calculated are as follows: 8% for Jail tract, 17% for Siquerim tract, 2% for Vagator tract and 3% for Arambol tract (*Table 3.2*).

**Table 3.2** Details of the dilation profiles, traverse lengths, dykes encountered and calculated dilation (Gadgil et al. 2019)

Particulars	Aguada		Vagator	Arambol
	Jail	Sinquerim		
Total traverse length (m)	536	245	1096	671
Total width of dykes (m)	41.9	34.9	22.0	19.6
Dyke numbers	AG15, AG16, AG17 AG19, AG21,	AG22, AG23, AG24, AG42, AG43, AG44	VG3, VG4, VG31, VG30, VG24	AR5, AR14, AR8, AR10
Effective traverse length (m)	494.1	210.1	1074	651.4
<b>Dilation</b>	<b>9 %</b>	<b>17 %</b>	<b>2 %</b>	<b>3 %</b>

### 3.2.2.2 Magmatic overpressures and source depths

Aspect ratios of dykes combined with reasonable values of mechanical properties of their host rocks can be used to calculate magmatic overpressures and thereby the source depths to the magma chamber (Gudmundsson 1983; Babiker and Gudmundsson 2004; Ray et al. 2007). These calculations assume

- (i) the exposed thickness of dyke equals the elastic opening at the time of emplacement, and
- (ii) the dykes, which are probable feeders to a now-eroded lava pile (Widdowson et al. 2000; Vanderkluyzen et al. 2011) represent through-the-thickness cracks between two free surfaces, these being the top of the source magma chamber and the Earth's surface.

The strike dimension (trace length),  $L$ , for such dykes is less than its dip dimension (vertical dimension or the height of the dyke), which I treated as being effectively infinite (Gudmundsson and Loetveit 2005). The Goa dykes are theoretically suitable for such calculations as they have a strike dimension (trace length) which is much shorter than the

expected dip dimension (a few kilometres depth to the magma chamber), implying that they should have got formed by vertical injection from such a chamber and not by lateral injection.

I calculated the magmatic overpressure  $P_o$  using the equation (Sneddon and Lowengrub 1969; Babiker and Gudmundsson 2004):

$$P_o = (b_{max}E) / 2L(1 - v^2) \quad (2)$$

where  $b_{max}$  is the maximum dyke thickness, and  $E$  and  $v$  are Young's modulus and Poisson's ratio of the host rock, respectively.  $P_o$  is also called net pressure or the driving pressure and is the pressure available at any point to drive open the walls of the dyke fracture.

The host rocks of the Goa dykes are Proterozoic-age metagreywackes, overlying granitic basement (Dessai, 2011). This situation is different from that in the Nandurbar-Dhule area of the Deccan Traps where the dykes are exposed within Deccan basalt lava flows (Ray et al. 2007). However, it is very similar to that in Sudan where Early Cretaceous and Late Proterozoic mafic dykes have been emplaced in much older granite (Babiker and Gudmundsson 2004). Therefore, in situ  $E$  values of 20-30 GPa are appropriate for the basement granitoids in my study area. Using these values and a corresponding Poisson's ratio of 0.25 for granitic rocks (Hansen et al. 1998; Babiker and Gudmundsson 2004) in equation (2), I calculated the magmatic overpressures of the Goa dykes. As noted, only one dyke (BG-3) has a relatively high aspect ratio of 767; I contrast this situation with the Nandurbar-Dhule dykes (Ray et al. 2007) the aspect ratios of which frequently run into several thousand. Dyke BG-3 gives a magmatic overpressure  $P_o$  from ~12 MPa (for  $E = 20$  GPa) to ~18 MPa (for  $E = 30$  GPa). Using these values of  $P_o$ , I calculate the depth to the source magma chamber using the equation of Gudmundsson (1983):

$$z = P_o / (\rho_r - \rho_m)g \quad (3)$$

where  $\rho_r$  is the average crustal density (assumed to be 2,800 kg/m<sup>3</sup>),  $\rho_m$  is magma density (2,700 kg/m<sup>3</sup>, Pinel and Jaupart, 2004) and  $g$  is the acceleration due to gravity. The calculated magma chamber depth for the dyke BG-3 is ~12 km. I consider this a reasonable value, noting from the petrographic observation that the dyke is relatively evolved in composition and has undergone considerable olivine fractionation, most likely at shallow depth.

For all the other dykes, the above two equations yield unrealistic (impossible) values of magmatic overpressures and depths to the magma chamber. For example, for dyke BG25 (aspect ratio of 133), the calculated magmatic overpressure is 70 MPa (for  $E = 20$  GPa) and 105 MPa (for  $E = 30$  GPa), with corresponding source depths of 70 km and 110 km. These extreme values for most study area dykes (except BG-3) are due to their very low aspect ratios. I attempted to laterally connect a few of the colinear dykes in the area to longer dykes, but their aspect ratios remain small enough to yield impossibly high magmatic overpressures and source magma chamber depths. This could also imply that the exposed thickness of the dykes may not merely reflect the elastic opening, but a component of the thickness maybe because of the thermal erosion of the wall rocks by the flowing dyke magma (see also Ray et al. 2007).

### **3.3 Discussion**

#### ***3.3.1 Interpretations of field structures of country rocks:***

##### ***3.3.1.1 The sequence of deposition of sediments***

From the field observations, I see that the country rocks exposed in the study area have gentle dips towards N-NW (*Fig. 3.1a-d*). It is also noted that the southern part of the study area is dominated by metagreywacke-argillite assemblage, while this transitions to an assemblage of metagreywackes with intercalations of white quartzite in the central region with the northern part dominated by quartzites with calcareous sediment assemblage. It is

evident from this observation that the metagreywacke-argillite represents slightly deeper facies than that of quartzites with calcareous sediments which represents a shallower depositional environment. I regard the former as a deeper part of the continental shelf and, the latter as more superficial part of the continental shelf—something like proximal part and distal turbidite. The metagreywackes and argillites, could be deposited under an unstable shelf environment owing to the abundance of SSD structures. At the same time, the basin got shallower towards North leading to the deposition of shallow water quartzites and carbonates. The association of metagreywackes and argillites in the form of interlaminations is common and is attributed to the quieter intervals between turbid periods when the fine-grained clays were deposited (Naqvi et al., 1988; Devaraju et al., 2010).

### *3.3.1.2 Soft-sediment deformation structures (SSDs)*

As many as 120 different types of SSDs have been described worldwide from sediments as old as the Paleoproterozoic to the present time (Shanmugam, 2017). The primary factors that form the SSDs are prelithification deformation and liquefaction (Shanmugam, 2017). Earthquake is not the only reason for the formation of SSDs (Alfaro, 1995; Shanmugam, 2017) but rapid deposition, differential compaction, slope stability are also responsible (Bowman et al., 2004; Majumder et al., 2009). Hence, independent verification of the seismic origin of the deformation structures is needed in every individual case (Seilacher, 1984).

The majority of the study area, has a metagreywacke-argillite association that represents a typical turbidite deposit. Such deposits form due to turbidity currents which may be generated by earthquake shocks, but the earthquake by itself is not the depositional process (Shanmugam, 2016). Hence, the SSDs owe cause of formation to the process of liquefaction (Shanmugam, 2016) or the slope instability on the shelf. Convolute laminations occurring together with ball-and-pillow structures, could be formed due to loss

of shear strength through a fluidization/liquefaction event (Toro and Pratt, 2015) and a concomitant expulsion of pore water (Kale et al., 2016).

I note that slump folds observed in Arambol (*Fig. 3.7*) are similar to those seen in Khari River section of Jhuran Formation, Kutch (Kale et al., 2016). These intricate folds consisting of anticlines and synclines with fold axes, assume mostly subhorizontal form when the sediments are poorly consolidated (Woodcock, 1976a, b; 1979; Maltman, 1984, 1994a, 1994b; Elliot and Williams, 1988; Collinson, 1994). Increase in pore fluid pressure facilitates such SSD which is responsible for reducing the shear strength of sediments (Maltman, 1994a, 1994b). In the case of Arambol, the unconsolidated calcareous sand layers must have moved downslope over relatively plastic clay layers in westerly direction under the effect of gravity when the slope exceeded the angle of repose of sediment (Mills, 1983).

The sand injections can primarily have two triggering mechanisms, namely earthquakes and depositional processes (Jolly and Lonergran, 2002). In the study area, the various clastic injections could be ascribed to the depositional process because earthquake-induced sand-injections contain angular mud fragments (Obermeier et al., 2005) which I have not seen in the study area.

### 3.3.1.3 Breccia

The post-consolidation structural features of the country rocks include the formation of breccia. The breccia zone orientation matches well with that interpreted from seismic and Landsat studies along the western coast of India, particularly with the fault zone passing through Panjim (Varadarajan and Ganju, 1989). Various types of fault breccia are recognized in the literature (Woodcock et al., 2014). Vagator-Chapora Headland has exposed a *megabreccia* (informal term), sedimentologically called as ‘boulder breccia’ (Woodcock et al., 2014) (*Fig. 3.18*). These breccias have angular to sub-angular clasts

(>1m), lack a fitted-fabric texture, and the clasts have been rotated and translated enough (Woodcock et al., 2014). It is observed here that there is similarly described breccia from Pembroke Peninsula, South Wales (Woodcock et al., 2014). In Aguada (*Fig. 3.17a-c*), what I observed is a ‘mosaic breccia’ recognized from its angular clasts and fitted-fabric texture with limited separation and rotation of clasts. Sometimes, normal and reverse micro-faults also occur in such breccia (*Fig. 3.17d*). Unlike in Aguada area, I note mosaic breccia in the Vagator-Chapora Headland in strong linear zones (*Fig. 3.19*) which is parallel to the megabreccia earlier described (*Fig. 3.18*). The breccia, at both the localities, i.e. Aguada and Vagator-Chapora have the voids filled with silica. Though various mechanisms are suggested for the formation of such structures, I attribute phreatic explosions/hydraulic fracturing (Bons et al., 2012; Woodcock et al., 2014; Shanmugam, 2016) to the formation of breccia in the study area.

#### 3.3.1.4 Mineral veins

Mineral-filled sigmoidal gash veins are excellent shear sense indicators because instantaneous stretching axis controls their opening and mineral growth. These form en echelon arrays along the shear zone. As tensional gashes form perpendicular to maximum stress, veins get oriented at  $45^\circ$  to non-coaxial deformation in simple shear (Jain, 2014). In the brittle-ductile shear zone, veins form progressively and continuously (Ramsay, 1980), hence these may shorten and rotate partially in the direction of shear near the centre of the shear zone, whereas newly formed veins will be  $\sim 45^\circ$  near its margin. Further, new veins may nucleate and form in the same original orientation, though early-formed veins got rotated with a change in the orientation of finite strain ellipse. The sequential propagation of shearing may thus produce multiple generations of veins, getting superposed on each other. The sigmoid form of en-echelon tension gashes reflects the fact that the younger, narrower tips form as fractures initially oriented perpendicular to the maximum

instantaneous stretching axis of the flow. At the same time, the older dilated central portion rotates with the same sense as the vorticity of the flow during progressive deformation (Hanmer and Passchier, 1991). The sigmoid shape of the veins is an excellent shear-sense indicator (Ramsay and Graham, 1970). I have noted several occurrences of a *tension gash* with negative dilatation (Ramsay and Huber, 1987) encompassing brittle-ductile shear indicators in the greywackes (*Fig. 3.15a*).

### **3.3.2 Interpretations of the field structures of the dykes:**

#### *3.3.2.1 Thermal erosion*

The propagation of dykes is governed by either along pre-existing fractures or by generating own hydraulic fractures (e.g., Gudmundsson 1984, 1995, 2011). Once a dyke forms with a particular thickness, its width may be widened by long-lived magma flow into it by thermal erosion of wall rocks. In such cases, its final thickness is more than the elastic opening during fracture formation (Fialko and Rubin 1999). Hence, thermal erosion of wall rocks widens the dyke thickness by a non-dilatational process (Fialko and Rubin 1999) and leads to an overestimate of the dilation. Thermal erosion is most common in dykes >7 m in thickness and involving turbulent magma flow (Fialko and Rubin 1999). Though 20% of the dykes in my study area are >10 m in thickness, no conclusive field evidence is available for the thermal erosion of their Proterozoic host rocks. I note here that chilled margins of dykes do not provide evidence for lack of thermal erosion (Fialko and Rubin 1999), and I cannot rule it out for some of the Goa dykes.

#### *3.3.2.2 Dyke trends and palaeostresses*

Undeformed dykes are very useful palaeostress indicators (e.g., Marinoni and Gudmundsson 2000; Babiker and Gudmundsson 2004; Ray et al. 2007). Wagle and Rajamanickam (1980) reported 43 dykes in the present study area, though without any

information on the dyke features. These dykes belonged to two magmatic episodes (Iyer et al. 1990), as the trends of these dykes correlated well with the regional Precambrian Dharwar trend (NNW-SSE) (Peshwa et al., 1987; Dessai 2018) and with the second folding (F<sub>2</sub>) episode of the Goa Group of rocks (Iyer et al. 1990). Whether these dykes have passively occupied pre-existing joints in the host rock or whether they reflect the contemporaneous stress fields is a question that is yet unanswered. I note that the dykes of highly irregular shapes and only a few centimeters thick follow fracture sets in their host rocks rather than the regional stress field.

As the trends of the Goa dykes were examined, it was noted that there is a significant spatial pattern in the dyke orientations. Though the majority of the dykes trend ~NW-SE and ~NNW-SSE in the study area, I note ~N-S trending dykes only at Aguada (*Fig. 3.1a*), whereas there are ~WSW-ENE-trending dykes at Baga (*Fig. 3.1b*) and Vagator (*Fig. 3.1c*), and a small number of ~E-W trending dykes at Aguada (*Fig. 3.1a*). The spread in the dyke strike (*Fig. 3.22a*) may reflect fluctuations in the direction of  $\sigma_3$  over time, though of a much larger magnitude than observed in the sizeable Nandurbar-Dhule swarm (Ray et al. 2007), for example. In my study area, though there are dominant dyke trends in select areas, small numbers of dykes striking in other directions than the dominant one are also noted. Perhaps, the variable strikes of the dyke either reflect a periodically changing  $\sigma_3$  direction or control by host rock joints, or both processes.

In the Aguada area (*Fig. 3.1a*), very few dykes strike E-W, which is the dominant joint trend. On the other hand, there are a large number of dykes that strike ~N-S and ~NW-SE, which are the least prevailing joint trends. This is overwhelming evidence that the dyke trends are unrelated to and unaffected by the pre-existing fracture fabric but must reflect the tectonic stress field at the time of their emplacement, which had ~E-W  $\sigma_3$  direction.

At Baga (*Fig. 3.1b*), the situation is different. There are both NNW-SSE-trending dykes and host rock joints in a large number, providing an argument for dyke trend control

by fracture fabric. However, even here, the most dominant joint set is ~NE-SW, and not a single dyke follows this trend. On the other hand, the different dyke trend observed at Baga (~WSW-ENE) has no matching joints. These observations again indicate a significant control of the contemporaneous stress field on dyke trends.

At Vagator-Chapora (*Fig. 3.1c*), ~WSW-ENE-trending dykes correspond to joints in roughly the same direction, but the NW-SE-trending dykes are oblique, by a few tens of degrees, to NNW-SSE-trending joints. At Arambol-Keri (*Fig. 3.1d*), I note a complete mismatch of the dyke and joint trends; the dominant joint trend of NNE-SSW has no matching dykes, and few joint trends match the dominant trend of the dykes of NW-SE.

Since the studied dykes do not occupy faults, and generally do not occupy pre-existing joints, they yield the minimum principal compressive stress direction ( $\sigma_3$ ) present during dyke emplacement. I believe that dykes having similar orientations may have been emplaced contemporaneously throughout the study area. The dykes' cross-cutting relationships can constrain their relative order. Based on these relationships I infer that ~E-W-trending  $\sigma_3$  forming ~N-S-oriented dykes existed first, followed by broadly NE-SW, but fluctuating,  $\sigma_3$  to cause dykes to trend from NNW-SSE to WNW-ESE. This  $\sigma_3$  seems to have stabilized in the last phase of dyke emplacement to a ~N-S-trending direction leading to the intrusion of ~E-W-trending dykes. The  $\sigma_3$  remained essentially horizontal throughout, as shown by the dominantly vertical and some steeply dipping dykes.

Thus, it is amply clear from the preceding discussion that the general trend of dykes in this study area is not E-W as perceived by Dessai (2018), but has three trends that have temporal variability. Dessai (2018) attributes the emplacement of the Goa dykes to the rejuvenation of basement weaknesses, specifically along the ancient Dharwar structural trend. However, my data of dyke and host rock joint trends show that, whereas there was some control exerted by the joints on dyke emplacement, particularly at Baga, overall there was a real control on the dyke trends by the contemporaneous stress fields.

### 3.3.2.3 *Inclined dykes*

A very few dykes in the study area dip at moderate angles (*Fig. 3.22b*) and cannot be considered sub-vertical. However, they do not resemble inclined sheets found in so-called sheet swarms, described from central volcanoes in Iceland (Gautneb et al. 1989) or Japan (Geshi 2005). These swarms contain sheets dipping inwards and converging on a shallow-level magma chamber, and the local stress field governs their structure around the chamber (Schirnick et al. 1999; Ancochea et al. 2003). The inclined dykes in the study area are simply too few to represent an inclined sheet swarm, and do not converge on a central magma source. These dykes (such as the one in *Fig. 3.24b*; and dyke AR4 in *Fig. 3.1d*) can be ascribed to local changes in stress fields in the shallowest (and mechanically most heterogeneous) part of the crust, or to control by pre-existing fractures (*Fig. 3.22c*), as seems to be the case in the Chimei island arc complex in eastern Taiwan (Song and Lo 2002).

### 3.3.2.4 *Nature of vesicles*

Vesicles are known to form at two stages during magma emplacement: (i) During the rise and decompression of a volatile-rich magma leading to volatile oversaturation, and (ii) crystallization of anhydrous phases from a magma with decreasing temperature (cooling), which raises the volatile content of the residual liquid to above saturation level (e.g., Sparks 1978; Wilson and Head 1981; Parfitt and Wilson 2008; Su et al. 2016). Both processes should lead to the formation of abundant vesicles that could be potentially sorted or segregated during the flow of magma in a fracture. My observations of the vesicle types and distribution in these dykes suggest similar processes. Vesicular dykes such as shown in *Fig. 3.27c* represents volatile-rich magmas that solidified above the depth of bubble nucleation (cf. Paquet et al. 2007). Estimated depths of basalt magma degassing range from

as shallow as 2-3 m (Galindo and Gudmundsson 2012), to as deep as 1.8 km, provided the magma has intruded into similar host rocks (Greenland et al. 1988; Paquet et al. 2007). In the case of fractured and low-density sedimentary host rocks, this degassing may have occurred even deeper.

Considering the overburden removal of 1 to 1.5 km from above the present exposures of the Goa dykes (Widdowson et al. 2000), and the generally volatile-poor nature of mafic melts, retrograde boiling resulting crystallization, rather than an originally volatile-rich magma, appears to be a plausible mechanism. The bubbles in a dyke magma should migrate upwards and, in a dyke inclined 50° (dyke AR-4 in *Fig. 3.1b*), should become concentrated along its hanging wall interface (Platten 1995). The high vesicle concentration along the central plane of the dyke AR-4 with its margins nearly free of vesicles may indicate that chilled margins developed on either side and the volatile-saturated magma being supplied was forced to flow along the central zone of the dyke, which was the last part to solidify.

#### 3.3.2.5 Feeder or non-feeder dykes?

I emphasize here that none of the dykes terminates in vertical sections, and it cannot be inferred, from field observations alone, whether these dykes fed Deccan flood basalt lava flows, now removed by erosion from much of Goa but still exposed in sections in the Western Ghats escarpment ~100 km to the east. Widdowson et al. (2000) provided  $^{40}\text{Ar}/^{39}\text{Ar}$  ages of ~62 Ma on some of the dykes in the coastal part of Goa, and based on geochemical-isotopic data, suggested the dykes to be potential feeders of some of the youngest Deccan basalts (Wai Subgroup). Baksi et al. (2014) proved that none of the  $^{40}\text{Ar}/^{39}\text{Ar}$  plateau or isochron ages of Widdowson et al. (2000) satisfies the essential statistical criteria for acceptance as crystallization ages. I point out that because the entire thick Western Ghats sequence, including the Wai Subgroup, is now dated to have formed

within a short time interval at 66-65 Ma (Baksi 2014; Renne et al. 2015), the 62 Ma age given by Widdowson et al. (2000) cannot be correct if these dykes are indeed feeders, as inferred by them based on geochemical-isotopic data.

The next chapter describes the petrography of the country rocks and dykes.

## **CHAPTER 4**

# **Petrography of country rocks and dykes**

I describe petrographic characters of country rocks and dykes in this chapter. I have used a polarized light petrological microscope to achieve this.

Thirteen representative samples of unaltered country rocks were collected. Due to the proximity to the west coast, most of the dyke rocks are altered on the surface. As far as possible, I have collected fresh samples by breaking the altered dyke rock. Though rock samples from forty-five dykes were collected, I have prepared representative thirty-seven thin sections. I have sampled from the central portion of the dykes as well as margins, where there was a visible megascopic change in the dyke grain size.

I sent the selected samples to a commercial thin section maker in Kolkata. The sections were studied in detail under a Nikon Eclipse E200 microscope under 5x, 10x, 20x and 40x magnifications in the School of Earth, Ocean and Atmosphere Science, Goa University. Photomicrographs in-plane and cross-polarized light obtained from the Nikon camera fitted to the microscope. I have processed the images using a NIS Elements D software, and inserted a scale for each image.

## **4.1 Country Rocks**

In total, I studied thirteen samples of country rocks under the microscope. I have divided these rocks into metagreywackes, argillites, breccia and calcareous sediments. The metagreywackes and argillites occur in association with each other; hence I have described them together.

### **4.1.1 *Metagreywackes and Argillites***

Metagreywacke exhibits immature and poorly sorted texture and consists of angular and medium-grained fragments of monocrystalline and polycrystalline quartz (most dominant) (*Fig. 4.1a-d*), plagioclase (*Fig. 4.1a and d*), alkali feldspars, biotite (*Fig. 4.1b*),

chert, rock and schistose fragments in a matrix of biotite, muscovite and clay minerals. Incipient crystallization of chlorite (*Fig. 4.1c*) with pale green pleochroism and irregular-outline opaques has occurred in the matrix as a result of low-grade metamorphism. At one instance, the rock shows weak foliation (*Fig. 4.1d*) defined by the regular oriented arrangement of quartz clasts in a fine-grained clay matrix dotted with opaques. Biotite forms a substantial proportion of the clasts at one locality in Aguada headland (*Fig. 4.1a*). On rare occasions, schistose fragments (*Fig. 4.1e*) are present in biotite-rich clast metagreywackes.

Argillite mostly occurs interbedded with metagreywackes. It is poorly sorted, immature, very fine-grained and consists of clasts of biotite in a matrix of quartz, feldspars, skeletal opaques and clay minerals. The rock also has quartz and clay-rich lenses separated from biotite & opaque rich layers (*Fig. 4.2a-b*). In laminated argillites, biotite clasts in a matrix of quartz, clay and opaques are seen (*Fig. 3.4a-c*). The biotite contains radioactive mineral inclusions that have formed pleochroic halos (Poole, 1928). The biotite clasts also show bending of the grains due to elasticity.

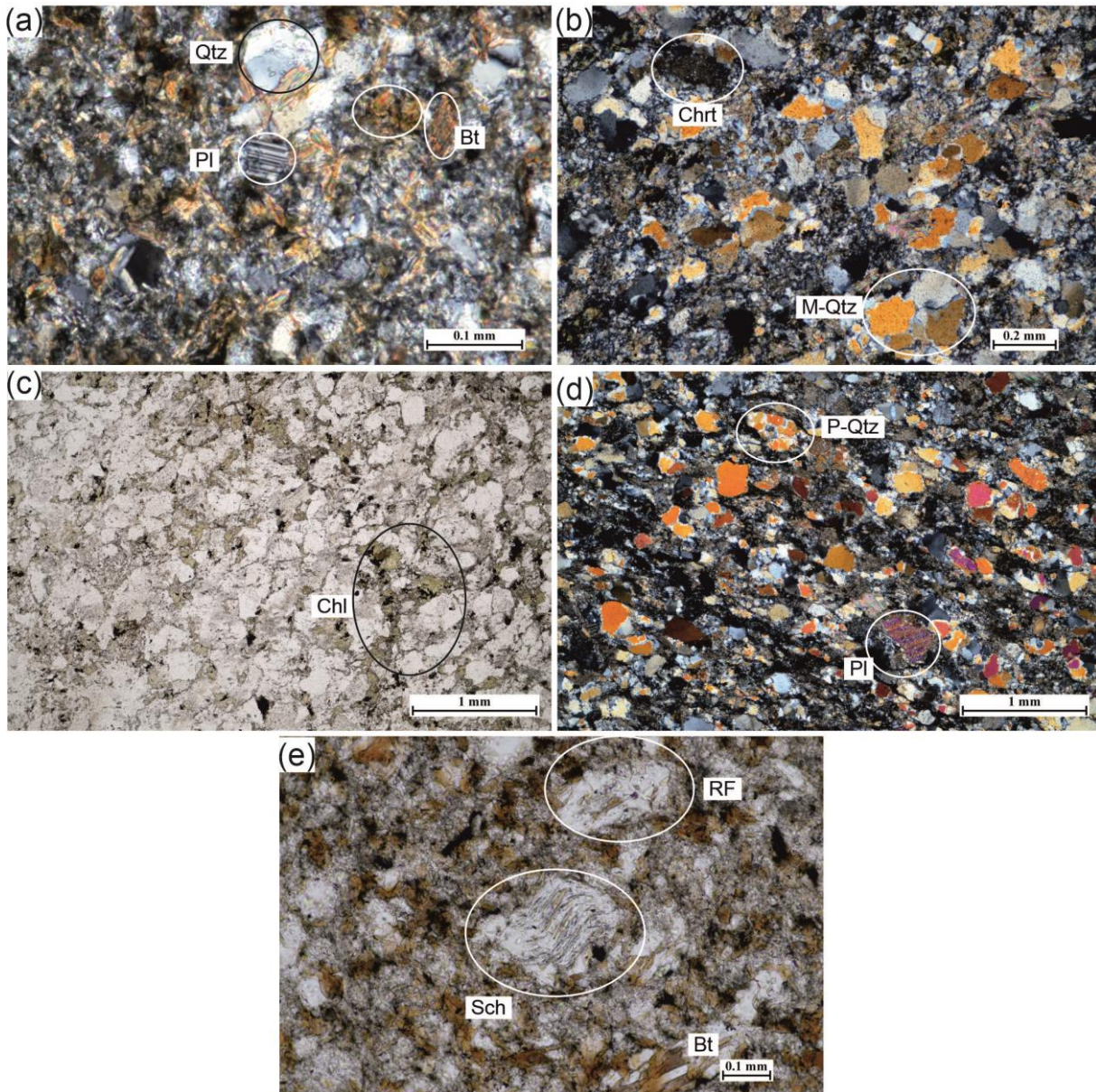


Fig. 4.1 (a) Cross-polarized light image of metagreywacke (BG-2) with biotite, quartz and plagioclase. Black and white coloured circles show the minerals. (b) Cross polarized light image of metagreywacke (BG-2) with monocrystalline quartz, chert, quartz, opaques and clay. (c) The plane-polarized light image of metagreywacke with secondary chlorite and specks of opaques. (d) The cross-polarized light image of metagreywacke (BG-3) showing faint foliation defined by oriented quartz grains and clayey matrix seen from the top left corner to the bottom right corner. Polycrystalline quartz and plagioclase are also present. (e) Metagreywacke (AG-30) having a schistose fragment of quartz-biotite along with a rock fragment in a matrix of biotite, quartz, chlorite and opaques. Abbreviations for all photos: Bt=biotite, Qtz=quartz, Pl=plagioclase, M-Qtz=monocrystalline quartz, P-Qtz=polycrystalline quartz, Chl=chlorite, Chrt=chert, RF=rock fragment, Sch=schistose.

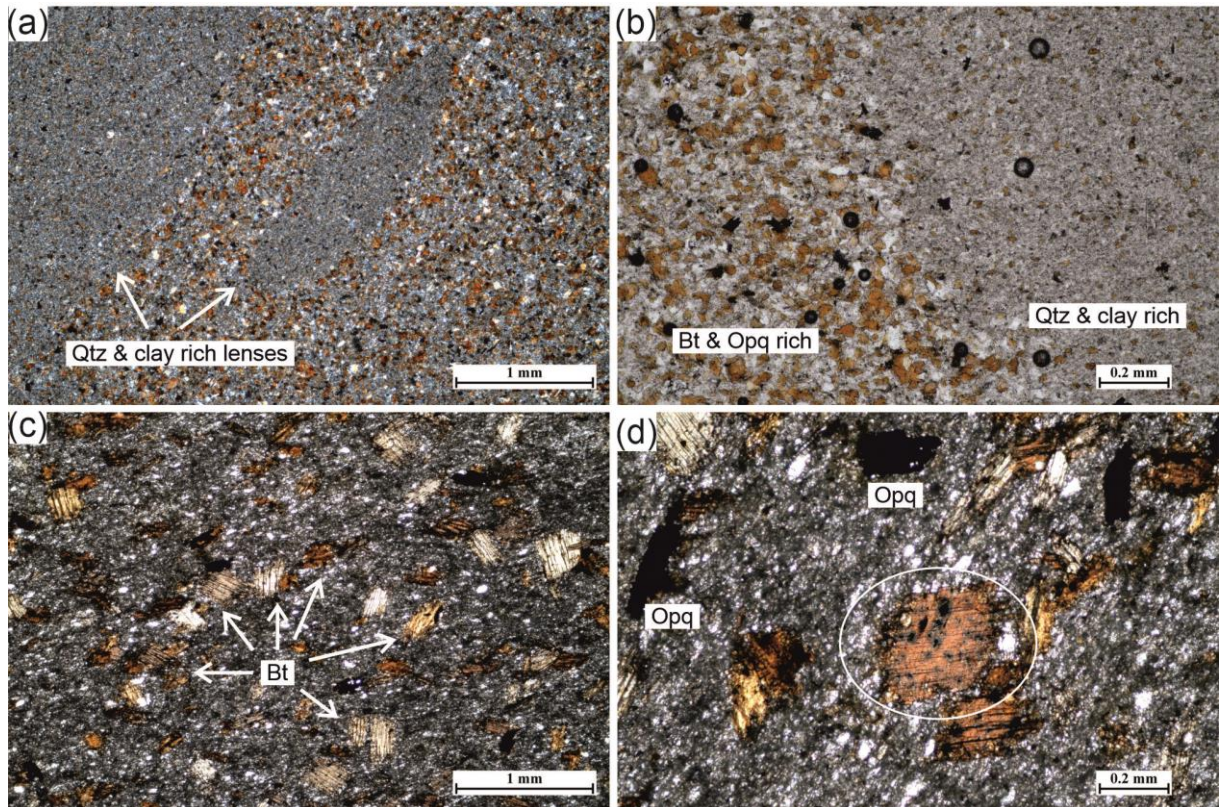


Fig. 4.2 (a) Plane-polarized light image of argillite (AG-40) having quartz and clay-rich lenses within a relatively coarser matrix of biotite, opaque and quartz. (b) A closer look at the figure in (a). Here there is a distinct boundary that separates biotite, opaque, rich areas from quartz and clay-rich areas. Flocculation could form these fine-grained lenses (Devaraju et al., 2010). (c) The cross-polarized light image of coarse biotite grains in a matrix of quartz, clay and opaques. Distinctly seen is one set cleavage of biotite. Sample VG-13. (d) Pleochroic halos (highlighted by a white ellipse) as seen in biotite. Picture (d) is a zoomed-in picture of (c). Abbreviations in all photos: Qtz=quartz, Bt=biotite, Opq=opaque.

#### 4.1.2 Breccia

This rock type has various types of clasts that include metagreywacke (Fig. 4.3a), argillite, and quartzite, dolerite (see Fig. 3.17d) in a matrix of quartz, clay and biotite. This rock is traversed by quartz veins that contain muscovite, biotite (Fig. 4.3b) and chlorite (Fig. 4.3c). Sometimes, the quartz veins show a comb structure (Fig. 4.3d).

Tourmaline rich quartzite clast consists of a mosaic of quartz (anhedral) and tourmaline (euhedral to subhedral, prismatic, tabular to triangular sections), both with planar grain boundaries (Fig. 4.3e-f). Volumetrically tourmaline makes up to 13 % in the rock. Tourmaline shows pale brown to pale yellow pleochroism with the triangular crystals

showing anomalous blue pleochroism. This quartzite has smooth boundary quartz grains meeting at planar triple junctions at grain boundaries (Fig. 4.4f).

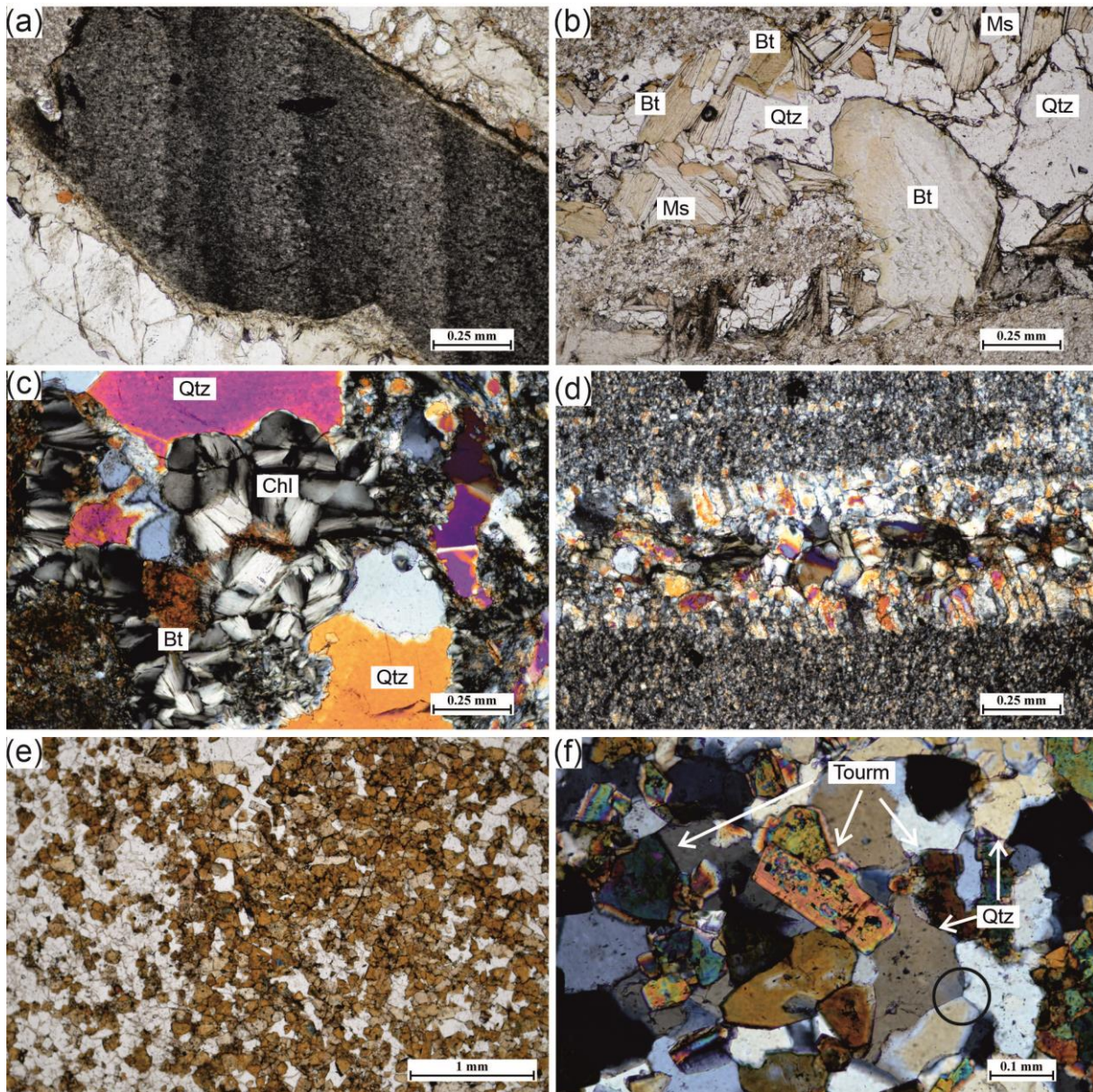


Fig. 4.3 (a) Plane-polarized light image of an argillite clast (VG-14-3) showing graded bedding. (b) Plane polarized light image of a quartz vein rich in biotite and muscovite. Sample VG-14-3. (c) The cross-polarized light image of a quartz vein and recrystallized flakes of biotite and chlorite. Sample VG-14-3. (d) The cross-polarized light image of a quartz vein that exhibits a comb structure. Sample VG-14-3. (e) Plane polarized light image of quartzite rich in tourmaline crystals (VG-14-1). Tourmaline exhibits brownish-bluish pleochroic colours. (f) A close up of (e) in cross-polarized light showing triangular and tabular sections of tourmaline. The black circle shows the planar triple point junction between quartz grains. Abbreviations in all photos: Qtz=quartz, Bt=biotite, Ms=muscovite, Chl=chlorite, Tourm=tourmaline.

### **4.1.3 Calcareous rocks**

These rock types are present only on the Arambol headland. Microscopic examination reveals that these rocks are uniform-grained with no distinction between clasts and matrix. Nevertheless, the rocks consist of muscovite and biotite, quartz, epidote whereas, at one occurrence, the rock showed the presence of calcite, muscovite and quartz. At places in the rock, muscovite flakes are abundant. The rock is brecciated; veins of quartz + muscovite disrupt fine-grained laminations.

## **4.2 Petrography and nomenclature of dykes**

In total, I studied thirty-seven dyke rocks under the microscope. I divided these rocks into tholeiitic basalts and dolerites, tholeiitic hypersthene dolerites and tholeiitic picrite basalts based on their mineralogy and textures. Tholeiitic basalts and dolerites are mineralogically similar but differ only in grain size, therefore described together. Table 4.1 gives the modal composition of the dyke rocks.

### **4.2.1 Tholeiitic basalts and dolerites**

Both, basalts and dolerites, are mineralogically similar but differ in grain size viz. basalts are fine-grained (< 1 mm) while dolerites are medium-grained (1-5 mm). I have classified the majority of the dykes from the study area under this category. The hand specimens of these rock types are greyish coloured, sometimes displaying clusters of >1 mm long plagioclase grains. All the rocks in this category are medium-fine grained, microporphyratic, and have hemicrystalline-holocrystalline and hypidiomorphic granular texture. They are primarily composed of calcic plagioclase, clinopyroxene (augite), olivine and opaques.

Plagioclase is the most abundant amongst all the phenocrysts. It also occurs abundantly in groundmass signalling towards its bimodal crystallization process. The size distribution of plagioclase phenocrysts ranges from 0.1 to 2.2 mm. It is lath shaped, pericline and albite twins are common, penetration twins are rare (*Fig 4.4a*); some of them are zoned while others altered to sericite. Other phenocrysts comprise olivine, in about 25 dykes, where it is rarely fresh. It is commonly altered to iddingsite, bowlingite and, less often to an aggregate of chlorite, serpentine, calcite and opaques (*Fig 4.4b-c*). They have a size distribution of 0.1 to 0.4 mm (average of 0.3 mm). Olivine phenocrysts are generally half the size of the most common plagioclase phenocrysts. In addition to these, microphenocrysts of plagioclase and pyroxene are also common. They average about 0.25 mm in size, suggesting that these crystals started crystallising slightly earlier than the groundmass.

In a few instances, I noticed up to three size populations (~1.3 mm, ~0.3 mm and ~0.1 mm) of plagioclase (*Fig 4.4d*). Zoning is more common in phenocrystic plagioclase rather than in groundmass (*Fig 4.4e-f*) and points towards the fluctuating conditions during magmatic crystallization. The glomerophyric texture so typical in basalts as well as dolerites, and does not appear to depend on overall grain size (*Fig 4.5a-b*). Few dykes have equigranular grains and are devoid of phenocrysts (*Fig. 4.5d*). Clinopyroxene (augite) forms phenocrysts in sporadic cases, otherwise restricted to groundmass. Sometimes augite forms long lath shaped crystals whereas plagioclase forms a directive (flow) texture (*Fig 4.5d*).



Fig 4.4 (a) Cross-polarized light image of penetration twin of plagioclase in a groundmass of a finer aggregate of augite and plagioclase. (AG-9) (b) The cross-polarized light image of interlocking texture is exhibited by iddingsitised olivine along with augite and plagioclase. (AG-17) (c) The plane-polarized light image of olivine (relict shape) altered to dusty and radiating opaques rimmed by pale green chlorite. Square and polygonal opaques could be magnetite. (AG-44) (d) The cross-polarized light image of three size populations of plagioclase (two of them form phenocrysts and the third forms groundmass). These phenocrysts also define glomerophytic texture. (AG-9) (e) And (f) Cross-polarized light image of zoning in plagioclase is prevalent in phenocrysts rather than in groundmass. Photo in (e) is AG-9 and in (f) is AG-21. Abbreviations for all photos: Pl=Plagioclase, Au=Augite, Chl=Chlorite, Op=Opaques, Mt=Magnetite.

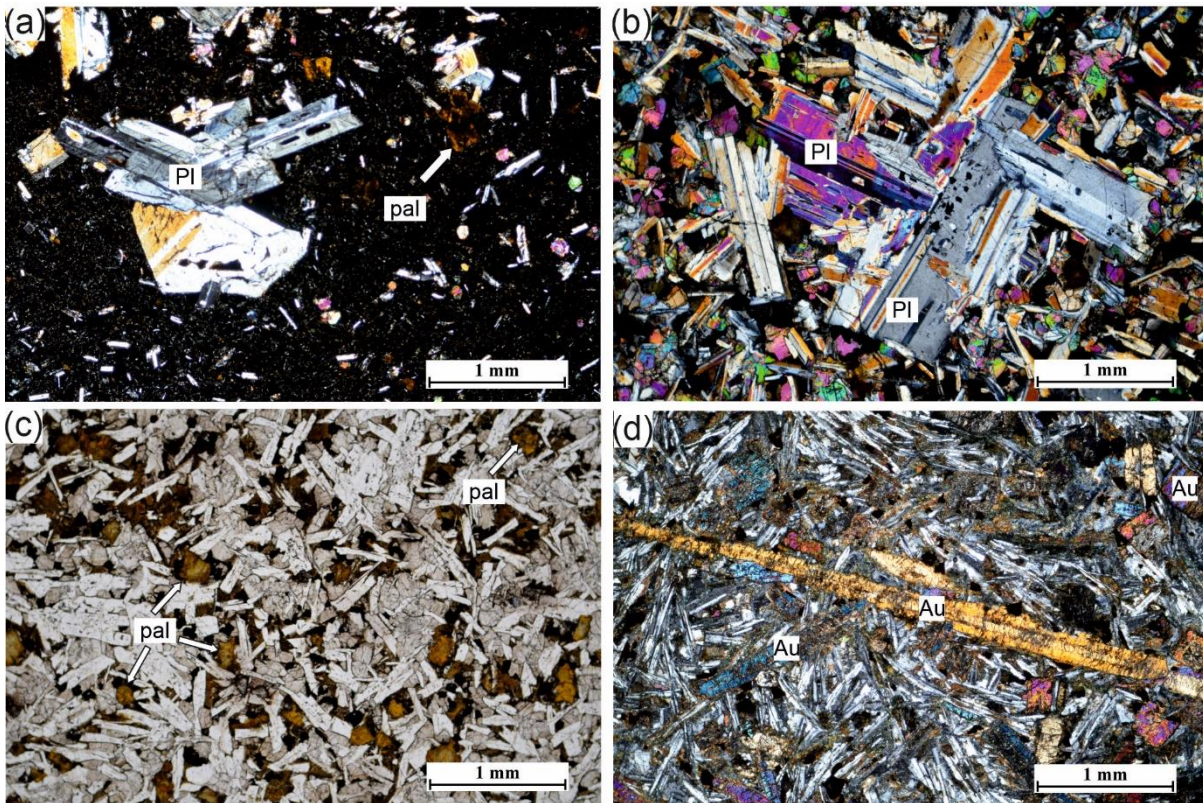
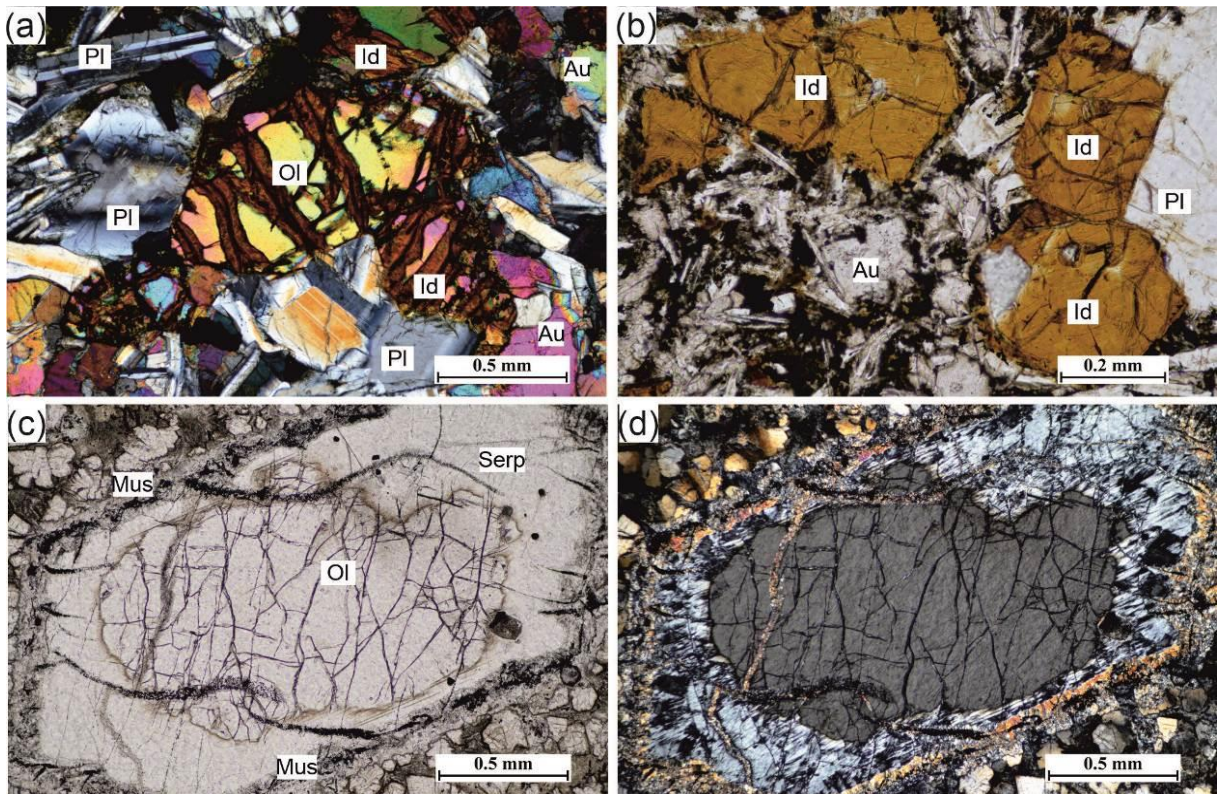


Fig. 4.5 (a) Cross-polarized light image of glomerophytic plagioclase in basalt (BG-3) with palagonite formed after glass. Plagioclase shows yellow colour as the section is thick. (b) The cross-polarized light image of penetration twins in plagioclase in a matrix that is dominated by plagioclase and anhedral augite. Plagioclase shows orange and purple colours due to the high thickness of the section. Sample AG-9. (c) Plane polarized light image of intergranular to intersertal textures where plagioclase laths are associated with augite as well as palagonitised glass. This is an example of an equigranular rock (AG-12). (d) Cross polarized light image of very long plates of augite ( $\gg 5$  mm) in a groundmass of finer augite and needle-shaped plagioclase. Sample AG-16. Abbreviations for all photos: Pl=Plagioclase, Au=Augite, Pal=Palagonite.

Olivine occurs as colourless, untwinned, fractured, euhedral crystals and mostly in the form of section cut parallel to (100) (Fig 4.6a). The olivine ranges in size from 0.1 to 0.4 mm. Euhedral phenocrysts of olivine are the most common. Olivine phenocrysts are commonly altered, either in part or wholly to red-brown iddingsite (Fig 4.6b). Deuteric alteration of olivine governs the formation of iddingsite (Chesworth et al., 2004). The contact between iddingsite and olivine is, at times, sharp and sometimes fuzzy. Olivine phenocrysts are sometimes completely pseudomorphed by iddingsite (Fig 4.4b, 4.6b), while in others remnant patches of olivine are preserved between the curved cracks. Olivine is

also altered to a mixture of chlorite, serpentine and oxides (*Fig 4.4c*). In one sample, euhedral olivine is seen to have an unaltered core, followed by serpentine dotted with opaques and rimmed by biotite (*Fig 4.6c-d*).



*Fig 4.6 (a) Cross-polarized light image of euhedral olivine with wine-red iddingsite replacing along the cracks. Sample AG-17. (b) Plane polarized light image of olivine pseudomorphs after iddingsite. Sample AG-9. (c) Plane-polarized light image and (d) Cross-polarized light image of olivine with unaltered core and a rim of serpentine + muscovite. Both (c) and (d) are AG-7. Abbreviations for all photos: Pl=plagioclase, Ol=olivine, Id=iddingsite, Au=augite, Serp=serpentine, Musc=muscovite.*

I divide the plagioclase phenocrysts into two types (i) transparent plagioclase laths, show distinct twins and are sometimes zoned, (ii) plagioclase with brown to black patches of interstitial glass as well as pyroxene inclusions that are distributed in the core or sometimes throughout the lath (*Fig 4.7a-d*). The latter type is known as “tecoblasts” which are defined as “late phase crystals developed at the expense of the groundmass” (Augusthithis, 1978) or as melt inclusions representing primary magmas (Dungan and Rhodes, 1978) or post-crystallization melt inclusions” (Srivastava et al. 1988). Such

tecoblasts are also described from dolerite dykes of Pachmarhi area, Madhya Pradesh (Powar and Deshpande, 1970), Deccan basalts from Malwa plateau (Srivastava et al. 1988) and, Carlsberg ridge basalts (Mislankar and Iyer, 2001; Mudholkar et al. 2002). There are two types of entrapped melt inclusions in plagioclase (Dungan and Rhodes, 1978). I have observed both types in studied dykes. First, the melt inclusions occur in plagioclase cores that are mantled by inclusion free rims (*Fig. 4.7c*). Secondly, a grid-like pattern exists where the position of melt inclusions are controlled by intersecting cleavage planes (*Fig. 4.7a-b and d*).

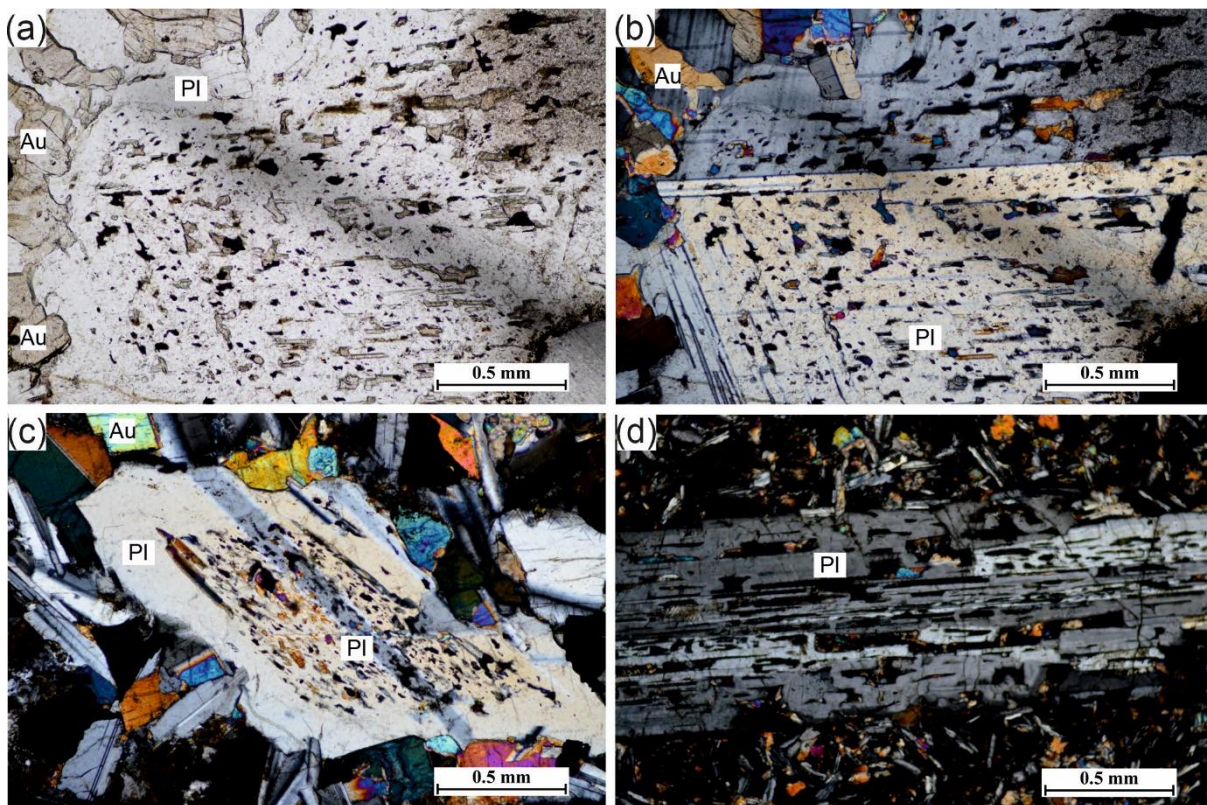


*Fig 4.7 (a) Plane polarized light image and (b) cross-polarized light image of a plagioclase phenocryst that has augite inclusions in it. Some of the melt inclusions cut through the grain boundaries of the twin. Sample AG-4 (c) Cross polarized light image of unique plagioclase with inclusion free rim. Sample AG-4 (d) Cross-polarized light image of plagioclase having pyroxene and opaque inclusions along its cleavage planes. Sample AG-9. Abbreviations in all photos: Pl=plagioclase, Au=augite.*

The groundmass is generally fine-grained, the average grain size is about 0.15 mm.

Usually, the grain size at the dyke contacts is minimum, but I note here quench zones in the

coarsest central part of the dyke. Plagioclase, pyroxene and opaques are the significant components, together with interstitial glass or palagonite, while olivine pseudomorphs are also noted. The texture is intersertal to intergranular. Interstitial glass or more commonly palagonite occur together, in quench zones of otherwise phaneritic basalt. The glass is usually a dirty brown or yellow colour, isotropic and frequently full of dusty opaques as well as other microlites. The palagonite is often a pale green colour and is feebly anisotropic.

By far, the ophitic (*Fig 4.8a-b*) to sub-ophitic (*Fig 4.8c-d*) textures are the most common and are associated with each other. The ophitic texture is when the plagioclase laths are entirely enclosed by the optically continuous pyroxene grains; while sub-ophitic is the one where there is the partial enclosure of plagioclase laths by pyroxene grains (Walker, 1957). In rare instances, I observe, the plagioclase laths taper towards the core of host pyroxene (Philpotts and Ague, 2009) (*Fig 4.8b*).

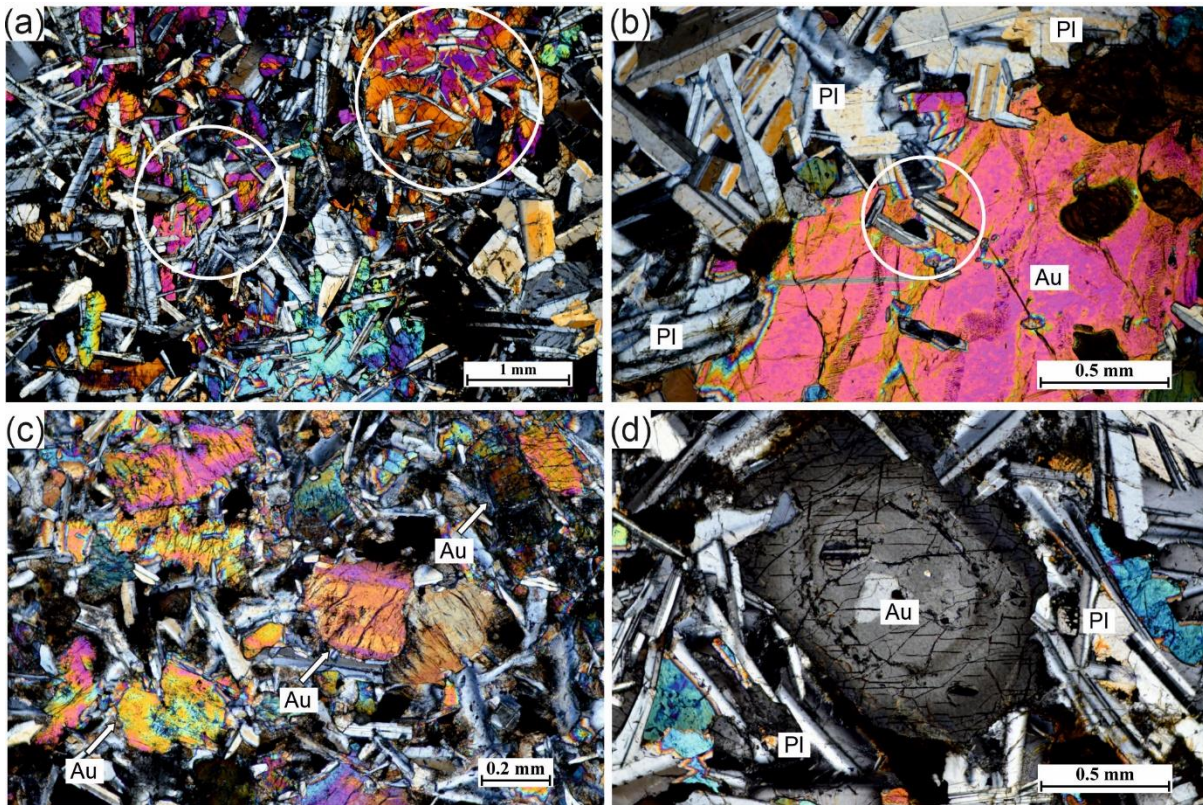


Fig 4.8 (a) Ophitic texture (marked by white circles) in a basalt (AG-19). (b) Partial to complete enveloping of plagioclase in augite. Note that the embedded plagioclase laths in augite are smaller than those outside the augite grain (marked by a white circle). Sample AG-17. (c) The sub-ophitic texture, where the augite shows zoning. Sample AR-4. (d) Zoned augite. Sample AG-4. All images in cross-polarized light. Abbreviations in all photos: Pl=plagioclase, Au=augite.

Clinopyroxene typically shows inclined ( $38-44^\circ$ ) extinction, and hence it is augite. Pyroxene exhibits alteration effects to chlorite. These pyroxenes, in general, show two sizes (0.3 mm and 0.7 mm) of distribution. In one of the dyke, the pyroxene (augite) is lath shaped and shows zoning (Fig 4.8c-d).

A common occurrence in the groundmass of these rocks is quenched glass and its devitrification products. Tholeiitic basaltic lavas often exhibit intersertal texture, that is, the presence of wedge-shaped patches of usually brown or greenish glass fitted between the groundmass plagioclase (Fig. 4.5c) (Cox et al., 1979). These quenched zones often consist of acicular/needle-shaped ilmenite, swallow-tailed to fibrous plagioclase and a feathery mineral which could be augite (Fig. 4.9a-c).

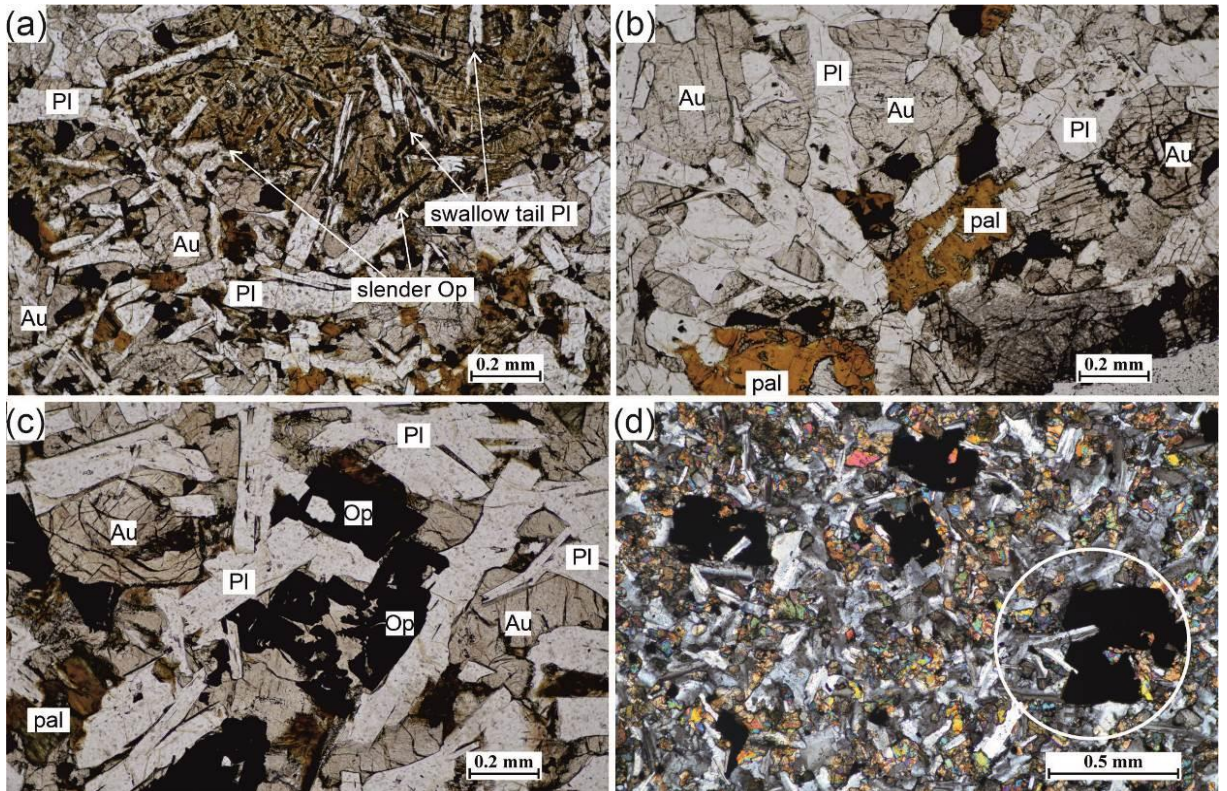


Fig 4.9 (a) Plane-polarized light image of a 'swallow-tail' plagioclase and 'slender' opaque within a quench zone. The rest of the area exhibits intergranular texture. Sample AG-25. (b) Plane-polarized light image of 'Golden Brown' palagonite formed after devitrification of glass in the quench zones. Note also well-crystallized plagioclase lath within palagonite. Sample BG-20. (c) Plane-polarized light image of skeletal opaques. Sample VG-4. (d) Cross polarized light image of opaques (marked in a white circle) having much larger sizes than the other mineral constituents. Sample BG-35. Abbreviations for all photos: PI=plagioclase, Au=augite, pal=palagonite, Op=opaques.

The opaques in the basalts are of small size and mainly confined to the groundmass; sometimes they have considerably higher sizes ( $>0.5$  mm) (Fig 4.9d) than any of its constituent minerals ( $<0.2$  mm). These large-sized opaques have probably grown later given their enveloping nature. The most common shapes of opaques are equant to rhomboid, whereas needle-shaped/acicular crystals (up to 0.6 mm long) are confined to the interstitial glass or quench zones. The equant shaped opaques are magnetites or titanomagnetites, and tabular ones are ilmenites. Apart from these common shapes, skeletal opaques are also dominant (Fig. 4.9c).

#### 4.2.2 *Tholeiitic hypersthene dolerites*

Only two dykes represent this variety of rocks, both are located in Arambol (AR-09 and AR-14). Both the dykes are medium to fine-grained, plagioclase phyrlic (2 mm x 1 mm), with hypersthene and augite occurring in interstices of the former, thus defining intergranular texture (*Fig 4.10c*). Hypersthene is identified by its pale green to pink pleochroism, higher-order interference colours (*Fig 4.10b*) high relief and straight extinction. The average mode of hypersthene is about 15-17 % (Table 4.1), and augite is about 10 %. At times, both the types of pyroxenes are partially to fully embedded in plagioclases defining the sub-ophitic texture. Plagioclase laths show reddish clouding due to dusty iron oxide inclusions, and this phenomenon is attributed to the entry of iron into the crystal lattice of feldspar under autothermal metamorphic effects or due to exsolution of Fe in feldspars (Halls and Zhang, 1995) (*Fig 4.10a* and *d*). Hypersthene and augite suffered deuteric alteration and breakdown to an aggregate of greenish chlorite, pale yellow to brown biotite and skeletal opaques (*Fig 4.10d*). Olivine (neither fresh nor altered) is conspicuously absent in these dykes.

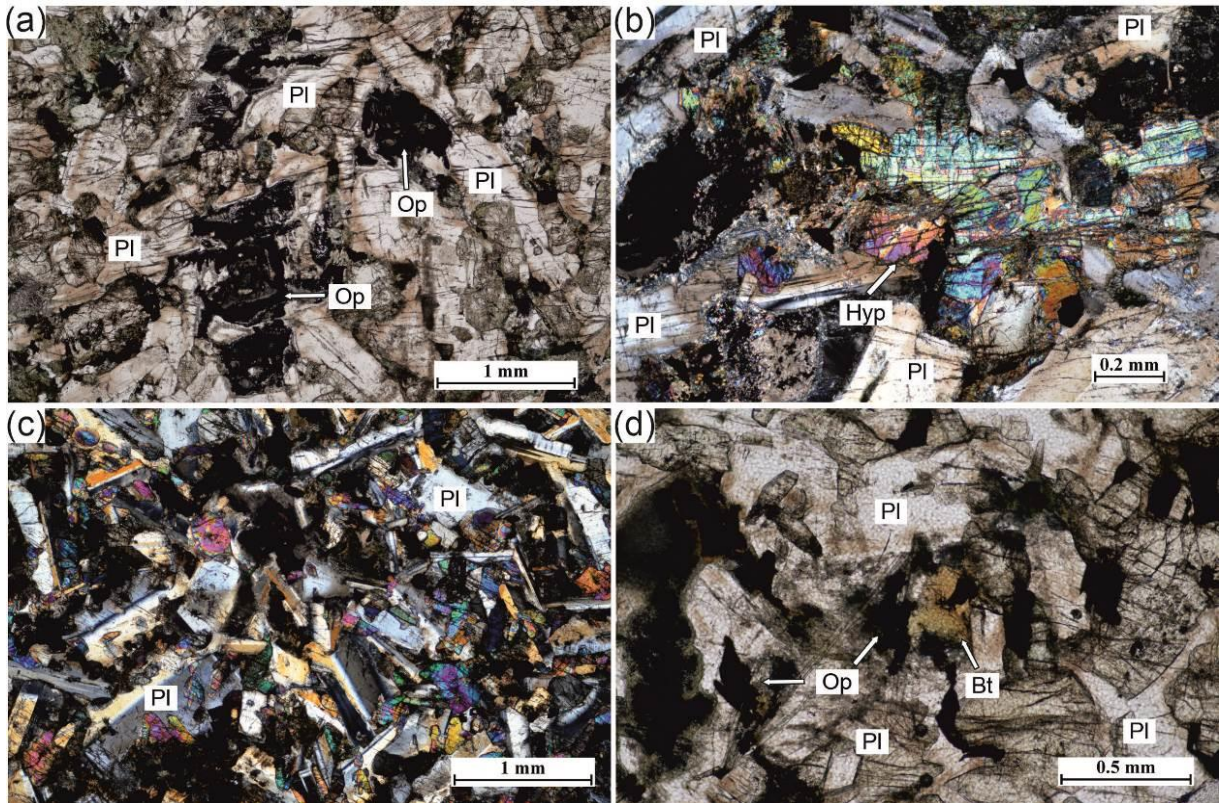


Fig 4.10 (a) Plane polarized light image showing reddish rimmed plagioclase and altered pyroxene with skeletal opaques. Sample AR-9. (b) Cross polarized light image shows higher-order interference colours for hypersthene, prominent cleavage planes and plagioclase. (c) Cross polarized light image showing anhedral pyroxene inclusions in plagioclase forming intersertal texture with accessory skeletal opaques. Sample AR-14. (d) Plane polarized light image showing alteration effects of some pyroxene grains to a mixture of opaques + biotite. Sample AR-14. Abbreviations: Pl: plagioclase, Hyp: hypersthene, Op: opaques, Bt: biotite.

### 4.2.3 Tholeiitic picrite basalts

Four dykes are representatives of this type (AG-23, AG-26, AG-39 and BG-11). The hand specimens of three of these dykes is a dense black rock and show rather abundant yellowish-green to a darker cluster of phenocrysts of pyroxene and olivine, set in a fine-grained groundmass. The hand specimen of one dyke shows coarse platy phenocrysts of pyroxene set in a darker groundmass (BG-11). Under the microscope, these are strongly porphyritic, medium to fine-grained bearing holocrystalline, hypidiomorphic inequigranular texture.

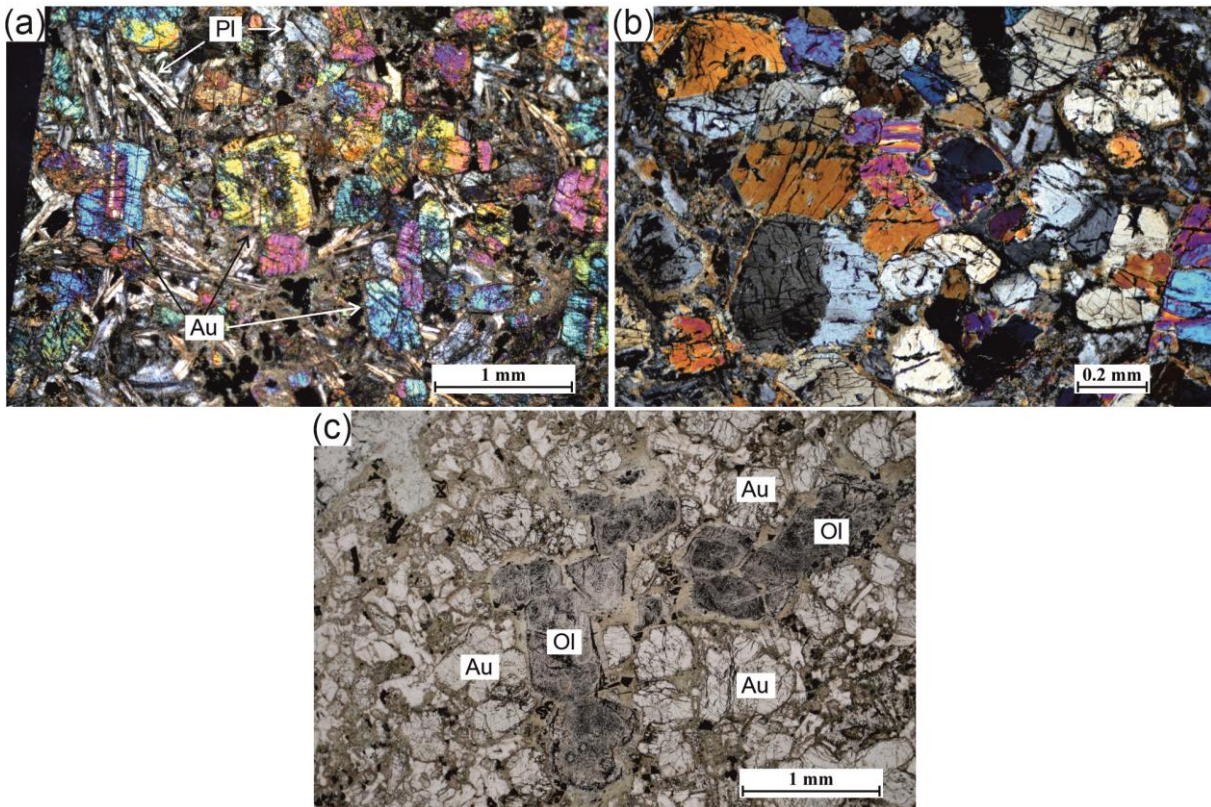


Fig 4.11 (a) Cross-polarized light image of BG-11 showing platy zoned augite dispersed in a groundmass containing needle-shaped and hollow plagioclase and opaques. (b) Cross-polarized image of AG-23 showing a cluster of euhedral to subhedral augite (some show two sets of perfect cleavage). The groundmass (not shown) consists of very fine-grained plagioclase and glass. (c) Plane-polarized image of AG-26 showing olivine phenocrysts pseudomorphed by chlorite + opaques in a groundmass of augite + chlorite. Abbreviations for all photos: Pl: plagioclase, Au: augite, Ol: olivine.

The phenocrysts in the three dykes (AG-23, AG-39, BG-11) are dominant of augite that vary in size from 0.2 mm to 0.5 mm (Fig. 4.11a-b), whereas olivine phenocrysts (now altered) is seen only in one dyke (Fig. 4.11c). Augite is euhedral-subhedral, has medium relief and possesses two sets of cleavage that intersect at 90°. It is fresh (sometimes uralitized) and occurs in clusters (Fig 4.11b). Olivine occurs as euhedral grains and has completely altered to a deuteric mixture of chlorite and opaques.

The texture in the dyke BG-11 roughly resembles cumulate consisting of pyroxene and plagioclase. The phenocrysts in this dyke comprise of augite (0.4 x 1.3 mm, up to 2.3

mm) that makeup ~54 % of the rock by volume. The augites are distinctly zoned, as recognized from the change of interference colours from the core to the rim (*Fig 4.11a*).

The groundmass of all four dykes is fine-grained, the average grain size being about 0.1 mm (up to 0.5 mm). It is composed principally of plagioclase laths, altered pyroxene (to chlorite + biotite + skeletal opaques) and equant opaques. The texture is intergranular.

#### **4.2.4 Alteration patches**

Two dykes in Baga (BG-9 and BG-35) show the occurrence of spherical to rectangular bodies of more acidic rock that are pinkish to more whitish than the host rock.

These patches dominantly consist of coarse hornblende (*Fig. 4.12a-b*) that shows pleochroism ranging from pale yellow to brown (sometimes green) with distinct two sets of cleavage intersecting at 56-124° angle, the average size of which is 0.5 mm (0.3 to 1 mm). Opaques are universal inclusions within hornblende. Next in abundance is feldspar of two varieties viz, alkali and sodic. Alkali feldspar shows characteristic clouding owing to secondary alteration, whereas sodic plagioclase has altered to sericite and epidote. This plagioclase also contains numerous crystals of apatite embedded in it. Apart from these minerals, it also consists of quartz, chlorite, serpentine and orthopyroxene, in decreasing abundance.

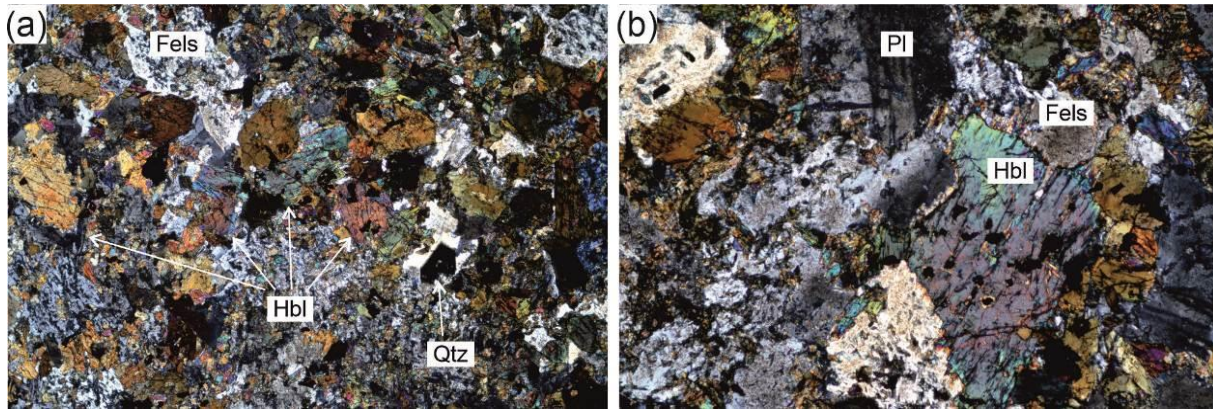


Fig 4.12 (a) Cross-polarized light image showing euhedral to subhedral hornblende, quartz forming triple junction and sericitised feldspar. (b) Subhedral hornblende with anomalous interference colours and opaque inclusions. It occurs in association with feldspar and plagioclase. Both the photos are in cross-polarized light. Abbreviations for all photos: Fels=feldspar, Hbl=hornblende, Qtz=quartz, Pl=plagioclase.

Table 4.1. Table showing modal mineralogy of the dyke rocks.

Sample	Plagioclase	Pyroxene	Olivine (Iddingsite)	Opaques	Palagonite	Glass	Groundmass (includes alteration)
AG4 Dolerite	41	20	--	5	4	9	21
AG7 Altered Basalt	--	40	--	4	--	--	56
AG9 Basalt	28	2	1	1	--	--	68
AG12 Basalt	35	53	--	4	8	--	--
AG13 Dolerite	28	62	2	4	--	--	3
AG15 Dolerite	51	37	4	5	--	--	3
AG16 Dolerite	80	18	--	2	--	--	--
AG17	45	28	15	--	--	--	2

Chapter 4 Petrography of country rocks and dykes

Dolerite							
AG19	45	35	5	5	--	--	15
Basalt							
AG21	49	29	4	2	--	6	66
Dolerite							
AG22	--	--	--	--	--	--	--
Basalt							
AG23	25	34	--	5	--	--	36
Picrite							
AG24	36	40	--	8	6	--	10
Basalt							
AG25	35	15	--	7	5	--	38
Basalt							
AG26	41	26	--	4	--	--	29
Picrite							
AG39	--	--	--	--	--	--	--
Picrite							
AG41	50	44	--	2	--	--	3
Dolerite							
AG42	33	39	--	5	3	--	20
Dolerite							
AG43	40	49	5	2	--	--	4
Basalt							
AG44	54	25	--	2	--	--	19
Basalt							
BG3	19	2	--	--	4	--	75
Basalt							
BG10	55	34	--	5	6	--	--
Basalt							
BG11	23	48	--	4	--	--	25
Picrite							
BG14	47	30	2	4	5	--	12
Basalt							

*Chapter 4 Petrography of country rocks and dykes*

BG20							
Basalt	37	46	3	6	--	--	8
BG35							
Basalt	57	40	--	3	--	--	--
BG36							
Basalt	38	36	--	4	4	--	18
BG37							
Basalt	--	--	--	--	--	--	--
VG1							
Basalt	29	34	--	4	--	--	33
VG2							
Basalt	43	40	3	5	2	--	10
VG3							
Basalt	35	40	7	5	7	--	6
AR4							
Basalt	55	35	2	3	5	--	2
AR5							
Basalt	36	47	--	3	--	--	14
AR7							
Dolerite	--	--	--	--	--	--	--
AR8							
Basalt	40	20	--	2	--	--	38
AR9							
Hyp Basalt	45	31	--	3	--	--	21
AR10							
Basalt	20	39	--	4	--	--	37
AR14							
Hyp Basalt	43	47	--	6	--	--	4

### 4.3 Discussion

The metagreywackes show sutured, fused and serrated quartz grains and chloritic matrix that point towards mild metamorphism of these rocks. Subparallel arrangement of quartz grains defines weak foliation, and the warping of the chlorite matrix around mineral and rock clasts points towards its mild deformation. The presence of idiomorphic quartz, chert and feldspar points towards volcanic source rocks. The sharp and angular clasts of quartz and plagioclase have given rise to breccia like texture, is evidence of deposition very close to provenance. The presence of biotite with pleochroic halos points towards its derivation from the granitic source rock.

The 60 dykes exposed on the coast of North Goa are divided into three rock types viz., tholeiitic basalts and dolerites, tholeiitic hypersthene dolerites and tholeiitic picrite basalts. The division envisaged is based on grain size and essential minerals. Grain size divides the rocks into basalts and dolerites whereas the mineralogy classifies them into tholeiitic basalts/dolerites, tholeiitic hypersthene dolerites and tholeiitic picrite basalts. Basalts/dolerites have plagioclase and augite as essential minerals while olivine, opaques occur as accessories. Besides plagioclase and augite, tholeiitic hypersthene dolerites contain hypersthene and olivine is absent. Tholeiitic picrite basalts have pyroxene >> plagioclase; while olivine, opaques and apatites comprise the accessories. The minerals in dykes are altered to chlorite, biotite, serpentine, sericite and opaques. Though the dyke rocks are essentially holocrystalline, some thin dykes are hemicrystalline. Some quench zones contain microlites, and acicular minerals from the well-crystallized dykes. Apart from ophitic and subophitic textures, other textures like intergranular, intersertal and glomerophytic are also common (*Fig. 4.4d, 4.4a-c, 4.5c, 4.8a-c, 4.9a, 4.10c*).

The fabric of the rock provides clues towards the crystallization process of constituent minerals, the mechanism of which is governed by, among others, cooling rate, nucleation and growth rate and settling or floating of crystals. It is usually accepted that the minerals that crystallized from the slightly undercooled magma tend to grow slowly from comparatively fewer nuclei to attain euhedral shapes. One of the typical textures is the porphyritic texture (*Fig. 4.4d, 4.5a-b*) that forms due to sudden changes in the freezing rates of the magma attributed to their rapid extrusion on the surface resulting into the contact with cooler rocks (Turner and Verhoogen, 1960).

Ophitic and subophitic textures form by simultaneous crystallization of augite and plagioclase in a static environment, where the growth rate of pyroxene exceeds its nucleation rate (Winter, 2011). Hence pyroxene grows in substantial size to include some of the plagioclases from the liquid (*Fig. 4.8a-b*) (cf. Fig. 4.11 in Gill, 2010). Simultaneous crystallization of plagioclase and pyroxene is also evident from the smaller and tapering ends of plagioclase within the pyroxene, as early enclosure prevents the growth of plagioclase that lies close to pyroxene's nucleus, while the other ends of which are outside the crystal boundary. The other type of ophitic texture is the one where the size of the enclosed plagioclase laths does not change from the rim of pyroxene towards its core. There are two possible explanations for such a texture (Gill, 2010):

- i) Augite nucleated along with the plagioclase but later engulfed plagioclase due to its growth tendency
- ii) Augite nucleated much later than most of the plagioclase in the rock but engulfed them subsequently.

The second process is possibly responsible for the tapering nature of plagioclase towards the core, whereas the latter process explains the constant size of the included

plagioclase grains. Hence, the assumption that plagioclase began to crystallize before augite is not true; instead, both crystallize together at a eutectic for most of the cooling history (Vernon, 2004). Further, as the growth of augite lags behind that of plagioclase, textures like the intergranular result.

The nucleation and growth rate of the minerals were in an imbalance in one rock type (AG16-tholeiitic basalt) where both pyroxene and plagioclase have high aspect ratios. It is possible that this disparity could arise when there is quenching of the magma leading to preferred growth in one dimension. The pyroxene crystals attain unusual lengths above 1 cm, and this could be an artefact of the procurement of the sample close to the margins.

Zoned plagioclases are not very abundant in the dykes studied. The reason behind zoning is the slow and challenging exchange of Si and Al that takes place in the tetrahedral framework of plagioclase. However, such zoned crystals are bound to be abundant in those rocks that cool rapidly. The scarcity of zoned plagioclase in the studied dykes suggests that the rates of cooling of magma were not fast enough to promote disequilibrium crystallization. Alternatively, the smaller size and homogeneity of the magma in the chamber supplying these dykes could be the reason for the non-zoning of the plagioclases (Iyer and Banerjee, 1998).

Quench zones within well-crystallized dykes could be a result of a sudden influx of water or due to magma intruding into shallow crustal fractures leading to heat loss. Sometimes these quench zones are comprised of swallow-tail plagioclase indicating that it formed during the last stage of lava solidification. The proposition that opaques are one of the first crystals in the melt may not be correct since these quench zones are full of acicular opaques which is possible only if these opaques have started crystallizing later in the series of the constituent minerals.

The alteration seen in these dykes isn't uniform. Some of the dykes have only ferromagnesian minerals like altered pyroxenes whereas other dykes have only plagioclases altered.

Plagioclase phenocrysts in a few dykes have inclusions (*Fig. 4.7a-d*). These inclusions can also be considered as liquid drops of magma (Mislankar and Iyer, 2001) and indicate that the plagioclase crystallized before/during the groundmass crystallization. Srivastava et al. (1988) suggest that there can be disequilibrium between plagioclase crystals and remaining melt due to sudden change in the physical condition of the magma, composition of magma or due to immersion of plagioclases in liquids with different composition. Dungan and Rhodes (1978) propose similar mechanisms for the formation of these melt inclusions. The melt inclusions found in cores of plagioclases were the result of entrapment during the growth of the crystal (*Fig. 4.7a-b, d*). Whereas those melt inclusions that were aligned, were trapped after an episode of corrosion of plagioclase phenocrysts. Dungan and Rhodes (1978) point towards resorption of the plagioclase that formed the interconnecting channel systems filled with melt from the surroundings.

Feldspar clouding process is commonly seen in Precambrian dykes, specifically those of early Proterozoic age (Pichamuthu, 1959; Halls and Palmer, 1990; Halls and Zhang, 1995). The explanation for feldspar clouding could be due to exsolution of Fe from primary feldspars.

Two possibilities could lead to the formation of alteration patches found in few dykes: either they are xenoliths or are altered parts of host rocks. The possibility of these features being xenoliths are rare due to the presence of gradational boundaries between these patches and the host rock. Secondly, there is no reaction texture at this boundary. Thirdly, I noted this feature in only two dykes where it is present on a minimal scale. Since

hornblende is a rare constituent of fresh and unaltered basalts, its occurrence is ascribed to deuteric alteration. Since the host rock is devoid of primary as well as secondary hornblende, such small portions in the host rock that comprises of coarse hornblende and feldspar are ascribed to late-stage processes (Moorhouse, 1959).

In the next chapter, I discuss the geochemical data of the country rocks and dykes.

## **CHAPTER 5**

# **Geochemistry of country**

# **rocks and dykes**

## 5.1 Introduction

The branch of Earth Science that uses chemical principles to understand the nature and working of the Earth System as well as of other planets is known as Geochemistry. Geochemistry deals with the mobility, transfer and substitution of chemical elements in the constituent rocks, minerals and fluids. The movement of chemical elements in rocks and minerals and their movement in soil and water systems are also studied.

There have been innumerable studies on the geochemical aspects of rocks, some of the earliest and significant ones being Harker (1909), Wager and Deer (1939), Walker and Poldervaart (1949), Macdonald and Katsura (1964). The mineralogy and chemical composition of the source region imposes excellent control over the chemistry of magmatic rocks. More importantly, the type of melting process and the degree (extent) of partial melting also constrain the major and trace element composition of a melt. The composition of the magma may also be modified *en route* to the surface (Rollinson, 1993). To resolve such chemical effects of different processes, we use a range of geochemical tools such as variation diagrams that relate the concentrations of major and trace elements combined with radiogenic and stable isotope compositions.

In igneous suites, the major elements show systematic variations in bulk rock chemistry. Hence, they play an essential role in determining the composition and classification of various rock types. The major oxides  $\text{SiO}_2$ ,  $\text{Al}_2\text{O}_3$ ,  $\text{TiO}_2$ ,  $\text{Fe}_2\text{O}_3$ ,  $\text{MgO}$ ,  $\text{FeO}$ ,  $\text{CaO}$ ,  $\text{Na}_2\text{O}$ ,  $\text{K}_2\text{O}$ , and  $\text{P}_2\text{O}_5$  are considered in the treatment of the dyke samples. The relationships between the major oxides are used to interpret the evolutionary trends of magmas, the degree of partial melting of, as well as physicochemical conditions during melting (Hanson and Langmuir, 1978; Sun et al., 1979) and the tectonic settings of the magmas (Rollinson, 1993).

A trace element is defined as an element whose concentration is less than 0.1 wt. % (or 1000 parts per million). The abundances and relative proportions of trace elements are widely used to understand genetic processes as they are sensitive to crystal fractionation, partial melting processes and source composition provided they are not a major stoichiometric component in a minor refractory phase. As trace elements tend to concentrate in fewer minerals than the major elements, they are more useful in deducing trends of magmatic differentiation, the extent of melting and in nature of the source of the magma. The trace elements have preferences to either crystal or melt or both, due to which they are subdivided into compatible and incompatible elements. In a system consisting of a silicate melt and minerals in equilibrium, those which preferentially get incorporated into the solid phases are the compatible elements, while the incompatible elements are those that have affinity to remain in the melt.

Compatible elements typically include those elements that have small ionic radii and higher charge. They show preferential partition into the solid phases that crystallize during early stages of magmatic evolution and are compatible in nature (Cox et al., 1979). LILE (large ion lithophile elements) are defined as those elements characterized by the large ionic radius to ionic charge ratio and are a subset of incompatible trace elements (Gast, 1972; White, 2013). They prefer to remain in the melt when partial melting occurs at the source. HFSE (high field strength elements) are those elements that have a high cationic charge ( $Z$ ) as compared to their small ionic radius ( $r$ ) due to which they have difficulty in achieving charge balance (Cox et al., 1979). They also prefer to remain in the melt during crystallisation. The REE (rare earth elements) are a group of elements with atomic numbers between 57 (La) and 72 (Lu) and possess large ionic radii and valences of either +2 or +3. They are subdivided into light REE (LREE, atomic numbers 57-62) and heavy REE

(HREE, atomic numbers 63-71). Y (atomic number = 39) is treated along with REE since it has an ionic radius similar to that of REE and behaves in a similar fashion (Winter, 2011).

## 5.2 Analytical techniques and Sample preparation

I took due care to collect fresh samples of all the dykes and country rocks. The specimens were chipped in the laboratory and crushed in a stainless-steel mortar and pestle to achieve the feed size of 1 mm for the ball mill. The small fragments produced were later powdered to 200 mesh size in an InSmart Systems Ball Mill with Twin Bowl holder having hardened stainless steel balls housed in the Department of Geology, Dhempe College of Arts and Science, Miramar (Fig. 5.1). In total, 36 dyke samples and six country-rock samples were crushed and powdered. The X-Ray Fluorescence (XRF) and Inductively Coupled Plasma-Mass Spectroscopy (ICP-MS) analyses of whole-rock samples are of splits from the same sample powder.



Fig 5.1 (a) InSmart systems ball mill twin bowl holder in Dhempe College of Arts and Science, Miramar (b) Closer look at the twin bowl holders with the balls and powder.

The whole-rock geochemical analysis was carried out in multiple laboratories namely Sophisticated Analytical Instrumentation Facility (SAIF) at the Indian Institute of Technology (IIT) at Bombay and at Roorkee, National Center for Polar and Oceanic Research (NCPOR) at Vasco and Drexel University, Philadelphia. For precision, accuracy

as well as consistency of the analytical values of samples, the same samples are analysed at the three labs. The samples analysed at three laboratories include AG-4, -11, -15, -16, -24, 30, -43, BG-4, -6, -10, -11, -13, -17, VG-1, -3, -24, AR-4, and -10. The samples analysed as duplicates are AG-24, -41, BG-11, -17, AR-7 and -10. The pressed pellets of samples are analysed at NCPOR and SAIF IIT Roorkee using X-ray Fluorescence methods for major element oxides.



Fig 5.2 (a) and (b) Sample powders kept in paper and glass trays and heated up to 100 degree Celsius in the oven for 1 hour to drive off volatiles. (c) InSmart systems hydraulic pellet maker (d) Aluminium cup (e) Borax powder (f) Prepared pellets are kept in glass boxes to avoid their breakage and contamination.

### 5.2.1 X-Ray Fluorescence

I analysed the majority of the dyke samples and the country rocks at NCPOR. I sorted out the samples, and selected sample powders were kept in paper trays in an oven at 100 °C for 1 hour to make them volatile free (Fig. 5.2a-b). Later, collapsible aluminium

cups were first rinsed in water and then cleansed with methanol. This cup was filled with Borax, Hi LR<sup>TM</sup> (di-Sodium Tetraborate decahydrate) up to the rim (*Fig. 5.2d and e*). About 1 g of the sample powder was evenly spread with the help of the flat end of a spatula. The sample was then compressed in an InSmart hydraulic pellet press at 20-ton pressure (*Fig. 5.2c*) to obtain pellets of 40 mm diameter. I preserved the prepared pellets in glass boxes (*Fig. 5.2f*). These pellets were analysed in Axios<sup>mAX</sup> PANalytical wavelength dispersive XRF spectrometer housed in NCPOR. The instrument measures complete major elemental oxide range, and total iron was measured as Fe<sub>2</sub>O<sub>3</sub>. International rock reference standards from the United States Geological Survey, namely BHVO1 and BCR2, were analysed in the same instrument to check the analytical precision.

Few samples were analysed in SAIF at IIT Bombay using PHILLIPS (now PANalytical, The Spectris Technology, The Netherlands) model PW 2404 that has an X-Ray tube with Rh target. The sample preparation method used here is similar to the one used at NCPOR for the preparation of pellets. Also, I analysed another set of samples at SAIF at IIT, Roorkee using the instrument Bruker S4 Pioneer (XRF). Here the powdered form of samples was converted to pressed pellets that were analysed in the instrument.

All the certified standards were measured in the instrument to check for accuracy and precision. (Table 6.1)

**Table 5.1.** Major element compositions obtained from XRF for USGS standard rocks.

Sample no.	BHVO1		DNC1		BHVO1		BIR1		BHVO1		BIR1		JSd-1	
	A	B	A	B	A	B	A	B	A	B	A	B	A	B
Laboratory (in wt.%)	NCPOR				IITR				IITB				NCPOR	
SiO <sub>2</sub>	48.61	49.94	47.54	47.15	46.82	49.94	47.96	48.93	48.20	49.94	47.90	48.93	66.284	66.42
TiO <sub>2</sub>	2.69	2.71	0.48	0.48	0.75	2.71	0.96	2.01	2.01	2.71	1.56	2.01	0.672	0.65
Al <sub>2</sub> O <sub>3</sub>	13.67	13.80	18.19	18.34	16.18	13.80	15.50	13.76	14.10	13.80	13.00	13.76	15.21	14.66
Fe <sub>2</sub> O <sub>3</sub>	12.03	12.23	10.02	9.97	10.58	12.23	11.30	12.02	11.25	12.23	12.96	12.02	5.145	5.11
MnO	0.17	0.17	0.15	0.15	0.06	0.17	0.18	0.06	0.09	0.17	0.20	0.06	0.101	0.093
MgO	7.14	7.23	10.14	10.13	8.08	7.23	9.70	6.74	7.95	7.23	7.01	6.74	1.892	1.85
CaO	11.06	11.40	11.45	11.49	13.45	11.40	13.30	11.68	12.00	11.40	12.25	11.68	3.124	3.07
Na <sub>2</sub> O	2.26	2.26	1.87	1.89	2.14	2.26	1.82	2.21	2.20	2.26	1.90	2.21	2.965	2.73
K <sub>2</sub> O	0.50	0.52	0.22	0.23	0.56	0.52	0.03	0.76	0.56	0.52	0.50	0.76	2.253	2.19
P <sub>2</sub> O <sub>5</sub>	0.27	0.27	0.07	0.07	0.14	0.27	0.02	0.18	0.25	0.27	0.09	0.18	0.124	0.12
Total	98.40	100.53	100.11	99.90	98.76	100.53	100.77	98.35	98.61	100.53	97.37	98.35	97.77	96.89

A: present study values; B: reported values from Govindaraju (1994)

NCPOR = National Center for Polar and Oceanic Research

IITR = Indian Institute of Technology, Roorkee

IITB = Indian Institute of Technology, Bombay

### 5.2.2 Inductively Coupled Plasma-Mass Spectroscopy (ICP-MS)

At SAIF IIT Bombay facility, sample preparation method involved weighing of 0.05 g of sample, and 3ml HNO<sub>3</sub> + 3mL H.F. was added in Teflon bombs and placed in a microwave digester. Step heating technique was used.

	Ramp	Temperature	Hold
Step 1	15 min	100°	30mins
Step 2	10 min	180°	30mins

Once the process of digestion was completed, it was allowed to cool at room temperature, and the contents were reheated on a hot plate at 75°C until dry. During the drying process, 3 ml of HNO<sub>3</sub> was added twice. The total volume was finally made into 25 ml with double distilled water. The blank solutions were prepared in the same way. The USGS certified standards used were BHVO1 and W2. The trace and REE were measured using the instrument Thermo Fisher Scientific Element XR, Germany, with double focussing Magnetic Sector (High Resolution) Inductively Coupled Plasma Mass Spectrometer System that has a quantification limit better than one ppt (parts per thousand).

The sample preparation procedure in Drexel University was according to the one given in Pyle et al. (1995). A quantity of ~70 mg of whole-rock powder was dissolved in tightly capped, 15-mL Savillex Teflon beakers with 800 µL of a (1:3) H.F.: HNO<sub>3</sub> acid mixture heated at 80°C overnight to prepare sample solutions. The beakers were uncapped upon dissolution, and the samples were dried on a hot plate to drive off H.F. Once this step was completed, the powders were again dissolved in 6 N HCl and redried. This cycle was repeated twice using 4 N HNO<sub>3</sub> to break down fluorosilicate precipitates. In the last step, the dried powder was dissolved in 10 mL of 2N HNO<sub>3</sub>, which was further diluted to 1:5 in 1% HNO<sub>3</sub> that was introduced into the ICP-MS instrument. The instrument drift was

monitored and corrected with multiple internal standard solutions of Be, In, and Bi added to each sample to attain a run concentration of 20 ppb for each element. Unknown element concentrations were determined using regression curves based on dissolved rock standards from the U.S. Geological Survey (BHVO-2; recommended values from Wilson, 1997) processed along with the samples. The samples were run on an Agilent 8800 (California, U. S. A.) triple-quadrupole ICP-MS.

I prepared the greywacke sample solutions at NCPOR. I mixed a quantity of ~50 mg of sample powder in 7:3:1 mixture of H.F.: HNO<sub>3</sub>: HCl in tightly capped Savillex Teflon beakers. Blank solution was prepared in this way. The beakers were kept on a hot plate for closed digestion for 24 hours at 120°C. Later, the bottles were uncapped and kept for further drying. Some samples required double digestion. After the sample had dried, the powder was dissolved in aquaregia (3:1 solution of HNO<sub>3</sub>: HCl), and I subjected them to further drying. In the end, I topped the beakers with 5N HNO<sub>3</sub> for its introduction into the ICPMS instrument. Along with the samples, I prepared International rock standards BIR1 and JSD-3 in the same way. I considered those analytical values for which the results were better than 10%.

Table 5.2 gives the entire dataset of standards analysed in the ICP-MS instruments of various laboratories.

Chapter 5 Geochemistry of country rocks and dykes

**Table 5.2** Trace and REE compositions for certified reference standards obtained from ICP-MS

Sample no.	BHVO2		BHVO1		W2		BIR1		JSd-3	
	A	B	A	B	A	B	A	B	A	B
Laboratory (in ppm)	Drexel University		IITB		IITB		NCPOR			
Sc	34.1	32	--	--	--	--	--	--	--	--
Cr	284	280	276	NA	91.6	91.51	488	382	34	35
Co	47.7	45	--	--	--	--	--	--	--	--
Ni	127	119	121	NA	70.4	70	177	166	19.6	19.6
Cs	0.13	NA	--	--	--	--	--	--	--	--
Rb	9.57	9.8	13.8	11	21	20.9	0.23	0.25	259	285
Sr	381	389	381	403	192	192	111.4	108	60.3	60
Ba	129	130	124	139	170	173.6	6.3	7	448	NA
Pb	2.38	NA	--	--	--	--	2.51	3	NA	NA
Nb	19.8	18	17.4	19	7.9	6.75	1.16	0.6	7.4	NA
Ta	2.58	1.4	0.97	1.2	0.5	0.52	--	--	--	--
Zr	168	172	166	179	90.6	100	12.8	13.3	60.8	129
Hf	4.05	4.1	4.91	4.4	2.6	2.6	--	--	--	--
Th	1.02	1.2	1.76	1.1	2.4	2.41	0.12	0.03	6.53	NA
U	NA	NA	--	--	--	--	0.01	0.01	1.36	NA
Y	25.4	26	26.9	28	23	23	--	--	--	--
La	15.2	15	14.5	16	10	10.36	0.63	0.62	19.7	20.1
Ce	38.3	38	37.8	39	23	23.37	1.94	1.95	40.2	41.4
Pr	18.5	NA	--	--	--	--	--	--	--	--
Nd	25.2	25	25.9	25	13	13.36	2.45	2.5	16.7	16.5
Sm	6.26	6.2	4.76	6.2	3.3	3.31	1.17	1.1	3.45	3.71
Eu	NA	NA	1.77	2.06	1	1.12	0.51	0.54	0.73	0.7
Gd	6.12	6.3	6.4	6.4	NA	3.9	--	--	--	--
Tb	0.84	0.9	--	--	--	--	--	--	--	--
Dy	5.02	NA	4.94	5.2	3.6	3.6	2.72	2.5	2.53	2.2
Ho	1	1.04	1	0.99	0.76	0.68	0.55	0.57	0.46	0.5
Er	2.3	NA	--	--	--	--	--	--	--	--
Tm	0.3	NA	0.27	0.33	0.38	0.38	--	--	--	--
Yb	1.98	2	2.09	2	2.1	2.14	1.72	1.65	1.47	1.21
Lu	0.25	0.28	0.27	0.29	0.33	0.33	0.28	0.26	0.25	0.2
Cu	136	127	--	--	--	--	--	--	--	--
Zn	106	103	--	--	--	--	--	--	--	--

NCPOR = National Center for Polar and Oceanic Research; IITR = Indian Institute of Technology, Roorkee; IITB = Indian Institute of Technology, Bombay  
A: present study values; B: reported values from Govindaraju (1994) for BHVO1, W2, BIR1 and JSd-3; from Wilson (1997) for BHVO2; dashes: Not Analysed

### 5.3 Geochemistry of country rocks:

#### 5.3.1 Major elements

I have sampled metagreywackes representative of the country rocks from Aguada, Baga and Vagator area and analyzed them for their major elemental oxides. This data is provided in Table 5.3. On the whole, all the analysis show limited variation in chemistry. This group of rocks have SiO<sub>2</sub> amount varying from 56 to 71.7 with an average of 64.8 wt. %; TiO<sub>2</sub> (0.43 to 0.7; avg. 0.55 wt. %); Al<sub>2</sub>O<sub>3</sub> (12.5 to 15; avg. 13.7 wt. %); Fe<sub>2</sub>O<sub>3</sub> (95.48 to 11.62; avg. 7.53 wt. %); MnO (0.05 to 0.17; avg. 0.1 wt. %); MgO (1.8 to 5.6; 3.2 wt. %), CaO (0.65 to 2.08; avg/ 1.3 wt. %), Na<sub>2</sub>O (1.6 to 4.5; avg. 3.24 wt. %); K<sub>2</sub>O (1.9 to 3.1; avg. 2.4 wt. %) and P<sub>2</sub>O<sub>5</sub> (0.1 to 0.15; avg. 0.12 wt. %).

Table 5.4 provides some major elemental oxide ratios. Among the ratios calculated, K<sub>2</sub>O/Na<sub>2</sub>O (0.5 to 1.9; avg. 0.9), SiO<sub>2</sub>/Al<sub>2</sub>O<sub>3</sub> (3.7 to 5.5; avg. 4.7), Al<sub>2</sub>O<sub>3</sub>/Na<sub>2</sub>O (3 to 9.1; avg. 4.8) and K<sub>2</sub>O/Al<sub>2</sub>O<sub>3</sub> (0.1 to 0.2; avg. 0.17).

The metagreywackes, in general, are sodic (Na<sub>2</sub>O/K<sub>2</sub>O > 1) in composition. The composition of these metagreywackes suggests that there is minimal postdepositional metasomatism, as shown by the negative correlation between MgO and Na<sub>2</sub>O and the low values of Mg/K and Na/K (< 2.7). Under metasomatic conditions, a large scatter is produced in Mg and Na distribution, resulting in low order or no correlation. Low values (< 4) of Mg/K and Na/K in the greywackes are characteristic of un-metasomatised rocks (Legault and Hattori, 1994). The K/Rb ratios of these metagreywackes are consistent with the K/Rb ratio of Tonalites (221-225) and basaltic rocks (196) of the western Dharwar craton (Jayaram et al., 1983; Rama Rao et al., 1991). These features are suggestive of minimal K-metasomatism of the metagreywackes under study.

I have used the weight percentages of the oxides to classify the greywackes using several classification schemes (Pettijohn et al., 1973; Marston, 1978; Bhatia and Crook, 1986). They have been compared with greywacke/metagreywacke occurrences from other areas [Archean greywackes of Fig Tree, Barberton, South Africa (Toukeridis et al., 1999), Late Archean (3.5-2.5 Ga) greywacke (Condie, 1993), greywacke with biotite, greywacke with chlorite-sericite and fine-grained greywacke of the Goa-Dharwar sector (GDS) (Devaraju et al., 2010) and argillite, metagreywacke, metagreywacke with biotite from Ribandar quarry, Goa (Fernandes et al., 2016)]. The comparative values are given in Table 5.4 and discussed in Section 6.1.

The plot of  $K_2O/Na_2O$  vs  $SiO_2/Al_2O_3$  (after Wimmenauer, 1984) (*Fig. 5.3a*) is of the samples studied. I observed that except one sample that falls in the field of "pelitic greywacke", all other samples distinctly fall in "greywacke" field. All other comparative values also plot in the "greywacke" field except metagreywacke with biotite (Fernandes et al., 2016) that falls in the "pelitic greywacke" field. A plot of log values of  $Na_2O/K_2O$  vs log values of  $SiO_2/Al_2O_3$  (Pettijohn et al., 1973) (*Fig. 5.3b*), clearly classifies all the rocks into the "greywackes" field except for one sample in the "litharenite" field. Most of the comparative values fall in the "greywackes" field, except for metagreywacke with biotite (Fernandes et al., 2016) and Greywacke with biotite of GDS (Devaraju et al., 2010) which fall in the "litharenite" field. *Fig. 5.3* shows the binary plot of  $\log(SiO_2/Al_2O_3)$  vs  $\log(Fe_2O_3/K_2O)$  by Pettijohn et al. (1973) modified by Herron (1988). On this plot, four samples under study fall in "wacke" field whereas two samples fall in the "shale" field. Most of the comparative values fall in "wacke" field except metagreywacke with biotite (Fernandes et al., 2016), Late Archean greywacke (Condie, 1993) and Fine-grained greywacke of GDS (Devaraju et al., 2010) which fall in the "shale" field. Hence from all the plots, it is evident that the rocks under study are distinctly greywackes. I used the Total

Alkali-Silica diagram (*Fig. 5.4*) to assess their chemical comparisons with the igneous rocks. It makes direct use of major element oxides  $\text{Na}_2\text{O}$ ,  $\text{K}_2\text{O}$  and  $\text{SiO}_2$  where the diagram is a total alkali ( $\text{Na}_2\text{O} + \text{K}_2\text{O}$ ) vs silica ( $\text{SiO}_2$ ) (TAS) (after Le Bas et al., 1986; Le Maitre et al., 1989, 2002). I observe here that the majority of the metagreywackes plot in the dacite field whereas one sample each plotted in the andesite field and the basaltic andesite field respectively.

**Table 5.3** Representative major (in wt. %) and trace element (in ppm) data for country-rock greywackes.

Sample no.	AG11	AG30	BG17	BG18	BG19	VCR1	VCR5
SiO <sub>2</sub>	66.83	56.01	71.72	66.59	59.4	68.07	64.97
TiO <sub>2</sub>	0.55	0.66	0.43	0.54	0.7	0.49	0.50
Al <sub>2</sub> O <sub>3</sub>	13.52	15.01	13.03	13.67	14.55	14.09	12.49
Fe <sub>2</sub> O <sub>3</sub>	7.7	11.62	5.48	6.55	9.16	5.73	6.44
MnO	0.17	0.07	0.09	0.11	0.13	0.06	0.05
MgO	1.8	5.6	2.8	2.97	3.85	2.34	2.79
CaO	0.65	1.13	1.26	2.08	1.59	1.21	1.22
Na <sub>2</sub> O	4.48	2.41	3.63	2.64	1.6	4.12	3.82
K <sub>2</sub> O	2.21	2.8	2.22	2.42	3.14	1.98	1.97
P <sub>2</sub> O <sub>5</sub>	0.1	0.15	0.1	0.12	0.14	0.1	0.12
Total	98.01	95.46	100.76	97.69	94.26	98.19	94.37
Cr	394.16	289.94	752.44	621.98	NA	549.34	NA
Ni	91.7	83.45	61.92	60.18	NA	51.68	NA
Rb	76.59	81.88	76.37	103.32	NA	75.96	NA
Sr	108.29	94	123.33	124.29	NA	204.54	NA
Ba	357.86	562.97	479.75	377.39	NA	338.86	NA
Nb	9.84	10.35	8.21	9.48	NA	11.91	NA
Zr	150.69	163.12	129.29	156.57	NA	162.43	NA
Th	10.8	18.44	11.6	12.14	NA	11.47	NA
U	3.46	4.73	3.29	3.84	NA	3.36	NA
La	21.4	23.3	37.25	31.32	NA	35.85	NA
Ce	42.97	47.38	72.2	65.51	NA	75.43	NA
Pb	6.26	8.94	9.66	15.9	NA	9.91	NA
Nd	18.1	21.72	25.87	24.55	NA	28.14	NA
Sm	3.39	4.47	4.89	4.73	NA	5.79	NA
Eu	0.76	0.89	1.11	0.99	NA	1.17	NA
Dy	2.55	3.74	3.54	3.28	NA	4.35	NA
Ho	0.48	0.68	0.61	0.57	NA	0.79	NA
Yb	1.82	2.09	2.02	2.08	NA	2.39	NA
Lu	0.28	0.32	0.29	0.34	NA	0.37	NA

Note: N.A. means Not Analysed

**Table 5.4** Average major oxides (in wt. %) of the metagreywackes under study as compared with other examples. Numbers in the brackets denote the number of samples, NA: Not Available

Elements	Metagreywacke under study (avg. of 7)	Greywacke from Merces, Goa (Widdowson, 2009) (avg. of 1)	Greywacke with biotite of Goa-Dharwar sector (GDS) (Devaraju et al., 2010) (avg. of 6)	Greywacke with chlorite- sericite of GDS (Devaraju et al., 2010) (avg. of 13)	Fine-grained greywacke of GDS (Devaraju et al., 2010) (avg. of 8)	Late Archaean (3.5-2.5 Ga) greywacke (Condie, 1993) (avg. of 1)	Archaean greywacke of Fig Tree, Barberton (South Africa) (Toulkeridis et al., 1999) (avg. of 12)	Argillite from Ribandar quarry, Goa (Fernandes et al., 2016) (avg. of 14)	Metagreywacke from Ribandar quarry, Goa (Fernandes et al., 2016) (avg. of 5)	Metagreywacke with biotite from Ribandar quarry, Goa (Fernandes et al., 2016) (avg. of 1)
SiO <sub>2</sub>	<b>64.8</b>	67.77	67.31	63.03	63.13	65.00	63.41	66.67	69.31	49.06
TiO <sub>2</sub>	<b>0.55</b>	0.56	0.79	0.59	0.61	0.61	0.54	0.63	0.5	3.03
Al <sub>2</sub> O <sub>3</sub>	<b>13.77</b>	14.65	12.13	14.16	15.18	15.2	11.85	15.7	13.71	12.9
Fe <sub>2</sub> O <sub>3</sub>	<b>7.53</b>	6.08	7.67	7.06	7.19	5.9	8.15	5.33	5.32	11.23
MnO	<b>0.1</b>	0.13	0.08	2.93	3.27	NA	0.18	0.06	0.08	0.56
MgO	<b>3.16</b>	3.07	3.9	0.11	0.11	3.30	6.16	3.52	2.54	5.29
CaO	<b>1.3</b>	0.95	1.37	2.83	2.22	2.6	2.48	1.11	0.92	11.86
Na <sub>2</sub> O	<b>3.24</b>	3.31	2.1	3.51	2.65	3.1	1.68	3.39	3.24	1.11
K <sub>2</sub> O	<b>2.39</b>	3.68	3.3	1.92	3.17	2.1	1.85	2.49	2.82	4.62
P <sub>2</sub> O <sub>5</sub>	<b>0.12</b>	0.12	0.11	0.14	0.16	0.14	0.09	0.11	0.09	0.35
K <sub>2</sub> O/Na <sub>2</sub> O	<b>0.88</b>	1.11	1.57	0.55	1.2	0.68	1.1	0.73	0.87	4.16
SiO <sub>2</sub> /Al <sub>2</sub> O <sub>3</sub>	<b>4.74</b>	4.63	5.55	4.45	4.16	4.33	5.35	4.24	5.05	3.8
Na <sub>2</sub> O/Al <sub>2</sub> O <sub>3</sub>	<b>0.24</b>	0.23	0.17	0.25	0.17	0.2	0.14	0.22	0.24	0.09
K <sub>2</sub> O/Al <sub>2</sub> O <sub>3</sub>	<b>0.17</b>	0.25	0.27	0.14	0.21	0.14	0.16	0.16	0.21	0.36

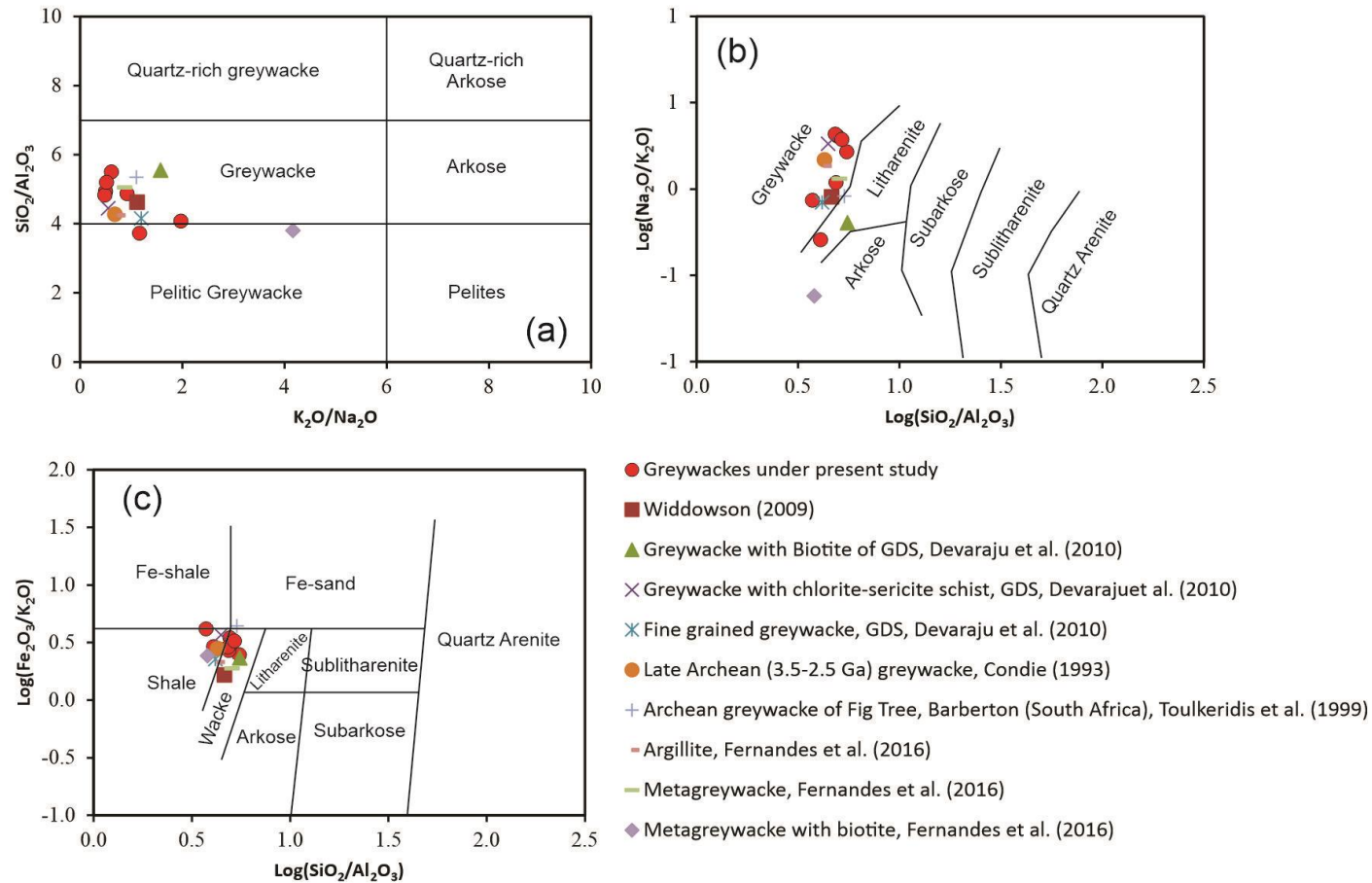


Fig. 5.3 (a) Binary plot of  $K_2O/Na_2O$  vs  $SiO_2/Al_2O_3$  (after Wimmenauer, 1984) showing all samples under study falling in the "greywacke" field except one falling in the "pelitic greywacke" field. (b) The binary plot of  $\text{Log}(SiO_2/Al_2O_3)$  vs  $\text{Log}(Na_2O/K_2O)$  (after Pettijohn et al., 1972) further confirms that all samples under study fall in the "greywacke" field except one falling in the "litharenite" field. (c) The binary plot of  $\text{Log}(SiO_2/Al_2O_3)$  vs  $\text{Log}(Fe_2O_3/K_2O)$  (after Pettijohn et al., 1972) shows that four samples plot in the "wacke" field while two samples plot in the "shale" field. The legend is given separately and is the same for all figures.

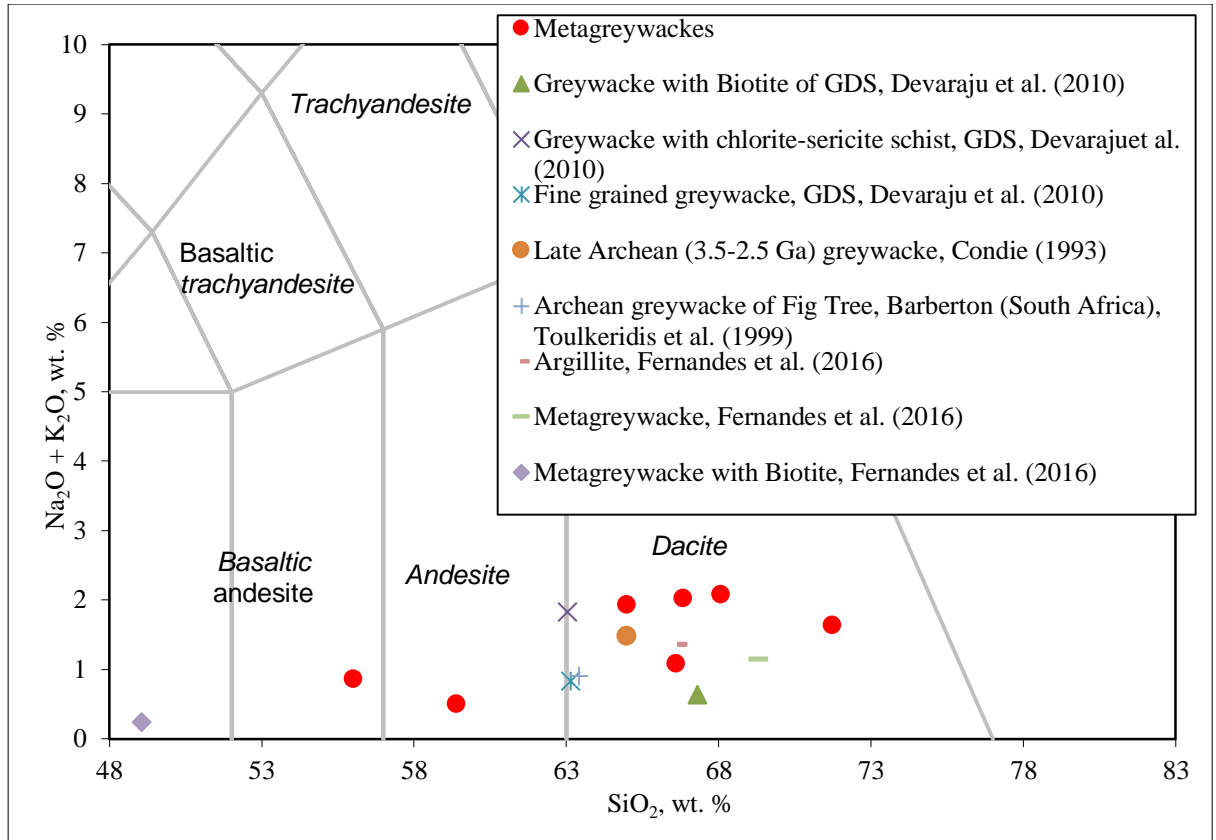


Fig. 5.4 Total Alkali-Silica (TAS) diagram after Le Maitre et al., (1989) showing metagreywacke samples in red filled circles. Other examples are also plotted.

### 5.3.2 Trace elements:

The trace elemental abundances of the greywackes (Table 5.3) are characterised by Cr that varies from 290-752 with an average of 522 ppm; Ni: 51.7-91.7 ppm, avg. 69.8 ppm; Rb: 75.7-103.3 ppm, avg. 82.8 ppm; Sr: 94-204 ppm, 131 ppm; Ba: 339-563 ppm, avg. 424 ppm; Nb: 8.2-11.9 ppm, avg. 9.9 ppm; Zr: 129-163 ppm, avg. 152 ppm; Th: 10.8-18.4 ppm, avg. 12.9 ppm; U: 3.3-4.7 ppm, avg. 3.7 ppm; La: 21.4-37.2 ppm, avg. 29.8 ppm; Ce: 42.9-75.4 ppm, avg. 60.7 ppm; Pb: 6.3-15.9 ppm, 10.1 ppm; Nd: 18.1-28.1 ppm, avg. 23.7 ppm; Sm: 3.4-5.8 ppm, avg. 4.6 ppm; Eu: 0.8-1.2 ppm, avg. 0.99 ppm; Dy: 2.5-4.3 ppm, avg. 3.5 ppm; Ho: 0.48-0.79 ppm, avg. 0.62 ppm; Yb: 1.8-2.39 ppm, avg. 2.08 ppm; and Lu: 0.28-0.37 ppm, avg. 0.32 ppm.

I have compared the trace element concentrations of the samples under study with greywackes from other areas. Table 5.5 gives the comparative values, and I discuss those in section 6.1.

**Table 5.5** Average trace element concentrations (in ppm) and ratios of the metagreywackes under study as compared with other examples. Numbers in the brackets denote the number of samples, NA: Not Available

Elements/Ratios	Metagreywacke under study (avg. of 5)	Greywacke from Merces, Goa (Widdowson, 2009) (avg. of 1)	Greywacke with biotite of Goa-Dharwar sector (GDS) (Devaraju et al., 2010) (avg. of 6)	Greywacke with chlorite- sericite of GDS (Devaraju et al., 2010) (avg. of 13)	Fine-grained greywacke of GDS (Devaraju et al., 2010) (avg. of 8)	Late Archaean (3.5-2.5 Ga) greywacke (Condie, 1993) (avg. of 1)	Archaean greywacke of Fig Tree, Barberton (South Africa) (Toulkeridis et al., 1999) (avg. of 12)	Argillite from Ribandar quarry, Goa (Fernandes et al., 2016) (avg. of 14)	Metagreywacke from Ribandar quarry, Goa (Fernandes et al., 2016) (avg. of 5)
Cr	<b>522</b>	108	152	108	108	175	539	123	77
Ni	<b>70</b>	33	58	52	54	75	336	43.9	35
Rb	<b>83</b>	118	106	80	161	70	94	136	128
Sr	<b>131</b>	114	90	292	390	265	77	112	141
Ba	<b>423</b>	721	356	419	713	390	291	458	644
Nb	<b>10</b>	13	9	9	14	11	7	17.9	21.1
Zr	<b>152</b>	191	166	215	271	160	111	150	105
Th	<b>13</b>	16	8	10	13	8	5	8.9	7.9
U	<b>3.74</b>	6	2	3	5	2	1	4.1	3.7
La	<b>29.8</b>	NA	25.7	30.9	35.1	26	16.2	33.7	28.3
Ce	<b>60.7</b>	NA	57.9	72.1	85.2	52	31.8	72	56
Pb	<b>10</b>	12	7	12	14	20	15	4.27	3.23
Nd	<b>23.7</b>	NA	20.1	24.7	23.7	22	14.1	30.3	24.6
Sm	<b>4.6</b>	NA	3.7	4.6	3.1	3.9	2.9	4.8	3.8
Eu	<b>0.98</b>	NA	1.02	1.28	0.69	1.1	0.68	0.94	0.94
Dy	<b>3.49</b>	NA	4.32	3.4	4.27	NA	2.85	3.63	3.02
Ho	<b>0.62</b>	NA	0.76	0.65	0.49	NA	0.61	0.75	0.65
Yb	<b>2.1</b>	NA	2.2	1.71	1.33	1.4	1.67	2.11	2.17
Lu	<b>0.32</b>	NA	0.3	0.24	0.19	0.25	0.26	0.36	0.34
Rb/Sr	<b>0.63</b>	1.03	1.18	0.27	0.41	0.26	1.22	1.22	0.91
Ba/Rb	<b>5.11</b>	6.11	3.36	5.24	4.43	5.57	3.10	3.36	5.01
Ba/Sr	<b>3.23</b>	6.32	3.96	1.43	1.83	1.47	3.78	4.09	4.58
Th/U	<b>3.44</b>	2.67	4.00	3.33	2.6	4	5	2.17	2.14
Zr/Nb	<b>15.3</b>	14.69	18.44	23.89	19.36	14.55	15.86	8.36	4.97
La <sub>N</sub> /Yb <sub>N</sub>	<b>10.2</b>	NA	8.38	12.96	18.93	13.32	6.96	11.46	9.35
La <sub>N</sub> /Sm <sub>N</sub>	<b>4.13</b>	NA	4.48	4.34	7.31	4.30	3.61	4.53	4.81

## 5.4 Geochemistry of dykes

### 5.4.1 Major elements

The major element oxide data of all the dykes were processed using “IgRoCs” computer programme (Verma et al., 2003; Verma and Rivera-Gomez, 2013) where I calibrated the data to 100% LOI-free basis (Loss On Ignition). This recalculated data is used for Harker and other plots. In addition to the standard CIPW Norm (Cross et al., 1902), this programme also computes the Mg number ( $Mg\# = (100 * Mg^{2+}) / (Mg^{2+} + Fe^{2+})$ ), Differentiation Index ( $D.I. = q + or + ab + ne + lc$ ) (Thornton and Tuttle, 1960), Crystallization Index [ $C.I. = an + 2.1570577(di-Mg) + fo + 0.7007616(hy-Fe)$ ] (Poldervaart and Parker, 1964), Solidification Index ( $S.I. = 100MgO / (MgO + FeO + Fe_2O_3 + Na_2O + K_2O)$ ) (Kuno, 1959; Hutchison, 1974), Alkalinity Ratio ( $A.R. = (Al_2O_3 + CaO + Na_2O + K_2O) / (Al_2O_3 + CaO - Na_2O - K_2O)$ ) (Wright, 1969) and provides a rock name consistent with the IUGS Sub-commission on the Systematics of Igneous Rocks and the Total Alkali-Silica diagram (Le Maitre et al., 1984; Le Bas et al., 1986). Since the total iron was determined as  $Fe_2O_3^T$ , the option of Middlemost (1989) was used, offered by the IgRoCs programme (Verma and Rivera-Gómez, 2013) to divide the total iron into  $Fe^{+2}$  and  $Fe^{+3}$ . The programme also calculates  $FeO^T/MgO [(2 * 71.8444 / 159.6882) * Fe_2O_3 + FeO] / MgO$ . All these data are presented in Table No 5.6 and 5.7.

Chapter 5 Geochemistry of country rocks and dykes

**Table 5.6** Representative major element oxide (in wt.%) and CIPW data of the Group 1 dykes in Goa

Sample no.	AG23	AG39	AG41	BG4	BG9	BG11	BG35	BG37	AR5	AR7	AR9
Rock Type	Basaltic Andesite	Basaltic Andesite	Basaltic Andesite	Basaltic Andesite	Subalkali Basalt	Picrite	Basaltic Andesite	Basaltic Andesite	Subalkali Basalt	Subalkali Basalt	Subalkali Basalt
SiO <sub>2</sub>	50.72	51.53	51.44	52.81	48.32	50.47	52.75	53.827	49.68	48.01	50.07
TiO <sub>2</sub>	1.22	1.22	1.23	1.7	1.91	0.74	1.47	1.47	0.52	0.86	0.7
Al <sub>2</sub> O <sub>3</sub>	10.68	10.11	10.76	13.32	17.72	9.36	12.50	12.93	12.84	14.59	12.29
Fe <sub>2</sub> O <sub>3</sub> <sup>T</sup>	12.89	13.20	13.06	15.49	14.97	12.85	16.31	15.22	11.61	11.28	12.36
MnO	0.2	0.21	0.19	0.20	0.20	0.19	0.08	0.08	0.19	0.15	0.22
MgO	10.36	12.39	11.13	3.67	3.20	15.48	3.80	3.42	10.35	9.45	10.26
CaO	7.43	7.95	7.94	7.31	7.86	9.24	7.38	7.51	9.89	8.95	9.57
Na <sub>2</sub> O	2.33	2.26	2.45	3.21	3.24	1.54	2.96	3.15	1.88	2.70	1.79
K <sub>2</sub> O	1.02	1.08	0.94	1.34	1.53	0.54	1.36	1.47	0.46	0.54	0.89
P <sub>2</sub> O <sub>5</sub>	0.14	0.11	0.13	0.18	0.16	0.08	0.16	0.19	0.10	0.09	0.13
Total	96.99	100.06	99.27	99.23	99.11	100.49	98.77	99.27	97.52	96.62	98.28
FeO <sup>T</sup>	9.52	9.45	9.41	10.87	11.67	9.86	11.85	11	9.17	8.99	9.69
<i>CIPW Norm (IgRoCS, Verma &amp; Rivera-Gomez, 2013)</i>											
Quartz	0.83	0	0	6.47	0	0	6.19	6.72	0	0	0
Plagioclase	36.88	33.73	36.97	44.87	57.96	30.24	42.93	44.31	42.62	51.16	39.10
Orthoclase	6.27	6.42	5.65	8.03	9.24	3.21	8.24	8.85	2.82	3.34	5.41
Diopside	17.11	19.93	18.89	14.71	7.50	22.91	16.21	16.55	19.49	15.05	19.87
Hypersthene	32.01	28.84	30.06	17.77	8.41	28.35	18.03	15.50	28.79	12.11	28.70
Olivine	0.00	4.39	1.65	0.00	9.42	10.83	0.00	0.00	2.36	13.81	2.43
Ilmenite	2.41	2.33	2.38	2.94	3.71	1.41	2.86	2.85	1.02	1.71	1.37
Magnetite	4.14	4.11	4.10	4.78	3.38	2.86	5.16	4.78	2.66	2.61	2.81
Apatite	0.33	0.25	0.31	0.43	0.38	0.19	0.38	0.45	0.24	0.22	0.31
Mg#	67	70	68	41	33	74	37	36	67	66	66
D.I.	27.66	25.73	26.75	40.69	37.26	16.32	40.12	42.75	19.29	27.21	20.98
C.I.	57.02	62.83	60.19	36.77	40.58	75.39	36.01	35.27	68.93	63.02	66.02
S.I.	40.50	44.42	41.92	17.55	14.77	52.80	16.42	15.53	44.39	41.06	42.30
CaO/Al <sub>2</sub> O <sub>3</sub>	0.69	0.78	0.73	0.54	0.44	0.98	0.59	0.58	0.77	0.61	0.77
FeO <sup>T</sup> /MgO	1.12	0.959	1.06	3.48	4.21	0.747	3.86	3.99	1.01	1.07	1.08

Chapter 5 Geochemistry of country rocks and dykes

**Table 5.7** Representative major element oxide (in wt.%) and CIPW data of the Group 2 dykes in Goa

Sample no.	AG4	AG9	AG13	AG15	AG16	AG17	AG19	AG24	AG43	BG2	BG6
Rock Type	Basaltic Andesite	Subalkali Basalt	Subalkali Basalt	Subalkali Basalt	Basaltic Andesite	Subalkali Basalt					
SiO <sub>2</sub>	51.04	45.11	45.84	49.82	51.25	45.18	48.82	49.77	49.85	50.14	49.8
TiO <sub>2</sub>	2.21	1.51	1.75	2.17	1.07	2.04	3.05	2.07	2.08	1.32	2.36
Al <sub>2</sub> O <sub>3</sub>	12.01	20.06	18.11	13.50	12.68	17.93	13.39	13.44	12.81	12.26	13.01
Fe <sub>2</sub> O <sub>3</sub> <sup>T</sup>	14.22	12.53	13.93	15.52	14.03	13.91	12.46	14.80	14.35	15.02	15.36
MnO	0.26	0.21	0.22	0.21	0.21	0.23	0.19	0.21	0.22	0.28	0.23
MgO	6.80	6.23	6.22	7.08	6.92	6.11	6.66	6.66	6.34	6.76	6.37
CaO	9.31	11.72	11.11	9.53	6.79	10.80	9.70	9.21	10.62	10	10.01
Na <sub>2</sub> O	2.12	2.15	2.24	2.25	2.44	2.34	2.14	2.29	2.33	2.35	2.26
K <sub>2</sub> O	0.42	0.20	0.26	0.46	1.34	0.38	0.57	0.41	0.39	0.39	0.4
P <sub>2</sub> O <sub>5</sub>	0.28	0.20	0.14	0.20	0.16	0.14	0.20	0.21	0.30	0.27	0.2
Total	98.67	99.92	99.82	100.74	96.89	99.06	97.18	99.07	99.29	98.79	100
FeO <sup>T</sup>	10.33	9.66	10.76	11.90	10.38	9.84	11.49	11.54	10.76	11.75	11.81
<i>CIPW Norm (IgRoCS, Verma &amp; Rivera-Gomez, 2013)</i>											
Quartz	6.95	0	0	1.46	1.51	0	3.76	2.79	2.45	1.96	2.66
Plagioclase	40.96	63.48	58.34	44.67	43.23	58.33	45.10	45.56	43.90	42.70	43.87
Orthoclase	2.54	1.20	1.56	2.73	9.16	2.29	3.50	2.48	2.35	2.36	2.40
Diopside	18.78	10.29	13.09	17.10	11.86	12.98	18.33	16.16	23.06	22.17	20.28
Hypersthene	21.31	3.12	7.59	25.96	26.71	4.28	19.94	25.15	20.24	24.20	22.34
Olivine	0.00	15.80	12.60	0	0	14.68	0	0	0	0	0
Ilmenite	4.30	2.90	3.37	4.15	2.40	3.96	6.03	4.02	4.02	2.57	4.54
Magnetite	4.49	2.81	3.12	3.45	4.79	3.14	2.87	3.35	3.23	3.41	3.44
Apatite	0.67	0.46	0.33	0.47	0.34	0.33	0.48	0.50	0.71	0.64	0.47
Mg#	55	54	51	51	52	51	55	51	51	51	50
D.I.	27.88	19.59	20.77	23.34	32.34	22.52	26.10	25.08	24.90	24.71	23.71
C.I.	55.45	66.6	63.02	55.17	45.13	61.88	59.50	53.79	58.03	55.72	54.79
S.I.	30.30	31.08	28.97	29.50	29.29	28.34	32.06	29.07	28.57	29.08	27.59
CaO/Al <sub>2</sub> O <sub>3</sub>	0.78	0.58	0.61	0.71	0.53	0.60	0.72	0.68	0.83	0.81	0.77
FeO <sup>T</sup> /MgO	1.88	1.81	2.01	1.97	1.82	2.048	1.75	1.99	2.04	1.99	2.1

Chapter 5 Geochemistry of country rocks and dykes

**Table 5.7, Contd**

Sample no.	BG7	BG10	BG13	BG14	BG20	VG1	VG2	VG3	VG23
Rock Type	Basaltic Andesite	Subalkali Basalt	Basaltic Andesite						
SiO <sub>2</sub>	53.26	48.97	49.01	49.58	51.21	50.07	49.34	51.17	51.55
TiO <sub>2</sub>	1.63	1.23	1.23	1.78	1.84	1.93	2.38	2.14	2.21
Al <sub>2</sub> O <sub>3</sub>	13.16	14.33	12.70	12.30	13.86	13.30	15.11	13.36	10.95
Fe <sub>2</sub> O <sub>3</sub> <sup>T</sup>	13.17	11.60	14.20	14.60	14.26	13.76	11.34	15.19	16.23
MnO	0.08	0.17	0.32	0.08	0.08	0.14	0.18	0.14	0.20
MgO	6.45	7.68	8.10	6.40	6.42	6.48	7.19	5.72	6.45
CaO	10.32	10.31	11.15	10.83	11.07	10.03	11.59	8.81	7.94
Na <sub>2</sub> O	1.99	2.27	1.84	2.03	2.24	2.15	2.24	2.47	1.77
K <sub>2</sub> O	0.11	0.18	0.05	0.19	0.19	0.29	0.32	0.51	2.04
P <sub>2</sub> O <sub>5</sub>	0.17	0.14	0.11	0.16	0.18	0.18	0.17	0.22	0.23
Total	100.34	96.88	98.71	97.95	101.35	98.33	99.86	99.73	99.57
FeO <sup>T</sup>	9.40	9.22	11.1	11.51	10.86	10.80	8.74	11.77	11.70
<i>CIPW Norm (IgRoCS, Verma &amp; Rivera-Gomez, 2013)</i>									
Quartz	9.55	0.73	1.02	3.89	3.44	4.20	0.74	4.79	5.48
Plagioclase	43.80	49.62	42.89	42.46	46.09	45.26	45.10	45.47	31.42
Orthoclase	0.65	1.11	0.30	1.16	1.12	1.76	1.91	3.06	12.27
Diopside	19.36	18.62	23.90	24.63	21.90	19.35	21.52	15.54	18.46
Hypersthene	19.04	24.46	26.01	20.64	20.40	22.09	18.60	23.08	22.47
Olivine	0	0	0	0	0	0	0	0	0
Ilmenite	3.12	2.44	2.40	3.50	3.49	3.77	4.58	4.13	4.27
Magnetite	4.09	2.67	3.22	3.34	3.15	3.13	2.54	3.41	5.09
Apatite	0.40	0.34	0.26	0.38	0.42	0.43	0.39	0.52	0.54
Mg#	55	61	57	51	51	52	60	47	50
D.I.	27.16	21.86	17.29	22.81	23.48	24.68	21.79	29.08	32.98
C.I.	59.45	64.95	66.88	60.44	60.23	57.99	69.09	48.72	46.29
S.I.	31.19	37.02	35.21	29.11	29.32	30.12	35.74	25.30	25.58
CaO/Al <sub>2</sub> O <sub>3</sub>	0.78	0.72	0.88	0.88	0.80	0.75	0.77	0.66	0.72
FeO <sup>T</sup> /MgO	1.84	1.36	1.58	2.05	1.99	1.91	1.43	2.39	2.26

**Table 5.7, Contd...**

Sample no.	VG24	AR4	AR8	AR10	AR14
Rock Type	Subalkali Basalt	Subalkali Basalt	Basaltic Andesite	Subalkali Basalt	Subalkali Basalt
SiO <sub>2</sub>	50.06	49.55	51.75	49.91	51.06
TiO <sub>2</sub>	2.01	1.45	1.04	1.52	0.99
Al <sub>2</sub> O <sub>3</sub>	11.71	14.62	13.54	12.91	14.07
Fe <sub>2</sub> O <sub>3</sub> <sup>T</sup>	17.07	12.38	14.75	13.94	14.21
MnO	0.25	0.18	0.26	0.21	0.24
MgO	6.36	7.70	6.41	8.31	6.86
CaO	8.33	10.63	7.18	10.80	9.24
Na <sub>2</sub> O	2.00	2.32	2.74	1.88	2.62
K <sub>2</sub> O	1.30	0.27	1.08	0.17	0.90
P <sub>2</sub> O <sub>5</sub>	0.27	0.13	0.23	0.12	0.47
Total	99.36	99.23	98.98	99.77	100.66
FeO <sup>T</sup>	13.04	9.61	10.68	10.53	10.90
<i>CIPW Norm (IgRoCS, Verma &amp; Rivera-Gomez, 2013)</i>					
Quartz	2.74	0.84	3.19	0.39	0.03
Plagioclase	36.83	47.06	45.64	45.51	46.40
Orthoclase	7.85	1.09	6.52	0.98	5.35
Diopside	17.36	22.51	10.70	21.14	15.63
Hypersthene	26.82	22.45	26.74	25.80	26.45
Olivine	0	0.11	0	0	0
Ilmenite	3.90	2.73	2.02	2.87	1.89
Magnetite	3.85	2.88	4.65	3.03	3.16
Apatite	0.64	0.33	0.54	0.26	1.09
Mg#	46	59	52	59	53
D.I.	27.87	21.60	33.41	18.49	27.66
C.I.	46.47	64.71	44.02	66.43	51.51
S.I.	26.81	35.63	26.91	36.50	29.33
CaO/Al <sub>2</sub> O <sub>3</sub>	0.71	0.73	0.53	0.84	0.66
FeO <sup>T</sup> /MgO	2.41	1.45	2.07	1.43	1.86

Before delving into the descriptions of the major oxides of the dykes, some clarifications about the hypothesis of all dykes belonging to the Deccan phase proposed in *Chapter 3* based on field relationships and the current observations after the scrutiny of geochemical data, needs attention. This has major ramifications on how these dykes are being dealt henceforth.

The field relationships in *Chapter 3* revealed that there are three episodes of dyking events that have intruded the country rocks, each separated in time. These dykes have orientations of, ~N-S, ~NNW-SSE/~WNW-ESE and ~E-W, arranged in ascending order, each corresponding to the variation of minimum principal compressive stress direction ( $\sigma_3$ ) that has changed over time from dominantly ~E-W, to ~NE-SW and finally settling in N-S direction respectively. The field data reveal that there is a clear cross-cutting relationship where the ~N-S trending dykes are cross-cut by the dykes in the other two directions. The petrographic data from *Chapter 4* when combined with the field data, reveals that the ~N-S trending dykes have distinct petrography from the dykes in other directions. The geochemical data also concurs with the field and petrographic data. Hence, I put all ~N-S dykes into Group 1 dykes while the ~NNW-SSE/~WNW-ESE and ~E-W dykes are into Group 2.

A total of thirty-six dyke rocks are analysed. The Group 1 comprises of eleven dykes striking N-S, whereas Group 2 comprises of twenty-five dykes that strike NW-SE and E-W.

Group 1 dykes are further sub-classified into Type 1 (four dykes) and Type 2 (seven dykes) based on their major oxide composition. Group 1 Type 1 dykes (BG-4, -9, -35, -37) have low MgO (3.2 to 3.8 with an average of 3.5 wt. %), low CaO (7.3-7.9; avg. 7.5 wt. %), high in Na<sub>2</sub>O (2.9-3.2; avg. 3.1 wt. %), high in K<sub>2</sub>O (1.3-1.5; avg. 1.4 wt. %), high in TiO<sub>2</sub>

(1.5 to 1.9; avg. 1.6 wt. %), high in  $\text{Al}_2\text{O}_3$  (12.5 to 17.7; avg. 14.1 wt. %), high in  $\text{Fe}_2\text{O}_3$  (14.9 to 16.3; avg. 15.5 wt. %), low  $\text{MnO}$  (0.08 to 0.2; avg. 0.14 wt. %), high  $\text{P}_2\text{O}_5$  (0.16 to 0.18; avg. 0.17 wt. %) and similar  $\text{SiO}_2$  (48.3-53.8; avg. 51.9 wt. %) and  $\text{FeO}^{\text{T}}$  (10.9 to 11.8; avg. 11.4 wt. %) in comparison with the Group 1 Type 2 dykes.

For other parameters,  $\text{Mg\#}$  varies from 33-41; avg. 37 (the lowest among all dykes), Differentiation Index (D. I.) varies from 37.3-42.8; avg. 40.2 (indicating that they are basic differentiates), and Solidification Index (S. I.) varies from 14.8-29.1; avg. 18.9. The  $\text{CaO}/\text{Al}_2\text{O}_3$  ratio varies from 0.4-0.6; avg. 0.5 and  $\text{FeO}^{\text{T}}/\text{MgO}$  varies from 3.5 to 4.2; avg. 3.9.

The Group 1 Type 2 dykes (AG-23, -39, -41, BG-11, AR-5, -7, -9) have high  $\text{MgO}$  (9.5 to 15.5 with an average of 11.3 wt. %), high  $\text{CaO}$  (7.4 to 9.9; avg. 8.7 wt. %), low  $\text{Na}_2\text{O}$  (1.5 to 2.7; avg. 2.1 wt. %), low  $\text{K}_2\text{O}$  (0.5 to 1.1; avg. 0.8 wt. %), low in  $\text{Fe}_2\text{O}_3$  (11.3 to 13.2; avg. 12.5 wt. %), low  $\text{TiO}_2$  (0.5 to 1.2; avg. 0.9 wt. %), low in  $\text{Al}_2\text{O}_3$  (9.4 to 14.6; avg. 11.5 wt. %), high in  $\text{MnO}$  (0.15 to 0.22; avg. 0.19 wt. %), low in  $\text{P}_2\text{O}_5$  (0.08 to 0.14; avg. 0.11 wt. %) and similar  $\text{SiO}_2$  (48 to 51.5; avg. 50.8 wt. %), and  $\text{FeO}^{\text{T}}$  (10.6 to 12.1; avg. 11.5 wt. %) than Group 1 Type 1 dykes. This characteristic is supported by the presence of olivine and pyroxene phenocrysts and a lower content of plagioclase. The Mg-rich composition of BG-11 and AG-39 is likely the result of an accumulation of pyroxene and olivine respectively, in addition to Cr-spinel.

For other calculated parameters,  $\text{Mg\#}$  varies from 66-74; avg. 68, and Differentiation Index (D. I.) varies from 16.3-27.7 (avg. 23.2) suggesting that they are middle stage differentiates, Solidification Index (S. I.) varies from 40.5-52.8; avg. 43.9. The  $\text{CaO}/\text{Al}_2\text{O}_3$  ratio varies from 0.6-0.9; avg. 0.8 and  $\text{FeO}^{\text{T}}/\text{MgO}$  varies from 0.75-1.12; avg. 1.

The values of Mg# higher than 65 and low  $\text{FeO}^{\text{T}}/\text{MgO}$  ratios bolster their origin being from a more primitive mantle (Wilson, 1989).

The geochemistry of Group 2 dykes allows further sub-classification into Type 1 (three dykes) and Type 2 (twenty-two dykes) based on their major oxide contents. The Group 2 Type 1 dykes (AG-9, -13, -17) have low and restricted  $\text{SiO}_2$  (45.1-45.8 with an average of 45.4 wt. %), high  $\text{Al}_2\text{O}_3$  (17.9-20.1; avg. 18.7 wt. %), low in  $\text{MgO}$  (6.11-6.23; avg. 6.19 wt. %), high in  $\text{CaO}$  (10.80-11.72; avg. 11.21 wt. %), low in  $\text{P}_2\text{O}_5$  (0.14-0.20; avg. 0.16 wt. %) and similar in  $\text{TiO}_2$  (1.51 to 2.04; avg. 1.77 wt. %),  $\text{Fe}_2\text{O}_3$  (12.53-13.93; avg. 13.46 wt. %),  $\text{MnO}$  (0.21-0.23; avg. 0.22 wt. %),  $\text{Na}_2\text{O}$  (2.15-2.34; avg. 2.24 wt. %),  $\text{K}_2\text{O}$  (0.20-0.38; avg. 0.28 wt. %), and  $\text{FeO}^{\text{T}}$  (9.65-10.84; avg. 10.42 wt. %) in comparison with the Group 2 Type 2 dykes.

For other calculated parameters, Mg# varies from 51-54; avg. 52, and Differentiation Index (D. I.) varies from 19.59-22.52; avg. 20.96 suggesting that they are middle stage differentiates, Solidification Index (S. I.) varies from 28.34-31.08 (avg. 29.46). The ratio  $\text{CaO}/\text{Al}_2\text{O}_3$  varies from 0.58-0.61 (avg. 0.60) and  $\text{FeO}^{\text{T}}/\text{MgO}$  varies from 1.81-2.05 (avg. 1.96).

The Group 2 Type 2 dykes (AG-4, -15, -16, -19, -24, -43, BG-2, -6, -7, -10, -13, -14, -20, VG-1, -2, -3, -23, -24, AR-4, -8, -10 and -14) have high  $\text{SiO}_2$  (48.8-53.3 with an average of 50.3 wt. %), low  $\text{Al}_2\text{O}_3$  (10.9-15.1; avg. 13.1 wt. %), high  $\text{MgO}$  (5.7-8.3; avg. 6.8 wt. %), low  $\text{CaO}$  (6.8-11.6; avg. 9.7 wt. %), high  $\text{P}_2\text{O}_5$  (0.1-0.47; avg. 0.21 wt. %), similar  $\text{TiO}_2$  (0.99-3.1; avg. 1.8 wt. %),  $\text{Fe}_2\text{O}_3$  (11.3-17.1; avg. 14.2 wt. %),  $\text{MnO}$  (0.08-0.32; avg. 0.20 wt. %),  $\text{Na}_2\text{O}$  (1.8-2.7; avg. 2.2 wt. %),  $\text{K}_2\text{O}$  (0.05-2.04; avg. 0.21 wt. %),  $\text{FeO}^{\text{T}}$  (8.7-13.3; avg. 10.9 wt. %) in comparison with the Group 2 Type 1 dykes.

For other calculated parameters, Mg# varies from 46-61; avg. 53, and Differentiation Index (D. I.) varies from 17.3-33.4; avg. 25.4 suggesting that they are middle stage differentiates. Solidification Index (S. I.) varies from 25.3-37; avg. 30.4, CaO/Al<sub>2</sub>O<sub>3</sub> varies from 0.5-0.9; avg. 0.7 and FeO<sup>T</sup>/MgO varies from 1.2-3.9; avg. 1.97.

The high Mg# dykes of Group 1 Type 2 also correspondingly have higher S. I. whereas the low Mg# dykes of Group 1 Type 1 have the lowest S. I. The dykes in Group 2 show a reasonably close value for S. I. for the corresponding similar Mg# values. It is apparent that the CaO/Al<sub>2</sub>O<sub>3</sub> values of Group 1 Type 2 dykes are the highest and FeO<sup>T</sup>/MgO ratio is the lowest amongst all groups. The total alkalis of Group 1 Type 1 are the highest due to which they occupy alkaline fields in various classification diagrams. CaO/Al<sub>2</sub>O<sub>3</sub> ratio is a significant characteristic of mafic rocks since in the primary melts it reflects the ratio of their mantle source (Cawthorn and Strong, 1974; Perfit et al., 1980) but this ratio is also controlled by plagioclase/clinopyroxene crystallization. All of the values in the dykes studied are lower than chondrite or primitive upper mantle CaO/Al<sub>2</sub>O<sub>3</sub> value of 0.9 (Sun and McDonough, 1989). According to Kuno (1962), Solidification Index (S. I.) tends to decrease during the formation of most igneous rocks. He proposed that the magmas of primary origin have S. I. values of 35-40, whereas those produced by fractionation in the middle stage have a value of 25. In case of those rocks where olivine accumulation has taken place, the S. I. values tend to be higher than 40. Hence, the Group 1 Type 2 dykes with the highest S. I. are of primary origin, whereas all Group 2 types are produced by fractionation in the middle stage. Group 1 Type 1 dykes are of late stage.

The Alteration Index [A. I. = 100 \* (MgO + K<sub>2</sub>O) / (MgO + K<sub>2</sub>O + Na<sub>2</sub>O + CaO)] (Hashiguchi et al., 1983) is used to assess the degree of alteration of rocks. The resulting values, however, cannot be used in rocks with abundant cumulative olivine or komatiites where it may reach values of 85 ± 10 (which is close to the average value of 90 ± 2 for

mantle lherzolite; Laflèche et al., 1992). The A. I. is higher than 50 for those affected by chloritization and /or sericitization whereas, in albitised samples, the value of A. I. is much lower than 30 (Laflèche et al., 1992). The A. I. values for Group 1 Type 1 dykes vary from 29.9-33.3; avg. 31.7 which are similar to Group 2 Type 1 dykes where A. I. varies from 31.7 to 33.1; avg. 32.5. These values approach those samples that are albitised. The A. I. values for Group 1 Type 2 vary from 46.2-59.8; avg. 52.5, which points towards their low level of chloritization and/or sericitization. Petrographic studies have also revealed this type of minor alteration in the dykes. The A. I. values for Group 2 Type 2 vary from 33.2-47.2; avg. 38.3. These values fall much within the expected values for the unaltered samples. Hence I consider these dykes to be largely pristine.

I use the weight percentages of major elements for both the Groups of dykes to classify and distinguish them. One of the diagrams used is the Total Alkali-Silica plot (*Fig. 5.3*). It makes direct use of major element oxides  $\text{Na}_2\text{O}$ ,  $\text{K}_2\text{O}$  and  $\text{SiO}_2$  where the diagram is a total alkali ( $\text{Na}_2\text{O} + \text{K}_2\text{O}$ ) vs silica ( $\text{SiO}_2$ ) (TAS) (after Le Bas et al., 1986; Le Maitre et al., 1989).

For regional correlations, I plotted the dykes under study with dykes from Goa's coast and in the vicinity (Widdowson et al., 2000; Fernandes et al., 2016), dyke from Dandeli (JEF-00-1; French and Heaman, 2010), dykes from Kalyadi (Chandrasekharam et al., 2008), dykes from Goa-Dharwar sector (Devaraju et al., 2008), Desur Formation (Hegde et al., 2014; Verma and Khosla, 2019) (It is considered as Unit of Panhala Formation by few; Sheth et al., 2014; Patel et al., 2020) basalt flows from Belgaum and the Deccan Formation averages of Ambenali, Poladpur and Mahabaleshwar (Vanderkluyzen et al., 2011).

The majority of the samples of both the groups plot in the basalt field. Samples AG-9 and -17 (Group 2 Type 1) plot very close to the boundary of micro-basalt since their SiO<sub>2</sub> value only marginally exceeds the lower SiO<sub>2</sub> limit for basalts, but their MgO contents are too low (6.23 and 6.11 wt. % respectively) for them to be classified as micro-basalts. Dykes BG-4, -35, -37 (all Group 1 Type 1) and BG-7 (Group 2 Type 2) plots in the basaltic andesite field. In the TAS diagram (Fig. 5.5) alkaline-sub-alkaline subdivision line (after Irvine and Baragar, 1971) is plotted, apart from AG-9 and BG-9 which are alkaline, all other dykes plot in the sub-alkaline field. The other samples plotted for comparison also show coherence to the dykes studied.

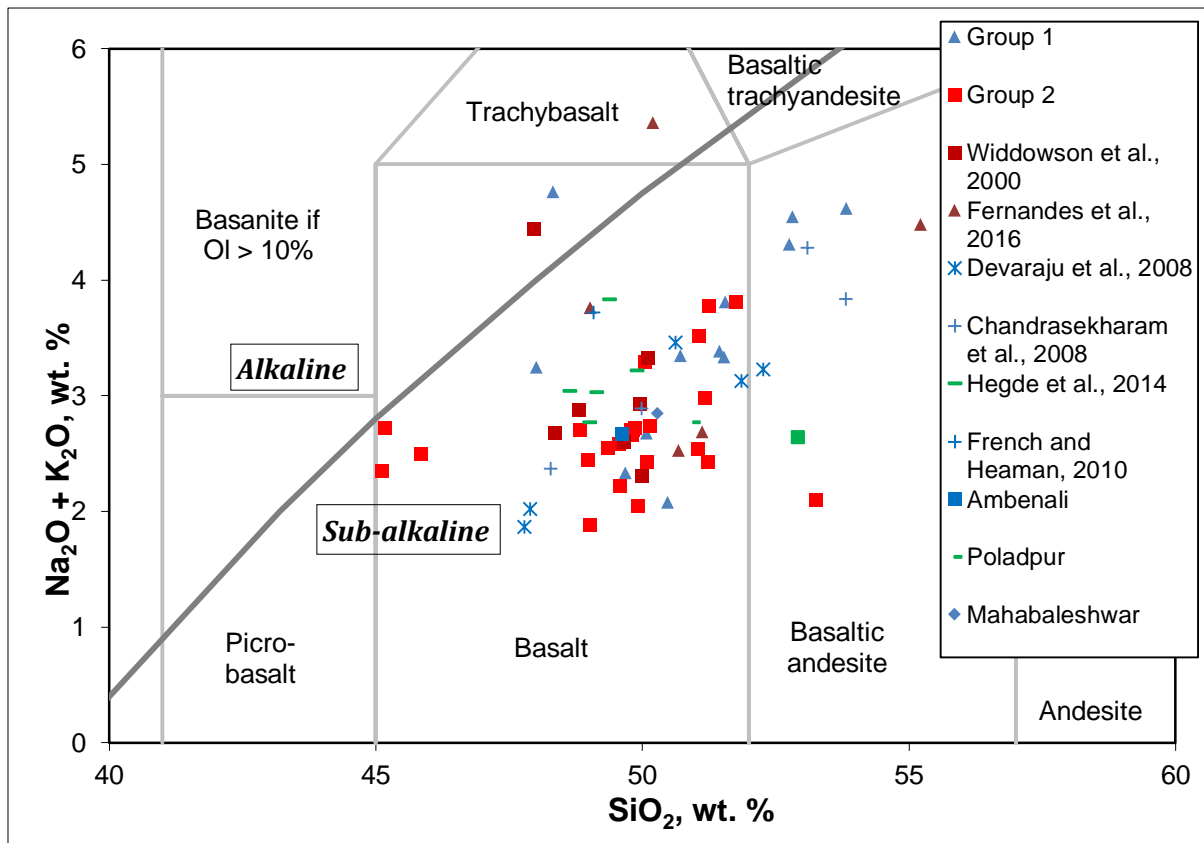


Fig 5.5 Total Alkali-Silica (TAS) diagram after Le Maitre et al., (1989) showing Group 1 and Group 2 dykes. (Alkaline-sub-alkaline division after Irvine and Baragar, 1971).

In the AFM diagram  $(\text{Na}_2\text{O} + \text{K}_2\text{O})\text{-FeO}^{\text{T}}\text{-MgO}$  (*Fig. 5.6a*) (after Irvine and Baragar, 1971), dykes from both the groups define a distinct tholeiitic trend, wherein Group 1 Type 2 dykes are closer to the magnesian end, Group 2 are in the middle, and Group 1 Type 1 is more iron-rich. All the dyke values are plotted on Al-Mg-(Fe\*+Ti) cation mole % diagram (*Fig. 5.6b*) (Jensen, 1976) that has sharply demarcated fields for several subtypes of basalts namely tholeiitic, calc-alkaline, high Mg tholeiite, high Fe tholeiite, Basaltic komatiite and Komatiite. As seen from the diagram, the majority of the dykes fall in the High-Fe tholeiitic basalt field except for AG-41, -39 and BG-11 (All Group 1) that plot in the Komatiitic basalt field and AG-9 (Group 2) that falls in the Andesite field with tholeiite affinity. Hence, the dykes belonging to both the Groups are broadly classified as basalts in general, with some varieties of basaltic andesite, high Mg and high Fe varieties of tholeiitic basalt.

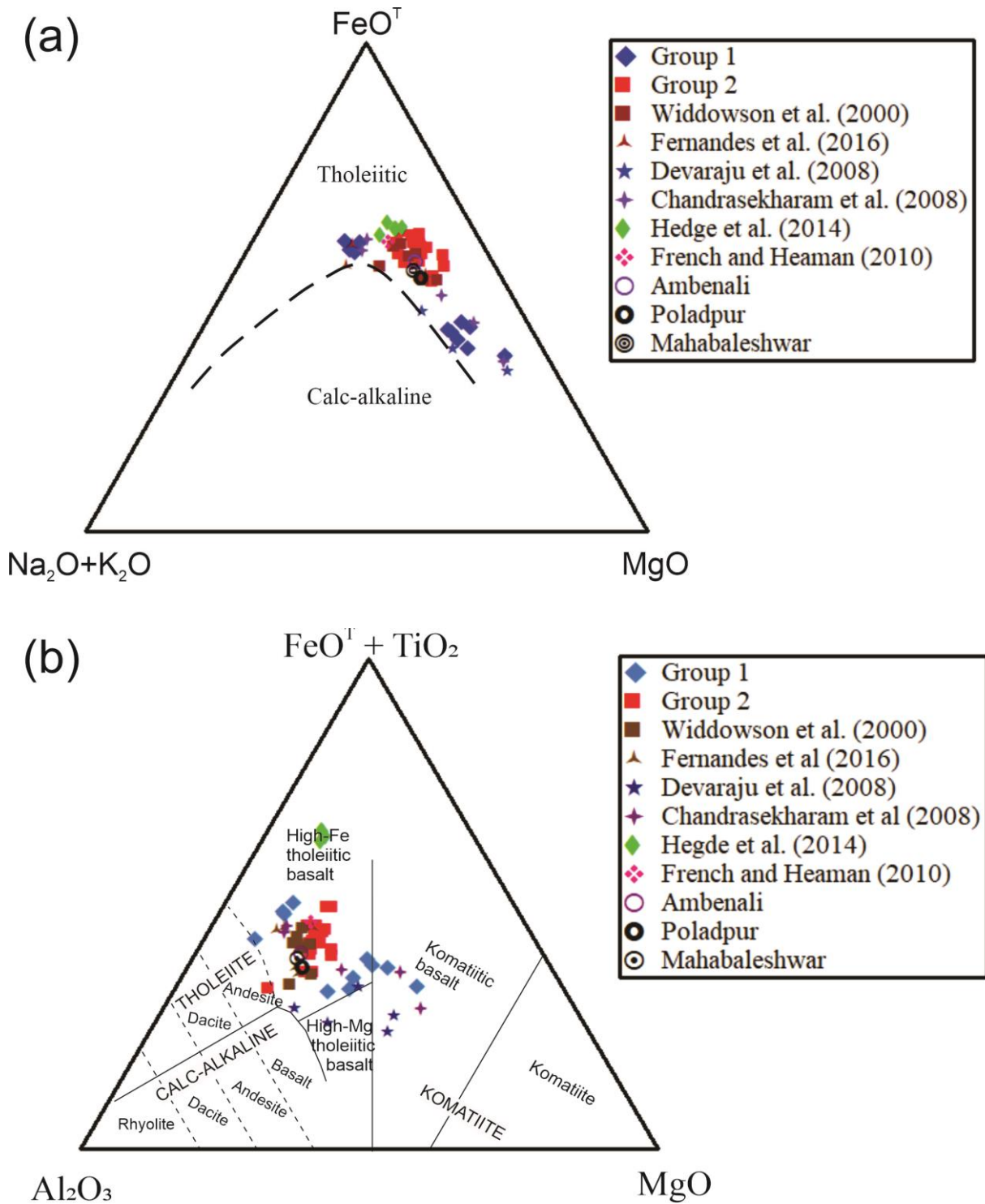


Fig. 5.6 (a) The dykes from Goa showing a distinct tholeiitic trend ( $\text{Na}_2\text{O}+\text{K}_2\text{O}$ )- $\text{FeO}^T$ - $\text{MgO}$  (AFM) diagram (after Irvine and Baragar, 1971). (b) Plots of the dykes of Goa showing High-Fe tholeiitic character along with Komatiitic basalt and Andesite varieties in  $\text{TiO}_2$ - $\text{Al}_2\text{O}_3$ - $\text{MgO}$  diagram (after Jensen, 1976)

#### **5.4.2 Trace elements**

Tables 5.5 a-b and 5.6 a-b contain the trace elemental data (including REE) and the ratios of the seventeen dykes from my study area. Trace element chemistry of the sampled dykes will be discussed by the compositions of compatible trace elements like Sc, Cr, Co and Ni; incompatible trace elements including LILE like Rb, Sr, Ba and HFSE like Nb, Ta, Zr, Hf, Th, U, Pb, and REE. The REE are further subdivided into LREE (LREE: La, Ce, Pr, Nd), MREE (Sm, Eu, Gd, Dy) and HREE (Tb, Ho, Er, Tm, Yb, Lu). Major elements such as K and P can also be considered along with the trace elements. Several factors such as source composition, residual mineralogy, degree of partial melting and the extent of subsequent fractional crystallisation of basaltic magmas control the elemental abundances of LILE, HFSE and REE.

**Table 5.8a** Representative trace element data of the Group 1 dykes in Goa. (NA: Not Analysed)

Sample no.	AG23	AG41	BG4	BG11	BG35	BG37
Sc	NA	24.2	25.3	26.6	25.2	24.6
Cr	807	771	89.7	1430	89.7	107
Co	NA	63.3	50	68.2	51.9	51.5
Ni	280	342	79.5	432	80.5	89.4
Cs	NA	2.72	1.96	2.39	1.95	1.94
Rb	46.4	50.5	46.9	25.1	50.5	49.6
Sr	301	320	235	132	239	247
Ba	213	217	295	120	315	312
Nb	8.22	8.58	8.72	3.46	9.3	9.53
Ta	0.44	0.99	1.14	0.5	1.33	1.35
Zr	117	121	167	53.7	165	172
Hf	2.55	2.8	4.11	1.29	4.41	4.09
Th	2.17	2.48	4.43	1.67	4.99	4.76
U	NA	0.65	1.27	0.42	1.43	1.36
Y	17.2	19.2	30.4	11.5	30.9	31.2
La	18.3	17.1	22.8	9.12	23.9	23.8
Ce	21.6	39.8	49.8	20.3	52	52
Pb	NA	6	10.9	4.15	12.4	11.3
Pr	NA	5.15	6.18	2.42	6.40	6.36
Nd	17.1	22.1	26	10.7	27.2	27.1
Sm	2.57	5.04	5.87	2.42	6.22	6.28
Eu	1.07	1.42	1.71	0.66	1.81	1.79
Gd	3.43	4.59	6.25	2.43	6.62	6.55
Tb	NA	0.59	0.89	0.33	0.98	0.96
Dy	3.89	3.73	5.68	2.14	5.92	5.93
Ho	0.62	0.72	1.2	0.41	1.23	1.22
Er	NA	1.81	3.01	1.05	3.17	3.1
Tm	NA	0.2	0.4	0.1	0.42	0.42
Yb	1.25	1.52	2.71	0.89	2.78	2.78
Lu	0.24	0.17	0.39	0.09	0.38	0.37
Cu	NA	188	211	95.4	224	226
Zn	NA	94.8	130	70	135	134

**Table 5.8b** Trace element ratios of Group 1 dykes in Goa

Sample no.	AG23	AG41	BG4	BG11	BG35	BG37
(Ce/Yb) <sub>N</sub>	4.81	7.26	5.10	6.34	5.20	5.20
(La/Lu) <sub>N</sub>	8.29	10.93	6.23	11.03	6.81	6.90
(La/Sm) <sub>N</sub>	4.60	2.19	2.51	2.44	2.48	2.45
(Gd/Yb) <sub>N</sub>	2.27	2.49	1.91	2.26	1.97	1.95
(Sm/Yb) <sub>N</sub>	2.29	3.68	2.40	3.02	2.48	2.51
(La/Sm) <sub>PM</sub>	4.55	2.16	2.48	2.41	2.45	2.42
(Nb/Th) <sub>PM</sub>	0.52	0.47	0.27	0.28	0.25	0.27
(Th/Nb) <sub>PM</sub>	1.93	2.13	3.74	3.54	3.94	3.67
(Nb/La) <sub>PM</sub>	0.50	0.55	0.42	0.42	0.43	0.44
Eu/Eu*	1.10	0.88	0.86	0.82	0.86	0.85
Zr/Nb	14.25	14.06	19.13	15.55	17.73	18.07
Zr/Sm	45.57	23.93	28.42	22.23	26.50	27.43
Zr/Y	6.82	6.29	5.49	4.66	5.33	5.53
Zr/Ba	0.55	0.56	0.57	0.45	0.52	0.55
Nb/La	0.45	0.50	0.38	0.38	0.39	0.40
Nb/Y	0.48	0.45	0.29	0.30	0.30	0.31
Nb/Yb	6.59	5.63	3.21	3.88	3.34	3.43
Nb/Ta	18.86	8.67	7.67	6.86	6.99	7.06
Nb/Th	3.80	3.46	1.97	2.07	1.86	2.00
Th/Yb	1.74	1.63	1.63	1.87	1.79	1.71
Th/Nb	0.26	0.29	0.51	0.48	0.54	0.50
Th/Ta	4.97	2.51	3.90	3.31	3.75	3.53
La/Sm	7.13	3.39	3.90	3.77	3.84	3.79
La/Yb	10.54	8.05	6.04	7.35	6.15	6.14
Ce/Nb	2.63	4.64	5.71	5.88	5.60	5.46
Sm/Yb	2.06	3.31	2.16	2.72	2.23	2.26

Chondrite (N) normalization factors after Sun and McDonough (1989)

Primitive Mantle (PM) normalization factors after Lyuetskaya and Korenaga (2007)

$$Eu/Eu^* = Eu_N[(Sm_N) + (Gd_N)/2]$$

(Ragland, 1989)

Chapter 5 Geochemistry of country rocks and dykes

**Table 5.9a** Representative trace element data of the Group 2 dykes in Goa. (NA: Not Analysed)

Sample no.	AG4	AG9	AG15	AG19	AG24	BG6	BG7	BG13	BG20	VG1	VG2
Sc	42.6	38.9	36	41.7	NA	40.6	38.8	20.3	41.4	39.4	43.5
Cr	150	323	98.3	127	160	118	148	82.7	156	167	167
Co	53.6	51.6	44.8	52.6	NA	49.9	47.6	25.9	50.3	46.8	51
Ni	103	133	69	86.3	79.5	87.8	89.7	59.3	86.4	108	109
Cs	0.23	0.26	0.26	0.32	NA	0.67	0.19	5.34	0.30	0.72	2.89
Rb	13	8.88	14.3	16.1	5.02	9.77	9.53	27.5	11.3	12	11.6
Sr	183	164	161	186	157	199	161	124	168	156	188
Ba	86.3	44.6	102	127	86	89.6	72	66	81.6	107	116
Nb	12.9	7.11	12.9	14.9	9.74	13.8	10.6	7.80	12.1	11	12.5
Ta	1.64	0.98	1.48	1.70	0.70	1.63	1.29	1.00	1.52	1.26	1.41
Zr	128	88.5	131	144	112	140	114	71.7	127.5	120.8	144
Hf	3.08	2.21	3.15	3.51	2.57	3.39	2.79	1.79	3.10	2.97	3.54
Th	1.54	0.65	1.64	1.77	1.44	1.44	1.11	0.83	1.26	1.17	1.32
U	0.36	0.14	0.37	0.42	NA	0.34	0.25	0.20	0.31	0.28	0.33
Y	30.1	24.7	28.1	33.7	22.8	33.9	28.1	16.7	33.8	29.3	34
La	12.1	6.78	13.1	15	8.39	12.5	10	6.92	11.1	10.4	12.3
Ce	28.9	16.8	31	35.3	16.6	30.4	24.8	16.4	27.2	25.7	30
Pb	2.58	1.26	2.61	3.18	NA	2.02	1.74	1.26	2.04	2.09	2.03
Pr	3.91	2.40	4.12	4.70	NA	4.20	3.39	2.20	3.79	3.61	4.22
Nd	18.3	11.9	18.9	21.7	12.8	19.8	16.3	10.3	18	16.9	20
Sm	4.76	3.39	4.84	5.43	2.90	5.28	4.42	2.68	4.76	4.48	5.25
Eu	1.53	1.13	1.45	1.69	1.03	1.65	1.39	0.82	1.51	1.41	1.67
Gd	5.41	4.04	5.19	6.03	3.58	5.80	4.99	2.97	5.51	5.13	5.93
Tb	0.82	0.62	0.77	0.91	NA	0.90	0.74	0.45	0.85	0.79	0.90
Dy	5.34	4.15	5.07	6.01	4.47	5.93	5.02	2.96	5.71	5.26	5.99
Ho	1.17	0.92	1.07	1.33	0.83	1.28	1.07	0.64	1.24	1.09	1.29
Er	3.09	2.42	2.86	3.44	NA	3.32	2.88	1.70	3.34	2.94	3.41
Tm	0.41	0.33	0.39	0.49	NA	0.45	0.37	0.23	0.46	0.39	0.46
Yb	2.80	2.22	2.65	3.22	1.98	3.08	2.60	1.61	3.07	2.68	3.18
Lu	0.40	0.30	0.37	0.46	0.27	0.43	0.37	0.23	0.43	0.36	0.43
Cu	225	172	225	254	NA	248	211	116	232	238	267
Zn	124	90	111	134	NA	124	101	59.6	114	111	124

Chapter 5 Geochemistry of country rocks and dykes

**Table 5.9b** Trace element ratios of Group 2 dykes in Goa

Sample no.	AG4	AG9	AG15	AG19	AG24	BG6	BG7	BG13	BG20	VG1	VG2
(Ce/Yb) <sub>N</sub>	2.87	2.11	3.26	3.05	2.33	2.75	2.65	2.84	2.46	2.67	2.63
(La/Lu) <sub>N</sub>	3.23	2.39	3.78	3.51	3.29	3.09	2.91	3.28	2.80	3.07	3.10
(La/Sm) <sub>N</sub>	1.64	1.29	1.75	1.79	1.87	1.53	1.47	1.67	1.52	1.50	1.52
(Gd/Yb) <sub>N</sub>	1.60	1.51	1.62	1.55	1.50	1.56	1.59	1.53	1.48	1.58	1.54
(Sm/Yb) <sub>N</sub>	1.89	1.70	2.03	1.88	1.63	1.91	1.89	1.85	1.72	1.86	1.84
(La/Sm) <sub>PM</sub>	1.62	1.27	1.73	1.77	1.84	1.51	1.51	1.65	1.50	1.48	1.50
(Nb/Th) <sub>PM</sub>	1.14	1.48	1.07	1.15	0.92	1.30	1.30	1.28	1.31	1.29	1.29
(Th/Nb) <sub>PM</sub>	0.87	0.68	0.93	0.87	1.09	0.77	0.77	0.78	0.76	0.78	0.78
(Nb/La) <sub>PM</sub>	1.18	1.16	1.08	1.09	1.28	1.22	1.22	1.24	1.20	1.17	1.12
Eu/Eu*	0.92	0.93	0.88	0.91	0.98	0.91	0.90	0.88	0.90	0.90	0.91
Zr/Nb	9.90	12.46	10.15	9.67	11.54	10.14	10.81	9.20	10.51	10.91	11.59
Zr/Sm	27.01	26.09	27.00	26.58	38.71	26.49	25.89	26.80	26.81	26.96	27.57
Zr/Y	4.27	3.59	4.64	4.28	4.92	4.13	4.07	4.28	3.77	4.12	4.25
Zr/Ba	1.49	1.99	1.28	1.14	1.31	1.56	1.59	1.09	1.56	1.13	1.24
Nb/La	1.07	1.05	0.98	0.99	1.16	1.10	1.05	1.13	1.09	1.06	1.01
Nb/Y	0.43	0.29	0.46	0.44	0.43	0.41	0.38	0.47	0.36	0.38	0.37
Nb/Yb	4.63	3.20	4.86	4.64	4.93	4.49	4.07	4.85	3.95	4.13	3.93
Nb/Ta	7.93	7.23	8.70	8.78	13.99	8.48	8.20	7.76	7.96	8.80	8.82
Nb/Th	8.41	10.87	7.87	8.44	6.76	9.57	9.53	9.44	9.66	9.45	9.47
Th/Yb	0.55	0.29	0.62	0.55	0.73	0.47	0.43	0.51	0.41	0.44	0.42
Th/Nb	0.12	0.09	0.13	0.12	0.15	0.10	0.10	0.11	0.10	0.11	0.11
Th/Ta	0.94	0.67	1.11	1.04	2.07	0.89	0.86	0.82	0.82	0.93	0.93
La/Sm	2.55	2.00	2.71	2.78	2.89	2.37	2.27	2.58	2.35	2.33	2.35
La/Yb	3.10	2.19	3.55	3.36	3.05	2.92	2.77	3.09	2.61	2.79	2.78
Ce/Nb	2.23	2.37	2.41	2.37	1.70	2.20	2.34	2.11	2.25	2.32	2.41
Sm/Yb	1.70	1.53	1.83	1.69	1.47	1.72	1.70	1.67	1.55	1.67	1.65

Calculation of Eu anomaly is the same way as given in Table 5.8b

The trace elemental abundances of Group 1 dykes consist of Sc which varies from 24.2-26.6 ppm with an average of 25.2 ppm, Cr: 89-1429 ppm; avg. 549 ppm, Co: 50-68.2 ppm; avg. 57 ppm and Ni: 79-432 ppm; avg. 217 ppm. The Large Ion Lithophile Elements (LILE) such as Cs varies from 1.94-2.72 ppm; avg. 2.19 ppm, Rb: 25.6-50.5 ppm; avg. 44.9 ppm, Sr: 132-320 ppm; avg. 246 ppm and Ba: 120-315 ppm; avg. 245 ppm. The higher concentrations of Ba and Sr indicate that these elements were preferentially incorporated into early-crystallizing calcic plagioclase phenocrysts and the variation in their compositional range is a function of low-pressure fractional crystallization.

The High Field Strength Elements (HFSE) are immobile, and alteration-resistant elements and their concentrations in the investigated samples are: Nb varies from 3.45-9.53 ppm; avg. 7.96 ppm, Ta: 0.44-1.35; avg. 0.96 ppm, Zr: 54-172 ppm; avg. 136, Hf: 1.29-4.41 ppm; avg. 3.2 ppm, Th: 1.67-4.99 ppm; avg. 3.41 ppm, U: 0.42-1.43 ppm; avg. 1.02 ppm, and Y: 11.5-31.8 ppm; avg. 23.4 ppm.

The Rare Earth Element (REE) abundances of these dykes are characterised with La that varies from 9.1-23.9 ppm; avg. 19.2 ppm, Ce: 20.3-52.1 ppm; avg. 39.3 ppm, Pb: 4.15-12.36; avg. 8.95 ppm; Pr: 2.4-6.4 ppm; avg. 5.3 ppm, Nd: 10.7-27.2 ppm; avg. 21.7 ppm and Sm: 2.4-6.3 ppm; avg. 4.7 ppm, Eu: 0.66-1.81 ppm; avg. 1.4 ppm, Gd: 2.4-6.6 ppm; avg. 4.9 ppm, Tb: 0.33-0.98 ppm; avg. 0.75 ppm, Dy: 2.1-5.9 ppm; avg. 4.6 ppm, Ho: 0.41-1.23 ppm; avg. 0.89 ppm, Er: 1.05-3.2 ppm; avg. 2.4 ppm, Tm: 0.1-0.4 ppm; avg. 0.3 ppm, Yb: 0.9-2.8 ppm; avg. 1.9 ppm, Lu: 0.09-0.39 ppm; avg. 0.27 ppm. Metals like Cu vary from 95-226 ppm; avg. 189 ppm and Zn varies from 70-136 ppm; avg. 113 ppm.

The compatible trace elemental abundances of Group 2 are represented by Sc that varies from 20.3-43.5 ppm; avg. 38.3 ppm, Cr: 83-323 ppm; avg. 154 ppm, Co: 25.9-53.6 ppm; avg. 47.4 ppm, and Ni: 59-133 ppm; avg. 92 ppm. The Sc and Co concentrations are

comparable with that of CFB/OIB (Continental Flood Basalts/Ocean Island Basalts) (Sc: 34-37 ppm; Co: 38 ppm) (BVSP, 1981; Thompson et al., 1984; Wilson, 1989). Slightly higher values of Sc are suggestive of crystallisation of clinopyroxene phenocrysts in these dykes. Except for sample AG-9 with Cr concentrations of 322.97 ppm, the remaining samples are close to the Cr: 81-160 ppm of CFB/OIB (BVSP, 1981; Thompson et al., 1984; Wilson, 1989). The concentrations of Ni are far higher than the expected Ni: 15-78 ppm for CFB/OIB (BVSP, 1981; Thompson et al., 1984; Wilson, 1989) and could be due to accumulation of olivine phenocrysts in these dykes (*refer chapter 4*). In LILE, concentrations of Cs vary from 0.19-5.34 ppm; avg. 1.12 ppm, Rb: 5.0-27.5 ppm; avg. 12.6 ppm, Sr: 124-199 ppm; avg. 168 ppm, and Ba: 44.6-126 ppm; avg. 89 ppm. The average concentrations of Rb, Sr and Ba in the dykes studied match fairly well with the ranges Rb: 5-15.4 ppm, Sr: 150-400 ppm and Ba: 70-200 ppm for CFB/OIB (BVSP, 1981). Comparative values of Ba and Sr reflect their preferential incorporation into early crystallizing calcic plagioclase phenocrysts.

The HFSE concentrations of the dykes investigated are represented by Nb varying between 7.1-14.9 ppm; avg. 11.4 ppm, Ta: 0.69 (Only AG-24), Zr: 72-145 ppm; avg. 120.3 ppm, Hf: 1.79-3.6 ppm; avg. 2.9 ppm, Th: 0.65-1.77 ppm; avg. 1.29 ppm, U: 0.14-0.42 ppm; avg. 0.31 ppm and Y: 16.7-34 ppm; avg. 28.7 ppm. For comparison, the CFB/OIB HFSE compositions are Nb: 5-25 ppm, Ta: 0.9-1.5 ppm, Zr: 100-300 ppm, Hf: 3-5.95 ppm, Th: 0.67-1.64 ppm, U: 1.18-1.8 ppm, Y: 37-42 ppm (BVSP, 1981; Thompson et al., 1984; Wilson, 1989). It is seen that apart from lower values for U and Y for the studied dykes, all other HFSE are well within those constrained for CFB/OIB.

The REE abundances of the dykes are marked by higher concentrations of La that vary from 6.8-15 ppm; avg. 10.8 ppm, Ce: 16.4-35.3 ppm; avg. 25.8 ppm, Pb: 1.26-3.18; avg. 2.1 ppm, Pr: 2.2-4.7 ppm; avg. 3.7 ppm, Nd: 10.3-21.7 ppm; avg. 16.8 ppm, Sm: 2.7-

5.4 ppm; avg. 4.4 ppm, Eu: 0.82-1.69 ppm; avg. 1.39 ppm, Gd: 2.9-6 ppm; avg. 4.96 ppm, Tb: 0.45-0.91 ppm; avg. 0.78 ppm, Dy: 2.95-6 ppm; avg. 5.1 ppm, Ho: 0.6-1.3 ppm; avg. 1.08 ppm, Er: 1.7-3.4 ppm; avg. 2.9 ppm, Tm: 0.1-0.49 ppm; avg. 0.38 ppm, Yb: 1.6-3.2 ppm; avg. 2.6 ppm and Lu: 0.2-0.46 ppm; avg. 0.37 ppm. Metals like Cu vary from 117-267 ppm; avg. 220 ppm and Zn varies from 60-135 ppm; avg. 110 ppm.

The next chapter discusses the geochemical aspects of the country rocks and dykes in detail.

## **CHAPTER 6**

**Petrogenesis of country**

**rocks and dykes**

Through this chapter, I will use the term “enriched” to describe enrichments in incompatible elements compared to estimates of primitive mantle or chondritic compositions, and “depleted” to mean the opposite.

## 6.1 Country rock

### 6.1.1 Comparisons to other greywackes

I determined major oxide compositions on seven metagreywacke samples, and trace element compositions for five samples. The plot of Harker variation diagrams (*Fig.6.1*), shows decreasing concentrations of  $\text{Al}_2\text{O}_3$ ,  $\text{TiO}_2$ ,  $\text{Fe}_2\text{O}_3^{\text{T}}$  and  $\text{MgO}$  with increasing  $\text{SiO}_2$  in contrast to the increasing concentration of  $\text{Na}_2\text{O}$ , and stable concentration of  $\text{CaO}$  against increasing  $\text{SiO}_2$ . This correlation is consistent with greywackes of Goa (Fernandes et al., 2016) and points towards increase in quartz content with decreasing phyllosilicates while the weak correlation of  $\text{CaO}$  could be attributed to the presence of variable feldspar proportions in the rocks. There is a positive correlation of Cr and Ni with  $\text{MgO}$  (*Fig. 6.2a-b*), Rb with K (*Fig. 6.2c*) and, U with Th (*Fig. 6.2d*) in the metagreywackes under study and it conforms with previous studies on greywackes of the Goa-Dharwar sector (Devaraju et al., 2010) and the Archaean Barberton greenstone belt of South Africa (Toulkeridis et al., 1999).

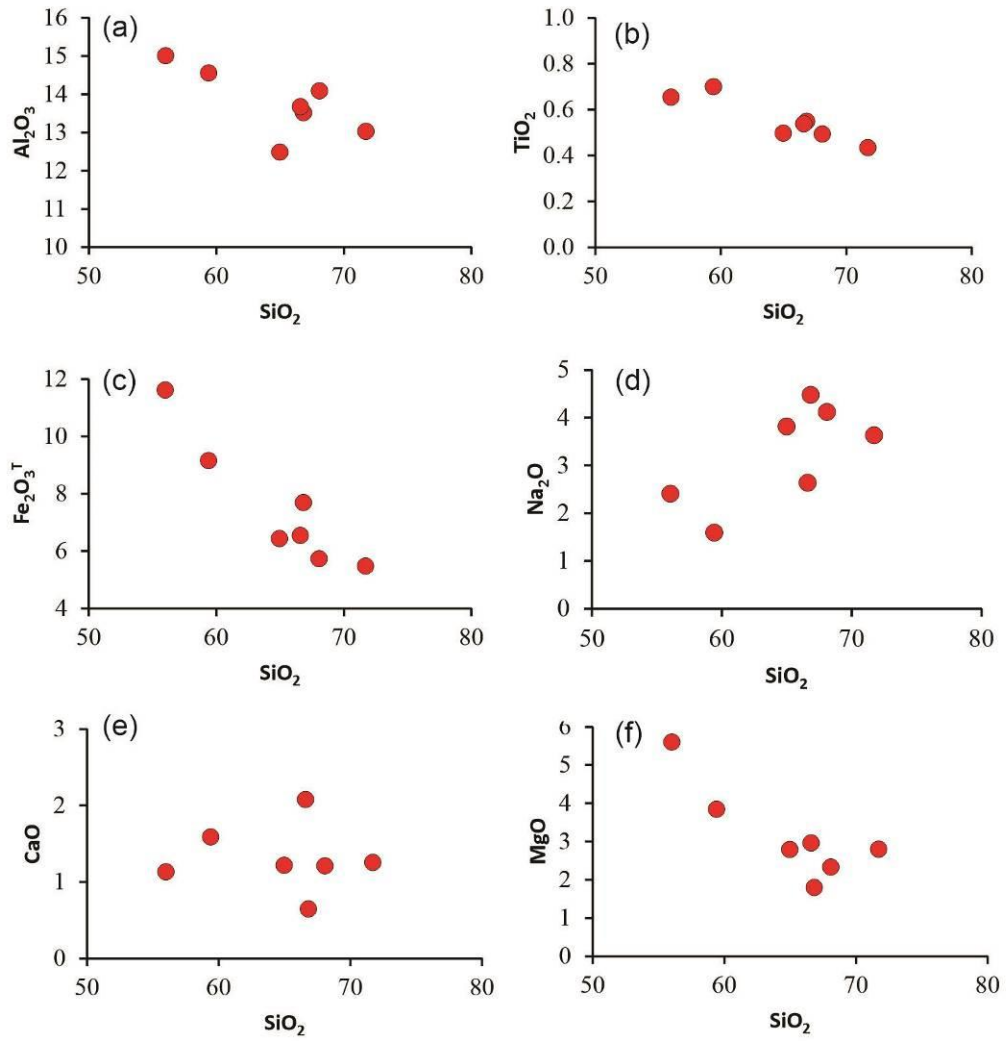


Fig. 6.1 Variation of major oxides (a)  $Al_2O_3$  (b)  $TiO_2$  (c)  $Fe_2O_3^T$  (d)  $Na_2O$  (e)  $CaO$  (f)  $MgO$ . All are plotted against  $SiO_2$  in the metagreywackes of the study area. All oxides show a decreasing trend with increasing  $SiO_2$ , except for  $Na_2O$  (negative trend) and  $CaO$  (stable trend).

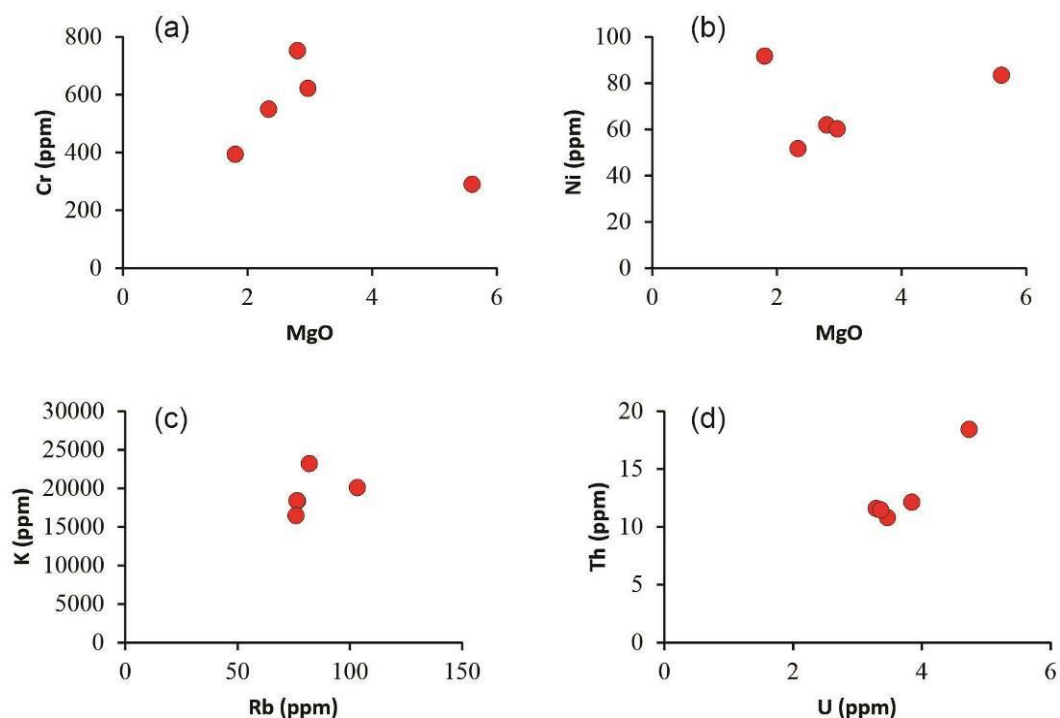


Fig. 6.2 Variation of (a) Cr and (b) Ni vs MgO (wt. %), (c) Rb vs K (d) U vs Th

In terms of major oxides and their ratios (*Table. 5.4*), the metagreywackes in this study have comparable SiO<sub>2</sub>, MnO, MgO, Na<sub>2</sub>O and P<sub>2</sub>O<sub>5</sub> to Late Archaean (3.5-2.5 Ga) greywacke (Condie, 1993), while they have more Fe<sub>2</sub>O<sub>3</sub>, and higher K<sub>2</sub>O/Na<sub>2</sub>O, SiO<sub>2</sub>/Al<sub>2</sub>O<sub>3</sub>, Na<sub>2</sub>O/Al<sub>2</sub>O<sub>3</sub> and K<sub>2</sub>O/Al<sub>2</sub>O<sub>3</sub>, and lesser TiO<sub>2</sub>, Al<sub>2</sub>O<sub>3</sub> and CaO. When the metagreywackes are compared with Archaean greywacke of Fig Tree, Barberton, South Africa (Toulkeridis et al., 1999) (*Table. 5.4*), they are found to have similar SiO<sub>2</sub>, TiO<sub>2</sub>, Fe<sub>2</sub>O<sub>3</sub>, MnO and K<sub>2</sub>O/Al<sub>2</sub>O<sub>3</sub>, and higher Al<sub>2</sub>O<sub>3</sub>, Na<sub>2</sub>O, K<sub>2</sub>O, P<sub>2</sub>O<sub>5</sub> and Na<sub>2</sub>O/Al<sub>2</sub>O<sub>3</sub> and lower MgO, CaO, K<sub>2</sub>O/Na<sub>2</sub>O and SiO<sub>2</sub>/Al<sub>2</sub>O<sub>3</sub>. These metagreywackes bear broad resemblance to the greywackes from the Goa-Dharwar sector (Devaraju et al., 2010) (which includes greywackes with biotite, greywacke with chlorite-sericite and fine grained greywacke), greywackes from Merces (Widdowson, 2009), argillite and metagreywacke from Ribandar (Fernandes et al., 2016) (*Table 5.4*).

The comparative values of trace element concentrations and trace element ratios are presented in *Table 5.5*. These greywackes have exceptionally high contents of Cr in comparison to the Archaean (3.5-2.5 Ga) greywackes (Condie, 1993). In contrast to this, the contents of Ba, Th, U, La, Ce, Sm, Yb, Lu, and ratios of Rb/Sr, Ba/Rb, Ba/Sr, Zr/Nb,  $La_N/Yb_N$  are marginally higher, and the contents of Sr, Nb, Pb, Eu and, the ratio of Th/U slightly lower. The contents of Ni, Rb, Zr, Nd and the ratio of  $La_N/Sm_N$  are comparable with the Archaean (3.5-2.5 Ga) greywackes (Condie, 1993). Note the N subscript refers to chondrite normalized concentrations (using values from Sun and McDonough, 1989). In comparison to the Archaean greywackes of Fig Tree, Barberton, South Africa (Toukeridis et al., 1999), the metagreywackes in this study have extremely high contents of Sr, Ba and marginally higher Nb, Zr, Th, U, La, Ce, Nd, Sm, Eu, Dy, Yb, Lu, Ba/Rb,  $La_N/Yb_N$  and  $La_N/Sm_N$ . They have much less Ni, marginally lower Rb, Pb, Rb/Sr, Th/U, and comparable Cr, Ho, Zr/Nb and Ba/Sr. My metagreywacke samples match fairly well with the greywackes from the Goa-Dharwar sector (Devaraju et al., 2010) (which includes greywacke with biotite, greywacke with chlorite-sericite and fine grained greywacke), greywacke from Merces (Widdowson, 2009), argillite and metagreywacke from Ribandar (Fernandes et al., 2016).

### **6.1.2 Tectonic setting and provenance**

As the framework grains of greywackes are liable to be modified with burial and metamorphism, one cannot infer tectonic settings and provenance type from the framework grains of the same (Bhatia and Crook, 1986). The major element geochemistry (Bhatia, 1983) along with immobile trace elements (La, Ce, Nd, Th, Zr, Nb and Ti) are most suited for provenance and tectonic setting determination (Holland, 1978). The immobile trace elements

are preferred because of their relatively low mobility during sedimentary processes and their low residence time in sea water (Holland, 1978).

I constructed tectonic discrimination plots using ratios of major oxides shown in *Fig. 6.3*. All the four diagrams have  $\text{Fe}_2\text{O}_3^{\text{T}}+\text{MgO}$  on the X-axis plotted against  $\text{Al}_2\text{O}_3/\text{SiO}_2$  (*Fig. 6.3a*),  $\text{TiO}_2$  (*Fig. 6.3b*),  $\text{K}_2\text{O}/\text{Na}_2\text{O}$  (*Fig. 6.3c*) and  $\text{Al}_2\text{O}_3/(\text{CaO}+\text{Na}_2\text{O})$  (*Fig. 6.3d*) on the Y-axis (After Bhatia, 1983; Banerjee and Bhattacharya, 1994). Bhatia and Crook (1986) envisaged four broad tectonic settings, the oceanic island-arc (OIA), the continental island-arc (CIA), the active continental margin (ACM) and the passive margin (PM) to describe the sedimentary fill of some Australian basins (*Table 6.1*). I have retained the same nomenclature here.

I have noted that, in all these diagrams that the metagreywacke samples in this study were laid down in a continental island-arc setting. This observation is corroborated by a positive correlation in Th vs La plot (after Bhatia and Crook, 1986) (*Fig. 6.4*), and the metagreywackes under study depict an average La/Th ratio of 2.43 that matches with the continental island arc value of  $2.4 \pm 0.3$  (Bhatia and Crook, 1986). There are other trace elements and their ratios that are a very sensitive pointer of tectonic settings (Bhatia and Crook, 1986); some of them are listed in *Table 6.2*. I observed from this table that, the tectonic settings of the metagreywackes under study compare very strongly with the continental island-arc and active continental margin setting. This interpretation also corroborates well with that of greywackes in Goa (Fernandes et al., 2016) and greywackes in the Goa-Dharwar Sector (Devaraju et al., 2010). Devaraju et al. (2010) suggested that the greywackes were formed by submarine weathering of felsic volcanics from a magmatic arc, and that they were deposited in a basin, which progressively changed from a passive to an active island arc-continental margin setting. Hegde and Chavadi (2009) and also concluded that the metagreywackes from Ranibennur were deposited in proximity of the arc in a continental island arc setting.

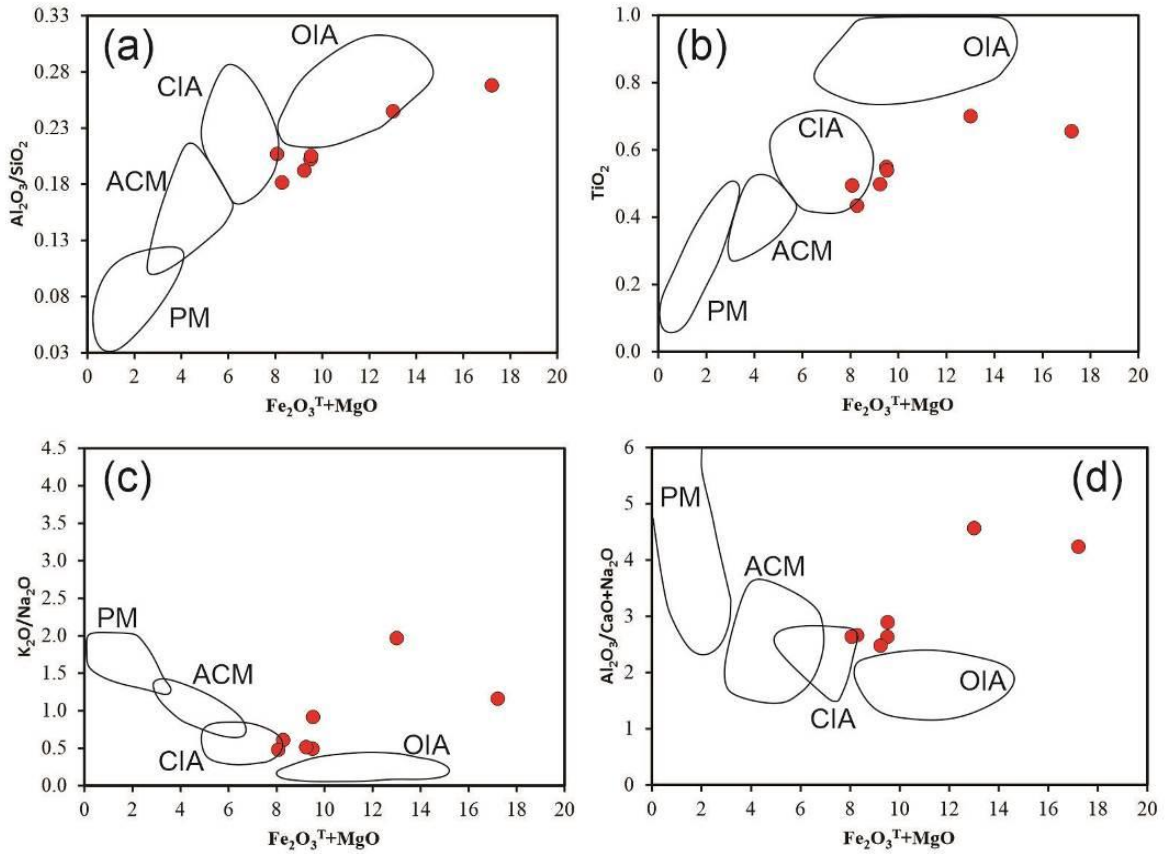


Fig. 6.3 Tectonic setting discrimination of the metagreywackes under study using  $Fe_2O_3^T + MgO$  vs (a)  $Al_2O_3/SiO_2$  (b)  $TiO_2$  (c)  $K_2O/Na_2O$  (d)  $Al_2O_3/(CaO+Na_2O)$  plots (after Bhatia, 1983; Banerjee and Bhattacharya, 1994). The fields denote: OIA-oceanic island-arc; CIA-continental island-arc; ACM-active continental margin; and PM-passive margin. The metagreywackes under study are represented by red circles with black border.

**Table 6.1** Plate tectonic classification of continental margins and oceanic basins (adopted from Bhatia and Crook, 1986)

Tectonic setting	Dominant depositional basin(s)	Nature of crust adjacent to basin	Provenance type	Modern example
Oceanic island arc	Forearc, back-arc	Oceanic island arc or island arc partly formed on thin continental crust	Undissected magmatic arc	Western North-Pacific Aleutians; Lesser Antilles; Marianas
Continental island arc	Apical inter-arc, back-arc, forearc	Island arc formed on well-developed continental crust or on thin continental margin	Dissected magmatic arc-recycled orogen	Havre Trough; Puerto Rico shelf; Cascades W. USA; Sea of Japan
Active continental margin	Retro-arc foreland; marginal basins, oblique-slip basins (sags, pull-aparts)	Thick continental margin; crystalline basement	Uplifted basement	N. Chile, Peru; S. California borderland
Passive margins	Major peri-cratonic depocenters on trailing edges Rifted continental margin (miogeosynclines and abyssal plains)	Normal continental crust Extended continental crust	Recycled and collision orogens Craton-interior	Bengal-Nicobar Fan and Nicobar Basin Atlantic Ocean

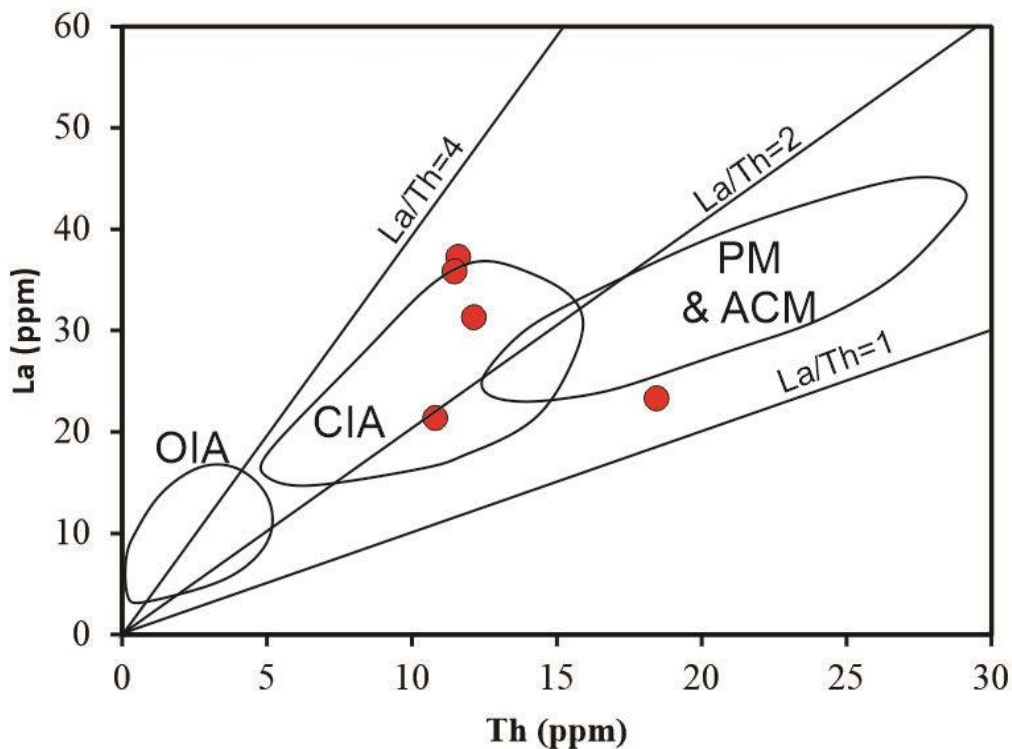


Fig. 6.4 Plot of Th vs La (after Bhatia and Crook, 1986) showing metagreywackes under study (red filled circles with black border) for their tectonic discrimination. The fields denote: OIA-oceanic island-arc; CIA-continental island-arc; ACM-active continental margin; and PM-passive margin. In this diagram, ACM and PM cannot be distinguished from each other.

**Table 6.2** Comparison of trace element characteristics of metagreywackes from the study area to other tectonic settings. Majority of the parameters used here are the most sensitive discriminator of tectonic setting (adapted from Bhatia and Crook (1986), Table 5)

Parameters	Metagreywacke under study	Oceanic Island Arc (OIA)	Continental Island Arc (CIA)	Active Continental Margin (ACM)	Passive Margin (PM)
Nb	9.96	2 ±0.4	8.5 ±0.8	10.7 ±1.4	7.9 ±1.9
Zr	152	96 ±20	229 ±27	179 ±33	298 ±80
Th	12.9	2.27 ±0.7	11.1 ±1.1	18.8 ±3	16.7 ±3.5
U	3.74	1.09 ±0.21	2.53 ±0.24	3.9 ±0.5	3.2 ±0.8
La	29.8	8.72 ±2.5	24.4 ±2.3	33 ±4.5	33.5 ±5.8
Ce	60.7	22.53 ±5.9	50.5 ±4.3	72.7 ±9.8	71.9 ±11.5
Pb	10.1	6.9 ±1.4	15.1 ±1.1	24 ±1.1	16 ±3.4
Nd	23.7	11.36 ±2.9	20.8 ±1.6	25.4 ±3.4	29 ±5.03
Rb/Sr	0.68	0.050 ±05	0.65 ±0.33	0.89 ±0.24	1.19 ±0.4
K/Th	1527	4055 ±1526	1296 ±250	1252 ±360	681 ±194
Th/U	3.42	2.1 ±0.78	4.6 ±0.45	4.8 ±0.38	5.6 ±0.7
La/Th	2.43	4.26 ±1.2	2.36 ±0.3	1.77 ±0.1	2.2 ±0.47
Zr/Nb	15.4	49.3 ±10.2	31.5 ±9.9	16.7 ±1.8	37.2 ±8

The REE are reliable provenance indicators, as they are considered to be transferred unfractionated into the sediment (Taylor and McLennan, 1985) and, therefore, reflect the average REE composition of the source material (McLennan, 1989). The chondrite normalised (values from Sun and McDonough, 1989) patterns of the metagreywackes under study (*Fig. 6.5*) are steep with LREE enrichment and HREE depletion, average  $La_N/Yb_N$  ratios of 10.25 being slightly higher than typical Archaean clastic sediments (e.g.  $La_N/Yb_N=6.8$ ; Toulkeridis et al., 1999), lower than argillites [ $(La_N/Yb)_N=15.5$ ; Fernandes et al., 2016], metagreywackes [ $(La_N/Yb)_N=13.47$ ; Fernandes et al., 2016] and are comparable with the greywackes in the Goa-Dharwar Sector ( $La_N/Yb_N=12.02$ , Devaraju et al., 2010). The La content varies from 90-157 times and the Yb content 10-14 times, from the chondrite values (*Fig. 6.5*). The average  $La_N/Sm_N$  ratios are 4.13, slightly higher than the ratios in the Archaean sedimentary rocks (e.g.,  $La_N/Yb_N=3.6$ ; Toulkeridis et al., 1999) lower than argillites ( $La_N/Sm_N=4.50$ ; Fernandes et al., 2016), metagreywackes ( $La_N/Sm_N=4.87$ ; Fernandes et al., 2016) and are comparable to the ratios in the greywackes in the Goa-Dharwar Sector ( $La_N/Sm_N=4.80$ , Devaraju et al., 2010). The  $Ce/Ce^*$  [ $Ce_N/(La_N^{2/3}*Nd_N^{1/3})$ ] is an indicator of Ce enrichment relative to the

smooth REE pattern. The Ce/Ce\* of the metagreywackes under study does not present significant anomalies and is 1.06, which is much lower than that of the greywackes in the Goa-Dharwar Sector (Ce/Ce\*=1.27; Devaraju et al., 2010). The greywackes also show a slight negative Eu anomaly which could be related to the Eu-depleted granitoids/felsic rocks in the source area.

The abundance of LILE, notably comparable Sr (94-204 ppm) and high Rb (75-103 ppm) with regard to Archean Upper Crustal Composition (AUCC) (Taylor and McLennan, 1985) points towards a granitic source. The Rb contents are similar to those of tonalites of the WDC (Jayaram et al., 1983). The average Th/U ratio of greywackes (3.42) is lower than that of Archaean (3.5-2.5 Ga) greywacke (Condie, 1993), Archaean greywackes of Fig Tree, Barberton, South Africa (Toukeridis et al., 1999) and that of AUCC (Taylor and McLennan, 1985). This ratio suggests a comparative enrichment of U in the greywackes (similar to Ranibennur metagreywackes; Hegde and Chavadi, 2009). Hence this ratio also points towards a provenance of K-rich granites, which the LILE data also supports.

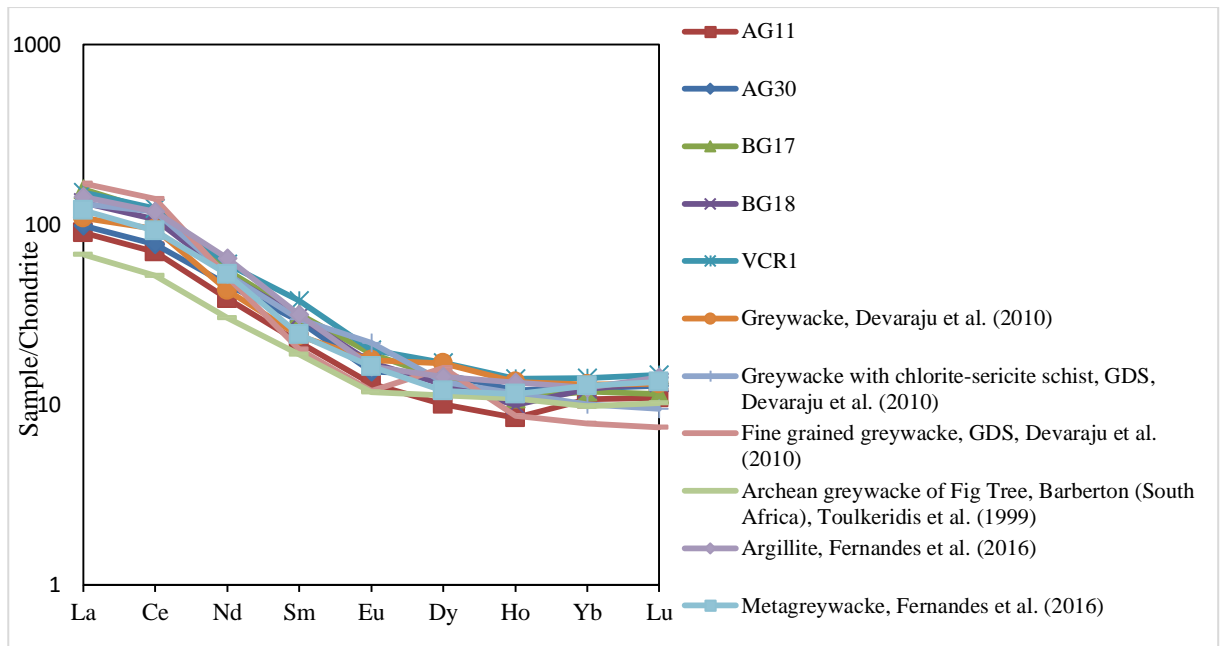


Fig. 6.5 Chondrite normalised REE patterns for the studied metagreywackes (individual samples are named). These values are compared with other localities as shown. Chondrite normalising values are from Sun and McDonough (1989).

I use the CaO-Na<sub>2</sub>O-K<sub>2</sub>O triangular plot (after Condie, 1967) to indicate the provenance rocks in the study area (Fig. 6.6). It is observed that the metagreywacke studied has affinities to felsic granodiorite and granite to quartz monzonitic source rocks. The presence of garnet in the source rock is also precluded owing to low MREE/HREE ratio (Dy/Yb = 1.39-1.82) (Jung et al., 2006).

To summarize, the provenance rocks that served the detrital material for the metagreywackes in the study area are felsic rocks which could be sourced from neighbouring granites (Quepem granitoid, Dudhsagar granitoid) or Vengurla granite (Chavadi, 1974) or rocks as old as Trondhjemite-Tonalite-Granodiorite basement rocks that are abundantly present in and around the study area. This observation is consistent with that made by Fernandes et al. (2016) and Armistead et al. (2018).

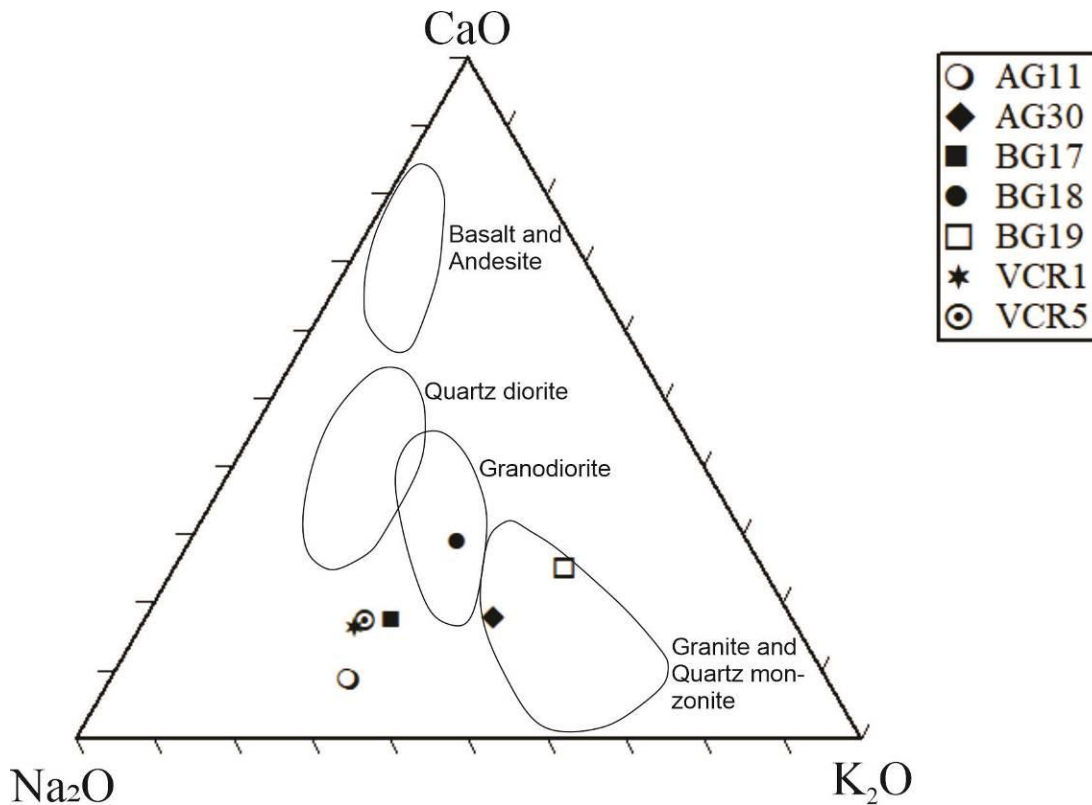


Fig. 6.6 CaO-Na<sub>2</sub>O-K<sub>2</sub>O triangular plot for the metagreywackes under study (legend displays the name of the samples) in relation to the compositional fields of common igneous rocks (after Condie, 1967).

## 6.2 Dykes

### 6.2.1 Crystallization Process

Olivine, clinopyroxene and plagioclase typically control tholeiitic fractionation trends. Since the highly compatible elements preferentially incorporate into mineral phases, they are good qualitative indicators of the extent of fractional crystallization (White, 2013). The Ni content in some Group 1 dykes, namely, AG-23, -41 and BG-11, is >200 ppm, whereas the Cr content for the same samples is >400 ppm which perfectly matches the values expected for primary melts (Song et al., 2008; Lai et al., 2012), with the SiO<sub>2</sub> contents marginally exceeding 50 wt. % limit for such mantle rocks (Wilson, 1989). Crystal accumulation is present only in BG-11 (refer to *Section 4.2.3*). The Group 2 dykes are characterised by low concentrations of compatible trace elements such as Ni (59-133 ppm), which supports that they are not primary

magmas, but instead, they have experienced olivine fractionation on their way up to the surface (Thompson et al., 1984; Wilson, 1989). In the mafic rocks, Co and Ni occupy the octahedral coordination sites in olivine (Wilson, 1989) and both these elements enter together, albeit Co being less frequently (Burns and Fyfe, 1966). Therefore during magmatic differentiation, it is expected that these elements should exhibit similar geochemical behaviour. When I plotted Co vs Ni (*Fig. 6.7a*), I observed that there is an increase in Ni commensurate with increasing Co in both the Groups of dykes, albeit with different slopes. Hence, I infer that in both the Groups, they acted like a couple and entered in a single mineral phase.

To quantify the clinopyroxene fractionation process, I plotted the Cr/Ni ratio against their CaO/Al<sub>2</sub>O<sub>3</sub> ratios (*Fig. 6.7b*). I observed two opposing trends, Group 1 showing a positive trend and Group 2 showing a negative trend. Positive trends reflect clinopyroxene fractionation responsible for Cr variation in Group 1 dykes (89-1429 ppm) while the negative trend reflects olivine fractionation instead of clinopyroxene for Group 2 dykes. In thin sections, the dykes of Group 1 with highest CaO/Al<sub>2</sub>O<sub>3</sub> have the highest Cr/Ni ratio, subsequently, have clinopyroxene phenocrysts accompanied by altered olivine (*See sec. 4.1.3*). With decreasing Cr/Ni, clinopyroxene fractionates and the rocks are more abundant in plagioclase (*Fig. 4.6d*). On the other hand, Group 2 dykes mostly show altered olivine to iddingsite/palagonite phenocrysts, occasionally fresh, and rich in clinopyroxene and plagioclase attesting to olivine fractionation (*Fig. 4.1b; 4.3a-b*).

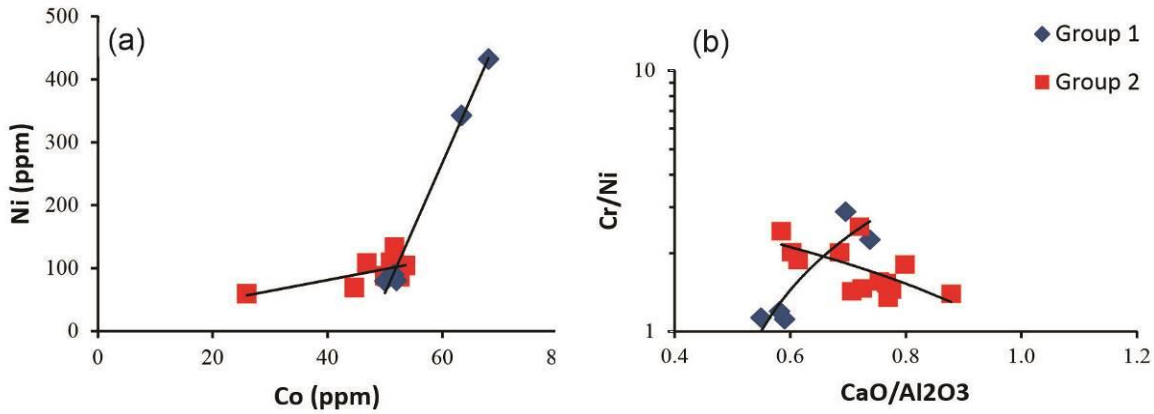


Fig 6.7 (a) Co vs Ni (ppm) binary diagram for both Groups of dykes. (b) CaO/Al<sub>2</sub>O<sub>3</sub> vs Cr/Ni for both Groups of dykes.

CaO/Al<sub>2</sub>O<sub>3</sub> ratio is a significant characteristic of mafic rocks since in the primary melts, it reflects the ratio of their mantle source (Cawthorn and Strong, 1974; Perfit et al., 1980). All of the values in the dykes studied (0.6-0.9) are lower than chondrite or primitive upper mantle value (0.9; Sun and McDonough, 1989). The relationship between the CaO/Al<sub>2</sub>O<sub>3</sub> ratio and TiO<sub>2</sub> contents of all the dykes is shown in Fig. 6.8. The CaO/Al<sub>2</sub>O<sub>3</sub> ratio increases with plagioclase removal, whereas it remains constant during olivine fractionation (Dungan and Rhodes, 1978). From Fig. 6.8, it is evident that all dykes show a olivine removal trend.

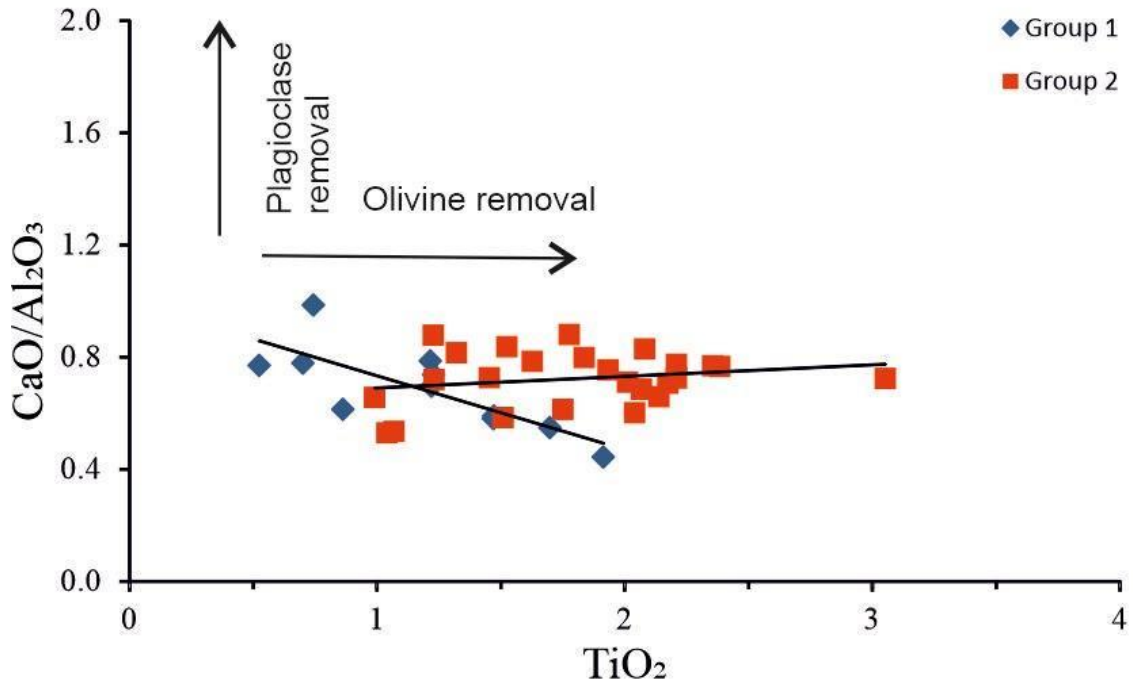


Fig 6.8  $\text{TiO}_2$  versus  $\text{CaO}/\text{Al}_2\text{O}_3$  variation diagram (after Dungan and Rhodes, 1978) showing relative olivine fractionation in both the groups of dykes.

The MgO content is considered a suitable index of differentiation for these dykes due to the restricted range of their  $\text{SiO}_2$  content (Cox et al., 1979; Wilson, 1989). I have used the variation plots of major element oxide variations versus the MgO content to decipher the nature of the evolution of magma in turn controlled by the crystallisation of the constituent mineral phases. As mentioned earlier, all the plots contain the Groups as a whole instead of their subgroupings. Fig. 6.9 depicts variations of major oxides with MgO on the X-axis. The wide change in MgO content of Group 1 dykes points towards the presence of a range of parental liquids in various melting conditions.

The CaO concentrations of Group 2 in Fig. 6.9a have correlated positively with MgO content suggesting crystal-liquid control by clinopyroxene and plagioclase during crystal fractionation (Wilson, 1989). The Group 1 Type 1 dykes indicate clinopyroxene and plagioclase fractionation control owing to their low CaO values, whereas Type 2 dykes show

a CaO enrichment with decreasing MgO content that collectively points towards olivine fractionation. As seen from Al<sub>2</sub>O<sub>3</sub> variation (*Fig. 6.9b*), the Group 1 and Group 2 dykes depict a progressive increase in Al<sub>2</sub>O<sub>3</sub> content with decreasing MgO suggesting the absence of significant plagioclase fractionation similar to Karoo and Emeishan flood basalts (Wilson, 1989; Song et al., 2001; 2008). The variation of SiO<sub>2</sub> content (*Fig. 6.9c*) for Group 1 types shows a scatter but for Group 2 dykes, the trend is more or less towards increasing SiO<sub>2</sub> content with decreasing MgO content again pointing towards olivine-clinopyroxene fractionation (Wilson, 1989). There is a concurrent rise in Na<sub>2</sub>O, K<sub>2</sub>O and P<sub>2</sub>O<sub>5</sub> with decreasing MgO (*Fig. 6.9d-f*) in both the Groups of dykes indicating that these elements are progressively enriched in the residual liquids during fractional crystallization (Cox et al., 1979). The variation of Fe<sub>2</sub>O<sub>3</sub><sup>T</sup> versus MgO shows that one dyke (BG11) has the effect of olivine accumulation in its evolutionary history. Lastly, the trend of decreasing CaO/Al<sub>2</sub>O<sub>3</sub> with decreasing MgO content owes its reason to the importance of plagioclase and clinopyroxene as a fractionating phase in both the Groups of dykes. In summary, it is amply clear that the fractional crystallization process applicable for both the Groups of dykes shows a typical tholeiitic lineage with an iron enrichment trend.

In summary, the dykes belonging to both the Groups show typical tholeiitic lineage with few exceptions. The low-MgO varieties in the Group 1 dykes show characteristics similar to most of the Group 2 dykes; however, they are more abundant in alkalis compared to the Group 2. The high-MgO varieties of Group 1 dykes provide evidence of having olivine crystallisation (*Fig. 6.9a and g*) over their evolutionary history. This partly conforms to the observation of the presence of abundant clinopyroxene and olivine phenocrysts in these rocks (*Fig. 4.8a-c*). These rocks (Group 1) have plagioclase restricted to the groundmass phase. The Group 2 dykes show geochemical evidence of clinopyroxene and plagioclase fractionation that controlled their evolutionary history.

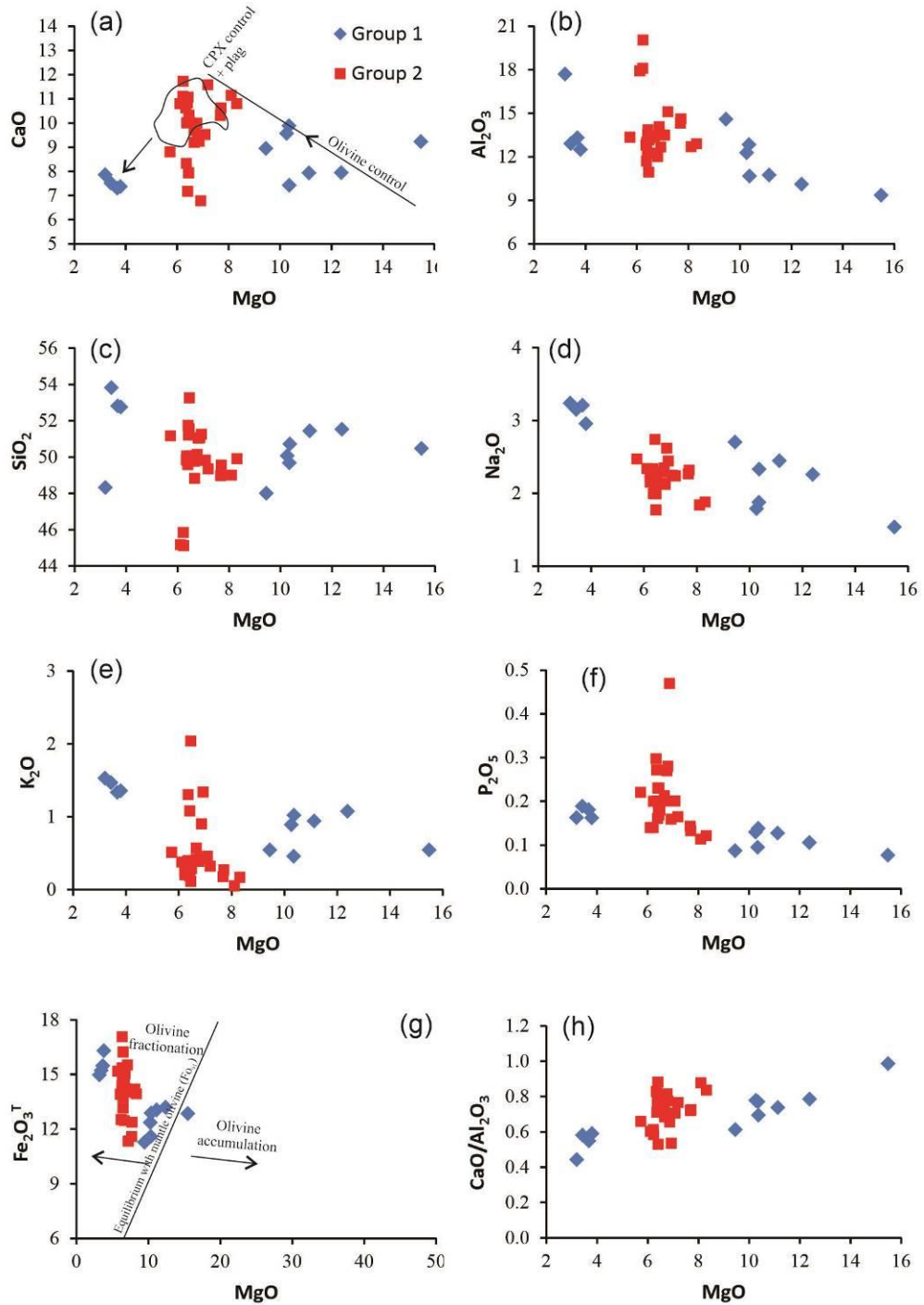


Fig. 6.9 (a) to (g) Variation of major elements with respect to MgO in both the Groups of dykes. The legend is displayed in (a) and is applicable to all the plots. The marked field in (a) is for the Deccan Traps. (h) Variation of MgO vs CaO/Al<sub>2</sub>O<sub>3</sub>.

Fig. 6.10a-w plots the trace element concentrations vs MgO. In the MgO versus Ni, Cr and Co diagrams (Fig. 6.10a-c), though there is wide scatter in Group 1 dykes, they generally

exhibit a decrease in the concentration of these elements with decreasing MgO. This indicates extensive fractionation of olivine and pyroxene in these dykes. However, a distinct reverse trend as compared to Group 1, of increasing concentrations of these elements with decreasing MgO is seen in Group 2 dykes. Barium and Sr concentrations (*Fig. 6.10d-e*) in Group 1 dykes both increase with decreasing MgO. In Group 2 dykes, Sr concentration also increases with decreasing MgO, but Ba concentrations show more scatter. Rb concentrations (*Fig. 6.10f*) show a gradual increase in Group 1, but decreases in Group 2 with decreasing MgO. The variation patterns of Zr, Nb, Y, Hf, Th and REE are plotted versus Mg#. All these elements depict increasing patterns with decreasing Mg#, and this is concomitant with typical magmatic fractionation. Ba, Sr and Hf show positive correlation when plotted against Zr, and it points towards plagioclase crystallisation in the early history of both the groups of dykes (*Fig. 6.11a-c*). Lastly, Sc/Y is plotted against MgO, which points towards significant clinopyroxene fractionation in Group 1 dykes in the history of their evolution (*Fig. 6.11d*).

In summary, decreasing concentrations of Cr, Ni and Co with decreasing MgO indicates fractionation of olivine and pyroxene in the Group 1 dykes. This is manifested by the abundance of clinopyroxene and olivine phenocrysts in the high-MgO dykes as studied in petrography. The increasing relationship of Ba, Sr and Hf with increasing MgO is commensurate with normal fractionation-controlled magmatic evolution. Clinopyroxene causes lowering in CaO over Al<sub>2</sub>O<sub>3</sub> at high pressures (Schilling et al., 1983) (*Fig. 6.10h*) but a similar trend can result from plagioclase accumulation (le Roex et al., 1996). Plagioclase accumulation can be possible for Group 2 dykes since these are phyrlic and contain phenocrystal plagioclase, as well as in the groundmass, while in the Group 1 dykes, plagioclase is restricted to the groundmass. MgO vs Sc/Y plot is used to further quantify clinopyroxene fractionation as Sc and Y have similar distribution coefficients in plagioclase and olivine but Sc is compatible in augite and Y is not (Mattsson and Oskarsson, 2005). Hence, a decreasing

trend of Sc/Y with decreasing MgO in Group 1 dykes points towards clinopyroxene fractionation, whereas significant clinopyroxene fractionation did not take place in Group 2 dykes.

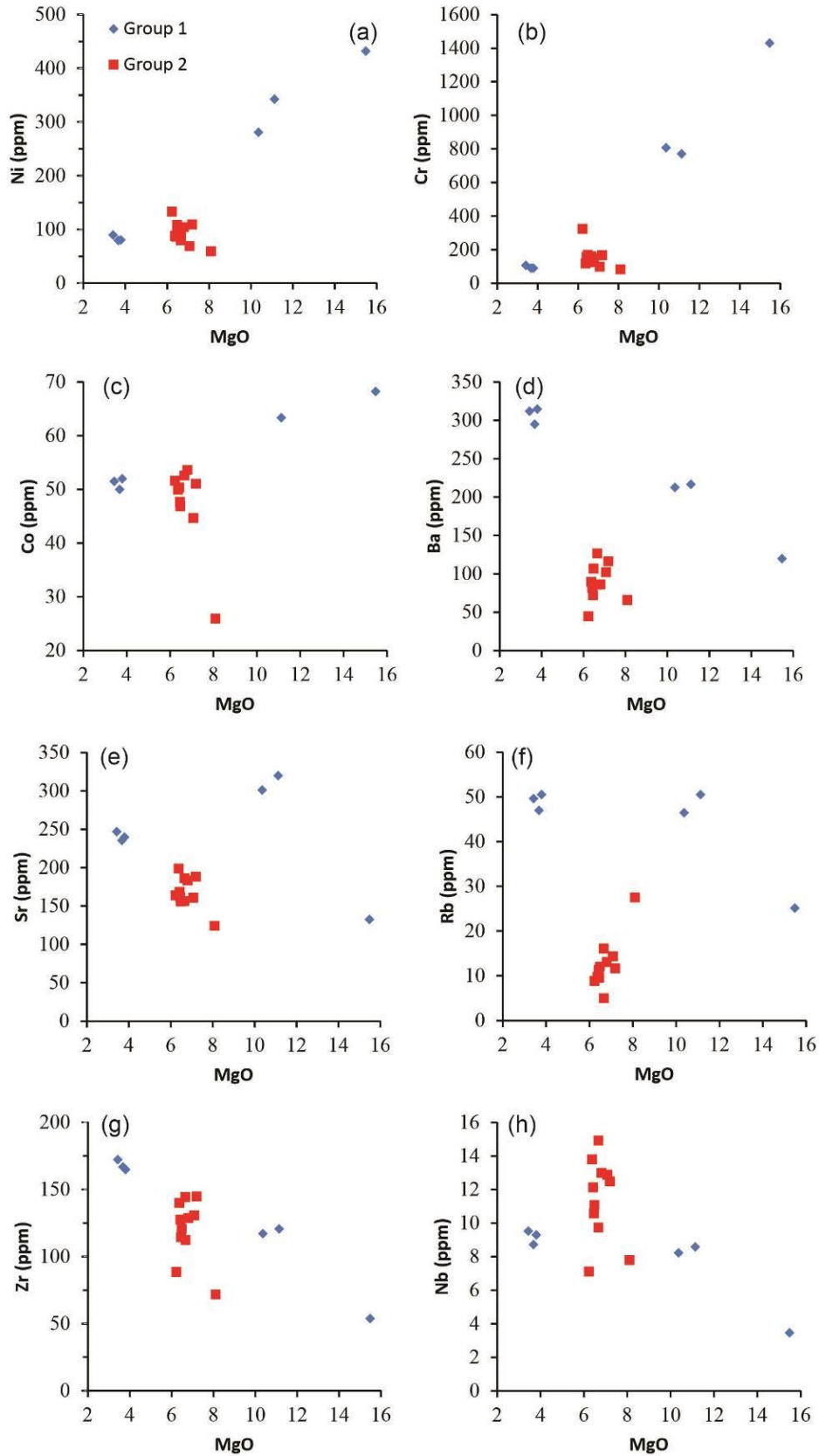


Fig. 6.10 Variations of trace elements and the REE's with respect to MgO for both the Groups of dykes. The legend is shown in (a) and is applicable to all the plots from b-w.

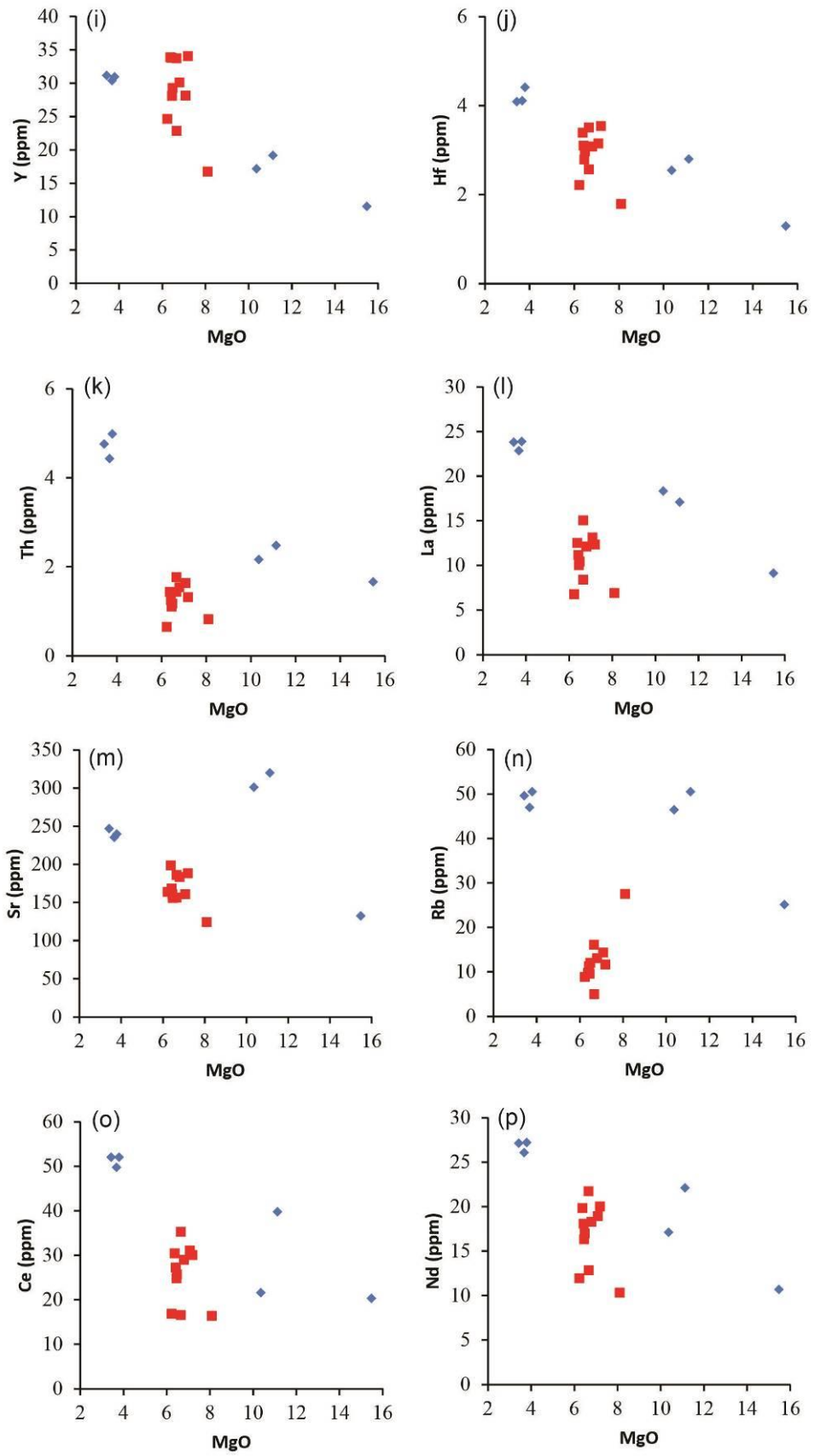


Fig. 6.10 continued...

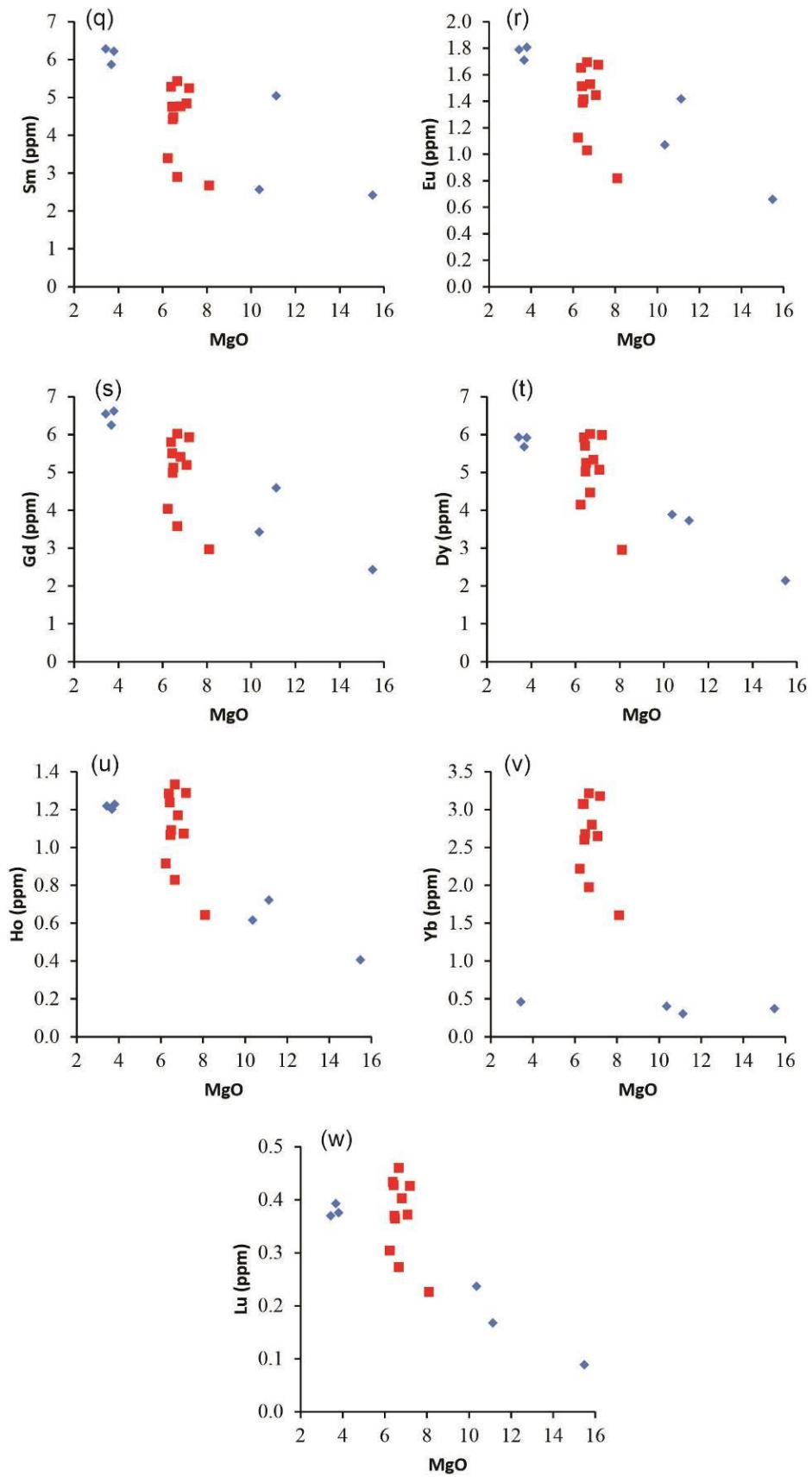


Fig. 6.10 continued...

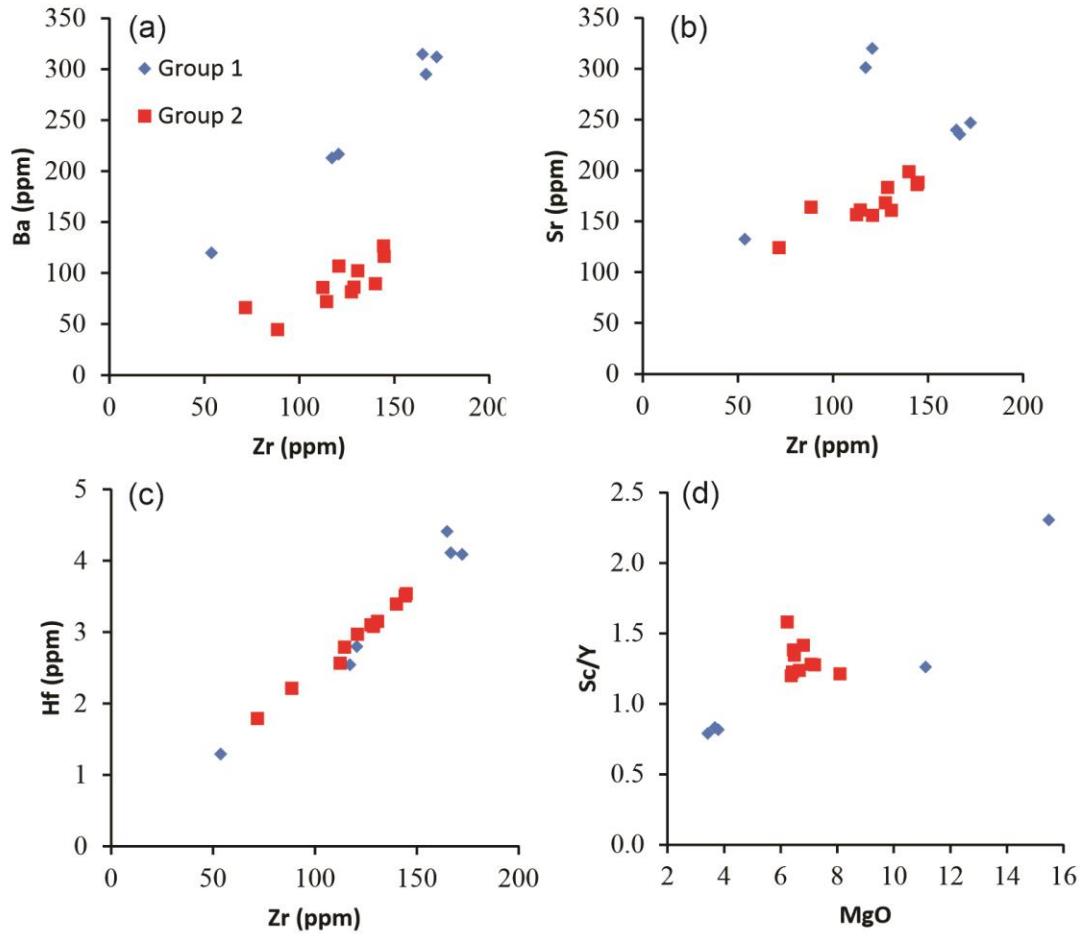


Fig. 6.11 Variations of (a) Ba, (b) Sr and (c) Hf with respect to Zr. (d) Variation of Sc/Y vs MgO. The legend for symbols is shown in (a) and is applicable to b, c and d.

### 6.2.2 Mantle source characteristics and Tectonic implications

Incompatible trace element ratios (as opposed to absolute abundances) are usually insensitive to fractional crystallization and partial melting processes, especially if they are of a similar incompatibility (White, 2013). In the case of larger degrees of melting, the ratios of two incompatible elements in a magma will be similar to their ratio in the magma source, as long as the magmas are not contaminated; for this reason, ratios of elements are preferred to their absolute abundances (White, 2013). Trace element ratio plots constrain mantle source characteristics (Rollinson, 1993; Condie, 2005). However, as much as it is feasible, plotted

ratios should not have an element in common, as this may produce spurious correlations (Rollinson, 1993).

Based on these considerations, to decipher the tectonic setting of the dykes, I use the immobile element plot of Zr vs Zr/Y (*Fig. 6.12*), following Pearce and Norry (1979). The parameters used in this diagram are effective in discriminating between various tectonic fields. Majority of the Group 1 and Group 2 dykes plot in within plate basalts field, except few samples in MORB (AG-9 and BG-20) and BG-13, AG-23, BG-11 plotting outside the fields (have less Zr). I observe here that this diagram does not differentiate between Group 1 and 2 dykes, concurrent with other examples plotted (*Fig. 6.12*). Majority of the dykes from Kalyadi (Chandrasekharam et al., 2008), the Goa-Dharwar Sector (Devaraju et al., 2008), those dykes in Goa (Widdowson et al., 2000; Fernandes et al., 2016), the Desur Formation (Hegde et al., 2014) and the Deccan formations (Ambenali, Poladpur and Mahabaleshwar) (Vanderkluyzen et al., 2011) plot in within plate basalt and MORB setting with few exceptions. The dyke from Dandeli (French and Heaman, 2010) has a mixed character of island arc basalt and MORB.

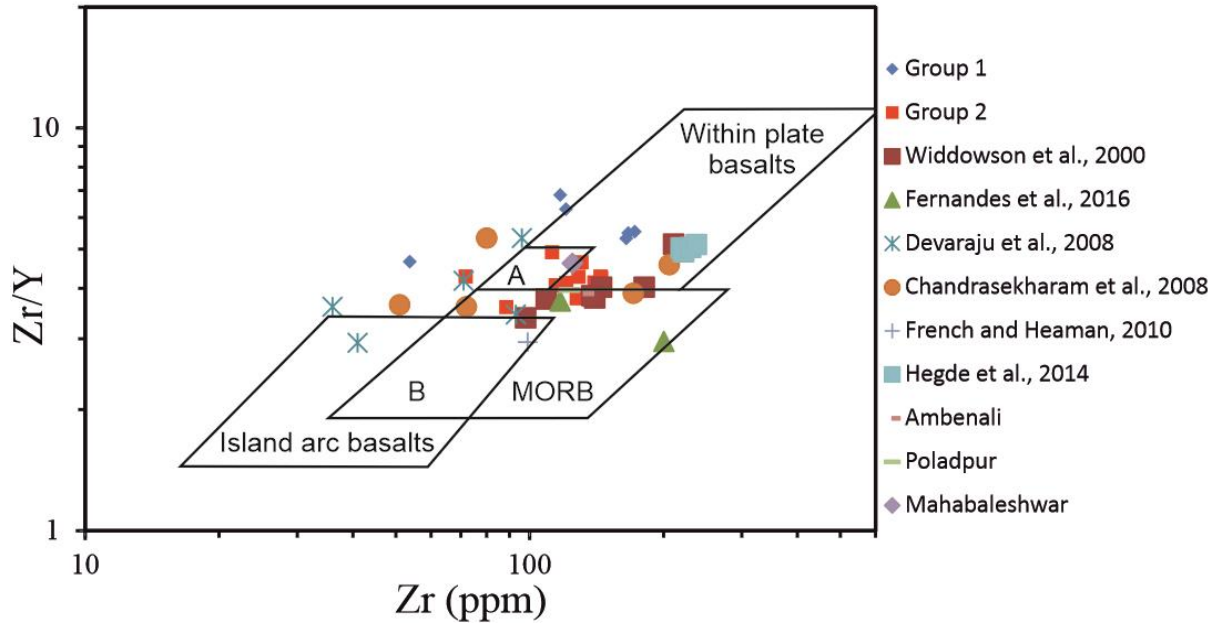


Fig. 6.12 A plot of Zr (ppm) vs Zr/Y that shows majority of Group 1 and 2 dykes restricted to within plate basalt setting (after Pearce and Norry, 1979). Field A: MORB and within plate basalts, B: MORB and island arc basalts. MORB: Mid Ocean Ridge Basalt.

Fig. 6.13a shows Primitive mantle (PM)-normalized multi-element patterns for the incompatible trace element abundances in Group 1 dykes. The element contents are normalized using PM values from Lyubetskaya and Korenaga (2007). In terms of the abundances of LILE, the dyke samples studied depict positive Rb and negative Sr, P anomalies while a flat pattern exists at Ba and K. The HFSE pattern of all dykes illustrates strong negative anomaly at Nb while only one dyke analysed for Ta shows Nb-Ta trough. There is a strong positive anomaly at Pb while Zr, Hf, Th and U show flat patterns. Minor troughs for Tm and minor peaks for Yb are also evident. The plot also shows relative enrichment of LREE with those of HREE. Also plotted for comparison (Sun and McDonough, 1989) are N-MORB, E-MORB, OIB and Upper Continental Crust (UCC) (Rudnick and Gao, 2013) patterns. Group 1 dykes show a pattern more akin to UCC.

Fig. 6.13b shows PM-normalised multi-element pattern for the incompatible trace element abundances for Group 2 dykes. Group 2 dykes depict positive anomaly for Rb (except

AG-24) amongst the LILE. In contrast, the dykes display negative anomaly for P, Sr and K (BG-13 shows very prominent K anomaly). The HFSE pattern for Nb, Ta, Zr, Hf, Pb, Y and U is flatter with slight positive anomalies at Th (except BG-13 and VG-1). Positive anomalies for Ti, Nd and Yb are also very evident. The plot also shows relative enrichment of LREE with that of HREE. Also plotted for comparison (Sun and McDonough, 1989) are N-MORB, E-MORB and OIB, and it is found that Group 2 dykes are akin to E-MORB.

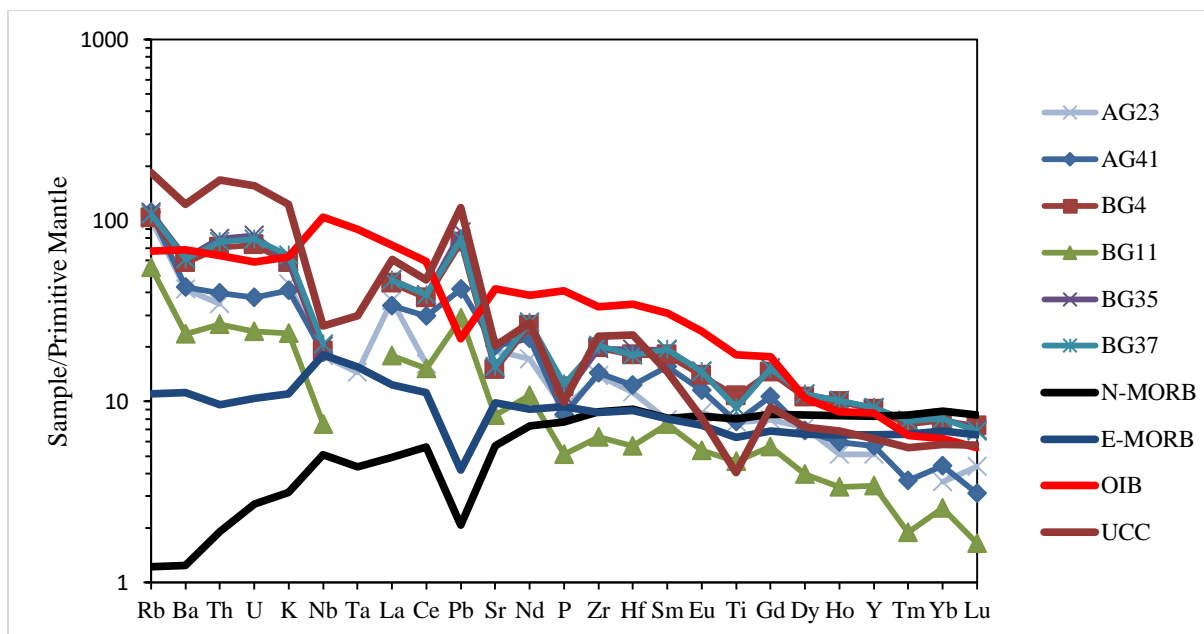


Fig. 6.13a Primitive mantle normalized multi-element diagram for Group 1 dykes. Normalization values are from Lyubetskaya and Korenaga (2007).

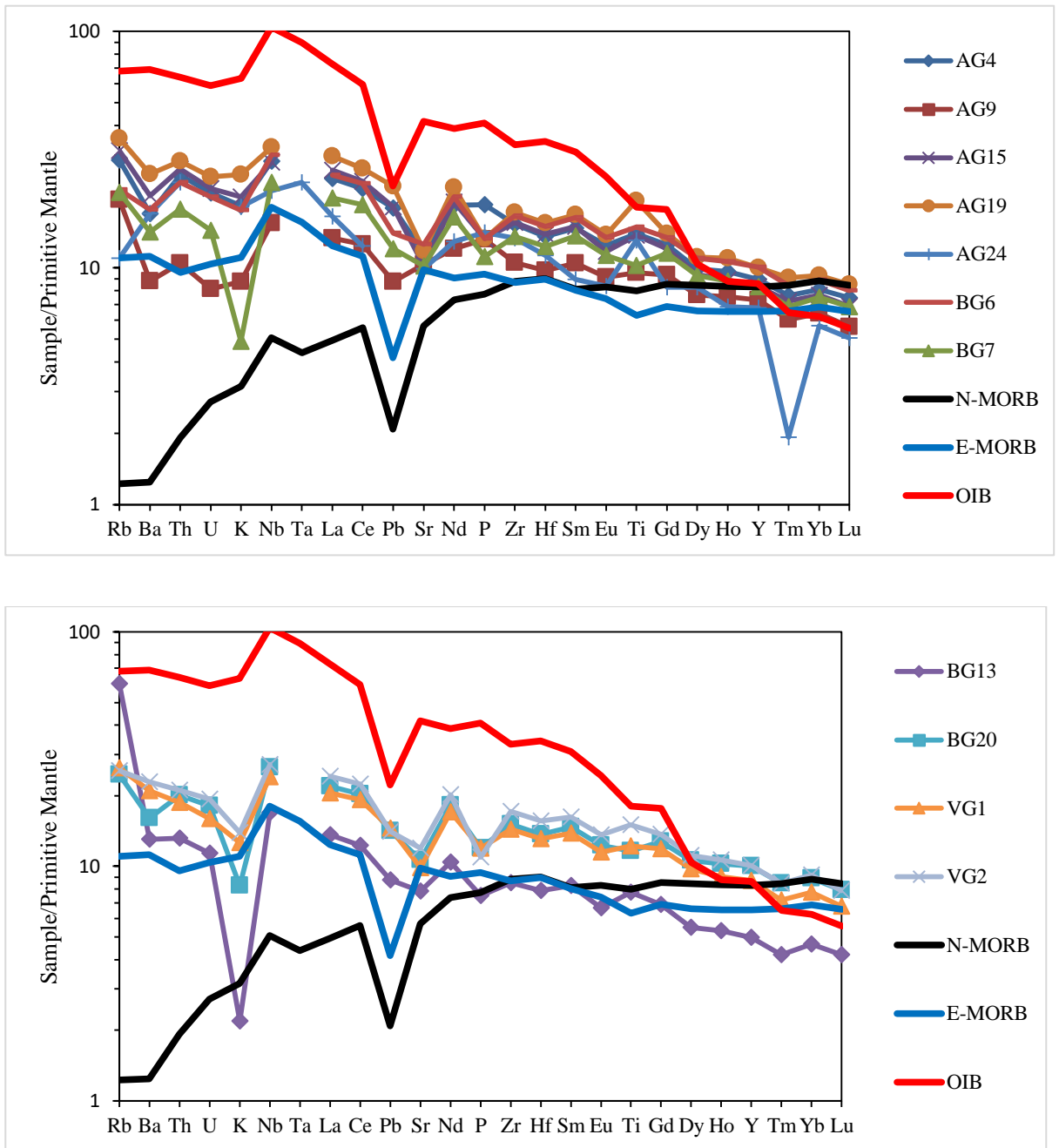


Fig. 6.13b Primitive mantle normalized multi-element diagram for Group 2 dykes (the samples have been split here between two panels for simplicity). Normalization values are from Lyubetskaya and Korenaga (2007).

Fig. 6.14a-b show Chondrite normalized REE patterns (Fig. 6.14a) (Sun and McDonough, 1989) for both groups of dykes. Both the groups of dykes show a prominent LREE enrichment. Dykes from both the Groups show negligible Eu anomalies ( $\text{Eu}/\text{Eu}^*$  of

0.83 to 1.10; avg. 0.90 for Group 1) (*Table 5.8b*) ( $\text{Eu}/\text{Eu}^*$  of 0.89 to 0.98; avg. 0.91 for Group 2) (*Table 5.9b*) on a chondrite-normalized REE diagram. This indicates that there is little plagioclase fractionation in these three dykes. The LREE/HREE fractionation can be quantified by  $(\text{Ce}/\text{Yb})_N$  values, the range for Group 1 dykes (4.81-7.26) is higher than that for Group 2 dykes (2.10-3.26), thereby suggesting pronounced LREE/HREE fractionation for Group 1 and moderate fractionation for Group 2. Similarly, the  $(\text{La}/\text{Sm})_N$  ratio quantifies LREE/MREE fractionation; this ratio ranges from 2.19-4.60 for Group 1 and 1.29-1.87 for Group 2 further attesting that Group 1 dykes show strong LREE/MREE fractionation. In contrast, Group 2 dykes show moderate LREE/MREE fractionation.

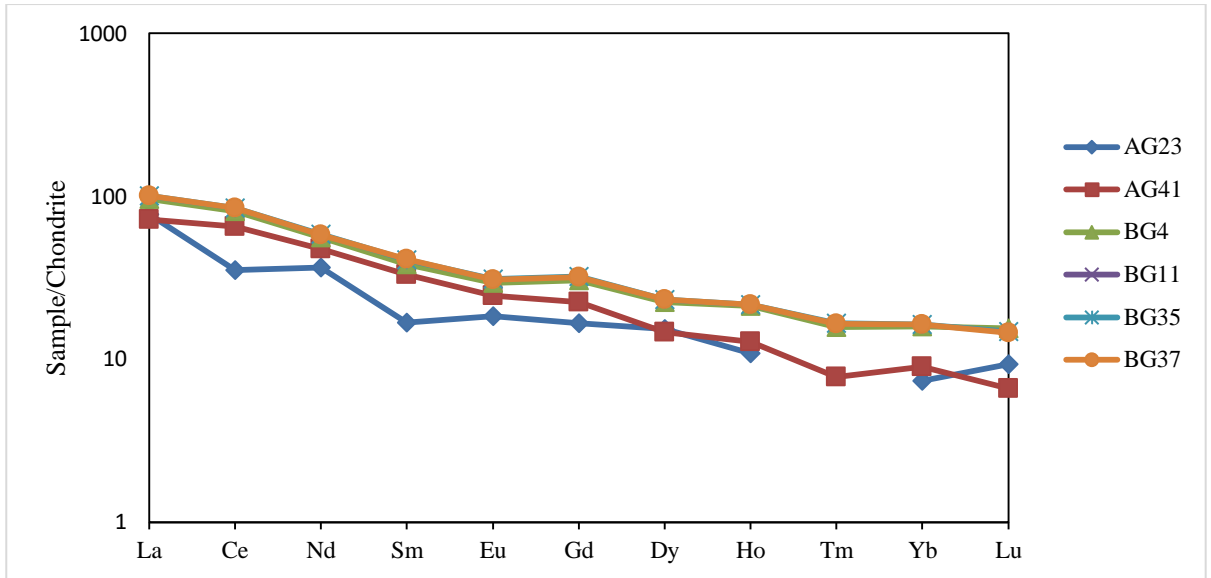


Fig. 6.14a Chondrite normalized multi-element diagram for Group 1 dykes. Normalizing values are from Sun and McDonough (1989).

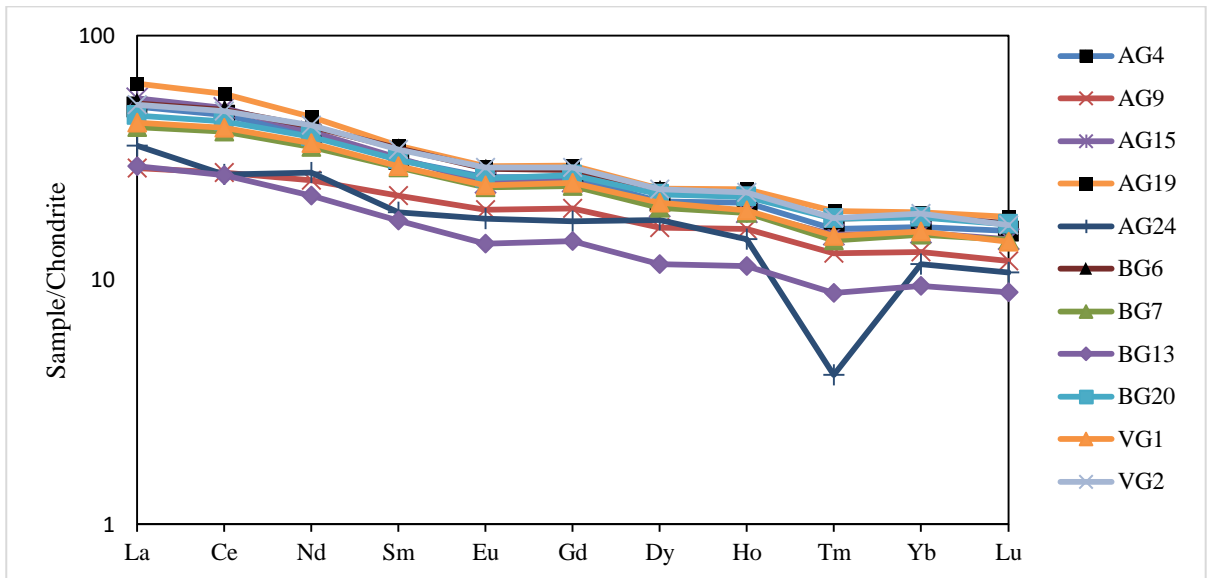


Fig. 6.14b Chondrite normalized multi-element diagram for Group 2 dykes. Normalizing values are from Sun and McDonough (1989).

Under normal conditions, the magmatic evolution for CFB's takes place under a lithospheric lid, and the subsequent magma batches interact with the lithospheric mantle during the evolution of the magma chamber and the travel of magma up to the surface. Hence, owing to the contamination of plume melts derived from continental crust and/or lithospheric

mantle, these CFB magmas have a much greater scatter in their REE profiles (Lassiter and DePaulo, 1997). Such type of scatter is noted in the Bushe lavas of Deccan Traps as opposed to the least contaminated Ambenali lavas (Peng et al., 1994). A manifestation of this type of contamination in CFB is the depletion in HFSE, particularly Nb and Ta relative to other similarly incompatible elements (Lassiter and DePaulo, 1997).

The normalized trace element diagrams for both groups reveal the enrichment pattern of LREE whereas there is depletion of the HREE. The strong negative anomalies at Nb, Ti and P and positive anomalies at Pb for Group 1 dykes which are absent for Group 2 is a very significant feature. A strong negative anomaly for Ta for one sample in Group 1 is also essential. Nb and Ta are insoluble and highly incompatible in the presence of water (White, 2013). Therefore, owing to their immobility during weathering and metamorphism, these elements are regarded as extremely useful in studying ancient environments in which the rocks were formed (White, 2013). Though depletion in Nb is a diagnostic feature of subduction-related volcanism (White, 2013), a strong crustal contamination process seems more plausible owing to a very close fit for UCC multi-element pattern. Also, the trough at Ti hints at crustal contamination (Carlson, 1991; Peate, 1997; Ewart et al., 2004). Hence, the magma of Group 1 dykes is likely to have been affected by crustal contamination.

Asthenospheric mantle melts that have erupted in ocean basins have Nb/Th ratios close to, or greater than, the PM value of 8, whereas the continental crust, and all arc related magmas, are enriched LREE with Nb/Th < 8 (Sun and McDonough, 1989; Rudnick and Gao, 2013; Manikyamba and Kerrich, 2012). The Group 1 dykes do show an enriched LREE with Nb/Th < 8 (0.2-3.8), whereas the majority of Group 2 dykes show Nb/Th > 8 (6.8-10.9). The Nb/Th ratio is considered robust in determining the mantle source areas (Kerrich and Xie, 2002; Said et al., 2012; Jowitt and Ernst, 2013; Ernst, 2014).

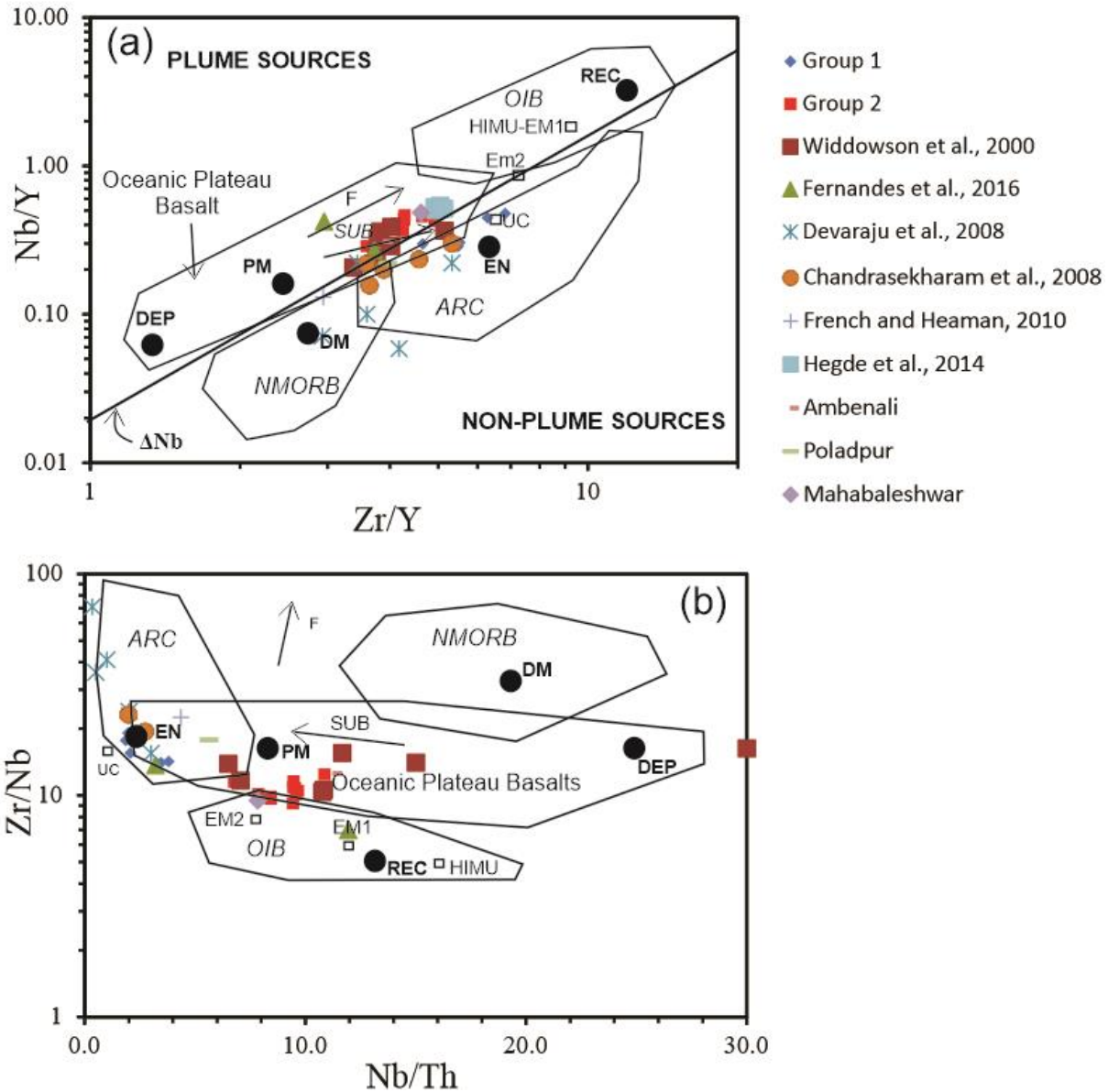


Fig. 6.15 Diagram showing mantle compositional components and fields for basalts from various tectonic settings (a) Zr/Y-Nb/Y and (b) Nb/Th-Zr/Nb. Arrows indicate the effects of batch melting (F) and subduction (SUB). Abbreviations: UC, upper continental crust; PM, primitive mantle; DM, shallow depleted mantle; HIMU, high mu (U/Pb) source; EM1 and EM2, enriched mantle sources; ARC, arc-related basalts; NMORB, normal ocean ridge basalt; OIB, oceanic island basalt; DEP, deep depleted mantle; EN, enriched component, REC, recycled component. References: Weaver (1991), Condie (2003).  $\Delta Nb = 1.74 + \log(Nb/Y) - 1.92\log(Zr/Y)$  (Fitton et al., 1997).

I consider four ratios of HFSE to constrain mantle sources of the dykes studied (Condie, 2005). Nb/Th vs Zr/Nb and Zr/Y vs Nb/Y are the ratio-ratio plots used for the dykes of Goa (Fig. 6.15a-b). Out of these four ratios, insensitivity to the degree of melting of garnet

lherzolite is shown only by the ratios of Nb/Th, restricting only tholeiites to be plotted on these ratio diagrams (Condie, 2005). The  $\Delta\text{Nb}$  line is a robust measure of separating the plume from non-plume basaltic sources (Condie, 2005). When the dyke data are plotted on the diagram (*Fig. 6.15a-b*), the Group 1 dykes plot below the  $\Delta\text{Nb}$  line in ARC field (close to UC value) in *Fig. 6.15a* and the same dykes plot in overlapping field of oceanic plateau basalts and ARC (close to EN and UC value) in *Fig. 6.15b*. It points towards either involvement of subduction zone induced fluids or they represent plume-derived basalts that have been contaminated by continental crust and/or subcontinental lithosphere. This diagram also hints at the non-plume source for Group 1 dykes. They have a significant contribution from the enriched component (EN). At least some of the EN contribution appears to have come directly from contamination by upper continental crust; while the Group 2 dykes, plot mainly above the  $\Delta\text{Nb}$  line (Fitton et al., 1997) in the Oceanic Plateau Basalt field thereby hinting at their plume source.

HFSE and REE being, to some degree, resistant to alteration can be successfully used to distinguish different possible melt sources and mantle-borne characters of basalts (Erlank and Kable, 1976; Pearce and Norry, 1979; Le Roex et al., 1983). The enrichment or depletion characters of the mantle source for the coastal dykes of Goa (relative to a primitive mantle reference) have been assessed in terms of HFSE concentrations and HFSE/HFSE ratios (c.f. Pearce and Parkinson, 1993; Pearce, 2008).

The average content of Nb in Group 1 dykes is 7.9 (Range: 3.5-9.5) whereas it is 11.4 in Group 2 (Range: 7.1-14.9). The average Zr content in Group 1 dyke is 132 (53-172) and 120 in Group 2 (71-144). Hence, the concentrations of Nb and Zr in both the groups of dykes are higher than that of N-MORBs (Nb = 2.33 ppm, Zr = 74 ppm) and lower than OIBs (Nb = 48 ppm, Zr = 280 ppm), implying their generation from a mantle source enriched in incompatible elements relative to estimates of the primitive mantle (Sun and McDonough, 1989). The average Zr/Sm for Group 1 is 29 (Range: 22.2–45.5) and 28 in Group 2 (Range:

26–39) is higher than that of primitive mantle (Zr/Sm: 25) (Frey et al., 1980; Menzies et al., 1991). This ratio corroborates an enriched mantle affinity of the dykes investigated from both groups.

The ratio of Zr/Ba can be considered as a useful parameter to distinguish lithospheric sources (Zr/Ba: 0.3-0.5) from asthenospheric sources (Zr/Ba: >0.5) of the parent melt (Menzies et al., 1991; K rk ođlu, 2010). In my study, the average Zr/Ba ratio of Group 1 dykes at 0.53 (Range: 0.45-0.56) coupled with high Zr/Hf ratio (37-46), points towards an average asthenospheric source, but with a mild lithospheric component. The average value of Zr/Ba for Group 2 dykes is 1.39 (Range: 1.1-1.99) coupled with high Zr/Hf ratio (40-43), clearly indicating the asthenospheric mantle source in the melting process. The Nb/U ratio provides additional evidence to the source of magmas: it is  $47 \pm 10$  for MORBs,  $25 \pm 5$  for OIBs, 30 for PM, and 10 for CC (Condie, 2001). The average ratio of Group 1 dykes is 8.4 (Range: 6.5-13.2) that is close to CC while the ratio of Group 2 is 39 (Range: 34-50) that is close to MORB affinity. Incidentally, the Nb/U ratio of Group 1 dykes is similar to Bushe lavas (Nb/U: 6.7; Vanderkluysen et al., 2011), indicating the possibility of crustal contamination for Group 1 dyke magmas. I do consider here the mobile nature of U during alteration processes, and hence Nb/U is only an indicative ratio.

Specific critical trace element ratios like Zr/Nb, La/Nb, Ba/Nb, Ba/Th, Rb/Nb, K/Nb, Th/Nb, Th/La and Ba/La maintain distinctive values corresponding to different mantle sources and provide fruitful constraints on the mantle source components (Weaver, 1991) (*Table 6.3*). On a general note, there are three end member compositions for OIB magmas i.e. HIMU, EM 1 and EM 2 (Zindler and Hart, 1986; Weaver, 1991). The best proxies for these end members are isotopes, but some general comments can be made based on trace elemental studies. HIMU has significant relative enrichment of highly incompatible HFSE Nb and Ta compared to the LREE and LILE suggesting that HIMU OIB lavas are derived from mantle source which is

complimentary to the Nb-Ta depleted continental crust. EM 1 contains entrained ancient oceanic sediments with higher Ba concentrations, while EM 2 carries ancient continental sediments having high LILE/Nb and LREE/Nb ratios, but is characteristically lacking relative Ba enrichment (Zindler and Hart, 1986; Hart, 1988; Loubet et al., 1988; Weaver, 1991). In the succeeding paragraphs, I will examine the affinity of Group 1 and 2 dykes to the OIB sources.

Erlank and Kable (1976), Pearce and Norry (1979) and Le Roex et al., (1983) have emphasised the importance of Zr/Nb ratio as an indicator of the 'depleted' or 'enriched' nature of the source region for basaltic magmas. The average Zr/Nb ratio of Group 1 is 16 (Range: 14–19) whereas the average value for Group 2 is 11 (Range: 9.2–12.5) (*Table 6.3*). The Zr/Nb ratio of Group 1 dykes is a close match with that of the continental crust and the upper limit of EM 1 OIB and PM, whereas Group 2 matches closely with the Within-Plate Tholeiite, OIT and E-MORB value. The Group 2, however, also falls within the broad range of the EM 1 mantle end-member found in many OIBs (*Table 6.3*).

The average La/Nb ratio for Group 1 dykes is 2.42 (Range: 1.99-2.64), which is close to that of continental crust. For Group 2, the average La/Nb is 0.9 (Range: 0.86-1.02), which is close to the EM 1 and EM 2 source end-members found in OIBs (there is an overlap in the La/Nb between EM 1 and EM 2 and hence it cannot be used to distinguish between the two; Weaver, 1991) (*Table 6.3*).

The average Ba/Nb ratio of Group 1 is 31 (Range: 25-35) while it is 7.8 for Group 2 (Range: 6.3-9.6). The range in Ba/Nb in Group 1 is slightly higher than the upper limit of EM 1 while that of Group 2 matches EM 2 values closely (*Table 6.3*). Moreover, Ba concentrations in Group 1 are close to OIB values, and those of Group 2 are close to those of E-MORBs (Sun and McDonough, 1989). The Nb content in Group 1 is much lower than found in OIBs (Nb $\approx$ 48 ppm) while Nb in Group 2 is slightly higher than the E-MORB average (Nb=8.3 ppm) (Sun

and McDonough, 1989). Hence, the ratio of Ba/Nb for Group 2 cannot be compared with an EM 2 source since the Group 2 dykes show Ba concentrations that are 8-20 times that of PM (*Fig. 6.13b*) as opposed with 30-90 times Ba enrichment in EM 2 magmas (Weaver, 1991) (*Table 6.3*).

The average value of Ba/Th for the Group 1 is 76 (Range: 63-98), whereas it is 70 for Group 2 (range: 56-91). The Ba/Th ratio of Group 1 and 2 dykes shows considerable overlap, and thus does not point towards a particular source (*Table 6.3*).

The average Ba/La ratio for Group 1 dykes is 12.8 (Range: 11.6-13.2) while the ratio for Group 2 is 8.2 (Range: 6.8-10.2). The Group 1 ratio is comparable to the EM 1 source whereas Group 2 is comparable to EM 2 (*Table 6.3*). The Ba concentrations in Group 1 dykes are likely to have been enriched by crustal contamination effects by the UCC or even due to the partly altered nature of the mineralogy due to weathering effects.

In summary, the Group 1 dykes have probably originated at a source which is EM 1 OIB with an influence of continental crust whereas the Group 2 dykes have an E-MORB source with least crustal interference.

Table 6.3 Incompatible trace element ratios in the major chemical reservoirs and their comparison with Group 1 and 2 dykes (Weaver 1991)

Ratio	Zr/Nb	La/Nb	Ba/Nb	Ba/Th	Rb/Nb	Th/Nb	Th/La	Ba/La
Primordial mantle	14.8	0.94	9	77	0.91	0.117	0.125	9.6
N-MORB	>30	1.07	4.3	60	0.36	0.071	0.067	4
E-MORB	~10	0.78	8.39	123.63	0.48	0.068	0.087	5.49-11.17
Within Plate Tholeiite	11.46	0.69	7.69	-	0.58	-	-	11.11
OIT	10.56	1.12	8.88	116.46	0.72	0.076	0.068	7.96
Con. Crust	16.2	2.2	54	124	4.7	0.44	0.204	25
GLOSS	14.54	3.2	86.8	112	6.4	0.77	0.24	25
HIMU OIB	3.2-5.0	0.66-0.77	4.9-5.9	63-77	0.35-0.38	0.078-0.101	0.107-0.133	6.8-8.7
EM 1 OIB	5.0-13.1	0.78-1.32	9.1-23.4	80-204	0.69-1.41	0.094-0.130	0.089-0.147	11.2-19.1
EM 2 OIB	4.4-7.8	0.79-1.19	6.4-11.3	57-105	0.58-0.87	0.105-0.168	0.108-0.183	7.3-13.5
<b>Group 1 Dykes</b>	<b>14.05-19.12</b>	<b>1.99-2.63</b>	<b>25.26-34.69</b>	<b>63.09-98.29</b>	<b>5.21-7.28</b>	<b>0.26-0.54</b>	<b>0.12-0.21</b>	<b>11.61-13.18</b>
<b>Group 2 Dykes</b>	<b>9.19-12.46</b>	<b>0.86-1.02</b>	<b>6.27-9.65</b>	<b>55.90-91.21</b>	<b>0.52-3.53</b>	<b>0.09-0.15</b>	<b>0.09-0.17</b>	<b>6.57-10.25</b>

PM: Primitive Mantle, N-MORB: Normal Mid Ocean Ridge Basalt, continental crust, HIMU OIB: High  $\mu^{238}\text{U}/^{204}\text{Pb}$  Ocean Island Basalt, EM1 OIB: Enriched Mantle 1 Oceanic Island Basalt, and EM 2 OIB: Enriched Mantle 2 Oceanic Island Basalt are from Weaver (1991); E-MORB: Enriched Mid Ocean Ridge Basalt is from Wilson (1989), OIT: Ocean Island Tholeiite is from Thompson et al., (1984)

In a Th vs Nb diagram (Pearce, 2008) (*Fig. 6.16*), the Group 1 dykes plot above the MORB-OIB array indicating upper crustal interactions or interactions with mantle lithosphere containing an inherent subducted component, whereas Group 2 dykes plot within the MORB-OIB array. Majority of the Group 2 dykes plotted close to the MORB-OIB array except three samples, indicating the little involvement of slab-derived components in the magmatic source (Pearce, 2008). This diagram is also useful for the cumulate rocks (except cumulate oxides) as it uses ratios of immobile incompatible elements that are transparent to cumulate effects (Pearce, 2008; Ernst, 2014). Hence, BG-11 can also be plotted on this. The Group 1 dykes show higher Th due to a possibility of crustal contamination. Other examples include dykes from Goa-Dharwar Sector (Devaraju et al., 2008), Kalyadi (Chandrasekharam et al., 2008), Dandeli (French and Heaman, 2010), One dyke from Goa (Fernandes et al., 2016) conform to the Group 1 dyke data. The other dykes from Goa (Widdowson et al., 2000; Fernandes et al., 2016), Ambenali, Poladpur and Mahabaleshwar formations of the Deccan (Vanderkluyzen et al., 2011) conform well to the Group 2 dykes.

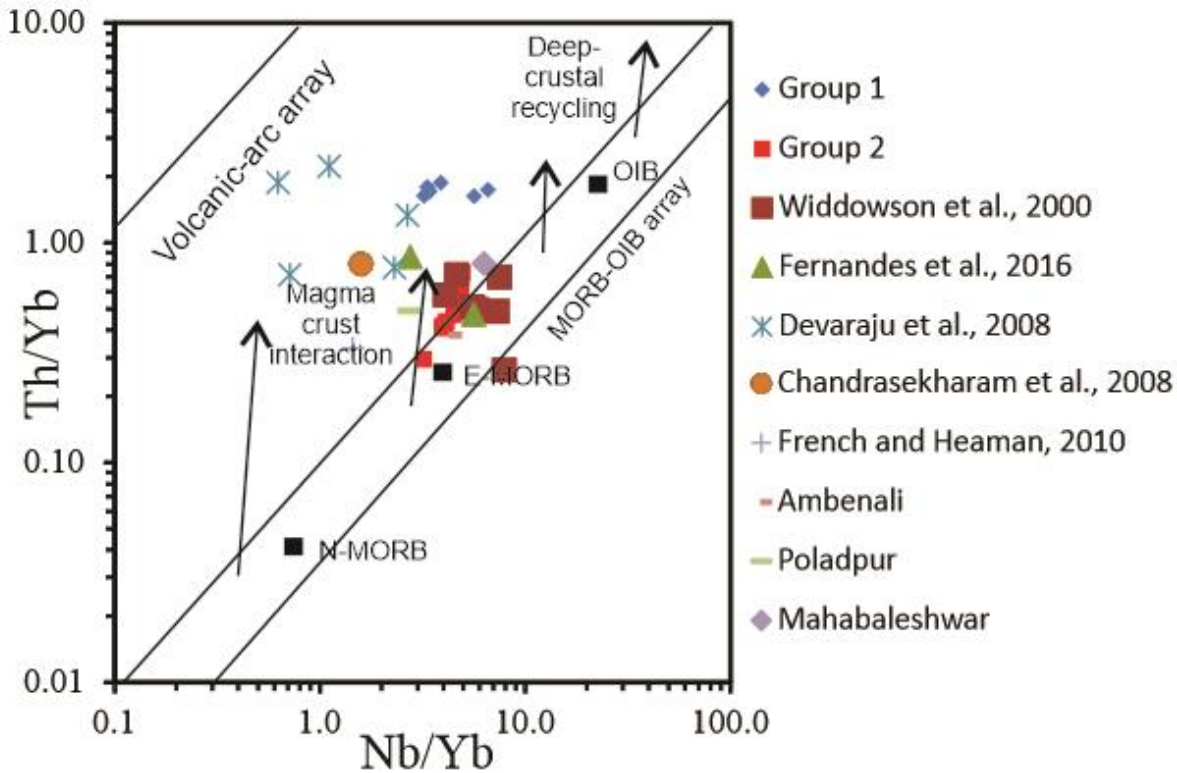


Fig. 6.16 Plot of both Groups of dykes on Nb/Yb vs. Th/Yb diagram (after Pearce, 2008) where the Group 1 dykes profoundly show magma-crust interaction and crustal contamination whereas majority of the Group 2 dykes fall in the MORB-OIB array with few of them slightly above the array. OIB: Ocean Island Basalts, NMORB: Normal mid-oceanic ridge basalts, EMORB: Enriched mid-oceanic ridge basalts, PM: Primitive mantle.

### 6.2.3 Mantle melting conditions

Continental Flood Basalt (CFB) magmas are thought to be the products of asthenospheric melting from adiabatic decompression of anhydrous mantle peridotite, and many authors have linked their formation to the impingement of the head of a mantle plume upon the lithosphere (e.g., White and McKenzie, 1989; Campbell and Griffiths, 1990; Richards et al., 1989; Garfunkel, 2008; Song et al., 2008; Lai et al., 2012). Previous workers have constrained the extent of mantle melting using trace element compositions of CFB samples (e.g., Lassiter et al., 1995; Reichow et al., 2005). REE compositions and their ratios are extremely useful in constraining mantle melting conditions because the degree of partial melting and the nature of aluminous phase (plagioclase, spinel, or garnet) in the mantle

source governs the relative abundance of the REEs in the melts (e.g., Lassiter et al., 1995; Reichow et al., 2005; He et al., 2010).

Heavy REE's are highly compatible in peridotites. Hence, plots based on ratios of REE such as La, Dy, Sm, Tb and Yb can be used to evaluate the depth of melting in uncontaminated melt products. This is possible because the relative abundance of these elements is strongly dependent on the degree of partial melting and, to a lesser degree, the nature of the Al-bearing accessory phase (garnet, spinel, or plagioclase) in the mantle source (e.g., Thirlwall et al., 1994; Furman, 1995; Kinzler, 1997; Van Westrenen et al., 2001; Bogaard and Wörner, 2003; Rajesh et al., 2013). Contaminated magmas like those of Group 1 dykes, have a limited utility in such diagrams that discuss about mantle melting. In a La/Yb vs Dy/Yb plot (*Fig 6.17*), Group 1 dykes are scattered between the garnet and spinel curves, whereas Group 2 clusters at the spinel curve. In addition to distinguishing between garnet and spinel peridotite melting, this diagram produces linear arrays for the melts resulting from mixing of garnet and spinel peridotite (Jung et al., 2006). Within Group 1, AG-23 is midway towards garnet curve, while AG-41 and BG-11 are lower than AG-23 and the rest BG-4, -35 and -37 are leaning more towards spinel curve, altogether forming a linear array. It can also be noted that the Group 1 dykes got formed due to mixing of melts of garnet-spinel peridotite with ~3-4% of melting, while Group 2 have resulted from ~4% of spinel peridotite melting, consistent with the limits of the tholeiitic magma generation (Langmuir et al., 1977; Bender et al., 1984). This percentage of melting is consistent with that calculated by Hegde et al. (2014) for the Desur lavas at Belgaum and as calculated by Chatterjee and Bhattacharji (2008) for Deccan basalts. As Tb is more incompatible than Yb in garnet, the near-constant  $(Tb/Yb)_N$  ratio for Group 2 (1.25-1.33) warrants an argument for the presence of a dominantly spinel-bearing source (Wang et al., 2002; Hazarika et al., 2020) and slight variable (1.49-1.78) for Group 1 hints at their source to be in slightly more in-depth, spinel-garnet transition

zone (e.g. Van Westrenen et al., 2001). However, I note here that this observation is doubtful given contaminated nature of Group 1 magmas. The Desur Formation falls close to the Group 2 dykes and the degree of melting matches with the previous study from the Belgaum area (Hegde et al., 2014).

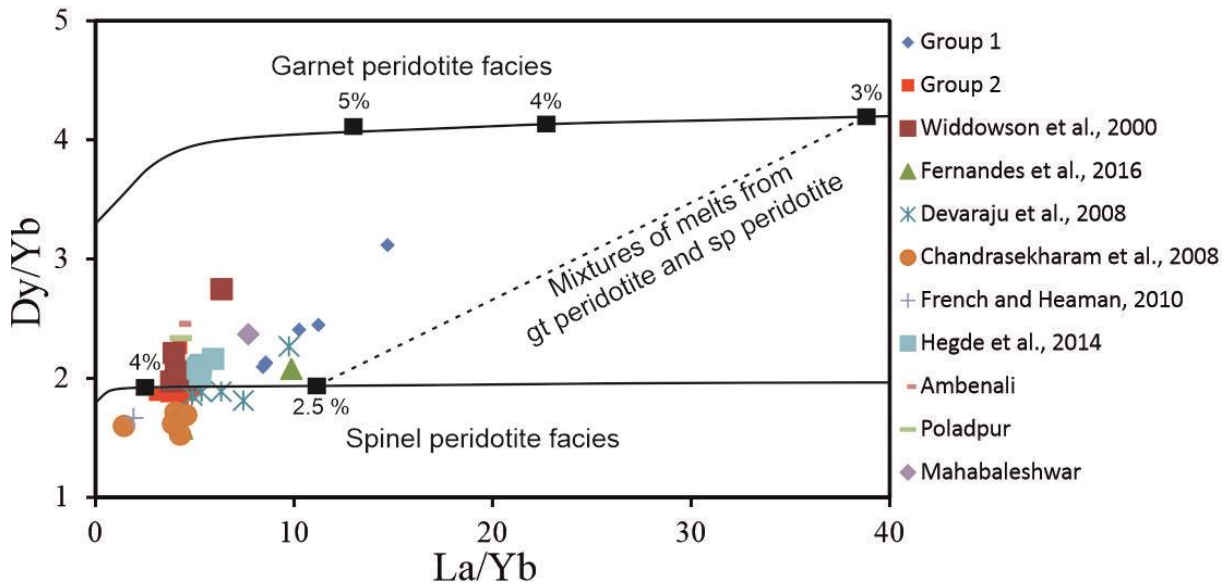


Fig. 6.17 Plot of  $La/Yb$  vs  $Dy/Yb$  (Jung et al., 2006) where both the Groups of dykes have been plotted. Numbers on model curves indicate percent melting. Comparative examples are also plotted.

The partition coefficients for different trace elements are different for different minerals that exist at variable depths. Within the HREE, Yb has high (8) garnet/melt partition coefficient, whereas Sm (MREE) is incompatible and has a low (0.131) garnet/melt partition coefficient (Irving and Frey, 1978; Kelemen, 1990; Aldanmaz et al., 2000). These two elements are combined with Ce (LREE) to form element ratios  $(Ce/Sm)_N$  vs  $(Yb/Sm)_N$  normalized (N) to PM values of Lyubetskaya and Korenaga (2007) (Fig. 6.18). This plot also contains calculated compositions of aggregated melts produced by fractional melting of garnet lherzolite and spinel lherzolite (Storey et al., 1997). The Group 2 dykes are staggered near the spinel-lherzolite melting trend pointing to 3-5% melting that generated the magmas. Since this diagram has ratios on each axis with a common denominator, Thirlwall et al.

(1994) asserted that trends caused by mixing of melts produced from garnet lherzolite with melts from spinel lherzolite will be linear, as shown by the Group 1 dykes. The intercepts on melting curves suggest that the Group 1 dykes formed by mixing of melts produced by ~2-3% melting of spinel lherzolite and ~3-5% of garnet lherzolite. This observation matches well with that plotted in *Fig. 6.17*. The average  $(\text{Gd}/\text{Yb})_{\text{N}}$  for Group 2 dykes is 1.50 which is  $>1.6$  indicating a spinel-bearing source implying greater degrees of melting and is in concordance with the earlier observations (made in *Fig. 6.17 & 6.18*). The  $(\text{Gd}/\text{Yb})_{\text{N}}$  ratio of Group 1 dykes cannot be used because of their contaminated nature. The transition from spinel lherzolite to garnet lherzolite occurs between 20 kbar at  $1200^{\circ}$  and between 26-27 kbar at  $1500^{\circ}\text{C}$  (Klemme and O'Neill, 2000). Garnet is only stable in the mantle at depths greater than ~75 km (Lassiter and DePaulo, 1997). Hence, the REE data point towards possible ~75 km origin of the melting for magma generation of Group 1 dykes (owing to uncertainties arising due to crustal contamination), as against  $<75$  km depth of origin for the magma in Group 2 dykes under lithospheric lid.

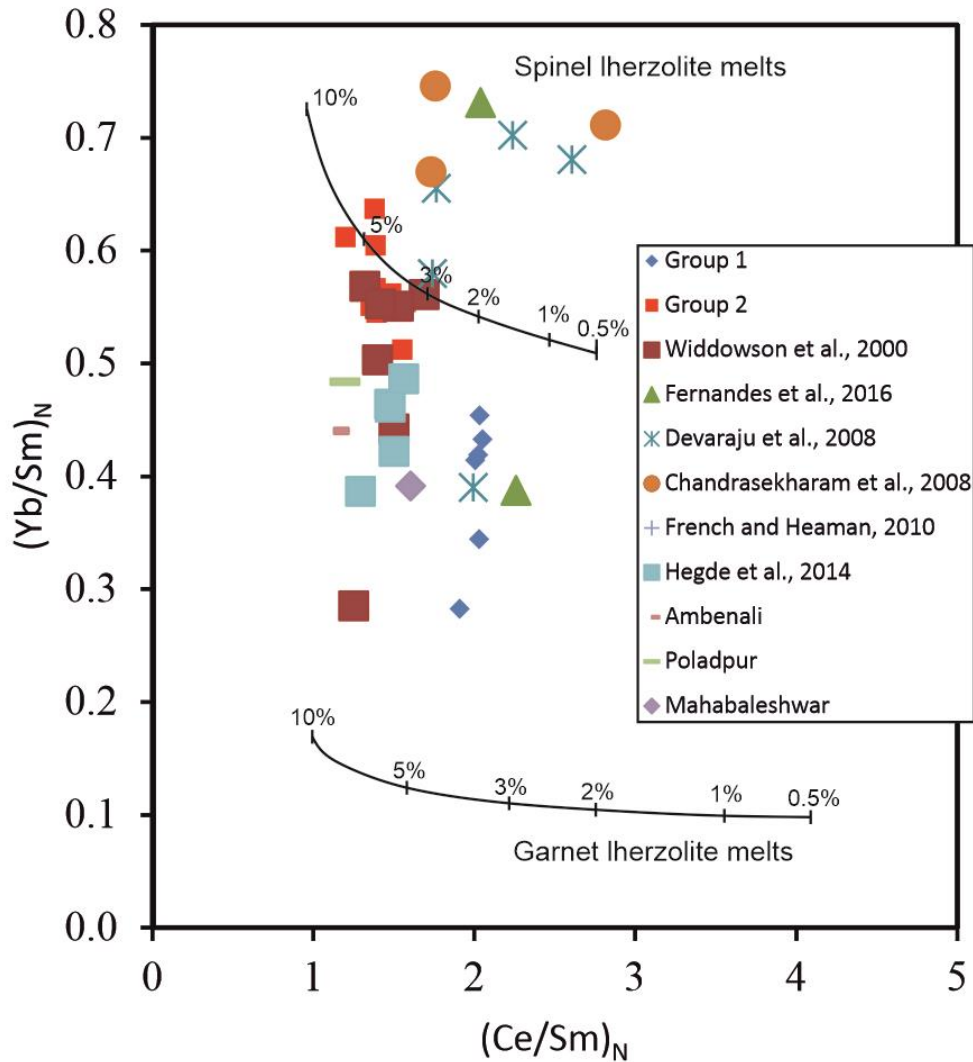


Fig. 6.18 Plot of  $(Ce/Sm)_N$  vs  $(Yb/Sm)_N$  (Storey et al., 1997) normalized (N) to PM values (Lyubetskaya and Korenaga, 2007) consisting of Group 1 and 2 dykes and other comparative values.

#### 6.2.4 Crustal contamination

Geochemical attributes for Group 1 dykes such as high  $Al_2O_3$ ,  $SiO_2$ ,  $K_2O$ , marked enrichment of Rb-Th associated with positive Rb and Th anomalies, negative K, Sr and Ti anomalies, Nb-Ta depletion relative to La on primitive mantle-normalized multi-element diagrams (Wilson, 1989) show effects of contamination from continental crustal materials in the evolution of these dykes of Goa. When the PM-normalized multi-element diagrams are

examined, it is seen that, though there are Rb and Sr anomalies and negative K, not all samples show negative anomalies for Ti, none for Th and there is no Nb depletion relative to La for Group 2 dykes. However, all the crustal contamination in the Group 1 dykes is evident.

Thompson et al. (1984) have considered La/Nb ratio as a suitable index of crustal contamination in magmas, while the same ratio can be used to distinguish between asthenospheric and lithospheric mantle sources (Fitton et al., 1988; Saunders et al., 1991; Wang et al., 2008). The La/Nb ratio is  $<1.5$  for uncontaminated asthenospheric sources whereas it is  $>1.5$  for lithospheric sources. In this case, the average ratio of La/Nb for Group 1 dykes is 2.42 whereas the ratio for Group 2 dykes is 0.94. This is also corroborated by La/Nb value of 1.90 (French and Heaman, 2010), 6.07 (Devaraju et al., 2008), 1.9 (Chandrasekharam et al., 2008), 0.89 (Hegde et al., 2014), 1.67 (Fernandes et al., 2016), 0.75 (Widdowson et al., 2000), 0.9 for the Ambenali Formation, 1.56 for the Poladpur Formation and 1.22 for the Mahabaleshwar Formation (Vanderkluyesen et al., 2011). It can be noted here that though there is no close match for the La/Nb ratio for Group 1 dykes, the Ambenali Formation and the Desur Formation of the Deccan traps are a close match for Group 2 dykes.

As shown in section 6.2.2, Group 1 dykes have Ba/Y and Th/Nb resembling continental crust, negative anomalies of Nb, Ta, Ti and P, and strong positive peaks of Pb on normalized trace element diagrams (Song et al., 2008; Lai et al., 2012) suggesting contamination of magma during ascent through continental crust (Huppert et al., 1985). In comparison, the Group 2 dykes suggest minimum contamination of magma during their ascent. Nb, Th and Ta serve as suitable geochemical proxies particularly for understanding the nature of crustal inputs during magma genesis manifested in terms of magma-crust interaction (assimilation and contamination), crustal recycling and subduction (Pearce, 2008). As shown in section 6.2.2, the Group 1 dykes have average Nb/Th ratio of 2.5 (Range: 1.9-3.8) and, Group 2 dykes have an average Nb/Th ratio of 9 (Range: 6.8-10.9). This Nb/Th

ratio is  $< 8$  (the PM value) for Group 1 dykes implying contamination of magma by continental crust, while the ratio of Nb/Th is  $> 8$  for Group 2 dykes hinting at minimum crustal contamination. Using Nb/Th, crustal contamination is attested in the Dandeli dyke (Nb/Th=4.35; French and Heaman, 2010), Goa-Dharwar Sector dykes (Nb/Th=1.38; Devaraju et al., 2008), and Kalyadi dykes (Nb/Th=2.35; Chandrasekharam et al., 2008). The Nb/Th ratio of Group 1 dykes most closely matches that of the Kalyadi dykes. Interestingly, the Nb/Th ratios of the Group 1 dykes also match those of the Bushe Formation (Nb/Th: 1.97) and the Khandala Formation (Nb/Th: 3.88) (Vanderkluysen et al., 2011) which are known to have been contaminated by lower crustal contaminants (Peng et al., 1994). By contrast, the other examples are uncontaminated, like the Desur Formation (Nb/Th=10.84; Hegde et al., 2014), Goa dykes (Nb/Th=7.56; Fernandes et al., 2016; and Nb/Th=13.11; Widdowson et al., 2000), the Ambenali Formation (Nb/Th=11.25), the Poladpur Formation (Nb/Th=5.62), or the Mahabaleshwar Formation (Nb/Th=7.83; Vanderkluysen et al., 2011). Of these, the Desur Formation (Hegde et al., 2014) matches closely with the Group 2 dykes.

At least three CFBs, Central Atlantic Magmatic Province, Siberian Trap LIP and the Lesotho Basalt province (of the Karoo LIP), have negative Nb, Ta anomalies. This is true for both, low-Ti and high-Ti basalts within these three provinces. Ernst (2014) suggested that this anomaly may not be reflective of subduction-setting but instead could indicate interaction with lithospheric mantle modified by an earlier subduction event (perhaps by hundreds of millions of years previously). This is also true in the case of Group 1 dykes. Ernst (2014) has discussed in detail about aspects of negative Nb-Ta anomaly in CFBs and the proposed models for their magma generation.

The Th vs Nb diagram can be used as a proxy for crustal contamination when the elements are normalised by Yb (Pearce, 2008). Fig. 6.16a is a plot of Nb/Yb vs Th/Yb, where present-day MORBs and OIBs form a diagonal array, whereas lavas that have interacted with

the continental crust or have subduction component (Pearce and Peate, 1995) are shifted above the array. When both the dyke groups are plotted, Group 1 samples plot on the upper side of the array, hinting at either their interaction with the continental crust, or that they have a subduction component (Pearce and Peate, 1995). By contrast, most of the Group 2 dykes fall on the MORB-OIB array. Few Group 2 samples are Yb-depleted, which indicates partial or negligible crustal involvement either by direct crustal contamination or via inherited subduction components in the lithosphere (Pearce, 2008). For comparison, the Dandeli dyke (French and Heaman, 2010), Goa-Dharwar Sector dykes (Devaraju et al., 2008), Kalyadi dykes (Chandrasekharam et al., 2008), Poladpur Formation (Vanderkluyzen et al., 2011) fall away from the mantle array showing crustal contamination effects similar to Group 1 dykes. By contrast, the Desur Formation (Hegde et al., 2014), the Goa dykes (Widdowson et al., 2000; Fernandes et al., 2016), and the Ambenali and Mahabaleshwar formations (Vanderkluyzen et al., 2011) are approximately arranged along the upper limit of the mantle array, together with Group 2 dykes.

*Fig. 6.13a* shows that Group 1 dykes have PM-normalised multi-element patterns that match with those of the UCC (Rudnick and Gao, 2013). These Group 1 patterns also match with those of the country-rock greywackes exposed in the study area (*Fig. 6.19*). This provides further evidence of contamination of Group 1 magmas by greywacke or other upper crustal rocks. Gadgil et al. (2019) did not rule out thermal erosion of wall rocks during emplacement of the dykes of Goa (see also *Sec. 3.3.2.1*), which is consistent with the contamination observed in Group 1 dykes. Huppert et al. (1985) demonstrated that thermal erosion of wall rocks by ascending high-Mg (hot) magmas can be rapid and efficient, as opposed to low-Mg, cooler basaltic magmas that retain their pristine state during ascent.

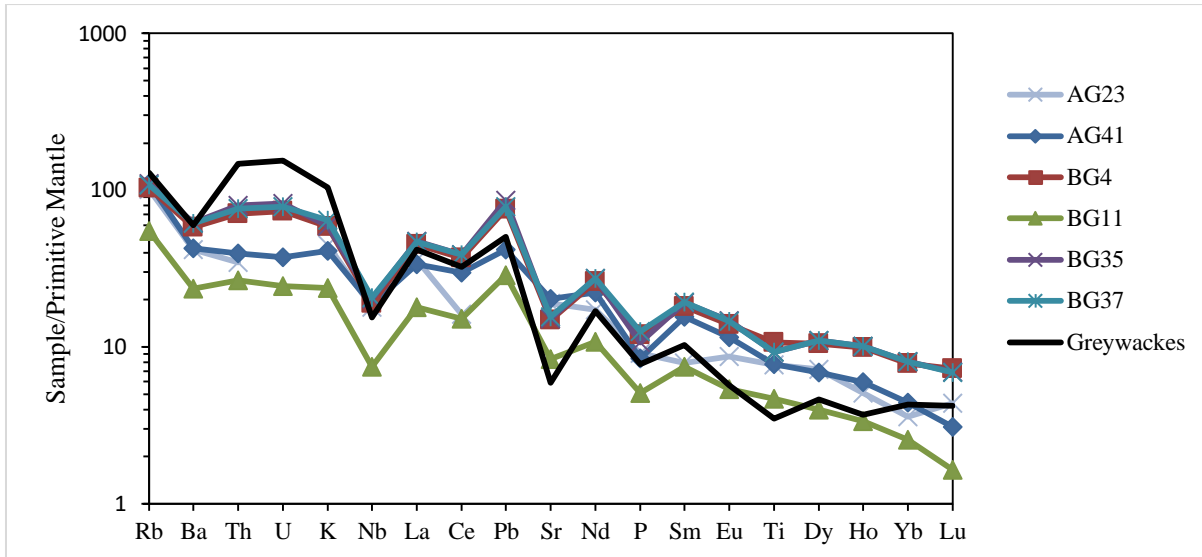


Fig. 6.19 Figure depicting PM-normalised multi-element pattern for Group 1 dykes compared with the country-rock metagreywackes. Profound similarities are seen in the many troughs and peaks of elemental abundances. Normalization factors after (Lyubetskaya and Korenaga (2007)).

### 6.3 The need for geochemical correlations

The objective here is to evaluate whether (i) the Group 1 dykes correlate with their Proterozoic equivalents from the Dharwar craton, (ii) the Group 2 dykes bear any semblance to the Deccan Traps exposed several tens of kilometres north of the study area (iii) these dykes were indeed feeders to some of the Western Ghat (WG) stratigraphic formations. To understand the Group 1 relations, I compare their multi-element patterns to their hypothesized Dharwar equivalents. On the other hand, for the Group 2 dykes, a two-pronged approach is followed: (i) binary plots of incompatible element abundance and element-element ratios (ii) comparison of primitive-mantle-normalized multi-element patterns of the Group 2 dykes with patterns of the southwestern Deccan formations.

### 6.3.1 Comparison of multi-element patterns for Group 1 dykes

As seen from the previous discussion, the Group 1 dykes are represented by geochemically distinct, magma modified, upper crustal contamination. The other Proterozoic dykes used for correlation in the diagrams also attest to the same. Here, the multi-element patterns of Group 1 dykes are compared with the earlier stated equivalents from the Dharwar craton to demonstrate their affinity further. I do this by using PM-normalized (Lyubetskaya and Korenaga, 2007) multi-element patterns in turn normalized to Lu=5. The normalization of all the REE patterns to an element with fixed abundance (in this case Lu=5) helps minimise effects of fractional crystallization on the patterns and enables better correlation (e.g., Sheth et al., 2004; Vanderkluysen et al., 2014).

I compare the PM-normalized multi-element patterns of Group 1 dykes with a 2.18 Ga dyke from Dandeli (French and Heaman, 2010) (*Fig. 6.20a*). I note that the pattern in Group 1 does not match well; except for some peaks for K and Rb, and a trough at Nb. The HREE pattern for the Dandeli dyke is flatter, and the abundances of all REE is much lower than in Group 1 dykes. I compare Group 1 dykes with the dykes from Kalyadi (Chandrasekharam et al., 2008) that have an age of 2.3-2.4 Ga (Halls et al., 2007) (*Fig. 6.20b*). The troughs in Nb, Sr and Ti, and peaks in Rb, K, La, Ce and Gd match well between Group 1 and Kalyadi dykes. When I compared dykes of Group 1 with the quartz dolerite and olivine dolerite dykes from the Goa-Dharwar sector (undated; Devaraju et al., 2008) (*Fig. 6.20c*), many similarities are found. The peaks in Rb, K, La, Ce, Nd, Gd and Y and troughs in Ti, P, Sr, Nb, Ba and Tm match well with Group 1 dykes. Overall, the Goa-Dharwar quartz dolerite is a close match for the Group 1 dykes.

Interestingly, the multi-element patterns of Group 1 dykes match very well with that of the Bushe Formation of the Deccan Traps (*Fig. 6.20d*), which I interpret as being

particularly contaminated by UCC (e.g., Peng et al., 1994). This provides evidence that magmatic conditions required for the formation of Bushe magmas were similar to those of Group 1 Goa dykes. Apart from multi-element patterns, a close match of Group 1 dykes with the Bushe Formation is also observed in Ti/Y (349 for Group 1; (370 in the Bushe Formation according to Patil et al. [2020]; and 279 in Vanderkluyesen et al. [2011]); in Zr/Nb (16.46 for Group 1; 16.15 in the Bushe Formation according to Patil et al. [2020] and 17.34 in Vanderkluyesen et al. [2011]), and in Nb/Y (0.35 in Group 1, vs 0.29 for the Bushe Formation in samples from Patil et al. [2020] and 0.25 in Vanderkluyesen et al. [2011]).

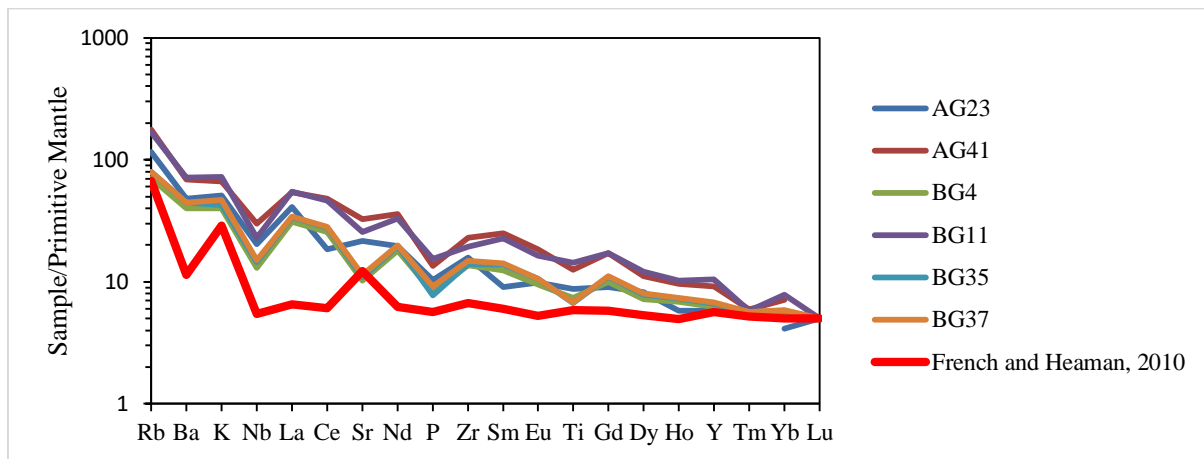


Fig. 6.20a Comparison of PM-normalized multi-element patterns of the Group 1 dykes with that of Dandeli dyke (French and Heaman, 2010). The patterns are compared with the same Lu=5 value.

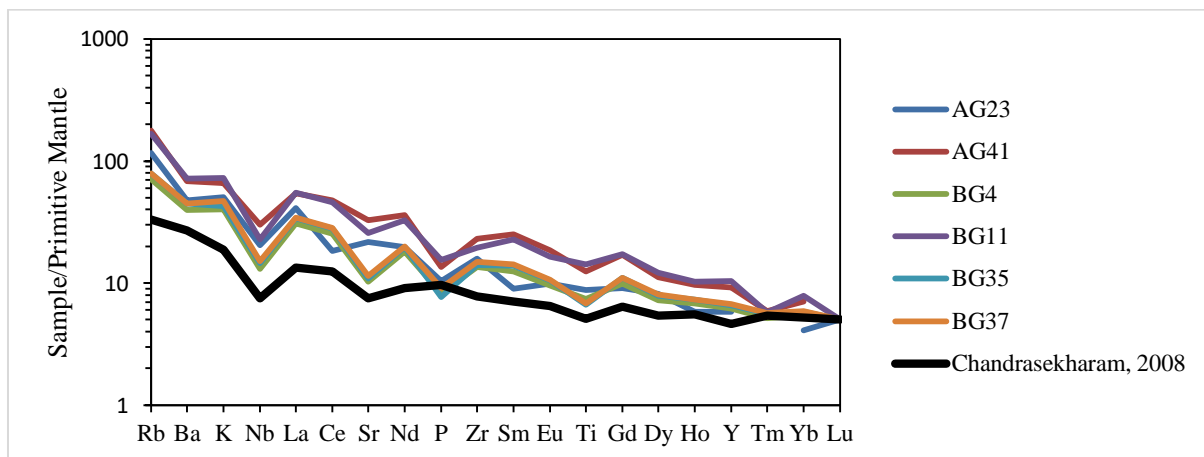


Fig. 6.20b cont... comparison with the Kalyadi dyke averages (of 5) (Chandrasekharam, 2008)

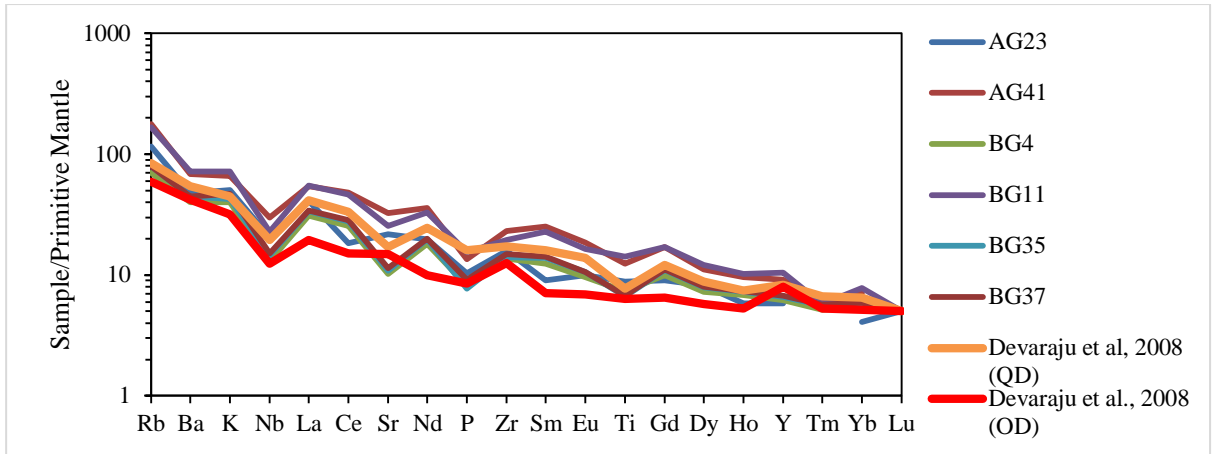


Fig. 6.20c cont... comparison with the Goa-Dharwar sector dyke average (Devaraju et al., 2008). Qtz D: Quartz Dolerite, Ol D: Olivine Dolerite.

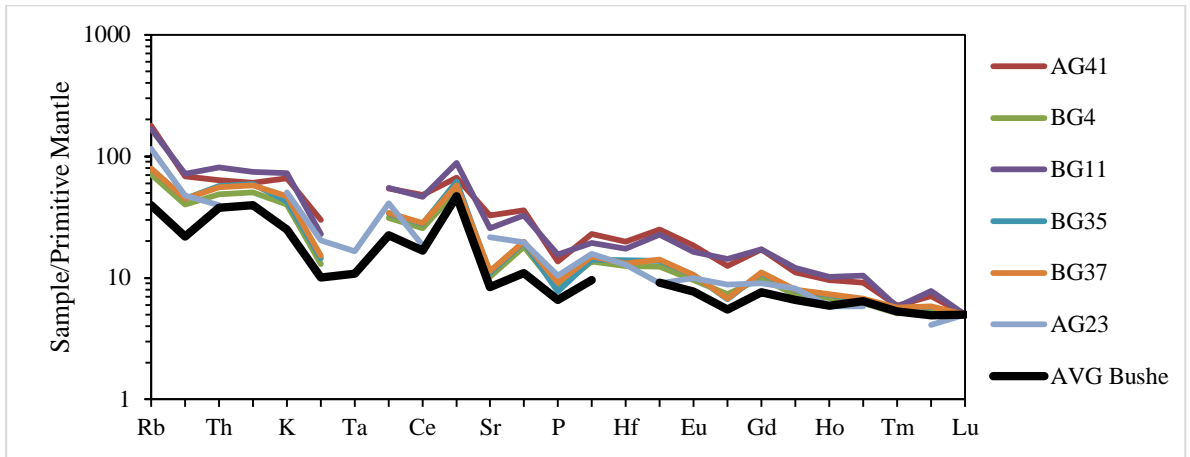


Fig. 6.20d cont... comparison with an average of the Bushe Formation of Deccan Traps (Vanderkluyssen et al., 2011).

### 6.3.2 Group 1 dykes as feeders to the Bushe Formation of the Deccan Traps?

Among CFB provinces preserved in India, which include the Rajmahal and Sylhet traps, the Deccan Traps are the most extensive. The Deccan Traps currently occupy an area of  $\sim 500,000 \text{ km}^2$ , with an original area of  $1,000,000 \text{ km}^2$  (Courtillet et al., 1986) when accounting for erosion, extending up to now-rifted Seychelles (Devey and Stephens, 1991, 1992). There is ample evidence suggesting that relatively thinner, fewer and younger formations (Panhala and Desur) are present in the southeastern Deccan Volcanic Province

(DVP) (thickness < 500 m at the Killari borehole, Jay and Widdowson, 2008) and towards Belgaum (Widdowson et al., 2000, Vanderkluyesen et al., 2011; Hegde et al., 2014) (*Fig. 6.21*). It is here that the younger formations progressively overstep the older formations (Devey and Lightfoot, 1986; Lightfoot et al., 1990) and the successive formations increasingly lie directly on the basement (Lightfoot et al., 1990). For example, the nonconformity between the basement and the Deccan lies at 25 m above sea level at Bavda and Phonda ghats. In comparison, it reaches to 550 m at Amboli, Isapur and Tilari ghats, near Belgaum (Lightfoot et al., 1990). This lends credence to model B (Mitchell and Widdowson, 1991) of the evolution of the Deccan Traps. In this model, the authors state that there was southerly migration of the eruptive focus as India moved northward over a fixed hotspot (Cox, 1983; Watts and Cox, 1989, Mitchell and Widdowson, 1991; Chenet et al., 2007; Schoene et al., 2015). Feeder dykes for the older Kalsubai and Lonavala Subgroups are present further north, primarily along the Narmada-Tapi dyke swarm, which restricts these formations' overall extent (e.g., Jerram and Widdowson, 2005; Vanderkluyesen et al., 2011).

The N-S cross-section of the Western Ghats (WG) sequence (Beane et al., 1986; Mahoney, 1988; Mitchell and Widdowson, 1991; Peng et al., 1994) shows the wedge-shaped nature of various subgroups of the Deccan and, particularly, the Lonavala Subgroup (~500 m thick) that dwindle to their thinnest, southwest of Mahabaleshwar. In an E-W section that stretches from Gulbarga to Ratnagiri (Mitchell and Widdowson, 1991; Peng et al., 2014), it is amply clear that the base of the Wai Subgroup (Poladpur Formation) lies directly on the basement, excluding all the older formations, over large swaths of the Deccan. Because the Kalsubai and Lonavala Subgroups erupted earlier in the history of the extrusive episode of the Deccan, their eruptive centres being located north of Nasik (Mitchell and Widdowson, 1991; Vanderkluyesen et al., 2011), the distant location of these flows from the present study area, and the rising elevation of the basement southwards prompts me to believe that the

dykes under study from Goa cannot be feeder dykes to either of the Kalsubai and Lonavala Subgroups or particularly to the Bushe Formation.

Hence these dykes have evolved on a near similar genetic history as that of the Bushe Formation. It is likely that this is a result of the contamination of granites coupled with sediment inputs. Goutham et al. (2011) has made similar observations for the Proterozoic age Cuddapah dykes. In any case, field observations made in Chapter 4 stand true in the sense that the N-S dykes (Group 1) have been emplaced first followed by the ~NNW-SSE/~WNW-ESE dykes and the ~E-W dykes (Group 2).

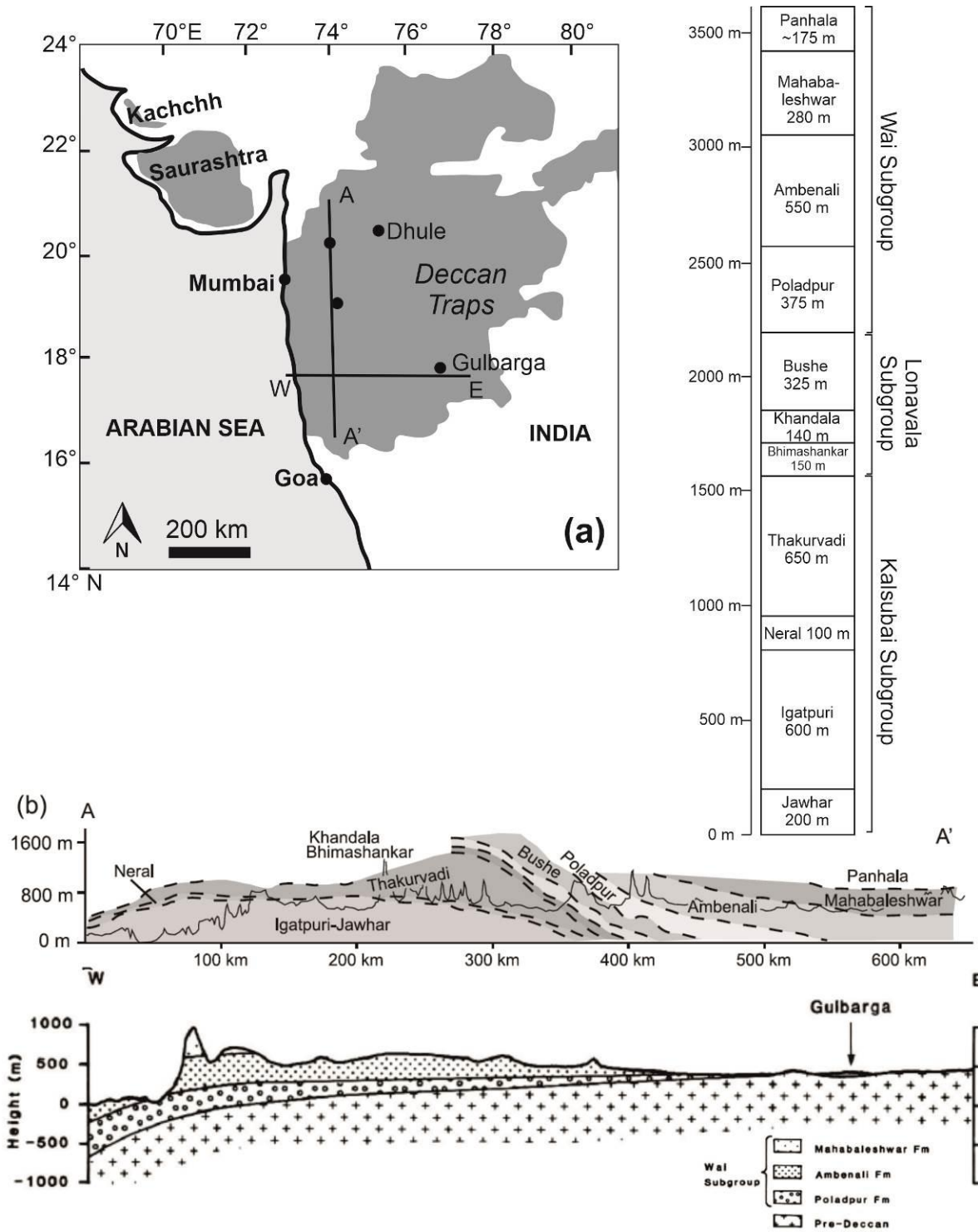


Fig. 6.21 (a) (left) Schematic diagram of the distribution of Deccan Traps (Modified after Vijayan et al., 2016). (right) Simplified stratigraphic column (formation thicknesses are maximum observed values). Compiled from Beane et al. (1986), Devey and Lightfoot (1986), Mitchell and Widdowson (1991), Mahoney et al. (2000), Vanderkluyesen et al. (2011), Schoene et al. (2015). (b) Schematic cross-sections along A-A' (from Vanderkluyesen et al., 2011) and E-W (from Mitchell and Widdowson, 1991).

### 6.3.3 Binary geochemical diagrams for Group 2 dykes

In comparison to the multi-element patterns, binary plots of major and trace elements (and their ratios) prove to be less diagnostic for stratigraphic correlations in the Deccan Trap formations because of the substantial overlap between the WG formations in these plots (e.g., Sheth et al., 2014). Therefore, such plots by themselves are insufficient to discriminate between them. Besides this, elements such as Rb, K and Sr are highly mobile during alteration and weathering and hence are avoided.

Here, the Nb/Zr ratio (Mitchell and Widdowson, 1991, Sheth et al., 2004; 2014) is used owing to its strong stability even during extreme alteration. Along with this, Y is used as it is also resistant to alteration, and Ba is less mobile than K or Rb. *Fig. 6.22a* shows a plot of Nb/Zr vs Ba/Y, wherein both these ratios are insensitive to fractional crystallization of minerals common in basalt. When Group 2 dykes are plotted, BG-6, BG-7 and BG-20 plot clearly in the Ambenali Formation field, whereas BG-13 falls in the Mahabaleshwar Formation field. The data points for AG-9, AG-15, AG-24, VG-1 and VG-2 plot in the overlap between the Ambenali and Poladpur Formation fields, while AG-4 falls in the overlap between Mahabaleshwar and Ambenali. Dyke AG-19 falls at the triple junction between the Ambenali, Mahabaleshwar, and Poladpur formations.

The plot of Zr/Nb vs Ti/Y (Cucciniello et al., 2015; Sheth et al., 2019) (*Fig. 6.22b*) consistently demonstrates the affinities of all the Group 2 dykes for the Wai Subgroup, while there is no similarity to the Bushe Formation. This ratio pair is insensitive to the olivine-gabbro fractionation well known for the WG sequence (Cox and Hawkesworth, 1985; Devey and Cox, 1987). Thus, this diagram emphasises the robust affiliation of these dykes to the younger formation of the Deccan Traps.

The plot of Zr (ppm) vs Th (ppm) (Sheth et al., 2019) (*Fig.6.22c*) shows that samples AG-4, BG-6, BG-7, BG-20 and VG-1 clearly plot in the Panhala Formation field, whereas AG-15, AG-19 and AG-24 have Poladpur Formation affinities. VG-2 is restricted to the Ambenali Formation field.

Such multi-element diagrams have proved to be useful in broadly assigning geochemical characters of given samples to any of the Deccan formations, rather than sharp correlations (Mitchell and Widdowson, 1991, Sheth et al., 2004, Bondre et al., 2006).

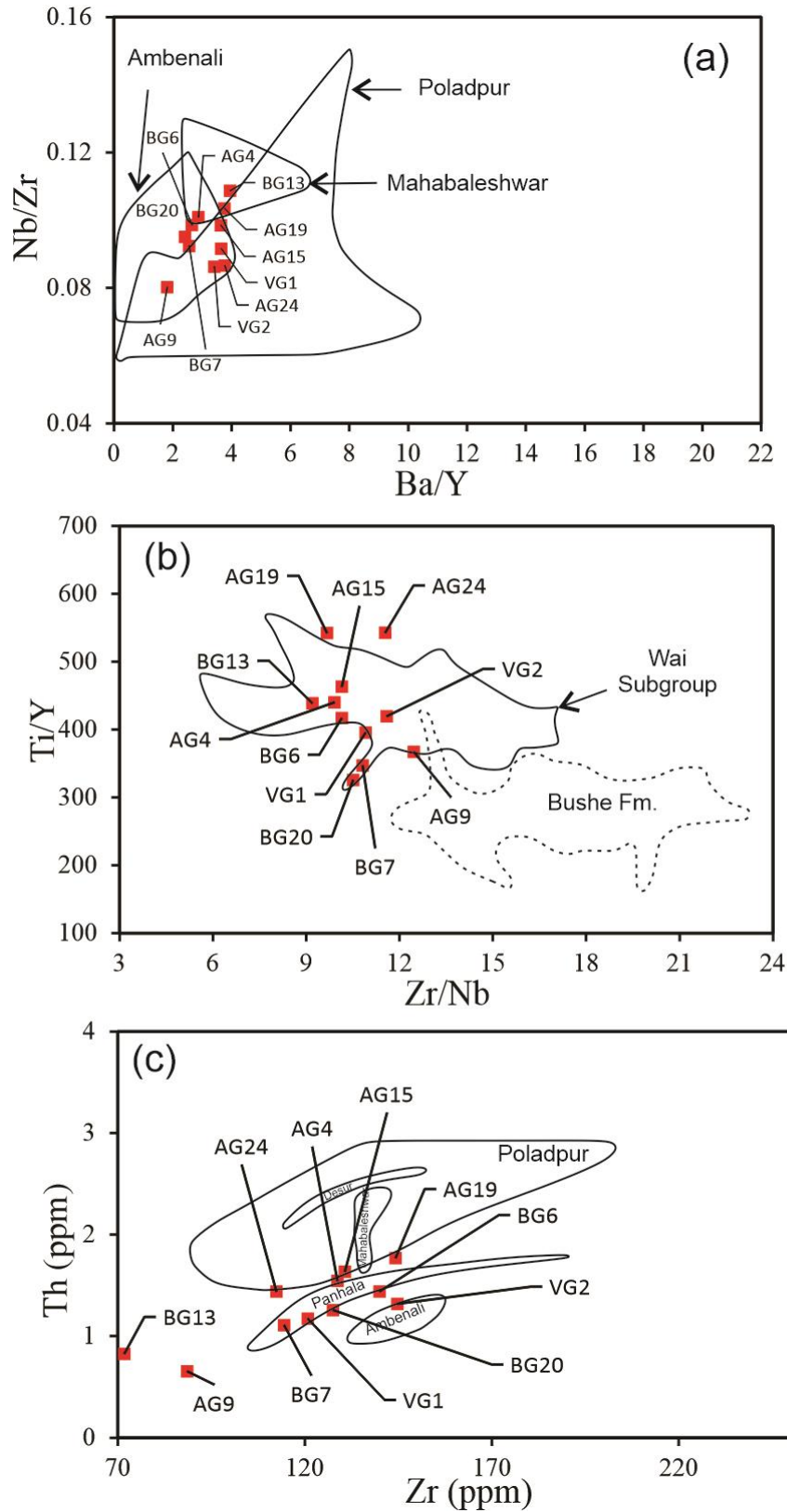


Fig. 6.22 Variation diagrams of (a) Ba/Y vs Nb/Zr, (b) Zr/Nb vs Ti/Y, (c) Zr (ppm) vs Th (ppm) for the Group 2 dykes. Fields for several southwestern Deccan formations are from Devey and Lightfoot (1986), Lightfoot et al. (1990), Sheth et al. (2004, 2019) and Mitchell and Widdowson (1991).

### 6.3.4 Comparison of multi-element patterns for Group 2 dykes

To further strengthen their stratigraphic affinities to the Deccan, the Group 2 dykes are compared with the average values of the Wai Subgroup formations using PM-normalized (Lyubetskaya and Korenaga, 2007) multi-element patterns, in turn, normalized to Lu=5. The normalization of all the REE patterns to an element with fixed abundance (in this case Lu=5) helps to minimise effects of fractional crystallization and enables better correlation (Sheth et al., 2004; Vanderkluyesen et al., 2014).

The PM-normalized multi-element patterns for AG-4, AG-15, AG-19, BG-6, BG-7, BG-20, VG-1 and VG-2 (*Fig. 6.23a-c*) show that these match closely with the Desur Formation for most of the elements. The peak in Ba and trough for Rb seen in the Desur Formation isn't seen in the dykes studied of the Goa coast, but the lack of Eu anomaly and a sharp trough at Sr perfectly match. However, all the dykes as mentioned earlier, along with AG-9, also show a close match with the Ambenali Formation (*Fig. 6.24a-c*). All these dykes broadly match the element patterns of the Ambenali Formation, except for Rb (this element is low in Ambenali Formation). The dyke AG-24 pattern is a bit offset with respect to trough in Tm, and peaks at Ti, whereas the concentrations of K and Th are much higher than typical of the Ambenali Formation. The dykes VG-1 and VG-2 are much better correlated with the Ambenali Formation than the Desur Formation. The only dyke showing affinity to the Poladpur Formation is BG-13 (*Fig. 6.25*); however, this dyke is multiple times rich in Rb and depleted of K as compared to the Poladpur Formation and could be an artefact of weathering.

Sheth et al. (2014) presented chemical and isotopic data on tholeiitic flows and dykes from the Ghatkopar-Powai areas of Mumbai. These samples yielded much younger ages of  $62.4 \pm 0.1$  Ma compared to the main Deccan event (66-65 Ma; Sprain et al., 2019; Schoene

et al., 2019). Though the age of  $62.8 \pm 0.2$  Ma for some of the coastal Goa dykes has been disputed (Baksi et al., 2014), the Goa dykes could not be older than 62.8 Ma (Sheth et al., 2001). One Ghatkopar-Powai sample similar to the Ambenali Formation in its isotopic ratios and multi-element patterns, MMD13, does not have the distinct trace element ratios of this formation. Sheth et al. (2014) suggest that though these dykes have similarities with the formations of the WG, they are not feeders. Hence, as these Goa dykes could represent the late phases of Deccan volcanism, it is prudent to compare the dykes from the study area to this phase of volcanism.

The dykes AG-4, -15, -19, BG-6, -7, -13, -20, VG-1 and -2 are plotted and compared with the MMD13 dyke of the Ghatkopar-Powai tholeiite sequence (*Fig. 6.26a-c*). MMD13 has unusually high Pb (83 ppm) ascribed to hydrothermal enrichment, and I exclude Pb from the multi-element pattern. All elements except Rb, Ba from MMD13 match very well with those dykes in the study area.

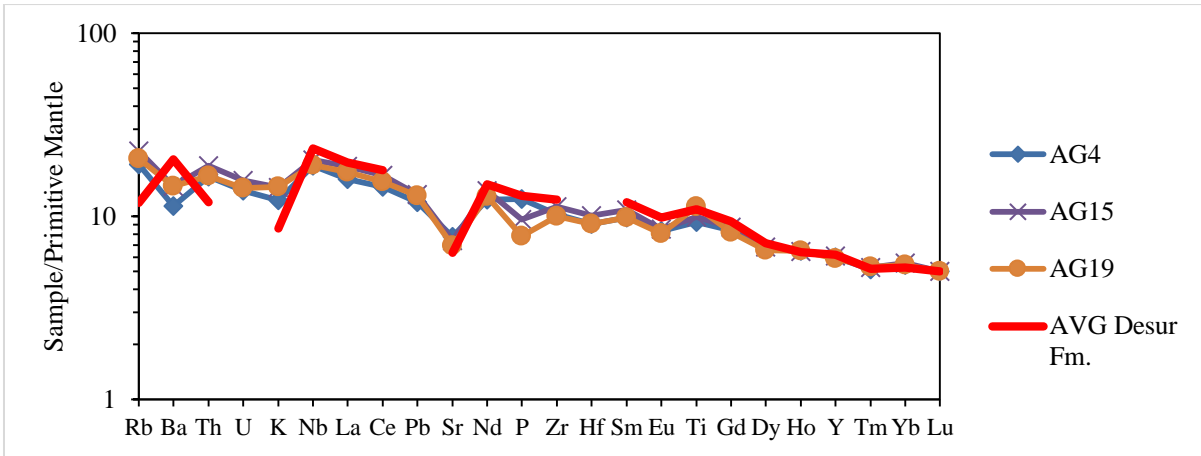


Fig. 6.23a Comparison of PM-normalized multi-element patterns of the Group 2 dykes with those of the Desur Formation average (Hegde et al., 2014). The patterns are compared with the same  $Lu=5$  value.

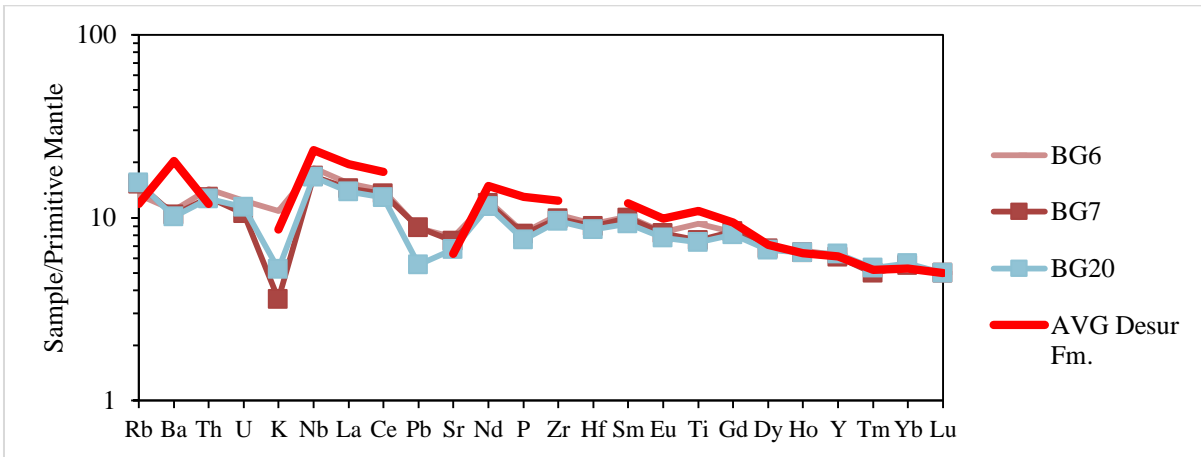


Fig. 6.23b cont...

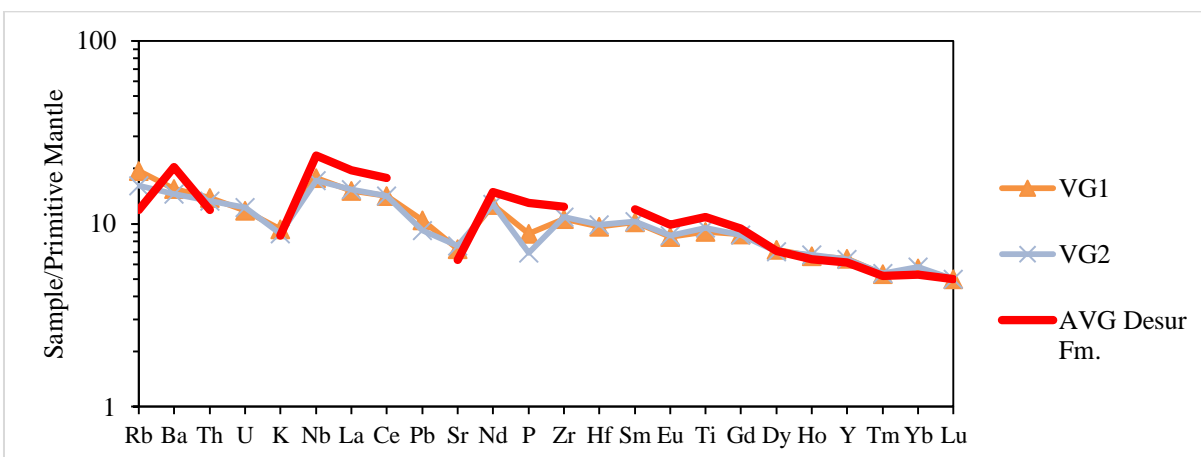


Fig. 6.23c cont...

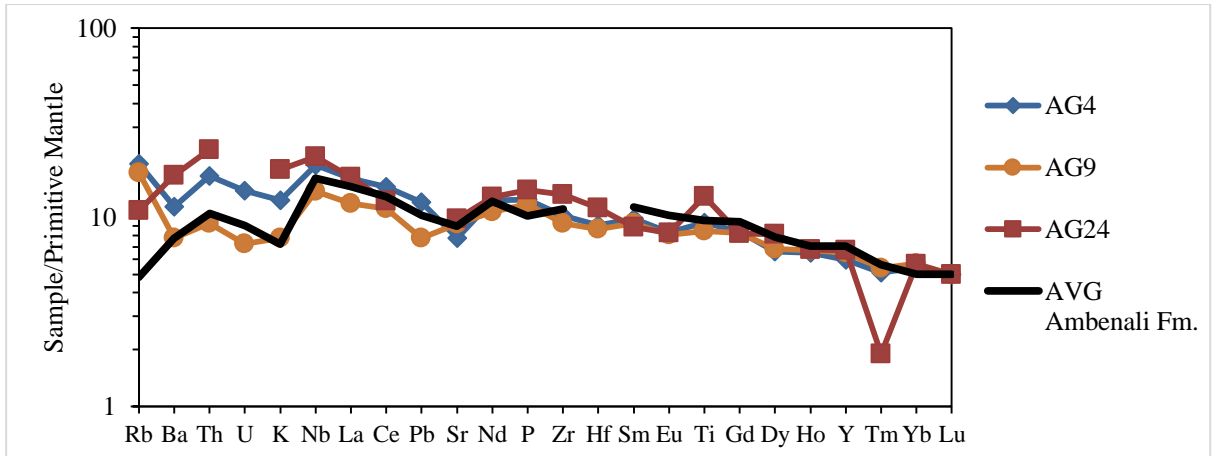


Fig. 6.24a Comparison of PM-normalized multi-element patterns of the Group 2 dykes with those of the Ambenali Formation averages (Vanderkluyesen et al., 2011). The patterns are compared with the same Lu=5 value.

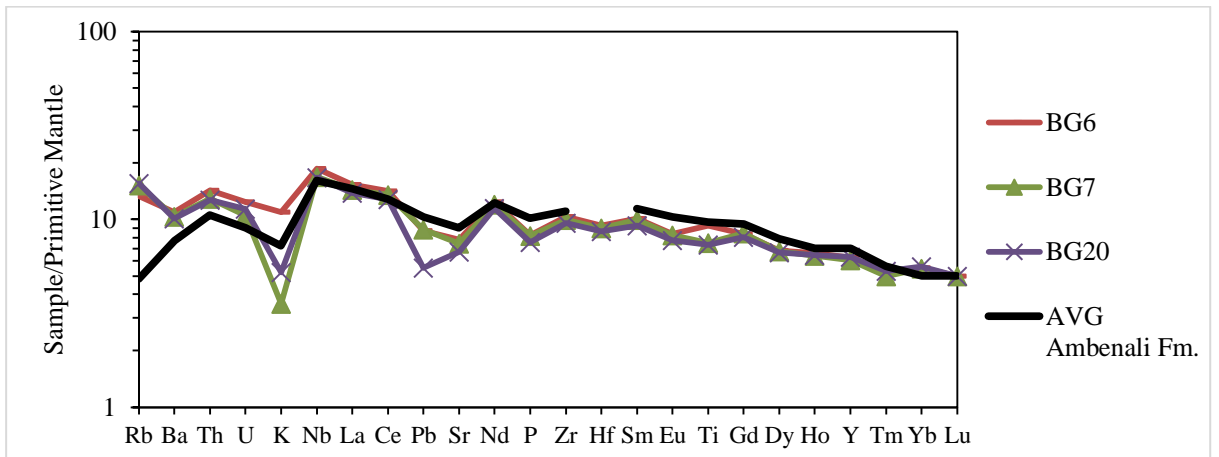


Fig. 6.24b cont...

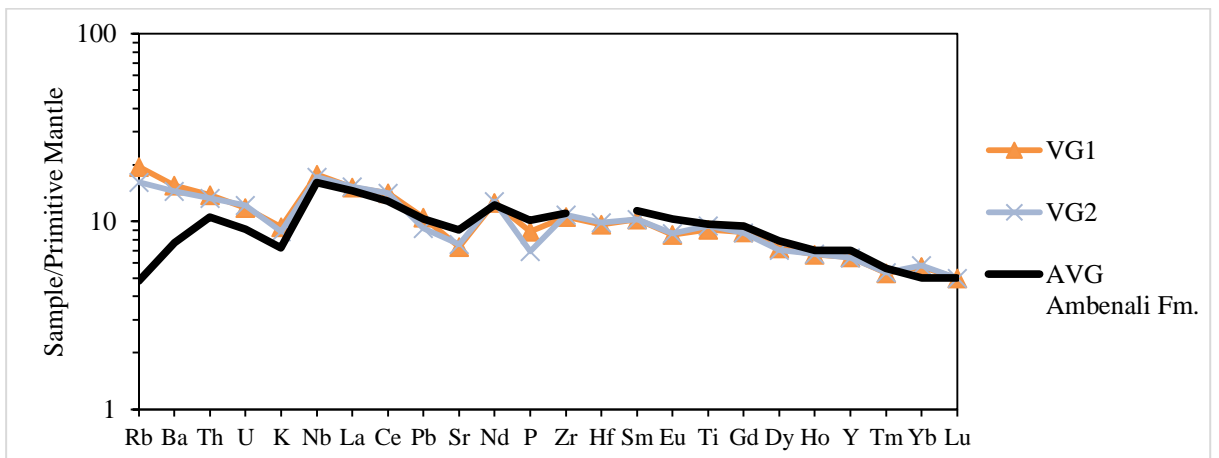


Fig. 6.24c cont...

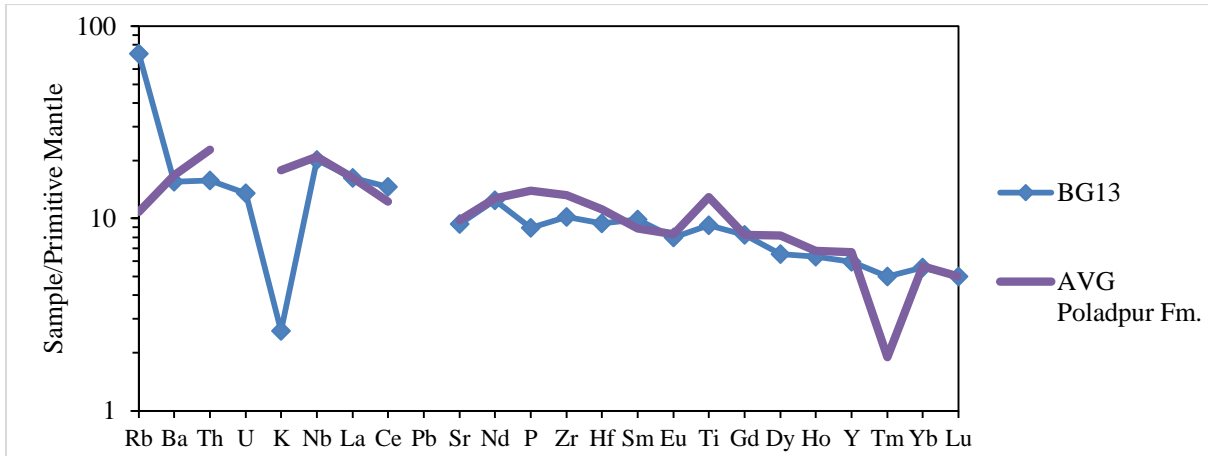


Fig. 6.25 Comparison of PM-normalized multi-element patterns of the Group 2 dyke with those of the Poladpur Formation averages (Vanderkluyssen et al., 2011). The patterns are compared with the same  $Lu=5$  value.

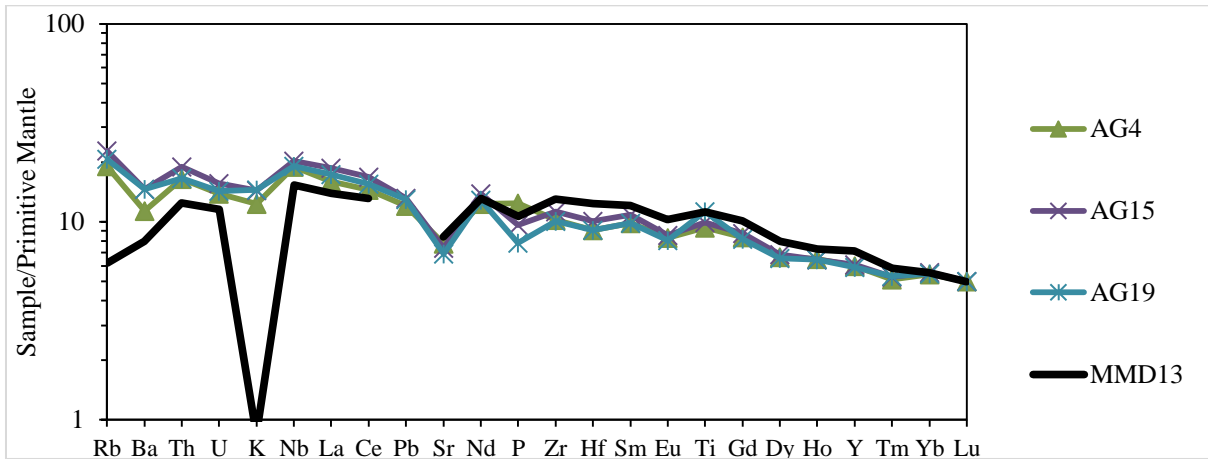


Fig. 6.26a Comparison of PM-normalized multi-element patterns of the Group 2 dykes with those of MMD13 (Sheth et al., 2014). The patterns are compared with the same  $Lu=5$  value.

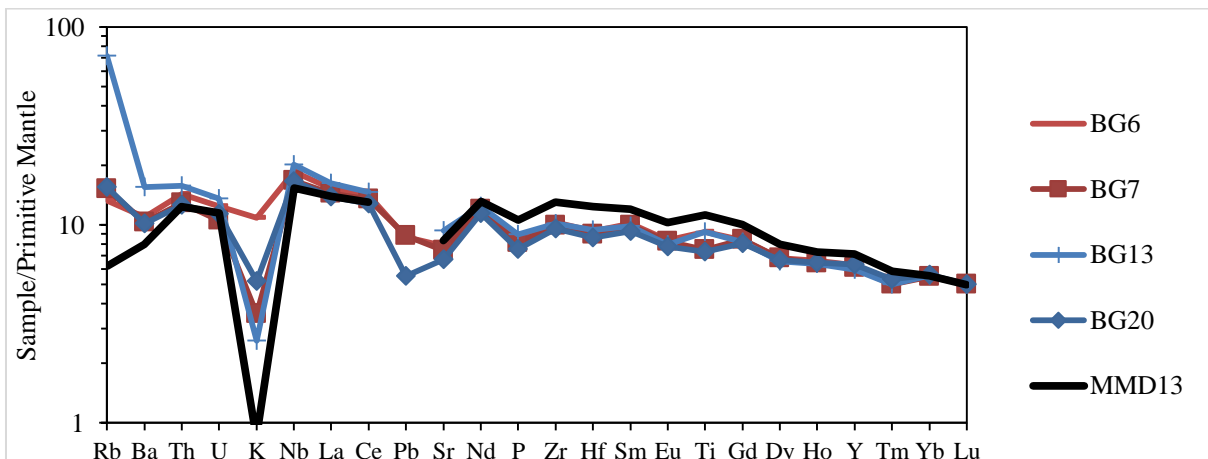


Fig. 6.26b cont...

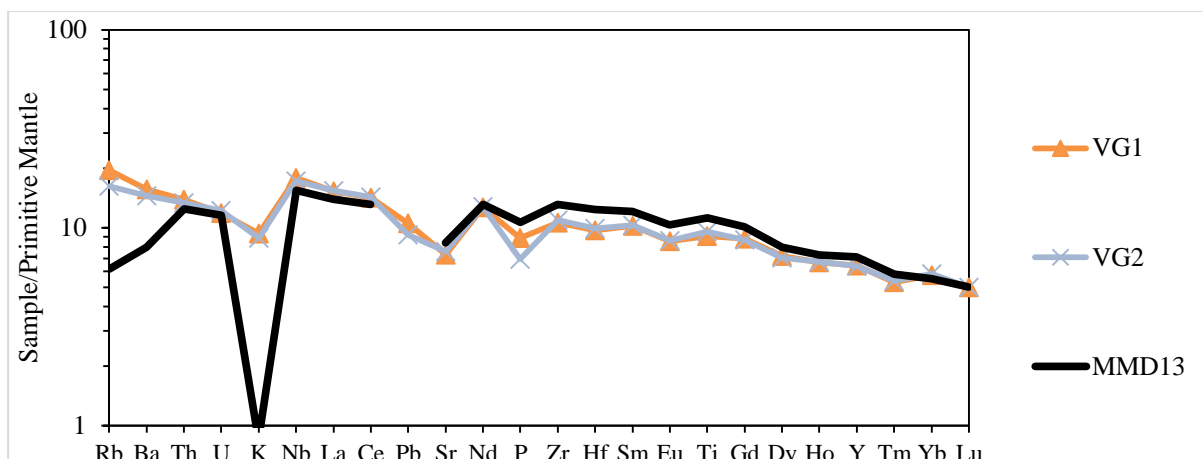


Fig. 6.26c cont...

### 6.3.5 Affinities of Group 2 dykes to Deccan Traps

From the preceding observations, I interpret dykes from Group 2 as having a robust geochemical affinity to the younger Deccan Formations belonging especially to the Wai Subgroup (Mahabaleshwar, Poladpur, Ambenali and Panhala). Some of the Group 2 dykes are also akin to the Ghatkopar-Powai tholeiite sequence that is a few millions years younger than the main phase of Deccan volcanism, and got formed at the same time as the Panvel flexure along India's west coast (Sheth et al., 2014, Pande et al., 2017).

The multi-element pattern of AG-4 shows affinities with both the Ambenali and Desur formations, with some similarities to the Ghatkopar-Powai tholeiite sequence (dyke MMD-13). In the Zr vs Th plot, it is close to the boundary of the Poladpur and Panhala formation fields. However, though Nb/Zr of AG-4 is consistent with that of the Mahabaleshwar Formation, its Ba/Y is more like that of the Ambenali Formation. Sr, Ba and TiO<sub>2</sub> are akin to the Panhala Formation (Table 6.4).

The multi-element pattern of dyke AG-9 is similar to the Ambenali Formation, but concentrations of diagnostic elements (such as Sr and Ba) match those of the Panhala

Formation, and Zr/Nb is within the Ambenali Formation range. Its TiO<sub>2</sub> content is very low and comparable to that of some Bushe lavas (Table 6.4).

The multi-element pattern, TiO<sub>2</sub>, Sr contents, and the Zr/Nb ratio of AG-15 match well with those of the Desur Formation. At the same time, it is also comparable to dyke MMD-13 from the Ghatkopar-Powai tholeiite sequence. The dyke AG-15 has Ba and Ba/Y like that of the Poladpur Formation, which is in line with results from the Zr vs Th plot.

The AG-19 dyke has a multi-element pattern matching that of the Desur Formation, while it is also analogous to dyke MMD-13 from the Ghatkopar-Powai tholeiite sequence. This dyke (AG-19) has Sr equivalent to that of Panhala Formation lavas, Ba, Zr/Nb, and TiO<sub>2</sub> within the range of Mahabaleshwar Formation Lavas, and Ba/Y similar to that of the Poladpur Formation. The dyke AG-19 plots between Poladpur and Panhala Formation fields on a Zr vs Th plot.

Dyke AG-24 roughly matches the Ambenali Formation in its multi-element pattern. However, its elemental abundances and ratios have mixed affinities to formations from the Poladpur upwards to the Desur.

Dykes BG-6, BG-7 and BG-20 have a triple geochemical affinity: to the Ambenali Formation, the Desur Formation, and Ghatkopar-Powai tholeiite sequence dyke MMD-13. The Sr and Ba contents of BG-6, BG-7 and BG-20 dykes closely match the Panhala Formation, while Zr/Nb and TiO<sub>2</sub> of BG-6 closely resemble the Mahabaleshwar Formation. Dykes BG-7 and BG-20 have Ba/Y, Zr/Nb similar to that of the Ambenali Formation, and TiO<sub>2</sub> is very low as also found in some Bushe Formation lavas. The BG-6, BG-7 and BG-20 dykes lie on the curved field of the Panhala Formation on a Zr vs Th plot.

Table 6.4 Geochemical criteria used to distinguish the younger stratigraphic units, WG (Sheth et al., 2014)

Formation	Sr (ppm)	Ba (ppm)	Ba/Y	Zr/Nb	TiO <sub>2</sub> (wt.%)
Desur	>230	>150	-	<12.5	Low (<2.25)
Panhala	<200	<90	-	>13	Low (<2.2)
Mahabaleshwar	>250	>100	>4	<10.5	>2.0
Ambenali	200-250	<100	<3.5	10.5-15	<2.7
Poladpur	-	>100	>3.5	15-20	-
Bushe	-	>100	-	>20	Very low (<1.5)

This table is based on the data from Devey and Lightfoot (1986), Lightfoot et al. (1990), Mitchell and Widdowson (1991) and Jay and Widdowson (2008). The Desur is considered as a Unit of Panhala Formation by some (Lightfoot et al., 1990; Sheth et al. 2004, 2014), while others designate it as a Formation (Hegde et al., 2014; Verma and Khosla, 2019).

BG-13 is the only dyke sample from this study that has a crude affiliation to the Poladpur Formation, principally in its multi-element pattern. Its Ba/Y is little less than the lower limit of Poladpur range, and Zr/Nb is within the upper bounds of the Mahabaleshwar Formation range. BG-13 has TiO<sub>2</sub> consistent with low-Ti Bushe Formation units, while its Ba and Sr content is within the limits of the Panhala Formation. This dyke has very low contents of Zr and Th; such signature is rarely found in the Deccan, except for few dykes of the Ghatkopar-Powai tholeiite sequence, which have low Th (~67 ppm). However, Ghatkopar-Powai dykes have Zr (~110-120 ppm) much higher than BG-13. Interestingly, the BG-13 dyke sample matches the multi-element pattern of a Ghatkopar-Powai tholeiite sequence dyke (MMD-13).

Dyke samples VG-1 and VG-2 very closely match the multi-element pattern of the average Ambenali Formation, while they are also similar to the Desur Formation and the Ghatkopar-Powai tholeiite sequence dyke MMD-13. Both VG-1 and VG-2 have Sr within the range of the Panhala Formation, while their Ba contents (~110 ppm) are higher than the upper limit of the Ambenali Formation (<100 ppm). The Zr/Nb of VG-1 and VG-2 is within limits of the Ambenali Formation while Ba/Y (VG-1: 3.6 and VG2: 3.4), is at the upper limit of the Ambenali Formation. In Zr vs Th, dyke VG-1 occupies the field of the Panhala Formation, and VG-2 falls in the Ambenali Formation field.

### 6.3.6 Stratigraphic implications

Of all the Deccan subgroups, the Wai Subgroup constitutes more than 50% of the total thickness of the Deccan basalts as measured in the WG (e.g., Beane et al., 1986) and is the only subgroup that extends to the southwestern Deccan (Lightfoot et al., 1990). Recent geochronological studies have constrained the total duration of the Deccan volcanism, and have dated the upper Deccan formations (Renne et al., 2015; Schoene et al., 2015; 2019; Sprain et al., 2019). The Deccan Trap lavas erupted continuously for 991,000 years from ~66.413 Ma ago (Jawhar Formation) to ~65.422 Ma ago (upper Mahabaleshwar Formation) (Sprain et al., 2019). Specifically, ~85% of the Kalsubai Subgroup erupted in  $242,000 \pm 101,000$  years, that ~95% of the Lonavala Subgroup erupted in  $46,000 \pm 129,000$  years and, that ~95% of the Wai Subgroup erupted in a period of  $690,000 \pm 185,000$  years. More than 75% of the Deccan Traps volume erupted within ~650,000 years around or after the KPB (Cretaceous-Paleogene Boundary;  $66.052 \pm 0.008$  Ma; Sprain et al., 2018). Also, the concept of three discrete phases of Deccan eruptions (Chenet et al., 2007) is obsolete, and the eruptions were continuous (Sprain et al., 2019).

The chemical plots and multi-element patterns discussed so far show that the Group 2 dykes, though with close similarities to the Ambenali, Panhala and Desur formations of the WG sequence, have no exact geochemical equivalents in the WG stratigraphy. Such affiliations are inconclusive because this part of the west coast of India is deeply eroded (up to 1.25 km; Widdowson, 1997) to expose the basement and plumbing system represented by dykes. These dykes may or may not have led to the surface forming basaltic flows, and maybe hypabyssal. In Goa, there are no flows to which these dykes unambiguously feed from depth. Some of the Goa dykes are similar to a Ghatkopar-Powai tholeiite sequence dyke, which is younger ( $62.4 \pm 0.1$  Ma; Pande et al., 2017) than the main Deccan eruptive sequence, and is chemically and isotopically akin to the Ambenali Formation. The sheer number of dykes

(Fig. 3.1a-d) observed along the coast of Goa occupying such a small area point towards magmatic reservoirs at depth as opposed to having been propagated from distant reservoirs. But, considering the geographical proximity of the dykes of the Goa coast to the Deccan basalts (Wai Subgroup) to the north and east (~150 km) (Fig. 6.25a), the vigorous eruption rates, and the compelling similarities between the Group 2 dykes and the uppermost Deccan flows, this part of the western continental margin of India in Goa could have very well been a part of the feeder system of the Deccan dykes. The new date for the Mahabaleshwar Formation (just below contact with the Panhala Formation at ~730 m above MSL) of  $65.422 \pm 0.103$  Ma (Sprain et al., 2019) in the Belgaum-Sankeshwar area in Karnataka makes way for 65-62 Ma magmatism in this part of Goa.

I discuss the tectonomagmatic evolution of the western Indian continental margin in the next chapter.

## **CHAPTER 7**

# **Tectono-magmatic evolution of the western Indian continental margin**

## **7.1 Introduction**

The west coast of India and the continental margin have a very striking straight-line configuration that has interested the geological fraternity for decades. There is an abrupt termination of the Deccan Trap flows along the line of WG indicating Cenozoic uplift, rifting and down-faulting. This is a volcanic passive margin that developed during India-Madagascar breakup in the Late Cretaceous (Ajay et al., 2010). The WG represented the receded margin of an uplifted landmass, the complimentary graben represented by Arabian Sea (Radhakrishna, 1993). This graben-structure is suggested for the formation of Panvel “flexure” and is a consequence of lithospheric stretching and thinning (Dessai and Viegas, 1995). Norton and Sclater (1979) suggested that India lay to the east of Seychelles before being rifted apart at 64 Ma (LaBrecque et al., 1977). The analogue of the tholeiitic west coast dyke swarm identified from Praslin and Felicite Island of Seychelles is compositionally similar to the Bushe Formation of the Deccan Traps (Devey and Stephens, 1991; 1992). Deccan related flows are also found to be located on the continental shelf south and east of Seychelles (Leg 115 Shipboard Scientific Party, 1987) during ODP leg 115. This gives a clear picture for the formation of WG, and the spatial extent of the Deccan Traps.

The western Indian continental margin has evolved after the eastern continental margin and has undergone several stages of rifting (Chandrasekharam, 1985), magmatism (Reunion &/or Marion) and isostatic adjustments (Widdowson and Cox, 1996; Subrahmanya, 1998). The earliest stage in the evolution of the western continental margin of India can be traced back to the fragmentation of Gondwanaland to East Gondwanaland (consisting of Antarctica, Australia, Madagascar, India and Sri Lanka) and West Gondwanaland (Africa, Arabia and South America) which started ~152 Ma (Late Jurassic) (Yatheesh et al., 2013). Geochemical and geophysical studies indicate the two events of basic magmatism (93 Ma and 65 Ma) evolved over an

attenuated and foundered continental crust of about 15 km thickness (Chandrasekharam and Parthasarathy, 1978).

A majority of the lineaments in the Indian subcontinent trend in N-S and NW-SE directions and bear similarities with the gravity, seismic and earthquake epicentres. Hence, a non-orogenic warping mechanism along the west coast is advocated (Qureshy, 1982). Further seismic and magnetic studies revealed that the tectonic features aligned parallel to the continental margin of India formed during the northward drift of the Indian plate and those that traverse the continent were formed before the drift (Chandrasekharam, 1985). The positive gravity anomaly around 19° N is due to up warping of the basic crust/mantle into overlying sialic crust. This happened during the Deccan Trap activity when a vast amount of basic material poured over the surface through fissures along the coast (Glennie, 1932; Chandrasekharam, 1985). Subsurface lithology offshore between 10° N and 19° N consists of Tertiary sediments overlying the basalt flows (Chandrasekharam, 1985). The west coast fault was formed in two stages, first as a narrow fracture along the northern part of the margin during the Late Jurassic-Early Cretaceous (Owen, 1976; Biswas, 1982), and extended further south during the Tertiary (Owen, 1976). Accretion of a high-density igneous layer having a thickness of ~3 km and about 40 km wide beneath the Konkan Coast, was probably due to the imprint of Deccan magmatism caused by the deep mantle plume, when the northward migrating Indian plate passed over the Reunion hotspot (Singh, 2002).

## 7.2 Stages in the development of western Indian continental margin

### 7.2.1 Stage 1: felsic magmatism (93 Ma), mafic magmatism (88 Ma), the origin of the Western Ghats of India

It all started with the breakup of Gondwanaland in the Late Triassic with a sinistral rotation of India (Biswas, 1987). Madagascar separated from Africa around ~152 Ma (Yatheesh et al., 2013) and in turn, began separating from India at ~88 Ma (Late Cretaceous) (Storey et al., 1995; Yatheesh et al., 2006; 2013; Bhattacharya & Yatheesh, 2015; Pande et al., 2017). A group of volcanic islands (St. Mary) exist at 13° 22' N consisting of rhyodacites (Naganna, 1966) ( $85.7 \pm 0.9$  Ma; Pande et al., 2001) showing columnar joints certifying that the extrusion was subaerial. The volcanic islands trend NNW-SSE in general and are related to the igneous activity resulting from partial melting and doming of the lithosphere between India and Madagascar (93 Ma; Subrahmanya, 1998; Arora et al., 2011). The breakup of Madagascar and India took place at 86.5 Ma with widespread basaltic volcanism on the eastern margin of Madagascar, and associated rhyodacites that are related to the Marion hotspot. The Sarnu-Dandali alkaline complex contains syenites, nephelinites, phonolites and rhyolites that are 88.9-86.8 Ma and some melanephelinites that are  $66.3 \pm 0.4$  Ma, proving that it is a periodically rejuvenated alkaline igneous complex (Sheth et al., 2017). The older ages of the Sarnu-Dandali complex overlap with the separation of India-Madagascar. A representational tectonic scenario is shown in *Fig. 7.1a-b* for the above discussed period.

Much similarity exists between the east-facing Great Escarpment of Madagascar running for 1500 km and that of the western continental margin of India that runs for a similar length (Radhakrishna et al., 2019). Melluso et al (2009) postulated that the St Mary's rhyodacites and the Vatmandry-Ilaka-Mananjary rhyolites in eastern Madagascar were adjacent before the Late Cretaceous rifting that split Madagascar from India. Another conspicuous similarity is the possession of gentle slopes towards the east for Madagascar and

west for India and consequent drainage directed away from their scarps. Also, the Precambrian structural trends are directed NNW in both the landmasses, which is nearly parallel to the trend of the continental margins (Subrahmanya, 1998). Hence the timing of formation of the western continental margin of India is ~86.5 Ma.

### **7.2.2 Stage 2: India's interaction with the Reunion hotspot leading to Deccan volcanism (mafic) (~70-65 Ma)**

After the formation of the western continental margin of India, this part witnessed the outpourings of a voluminous amount of tholeiitic basalts known as the Deccan Traps (peak at ~65 Ma) as the Seychelles-India block moved over the Reunion hotspot at ~70 Ma (Subrahmanya, 1998; Yatheesh et al., 2013; Jain et al. 2020). These eruptions are unique in many ways: (a) The stratigraphic position is within the K/T (Cretaceous/Tertiary) boundary (b) They have a vast area and a maximum thickness of 3 km in the WG (c) These basalts, Mascarene Plateau and Laccadive-Chagos Ridge represent the trail of the Reunion hotspot as India moved northward (Jason Morgan, 1983; Cox, 1988; Todal and Edholm, 1998; Vanderkluyesen et al., 2011; Richards et al., 2015). Richards et al. (2015) suggested that >70% of the Deccan Traps contained in the Wai Subgroup, erupted at approximately the time of K/T mass extinction and the Chicxulub impact, supplemented by U/Pb dating techniques (Renne et al., 2015). A representational tectonic scenario is shown in *Fig. 7.1c-d* for the above discussed period.

Pre-rift magmatism is abundant. Earliest magmatism is manifested in the form of lamproites in Kachchh and the Narmada valley (Karmalkar et al., 2000; 2014). It also includes Elephanta sequence (chemically akin to Khandala and Ambenali Fm; Patel et al., 2020) located near Mumbai consisting of subaerially erupted tholeiitic lava flows and dykes (66-65 Ma) contemporaneous with the main Deccan sequence in the WG (~60 km eastwards) (Samant et al., 2019). The younger dates for the ankaramite dyke ( $61.6 \pm 0.4$  Ma) in the same area point

the total duration of the Elephanta magmatism to be as much as 6 Ma (Samant et al., 2019). The Jogeshwari basalt flow dates at  $64.55 \pm 0.59$  Ma (Hooper et al., 2010). Cucciniello et al. (2019) reported older ages for granophyres (69.5-68.5 Ma) from Barda (Saurashtra) that predate (by 3-4 Ma) the intense 66-65 Ma Deccan Flood Basalts; generally, silicic magmatism post-dates the bulk of the Deccan Traps. Advanced (70-75 %), nearly-closed system fractional crystallisation in massive crustal magma chambers leads to the formation of Barda granophyres (Cucciniello et al., 2019). Some E-W trending dykes (higher width of 2.5-45 m) and N-S trending dykes (lower width 0.5-3 m) at Borlai and Uran are also part of this phase (Dessai and Viegas, 1995).

### 7.2.3 Stage 3: India-Seychelles micro-continent rifting

As a consequence of the Deccan eruptions under the influence of Reunion hotspot, the spreading centre initiated between Seychelles and India gradually diminished under the Mascarene Basin (Norton and Sclator, 1979; Yatheesh et al., 2013; Radhakrishna et al., 2019). At around 68 Ma, this process in the northern part of the western continental margin of India lead to the opening of Carlsberg Ridge (Royer et al., 1992; Müller et al., 2001). India-Seychelles rifting occurred in two phases: (a) First, a rift between India and the Laxmi Ridge at 67.6 Ma that formed the Gop Rift at 64.7 Ma (Bhattacharya and Yatheesh, 2015) and, (b) Second, rift and seafloor spreading between Laxmi Ridge and Seychelles (62.5 Ma; Bhattacharya and Yatheesh, 2015). The formation of younger volcanics due to the Reunion hotspot continued after this and, the Laccadive-Chagos ridge represents the trail of the hotspot as the Indian plate moved northward (Subrahmanya, 1998). At this stage, the Reunion hotspot shifted its place from the Indian subcontinent to offshore. A representational tectonic scenario is shown in *Fig. 7.1d* for the above discussed period.

Post-rift magmatism represented by Saki Naka trachyte intrusion at  $61.8 \pm 0.6$  Ma, the Manori trachyte intrusion at  $60.4 \pm 0.6$  Ma and the Gilbert Hill basalt intrusion at  $60.5 \pm 1.2$  Ma, is significant (Sheth et al., 2001a, b). The Mumbai trachytes formed by remelting of mafic sill complexes in the crust (Lightfoot et al., 1987), and the Manori-Gorai trachytes themselves contain mingled alkali basalt enclaves produced by mafic recharge in trachytic magma chambers (Zellmer et al., 2012). This shows the felsic-alkalic magmatism (the various trachytic intrusions), alkali basalt magmatism (mafic enclaves in the Manori-Gorai trachytes) and tholeiitic basalt magmatism (represented in the Gilbert Hill intrusion) were active as late as 60.8–60.9 Ma, a post-rift and syn-drift stage of Seychelles-Laxmi Ridge/India breakup. There was the intrusion of Dongri rhyolite flow ( $62.6 \pm 0.6$  and  $62.9 \pm 0.2$  Ma; Sheth and Pande, 2014) part of the Mumbai stratigraphic sequence. Alkaline magmatism (lamprophyres) along the coast south of Mumbai is an expression of the waning of Deccan magmatism (Dessai and Viegas, 1995).

#### **7.2.4 Stage 4: Formation of the Panvel flexure**

Panvel “Flexure” was initially described by Auden (1949), as a monoclonal bend of the Deccan lava pile or as a result of the warping of the crust in response to rifting (Devey and Lightfoot, 1986) or due to uplift of the WG and consequent subsidence of the continental margin (Watts and Cox, 1989). Field evidence ascribed the cause to normal faulting and tilting followed by attenuation and foundering of the continental crust due to crustal thinning and loading by a dyke-swarm followed by a period of massive magmatic discharge accompanying the continental breakup and opening of the Indian Ocean during the early Tertiary (Dessai and Bertrand, 1995). Sheth (1998) interpretes the formation of Panvel flexure as a reverse drag structure on an east-dipping listric master fault lying at offshore Bombay, with numerous, subsidiary, antithetic (west-dipping) and sympathetic (east-dipping) faults. Based on a recent study of Ghatkopar-Powai tholeiite flows and dykes, the formation of Panvel flexure was found

to be very rapidly, practically instantaneously at 62.5 Ma. Mutually same  $^{40}\text{Ar}/^{39}\text{Ar}$  ages of westerly dipping Ghatkopar-Powai tholeiite flows and those of vertical dykes in the same area (Pande et al., 2017) indicated the timing of formation of the Panvel flexure.

#### ***7.2.5 Stage 5: Isostatic subsidence/thermal collapse relating to the loading/eruption of Deccan basalts***

Subrahmanya (1998) proposed isostatic subsidence of the crust by 2.2 km and subsequent elevation of the WG to be 1.3 km. He ascribed this subsidence to thermal contraction of the upper mantle due to cooling after eruptions. The supporting evidence is the northward slope of the Precambrian basement rocks in the south of the DVP. There has been anomalous thinning of the lithosphere in the northern DVP due to the passage of the Indian continent over the Reunion hotspot (Patro et al., 2018). Radhakrishna et al. (2019) attributed the slumping of basalt basement below sea level up to -300 m (at Koyna) to thermal collapse and subsidence experienced by the lithosphere beneath the continental margin while returning to normal temperatures following the India-Seychelles breakup.

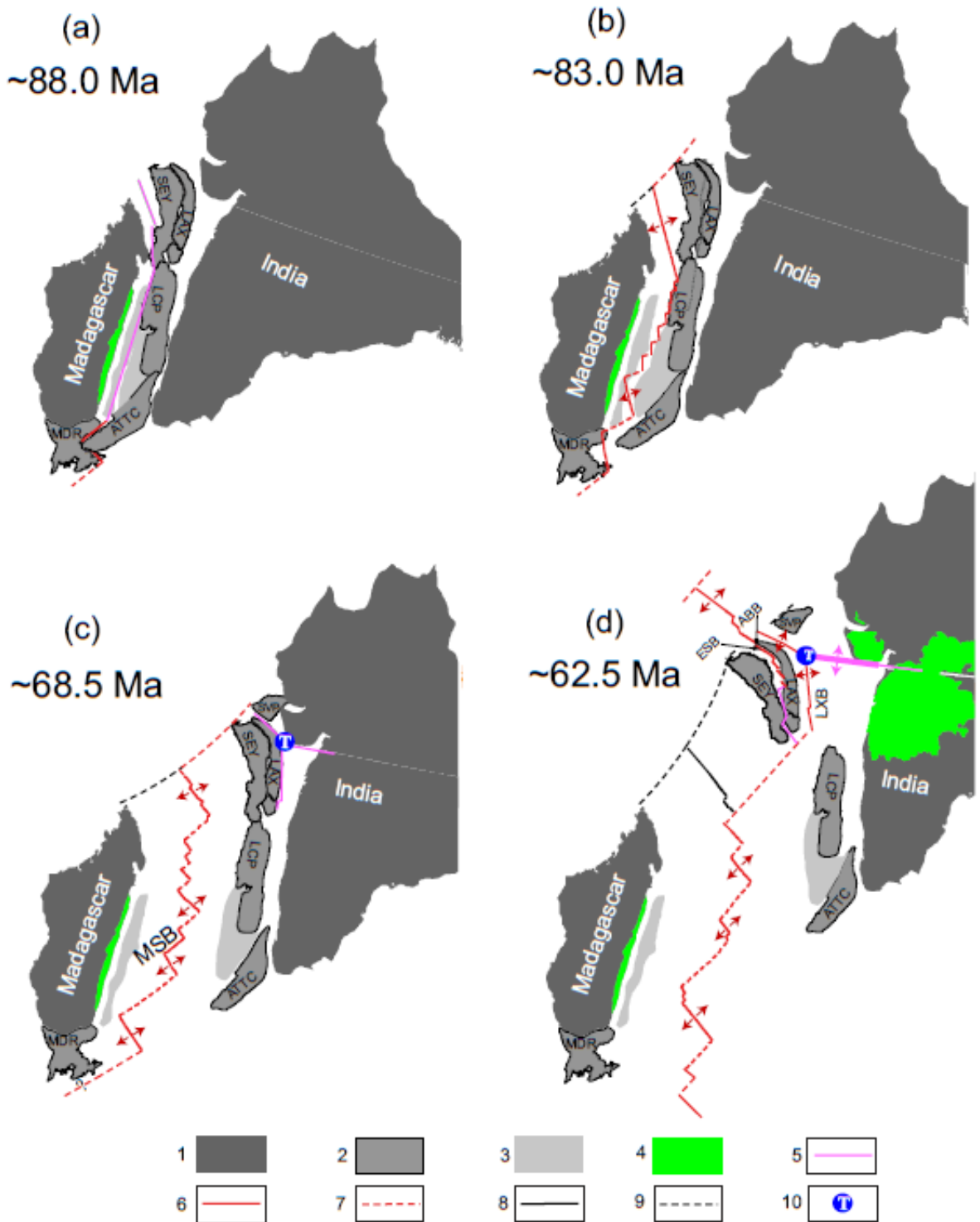


Fig. 7.1 Schematic diagrams adapted from Pande et al. (2017) depicting the major stages of India-Seychelles-Madagascar breakup and the early opening history of the Arabian Sea. (a) ~88 Ma; (b) ~83 Ma; (c) ~68.5 Ma and (d) ~62.5 Ma. The legend is explained as: (1) Major continental blocks, (2) Microcontinents, (3) Ultra-thinned continental crust, (4) Volcanics, (5) Rift axis, (6) Ridge axis, (7) Transform fault, (8) Extinct spreading centre, (9) Paleo-transform fault, (10) The Gop-Narmada-Laxmi fossil Triple Junction off the Saurashtra peninsula. Red and pink coloured arrows represent the directions of spreading and rifting, respectively. The names of geographical domains or topographical features (after Bhattacharya and Chaubey, 2001) are abbreviated as follows: ABB-Arabian Basin; ATTC-Alleppey-Trivandrum Terrace Complex; ESB-Eastern Somali Basin; LAX-Laxmi Ridge continental sliver; LCP-Laccadive Plateau; LXB-Laxmi Basin; MDR-Madagascar Ridge; MSB-Mascarene Basin; SEY-Seychelles Plateau and SVP-Saurashtra Volcanic Platform.

### **7.2.6 Stage 6: Subsidence of Bombay offshore region due to reactivation of SONATA rift**

The offshore region south of Saurashtra underwent subsidence due to downfaulting of the continental margin. As proposed, these faults could either be related to the Narmada-Son lineament (Bhattacharya and Subrahmanya, 1986) or to the meteorite impact that formed the Shiva crater (Chatterjee and Rudra, 1996). The Bombay offshore region has Eocene sediments overlying the Deccan Basalts that attest to the subsidence. Also, the lava pile south of SONATA, has a downthrow of 243 m relative to its northern counterpart (Prasad et al., 1995).

### **7.2.7 Stage 7: Buckling of south India**

At ~50-55 Ma (Middle Eocene), the spreading rate at the Carlsberg, Central Indian and Southeast Indian ridges slowed down due to India's collision in the north with an intra-oceanic island arcs system (Yatheesh et al., 2013). The Indian continent experienced compressional forces in NNE direction due to ridge-push in the south and resistive force in the north collisional zone (Gowd et al., 1996; Subrahmanya, 1998). Large wavelength undulations traversed southern India, one of which runs close to 13°N (Mangalore-Madras axis) and has created a drainage divide (Subrahmanya, 1998). This part has characteristics like gravity high, relatively thinner crust, microseismicity, the shoreline at either end is convex towards the sea, the coast has a relative fall in sea level, river channels migrate away from the axis of uplift, and hence this part has been interpreted as a zone of active deformation (Subrahmanya, 1996). Bendick and Bilham (2001) consider the view of buckling with suspicion and, instead believe that the Indian craton cannot buckle under collisional stresses owing to its high thickness. Bilhem et al. (2003) contrasts with this view and suggests that the buckling of central India having a wavelength of 670 km has taken place due to India's collision with the Asian continent.

**7.2.8 Stage 8: Separation of Laccadive-Chagos ridge from the southern part of the Mascarene plateau because of shifting of the Central Indian Ridge (40 Ma)**

A significant reorganisation of spreading centres took place in the Indian Ocean due to the collision of India with Asia during the middle Eocene leading to the formation of the Himalayas. At this stage, a part of the Mascarene plateau separated from Laccadive-Chagos Ridge at 40 Ma (Fisher et al., 1971; McKenzie and Sclater, 1971). The Reunion hotspot shifted its place from east to west of the spreading ridge (Subrahmanya, 1996).

**7.2.9 Stage 9: Tilting of the Peninsula northward due to collision and subduction**

The western continental margin of India is divided into Konkan coast in the north and Malabar Coast in the south. The Konkan coast (between 14°N and 20°N) is cliffed with headlands and embayments, and the Malabar Coast (between 8°N and 11°N) has alluvial plains and lagoons (Geological Survey of India, 1972). This indicates that the northern coast has a submergent character while the southern coast is emergent. But as the coast in Goa is neither submergent nor emergent, this state lies in the transitional type of coast (Wagle, 1993; Martha et al., 2013). An inverse relationship exists between the width of the continental shelf and coastal plain in the east and west coasts and the occurrence of Holocene terraces at a depth of 55-60 m in the south and 65-70 m in the north (Wagle et al., 1994). These pieces of evidence indicate that the western margin and the crust/lithosphere is sloping towards the north (Subrahmanya, 1996).

### **7.3 Tectono-magmatic evolution of the western Indian continental margin**

With the ongoing discussion about the tectono-magmatic evolution, it is amply clear that after the Gondwanaland broke up, felsic-mafic magmatism punctuated the western Indian continental margin. The Marion hotspot gave rise to rhyodacites in St Mary's islands that was followed by rhyolitic intrusions in Saurashtra, after which the main phase of Deccan tholeiitic magmatism erupted pre-India-Seychelles rifting, under the influence of Reunion hotspot. The formation of "Panvel flexure" (Auden, 1949; Dessai and Bertrand, 1995) is a major tectonic event characterising the evolution of this margin which constitutes blocks of lava tilted westwards along a system of N-S trending normal faults/fracture zones. Ghatkopar-Powai tholeiites formed simultaneously with the formation of the Panvel flexure (Pande et al., 2017). The Deccan lava pile is at its thickest in the vicinity of this "flexure" thinning both towards east and west. Around this time, the Reunion plume had shifted its place southwards; near Goa (Bhattacharya and Yatheesh, 2015). The shift in the dominant dyke directions from coast parallel N-S in Mumbai (Dessai and Viegas, 1995; Hooper et al., 2010) to ~NW-SE and ~E-W in Goa (Gadgil et al., 2019) could be due to the advanced stage of Mascarene Basin and Laxmi-Ridge spreading ridge exerting NE-SW to N-S extension forces on the continental margin of India. The petrogenetic aspects of Group 2 dykes indicate an intraplate tectonic scenario, with rift controlled magmatic intrusions. As the geochemical expression of Group 2 dykes is akin to the younger basalts in Mumbai (Ghatkopar-Powai tholeiites) as well as Desur lavas in Belgaum, the dykes studied represent a magmatic event active between 65-62 Ma. The waning phase of Deccan magmatism marked by trachytic, rhyolitic and alkaline intrusions along the west coast is a characteristic of extension type of margins.

Next chapter concludes the entire study.

## **CHAPTER 8**

# **Conclusions**

The concept of this thesis entitled “Structure, petrology and geochemistry of the coastal dyke swarm in Goa: Tectono-magmatic evolution of the western Indian continental margin” is based on assessing the mutual relationships of the dykes in the swarm, addressing their geochemical characteristics, searching for a clue to their stratigraphic position and their role in the evolution of the continental margin. The study area to evaluate this concept lies along the ~26 km long coastal tract of North Goa district in the state of Goa.

The first chapter introduces the dykes and the dyke swarms of the world, their emplacement mechanisms and the research problem while defining the objectives and the workflow. The second chapter discusses the regional geological and local geological set up along with a comprehensive literature review.

Chapter three describes the field occurrence of country rocks and dykes and their mutual correlation. The petrographical observations of country-rocks and dykes, along with their discussions, are incorporated in chapter four. The methodology adopted for the preparation of samples and the primary geochemical data is presented in chapter 5. Petrogenesis of country rocks and dykes forms chapter 6, which also discusses the possible stratigraphical positions of the dyke swarm. The last chapter puts forth the tectono-magmatic evolution of the western Indian continental margin.

The salient objectives of the study include identifying the sub-populations of dykes, understanding spatial and temporal variation in dyke orientations to measure paleo-tectonics, compositional variability of the dykes and country rocks followed by petrogenesis and finally to comment on tectono-magmatic evolution of the western Indian continental margin.

The findings of this study are as under:

1. Sixty dykes were observed and recorded in the study area; twenty-one dykes are in Aguada, twenty-three in Baga, nine are seen in Vagator and seven are exposed in Arambol. There is a tendency of the dykes to occur in pairs, separated from each other by a common chilled margin. Single, double and multiple-injection dykes are also observed where individual injections either are juxtaposed or are separated by a thin screen of country-rock. The dykes trend in various directions, but 70% of the them trend between ~E-W and N-S and, 87% of them are sub-vertical with the remaining dipping at various angles that vary from 50 to 85°. Majority of the dykes have an exposed length of <100 m with the most extended length being ~222 m. The thickness of the dykes ranges between 3 cm to as much as 20 m with an average thickness of ~6 m. Some dykes exhibit a 'horn' feature while a few others show a 'rock-bridge' feature. On an average, the area has suffered a crustal dilation of ~8%.
2. Owing to the gentle dip of the rocks towards N-NW, I infer that the sedimentary depositional sequence gets younger in this direction. On a general note, the metagreywacke-argillite association is at the bottom of the sequence, it transits to an assemblage of metagreywackes with intercalations of white quartzite in the middle, and quartzites occupy the upper part with calcareous sediment assemblage. The entire succession is abundant in various Soft Sediment Deformation structures (convolute laminations, slump folds, sand injections, sand ridges, water-escape structures, syndimentary faults). The features hint that the succession is deposited in a progressively shallower-basin, particularly along the unstable continental shelf setting.

3. There exists a significant spatial pattern in the dyke orientations in the study area, which may reflect fluctuations in the direction of  $\sigma_3$  over time. This is manifested by the presence of dominant dyke trends in select areas, but a small number of dykes striking in directions other than the dominant one are also noted. At various instances, the mismatch of dyke and joint trends prove that both are unrelated to each other, indicating a significant control of the contemporaneous stress field on the dyke trends.
  
4. Based on the cross-cutting relationships of the dykes, it is inferred that an ~E-W-trending  $\sigma_3$  forming ~N-S-oriented dykes existed first, followed by a broadly NE-SW, but fluctuating,  $\sigma_3$  to cause dykes to trend from NNW-SSE to WNW-ESE. This  $\sigma_3$  seems to have stabilized in the last phase of dyke emplacement to a ~N-S-trending direction leading to the intrusion of ~E-W-trending dykes. The  $\sigma_3$  remained mostly horizontal throughout, as shown by the dominantly vertical and some steeply dipping dykes. This field distinction is also reflected in petrographic characters, in that the ~N-S dykes have unique mineralogy and textures as compared to the remaining two orientations. The geochemistry is not an exception to this, which lets discrimination into two groups, Group 1 with ~N-S trending dykes and Group 2 with ~NNW-SSE/~WNW-ESE and ~E-W dykes. This also belies the belief that the dyke swarm in Goa has a monotonous trend of ~E-W as perceived earlier, it instead has three trends that have temporal variability. The data presented in this thesis hints that whereas there was some control exerted by the joints on dyke emplacement, particularly at Baga, overall there was a real control on the dyke trends by the contemporaneous stress fields.

5. The dykes, specially belonging to Group 2, have central vesicular zones that sometimes form furrows due to weathering effects. Considering the overburden removal of about 1 to 1.5 km from above the present exposures of the dykes, and the generally volatile-poor nature of mafic melts, retrograde boiling resulting crystallization, rather than an originally volatile-rich magma, appears to be a plausible mechanism for the formation of these gas vesicles. The profuse vesicle concentration along the central plane of one inclined dyke with its margins nearly free of vesicles may indicate that chilled margins developed on either side and the volatile-saturated magma being supplied was forced to flow along the central zone of the dyke, which was the last part to solidify.
  
6. The metagreywackes show sutured, fused and serrated quartz grains and chloritic matrix that hints at low-grade metamorphic effects. The subparallel arrangement of quartz grains defines a weak foliation, and the warping of the chlorite matrix around the mineral and rock clasts points towards its mild deformation. Immature, angular clasts and presence of biotite with pleochroic halos point towards its derivation from the granitic source rock. The overall dacitic affinity of these rocks in Total-Alkali Silica diagram also points to the same source rocks. Presence of slight negative Eu anomaly, comparable Sr, Rb with that of AUCC, enrichment in U and LILE suggests at a provenance of K-rich granitoids in an active continental margin setting. These source rocks could be Quepem granitoid or Dudhsagar granitoid that lie in the vicinity areas.
  
7. Microscope studies permit dyke rocks to be divided into three types, namely tholeiitic basalts and dolerites, tholeiitic hypersthene dolerites and tholeiitic picrite basalts.

Corroborating this, the major element oxide classification places the rocks primarily into subalkali basalts and basaltic andesites, with one sample as a picrite. Apart from ophitic and sub-ophitic textures, other textures like intergranular, intersertal and glomerophyric are also typical. The rocks are distinctly sub alkaline, having a characteristic tholeiitic trend.

8. Both the groups of dykes show typical tholeiitic lineage with iron enrichment trend. The major and trace elemental data for both the groups of dykes shows that the fractionation trend is overall controlled by olivine, clinopyroxene and plagioclase. In the Group 1 dykes the major control is exerted by clinopyroxene and olivine whereas in Group 2 dykes, it is olivine that exerts the major control.
9. Trace element ratios constrain the tectonic setting of the dykes to within plate settings with few related to MORB. All the dykes show enrichment in LREE and depletion in HREE on PM-normalized spider diagrams. On a general note, Group 1 dykes show pronounced LREE/MREE fractionation whereas the Group 2 dykes show moderate fractionation. The REE pattern of Group 1 is similar to UCC, whereas Group 2 dykes' pattern is akin to E-MORB. The strong negative anomaly for Nb and Ta shown by Group 1 dykes is attributed to substantial crustal contamination. In addition, these dykes also show negative anomalies at Ti and P and strong positive anomaly at Pb, which again hints at crustal contamination. In comparison, Group 2 dykes are the least contaminated. All the dykes are generated from a mantle enriched in incompatible elements. The Group 1 dykes have probably originated at a source which is EM 1 OIB with an influence of continental crust whereas the Group 2 dykes have an E-MORB source with least crustal interference.

10. Though there are limited interpretations of the mantle melting mechanisms of contaminated Group 1 dykes, this process can fairly be commented for Group 2 dykes. The Group 1 dykes are scattered between garnet and spinel curves, while Group 2 dykes forms a cluster at the spinel curve. It is also noted that the Group 1 dykes were formed due to mixing of melts of garnet-spinel peridotite with ~3-4% melting, while Group 2 have resulted from ~4% spinel peridotite melting. The transition from spinel lherzolite to garnet lherzolite occurs between 20 kbar at 1200° and between 26-27 kbar at 1500°C. Garnet is only stable in the mantle at depths higher than ~75 km. Hence, the REE data point towards possible ~75 km origin of the melting for magma generation of Group 1 dykes (owing to uncertainties arising due to crustal contamination), and <75 km depth of origin for the magma for Group 2 dykes under the lithospheric lid.
  
11. Group 1 dykes compare well with the Proterozoic dykes from the WDC, particularly with the quartz-dolerite dyke from the Goa-Dharwar sector (Devaraju et al., 2008). Interestingly, the multi-element pattern of Group 1 also matches very well with that of the Bushe Formation lavas of the Deccan Traps. As the Kalsubai and Lonavala Subgroups of the Deccan Traps erupted earlier in the history of the extrusive episode of the Deccan, their eruptive centres being located north of Nasik, the distant location (>200) of these flows from the present study area, and the rising elevation of the basement southwards prompts me to believe that the Group 1 dykes studied from Goa cannot be feeder dykes to either the Kalsubai and Lonavala Subgroups or particularly to Bushe Formation.

12. Binary geochemical plots and multi-element pattern comparison for Group 2 dykes establish the general similarity of these dykes with the younger formations (Ambenali, Poladpur, Panhala and Desur) of the WG sequence of the Deccan Traps but have no exact geochemical equivalents in the WG stratigraphy. Such affiliations are inconclusive because this part of the west coast of India is deeply eroded (up to 1.25 km) to expose the basement and plumbing system represented by dykes. In Goa, there are no flows for which these dykes unambiguously feed from depth. Some of the Goa dykes are similar to a Ghatkopar-Powai tholeiite sequence dyke, which is younger ( $62.4 \pm 0.1$  Ma) than the main Deccan eruptive sequence, and is chemically and isotopically akin to the Ambenali Formation. The sheer number of dykes observed along the coast of Goa occupying such a small area point towards magmatic reservoirs at depth as opposed to having been propagated from distant reservoirs. But, considering the geographical proximity of the dykes of the Goa coast to the Deccan basalts (Wai Subgroup) to the north and east (~150 km), the vigorous eruption rates, and the compelling similarities between the Group 2 dykes and the uppermost Deccan flows, this part of the western continental margin of India in Goa could have very well been a part of the feeder system of the Deccan dykes. Recent dates for Mahabaleshwar Formation of  $65.422 \pm 0.103$  Ma in the Belgaum-Sankeshwar area in Karnataka makes way for 65-62 Ma magmatism in this part of Goa.

13. During the break-up of Gondwanaland in the Late Jurassic, felsic-mafic magmatism punctuated the western Indian continental margin. The Marion hotspot gave rise to rhyodacites in St Mary's islands followed by rhyolitic intrusions in Saurashtra after which the main phase of Deccan tholeiitic magmatism erupted pre-India-Seychelles

rifting under the influence of the Reunion hotspot. Ghatkopar-Powai tholeiites were formed simultaneously with the formation of the Panvel flexure. Around this time, the Reunion plume had shifted its place southwards; near Goa. The shift in the dominant dyke directions from the coast parallel N-S in Mumbai to ~NW-SE and ~E-W in Goa could be due to the advanced stage of the spreading in the Mascarene Basin and the Laxmi-Ridge exerting NE-SW to N-S extension forces on the continental margin of India. The petrogenetic aspects of Group 2 dykes indicate an intraplate tectonic scenario, with rift controlled magmatic intrusions. As the geochemical expression of Group 2 dykes is akin to the younger basalts in Mumbai (Ghatkopar-Powai tholeiites) as well as Desur lavas in Belgaum, the dykes under study potentially represent a magmatic event active between 65-62 Ma. The waning phase of Deccan magmatism marked by trachytic, rhyolitic and alkaline intrusions along the west coast is a characteristic of extension type of margins.

Future work could involve a detailed sequence stratigraphy of the Sanvordem Formation rocks to understand the nature of sedimentation and processes leading to the development of the SSDs. A further detailed isotopic study of the dykes coupled with geochronology will help to establish its accurate position in the stratigraphic framework of Goa.

# References

- Agashe, L.V., Gupte, R.B. (1971) Mode of eruption of the Deccan Trap basalts. *Bulletin of Volcanology*, 35, 591–601.
- Ajay, K. K., Chaubey, A. K., Krishna, K. S., Rao, D. G., & Sar, D. (2010). Seaward dipping reflectors along the SW continental margin of India: Evidence for volcanic passive margin. *Journal of Earth System Science*, 119(6), 803–813.
- Alfaro, P., (1995). *Neotectonica en la Cuenca del Bajo Segura* (Cordillera Betica oriental) (Ph.D. thesis). Universidad de Alicante, Spain, pp219.
- Anjanappa, K. (1972) Application of Palaeomagnetism in estimating the age of the dolerite dykes of Peninsular India. *Current Science*, 41, 106-108.
- Anderson E, M. (1951) *The Dynamics of Faulting and Dyke Formation with Application to Britain*, Oliver and Boyd, Edinburgh, 2<sup>nd</sup> Edition, 206.
- Abdel-Rahman, A. F. M., & Nassar, P. E. (2004). Cenozoic volcanism in the Middle East: Petrogenesis of alkali basalts from northern Lebanon. *Geological Magazine*, 141(5), 545–563.
- Absar, N., & Sreenivas, B. (2015). Petrology and geochemistry of greywackes of the ~1.6 Ga Middle Aravalli Supergroup, northwest India: evidence for active margin processes. *International Geology Review*, 57(2), 134–158.
- Aldanmaz, E., Pearce, J. A., Thirlwall, M. F., & Mitchell, J. G. (2000). Petrogenetic evolution of late Cenozoic, post-collision volcanism in western Anatolia, Turkey. *Journal of Volcanology and Geothermal Research*, 102(1–2), 67–95.
- Allègre, C. J., Poirier, J. P., Humler, E., & Hofmann, A. W. (1995). The chemical composition of the Earth. *Earth and Planetary Science Letters*, 134(3-4), 515-526.
- Ancochea, E., Brändle, J. ., Huertas, M. ., Cubas, C. ., & Hernán, F. (2003). The felsic dikes of La Gomera (Canary Islands): identification of cone sheet and radial dike swarms. *Journal of Volcanology and Geothermal Research*, 120(3–4), 197–206.
- Armistead, S. E., Collins, A. S., Payne, J. L., Foden, J. D., De Waele, B., Shaji, E., & Santosh, M. (2018). A re-evaluation of the Kumta Suture in western peninsular India and its extension into Madagascar. *Journal of Asian Earth Sciences*, 157(June), 317–328.
- Arora, K., Tiwari, V. M., Singh, B., Mishra, D. C., & Grevemeyer, I. (2012). Three dimensional lithospheric structure of the western continental margin of India

- constrained from gravity modelling: Implication for tectonic evolution. *Geophysical Journal International*, 190(1), 131–150.
- Athavale, R. N. and Verma, R. K. (1970) Palaeomagnetic results on Gondwana dykes from the Damodar valley coal fields and their bearing on the sequence of Mesozoic igneous activity in India. *Geophysical Journal of Royal Astrological Society of London*, 20, 303-316.
- Augustithis S S, (1978) *Atlas of the Textural Patterns of Basalts And Their Genetic Significance*, Elsevier Science Publishing Company, Amsterdam, 323.
- Auden, J. B. (1949) Dykes in western India- a discussion of their relationships with the Deccan Traps. *Transactions of National Institute of Science India*, 3, 123-157.
- Babiker, M., & Gudmundsson, A. (2004). Geometry, structure and emplacement of mafic dykes in the Red Sea Hills, Sudan. *Journal of African Earth Sciences*, 38(3), 279–292.
- Baer G., Beyth M. (1990) A mechanism of dyke segmentation in fractured host rock. In: Parker AJ, Rickwood PC, Tucker DH (eds) *Mafic Dykes And Emplacement Mechanisms*. Balkema, Rotterdam, pp 3–11
- Baksi, A. K. (1994). Geochronological studies on whole-rock basalts, Deccan Traps, India: evaluation of the timing of volcanism relative to the K-T boundary. *Earth and Planetary Science Letters*, 121(1–2), 43–56.
- Baksi, A. K. (2014). The Deccan Trap-Cretaceous-Paleogene boundary connection; new  $^{40}\text{Ar}/^{39}\text{Ar}$  ages and critical assessment of existing argon data pertinent to this hypothesis. *Journal of Asian Earth Sciences*, 84, 9–23.
- Balasubrahmanyam, M. N. (1975) The age of the dykes of south Kanara, Mysore state. *Geological Survey of India Miscellaneous Publication*, 23, 236-239.
- Banerjee, D. M., & Bhattacharya, P. (1994). Petrology and geochemistry of greywackes from the Aravalli Supergroup, Rajasthan, India and the tectonic evolution of a Proterozoic sedimentary basin. *Precambrian Research*, 67(1–2), 11–35.
- Baragar, W. R. A., Ernst, R. E., Hulbert, L., & Peterson, T. (1996). Longitudinal Petrochemical Variation in the Mackenzie Dyke Swarm, Northwestern Canadian Shield. *Journal of Petrology*, 37(2), 317–359.
- Barth, T. F. W. 1962. *Theoretical Petrology*, 2<sup>nd</sup> edition, John Wiley & Sons, NY, 416.

- Basavaiah, N., Satyanarayana, K. V. V., Deenadayalan, K., & Prasad, J. N. (2018). Does Deccan Volcanic Sequence contain more reversals than the three-Chron N-R-N flow magnetostratigraphy?-a palaeomagnetic evidence from the dyke-swarm near Mumbai. *Geophysical Journal International*, 213(3), 1503–1523.
- Beane, J. E., Turner, C. A., Hooper, P. R., Subbarao, K. V., & Walsh, J. N. (1986). Stratigraphy, composition and form of the Deccan Basalts, Western Ghats, India. *Bulletin of Volcanology*, 48(1), 61–83.
- Beckinsale, R. D., Drury, S. A., & Holt, R. W. (1980). 3,360-Myr old gneisses from the South Indian Craton. *Nature*, 283(5746), 469–470.
- Bendick, R. and Bilham, R. (2001) Search for buckling of the southwest Indian coast related to Himalayan collision. In: *Himalaya and Tibet: Mountain Roots To Mountain Tops*, (ed) A Macfarlane, R Sorkhabi, and J Quade; *Geological Society of America Special Paper*, 328, 313-323.
- Belica, M. E., Piispa, E. J., Meert, J. G., Pesonen, L. J., Plado, J., Pandit, M. K., Kamenov, G. D., & Celestino, M. (2014). Paleoproterozoic mafic dyke swarms from the Dharwar craton; paleomagnetic poles for India from 2.37 to 1.88Ga and rethinking the Columbia supercontinent. *Precambrian Research*, 244(1), 100–122.
- Bender, J. F., Langmuir, C. H., & Hanson, G. N. (1984). Petrogenesis of Basalt Glasses from the Tamayo Region, East Pacific Rise. *Journal of Petrology*, 25(1), 213–254.
- Bhaskar Rao, Y. J., Sivaraman, T. V., Pantulu, G. V. C., Gopalan, K., & Naqvi, S. M. (1992). Rb-Sr ages of late Archean metavolcanics and granites, Dharwar craton, South India and evidence for Early Proterozoic thermotectonic event (s). *Precambrian Research*, 59(1-2), 145-170.
- Bhatia, M. R. (1983). Plate tectonics and geochemical composition of sandstones. *Journal of Geology*, 91(6), 611-627.
- Bhatia, M. R., & Crook, K. A. W. (1986). Trace element characteristics of greywackes and tectonic setting discrimination of sedimentary basins. *Contributions to Mineralogy and Petrology*, 92(2), 181–193.
- Bhattacharji, S., Chatterjee, N., Wampler, J. M., Nayak, P. N., & Deshmukh, S. S. (1996). Indian intraplate and continental margin rifting, lithospheric extension, and mantle

- upwelling in deccan flood basalt volcanism near the K/T boundary: Evidence from mafic dike swarms. *Journal of Geology*, 104(4), 379–398.
- Bhattacharya, G. C., & Subrahmanyam, V. (1986). Extension of the Narmada — Son lineament on the continental margin off Saurashtra, Western India as obtained from magnetic measurements. *Marine Geophysical Researches*, 8(4), 329–344.
- Bhattacharya, H., & Bandyopadhyay, S. (1998). Seismites in a Proterozoic tidal succession, Singhbhum, Bihar, India. *Sedimentary Geology*, 119(3–4), 239–252.
- Bhattacharya, G. C. & Yatheesh, Y. V. (2015) Plate-Tectonic Evolution of the Deep Ocean Basins Adjoining the Western Continental Margin of India—A Proposed Model for the Early Opening Scenario. In: Mukherjee S. (eds) *Petroleum Geosciences: Indian Contexts*. Springer Geology. Springer, Cham, pp.1-61.
- Bilham, R., Bendick, R., & Wallace, K. (2003). Flexure of the Indian plate and intraplate earthquakes. *Journal of Earth System Science*, 112(3), 315–329.
- Biswas, S. K. (1982). Rift Basins in western margin of India and their hydrocarbon prospects with special reference to Kutch Basin. *American Association of Petroleum Geologists Bulletin*, 66.
- Biswas, S. K. (1987). Regional tectonic framework, structure and evolution of the western marginal basins of India. *Tectonophysics*, 135(4), 307–327.
- Blanford, W. T. (1869) On the geology of the Taptee and Lower Narmada valleys and some adjoining districts. *Geological Survey of India Memoirs, Number 6*, 163-384.
- Bogaard, P. J. F., & Wörner, G. (2003). Petrogenesis of Basanitic to Tholeiitic volcanic rocks from the Miocene Vogelsberg, Central Germany. *Journal of Petrology*, 44(3), 569-602.
- Boggs, S. J. (2009). *Petrology of Sedimentary Rocks* (2<sup>nd</sup> Edition). Cambridge University Press.
- Bondre, N. R., Duraiswami, R. A., & Dole, G. (2004a). Morphology and emplacement of flows from the Deccan Volcanic Province, India. *Bulletin of Volcanology*, 66(1), 29–45.
- Bondre, N. R., Duraiswami, R. A., & Dole, G. (2004b). A brief comparison of lava flows from the Deccan Volcanic Province and the Columbia-Oregon Plateau Flood Basalts: Implications for models of flood basalt emplacement. *Journal of Earth System Science*, 113(4), 809–817.

- Bondre, N. R., Hart, W. K., & Sheth, H. C. (2006). Geology and geochemistry of the Sangamner mafic dike swarm, western Deccan Volcanic Province, India: Implications for regional stratigraphy. *Journal of Geology*, *114*(2), 155–170.
- Bons, P. D., Elburg, M. A., & Gomez-Rivas, E. (2012). A review of the formation of tectonic veins and their microstructures. *Journal of Structural Geology*, *43*, 33–62.
- Bose, P. K., Banerjee, S., & Sarkar, S. (1997). Slope-controlled seismic deformation and tectonic framework of deposition: Koldaha Shale, India. *Tectonophysics*, *269*(1-2), 151-169.
- Bose, P. N. (1884) Geology of the Lower Narbada valley between Nimawar and Kawant. *Geological Survey of India Memoirs, Number 21*, 1-72.
- Bowman, D., Korjenkov, A., & Porat, N. (2004). Late-Pleistocene seismites from Lake IssykKul, the Tien Shan range, Kyrghyzstan. *Sedimentary Geology*, *163*(3–4), 211–228.
- Branquet, Y., Cheilletz, A., Giuliani, G., Laumonier, B., & Blanco, O. (1999). Fluidized hydrothermal breccia in dilatant faults during thrusting: the Colombian emerald deposits. *Geological Society, London, Special Publications*, *155*(1), 183–195.
- Buchan, K L, & Ernst, R. E. (2004). *Diabase dyke swarms and related units in Canada and adjacent regions*.
- Buchan, K. L., Mortensen, J. K., & Card, K. D. (1993). Northeast-trending early Proterozoic dykes of southern Superior Province: multiple episodes of emplacement recognized from integrated paleomagnetism and U-Pb geochronology. *Canadian Journal of Earth Sciences*, *30*(6), 1286-1296.
- Buchan, K. L., & Ernst, R. E. (2018). A giant circumferential dyke swarm associated with the High Arctic Large Igneous Province (HALIP). *Gondwana Research*, *58*, 39–57.
- Buchan, K. L., & Ernst, R. E. (2019). *Giant Circumferential Dyke Swarms: Catalogue and Characteristics* (pp. 1–44).
- Budkewitsch, P., & Robin, P. Y. (1994). Modelling the evolution of columnar joints. *Journal of Volcanology and Geothermal Research*, *59*(3), 219–239.
- Burns, R. G., & Fyfe, W. S. (1966). Distribution of elements in geological processes. *Chemical Geology*, *1*(C), 49–56.
- BVSP. (1981). *Basaltic Volcanism On The Terrestrial Planets*. Pergamon Press, 1286.

- Campbell, I. H., & Griffiths, R. W. (1990). Implications of mantle plume structure for the evolution of flood basalts. *Earth and Planetary Science Letters*, 99(1-2), 79-93.
- Carlson, R. W. (1991). Physical and chemical evidence on the cause and source characteristics of flood basalt volcanism. *Australian Journal of Earth Sciences*, 38, 525-544.
- Carmichael, I. S. E., Turner, F. J., & Verhoogen, J. (1974). *Igneous Petrology*, McGraw Hill, NY, 739.
- Chadwick, W. W., & Howard, K. A. (1991). The pattern of circumferential and radial eruptive fissures on the volcanoes of Fernandina and Isabela islands, Galapagos. *Bulletin of Volcanology*, 53(4), 259-275.
- Chadwick, B., Vasudev, V. N., Hegde, G. V. (2000). The Dharwar craton, southern India, interpreted as the result of late Archaean oblique convergence. *Precambrian Research* 99, 91-101.
- Chadwick, B., Vasudev, V. N., Hegde, G. V. (1997) The Dharwar Craton, southern India, and its late Archean plate tectonic setting: current interpretations and controversies. *Proceedings of the Indian Academy of Science (EPS)*, 106, 249-258.
- Chandrasekharam, D. & Parthasarathy, A. (1978). Geochemical and tectonic studies on the coastal and inland Deccan Trap volcanics and a model for the evolution of Deccan Trap volcanism. *Neues Jahrbuch Für Mineralogie - Abhandlungen*, 132(2), 214-229.
- Chandrasekharam, D. (1985). Structure and evolution of the western continental margin of India deduced from gravity, seismic, geomagnetic and geochronological studies. *Physics of the Earth and Planetary Interiors*, 41(2-3), 186-198.
- Chandrasekharam, D., Melluso, L., Cucciniello, C., Mathew, B., Perini, G. (2008) Petrogenesis of E-W trending dykes from Kalyadi, Dharwar Craton, southwestern India. In Srivastava, R. K., Sivaji, Ch., Chalapathi Rao, N. V. (Eds) *Indian Dykes: Geochemistry, Geophysics, Geochronology*. Narosa Publishing House, 199-214.
- Chavadi, V. C. (1974) Geology of the mafic and other associated rocks of Savantwadi, Ratnagiri District, Maharashtra State. *Unpublished PhD Thesis, Karnatak University, Dharwar*.
- Chardon, D., Jayananda, M., Chetty, T. R. K., & Peucat, J.-J. (2008). Precambrian continental strain and shear zone patterns: South Indian case. *Journal of Geophysical Research: Solid Earth*, 113(B8).

- Chardon, D., Jayananda, M., & Peucat, J.-J. (2011). Lateral constrictional flow of hot orogenic crust: Insights from the Neoproterozoic of south India, geological and geophysical implications for orogenic plateaux. *Geochemistry, Geophysics, Geosystems*, 12(2), Q02005, <https://doi.org/10.1029/2010GC003398>.
- Chatterjee, N., & Bhattacharji, S. (2008). Trace element variations in Deccan basalts: Roles of mantle melting, fractional crystallization and crustal assimilation. *Journal of the Geological Society of India*, 71, 171-188.
- Chatterjee, K. K., Deshmukh, S. S. (1996) Inferring palaeostresses from mafic dyke swarms in Deccan volcanics, Maharashtra and Madhya Pradesh, India. In: Deshmukh, S. S., Nair, K. K. K. (Eds.) Deccan Basalts. *Gondwana Geological Magazine Special Vol. 2*, 375-391.
- Chatterjee, S. and Rudra, D. K. (1996). K.T. events in India: Impact, Rifting, Volcanism and Dinosaur extinction. *Memoirs of the Queensland Museum*, Brisbane, 39, 489-532.
- Chenet, A. L., Quidelleur, X., Fluteau, F., Courtillot, V., & Bajpai, S. (2007).  $^{40}\text{K}$ - $^{40}\text{Ar}$  dating of the Main Deccan large igneous province: Further evidence of KTB age and short duration. *Earth and Planetary Science Letters*, 263(1-2), 1-15.
- Chesworth, W., Dejoux, J., Larroque, P., & Rodeja, E. G. (2004). Alteration of olivine in a basalt from central France. *CATENA*, 56(1-3), 21-30.
- Clark, G. T. (1869). Remarks upon the basalt dykes of the mainland of India, opposite to the Islands of Bombay and Salsette. *Quarterly Journal of the Geological Society of London*, 25, 163-168.
- Clemens, J. D., & Mawer, C. K. (1992). Granitic magma transport by fracture propagation. *Tectonophysics*, 204(3-4), 339-360.
- Coffin, M. F., & Eldholm, O. (1993). Scratching the surface: estimating dimensions of large igneous provinces. *Geology*, 21(6), 515-518.
- Coffin, Millard F., & Eldholm, O. (1992). Volcanism and continental break-up: A global compilation of large igneous provinces. *Geological Society Special Publication*, 68, 17-30.
- Coffin, Millard F., & Eldholm, O. (1994). Large igneous provinces: Crustal structure, dimensions, and external consequences. In *Reviews of Geophysics*, 32(4), 1-36.

- Coffin, M.F. & Eldholm, O. (2005). Large igneous provinces. In Selley, R.C., Cocks, R., & Plimer, I.R. (eds.), *Encyclopedia of Geology*. Elsevier: Oxford, 315–323.
- Collinson, J. (1994). Sedimentary deformational structures. In Maltman A. (Eds) *The Geological Deformation of Sediments*. Springer Dordrecht, 95-125.
- Condie, K. C. (1967). Geochemistry of early Precambrian graywackes from Wyoming. *Geochimica et Cosmochimica Acta*, 31(11), 2135-2136, IN1-IN2, 2137-2149.
- Condie, K. C. (1993). Chemical composition and evolution of the upper continental crust: Contrasting results from surface samples and shales. *Chemical Geology*, 104(1–4), 1–37.
- Condie, K. C. (2001). *Mantle Plumes and their Record in Earth History*. Cambridge University Press, 1-306.
- Condie, K. C. (2003). Incompatible element ratios in oceanic basalts and komatiites: Tracking deep mantle sources and continental growth rates with time. *Geochemistry, Geophysics, Geosystems*, 4(1), 1–28. <https://doi.org/10.1029/2002GC000333>
- Condie, K. C. (2005). High field strength element ratios in Archean basalts: A window to evolving sources of mantle plumes? *Lithos*, 79(3-4 SPEC. ISS.), 491–504.
- Coulson, A. L. (1933) Barytes in Ceded districts of Madras Presidency, with notes on its occurrence in other parts of India. *Geological Survey of India Memoirs, Number 64*(1), 114-115.
- Courtillot, V., Vandamme, D., Montigny, R., Jaegar, J. J., Capetta, H. (1986) Deccan flood basalts at the Cretaceous/Tertiary boundary? *Earth and Planetary Science Letters, Vol. 80*, 361-374.
- Courtillot, V., Féraud, G., Maluski, H., Vandamme, D., Moreau, M. G., & Besse, J. (1988). Deccan flood basalts and the Cretaceous/Tertiary boundary. *Nature*, 333(6176), 843–846.
- Cox, K. G. (1980). A model for flood basalt volcanism. *Journal of Petrology*, 21(4), 629–650.
- Cox, K. G. (1983) The Deccan Traps and the Karoo: stratigraphic implications of possible hot-spot origins, IAVCEI Abstracts, Hamburg, 96.
- Cox, K. G., Bell, J. D., & Pankhurst, R. J. (1979). *The Interpretation of Igneous Rocks*. Springer Netherlands, 1-450.

- Cox, K. G., & Hawkesworth, C. J. (1984). Relative contribution of crust and mantle to flood basalt magmatism, Mahabaleshwar area, Deccan Traps. *Philosophical Transactions of the Royal Society of London* 310 (1514), 627-641.
- Cox, K. G., & Hawkesworth, C. J. (1985). Geochemical stratigraphy of the deccan Traps at Mahabaleshwar, Western Ghats, India, with implications for open system magmatic processes. *Journal of Petrology*, 26(2), 355–377.
- Crawford, A. D. and Compston, W. (1970) The age of the Vindhyan system of Peninsular India. *Quaternary Journal, Geological Society of London*, 125, 351-372.
- Crookshank, H. (1936) Geology of the northern slopes of the Satpuras between Morand and Sher river. *Geological Survey of India Memoirs, Vol. 66*.
- Crookshank, H. (1963) Geology of southern Bastar and Jeypore from the Bailadila range to the Eastern Ghats. *Geological Survey of India Memoirs, Vol. 87*, 1-150.
- Cross, W., Iddings, J. P., Pirsson, L. V., & Washington, H. S. (1902). A Quantitative Chemicomineralogical Classification and Nomenclature of Igneous Rocks. *The Journal of Geology*, 10(6), 1-155.
- Cucciniello, C., Choudhary, A. K., Pande, K., & Sheth, H. (2019). Mineralogy, geochemistry and  $^{40}\text{Ar}$ - $^{39}\text{Ar}$  geochronology of the Barda and Alech complexes, Saurashtra, northwestern Deccan Traps: Early silicic magmas derived by flood basalt fractionation. *Geological Magazine*, 156(10), 1668–1690.
- Cucciniello, C., Demonerova, E. I., Sheth, H., Pande, K., & Vijayan, A. (2015).  $^{40}\text{Ar}/^{39}\text{Ar}$  geochronology and geochemistry of the Central Saurashtra mafic dyke swarm: insights into magmatic evolution, magma transport, and dyke-flow relationships in the northwestern Deccan Traps. *Bulletin of Volcanology*, 77(5), 1–19.
- Currie, K. L., & Ferguson, J. (1970). The mechanism of intrusion of lamprophyre dikes indicated by “Offsetting” of dikes. *Tectonophysics*, 9(6), 525-535.
- Daniels, K. A., Kavanagh, J. L., Menand, T., & Sparks, R. S. J. (2012). The shapes of dikes: Evidence for the influence of cooling and inelastic deformation. *Bulletin of the Geological Society of America*, 124(7–8), 1102–1112.
- Davis, G. H., Reynolds, S. J., & Kluth, C. (2012). *Structural Geology of Rocks and Regions*. Hoboken: Wiley.

- DeGraff, J. M., & Aydin, A. (1987). Surface morphology of columnar joints and its significance to mechanics and direction of joint growth. *Bulletin of the Geological Society of America*, 99(5), 605–617.
- Delaney, P. T., & Pollard, D. D. (1981). Deformation of host rocks and flow of magma during growth of minette dikes and breccia-bearing intrusions near Ship Rock, New Mexico. *U.S. Geological Survey Professional Papers*, 1202, 61p.
- Delaney, Paul T., Pollard, D. D., Ziony, J. I., & McKee, E. H. (1986). Field relations between dikes and joints: Emplacement processes and paleostress analysis. *Journal of Geophysical Research*, 91(B5), 4920.
- Delaney, Paul T., & Pollard, D. D. (1982). Solidification of basaltic magma in a dike. *American Journal of Science*, Vol. 282, 856–885
- Dessai, A. G. (2011). The Geology of Goa Group: Revisited. *Journal of the Geological Society of India*, Vol. 78(3), 233–242.
- Dessai, A. G. (2018). *Geology and Mineral Resources of Goa* (1st Edition). New Delhi Publishers.
- Dessai, A.G. and Peshwa, V.V. (1982) Manganese mineralization in the tropical forest area of Goa, India. In: D.J.C. Laming and A.K. Gibbs (Eds.), *Hidden Wealth: Mineral Exploration Techniques in Tropical Forest Areas*. Proc. Seminar of the Association of Geoscientists for International Development, Caracas, Venezuela, pp.170-175.
- Dessai, A. G., Viegas, A. A. A. A. (1995) Multi-generation mafic dyke swarm related to Deccan magmatism, south of Bombay: Implications on the evolution of the western Indian continental margin. In: Devaraju, T. C. (Ed.), *Dyke Swarms of Peninsular India. Geological Society of India Memoirs Vol. 33*, 435-451.
- Dessai, A. G., & Bertrand, H. (1995). The “Panvel Flexure” along the Western Indian continental margin: an extensional fault structure related to Deccan magmatism. *Tectonophysics*, 241(1–2), 165–178.
- Dessai, A. G., Rock, N. M. S., Griffin, B. J., & Gupta, D. (1990). Mineralogy and petrology of some xenolith-bearing alkaline dykes associated with Deccan magmatism, south of Bombay, India. *European Journal of Mineralogy*.

- Dessai, A. G., Downes, H., López-Moro, F. J., & López-Plaza, M. (2008). Lower crustal contamination of Deccan Traps magmas: Evidence from tholeiitic dykes and granulite xenoliths from western India. *Mineralogy and Petrology*, 93(3–4), 243–272.
- Dessai, A. G., Arolkar, D. B., French, D., Viegas, A., & Viswanath, T. A. (2009). Petrogenesis of the Bondla layered mafic-ultramafic complex, Usgaon, Goa. *Journal of the Geological Society of India*, 73(5), 697–714.
- Dessai, A. G., Viegas, A. (2010) Petrogenesis of alkaline rocks from Murud-Janjira, in the Deccan Traps, Western India. *Mineralogy & Petrology*, 98, 297–311.
- Deshmukh, S. S., Sehgal, M. N. (1988) Mafic dyke swarms in Deccan Volcanic Province of Madhya Pradesh and Maharashtra. In: Subbarao, K. V. (Ed.), Deccan Flood Basalts. *Geological Society of India Memoirs Vol. 10*, 323-340.
- Devaraju, T. C. (1995) Dyke swarms of Peninsular India (Editor). *Geological Society of India Memoirs Number 33*, 451.
- Devaraju, T. C., Alapeiti, T. T., Sudhakara, T. L., Kaukonen, R. J. (2008) Mafic dyke swarms of volcanic arc, ocean floor and N-MORB affinity with destructive plate margin emplacement features in the northern segment of the Western Dharwar Craton. In Srivastava, R. K., Sivaji, Ch., Chalapathi Rao, N. V. (Eds) *Indian Dykes: Geochemistry, Geophysics, Geochronology*. Narosa Publishing House. 215-237
- Devaraju, T. C., Huhma, H., Sudhakara, T. L., Kaukonen, R. J., & Alapieti, T. T. (2007). Petrology, geochemistry, model Sm-Nd ages and petrogenesis of the granitoids of the northern block of Western Dharwar Craton. *Journal of the Geological Society of India*, 70(6), 889–911.
- Devaraju, T. C., Sudhakara, T. L., Kaukonen, R. J., Viljoen, R. P., Alapieti, T. T., Ahmed, S. A., & Sivakumar, S. (2010). Petrology and geochemistry of greywackes from Goa-Dharwar sector, western Dharwar craton: Implications for volcanoclastic origin. *Journal of the Geological Society of India*, 75(3), 465–487.
- Devey, C. W. (1986). *Stratigraphy and geochemistry of the Deccan Trap lavas, western India*. D. Phil. Thesis, Oxford University.
- Devey, C. W., & Cox, K. G. (1987). Relationships between crustal contamination and crystallisation in continental flood basalt magmas with special reference to the Deccan Traps of the Western Ghats, India. *Earth and Planetary Science Letters*, 84(1), 59–68.

- Devey, C. W., & Stephens, W. E. (1991). Tholeiitic dykes in the Seychelles and the original spatial extent of the Deccan. *Journal of the Geological Society*, 148(6), 979–983.
- Devey, C. W., & Stephens, W. E. (1992). Deccan-related magmatism west of the Seychelles-India rift. *Geological Society Special Publication*, 68(68), 271–291.
- Devey, C. W., & Lightfoot, P. C. (1986). Volcanological and tectonic control of stratigraphy and structure in the western Deccan Traps. *Bulletin of Volcanology*, 48, 195–207.
- Dhondial, D. P., Paul, D. K., Sarkar, A., Trivedi, J. R., Gopalan, K., & Potts, P. J. (1987). Geochronology and geochemistry of Precambrian granitic rocks of Goa, SW India. *Precambrian Research*, 36(3–4), 287–302.
- Drury, S. A. (1983). The petrogenesis and setting of Archaean metavolcanics from Karnataka State, South India. *Geochimica et Cosmochimica Acta*, 47(2), 217–329.
- Duncan, R. A., & Pyle, D. G. (1988). Rapid eruption of the Deccan flood basalts at the Cretaceous/Tertiary boundary. *Nature*, 333(6176), 841–843.
- Dungan, M. A., & Rhodes, J. M. (1978). Residual glasses and melt inclusions in basalts from DSDP Legs 45 and 46: Evidence for magma mixing. *Contributions to Mineralogy and Petrology*, Vol. 67, 417–431.
- Dunn, J. A. (1929) Geology of northern Singhbhum, including parts of Ranchi and Manbhum districts. *Geological Survey of India Memoirs*, Vol. 54, 166.
- Durney, D.W., Ramsay, J.G., 1973. Incremental strains measured by syntectonic crystal growth. In de Jong, K.A., Scholten, R. (Editors), *Gravity and Tectonics*. Wiley, New York, 67–96.
- Elliott, C. G., & Williams, P. F. (1988). Sediment slump structures: a review of diagnostic criteria and application to an example from Newfoundland. *Journal of Structural Geology*, 10(2), 171–182.
- Erlank, A. J., & Kable, E. J. D. (1976). The significance of incompatible elements in mid-Atlantic ridge basalts from 45°N with particular reference to Zr/Nb. *Contributions to Mineralogy and Petrology*, 54(4), 281–291.
- Ernst, R., & Bleeker, W. (2010). Large igneous provinces (LIPs), giant dyke swarms, and mantle plumes: Significance for breakup events within Canada and adjacent regions from 2.5 Ga to the present. *Canadian Journal of Earth Sciences*, 47(5), 695–739.

- Ernst, R. E., Head, J. W., Parfitt, E., Grosfils, E., & Wilson, L. (1995). Giant radiating dyke swarms on Earth and Venus. *Earth Science Reviews*, 39(1–2), 1–58.
- Ernst, R. E. (2014). *Large Igneous Provinces*. Cambridge University Press.
- Ernst, R. E., & Baragar, W. R. A. (1992). Evidence from magnetic fabric for the flow pattern of magma in the Mackenzie giant radiating dyke swarm. *Nature*, 356, 511–513.
- Ernst, R. E., & Buchan, K. L. (1997). Giant radiating dyke swarms: Their use in identifying pre-Mesozoic large igneous provinces and mantle plumes. In *Geophysical Monograph Series*.
- Ernst, R. E., & Buchan, K. L. (2001). The use of mafic dike swarms in identifying and locating mantle plumes. *Special Paper of the Geological Society of America*, 352, 247–265.
- Ernst, R. E., & Srivastava, R. K. (2008). India's place in the Proterozoic world: constraints from the Large Igneous Province (LIP) record. *Indian Dykes. Edited by RK Srivastava, Ch. Sivaji, and NV Chalapathi Rao. Geochemistry, Geophysics, and Geochronology, Narosa Publishing House Pvt. Ltd, New Delhi, India.*
- Ernst, R.E., Buchan, K.L. 1998. Arcuate dyke swarms associated with mantle plumes on Earth: implications for Venusian coronae. Lunar and Planetary Science Conference #29, abstract #1021.
- Ernst, R.E. & Buchan, K.L. (2004). Dyke (dike) swarm. In Goudie, A.S. (ed.), *Encyclopedia of Geomorphology*. London: Routledge, p. 305.
- Ewart, A. (2004). Petrology and Geochemistry of Early Cretaceous Bimodal Continental Flood Volcanism of the NW Etendeka, Namibia. Part 1: Introduction, Mafic Lavas and Re-evaluation of Mantle Source Components. *Journal of Petrology*, 45(1), 59–105.
- Fahrig, W.F. (1987). The tectonic setting of continental mafic dyke swarms: failed arm and early passive margin. In Halls, H.C. & Fahrig, W.F. (eds.), *Mafic Dyke Swarms*. St John's, NL: Geological Association of Canada, Special Publication 34, 331–348.
- Fahrig, W. F., Christie, K. W., Chown, E. H., Janes, D., & Machado, N. (1986). The tectonic significance of some basic dyke swarms in the Canadian Superior province with special reference to the geochemistry and paleomagnetism of the Mistassini swarm, Quebec, Canada. *Canadian Journal of Earth Sciences*, 23(2), 238–253.

- Feng, R., & Kerrich, R. (1990). Geochemistry of fine-grained clastic sediments in the Archean Abitibi greenstone belt, Canada: Implications for provenance and tectonic setting. *Geochimica et Cosmochimica Acta*, 54(4), 1061–1081.
- Fernandes, G. Q. (2018). *Geology and characteristics of metagreywacke and associated rocks of Goa Group, India*. PhD Thesis, Goa University, 1-195.
- Fernandes, G. Q., Iyer, S. D., & Kotha, M. (2016). The origin and tectonic setting of Precambrian greywacke of Ribandar-Chimbel, Goa, India: petrological and geochemical evidence. *Acta Geologica Sinica*, 90(6), 2036–2048.
- Fernandes, O. A. (2009). Physiography and General Geology of Goa, In *Natural resources of Goa: a geological perspective*, Mascarenhas, A. & Kalavampara, G. (Editors), 11–23.
- Fernandes, O. A. & Widdowson, M. (2009) Petrogenesis, geochronology and crustal evolution of Canacona region of southern Goa. In *Natural resources of Goa: a geological perspective*, Mascarenhas, A. & Kalavampara, G. (Editors), 69-96
- Fermor, L. L. (1938) Origin of ultramafic lavas: Kathiawar. *Record of Geological Survey of India, Vol. 66*, 18-21.
- Fialko, Y. A., & Rubin, A. M. (1999). Thermal and mechanical aspects of magma emplacement in giant dike swarms. *Journal of Geophysical Research: Solid Earth*, 104(B10), 23033–23049.
- Fisher, R. L., Sclater, J. G. and McKenzie, D. P. (1971). Evolution of the Central Indian Ridge, Western Indian Ocean. *Bulletin of the Geological Society of America, Vol 82*, 553-562.
- Geological Survey of India., (1972). Map of coastal landforms of India, first edition. *Geological Survey of India*, Calcutta.
- Fitton, J. G., James, D., Kempton, P. D., Ormerod, D. S., & Leeman, W. P. (1988). The role of lithospheric mantle in the generation of late cenozoic basic magmas in the western united states. *Journal of Petrology, Special Vol(1)*, 331–349.
- Fitton, J. G., Saunders, A. D., Norry, M. J., Hardarson, B. S., & Taylor, R. N. (1997). Thermal and chemical structure of the Iceland plume. *Earth and Planetary Science Letters*, 153(3–4), 197–208.
- Forslund, T., & Gudmundsson, A. (1991). Crustal spreading due to dikes and faults in southwest Iceland. *Journal of Structural Geology*, 13(4), 443–457.

- Fossen, H. (2010). *Structural Geology*. Cambridge University Press.
- French, J. E., & Heaman, L. M. (2010). Precise U-Pb dating of Paleoproterozoic mafic dyke swarms of the Dharwar craton, India: Implications for the existence of the Neoproterozoic supercraton Sclavia. *Precambrian Research*.
- Frankel, J.J. (1967). Forms and structures of intrusive basaltic rocks. In: *Basalts, Vol. 1* (Eds.: Halls, H.C. and Poldervaart, A.) Interscience – New York, 63-102.
- Frey, F. A., Dickey, J. S., Thompson, G., Bryan, W. B., & Davies, H. L. (1980). Evidence for heterogeneous primary MORB and mantle sources, NW Indian Ocean. *Contributions to Mineralogy and Petrology*, 74, 387-402.
- Furman, T. (1995). Melting of metasomatized subcontinental lithosphere: Undersaturated mafic lavas from Rungwe, Tanzania. *Contributions to Mineralogy and Petrology*, Vol. 122, 97-115.
- Gadgil, R., Miranda, M. A., Viswanath, T. A. (2018) Deformational features of intraformational para-conglomerate of the Palaeoproterozoic Sanvordem formation, Goa group indicates a brittle-ductile dextral shear. *International Journal of Geomatics and Geosciences*, 8, 24–40
- Gadgil, R., Viegas, A., & Iyer, S. D. (2019). Structure and emplacement of the Coastal Deccan tholeiitic dyke swarm in Goa, on the western Indian rifted margin. *Bulletin of Volcanology*, 81(6). <https://doi.org/10.1007/s00445-019-1297-6>
- Galindo, I., & Gudmundsson, A. (2012). Basaltic feeder dykes in rift zones: Geometry, emplacement, and effusion rates. *Natural Hazards and Earth System Science*, 12(12), 3683–3700.
- Gast, P. W. (1972). The chemical composition and structure of the moon. *The Moon*, 5(1–2), 121–148.
- Garfunkel, Z. (2008). Formation of continental flood volcanism - The perspective of setting of melting. *Lithos*, 100(1-4), 59-65.
- Gautneb, H., Gudmundsson, A., & Oskarsson, N. (1989). Structure, petrochemistry and evolution of a sheet swarm in an Icelandic central volcano. *Geological Magazine*, 126(6), 659-673.
- Geshi, N. (2005). Structural development of dike swarms controlled by the change of magma supply rate: The cone sheets and parallel dike swarms of the Miocene Otoge igneous

- complex, Central Japan. *Journal of Volcanology and Geothermal Research*, 141(3-4), 267-281.
- Geshi, N., Kusumoto, S., & Gudmundsson, A. (2010). Geometric difference between non-feeder and feeder dikes. *Geology*, 38(3), 195–198.
- Ghosh, S. K., Pandey, A. K., Pandey, P., Ray, Y., & Sinha, S. (2012). Soft-sediment deformation structures from the Paleoproterozoic Damtha Group of Garhwal Lesser Himalaya, India. *Sedimentary Geology*, 261–262, 76–89.
- Gill, R. (2010). *Igneous Rocks and Processes: A Practical Guide*. Wiley-Blackwell.
- Glennie, E. A. (1932) Gravity anomaly and the structure of the Earth's crust. *Survey of India Professional Paper, Vol. 27*, 10-16.
- Gokul, A. R. (1985) Structure and tectonics of Goa. In: *Proceedings of the Seminar on Earth's resources for Goa's development*, Geological Survey of India, 14–21.
- Gokul, A. R., Srinivasan, M. D., Gopalkrishnan, K. and Vishwanathan, L. S. (1985) Stratigraphy and structure of Goa. In: *Proceedings of the Seminar on Earth's resources for Goa's development*, Geological Survey of India, 1-13.
- Goutham, M. R., Subbarao, K. V., Prasad, C. V. R. K., Walsh, J. N., and Damodara Reddy, V. (2011) Proterozoic mafic dikes from the southern margin of Cuddapah basin, India: Part 1 – Geochemistry and petrogenesis, in Srivastava, R.K., ed., *Dike swarms: Keys for geodynamic interpretation*: Berlin-Heidelberg, Springer-Verlag, p. 47–71
- Govindaraju, K. (1994). 1994 Compilation of Working Values and Sample Description for 383 Geostandards. *Geostandards Newsletter*, 18(July), 1–158.
- Gowd, T. N., Srirama Rao, S. V., & Chary, K. B. (1996). Stress Field and Seismicity in the Indian Shield: Effects of the Collision between India and Eurasia. In *Mechanics Problems in Geodynamics Part II* (pp. 503–531). Birkhäuser Basel.
- Cawthorn, R., & Strong, D. F. (1974). The petrogenesis of komatiites and related rocks as evidence for a layered upper mantle. *Earth and Planetary Science Letters*, 23(3), 369–375.
- Greenland, L. P., Okamura, A. T., & Stokes, J. B. (1988). Constraints on the mechanics of the eruption. *US Geological Survey Professional Paper*.

- Grossenbacher, K. A., & McDuffie, S. M. (1995). Conductive cooling of lava: columnar joint diameter and stria width as functions of cooling rate and thermal gradient. *Journal of Volcanology and Geothermal Research*, 69(1–2), 95–103.
- Gudmundsson, A. (1983). Stress estimates from the length/width ratios of fractures. *Journal of Structural Geology*, 5(6), 623–626.
- Gudmundsson, A. (1984). Formation of dykes, feeder-dykes, and the intrusion of dykes from magma Chambers. *Bulletin Volcanologique*, 47(3), 537–550.
- Gudmundsson, A. (1986). Formation of crustal magma chambers in Iceland. *Geology*, 14(2), 164–166.
- Gudmundsson, A. (1990). Emplacement of dikes, sills and crustal magma chambers at divergent plate boundaries. *Tectonophysics*, 176(3–4), 257–275.
- Gudmundsson, A. (1995). Stress fields associated with oceanic transform faults. *Earth and Planetary Science Letters*, 136(3-4), 603-614.
- Gudmundsson, A. (2002). Emplacement and arrest of sheets and dykes in central volcanoes. *Journal of Volcanology and Geothermal Research*, 116(3-4), 279-298.
- Gudmundsson, A. (2004). Effects of Young's modulus on fault displacement. *Comptes Rendus - Geoscience*, 336(1), 85-92.
- Gudmundsson, A. (2006). How local stresses control magma-chamber ruptures, dyke injections, and eruptions in composite volcanoes. *Earth-Science Reviews*, 79(1–2), 1–31.
- Gudmundsson, A. (2011). *Rock Fractures in Geological Processes*. Cambridge University Press.
- Gudmundsson, A. (2012). Magma chambers: Formation, local stresses, excess pressures, and compartments. *Journal of Volcanology and Geothermal Research*, 237–238, 19–41.
- Gudmundsson, A., & Loetveit, I. F. (2005). Dyke emplacement in a layered and faulted rift zone. *Journal of Volcanology and Geothermal Research*, 144(1-4 SPEC. ISS.), 311–327.
- Gudmundsson, A., Marinoni, L. B., 2002. Geometry, emplacement, and arrest of dykes. *Annales Tectonicae*, 13, 71–92.
- Hall, A. (1996). *Igneous Petrology*, 2<sup>nd</sup> Edition. Harlow: Longman Science & Technology.

- Halls, H. C. (1982). The importance and potential of mafic dyke swarms in studies of geodynamic processes. In *Geoscience Canada* (Vol. 9, Issue 3, pp. 145–154).
- Halls, H. C. (1986). Paleomagnetism, structure, and longitudinal correlation of Middle Precambrian dykes from northwestern Ontario and Minnesota (Canada, USA). *Canadian Journal of Earth Sciences*, 23(2), 142-157.
- Halls, H. C., & Palmer, H. C. (1990). The tectonic relationship of two Early Proterozoic dyke swarms to the Kapuskasing Structural Zone: a paleomagnetic and petrographic study. *Canadian Journal of Earth Sciences*, 27(1), 87-103.
- Halls, H.C., Zhang, B. (1995) Tectonic implications of clouded feldspar in Proterozoic mafic dyke swarms. *Geological Survey of India Memoirs*, Vol. 33, 65-80.
- Halls, H. C., Kumar, A., Srinivasan, R., & Hamilton, M. A. (2007). Paleomagnetism and U-Pb geochronology of easterly trending dykes in the Dharwar craton, India: feldspar clouding, radiating dyke swarms and the position of India at 2.37 Ga. *Precambrian Research*, 155(1-2), 47-68.
- Hanmer, S., Passchier, C. W. (1991) Shear sense indicators: a review. *Geological Survey of Canada Papers*, 90, 1–71.
- Hanmer, S., Mengel, F., Connelly, J., & Van Gool, J. (1997). Significance of crustal-scale shear zones and synkinematic mafic dykes in the Nagssugtoqidian orogen, SW Greenland: A re-examination. *Journal of Structural Geology*, 19(1), 59-75.
- Hansen, S. E., Sorlokk, T., Johannsson, A. E. (1998) Mechanical properties of rocks. SINTEF report, STF22 A98034, Trondheim.
- Hanson, G. N., & Langmuir, C. H. (1978). Modelling of major elements in mantle-melt systems using trace element approaches. *Geochimica et Cosmochimica Acta*, 42(6), 725-741.
- Harker, A. (1909) *The Natural History of Igneous Rocks*. London: Methuen & Co. pp.1-402.
- Hart, S. R. (1988). Heterogeneous mantle domains: signatures, genesis and mixing chronologies. *Earth and Planetary Science Letters*, 90(3), 273-296.
- Hashiguchi, H., Yamada, R., & Inoue, T. (1983). Practical Application of Low Na<sub>2</sub>O Anomalies in Footwall Acid Lava for Delimiting Promising Areas around the Kosaka and Fukazawa Kuroko Deposits, Akita Prefecture, Japan. In *The Kuroko and Related*

*Volcanogenic Massive Sulfide Deposits*. Society of Economic Geologists.  
<https://doi.org/10.5382/Mono.05.23>

- Hasnain, I., & Qureshy, M. N. (1971). Paleomagnetism and geochemistry of some dikes in Mysore State, India. *Journal of Geophysical Research*, 76(20), 4786–4795.
- Hastie, W. W., Watkeys, M. K., & Aubourg, C. (2014). Magma flow in dyke swarms of the Karoo LIP: Implications for the mantle plume hypothesis. In *Gondwana Research*, 25(2), 736–755.
- Hazarika, B., Malpe, D. B., & Dongre, A. (2020). Petrogenesis of mafic dykes from the western Bastar craton of Central India and their relation to outgrowth of Columbia supercontinent. *Mineralogy and Petrology*, 114, 243–262.
- He, Y., Zhao, G., & Sun, M. (2010). Geochemical and isotopic study of the Xiong'er volcanic rocks at the southern margin of the North China Craton: Petrogenesis and tectonic implications. *Journal of Geology*, 118(4), 417–433.
- Heaman, L. M. (2008). Precambrian large igneous provinces: An overview of geochronology, origins and impact on Earth evolution. In *Journal of the Geological Society of India*, 72(1).
- Hegde, V. S., & Chavadi, V. C. (2009). Geochemistry of late Archaean metagreywackes from the Western Dharwar Craton, South India: Implications for provenance and nature of the Late Archaean crust. *Gondwana Research*, 15(2), 178–187.
- Hegde, V. S., Koti, B. K., & Kruger, S. J. (2014). Geochemistry of the Desur lavas, deccan Traps: Case study from the vicinity of Belgaum, Karnataka and their petrogenetic inferences. *Journal of the Geological Society of India*, 83(4), 363–375.
- Heron, A. M. (1953) The geology of central Rajputana. *Geological Survey of India, Vol. 78*, 1–389.
- Herron, M. M. (1988). Geochemical classification of terrigenous sands and shales from core or log data. *Journal of Sedimentary Petrology*, 58(5), 820–829.
- Hoek, J. D. (1991). A classification of dyke-fracture geometry with examples from Precambrian dyke swarms in the Vestfold Hills, Antarctica. *Geologische Rundschau*, 80(2), 233–248.

- Hofmann, C., Féraud, G., & Courtillot, V. (2000).  $^{40}\text{Ar}/^{39}\text{Ar}$  dating of mineral separates and whole rocks from the Western Ghats lava pile: further constraints on duration and age of the Deccan Traps. *Earth and Planetary Science Letters*, 180(1–2), 13–27.
- Hogan, J. P., Price, J. D., & Gilbert, M. C. (1998). Magma Traps and driving pressure: Consequences for pluton shape and emplacement in an extensional regime. *Journal of Structural Geology*, 20(9–10), 1155–1168.
- Holland, H. D. (1978) *The Chemistry of the Atmosphere and Oceans*. Wiley, New York, 351.
- Hooper, P. R. (1990). The timing of crustal extension and the eruption of continental flood basalts. *Nature*, 345(6272), 246–249.
- Hooper, P. R. (1999). The wind of change, the Deccan Traps: a personal perspective. *Geological Society of India Memoirs*, Vol. 43, 153–165.
- Hooper, P., Widdowson, M., & Kelley, S. (2010). Tectonic setting and timing of the final Deccan flood basalt eruptions. *Geology*, 38(9), 839–842.
- Huppert, H. E., & Sparks, R. S. J. (1989). Chilled margins in igneous rocks. *Earth and Planetary Science Letters*, 92(3–4), 397–405.
- Huppert, H. E., Stephen, R., & Sparks, J. (1985). Cooling and contamination of mafic and ultramafic magmas during ascent through continental crust. *Earth and Planetary Science Letters*, 74(4), 371–386.
- Hutchison, C. S. (1974). *Laboratory Handbook of Petrographic Techniques*. New York: Wiley.
- Hutton, D. H. W. (1982) A tectonic model for the emplacement of the main Donegal granite. *Journal of the Geological Society of London*, Vol. 139, 615–631.
- Hutton, D. H. W. (1988) Granite emplacement mechanisms and tectonic controls: inferences from deformational studies. *Transactions of the Royal Society of Edinburgh Earth Science*, Vol. 79, 245–255.
- Ikramuddin, M., & Stueber, A. M. (1976). Rb-Sr ages of Precambrian dolerite and alkaline dikes, southeast Mysore state, India. *Lithos*, 9(3), 235–241.
- Irvine, T. N., & Baragar, W. R. A. (1971). A Guide to the Chemical Classification of the Common Volcanic Rocks. *Canadian Journal of Earth Sciences*, 8(5), 523–548.

- Irving, A. J., & Frey, F. A. (1978). Distribution of trace elements between garnet megacrysts and host volcanic liquids of kimberlitic to rhyolitic composition. *Geochimica et Cosmochimica Acta*, 42(6), 771–787.
- Ishwar-Kumar, C., Windley, B. F., Horie, K., Kato, T., Hokada, T., Itaya, T., Yagi, K., Gouzu, C., & Sajeev, K. (2013). A Rodinian suture in western India: New insights on India–Madagascar correlations. *Precambrian Research*, 236, 227–251.
- Ishwar-Kumar, C., Santosh, M., Wilde, S. A., Tsunogae, T., Itaya, T., Windley, B. F., & Sajeev, K. (2016). Mesoproterozoic suturing of Archean crustal blocks in western peninsular India: Implications for India–Madagascar correlations. *Lithos*, 263, 143–160.
- Iyer, L. A. N. (1932) Granitic intrusions and associated rocks in Ranchi and Singhbhum. *Records of the Geological Survey of India, Vol. 65*, 490-533.
- Iyer, S. D., Wagle, B. G., D'Cruz, E. E. (1990) Dyke swarms along the Goa coast, India. Nat Sem Rec Geol West Ind, MS Univ, Vadodara, p14.
- Iyer, S. D., & Banerjee, R. (1998). Importance of plagioclase morphology and composition in the magmagenesis of basalts.pdf. *Journal of Indian Geophysical Union*, 1, 63–72.
- Jaeger, J.-J., Courtillot, V., & Tapponnier, P. (1989). Paleontological view of the ages of the Deccan Traps, the Cretaceous/Tertiary boundary, and the India-Asia collision. *Geology*, 17(4), 316.
- Jain, A. K. (2014). *An Introduction to Structural Geology*. Geological Society of India.
- Jain, A. K., Banerjee, D. M., & Kale, V. S. (2020). *Tectonics of the Indian Subcontinent: An Introduction*. In: Tectonics of the Indian Subcontinent. Society of Earth Scientists Series. Springer, Cham., 1-16pp.
- Jason Morgan, W. (1983). Hotspot tracks and the early rifting of the Atlantic. *Tectonophysics*, 94(1–4), 123–139.
- Jay, A. E., & Widdowson, M. (2008). Stratigraphy, structure and volcanology of the SE Deccan continental flood basalt province: Implications for eruptive extent and volumes. *Journal of the Geological Society*, 165(1), 177–188.
- Jayaram, S., Venkatasubramanian, V.S., Radhakrishna, B.P., 1983. Geochronology and trace element distribution in some tonalite and granitic gneisses of the Dharwar craton. In:

- Naqvi, S.M., Rogers, J.J.W. (Eds.), *Precambrians of South India. Geological Society of India Memoir, Vol. 4*, 377–387.
- Jayananda, M., Moyen, J. F., Martin, H., Peucat, J. J., Auvray, B., & Mahabaleswar, B. (2000). Late Archaean (2550-2520 Ma) juvenile magmatism in the Eastern Dharwar craton, southern India: Constraints from geochronology, Nd-Sr isotopes and whole rock geochemistry. *Precambrian Research*, 99(3-4), 225-254.
- Jayananda, M., Chardon, D., Peucat, J. J., & Capdevila, R. (2006). 2.61 Ga potassic granites and crustal reworking in the western Dharwar craton, southern India: Tectonic, geochronologic and geochemical constraints. *Precambrian Research*, 150(1–2), 1–26.
- Jayananda, M., Kano, T., Peucat, J. J., & Channabasappa, S. (2008). 3.35 Ga komatiite volcanism in the western Dharwar craton, southern India: Constraints from Nd isotopes and whole-rock geochemistry. *Precambrian Research*, 162(1–2), 160–179.
- Jayananda, M., Tsutsumi, Y., Miyazaki, T., Gireesh, R. V., Kapfo, K. u., Tushipokla, Hidaka, H., & Kano, T. (2013). Geochronological constraints on Meso- and Neoproterozoic regional metamorphism and magmatism in the Dharwar craton, southern India. *Journal of Asian Earth Sciences*, 78(June 2015), 18–38.
- Jena, B.K. (1980) Basic intrusives in Pernem taluka. *Journal of the Geological Society of India, Vol. 21*, 142-145.
- Jena, B.K. (1985) Usgao ultramafic-gabbro complex. *Journal of the Geological Society of India, Vol. 26*, 492-495.
- Jerram, D. A., & Widdowson, M. (2005). The anatomy of Continental Flood Basalt Provinces: Geological constraints on the processes and products of flood volcanism. *Lithos*, 79(3-4 SPEC. ISS.), 385–405.
- Jensen, L. S. (1976). New cation plot for classifying subalkalic volcanic rocks. *Ontario Division of Mines Miscellaneous Paper*.
- Jolly, R. J. H., & Lonergan, L. (2002). Mechanisms and controls on the formation of sand intrusions. *Journal of the Geological Society*, 159(5), 605-617.
- Jowitt, S. M., & Ernst, R. E. (2013). Geochemical assessment of the metallogenic potential of Proterozoic LIPs of Canada. *Lithos*, 174, 291–307.
- Ju, W., Hou, G., & Hari, K. R. (2013). Mechanics of mafic dyke swarms in the Deccan Large Igneous Province: Palaeostress field modelling. *Journal of Geodynamics*, 66, 79–91.

- Jung, C., Jung, S., Hoffer, E., & Berndt, J. (2006). Petrogenesis of Tertiary Mafic Alkaline Magmas in the Hocheifel, Germany. *Journal of Petrology*, 47(8), 1637–1671.
- Kale, M. G., Pundalik, A. S., Duraiswami, R. A., & Karmalkar, N. R. (2016). Soft sediment deformation structures from Khari River section of Rudramata member, Jhuran Formation, Kutch: A testimony of Jurassic seismites. *Journal of the Geological Society of India*, 87(2), 194–204.
- Karmalkar, N. R., Griffin, W. L., & O'Reilly, S. Y. (2000). Ultramafic xenoliths from kutch, northwest india: Plume-related mantle samples? *International Geology Review*, 42(5), 416–444.
- Karmalkar, N. R., Duraiswami, R. A., Jonnalagadda, M. K., & Griffin, W. L. (2014). Mid-Cretaceous lamproite from the Kutch region, Gujarat, India: Genesis and tectonic implications. *Gondwana Research*, 26(3–4), 942–956.
- Kelemen, P. B. (1990). Reaction Between Ultramafic Rock and Fractionating Basaltic Magma I. Phase Relations, the Origin of Calc-alkaline Magma Series, and the Formation of Discordant Dunite. *Journal of Petrology*, 31(1), 51–98.
- Keller, G., Adatte, T., Bajpai, S., Mohabey, D. M., Widdowson, M., Khosla, A., Sharma, R., Khosla, S. C., Gertsch, B., Fleitmann, D., & Sahni, A. (2009). K-T transition in Deccan Traps of central India marks major marine Seaway across India. *Earth and Planetary Science Letters*, 282(1–4), 10–23.
- Kerrick, R., & Xie, Q. (2002). Compositional recycling structure of an Archean super-plume: Nb-Th-U-LREE systematics of Archean komatiites and basalts revisited. *Contributions to Mineralogy and Petrology*, 142, 476–484.
- Kinzler, R. J. (1997). Melting of mantle peridotite at pressures approaching the spinel to garnet transition: Application to mid-ocean ridge basalt petrogenesis. *Journal of Geophysical Research: Solid Earth*, 102(B1), 853–874.
- Klemme, S., & O'Neill, H. S. C. (2000). The near-solidus transition from garnet lherzolite to spinel lherzolite. *Contributions to Mineralogy and Petrology*, 138(3), 237–248.
- Krishnan, M. S. (1960). *Geology of India and Burma*. Higginbothams.
- Krishnan, M. S. (1935) The dyke rocks of Keonjhar state. Rec. *Geological Survey of India*, Vol.71, 105.

- Kumar, A., Pande, K., Venkatesan, T. R., & Bhaskar Rao, Y. J. (2001). The Karnataka late Cretaceous dykes as products of the Marion hot spot at the Madagascar - India breakup event: Evidence from  $^{40}\text{Ar}$ - $^{39}\text{Ar}$  geochronology and geochemistry. *Geophysical Research Letters*, 28(14), 2715–2718.
- Kumar, A., Hamilton, M. A., & Halls, H. C. (2012). A Paleoproterozoic giant radiating dyke swarm in the Dharwar Craton, southern India. *Geochemistry, Geophysics, Geosystems*, 13(1). <https://doi.org/10.1029/2011GC003926>
- Kumar, P., & Chaubey, A. K. (2019). Extension of flood basalt on the northwestern continental margin of India. *Journal of Earth System Science*, 128(4). <https://doi.org/10.1007/s12040-019-1089-6>
- Kuno, H. (1959). Origin of Cenozoic petrographic provinces of Japan and surrounding areas. *Bulletin Volcanologique*, 20, 37-76.
- Kürkcüoğlu, B. (2010). Geochemistry and petrogenesis of basaltic rocks from the Develidağ volcanic complex, Central Anatolia, Turkey. *Journal of Asian Earth Sciences*, 37(1), 42-51.
- Kusumoto, S., Geshi, N., & Gudmundsson, A. (2013). Aspect ratios and magma overpressures of non-feeder dikes observed in the Miyake-jima volcano (Japan), and fracture toughness of its upper part. *Geophysical Research Letters*, 40(6), 1065–1068.
- Lai, S., Qin, J., Li, Y., Li, S., & Santosh, M. (2012). Permian high Ti/Y basalts from the eastern part of the Emeishan Large Igneous Province, southwestern China: Petrogenesis and tectonic implications. *Journal of Asian Earth Sciences*, 47, 216–230.
- Lafleche, M. R., Dupuy, C., & Bougault, H. (1992). Geochemistry and petrogenesis of Archean mafic volcanic rocks of the southern Abitibi Belt, Québec. *Precambrian Research*, 57(3–4), 207–241.
- Langmuir, C. H., Bender, J. F., Bence, A. E., Hanson, G. N., & Taylor, S. R. (1977). Petrogenesis of basalts from the FAMOUS area: Mid-Atlantic Ridge. *Earth and Planetary Science Letters*, 33(1), 133-156.
- Le Maitre, R. W. (1984). A proposal by the IUGS Subcommittee on the Systematics of Igneous Rocks for a chemical classification of volcanic rocks based on the total alkali silica (TAS) diagram. *Australian Journal of Earth Sciences*, 31(2), 243–255.

- LaBrecque, J. L., Kent, D. V., & Cande, S. C. (1977). Revised magnetic polarity time scale for Late Cretaceous and Cenozoic time. *Geology*, 5(6), 330-335.
- Lassiter, J. C., Depaolo, D. J., & Mahoney, J. J. (1995). Geochemistry of the Wrangellia flood basalt province: Implications for the role of continental and oceanic lithosphere in flood basalt genesis. *Journal of Petrology*, 36(4), 983-1009.
- Lassiter, J. C., & DePaolo, D. J. (1997). Plume/lithosphere interaction in the generation of continental and oceanic flood basalts: Chemical and isotopic constraints. *Geophysical Monograph Series*, 100, 335–355.
- Lawson, A. C. (1893). *The geology of Carmelo Bay*. California University, Department of Geology Science Bulletin, 1-59
- Le Bas, M. J., Le Maitre, R. N., Streckeisen, A., & Zanettin, B. (1986). A chemical classification of volcanic rock based on total silica diagram. *Journal Petrology*, 27(3), 745-750.
- Le Maitre, R.W., Streckeisen, A., Zanettin, B., Le Bas, M.J., Bonin, B., Bateman, P., Bellieni, G., Dudek, A., Schmid, R., Sorensen, H., and Woolley, A.R., 1989, Igneous rocks. A classification and glossary of terms: recommendations of the International Union of Geological Sciences Subcommittee of the Systematics of Igneous Rocks: *Oxford, Blackwell Scientific Publications*, 193 pp.
- Le Maitre, R. W., Streckeisen, A., Zanettin, B., Le Bas, M. J., Bonin, B., & Bateman, P. (2002). Igneous Rocks: A Classification and Glossary of Terms (Recommendations of the IUGS Subcommittee on the Systematics of Igneous Rocks). In *Cambridge University Press*.
- Le Roex, A. P., Watkins, R. T., & Reid, A. M. (1996). Geochemical evolution of the Okenyena sub-volcanic ring complex, northwestern Namibia. *Geological Magazine*, 133(6), 645-670.
- Legault, M. I., & Hattori, K. (1994). Late Archaean geological development recorded in the Timiskaming Group sedimentary rocks, Kirkland Lake area, Abitibi greenstone belt, Canada. *Precambrian Research*, 68(1-2), 23-42.
- Lightfoot, P. C., Hawkesworth, C. J., & Sethna, S. F. (1987). Petrogenesis of rhyolites and trachytes from the Deccan Trap: Sr, Nd and Pb isotope and trace element evidence. *Contributions to Mineralogy and Petrology*, 95(1), 44–54.

- Lightfoot, P. C., Hawkesworth, C. J., Devey, C. W., Rogers, N. W., & Calsteren, P. W. C. V. (1990). Source and differentiation of Deccan Trap lavas: Implications of geochemical and mineral chemical variations. *Journal of Petrology*, *31*(5), 1165–1200.
- Lister, J. R., & Kerr, R. C. (1991). Fluid-mechanical models of crack propagation and their application to magma transport in dykes. *Journal of Geophysical Research*, *96*(B6), 10049-10077.
- Long, P. E., & Wood, B. J. (1986). Structures, textures, and cooling histories of Columbia River basalt flows (USA). *Geological Society of America Bulletin* *97*(9), 1144–1155.
- Loubet, M., Sassi, R., & Di Donato, G. (1988). Mantle heterogeneities: a combined isotope and trace element approach and evidence for recycled continental crust materials in some OIB sources. *Earth and Planetary Science Letters*, *89*(3-4), 299-315.
- Lyle, P. (2000). The eruption environment of multi-tiered columnar basalt lava flows. *Journal of the Geological Society*, *157*(4), 715-722.
- Lyubetskaya, T., & Korenaga, J. (2007). Chemical composition of Earth's primitive mantle and its variance: 1. Method and results. *Journal of Geophysical Research: Solid Earth*, *112*(3), 1–21.
- Mahoney, J. J. (1988). Deccan Traps. In: Macdougall, J. D. (ed) *Continental Flood Basalts*. Dordrecht: Kluwer Academic, pp. 151-194.
- Mahoney, J. J. & Coffin, M. F. (1997). *Preface*. AGU Geophysical Monograph 100, ix–x.
- Mahoney, J. J., Sheth, H. C., Chandrasekharam, D., & Peng, Z. X. (2000). Geochemistry of flood basalts of the Toranmal section, northern Deccan Traps, India: Implications for regional Deccan stratigraphy. *Journal of Petrology*, *41*(7), 1099–1120. <https://doi.org/10.1093/petrology/41.7.1099>
- Maltman, A. (1984). On the term “soft-sediment deformation.” *Journal of Structural Geology*, *6*(5), 589-592.
- Maltman, A. (1994a). Introduction and overview. In: Maltman, A. (Ed.), *The Geological Deformation of Sediments*. Chapman and Hall, London, 1-35.
- Maltman, A. (1994b). Deformation structures preserved in the rocks. In: Maltman, A. (Ed.), *The Geological Deformation of Sediments*. Chapman and Hall, London, 261-307.

- Marston, R. J. (1978). The geochemistry of archaean clastic metasediments in relation to crustal evolution, Northeastern Yilgarn Block, Western Australia. *Precambrian Research*, 6(2), 157-175.
- Melluso, L., Sethna, S. F., Morra, V., Khateeb, A., & Javeri, P. (1999). Petrology of the mafic dyke swarm of the Tapti River in the Nandurbar area (Deccan volcanic province). In *Geological Society of India Memoirs*, K. V. Subbarao (Editor), *Deccan volcanic province*, 43-2, 735-755.
- Macdonald, G. A., & Katsura, T. (1964). Chemical Composition of Hawaiian Lavas. *Journal of Petrology*, 5(1), 82-133. <https://doi.org/10.1093/petrology/5.1.82>
- Mandal, N. (1995). Mode of development of sigmoidal en echelon fractures. *Proceedings of the Indian Academy of Sciences - Earth and Planetary Sciences*, 104, 453-464.
- Mandal, N., Mitra, A. K., Misra, S., & Chakraborty, C. (2006). Is the outcrop topology of dolerite dikes of the Precambrian Singhbhum Craton fractal? *Journal of Earth System Science*, 115, 643-660.
- Manikyamba, C., & Kerrich, R. (2012). Eastern Dharwar Craton, India: Continental lithosphere growth by accretion of diverse plume and arc terranes. *Geoscience Frontiers*, 3(3), 225-240.
- Marinoni, L. B. (2001). Crustal extension from exposed sheet intrusions: Review and method proposal. *Journal of Volcanology and Geothermal Research*, 107(1-3), 27-46.
- Marinoni, L. B., & Gudmundsson, A. (2000). Dykes, faults and palaeostresses in the Teno and Anaga massifs of Tenerife (Canary Islands). *Journal of Volcanology and Geothermal Research*, 103(1-4), 83-103.
- Martínez-Poza, A. I., Druguet, E., Castaño, L. M., & Carreras, J. (2014). Dyke intrusion into a pre-existing joint network: The Aiguablava lamprophyre dyke swarm (Catalan Coastal Ranges). *Tectonophysics*, 630(C), 75-90.
- Mattsson, H. B., & Oskarsson, N. (2005). Petrogenesis of alkaline basalts at the tip of a propagating rift: Evidence from the Heimae volcanic centre, south Iceland. *Journal of Volcanology and Geothermal Research*, 147(3-4), 245-267.
- McLennan, S. M. (1989). Rare earth elements in sedimentary rocks: influence of provenance and sedimentary processes. In B. R. Lipin & G. A. McKay (Editors), *Geochemistry and Mineralogy of Rare Earth Elements*, 169-200. De Gruyter.

- Martha, T. R., Ghosh, D., Kumar, K. V., Lesslie, A., & Kumar, M. V. R. (2013). Geospatial technologies for national geomorphology and lineament mapping project - a case study of Goa state. *Journal of the Indian Society of Remote Sensing*, 41(4), 905–920.
- McKenzie, D., & Sclater, J. G. (1971). The Evolution of the Indian Ocean since the Late Cretaceous. *Geophysical Journal International*, 24(5), 437–528.
- Mazumder, R., Rodríguez-López, J. P., Arima, M., & van Loon, A. J. (2009). Palaeoproterozoic seismites (fine-grained facies of the Chaibasa formation, east India) and their soft-sediment deformation structures. *Geological Society Special Publication*, 323, 301-318.
- Mège, D., & Korme, T. (2004). Dyke swarm emplacement in the Ethiopian Large Igneous Province: Not only a matter of stress. *Journal of Volcanology and Geothermal Research*, 132(4), 283–310.
- Melluso, L., Sheth, H. C., Mahoney, J. J., Morra, V., Petrone, C. M. & Storey, M. (2009) Correlations between silicic volcanic rocks of St Mary's Islands (southwestern India) and eastern Madagascar: implications for Late Cretaceous India-Madagascar reconstructions. *Journal of the Geological Society*, 166, 283-294.
- Menzies, M. A., Kyle, P. R., Jones, M., & Ingram, G. (1991). Enriched and depleted source components for tholeiitic and alkaline lavas from Zuni-Bandera, New Mexico: inferences about intraplate processes and stratified lithosphere. *Journal of Geophysical Research*, 96(B8), 13645-13671.
- Middlemost, E. A. K. (1989). Iron oxidation ratios, norms and the classification of volcanic rocks. *Chemical Geology*, 77(1), 19-26.
- Mills, P. C. (1983). Genesis and diagnostic value of soft-sediment deformation structures-A review. *Sedimentary Geology*, 35(22), 83-104.
- Moorhouse, W. W. (1959) *The study of rocks in thin section*. Harper and Row, New York, 514.
- Mislankar, P. G., & Iyer, S. D. (2001). Petrographical indicators of petrogenesis: Examples from Central Indian Ocean Basin basalts. *Indian Journal of Marine Sciences*, 30(1), 1-8.
- Misra, A. A., & Mukherjee, S. (2017). Dyke-brittle shear relationships in the western Deccan strike-slip zone around Mumbai (Maharashtra, India). *Geological Society Special Publication*, 445(1), 269–295.

- Misra, K. S. (2008) Dyke swarms and dykes within the Deccan Volcanic Province, India. *In* Srivastava, R. K., Sivaji, Ch., Chalapathi Rao, N. V. (Eds) *Indian Dykes: Geochemistry, Geophysics and Geochronology*, Narosa Publishing House. 57-72.
- Mitchell, C., & Widdowson, M. (1991). A geological map of the southern Deccan Traps, India and its structural implications. *Journal of the Geological Society*, 148(3), 495–505.
- Moyen, J. F., Martin, H., Jayananda, M., & Auvray, B. (2003). Late Archaean granites: A typology based on the Dharwar Craton (India). *Precambrian Research*, 127(1–3), 103–123.
- Mudholkar, A. V., Kodagali, V. N., Kamesh Raju, K. A., Valsangkar, A. B., Ranade, G. H., & Ambre, N. V. (2002). Geomorphological and petrological observations along a segment of slow-spreading Carlsberg Ridge. *Current Science*, 82(8), 982–989.
- Müller, R. D., Gaina, C., Roest, W. R., & Hansen, D. L. (2001). A recipe for microcontinent formation. *Geology*, 29(3), 203-206.
- Murthy, N. G. K. (1995) Proterozoic mafic dykes in southern peninsular India: A review. *In*: Devaraju T. C. (Editor) *Mafic Dyke Swarms of Peninsular India*, Geological Society of India Memoirs Number 33, 81–98.
- Murthy, N. G. K. (1987) Mafic dyke swarms of the Indian Shield. *In*: H. C. Halls and W. F. Fahrig (Eds.), *Mafic Dyke Swarms*. Geological Association of Canada. Special Paper 34, 393-400.
- Naganna, C. (1966). Petrology of the rocks of St. Mary Islands, near Malpe, South Kanara District, Mysore State. *Journal of the Geological Society of India*, Vol. 7, 110- 117.
- Najafi, S. J., Cox, K. G., Sukheswala, R. N., (1981) Geology and geochemistry of the basalt flows (Deccan Traps) of the Mahad-Mahabaleshwar section, India. *In*: Subbarao, K. V., Sukheswala, R. N. (Eds.), *Deccan Volcanism and Related Basalt Provinces in Other Parts of the World*. *Geological Society of India*, Vol. 3, 300-315.
- Naqvi, S. M., Rao, V. D., Satyanarayana, K., & Hussain, S. M. (1974). Geochemistry of post-Dharwar basic dikes and the Precambrian crustal evolution of peninsular India. *Geological Magazine*, 111(3), 229–236.
- Naqvi, S. M., Sawkar, R. H., Subba Rao, D. V., Govil, P. K., & Ganeswar Rao, T. (1988). Geology, geochemistry and tectonic setting of Archaean greywackes from Karnataka nucleus, India. *Precambrian Research*, 39(3), 193–216.

- Naqvi, S.M., Rogers, J.J.W. (1987). *Precambrian Geology of India*. Oxford Monographs on Geology and Geophysics 6, 233.
- Neuendorf, K. K. E., Mehl, J. P., Jr., & Jackson, J. A., eds. (2011). *Glossary of Geology*, 5<sup>th</sup> edition. Alexandria, VA: American Geological Institute.
- Leg 115 Shipboard Scientific Party (1987) New studies of the Indian Ocean. *Nature* **329**, 586–587.
- Nicholson, R., & Pollard, D. D. (1985). Dilation and linkage of echelon cracks. *Journal of Structural Geology*, 7(5), 583–590.
- Nogueira, C. R., Terrinha, P., Moreira, M. (2009) Assessing magma flow direction in dykes from vesicle shapes and orientations. *Geophysical Research Abstracts* (EGU), 13369
- Norton, I. O., & Sclater, J. G. (1979). A model for the evolution of the Indian Ocean and the breakup of Gondwanaland. *Journal of Geophysical Research: Solid Earth*, 84(B12), 6803–6830.
- Nutman, A. P., Chadwick, B., Krishna Rao, B., Vasudev, V. N. (1996). SHRIMP U/Pb zircon ages of acid volcanic rocks in the Chitradurga and Sandur groups, and granites adjacent to the Sandur schist belt, Karnataka. *Journal of the Geological Society of India* 47, 153–164.
- Nutman, A. P., Chadwick, B., Ramakrishnan, M., Viswanatha, M. N. (1992). SHRIMP U–Pb ages of detrital zircons in Sargur supracrustal rocks in western Karnataka, Southern India. *Journal of the Geological Society of India* 39, 367–374.
- Obermeier, S. F., Olson, S. M., & Green, R. A. (2005). Field occurrences of liquefaction-induced features: A primer for engineering geologic analysis of paleoseismic shaking. In *Engineering Geology*, 76(3-4), 209-234.
- Oldham, R. D. (1893; Reprinted 1994) *Encyclopedia of Indian Geology (formerly Manual of Geology of India)*, 2<sup>nd</sup> Edition, Vol. 1, 254, Vol. 543, Cosmo Publications, New Delhi.
- Owen, G. (1995). Soft-sediment deformation in Upper Proterozoic Torridonian Sandstones (Applecross Formation) at Torridon, northwest Scotland. *Journal of Sedimentary Research A: Sedimentary Petrology & Processes*, A65(3), 495–504.
- Owen, H. G. (1976). Continental displacement and expansion of the earth during the Mesozoic and Cenozoic. *Philosophical Transactions of the Royal Society of London. Series A, Mathematical and Physical Sciences*, 281(1303), 223–291.

- Pande, K. (2002). Age and duration of the Deccan Traps, India: A review of radiometric and paleomagnetic constraints. In *Proceedings of the Indian Academy of Sciences, Earth and Planetary Sciences*, 111(2), 115.
- Pande, K., Sheth, H. C., Bhutani, R. (2001).  $^{40}\text{Ar}/^{39}\text{Ar}$  age of the St. Mary's Islands volcanics, southern India: record of India-Madagascar break-up on the Indian subcontinent. *Earth and Planetary Science Letters*, 193, 39-46.
- Pande, K., Yatheesh, V., & Sheth, H. (2017).  $^{40}\text{Ar}/^{39}\text{Ar}$  dating of the Mumbai tholeiites and Panvel flexure: Intense 62.5 Ma onshore-offshore Deccan magmatism during India-Laxmi Ridge-Seychelles breakup. *Geophysical Journal International*, 210(2), 1160–1170.
- Paquet, F., Dauteuil, O., Hallot, E., & Moreau, F. (2007). Tectonics and magma dynamics coupling in a dyke swarm of Iceland. *Journal of Structural Geology*, 29(9), 1477–1493.
- Parfitt, Liz; Wilson, L. (2008). *Fundamentals of Physical Volcanology*. Wiley-Blackwell.
- Parker, A. J., Rickwood, P. C. and Tucker, D. H. (1990) 2<sup>nd</sup> International Dyke Conference Australia, Adelaide. Rotterdam: Balkema, IGCP Project 257, Publication No. 23.
- Pascoe, E. H. (1950) *A manual of the Geology of India and Burma. Geological Survey of India, Vol. 1.*
- Patel, V., Sheth, H., Cucciniello, C., Joshi, G. W., Wegner, W., Samant, H., Sen, B., & Koeberl, C. (2020). Geochemistry of deccan tholeiite flows and dykes of elephanta island: Insights into the stratigraphy and structure of the panvel flexure zone, western Indian rifted margin. *Geosciences (Switzerland)*, 10(4), 118. <https://doi.org/10.3390/geosciences10040118>
- Paterson, S. R., & Fowler, T. K. (1993). Re-examining pluton emplacement processes. *Journal of Structural Geology*, 15(2), 191-206.
- Patil, S. K., & Rao, D. R. K. (2002). Palaeomagnetic and rock magnetic studies on the dykes of Goa, west coast of Indian Precambrian Shield. *Physics of the Earth and Planetary Interiors*, 133(1–4), 111–125.
- Patil, S. K., Gadpallu, P., Monteiro, A., Sepahi, M. N., & Duraiswami, R. A. (2020). Characterising the Bushe-Poladpur Contact across the Western Deccan Traps and Implications for Mapping the K-Pg Boundary? *Journal of the Geological Society of India*, 95(3), 227–240.

- Patro, P. K., Raju, K., & Sarma, S. V. S. (2018). Some Insights into the Lithospheric Electrical Structure in the Western Ghat Region from Magnetotelluric Studies. *Journal of the Geological Society of India*, 92(5), 529–532.
- Paquet, F., Dauteuil, O., Hallot, E., & Moreau, F. (2007). Tectonics and magma dynamics coupling in a dyke swarm of Iceland. *Journal of Structural Geology*, 29(9), 1477–1493.
- Pearce, J. A. (2008). Geochemical fingerprinting of oceanic basalts with applications to ophiolite classification and the search for Archean oceanic crust. *Lithos*, 100(1–4), 14–48.
- Pearce, J. A., & Peate, D. W. (1995). Tectonic implications of the composition of volcanic arc magmas. *Annual Review of Earth & Planetary Sciences*, 23, 251–285.
- Pearce, J. A., & Norry, M. J. (1979). Petrogenetic implications of Ti, Zr, Y, and Nb variations in volcanic rocks. *Contributions to Mineralogy and Petrology*, 69(1), 33–47.
- Pearce, J. A., & Parkinson, I. J. (1993). Trace element models for mantle melting: Application to volcanic arc petrogenesis. *Geological Society Special Publication*, 76, 373–403.
- Peate, D.W. (1997). The Paraná-Etendeka Province. In *Large Igneous Provinces: Continental, Oceanic, and Planetary Flood Volcanism* (eds J. J. Mahoney and M. F. Coffin), Vol 100, Geophysical Monograph Series, <https://doi.org/10.1029/GM100p0217>
- Peng, Z. X., Mahoney, J., Hooper, P., Harris, C., & Beane, J. (1994). A role for lower continental crust in flood basalt genesis? Isotopic and incompatible element study of the lower six formations of the western Deccan Traps. *Geochimica et Cosmochimica Acta*, 58(1), 267–288.
- Peng, Z. X., & Mahoney, J. J. (1995). Drillhole lavas from the northwestern Deccan Traps, and the evolution of Réunion hotspot mantle. *Earth and Planetary Science Letters*, 134(1–2), 169–185.
- Peng, Z. X., Mahoney, J. J., Vanderkluyzen, L., & Hooper, P. R. (2014). Sr, Nd and Pb isotopic and chemical compositions of central Deccan Traps lavas and relation to southwestern Deccan stratigraphy. *Journal of Asian Earth Sciences*, 84, 83–94.
- Perfit, M. R., Gust, D. A., Bence, A. E., Arculus, R. J., & Taylor, S. R. (1980). Chemical characteristics of island-arc basalts: Implications for mantle sources. *Chemical Geology*, 30(3), 227–256.

- Peshwa, V. V., Mulay, J. G. & Kale, V. S. (1987) Fracture zones in the Deccan Traps of Western and Central India: A study based on remote sensing techniques. *Journal of Indian Society of Remote Sensing* 15, 9–17.
- Pettijohn, F. J., Potter, P. E., & Siever, R. (1973). *Sand and Sandstone*. Springer US. <https://doi.org/10.1007/978-1-4615-9974-6>
- Peucat, J. J., Bouhallier, H., Fanning, C. M., & Jayananda, M. (1995). Age of the Holenarsipur Greenstone Belt, relationships with the surrounding gneisses (Karnataka, south India). *Journal of Geology*, 103(6), 701–710.
- Peucat, J. J., Mahabaleswar, B., & Jayananda, M. (1993). Age of younger tonalitic magmatism and granulitic metamorphism in the South Indian transition zone (Krishnagiri area); comparison with older Peninsular gneisses from the Gorur/Hassan area. *Journal of Metamorphic Geology*, 11(6), 879–888.
- Peucat, J. J., Jayananda, M., Chardon, D., Capdevila, R., Fanning, C. M., & Paquette, J. L. (2013). The lower crust of the Dharwar Craton, Southern India: Patchwork of Archean granulitic domains. *Precambrian Research*, 227, 4–28.
- Philpotts, A., & Ague, J. (2009). *Principles of Igneous and Metamorphic Petrology*. Cambridge University Press. <https://doi.org/10.1017/CBO9780511813429>
- Pichamuthu, C. S. (1959) The significance of clouded plagioclase in the basic dykes of Mysore state, India. *Journal Geological Society of India, Vol. 1*, 68-79.
- Pinel, V., & Jaupart, C. (2004). Likelihood of basaltic eruptions as a function of volatile content and volcanic edifice size. *Journal of Volcanology and Geothermal Research*, 137(1-3), 201-217.
- Pitcher, W. S. (1979) The nature, ascent and emplacement of granitic magmas. *Journal of Geological Society of London, Vol. 136*, 627-662.
- Piispa, E. J., Smirnov, A. V., Pesonen, L. J., Lingadevaru, M., Anantha Murthy, K. S., & Devaraju, T. C. (2011). An Integrated Study of Proterozoic Dykes, Dharwar Craton, Southern India. In *Dyke Swarms: Keys for Geodynamic Interpretation* (pp. 33–45). Springer Berlin Heidelberg.
- Platten, I. M. (1995) Flow and crystallization in dykes: a review of field and laboratory data in the light of recent advances in mathematical modelling. In: Devaraju, T. C. (ed) *Dyke swarms of peninsular India. Geological Society of India Memoirs Number 33*, 1–47

- Plummer, P. S., & Belle, E. R. (1995). Mesozoic tectono-stratigraphic evolution of the Seychelles microcontinent. *Sedimentary Geology*, 96(1–2), 73–91.
- Poldervaart, A., & Parker, A. B. (1964). The crystallization index as a parameter of igneous differentiation in binary variation diagrams. *American Journal of Science*, 262(3), 281–289.
- Pollard, D. D., Segall, P., & Delaney, P. T. (1982). Formation and interpretation of dilatant echelon cracks. *Geological Society of America Bulletin*, 93(12), 1291–1303.
- Pollard, D. D. (1973). Derivation and evaluation of a mechanical model for sheet intrusions. *Tectonophysics*, 19(3), 233–269.
- Pollard, D. D., Muller, O. H., & Dockstader, D. R. (1975). Geological Society of America Bulletin The Form and Growth of Fingered Sheet Intrusions. *Geological Society Of America Bulletin*, 86(3), 351–363.
- Pollard, D. D., Fink, J. H. and Delaney, P. T. (1984) Igneous dikes at Long Valley, CA; emplacement mechanisms and associated geologic structures. In *Proceedings of Workshop XIX*, 130–146.
- Poole, J. H. J. (1928). XLIV. Note on the formation of Pleochroic Halos in biotite. *The London, Edinburgh, and Dublin Philosophical Magazine and Journal of Science*, 5(28), 444–444.
- Powar, K. B., & Deshpande, G. G. (1970). Plagioclase tecoblasts in dolerite dyke of Panchmarhi area, Madhya Pradesh. *Current Science*, 39(22), 516.
- Prasad, V., Nair, K. K. K. and Jain, S. C. (1995). Geophysical studies in Central India - Paleomagnetic studies. In: B.D. Dungrakoti et al., (Eds). Geoscientific studies of the Son-Narmada-Tapti Lineament zone. *Geological Survey of India Special Publications Number 10*, 198–209
- Pyle, D. G., Christie, D. M., Mahoney, J. J., & Duncan, R. A. (1995). Geochemistry and geochronology of ancient southeast Indian and southwest Pacific seafloor. *Journal of Geophysical Research: Solid Earth*, 100(B11), 22261–22282.
- Qureshy, M. N. (1982). Geophysical and Landsat lineament mapping — An approach illustrated from west-central and south India. *Photogrammetria*, 37(3–5), 161–184.
- Radhakrishna, B. P. (1993). Neogene uplift and geomorphic rejuvenation of the Indian Peninsula. *Current Science*, 64(11–12), 787–793.

- Radhakrishna, T. (2007) Temporal variations and mantle sources of the mafic dyke swarms in south India. *Deep Continental Studies. News Letter, Vol.17, 2-7.*
- Radhakrishna, T., Mohamed, A. R., Venkateshwarlu, M., Soumya, G. S., & Prachiti, P. K. (2019). Mechanism of rift flank uplift and escarpment formation evidenced by Western Ghats, India. *Scientific Reports, 9(1), 1–7.*
- Ragland, P. C. (1989) *Basic Analytical Petrology*. Oxford University Press, Oxford. 369
- Raja Rao, C. S., Sahasrabudhe, Y. S., Deshmukh, S. S., Raman, R. (1978). Distribution, structure and petrography of the Deccan Trap, India. *Records of the Geological Survey of India, 43.*
- Rajesh, H. M., Chisonga, B. C., Shindo, K., Beukes, N. J., & Armstrong, R. A. (2013). Petrographic, geochemical and SHRIMP U-Pb titanite age characterization of the Thabazimbi mafic sills: Extended time frame and a unifying petrogenetic model for the Bushveld Large Igneous Province. *Precambrian Research, 230, 79–102.*
- Ramakrishnan, M., Vaidyanadhan, R. (2010). *Geology of India*, Vol. I. Geological Society of India, Bangalore, 557.
- Rama Rao, P., Naqvi, S.M., Govil, P.K., Balaram, V. (1991). Geochemistry of trondhjemites from Sigegudda, Hassan District, Karnataka. *Journal of the Geological Society of India 37, 351–358.*
- Ramesh Babu, N., Venkateshwarlu, M., Shankar, R., Nagaraju, E., & Parashuramulu, V. (2018). New paleomagnetic results on ~2367 ma dharwar giant dyke swarm, Dharwar Craton, southern India: Implications for Paleoproterozoic continental reconstruction. *Journal of Earth System Science, 127(1), 1–15.*
- Ramsay, J. G., & Graham, R. H. (1970). Strain variation in shear belts. *Canadian Journal of Earth Sciences, 7(3), 786–813.*
- Ramsay, J. G., Huber, M. I. (1987) *The techniques of modern Structural Geology*, Volume 2: Folds and fractures. Academic Press, London
- Ramsay, J. G., & Lisle, R. J. (2000). *The Techniques of Modern Structural Geology*, Volume 3: Applications of Continuum Mechanics in Structural Geology.
- Ramsay, J. G. (1980). Shear zone geometry: A review. *Journal of Structural Geology, 2(1–2), 83–99.*

- Ray, R., Sheth, H. C., & Mallik, J. (2007). Structure and emplacement of the Nandurbar-Dhule mafic dyke swarm, Deccan Traps, and the tectonomagmatic evolution of flood basalts. *Bulletin of Volcanology*, *69*(5), 537–551.
- Reichow, M. K., Saunders, A. D., White, R. V., Al’Mukhamedov, A. I., & Medvedev, A. Y. (2005). Geochemistry and petrogenesis of basalts from the West Siberian Basin: An extension of the Permo-Triassic Siberian Traps, Russia. *Lithos*, *79*(3-4), 425-452.
- Rekha, S., & Bhattacharya, A. (2013). Growth, preservation of Paleoproterozoic-shear-zone-hosted monazite, north of the Western Dharwar Craton (India), and implications for Gondwanaland assembly. *Contributions to Mineralogy and Petrology*, *166*(4), 1203–1222.
- Rekha, S., Bhattacharya, A., & Viswanath, T. A. (2013a). Microporosity linked fluid focusing and monazite instability in greenschist facies para-conglomerates, western India. *Geochimica et Cosmochimica Acta*, *105*, 187–205.
- Rekha, S., Viswanath, T. A., Bhattacharya, A., & Prabhakar, N. (2013b). Meso/Neoproterozoic crustal domains along the north Konkan coast, western India: The Western Dharwar Craton and the Antongil-Masora Block (NE Madagascar) connection. *Precambrian Research*, *233*, 316–336.
- Renne, P. R., Sprain, C. J., Richards, M. A., Self, S., Vanderkluysen, L., Pande, K. (2015). State shift in Deccan volcanism at the Cretaceous-Paleogene boundary, possibly induced by Impact. *Science*, *350*(6256), 76–78.
- Richards, M. A., Alvarez, W., Self, S., Karlstrom, L., Renne, P. R., Manga, M., Sprain, C. J., Smit, J., Vanderkluysen, L., & Gibson, S. A. (2015). Triggering of the largest Deccan eruptions by the Chicxulub impact. *Bulletin of the Geological Society of America*, *127*(11–12), 1507–1520.
- Richards, M. A., Duncan, R. A., & Courtillot, V. E. (1989). Flood basalts and hot-spot tracks: Plume heads and tails. *Science*, *246*(4926), 103-107.
- Rittmann, A. (1973) *Stable mineral assemblages of igneous rocks*. Springer, Berlin. 262 pp.
- Rivalta, E., Taisne, B., Bungler, A. P., & Katz, R. F. (2015). A review of mechanical models of dike propagation: Schools of thought, results and future directions. In *Tectonophysics*, *638*, 1-42.

- Rogers, J. (1986). The Dharwar Craton and the Assembly of Peninsular India. *The Journal of Geology*, 94(2), 129-143
- Rollinson, H. R. 1. (1993). *Using geochemical data: evaluation, presentation, interpretation*. Harlow, Essex, England: New York: Longman Scientific & Technical, 344.
- Ross C. S., and Shannon, E. V. (1925). The origin, occurrence, composition and physical properties of the mineral iddingsite. *Proceedings of the United States National Museum*. 67(2579), 1–19.
- Rogers, J. J. W. (1996). A history of continents in the past three billion years. *Journal of Geology*. <https://doi.org/10.1086/629803>
- Royer, J. Y, Sclater, J. G., and Sandwell, D. T. (1989). A preliminary Tectonic Fabric Chart of the Indian Ocean. *Proceedings of the Indian Academy of Science (Earth and Planetary Science)*, Vol. 98, 7-24.
- Rubin, A. M. (1993). Dikes vs. diapirs in viscoelastic rock. *Earth and Planetary Science Letters*, 117(3–4), 653–670.
- Rudnick, R. L., & Gao, S. (2013). Composition of the Continental Crust. In *Treatise on Geochemistry: Second Edition*. <https://doi.org/10.1016/B978-0-08-095975-7.00301-6>
- Saha, A. K., Sankaran, A. V. and Bhattacharyya, T. K. (1973) Geochemistry of the newer dolerite suite of intrusions within the Singhbhum granite - a preliminary study. *Journal Geological Society of India*, 14, 229-346.
- Said, N., Kerrich, R., Cassidy, K., & Champion, D. C. (2012). Characteristics and geodynamic setting of the 2.7 Ga Yilgarn heterogeneous plume and its interaction with continental lithosphere: Evidence from komatiitic basalt and basalt geochemistry of the Eastern Goldfields Superterrane. *Australian Journal of Earth Sciences*, 39, 737-763.
- Samant, H., Patel, V., Pande, K., Sheth, H., & Jagadeesan, K. C. (2019).  $^{40}\text{Ar}/^{39}\text{Ar}$  dating of tholeiitic flows and dykes of Elephanta Island, Panvel flexure zone, western Deccan Traps: A five-million-year record of magmatism preceding India-Laxmi Ridge-Seychelles breakup. *Journal of Volcanology and Geothermal Research*, 379, 12–22.
- Sant DA, Karanth RV (1990) Emplacement of dyke swarms in the Lower Narmada valley, western India. In: Parker AJ, Rickwood PC, Tucker DH (eds) *Mafic dykes and emplacement mechanisms*. Balkema, Rotterdam, pp 383–389

- Sarkar, S., Banerjee, S., Chakrabarty, S., 1995. Synsedimentary seismic signatures in the Mesoproterozoic Koldhaha shale, Kheinjua Formation, Central India. *Indian Journal of Earth Sciences*, Vol. 22, 158–164.
- Saunders, A. D., Norry, M. J., & Tarney, J. (1991). Fluid influence on the trace element compositions of subduction zone magmas. *Philosophical Transactions - Royal Society of London, A*, 335(1638), 377–392.
- Schilling, J. G., Zajac, M., Evans, R., Johnston, T., White, W., Devine, J. D., & Kingsley, R. (1983). Petrologic and geochemical variations along the Mid-Atlantic Ridge from 29°N to 73°N. *American Journal of Science*, 283(6), 510-586.
- Schirnack, C., Van Den Bogaard, P., & Schmincke, H. U. (1999). Cone sheet formation and intrusive growth of an oceanic island-the Miocene Tejada complex on Gran Canaria (Canary Islands). *Geology*, 27(3), 207-210.
- Schoene, B., Eddy, M. P., Samperton, K. M., Keller, C. B., Keller, G., Adatte, T., & Khadri, S. F. R. (2019). U-Pb constraints on pulsed eruption of the Deccan Traps across the end-Cretaceous mass extinction. *Science*, 363(6429), 862–866.
- Schoene, B., Samperton, K. M., Eddy, M. P., Keller, G., Adatte, T., Bowring, S. A., Khadri, S. F. R., & Gertsch, B. (2015). U-Pb geochronology of the Deccan Traps and relation to the end-Cretaceous mass extinction. *Science*, 347(6218), 182–184.
- Seilacher, A. (1984). Sedimentary structures tentatively attributed to seismic events. *Marine Geology*, 55(1-2), 1-12.
- Sen, G. (2001). Generation of Deccan Trap magmas. *Proceedings of the Indian Academy of Sciences, Earth and Planetary Sciences*, 110(4), 409–431.
- Seshadri, T. S., Chaudhuri, A., Harinadha Babu, P., Chayapathi, N., 1981. Chitradurga belt. In: Swaminanath, J., Ramakrishnan, M. (Eds.), Early Precambrian Supracrustals of Southern Karnataka. *Geological Survey of India Memoir* 112, 163–198.
- Seyum, S., Pollard, D.P. (2016) The mechanics of intersecting echelon veins and pressure solution seams in limestone. *Journal of Structural Geology*, Vol. 89, 250-263.
- Shanmugam, G. (2016). The Contourite Problem. In *Sediment Provenance: Influences on Compositional Change from Source to Sink*, 183-254.

- Shanmugam, G. (2017). The fallacy of interpreting SSDS with different types of breccias as seismites amid the multifarious origins of earthquakes: Implications. *Journal of Palaeogeography*, 6(1), 12–44.
- Shelley, D. (1993). *Igneous and metamorphic rocks under the microscope: Classification, textures, microstructures, and mineral preferred-orientations*. London: Chapman & Hall
- Sheth, H. c. (1998) A reappraisal of the coastal Panvel flexure, Deccan Traps, as a listric-fault-controlled reverse drag structure. *Tectonophysics*, 294, 143-149.
- Sheth, H. C. (2000). The timing of crustal extension, diking, and eruption of the deccan flood basalts. *International Geology Review*, 42(11), 1007–1016.
- Sheth, H. C., Pande, K., & Bhutani, R. (2001).  $^{40}\text{Ar}$ - $^{39}\text{Ar}$  age of a national geological monument: The Gilbert Hill basalt, Deccan Traps, Bombay. *Current Science*, 80(11), 1437–1440.
- Sheth, H. C., & Cañón-Tapia, E. (2015). Are flood basalt eruptions monogenetic or polygenetic? *International Journal of Earth Sciences*, 104(8), 2147–2162.
- Sheth, H. C., & Pande, K. (2014). Geological and  $^{40}\text{Ar}/^{39}\text{Ar}$  age constraints on late-stage Deccan rhyolitic volcanism, inter-volcanic sedimentation, and the Panvel flexure from the Dongri area, Mumbai. *Journal of Asian Earth Sciences*, 84, 167–175.
- Sheth, H. C., Mahoney, J. J., & Chandrasekharam, D. (2004). Geochemical stratigraphy of Deccan flood basalts of the Bijasan Ghat section, Satpura Range, India. *Journal of Asian Earth Sciences*, 23(1), 127–139.
- Sheth, H. C., Pande, K., Vijayan, A., Sharma, K. K., & Cucciniello, C. (2017). Recurrent Early Cretaceous, Indo-Madagascar (89–86 Ma) and Deccan (66 Ma) alkaline magmatism in the Sarnu-Dandali complex, Rajasthan:  $^{40}\text{Ar}/^{39}\text{Ar}$  age evidence and geodynamic significance. *Lithos*, 284–285(September), 512–524.
- Sheth, H., Meliksetian, K., Gevorgyan, H., Israyelyan, A., & Navasardyan, G. (2015). Intracanyon basalt lavas of the Debed River (northern Armenia), part of a Pliocene-Pleistocene continental flood basalt province in the South Caucasus. *Journal of Volcanology and Geothermal Research*, 295, 1-15.
- Sheth, H. C., Ray, J. S., Ray, R., Vanderkluisen, L., Mahoney, J. J., Kumar, A., Shukla, A. D., Das, P., Adhikari, S., & Jana, B. (2009). Geology and geochemistry of Pachmarhi

- dykes and sills, Satpura Gondwana Basin, central India: Problems of dyke-sill-flow correlations in the Deccan Traps. *Contributions to Mineralogy and Petrology*, 158(3), 357–380.
- Sheth, H. C., Vanderkluyesen, L., Demonterova, E. I., Ivanov, A. V., & Savatenkov, V. M. (2019). Geochemistry and  $^{40}\text{Ar}/^{39}\text{Ar}$  geochronology of the Nandurbar-Dhule mafic dyke swarm: Dyke-sill-flow correlations and stratigraphic development across the Deccan flood basalt province. *Geological Journal*, 54(1), 157–176.
- Sheth, H. C., Zellmer, G. F., Demonterova, E. I., Ivanov, A. V., Kumar, R., & Patel, R. K. (2014). The Deccan tholeiite lavas and dykes of Ghatkopar-Powai area, Mumbai, Panvel flexure zone: Geochemistry, stratigraphic status, and tectonic significance. *Journal of Asian Earth Sciences*, 84, 69–82.
- Sneddon, I. N., Lowengrub, M. (1969) *Crack problems in the classical theory of elasticity*. John Wiley, New York, 221.
- Shrivastava, J. P., Kumar, R., & Rani, N. (2017). Feeder and post Deccan Trap dyke activities in the northern slope of the Satpura Mountain: Evidence from new  $^{40}\text{Ar}-^{39}\text{Ar}$  ages. *Geoscience Frontiers*, 8(3), 483–492. <https://doi.org/10.1016/j.gsf.2016.04.001>
- Sibson, R. H. (1986). Brecciation processes in fault zones: Inferences from earthquake rupturing. *Pure and Applied Geophysics PAGEOPH*, 124(1–2), 159–175.
- Silpa, A. S., & Satish-Kumar, M. (2018). Dyke Swarms in the Dharwar Craton: A Key to Understanding the Late Archean to Early Proterozoic Cratonic Correlations. In *Journal of the Indian Institute of Science*, 98, 365-378.
- Singh, A. P. (2002). Impact of Deccan volcanism on deep crustal structure along western part of Indian mainland and adjoining Arabian Sea. *Current Science*, 82(3), 316–325
- Song, X. Y., Qi, H. W., Robinson, P. T., Zhou, M. F., Cao, Z. M., & Chen, L. M. (2008). Melting of the subcontinental lithospheric mantle by the Emeishan mantle plume; evidence from the basal alkaline basalts in Dongchuan, Yunnan, Southwestern China. *Lithos*, 100(1–4), 93–111.
- Song, X. Y., Zhou, M. F., Hou, Z. Q., Cao, Z. M., Wang, Y. L., & Li, Y. (2001). Geochemical constraints on the mantle source of the upper Permian Emeishan continental flood basalts, Southwestern China. *International Geology Review*, 43(3), 213–225.

- Song, S. R., & Lo, H. J. (2002). Lithofacies of volcanic rocks in the central Coastal Range, eastern Taiwan: Implications for island arc evolution. *Journal of Asian Earth Sciences*, 21(1), 23-38.
- Sparks, R. S. J. (1978). The dynamics of bubble formation and growth in magmas: A review and analysis. *Journal of Volcanology and Geothermal Research*, 3(1-2), 1-37.
- Sprain, C. J., Renne, P. R., Clemens, W. A., & Wilson, G. P. (2018). Calibration of chron C29r: New high-precision geochronologic and paleomagnetic constraints from the Hell Creek region, Montana. *Bulletin of the Geological Society of America*, 130(9–10), 1615–1644.
- Sprain, C. J., Renne, P. R., Vanderkluyzen, L., Pande, K., Self, S., & Mittal, T. (2019). The eruptive tempo of deccan volcanism in relation to the cretaceous-paleogene boundary. *Science*, 363(6429), 866–870.
- Spry, A. (1962). The origin of columnar jointing, particularly in basalt flows. *Journal of the Geological Society of Australia*, 8(2), 191-216.
- Sreeramachandra Rao, K., Murthy, T. S. S., Ramakrishna, T. L., Janardhan, K., Sundaram, V. (1996) Geological and mineral map of Goa (1:1, 25, 000). *Geological Survey of India Publications*.
- Srivastava, R. K., Pandit, M. K., Upadhyaya, R. (1988) Petrography and chemical stratigraphy of Deccan basalts from a part of the Malwa Plateau: use of cluster analysis in chemical stratigraphy. In *Deccan Flood Basalts (Subbarao, K. V., Ed)*, *Geological Society of India Memoirs Number 10*, 181-198.
- Srivastava, R. K. (2011). *Dyke Swarms: Keys for Geodynamic Interpretation*. Springer Berlin Heidelberg. <https://doi.org/10.1007/978-3-642-12496-9>
- Srivastava, R. K., Kumar, S., Sinha, A. K., & Chalapathi Rao, N. V. (2014). Petrology and geochemistry of high-titanium and low-titanium mafic dykes from the Damodar valley, Chhotanagpur Gneissic Terrain, eastern India and their relation to Cretaceous mantle plume(s). *Journal of Asian Earth Sciences*, 84(June 2015), 34–50.
- Srivastava, R. K., Sivaji, C., Rao, N. V. C., Shrivastava, J. P., Girdhar, M., & Kumar, R. (2008). Petrography, Composition and Petrogenesis of Basalts from Chakhla-Delakhari Intrusive Complex, Eastern Deccan Volcanic Province, India. In *Srivastava, R. K.,*

- Sivaji, Ch., Chalapathi Rao, N. V. (Eds) *Indian Dykes: Geochemistry, Geophysics, Geochronology*. Narosa Publishing House.
- Storey, M., Mahoney, J. J., & Saunders, A. D. (1997). Cretaceous basalts in Madagascar and the transition between plume and continental lithosphere mantle sources. *Geophysical Monograph Series*, 100, 95–122.
- Su, Y., Huber, C., Bachmann, O., Zajacz, Z., Wright, H., & Vazquez, J. (2016). The role of crystallization-driven exsolution on the sulfur mass balance in volcanic arc magmas. *Journal of Geophysical Research: Solid Earth*, 121(8), 5624-5640.
- Sun, S. S., & McDonough, W. F. (1989). Chemical and isotopic systematics of oceanic basalts: Implications for mantle composition and processes. *Geological Society Special Publication*, 42(1), 313–345.
- Subrahmanya, K. R. (1996). Active intraplate deformation in south India. *Tectonophysics*, 262(1–4), 231–241.
- Subrahmanya, K. R. (1998). Tectono-magmatic evolution of the west coast of india. *Gondwana Research*, 1(3–4), 319–327.
- Sun, S. S., Nesbitt, R. W., & Sharaskin, A. Y. (1979). Geochemical characteristics of mid-ocean ridge basalts. *Earth and Planetary Science Letters*, 44(1), 119-138.
- Subbarao, K. V., Hooper, P. R. (1988) Reconnaissance map of the Deccan Basalt Group in the Western Ghats, India. In: Subbarao, K. V. (Ed.) *Deccan Flood Basalts. Geological Society of India Memoir Number 10*.
- Swaminath, J., Ramakrishnan, M. (Eds.), 1981. Early Precambrian supracrustals of southern Karnataka. Geological Survey of India, Memoir 112, 350.
- Taylor, S. R., & McLennan, S. M. (1985). The Continental Crust: its Composition and Evolution. An Examination of the Geochemical Record Preserved in Sedimentary Rocks. In *The Continental Crust: its Composition and Evolution. An Examination of the Geochemical Record Preserved in Sedimentary Rocks*.
- Thirlwall, M. F., Upton, B. G. J., & Jenkins, C. (1994). Interaction between Continental Lithosphere and the Iceland Plume--Sr-Nd-Pb Isotope Geochemistry of Tertiary Basalts, NE Greenland. *Journal of Petrology*, 35(3), 839–879.

- Thompson, R. N., Morrison, M. A., Hendry, G. L., & Parry, S. J. (1984). An assessment of the relative roles of crust and mantle in magma genesis: an elemental approach. *Philosophical Transactions of the Royal Society of London*, 3(A310(1514)), 549–590.
- Thornton, C. P., & Tuttle, O. F. (1960). Chemistry of igneous rocks--[Part] 1, Differentiation Index. *American Journal of Science*, 258(9), 664–684.
- Todal, A., & Edholm, O. (1998). Continental margin off western India and Deccan Large Igneous Province. *Marine Geophysical Research*, 20(4), 273–291.
- Toulkeridis, T., Clauer, N., Kröner, A., Reimer, T., & Todt, W. (1999). Characterization, provenance, and tectonic setting of Fig Tree greywackes from the Archaean Barberton Greenstone Belt, South Africa. *Sedimentary Geology*, 124(1–4), 113–129.
- Törő, B., & Pratt, B. R. (2015). Eocene Paleoseismic Record of the Green River Formation, Fossil Basin, Wyoming, U.S.A.: Implications of Synsedimentary Deformation Structures In Lacustrine Carbonate Mudstones. *Journal of Sedimentary Research*, 85(8), 855–884.
- Turner, F.J. and Verhoogen, J. (1960) *Igneous and Metamorphic Petrology*. 2nd Edition, McGraw-Hill, New York, 694.
- Tucker, M. E. (2011). *Sedimentary Rocks in the Field: A Practical Guide* (4<sup>th</sup> Edition). Wiley.
- Ugarkar, A. G., Chandan Kumar, B., Malapur, M. A., Manuvachari, T. B., & Kerr, A. C. (2017). Petrography and geochemistry of Archaean greywackes from northern part of the Dharwar-Shimoga greenstone belt, western Dharwar craton: Implications for nature of provenance. *Journal of the Geological Society of India*, 89(5), 547–553.
- Valdiya, K. S. (2016). *The Making of India-Geodynamic Evolution* (2<sup>nd</sup> Edition). Springer International Publishing. <https://doi.org/10.1007/978-3-319-25029-8>
- Valentine, G. A., & Krogh, K. E. C. (2006). Emplacement of shallow dikes and sills beneath a small basaltic volcanic center - The role of pre-existing structure (Paiute Ridge, southern Nevada, USA). *Earth and Planetary Science Letters*, 246(3–4), 217–230.
- Valsangkar, A. B., Radhakrishna Murthy, C., Subbarao, K. V. and Beckinsale, R. D. (1981). Paleomagnetism and Potassium-Argon age studies of acid igneous rocks from St. Mary Islands. *Geological Society of India Memoirs Number 3*, 265-276
- Van Westrenen, W., Blundy, J. D., & Wood, B. J. (2001). High field strength element/rare earth element fractionation during partial melting in the presence of garnet:

- Implications for identification of mantle heterogeneities. *Geochemistry, Geophysics, Geosystems*, 2(7). <https://doi.org/10.1029/2000GC000133>
- Vandamme, D., Courtillot, V., Besse, J., & Montigny, R. (1991). Paleomagnetism and age determinations of the Deccan Traps (India): Results of a Nagpur-Bombay Traverse and review of earlier work. *Reviews of Geophysics*, 29(2), 159.
- Vanderkluysen, L., Mahoney, J. J., Hooper, P. R., Sheth, H. C., & Ray, R. (2011). The feeder system of the Deccan Traps (India): Insights from dike geochemistry. *Journal of Petrology*, 52(2), 315–343.
- Vanderkluysen, L., Mahoney, J. J., Koppers, A. A. P., Beier, C., Regelous, M., Gee, J. S., & Lonsdale, P. F. (2014). Louisville Seamount Chain: Petrogenetic processes and geochemical evolution of the mantle source. *Geochemistry, Geophysics, Geosystems*, 15(6), 2380–2400.
- Varadarajan, K. and Ganju, J. L. (1989) Lineament analysis of coastal belt of Peninsula India. Qureshy, M. N and Hinze, W. J. (Eds) *Geological Society of India Memoir Number 12*, 49-58.
- Varga, R. J., Gee, J. S., Staudigel, H., & Tauxe, L. (1998). Dike surface lineations as magma flow indicators within the sheeted dike complex of the Troodos Ophiolite, Cyprus. *Journal of Geophysical Research: Solid Earth*, 103(B3), 5241–5256.
- Venkatesan, T.R., Pande, K. (1996) A review of  $^{40}\text{Ar}$ - $^{39}\text{Ar}$  ages from the Western Ghats, Deccan Trap Province, India: Implications for K/T events, *Gondwana Geological Society Special Vol. 2*, 321-328
- Venkatesan, T. R., Pande, K., & Gopalan, K. (1993). Did Deccan volcanism pre-date the Cretaceous/Tertiary transition? *Earth and Planetary Science Letters*, 119(1–2), 181–189.
- Verma, O., & Khosla, A. (2019). Developments in the stratigraphy of the Deccan Volcanic Province, peninsular India. *Comptes Rendus - Geoscience*, 351(7), 461–476.
- Verma, S. P., & Rivera-Gómez, M. A. (2013). Computer programs for the classification and nomenclature of igneous rocks. In *Episodes*, 36(2), 115-124.
- Verma, S. P., Torres-Alvarado, I. S., & Velasco-Tapia, F. (2003). A revised CIPW norm. *Schweizerische Mineralogische Und Petrographische Mitteilungen*, 83(2), 197–216.

- Vernon, R. H. (2004). *A Practical Guide to Rock Microstructure*. Cambridge University Press.  
<https://doi.org/10.1017/cbo9780511807206>
- Vijayan, A., Sheth, H., & Sharma, K. K. (2016). Tectonic significance of dykes in the Sarnu-Dandali alkaline complex, Rajasthan, northwestern Deccan Traps. *Geoscience Frontiers*, 7(5), 783–791.
- Viswanatha, M.N., Ramakrishnan, M., 1981. Bababudan belt. In: Swaminanath, J., Ramakrishnan, M. (Eds.), *Early Precambrian Supracrustals of Southern Karnataka. Geological Survey of India Memoir Volume 112*, 91–114.
- Vredenburg, S. W. (1906) Suggestions for a classification of the Vindhyan System. *Records of the Geological Survey of India, Vol. 33(4)*, 261-314.
- Wadia, D.N. (1975) *Geology of India*, 4<sup>th</sup> Edition, Tata McGraw-Hill, New Delhi.
- Wager, L. R., Deer, W. A. (1939) Geological investigations in East Greenland, Part III, The petrology of the Skaergaard intrusion, Kangerdlugssuaq, East Greenland: *Meddl. Om Gronland*, V.105, 590-706.
- Wagle, B. G. (1993). Geomorphology of Goa and Goa Coast. *Giornale di Geologia*, 55(2), 19–24.
- Wagle, B. G., Rajamanickam, G. V. (1980) A petrographic study of Precambrian quartzites from Goa coast. *Mahasagar-Bulletin of National Institute of Oceanography*, 13, 9–21
- Wagle, B. G., Vora, K. H., Karisiddaiah, S. M., Veerayya, M., & Almeida, F. (1994). Holocene submarine terraces on the western continental shelf of India; Implications for sea-level changes. *Marine Geology*, 117(1–4), 207–225.
- Walker, F., Poldervaart, A. (1949) Karroo dolerites of the Union of South Africa. *Geological Society of America Bulletin*, 60(4), 591–706.
- Walker, F. (1957). Ophitic Texture and Basaltic Crystallization. *The Journal of Geology*, 65(1), 1-14
- Walker, G. P. L., Eyre, R., Spengler, S. R., Knight, M. D., Kennedy, K. (1995) Congruent dyke-widths in large basaltic volcanoes. In: Baer G, Heimann A (Editors) *Physics and chemistry of dykes*. Balkema, Rotterdam, pp 35–40
- Wang, K. L., Chung, S. L., Chen, C. H., & Chen, G. H. (2002). Geochemical constraints on the petrogenesis of high-Mg basaltic andesites from the Northern Taiwan volcanic zone. *Chemical Geology*, 182(2-4), 513-528.

- Wang, X. L., Zhou, J. C., Qiu, J. S., Jiang, S. Y., & Shi, Y. R. (2008). Geochronology and geochemistry of Neoproterozoic mafic rocks from western Hunan, South China: Implications for petrogenesis and post-orogenic extension. *Geological Magazine*, *145*(2), 215–233.
- Watanabe, T., Masuyama, T., Nagaoka, K., & Tahara, T. (2002). Analog experiments on magma-filled cracks: Competition between external stresses and internal pressure. *Earth, Planets and Space*, *54*(12), e1247–e1261.
- Watts, A. B., & Cox, K. G. (1989). The Deccan Traps: an interpretation in terms of progressive lithospheric flexure in response to a migrating load. *Earth and Planetary Science Letters*, *93*(1), 85–97.
- Weaver, B. L. (1991). The origin of ocean island basalt end-member compositions: trace element and isotopic constraints. *Earth and Planetary Science Letters*, *104*(2–4), 381–397.
- Weertman, J. (1971). Theory of water-filled crevasses in glaciers applied to vertical magma transport beneath oceanic ridges. *Journal of Geophysical Research*, *76*(5), 1171–1183.
- West, W. D. (1958) The petrography and petrogenesis of forty-eight flows of Deccan Trap penetrated by borings in Western India. Transactions of the National Institute of Science, India, IV, pp.1-56.
- West, W. D. (1959). The source of the Deccan Trap flows. *Journal of the Geological Society of India*, *1*, 44–52.
- White, R., & McKenzie, D. (1989). Magmatism at rift zones: the generation of volcanic continental margins and flood basalts. *Journal of Geophysical Research*, *94*(B6), 7685–7729.
- White, W. M. (2013). *Geochemistry*. Wiley-Blackwell.
- White, R.S., Westbrook, G.K., Fowler, S.R., et al. (1987). Hatton Bank (northwest U.K.) continental margin structure. *Geophysical Journal of the Royal Astronomical Society*, *Vol. 89*, 265–272.
- Widdowson, M. (1997). Tertiary palaeosurfaces of the SW Deccan, Western India: implications for passive margin uplift. *Geological Society, London, Special Publications*, *120*(1), 221–248.

- Widdowson, M. (2009). Evolution of Laterite in Goa. In *Natural resources of Goa: a geological perspective*, Mascarenhas, A. & Kalavampara, G. (Editors), 35-68.
- Widdowson, M., & Cox, K. G. (1996). Uplift and erosional history of the Deccan Traps, India: Evidence from laterites and drainage patterns of the Western Ghats and Konkan Coast. *Earth and Planetary Science Letters*, 137(1–4), 57–69.
- Widdowson, M., Pringle, M. S., & Fernandez, O. A. (2000). A post K-T boundary (early Palaeocene) age for Deccan-type feeder dykes, Goa, India. *Journal of Petrology*, 41(7), 1177–1194.
- Wilson, B. M., (1989) *Igneous Petrogenesises – A Global Tectonic approach*, Springer Netherlands, pp.466. <https://doi.org/10.1007/978-1-4020-6788-4>
- Wilson, L., & Head, J. W. (1981). Ascent and eruption of basaltic magma on the Earth and moon. *Journal of Geophysical Research*, 86(B4), 2971-3001.
- Wilson, S. A., 1997, Data compilation for USGS reference material BHVO-2, Hawaiian Basalt, U.S. Geological Survey Open-File Report xxxxx.
- Windley, B. F. (1984) *The Evolving Continents*; John Wiley and Sons, 2<sup>nd</sup> Edition.
- Winter, J. D. (2011). *Principles of Igneous and Metamorphic Petrology* (Second Edition). Pearson Prentice Hall.
- Wimmenauer, W., (1984). Das pravariskische Kristallin in Schwarzwald. *Fortschritt der Mineralogie*, 62, 6986.
- Woodcock, N. H. (1976a). Ludlow Series slumps and turbidites and the form of the Montgomery Trough, Powys, Wales. *Proceedings of the Geologists' Association*, 87(2), 169–182.
- Woodcock, N. H. (1976b). Structural style in slump sheets: Ludlow Series, Powys, Wales. *Journal of the Geological Society*, 132(4), 399–415.
- Woodcock, N. H. (1979). The use of slump structures as palaeoslope orientation estimators. *Sedimentology*, 26(1), 83–99.
- Woodcock, N. H., Miller, A. V. M., & Woodhouse, C. D. (2014). Chaotic breccia zones on the Pembroke Peninsula, south Wales: Evidence for collapse into voids along dilational faults. *Journal of Structural Geology*, 69(PA), 91-107.
- Wright, J. B. (1969). A simple alkalinity ratio and its application to questions of non-orogenic granite genesis. *Geological Magazine*, 106(4), 370–384.

- Xu, X. W., Zhang, B. L., Qin, K. Z., Mao, Q., & Cai, X. P. (2007). Origin of lamprophyres by the mixing of basic and alkaline melts in magma chamber in Beiya area, western Yunnan, China. *Lithos*, 99(3–4), 339–362.
- Yatheesh, V., Kurian, P. J., Bhattacharya, G. C., & Rajan, S. (2013). Morphotectonic architecture of an India-Madagascar breakup related anomalous submarine terrace complex on the southwest continental margin of India. *Marine and Petroleum Geology*, 46, 304–318.
- Yatheesh, V., Bhattacharya, G. C., & Mahender, K. (2006). The terrace like feature in the mid-continental slope region off Trivandrum and a plausible model for India-Madagascar juxtaposition in immediate pre-drift scenario. *Gondwana Research*, 10(1–2), 179–185.
- Yong Technology, Inc. (2014) GeoRose. Edmonton, Canada. <http://www.yongtechnology.com/download/georose>. Accessed 12 July 2016
- Zellmer, G. F., Sheth, H. C., Iizuka, Y., & Lai, Y. J. (2012). Remobilization of granitoid rocks through mafic recharge: Evidence from basalt-trachyte mingling and hybridization in the Manori-Gorai area, Mumbai, Deccan Traps. *Bulletin of Volcanology*, 74(1), 47–66.
- Zhang, C., Wu, Z., Gao, L., Wang, W., Tian, Y., & Ma, C. (2007). Earthquake-induced soft-sediment deformation structures in the Mesoproterozoic Wumishan Formation, North China, and their geologic implications. *Science in China Series D: Earth Sciences*, 50(3), 350–358.
- Zindler, A., & Hart, S. (1986). Chemical geodynamics. *Annual Review of Earth and Planetary Sciences*. Vol. 14, c, 493–571.
- Ziv, A., Rubin, A. M., & Agnon, A. (2000). Stability of dike intrusion along preexisting fractures. *Journal of Geophysical Research: Solid Earth*, 105(B3), 5947–5961.

# **Research Publications**

## Publication

Gadgil, R., Viegas, A. & Iyer, S.D. Structure and emplacement of the Coastal Deccan tholeiitic dyke swarm in Goa, on the western Indian rifted margin. *Bull Volcanol* **81**, 35 (2019). <https://doi.org/10.1007/s00445-019-1297-6> (Impact Factor: 2.582)

## Seminar/Conference attended

- 1) Attended and presented a paper titled “**Petrology and whole rock geochemistry of the dyke swarm in Goa, India**” at the National Seminar on “**Deccan magmatism and biotic events across the K/T boundary**” at the Dr. Harisingh Gour Vishwavidyalaya, Sagar, Madhya Pradesh from 26<sup>th</sup> to 28<sup>th</sup> October 2017.
- 2) Attended and presented a paper titled “**Tectonic aspects of dyke emplacements along the coast of Goa – a preliminary study**” at the 5<sup>th</sup> Conference and Workshop on “**Rock Deformation and Structures**” at the University of Delhi from 4<sup>th</sup> to 6<sup>th</sup> October 2018.



# Structure and emplacement of the Coastal Deccan tholeiitic dyke swarm in Goa, on the western Indian rifted margin

Raghav Gadgil<sup>1,2</sup> · Anthony Viegas<sup>1</sup> · Sridhar D. Iyer<sup>3</sup>

Received: 14 January 2019 / Accepted: 1 May 2019

© International Association of Volcanology & Chemistry of the Earth's Interior 2019

## Abstract

Mafic dyke swarms, when controlled by a regional stress field, are emplaced perpendicular to the minimum principal compressive stress direction. However, mafic dyke swarms may also exploit pre-existing structural fabric in their host rocks. Distinguishing between the two scenarios is important for correct geodynamic understanding of magmatic events. Continental flood basalt provinces such as the Deccan Traps of India represent huge fissure eruptions produced by swarms of mafic dykes. The Coastal dyke swarm of the Deccan, along the western Indian rifted margin, is one of its three major dyke swarms. We present a field study of the Goa dykes, part of the Coastal swarm. The dykes are typical dolerites and basalts exposed in Proterozoic-age basement; lava flows which these dykes may have once fed have been stripped away by erosion, though exposed in the Western Ghats escarpment ~ 100 km to the east. The Goa dyke swarm contains 60 dykes, some of which form larger multiple-injection dykes. The dykes are short compared to typical (kilometers or tens of kilometers long) dykes in flood basalt provinces such as the Deccan or Iceland, and range in length from ~ 15 to ~ 220 m and in thickness from 3 cm to 20 m. Most dykes are vertical and the others dip steeply in various directions. Their structural attributes and internal features (such as vesicular zones and columnar jointing) provide clues to the processes of magma flow and solidification in the dykes. Field measurements yield an average crustal dilation of 8% due to dyke emplacement. Calculations of magmatic overpressures and magma chamber depths generally yield unrealistic values owing to the low aspect ratios of the dykes. Based on comparisons between the dyke trends and the host rock joint trends, we consider that a few of the Goa dykes were emplaced along pre-existing fractures, but the orientations of the great majority of the dykes reflect contemporaneous stress fields. Based on crosscutting relationships, we infer that the regional minimum horizontal compressive stress ( $\sigma_3$ ) changed over time from a ~E-W orientation to a ~NE-SW orientation and finally to a ~N-S direction.

**Keywords** Volcanism · Continental flood basalt · Dyke swarm · Deccan traps · Goa

## Introduction

Continental flood basalt (CFB) provinces of the world represent fissure eruptions of a huge scale, produced by swarms of

mafic dykes (e.g., Swanson et al. 1975; Mège and Korme 2004; Ray et al. 2007). Mafic dyke swarms provide valuable information on the mechanics of magma transport in the crust and to the surface and crustal deformation during swarm emplacement (e.g., Currie and Ferguson 1970; Daniels et al. 2012; Gudmundsson and Loetveit 2005), as well as allowing palaeocontinental reconstructions (e.g., Halls 1982; Ernst et al. 1995; Park et al. 1995). Most dykes are magma-driven extension fractures (mode I cracks) that form in a direction perpendicular to the minimum principal compressive stress, with the maximum and intermediate principal stresses lying within the dyke plane (e.g., Gudmundsson 1995, 2011; Marinoni 2001). Dyke swarms can be useful kinematic indicators in deformed crust (e.g., Paquet et al. 2007; Hou et al. 2010; Airolidi et al. 2011). Whereas preexisting fracture fabrics in basement rocks sometimes exert a fundamental control

---

Editorial responsibility: V. Acocella

✉ Raghav Gadgil  
geology.raghav@unigoa.ac.in

<sup>1</sup> Department of Earth Science, Goa University, Taleigao Plateau, Goa 403206, India

<sup>2</sup> Department of Geology, Dhempe College of Arts and Science, Miramar, Panaji, Goa 403001, India

<sup>3</sup> Formerly with Geological Oceanography Division, CSIR-National Institute of Oceanography, Dona Paula, Goa 403004, India

on dyke swarm geometry (e.g., Baer et al. 1994; Mège and Korme 2004; Martinez-Poza et al. 2014), in many cases dyke swarm configurations reflect contemporaneous tectonic stress fields (e.g., Gudmundsson 1995; Ray et al. 2007; Vijayan et al. 2016). The shapes of dykes reflect the interplay of complex emplacement and eruptive processes wherein magma viscosity, host rock deformation, stress distribution, magma pressure variation, and heat transfer play essential roles (e.g., Cadman et al. 1990; Fialko and Rubin 1999; Daniels et al. 2012).

The Deccan Traps volcanic province of India is a major CFB province, ~65 million years in age (Baksi 2014). With a current exposed area of > 500,000 km<sup>2</sup> (Mahoney 1988), the Deccan province has been extensively studied for petrology, geochemistry, and volcanic stratigraphy (e.g., Cox and Hawkesworth 1984; Sheth and Melluso 2008; Cucciniello et al. 2014). The flood basalts are best exposed in the Western Ghats escarpment along the western Indian rifted continental margin, where they attain a stratigraphic thickness of > 3 km (Beane et al. 1986; Devey and Lightfoot 1986). The Deccan Traps contain three major mafic dyke swarms (Auden 1949; Deshmukh and Sehgal 1988; Vanderkluyzen et al. 2011; Ju et al. 2013; Fig. 1a). These are the ENE-WSW-trending Narmada-Tapi dyke swarm in the north-central Deccan and Saurashtra (Bhattacharji et al. 1996; Melluso et al. 1999; Ray et al. 2007; Sheth et al. 2009, 2013, 2019; Cucciniello et al. 2015), the more randomly oriented Nasik-Pune dyke swarm in the region of the Western Ghats (Bondre et al. 2006; Vanderkluyzen et al. 2011), and the NNW-SSE-trending Coastal dyke swarm along and parallel to the western Indian rifted continental margin (e.g., Dessai and Viegas 1995; Powar and Vadetwar 1995; Hooper et al. 2010; Sheth et al. 2014; Pande et al. 2017; Basavaiah et al. 2018; Samant et al. 2019).

Dykes of the three major Deccan mafic dyke swarms are usually seen cutting Deccan basalt lava flows (e.g., Melluso et al. 1999; Sheth et al. 2014; Cucciniello et al. 2015). However, mafic dykes in the coastal state of Goa in western India (Fig. 1a), part of the Coastal Deccan dyke swarm, are seen intruding Precambrian basement rocks (Widdowson et al. 2000; Dessai 2018). The Deccan basalt lava flows which once presumably covered these dykes have been removed by erosion, but are preserved in the Western Ghats escarpment to the east. Despite some geochemical, geochronological, and palaeomagnetic data available on some of the Goa dykes (Widdowson et al. 2000; Patil and Rao 2002), there is no study of the field geological and structural aspects of these dykes in the international literature comparable to studies of other Deccan dykes (e.g., Bondre et al. 2006; Ray et al. 2007; Vanderkluyzen et al. 2011). In this study, we present data on the field relationships and structural and volcanological features of these dykes, exposed in the coastal stretch from Aguada to Keri in Goa (Fig. 1b). We use these field data to

understand the emplacement mechanics of the Goa dykes during Deccan flood basalt volcanism, as has been done based on detailed structural data and geological mapping for dykes elsewhere in the Deccan Traps (e.g., Bondre et al. 2006; Ray et al. 2007; Sheth et al. 2013; Cucciniello et al. 2015). Our field data on the Goa dykes considerably improve our understanding of the interplay of tectonics and magmatism associated with the formation of the Coastal dyke swarm of the Deccan CFB province.

## Geological background

The coast of Goa state is situated ~150 km south of the southernmost exposures of the Deccan Traps (Fig. 1a). Goa's coastline is shaped by a set of NNW-SSE-trending fractures which have undergone lateral shifts along ENE-WSW-trending, Precambrian-age mega-lineaments traversing the Indian peninsular shield (Prabhakar Rao et al. 1985). The drainage patterns of Goan rivers (NW-SE, NNW-SSE, or E-W) follow Precambrian rock trends (strikes of strata, faults, fractures, shear zones). Lineament maps of Goa based on remote sensing images can be found in Iyer and Wagle (1987) and Martha et al. (2013). Iyer et al. (1989) treated the lineaments of Goa statistically and found three distinct peaks in lineament trends at N 40–45°, N 90–95°, and N 140–145° which they could correlate with the axial plane trends of various plunging folds in the Precambrian rocks.

Our study area is located along the coastline of Goa north of the capital city of Panjim (Fig. 1b). The host rocks of the mafic dykes are argillites, greywackes, and quartzites of the Sanvordem Formation belonging to the Proterozoic-age Goa Group (Fig. 2a–d) (Gokul 1985; Fernandez 2009; Gadgil et al. 2018; Dessai 2018). These rocks strike N-S to NNE-SSW with gentle eastward to westward dips, and thus form broad and open anticlines and synclines (Gokul 1985).

Widdowson et al. (2000) provided <sup>40</sup>Ar/<sup>39</sup>Ar ages of ~62 Ma on four Goa dykes, and based on geochemical and isotopic comparisons to the Deccan flood basalt lava sequence in the Western Ghats, considered the Goa dykes to be potential feeders of some of the youngest Deccan basalts (Wai Subgroup). This view contrasts with that of Gokul (1985), that the Goa region was a topographic high originally never covered by the Deccan flood basalts and the Goa dykes were not feeders to lava flows. Patil and Rao (2002) calculated a palaeomagnetic pole for the Goa dykes which was very close to the Deccan superpole.

Widdowson et al. (2000) claimed, quoting unpublished data, that not all Goa dykes were of Deccan age but some were of Proterozoic age. The features suggested by them to distinguish between Deccan and Proterozoic dykes, such as a greater degree of weathering and secondary amphibole in the latter are, however, ambiguous, especially as many of these dykes are found within the intertidal zone and may have also suffered

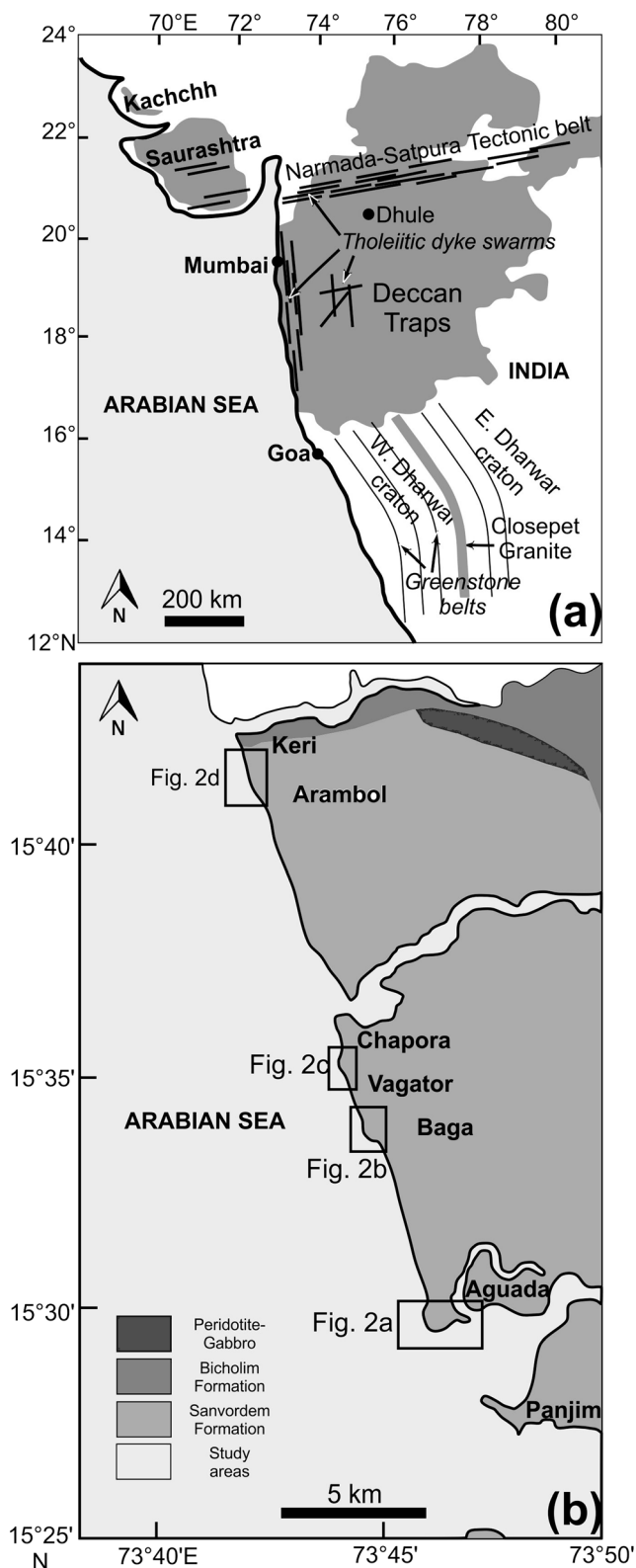


**Fig. 1** **a** Map of western India showing the present-day extent of Deccan Traps with some major features and localities mentioned in the text marked. The three major dyke swarms of the province (Satpura-Tapi, ENE-WSW; Coastal, NNW-SSE along the continental margin; and Nasik-Pune, inland) are shown. Modified from Vijayan et al. (2016). **b** Geological map of the part of northern Goa (north of the capital Panjim), showing the locations of the four individual study areas (rectangles). Modified from Dessai (2011)

Therefore, we treat all dykes in our study area as Deccan-age dykes, in the absence of evidence to the contrary.

## Field observations

The coastline of our study area is punctuated by rugged headlands characterised by cliffs and bays. The dykes are exposed along these headlands, and are easy to locate from their black colour, linear outcrop pattern, and frequently high relief relative to host rock, though parts of them are often concealed under beach deposits. Farther inland, they are even more difficult to identify due to a thick cover of laterite (ferricrete) (Widdowson and Gunnell 1999). The field observations presented in this study were made in four areas, namely the Aguada Headland (Fig. 2a), Baga Headland (Fig. 2b), Vagator-Chapora Headland (Fig. 2c) and Arambol-Keri Headland (Fig. 1b). We have found 60 mafic dykes that constitute the Goa dyke swarm, part of the Coastal Deccan dyke swarm, in this area. We measured their strike, dip, length, and thickness (Table 1), and carefully observed their geometric forms, contact relationships, and internal features such as vesicular zones and columnar jointing. Rose diagrams of dyke trends and host rock joint trends were prepared using GeoRose (Yong Technology Inc. 2014). Fresh, representative rock samples were collected for petrographic observations.

## Results

The dykes are typical dolerites and basalts, with medium to fine grain size; both aphyric and phyrlic varieties occur. Thin sections show microphenocrysts of plagioclase (sometimes zoned), clinopyroxene, and olivine, in a groundmass of the same minerals with Fe-Ti oxides (often skeletal). Some dykes contain platy aggregates of clinopyroxene while some others contain glomerocrysts of clinopyroxene in a groundmass dominated by plagioclase and clinopyroxene. Alteration minerals include chlorite, hornblende, and clays that have formed at the expense of clinopyroxene, plagioclase, and glass. Olivines, when present, are always partially or fully altered to wine-red iddingsite.

There are several cases of clear crosscutting relationships in the Goa dykes which provide the relative emplacement ages

deuteric alteration soon after emplacement. Also, to our knowledge, no radioisotopic age determinations on the Goa dykes yielding Proterozoic ages have been published.

(Fig. 3a). Individual dykes also show varied jointing patterns (Fig. 3b). Dyke margins against country rocks range from straight (Fig. 3a) to wavy (Fig. 3c). Almost all dykes are

vertical, with a very few steeply dipping ones. Several dykes form pairs sharing a common chilled margin. Examples are dykes AG19 and AG21, and AG43 and AG44, at Aguada

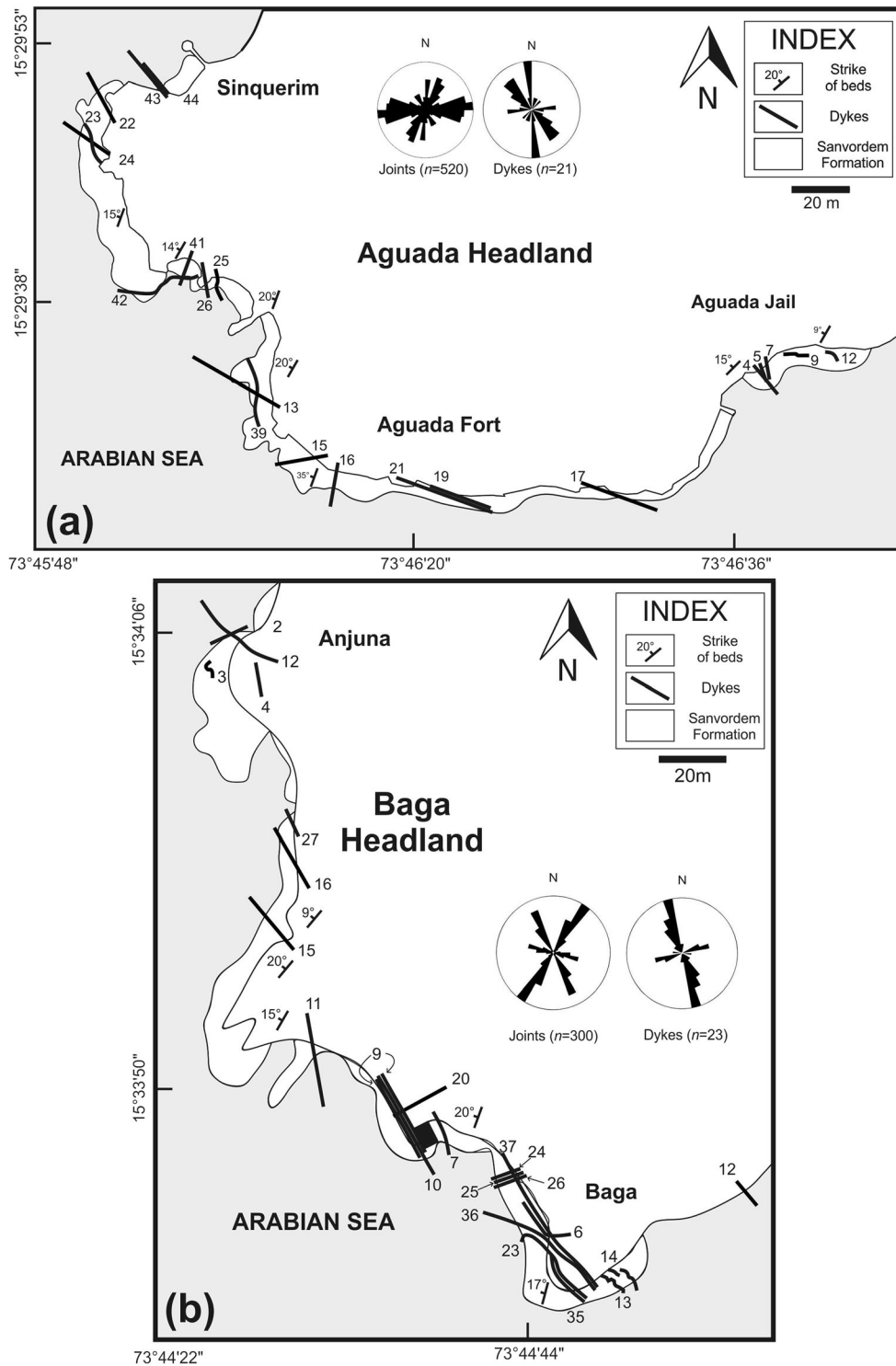


**Fig. 2** Dyke maps for the study areas. **a** Aguada Headland, **b** Baga Headland, **c** Vagator-Chapora Headland, **d** Arambol-Keri Headland. The dyke numbers are shown without the prefixes “AG,” “BG,” “VG,” and “AR” (abbreviations for Aguada, Baga, Vagator-Chapora, and Arambol-Keri, respectively) to avoid cluttering. These prefixes have been

used in Table 1. Rose diagrams for host rock joints and dykes are shown in each map; *n* is the number of measurements taken for the rose diagrams. The white patch delineated by a black line along the coastline shows a beach or rocky stretch

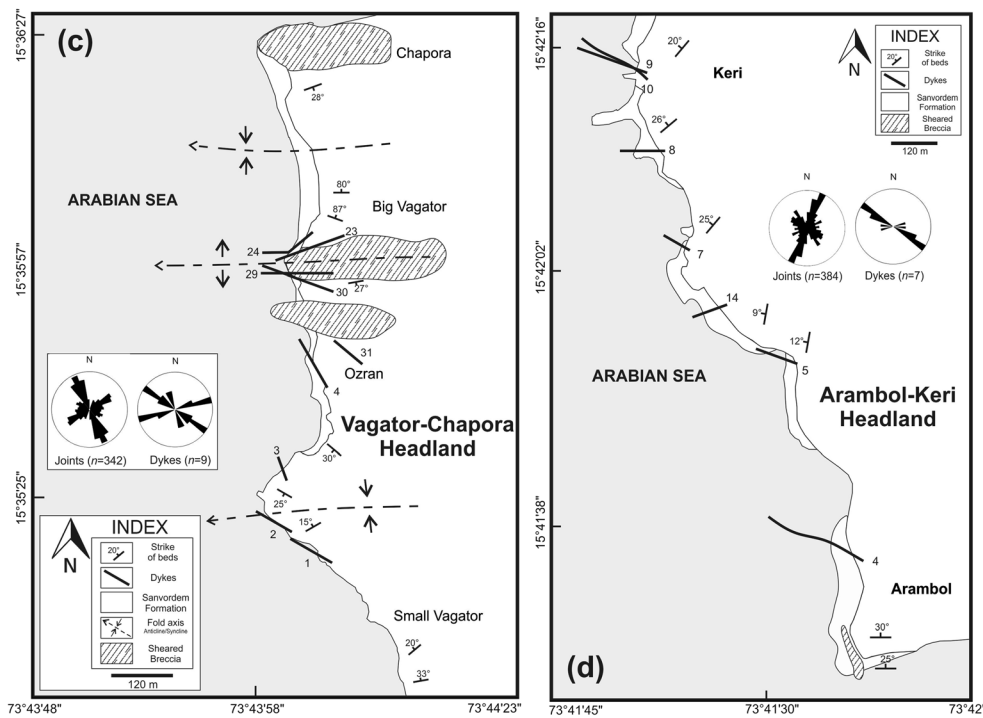


Fig. 2 (continued)

(Fig. 2a), and dykes BG09 and BG10 at Baga (Figs. 2b and 3b). A similar observation of dykes forming pairs has been made by Bondre et al. (2006) on the Sangamner dykes, part of the Nasik-Pune dyke swarm. Here, however, the two dykes of a pair tend to be separated by a screen of country rock a few meters wide.

Individual dykes can be a result of one or more magma injections. Those formed by a single magma injection typically show margin-perpendicular columnar jointing extending from one margin to the other, whereas those formed by multiple magma injections are identified by multiple rows of transverse columnar jointing (Gudmundsson 1995; Sheth and Cañón-Tapia 2015). At Baga, several instances of multiple-injection dykes are noted. Dykes BG6, BG30, BG36, and BG37 all trend ~NW-SE and have been mapped and named separately (Figs. 2b and 3d), and the first three of these show common chilled margins, central vesicular zones, and strike-perpendicular joints. Slightly north of the outcrop in Fig. 3d occur ENE-WSW-trending dykes BG24 (with four magma injections) and BG26 (with three magma injections) (Figs. 2b and 3e). The individual injections in BG24 and BG26 have a thickness between 8 and 26 cm. The multiple-injection dykes BG24 and BG26 have, between them, the relatively thick (30 cm), single-injection dyke BG25 (Figs. 2b and 3e), with a narrow screen of the country rock on either side. This situation is similar to that described in the Sangamner dykes (Bondre et al. 2006). Goa dykes BG09 and BG10 with the same trend, which appear to form a pair (Figs. 2b and 3b), may be considered a case of double

injection. Dyke BG10 branches into thin finger-like dykelets at its southern end and shows chilled margins throughout its length in contact with BG09. Again, dykes BG09-BG10 are separated from dyke BG07 by a 5-m wide screen of country rock (Fig. 2b; cf. Bondre et al. 2006).

### Structural attributes and internal features of the Goa dykes

It should be noted that in this paper, we treat all magma injections within a multiple-injection dyke as several dykes. The 60 dykes considered in this study include the single-injection dykes and all constituent parts of multiple-injection dykes. Thus, dykes BG09 and BG10, from a double-injection dyke (Fig. 3b), are counted as two dykes. This practice differs from that followed by, for example, Ray et al. (2007), who treated each multiple-injection dyke as a single dyke for the purpose of statistical treatment. Whereas they had 210 dykes of > 1-km length to perform statistics on, the practice followed here (of counting individual injections in multiple dykes as individual dykes) is partly governed and required by the relatively small number of Goa dykes that we have to work with.

### Strike and dip

The strike distribution for the 60 Goa dykes (Fig. 4a) shows that 42 dykes (70%) trend between N 100° and N 180° (~E-W to N-S). The mean and median strike directions are N 123° and N 130°, respectively, and the mode is N 160° (NNW-

**Table 1** Field data on the Goa dykes exposed in the four study areas

Sr. no.	Location	Dyke no.	Trend	Thickness (m)	Latitude (N)	Longitude (E)	Length (m)	Aspect ratio (length/thickness)
1	Aguada	AG4	140°	2.00	15 29 30.0	73 46 38.6	20.8	10.4
2	Aguada	AG5	160°	5.80	15 29 33.6	73 46 39.0	24.4	4.21
3	Aguada	AG7	170°	0.50	15 29 34.1	73 46 40.1	14.0	28.0
4	Aguada	AG9	90°/85° → 180°	0.50	15 29 34.5	73 46 41.7	45.8	91.6
5	Aguada	AG12	140°/75° → 230°	3.50	15 29 34.3	73 46 45.7	23.3	6.66
6	Aguada	AG13	120°	17.8	15 29 32.9	73 46 03.8	106	5.96
7	Aguada	AG15	80°	10.1	15 29 27.0	73 46 07.0	100	9.90
8	Aguada	AG16	10°	3.00	15 29 27.7	73 46 07.6	72.0	24.0
9	Aguada	AG17	110°	12.4	15 29 25.6	73 46 26.2	98.3	7.93
10	Aguada	AG19	130°	11.4	15 29 25.2	73 46 19.5	92.0	8.07
11	Aguada	AG21	130°	5.00	15 29 25.2	73 46 19.5	103	20.6
12	Aguada	AG22	170°	16.0	15 29 50.2	73 45 53.8	82.0	5.13
13	Aguada	AG23	170°/60° → 80°	2.60	15 29 47.1	73 45 53.2	61.3	23.6
14	Aguada	AG24	125°	5.00	15 29 47.3	73 45 53.4	58.0	11.6
15	Aguada	AG25	170°	1.50	15 29 39.5	73 46 01.3	20.3	13.6
16	Aguada	AG26	170°	2.20	15 29 39.5	73 46 00.0	29.7	13.5
17	Aguada	AG39	35° and 165°	3.50	15 29 33.8	73 46 03.8	72.0	20.6
18	Aguada	AG41	40°	18.0	15 29 40.4	73 45 59.9	34.4	1.91
19	Aguada	AG42	80°/74° → 350°	0.70	15 29 45.8	73 45 53.1	68.7	98.1
20	Aguada	AG43	240°/75° → 230°	3.50	15 29 52.5	73 45 55.1	53.0	15.1
21	Aguada	AG44	130°/75° → 230°	7.10	15 29 51.9	73 45 56.5	57.0	8.03
22	Baga	BG2	65°	1.20	15 34 6.60	73 44 29.8	58.0	48.3
23	Baga	BG3	~N-S	0.03	15 34 5.20	73 44 28.7	23.0	767
24	Baga	BG4	160°	12.0	15 34 2.70	73 44 31.4	36.1	3.01
25	Baga	BG6	170°	3.80	15 33 40.0	73 44 44.0	37.2	9.79
26	Baga	BG7	155°	3.50	15 33 48.0	73 44 37.8	36.8	10.5
27	Baga	BG9	150°	19.0	15 33 46.9	73 44 36.5	96.0	5.05
28	Baga	BG10	150°	15.5	15 33 47.2	73 44 36.8	96.0	6.19
29	Baga	BG11	160°	3.00	15 33 51.3	73 44 31.5	32.0	10.7
30	Baga	BG12	140°	1.30	15 33 44.4	73 44 51.4	21.7	16.7
31	Baga	BG13	90°	0.50	15 33 41.0	73 44 45.0	32.0	64.0
32	Baga	BG14	140°	1.50	15 33 40.9	73 44 45.5	37.6	25.1
33	Baga	BG15	140°	13.0	15 33 55.5	73 44 30.6	40.6	3.12
34	Baga	BG16	120°	20.3	15 33 57.2	73 44 31.2	35.0	1.72
35	Baga	BG20	60°	0.20	15 33 48.0	73 44 39.0	17.7	88.5
36	Baga	BG22	130°	5.10	15 34 07.4	73 44 29.0	187	36.7
37	Baga	BG23	160°	0.80	15 33 41.9	73 44 42.6	98.0	122
38	Baga	BG24	70°	0.62	15 33 44.0	73 44 41.6	38.0	61.2
39	Baga	BG25	70°	0.30	16 33 44.0	74 44 41.6	40.0	133
40	Baga	BG26	70°	0.49	17 33 44.0	75 44 41.6	35.0	71.4
41	Baga	BG27	155°	0.25	15 33 56.5	73 44 31.7	15.0	60.0
42	Baga	BG35	165°	19.5	15 33 40.0	73 44 43.0	105	5.38
43	Baga	BG36	160°	3.50	15 33 40.1	73 44 44.7	190	54.3
44	Baga	BG37	160°	2.50	15 33 41.0	73 44 44.0	222	88.8
45	Vagator	VG1	120°	8.00	15 35 19.9	73 44 00.0	57.0	7.13
46	Vagator	VG2	120°	1.90	15 35 22.8	73 43 56.4	59.0	31.1
47	Vagator	VG3	160°	7.00	15 35 30.4	73 43 58.5	56.3	8.04
48	Vagator	VG4	150°	5.10	15 35 45.2	73 44 1.70	64.4	12.6
49	Vagator	VG30	70°/75° → 340°	0.40	15 35 53.3	73 44 00.0	72.0	180
50	Vagator	VG31	130°	1.60	15 35 47.9	73 44 1.80	52.0	32.5
51	Vagator	VG23	70°	0.60	15 35 59.0	73 43 59.6	32.2	53.7
52	Vagator	VG24	60°	7.90	15 35 59.9	73 43 59.0	100	12.7
53	Vagator	VG29	110°	0.30	15 35 53.8	73 43 59.9	71.6	239
54	Arambol	AR4	120°/50° → 30°	13.0	15 41 38.1	73 41 53.5	153	11.8
55	Arambol	AR5	110°	5.40	15 41 59.0	73 41 45.8	66.2	12.3
56	Arambol	AR7	70°	7.00	15 42 00.0	73 41 43.6	62.0	8.86
57	Arambol	AR8	120°	3.00	15 42 14.3	73 41 38.1	50.0	16.7
58	Arambol	AR9	110°	3.40	15 42 16.5	73 41 38.3	58.7	17.3
59	Arambol	AR10	120°	7.20	15 42 15.8	73 41 37.6	60.0	8.33
60	Arambol	AR14	90°	4.00	15 42 11.3	73 41 38.9	42.0	10.5

The geographic coordinates are in degrees, minutes and seconds (dms). The trend should be read as strike°/amount of true dip°→dip direction°

SSE). Fifty-two of the 60 dykes (87%) are subvertical, and eight (13%) dip at various angles between 50° and 85°; the average value is 71° (Fig. 4b). Six of these eight inclined dykes dip due NNW-NNE, one dips due east and one due south.

### Length and thickness

The Goa dykes are generally short in length. The longest exposed dyke is 222 m long whereas the rest are < 100 m long (Fig. 4c). The exposed lengths of these dykes are significantly smaller than typical lengths of Icelandic dykes (Paquet et al. 2007; Gudmundsson 1984) or Deccan dykes such as the Nandurbar-Dhule dykes where lengths of many tens of kilometers are common (Ray et al. 2007). The dykes range in thickness from 3 cm to as much as 20 m and have an average thickness of ~6 m (Fig. 4d). Thirteen of the 60 dykes (22%) are > 10 m thick. Given the short lengths of the Goa dykes, their aspect ratios (length/thickness) are very small, compared to those of the Nandurbar-Dhule dykes for example (where aspect ratios reach as high as 11,630; Ray et al. 2007). For the Goa dykes, the low aspect ratios may be in part due to incomplete along-strike exposure, implying that all reported lengths are minimum lengths.

### Horns

Horns are defined as short branches of dykes located at dyke tips and also along the edges of dykes of any thickness (Hoek 1991; Martinez-Poza et al. 2014). Goa dykes thicker than 2 m have straight planar contacts and do not necessarily follow joint planes in the host rocks. The occurrence of a horn was noted in two dykes, AG22 at Aguada and BG6 at Baga. Dyke AG22 has dilated the locally dominant NW-SE joint set with its horn following a WNW-ESE joint (Fig. 5). The horn of the dyke BG6 intrudes into dyke BG35 along a prominent joint. Horns are formed either due to stress perturbations at the dyke tip or by magma moving along pre-existing fractures along dyke margins (Martinez-Poza et al. 2014). The horns observed in the Goa dykes appear to have originated by the latter process.

### Dykes along pre-existing anisotropies

Thin dykes (< 20 cm) are strongly controlled by the anisotropies within either the host rock greywacke (Fig. 6a) or another dyke (Fig. 6b). A similar situation is seen in the Chimei complex of eastern Taiwan, where thin diabase dykes abruptly change direction, apparently controlled by fractures in the altered andesite host (Fig. 6c). In Fig. 6a, it appears that two orthogonal joint sets (NW-SE and NE-SW) were perhaps utilised by the magma to cause dilation. A slightly thicker dyke (AG42, 50 cm) at Aguada is also seen to occupy a pre-

existing joint set that trends ~N90°. Occasionally, offshoots from thicker dykes occupy joints in the country rocks.

### Rock bridges

A rock bridge is a block of host rock bounded by two en echelon segments of a single dyke located at an offset of the dyke-fracture system (Hoek 1991). In subhorizontal outcrops where rock bridges are observed, both dyke segments become thinner (Babiker and Gudmundsson 2004). Though the segments seem disconnected at the present exposure level, they must be connected at a deeper level for the magma to be transported. There have been many studies of the occurrence and origin of rock bridges (Currie and Ferguson 1970; Pollard 1973; Pollard et al. 1982; Hoek 1991; Daniels et al. 2012). Sometimes, rotation and deformation of rock bridges occurs during an ongoing dilation event along en echelon dyke segments having either straight or curved propagation paths (Nicholson and Pollard 1985). Rock bridges indicate coeval tectonics and magmatism (Martinez-Poza et al. 2014).

Two instances of such rock bridges are observed at Baga. Two overlapping segments of dyke BG14 (Fig. 7a) are separated by a greywacke bridge that is highly fractured and magma has entered the fractures. In this outcrop, the far part of the left segment of the dyke (Fig. 7a) follows a NW-SE (N 140°) joint set that is not followed by the right segment of the same dyke. We have not come across any literature on the Deccan that shows such rock bridges in dykes of comparable width. In the other instance at Baga, an offshoot of dyke BG16 runs parallel to the main dyke and has two overlapping segments with a right-stepping geometry (Fig. 7b, note also the connection between the two segments).

### Contact relations and vesicles

Some of the dykes show evidence of chilling against the country rock (Fig. 8a). Glassy selvages at such dyke margins are generally < 1 cm thick but can be up to 9 cm thick. A majority of the dykes, however, do not show a glassy selvage but simply a finer grain size than the interior parts. The margins of these dykes have closely spaced transverse joints. In many instances, the country rock at the margins has been hardened by magmatic heat (though without mineralogical changes), developing very closely spaced jointing resulting in sharp-edged blocks. Sometimes magma has filled joints in the country rock forming a criss-cross network (Fig. 8b).

Vesicles are reported in feeder dykes, where they can be elliptical or even teardrop-shaped suggesting a subvertical movement of gas bubbles, and from their orientation, the magma flow direction can be inferred (Varga et al. 1998; Nogueira et al. 2009; Galindo and Gudmundsson 2012). Vesicles are common in the Goa dykes and tend to be concentrated along the central portions of the dykes (Figs. 8c and 9). Most

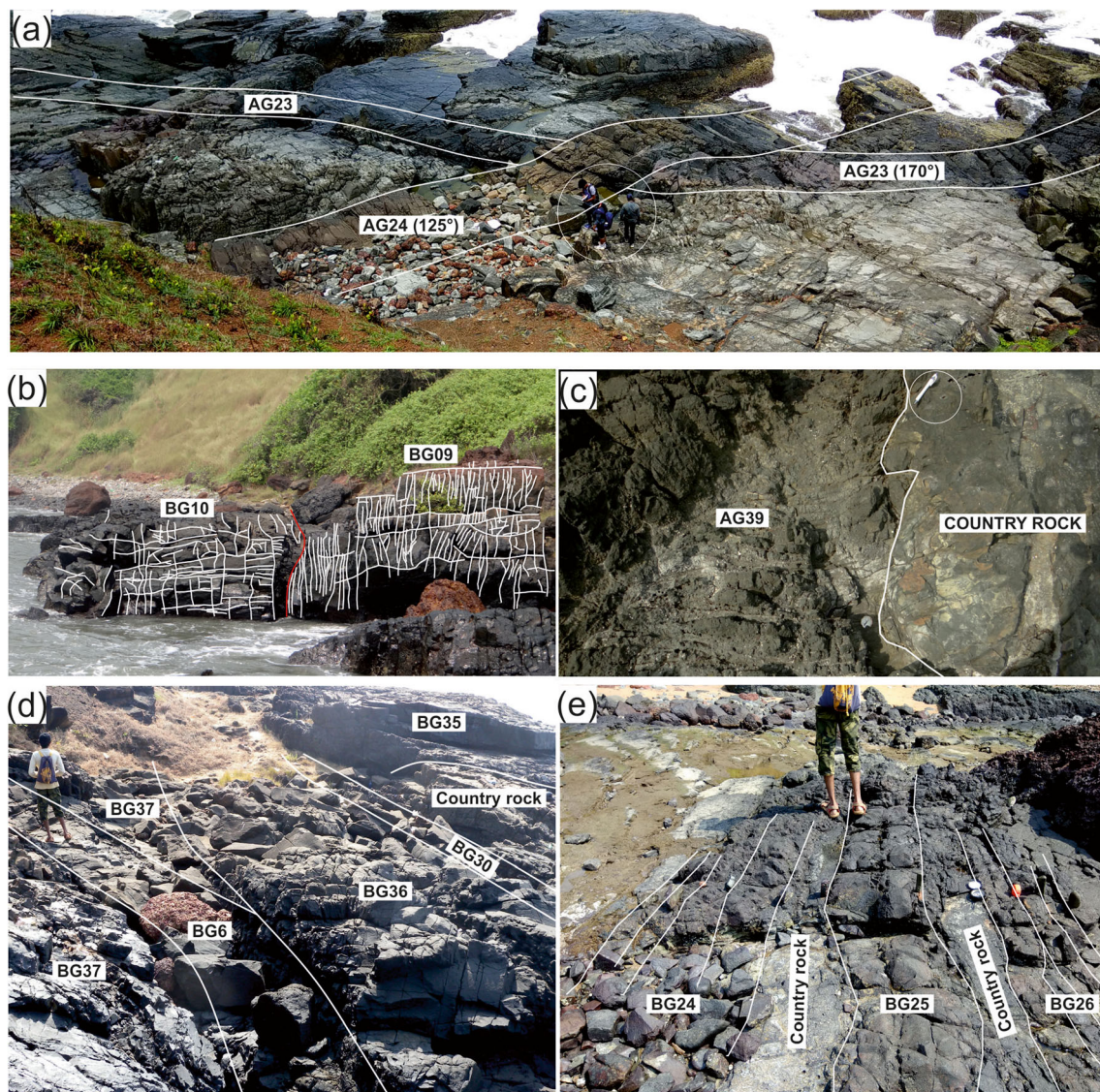


**Fig. 3** **a** Field photograph of dyke AG24 cutting dyke AG23 dyke at Aguada. A group of people (circled) standing at the dyke intersection provide a scale. **b** Baga dykes BG09 and BG10 showing variable joint pattern. BG10 shows more widely spaced joints whereas BG09 shows very closely spaced joints. BG10 is 15.5 m thick. **c** Angular contact between dyke AG39 and country rock at Aguada. In this case, contacts

follow joints in the host rock. White pen (encircled) is 9 cm long. **d** A multiple-injection dyke at Baga, with each injection named separately (BG30, BG36, BG37, and BG6). There is a country rock screen between BG35 and BG30. Person for scale is 1.7 m tall. **e** Multiple-injection dykes BG24 and BG26 at Baga, separated from dyke BG25 in the middle by screens of country rock. Person is 1.7 m tall

vesicles are circular and a few millimeters in diameter (centimeters when enlarged by weathering, Fig. 8c), and distributed in bands parallel to dyke margins. In all dykes, vesicles form a 2–40-cm wide band at the centre, which in some cases weathering has changed into a deep furrow (Fig. 9). Frequently, such outcrops give a false impression of multiple intrusions.

### Columnar jointing

Several dykes display well-developed transverse joints that are independent of the country rock joint systems. Well-formed columnar joints were observed only in a single

dyke, dyke AR4 at Arambol (Fig. 10). The joint columns are four- to six-sided polygons that run throughout the dyke thickness. Other, less well-developed jointing patterns in the Goa dykes include curving columns of irregular width that are found throughout the dykes. The columnar joints form under tensional stress that produces cracks caused by shrinkage of magma due to cooling, with the joint columns propagating inwards from either margin, perpendicular to the isotherms which are parallel to the margins (DeGraff and Aydin 1987; Grossenbacher and McDuffie 1995). The generally poorly developed and irregular columnar jointing in the Goa dykes may be due to the dyke magma encountering groundwater, which would

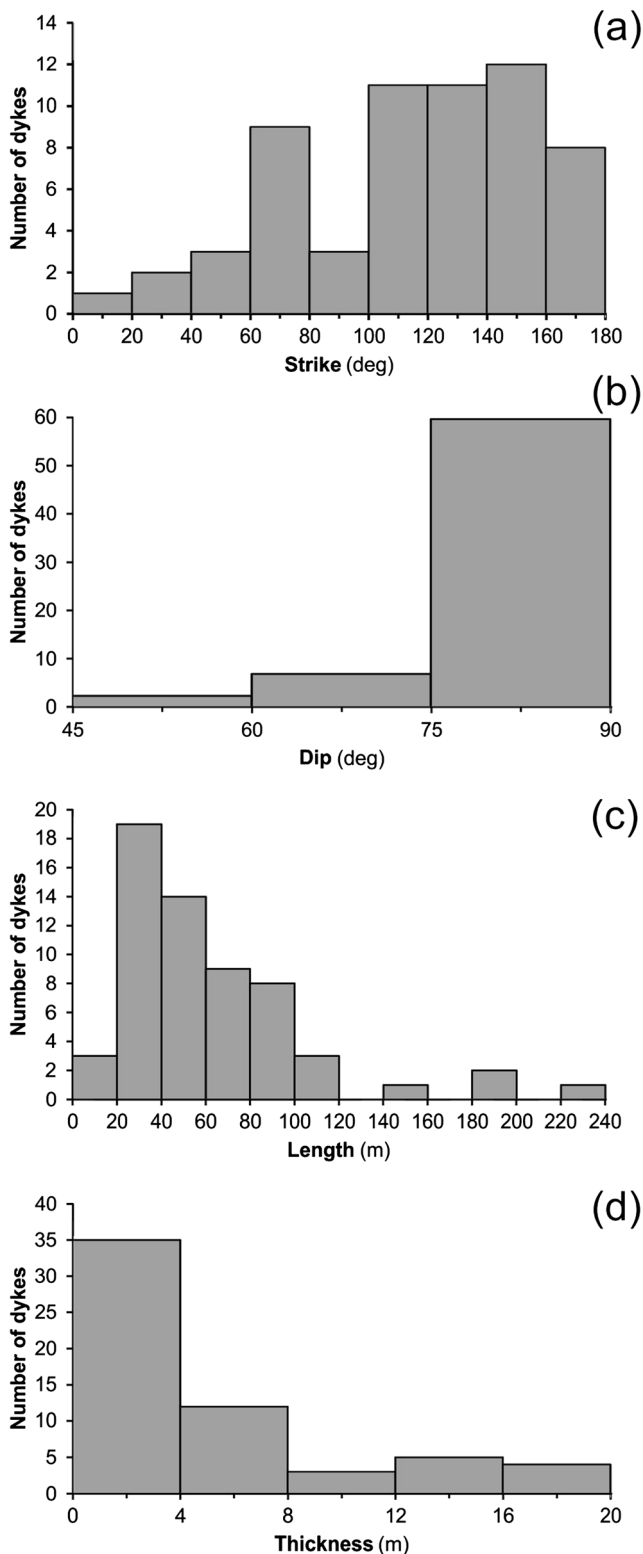


**Fig. 4** Plots of the number of dykes versus **a** dyke strike, **b** dyke dip, **c** dyke length, and **d** dyke thickness

distort the regular isotherms within the cooling dyke, much as occurs in lava flows (e.g., Lyle 2000; Long and Wood 1986; Sheth et al. 2015; Sheth 2018).

## Tectonic aspects of the Goa dykes

### Crustal dilation

Dykes are magma-driven extension fractures (mode I cracks, akin to hydraulic fractures) that form in a direction perpendicular to the minimum principal compressive stress, and dyke swarms produce significant crustal extension during emplacement (e.g., Gudmundsson 1995; Marinoni 2001; Ray et al. 2007). In regional-scale mafic dyke swarms such as those in Iceland or the Deccan Traps, most dykes are steep-dipping and subparallel since the regional stress field controls the major attitudes of dykes (e.g., Gudmundsson 1983; Ernst et al. 1995; Ray et al. 2007). However, there can be local deviations in the overall stress field, arising from factors such as shallow-level magma chambers or rock layers with anomalously high or low mechanical strength (Gudmundsson 1995, 2011). Methods for computing the crustal dilation associated with dyke swarm emplacement have been presented by Marinoni (2001). Given the nature of the terrain in our study area (rocky headlands and bays along the coastline, as well as beach deposits), there is no single straight traverse that would cut across all the exposed dykes. Two sizeable coastal stretches with either beach deposits or an intervening estuary (~7 km between Aguada and Baga headlands, and ~10 km between Vagator and Arambol headlands) provide no rock exposures and were therefore not included in the calculations. We also avoided selecting traverses where the dykes would be parallel to the traverse (e.g., Baga). With these inherent limitations, we took four *local* traverses, suitably oriented to cut across a maximum number of dykes. The thickness of the dykes was measured perpendicular to the dyke strike. The cumulative thickness of the dykes (T) and the traverse length (L) were determined, and the dilation was calculated using the equation (Marinoni 2001):

$$\%dilation = \frac{\text{(aggregate dyke thickness)}}{\text{(length of traverse - aggregate dyke thickness)}} \quad (1)$$

The traverses taken were from dyke AG15 to AG17 in the Jail profile at Aguada (Fig. 2a), dyke AG42 to AG43 in the Sinquerim profile at Aguada (Fig. 2a), dyke VG3 to VG24 in the Vagator profile (Fig. 2c), and dyke AR5 to AR10 in the Arambol profile (Fig. 2d). The Arambol traverse was not extended to dyke AR4 as there is a 600-m-long beach with no outcrops which separates this dyke from the others. The dilation values calculated are as follows: 9% for Jail profile, 17% for Sinquerim profile, 2% for Vagator profile, and 3% for Arambol profile (Table 2).

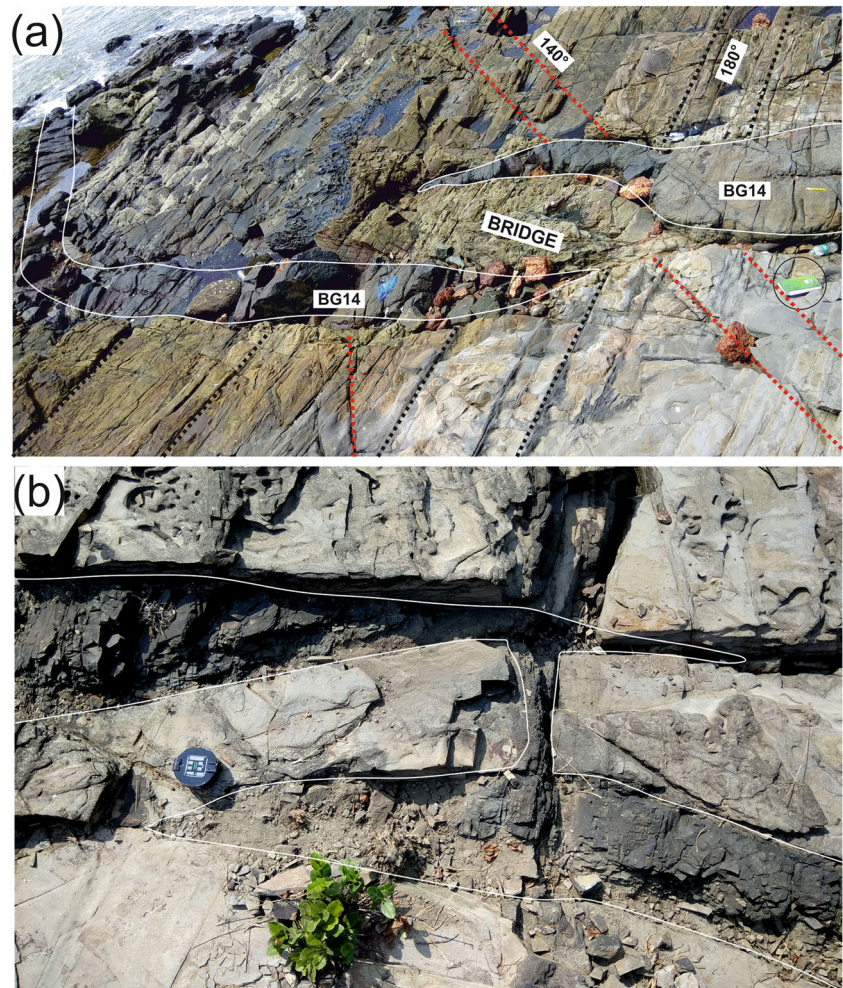
**Fig. 5** Dyke AG22 at Aguada, with its “horn” following country rock joints. Prominent joints can be seen in the upper half of the photo. The photo was taken in an oblique way standing on the Aguada Fort wall. Person (encircled) is 1.6 m tall



**Fig. 6 a** Control of pre-existing country rock joints on the emplacement of dyke BG3 at Baga. Pen (encircled) is 15 cm long. **b** Vertical section showing dyke BG20 at Baga occupying pre-existing weak planes within the dyke BG09. BG20 also shows a concentration of vesicles along its middle. **c** Vertical section showing a deflected diabase dyke cutting altered andesite, Chimei complex, eastern Taiwan. Note well-developed fractures in the andesite near and exactly parallel to the vertical and inclined segments of the dyke, suggesting that the dyke occupies a pre-existing fracture network. Photograph courtesy Hetu Sheth. Geologist is A. Alam.



**Fig. 7** View of the dyke BG14 in a flat outcrop on the wave-cut platform at Baga, taken in an oblique and inclined manner from a cliff so as to show all features of interest in the same photo. Note the overlapping dyke tips around a host rock “bridge.” The far end of the left segment of the dyke occupies a joint that trends  $140^\circ$ . Field notebook (encircled, with long dimension of 25 cm) near the right edge of the photo provides a scale and is horizontal. **b** Plan view of the offshoot of the dyke BG16. It shows two overlapping segments with right-stepping geometry and a mutual connection. Brunton compass provides a scale.



### Host rock joints

The gently-dipping metagreywackes along the Goa coast are criss-crossed by several fracture or joint sets which are dense in a few areas. We measured > 1500 host rock joints in our study area allowing good statistical treatment of the joint trends. The subvertical joint pattern consists of two systematic orthogonal sets, namely  $\sim$ NW-SE and  $\sim$ NE-SW, with subordinate joint sets being WNW-ESE, E-W, N-S, and ENE-WSW (Fig. 11a). These variably oriented, mutually crosscutting joints render a blocky appearance to the host rock, and the erosion of these rock blocks leaves rounded knobs. The joints, particularly those that trend  $N 0\text{--}30^\circ$  ( $\sim$ N-S) to  $N 255\text{--}290^\circ$  ( $\sim$ E-W), are occasionally filled with quartz and calcite, and rarely kyanite. These veins are offset by  $\sim$ NW-SE-striking joints that do not show any infillings (Fig. 11b). The  $\sim$ N-S trending joints frequently show an *en echelon* pattern (Fig. 11c). Several occurrences of gash veins, some of which are sigmoidal, also trend NNW-SSE (Fig. 11d). Rose diagrams of joints in the four individual study areas are shown in the maps

of Fig. 2a–d. These trends are individually dominant in certain parts of the study area.

### Magmatic overpressures and source depths

Aspect ratios of dykes combined with reasonable values of mechanical properties of their host rocks can be used to calculate magmatic overpressures and thereby the source depths to the magma chamber (Gudmundsson 1983; Babiker and Gudmundsson 2004; Ray et al. 2007). These calculations assume that (i) the exposed thickness of dyke equals the elastic opening at the time of emplacement, and (ii) the dykes, which are probable feeders to a now-eroded lava pile (Widdowson et al. 2000; Vanderkluyzen et al. 2011) represent through-the-thickness cracks between two free surfaces, these being the top of the source magma chamber and the Earth's surface. The strike dimension (trace length),  $L$ , for such dykes is less than its dip dimension (vertical dimension or the height of the dyke), which is treated as being effectively infinite (Gudmundsson and Loetveit 2005). The Goa dykes are theoretically suitable

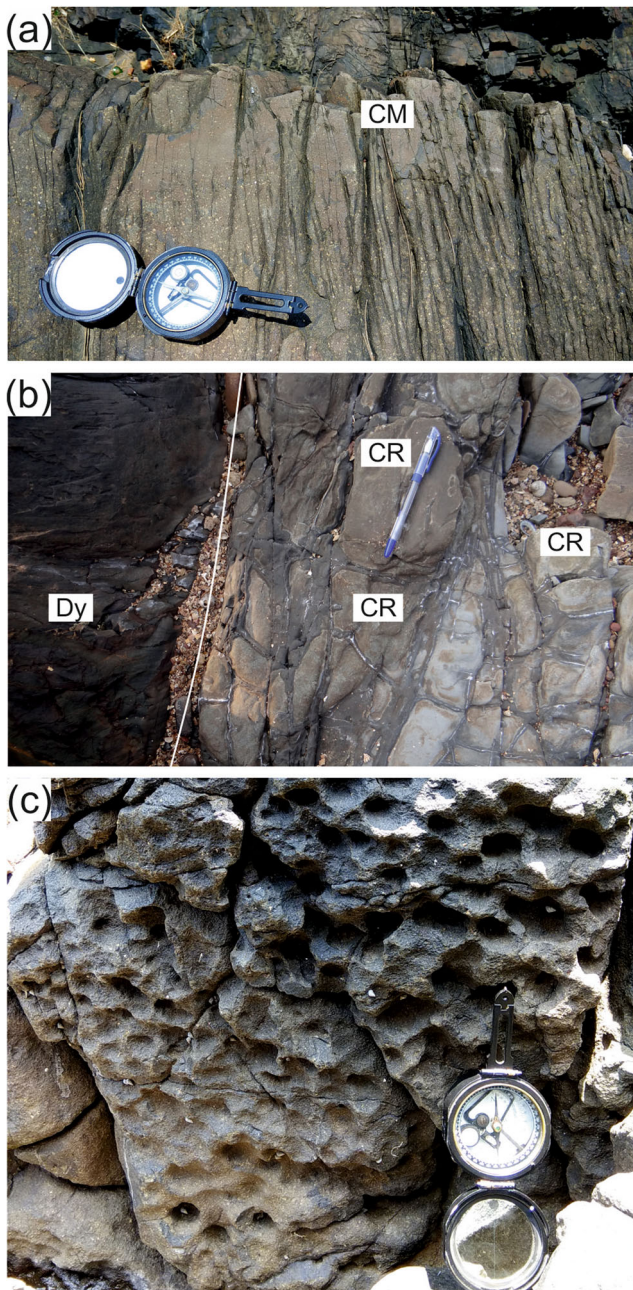


**Fig. 8** **a** Chilled margin (CM) of dyke BG36 at Baga, showing very fine grain size. Brunton compass provides a scale. **b** The contact of dyke VG3 with country rock at Vagator. Roughly orthogonal fractures have been filled with dyke magma, and the host rock is hardened by magmatic heat. Dy dyke, CR country rock. **c** A close-up of the central cross-section along the length of dyke BG23 shows the spherical shape of vesicles

for such calculations as they have a strike dimension (trace length) which is much shorter than the expected dip dimension (a few kilometers depth to the magma chamber), implying that they should have formed by vertical injection from such a chamber and not by lateral injection.

The magmatic overpressure  $P_o$  can be calculated using (Sneddon and Lowengrub 1969; Babiker and Gudmundsson 2004)

$$P_o = (b_{\max}E)/2L(1-\nu^2) \quad (2)$$

where  $b_{\max}$  is the maximum dyke thickness, and  $E$  and  $\nu$  are Young's modulus and Poisson's ratio of the host rock, respectively.  $P_o$  is also called as net pressure or the driving pressure and is the pressure available at any point to drive open the walls of the dyke fracture.

The host rocks of the Goa dykes are Proterozoic-age greywackes, overlying granitic basement. This situation is different from that in the Nandurbar-Dhule area of the Deccan Traps where the dykes are exposed within Deccan basalt lava flows (Ray et al. 2007). However, it is very similar to that in Sudan where Early Cretaceous and Late Proterozoic mafic dykes have been emplaced in much older granite (Babiker and Gudmundsson 2004). Therefore, in situ  $E$  values of 20–30 GPa are appropriate for the basement granitoids in our study area. Using these values and a corresponding Poisson's ratio of 0.25 for granitic rocks (Hansen et al. 1998; Babiker and Gudmundsson 2004) in Eq. (2), we calculated the magmatic overpressures of the Goa dykes. As noted, only one dyke (BG3) has a relatively high aspect ratio of 767; this situation can be contrasted with the Nandurbar-Dhule dykes (Ray et al. 2007) whose aspect ratios frequently are into several thousands. Dyke BG3 gives a magmatic overpressure  $P_o$  from ~12 MPa (for  $E = 20$  GPa) to ~18 MPa (for  $E = 30$  GPa). Using these values of  $P_o$ , the depth to the source magma chamber can be calculated using the equation of Gudmundsson (1983):

$$z = P_o/(\rho_r - \rho_m)g \quad (3)$$

where  $\rho_r$  is the average crustal density (assumed to be 2800 kg/m<sup>3</sup>),  $\rho_m$  is magma density (2700 kg/m<sup>3</sup>, Pinel and Jaupart 2004), and  $g$  is the acceleration due to gravity. The calculated magma chamber depth for the dyke BG3 is ~12 km. We consider this a reasonable value, noting from petrographic observation that the dyke is relatively evolved in composition and has undergone considerable olivine fractionation, most likely at shallow depth.

For all other dykes, the above two equations yield unrealistic (impossible) values of magmatic overpressures and depths to the magma chamber. For example, for dyke BG25 (aspect ratio of 133), the calculated magmatic overpressure is 70 MPa (for  $E = 20$  GPa) and 105 MPa (for  $E = 30$  GPa), with corresponding source depths of 70 km and 110 km. These excessive values for most Goa dykes (except BG3) are due to their very low aspect ratios. We attempted to laterally connect a few of the colinear dykes in our area into longer dykes, but their aspect ratios remain small enough to yield impossibly high magmatic overpressures and source magma chamber depths. This could also imply that the exposed thickness of the dykes may not simply reflect the elastic opening, but a component of the thickness may be because of the thermal

**Fig. 9** Dyke AG24 at Aguada showing a striking concentration of vesicles in a 1.6-m-wide zone along its central part. The vesicular zone has been eroded more than the vesicle-free zones on either side. Hammer is 0.36 m long



erosion of the wall rocks by the flowing dyke magma (see also Ray et al. 2007).

## Discussion

### Thermal erosion

Dykes propagate by intruding along pre-existing fractures or by creating their own fractures by hydraulic fracturing (e.g., Gudmundsson 1984, 1995, 2011). Once a dyke has formed, however, with a particular thickness (opening), long-lived magma flow in the dyke may widen it by thermally eroding the wall rocks, so that its final thickness as measured is greater than the elastic opening during fracture formation (Fialko and Rubin 1999). Thus, thermal erosion of wall rocks by magma

flowing in a dyke is a non-dilational process of dyke widening (Fialko and Rubin 1999) and leads to an overestimate of the dilation. Fialko and Rubin (1999) found that the thermal erosion is most common in dykes > 7 m in thickness and involving turbulent magma flow. Some 20% of the dykes in our study area are > 10 m in thickness, but there is no conclusive field evidence that thermal erosion of their Proterozoic host rocks occurred. We note however that chilled margins of dykes are not evidence for lack of thermal erosion (Fialko and Rubin 1999), and we cannot rule it out for some of the Goa dykes.

### Dyke trends and palaeostresses

Undeformed dykes are very useful palaeostress indicators (e.g., Marinoni and Gudmundsson 2000; Babiker and

**Fig. 10** Cross-section of joint columns, four to six-sided, in the Arambol dyke AR4. The view is perpendicular to the dyke walls. Hammer is 0.36 m long



**Table 2** Details of the dilation profiles, traverse lengths, dykes encountered, and calculated dilation

Particulars	Aguada		Vagator	Arambol
	Jail	Sinquerim		
Total traverse length (m)	536	245	1096	671
Total width of dykes (m)	41.9	34.9	22.0	19.6
Dyke numbers	AG15, AG16, AG17, AG19, AG21	AG22, AG23, AG24, AG42, AG43, AG44	VG3, VG4, VG31, VG30, VG24	AR5, AR14, AR8, AR10
Effective traverse length (m)	494.1	210.1	1074	651.4
Dilation (%)	9	17	2	3

Gudmundsson 2004; Ray et al. 2007). Wagle and Rajamanickam (1980) reported 43 dykes in the present study area, though without any information on the dyke features. Several of the dykes with similar petrographic characteristics were suggested as belonging to two magmatic episodes (Iyer et al. 1990), as it was deduced that the trends of dykes correlated well with the regional Precambrian Dharwar trend (NNW-SSE) (Dessai 2018) and with the second folding ( $F_2$ ) episode of the Goa Group of rocks (Iyer et al. 1990). Whether these dykes have passively occupied pre-existing joints in the host rock or whether they reflect the contemporaneous stress fields is a question that has not been discussed. We note that

dykes of highly irregular shapes and only a few centimeters thick have been argued to follow fracture sets in their host rocks rather than the regional stress field (Baer et al. 1994).

When the trends of the Goa dykes are examined, a significant spatial pattern is noted in the dyke orientations. Though the majority of the dykes trend  $\sim$ NW-SE and  $\sim$ NNW-SSE in all the study areas,  $\sim$ N-S trending dykes are only noted at Aguada (Fig. 2a), whereas  $\sim$ WSW-ENE-trending dykes are noted at Baga (Fig. 2b) and Vagator (Fig. 2c), and a small number of  $\sim$ E-W trending dykes at Aguada (Fig. 2a). The spread in the dyke strike (Fig. 4a) may reflect fluctuations in the direction of  $\sigma_3$  over time, though of a much larger

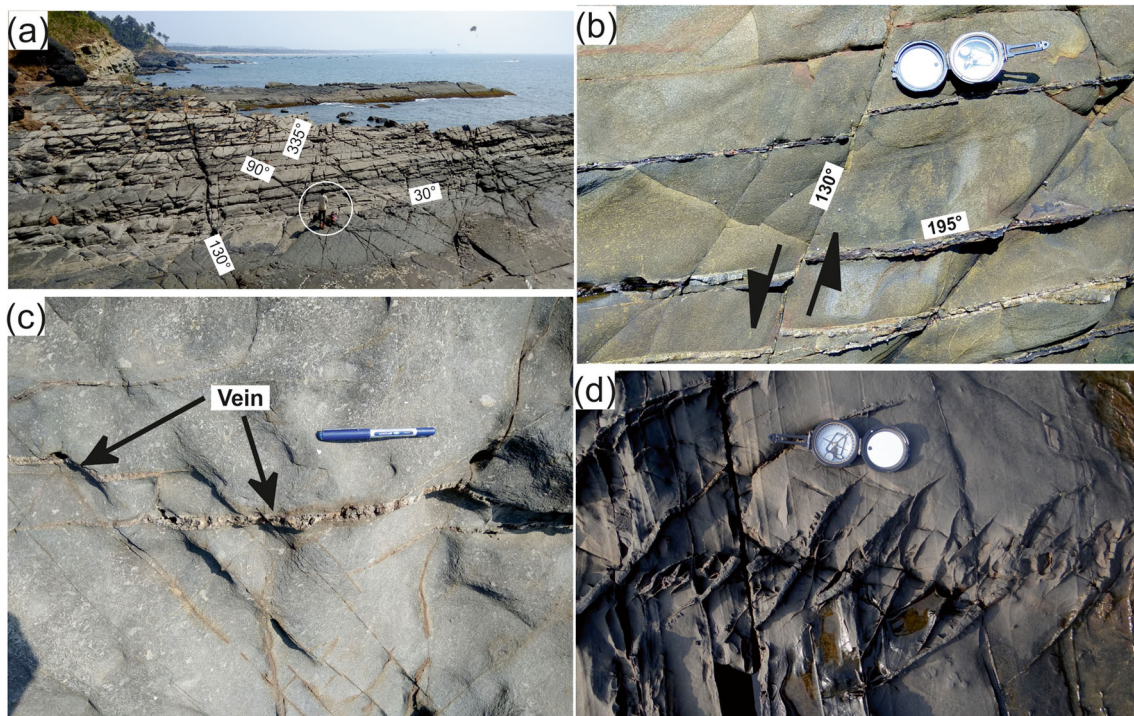


**Fig. 11** **a** Oblique aerial view of a part of Baga Headland, showing criss-cross joints on a subhorizontal outcrop. Numbers indicate the orientation of the major joint sets (whole circle reading). Person (encircled) just below the photograph centre is 1.7 m tall. **b** Country rock joints in plan view at Baga. Quartz-mineralised older joints ( $195^\circ$ ) and non-mineralised later joints ( $130^\circ$ ) are observed. There are also a few younger,  $\sim$ N-S joints

that are left unmineralised (upper part of photo). Brunton compass for scale. **c** En echelon segments of a quartz vein trending  $N 30^\circ$  on one of the subhorizontal wave-cut platforms at Baga. Pen is 15 cm long. **d** Plan view of sigmoidal tensional gash veins, filled by quartz, trending NNW-SSE. Brunton compass for scale

magnitude than observed in the large Nandurbar-Dhule swarm (Ray et al. 2007), for example. In our study area, though there are dominant dyke trends in individual areas, small numbers of dykes striking in other directions than the dominant one are also noted. Do these dyke strike variations reflect a periodically changing  $\sigma_3$  direction, control by host rock joints, or both?

In the Aguada area (Fig. 2a), very few dykes strike E-W, which is the dominant joint trend. On the other hand, there are a large number of dykes that strike ~N-S and ~NW-SE, which are the least dominant joint trends. This is strong evidence that the dyke trends are unrelated to and unaffected by the pre-existing fracture fabric but must reflect the tectonic stress field at the time of their emplacement, which had an ~E-W  $\sigma_3$  direction.

At Baga (Fig. 2b), the situation is different. There are both NNW-SSE-trending dykes and host rock joints in a large number, providing an argument for dyke trend control by fracture fabric. However, even here, the most dominant joint set is ~NE-SW, and not a single dyke follows this trend. On the other hand, the other dyke trend observed at Baga (~WSW-ENE) has no matching joints. These observations again indicate the ultimate control of contemporaneous stress field on dyke trends.

At Vagator-Chapora (Fig. 2c), ~WSW-ENE-trending dykes correspond to joints in roughly the same direction, but the NW-SE-trending dykes are oblique, by a few tens of degrees, to NNW-SSE-trending joints. At Arambol-Keri (Fig. 2d), a complete mismatch of the dyke and joint trends is seen; the dominant joint trend of NNE-SSW has no matching dykes, and the dykes dominantly trend NW-SE, along which there are only few joints.

Since the studied dykes do not occupy faults, and generally do not occupy pre-existing joints, they yield the minimum principal compressive stress direction ( $\sigma_3$ ) present during dyke emplacement. We believe that dykes having similar orientations may have been emplaced contemporaneously throughout the study area. High-temporal resolution radioisotopic dating, if carried out in future, can throw light on both the absolute and relative ages of emplacement in our study area, but for now, the dykes' crosscutting relationships can constrain their relative order. Based on these relationships, we infer that an ~E-W-trending  $\sigma_3$  forming ~N-S-oriented dykes existed first, followed by a broadly NE-SW, but fluctuating,  $\sigma_3$  to cause dykes to trend from NNW-SSE to WNW-ESE. This  $\sigma_3$  seems to have been stabilised in the last phase of dyke emplacement to a ~N-S-trending direction leading to the intrusion of ~E-W-trending dykes. The  $\sigma_3$  remained essentially horizontal throughout, as shown by the dominantly vertical and some steeply dipping dykes.

Workers such as Dessai (2018) attribute the emplacement of the Goa dykes to rejuvenation of basement weaknesses, specifically along the ancient Dharwar structural trend.

Instead, our data on dyke and host rock joint trends show that, whereas there was some control exerted by the joints on dyke emplacement, particularly at Baga, overall there was a real control on the dyke trends by the contemporaneous stress fields.

### Inclined dykes

A very few dykes in our study area dip at moderate angles (Fig. 4b) and cannot be considered subvertical. However, they do not resemble inclined sheets found in so-called sheet swarms, described from central volcanoes in Iceland (Gautneb et al. 1989) or Japan (Geshi 2005). These sheet swarms contain sheets dipping inwards and converging on a shallow-level magma chamber, and their structure is governed by the local stress field around the chamber (Schirmick et al. 1999; Ancochea et al. 2003). The inclined dykes in our study area are simply too few to represent an inclined sheet swarm and do not converge on a central magma source. These dykes (such as the one in Fig. 6b; and dyke AR4 in Fig. 2d) can be ascribed to local changes in stress fields in the shallowest (and mechanically most heterogeneous) part of the crust, or to control by pre-existing fractures (Fig. 6c), as seems to be the case in the Chimei island arc complex in eastern Taiwan (Song and Lo 2002).

### Nature of vesicles

Vesicles are known to form at two stages during magma emplacement: (i) During the rise and decompression of a volatile-rich magma leading to volatile oversaturation, and (ii) during crystallisation of anhydrous phases from a magma with decreasing temperature (cooling), which raises the volatile content of the residual liquid to above saturation level (e.g., Sparks 1978; Wilson and Head 1981; Parfitt and Parfitt and Wilson 2008; Su et al. 2016). Both processes should lead to the formation of abundant vesicles that could be potentially sorted or segregated during the flow of magma in a fracture. Our observations of the vesicle types and distribution in the Goa dykes suggest similar processes. Vesicular dykes such as shown in Fig. 8c represent volatile-rich magmas that solidified above the depth of bubble nucleation (cf. Paquet et al. 2007). Estimated depths of basalt magma degassing range from as shallow as 2–3 m (Galindo and Gudmundsson 2012), to as deep as 1.8 km, provided the magma has intruded into similar host rocks (Greenland et al. 1988; Paquet et al. 2007). In the case of fractured and low-density sedimentary host rocks, this degassing may occur even deeper. Considering the overburden removal of 1 to 1.5 km from above the present exposures of the Goa dykes (Widdowson et al. 2000), and the generally volatile-poor nature of mafic melts, retrograde boiling resulting from crystallisation, rather than an originally volatile-rich magma, appears a plausible mechanism.

Whereas bubbles in a dyke magma should migrate upwards and, in a dyke inclined  $50^\circ$  (dyke AR4 in Fig. 2b), should become concentrated along its hanging wall interface (Platten 1995), the high vesicle concentration along the central plane of this dyke with its margins nearly free of vesicles may indicate that chilled margins developed on either side and the volatile-saturated magma being supplied was forced to flow along the central zone of the dyke, which was the last part to solidify.

### Feeder or non-feeder dykes?

No Goa dykes are observed to terminate in vertical sections, and it cannot be inferred, from field observations alone, whether these dykes fed Deccan flood basalt lava flows, now removed by erosion from much of Goa but still exposed in sections in the Western Ghats escarpment  $\sim 100$  km to the east. Widdowson et al. (2000) provided  $^{40}\text{Ar}/^{39}\text{Ar}$  ages of  $\sim 62$  Ma on four Goa dykes, and based on geochemical-isotopic data, considered the Goa dykes to be potential feeders of some of the youngest Deccan basalts (Wai Subgroup). Baksi (2014) showed that none of the  $^{40}\text{Ar}/^{39}\text{Ar}$  plateau or isochron ages of Widdowson et al. (2000) satisfy the basic statistical criteria for acceptance as valid crystallisation ages. We point out that because the entire thick Western Ghats sequence, including the Wai Subgroup, is now dated within a short time interval at 66–65 Ma (Baksi 2014; Renne et al. 2015), the 62 Ma age given by Widdowson et al. (2000) cannot be correct if these dykes are indeed feeders, as inferred by them based on geochemical-isotopic data.

There is considerable scope for new geochronological and geochemical-isotopic work on the Goa dykes, which so far has been carried out only to a limited degree, and without matching work on the geological and structural aspects of these dykes. In this paper, we fill this gap and provide hitherto unavailable data on the structural attributes and internal features of the Goa dykes as well as detailed geological maps that give ground truth. These should serve as a solid base for future detailed field studies of specific dykes of interest, and for petrological, geochemical-isotopic, and geochronological work. These combined approaches will answer the question of the feeder or non-feeder nature of the Goa dykes.

### Conclusions

This study is the first detailed field investigation of the Goa dykes, part of the Coastal dyke swarm, one of the three major mafic dyke swarms in the Deccan flood basalt province of India. We have studied the structural attributes and internal features of 60 mafic dykes (dolerites and basalts), some of which together form multiple-injection dykes. We compute

an average crustal dilation of 8% for the Goa dykes, with the highest local dilation of 17% (Sinquerim section of Aguada Headland) and the lowest of 2% (Vagator section). Features such as vesicular zones and jointing patterns in the dykes provide information on magma flow in the dykes and its solidification. Calculations of magmatic overpressures and magma chamber depths generally yield unrealistic values owing to the low aspect ratios of the dykes. Several dykes show clear crosscutting relationships which establish the relative order of emplacement. The question of whether mafic dyke swarms reflect contemporaneous regional stress fields, or pre-existing basement fabric, is an important one, and there is evidence for both scenarios in different case studies (e.g., Baer et al. 1994; Mège and Korme 2004; Ray et al. 2007; Vijayan et al. 2016). We find that, whereas some of the Goa dykes have orientations apparently controlled by pre-existing joint sets in their Proterozoic host rocks, the configuration and emplacement of most Goa dykes reflect contemporaneous tectonic stress fields, with the minimum compressive stress  $\sigma_3$  having changed over time from  $\sim$ E-W to  $\sim$ NE-SW and finally stabilising in an  $\sim$ N-S direction. It is possible that the Goa dykes are feeders to some of the upper lava flow units exposed in the Western Ghats escarpment some 100 km to the east, as inferred from limited geochemical-isotopic and geochronological data, but there are weaknesses and contradictions in these datasets. The possibility that the Goa dykes fed Deccan flood basalt lavas is real, and now needs to be more rigorously evaluated than in the past with geochemical-isotopic and geochronological work on a substantial number of the Goa dykes. The present work provides a solid field geological base for such studies to be taken up in the future. It contributes new data to the existing literature on the shapes of mafic dykes, their propagation and linkage in the continental crust, and the magmatic processes which occur in them. It also contributes to the important question, in the geodynamics of flood basalt volcanism, of whether swarms of such mafic dykes reflect contemporaneous stress fields, control by pre-existing structural fabrics, or both of these (cf. Mège and Korme 2004; McHone et al. 2005; Ray et al. 2007).

**Acknowledgements** This work forms a part of the PhD dissertation of Raghav Gadgil at Goa University. Gadgil is grateful to all his dissertation and project students of 2014–2019 batches at Goa University and Dhempe College, and especially to Akshay Tari for the valuable field assistance on many occasions. He also thanks his wife Shweta Gadgil for domestic support and encouragement in this research. He is grateful to Tapas Kumar Biswal, Paul Bons, Elena Druguet, Agust Gudmundsson, and Hetu Sheth for the helpful email discussions over the past several years, Peter C. Rickwood and Rajesh K. Srivastava for providing relevant literature, and Hetu Sheth for the photograph in Fig. 6c. Goa University and Dhempe College of Arts and Science are acknowledged for hosting this study. Sridhar D. Iyer thanks the Director, CSIR-NIO for providing facilities. The authors thank Hetu Sheth and Agust Gudmundsson for the detailed and constructive reviews and Valerio Acocella and Andrew Harris for their editorial handling and valuable comments that greatly improved this manuscript.

## References

- Airoldi G, Muirhead JD, White J, Rowland J (2011) Emplacement of magma at shallow depth: insights from field relationships at Allan Hills, South Victoria Land, East Antarctica. *Antarct Sci* 23:281–296
- Ancochea E, Brändle JL, Huertas MJ, Cubas CR, Hernán F (2003) The felsic dykes of La Gomera (Canary Islands): identification of cone sheet and radial dyke swarms. *J Volcanol Geotherm Res* 120:197–206
- Auden JB (1949) Dykes in western India: a discussion of their relationships with the Deccan Trap. *Trans Nat Inst Sc India* 3:123–157
- Babiker M, Gudmundsson A (2004) Geometry, structure and emplacement of mafic dykes in the Red Sea hills, Sudan. *J Afr Earth Sci* 38:279–292
- Baer G, Beyth M, Rechis Z (1994) Dykes emplaced into fractured basement, Timna igneous complex, Israel. *J Geophys Res* 99:24039–24050
- Baksi AK (2014) The Deccan Trap – Cretaceous-Paleogene boundary connection; new  $^{40}\text{Ar}/^{39}\text{Ar}$  ages and critical assessment of existing argon data pertinent to this hypothesis. *J Asian Earth Sci* 84:9–23
- Basavaiah N, Satyanarayana KVV, Deenadayalan K, Prasad JN (2018) Does Deccan volcanic sequence contain more reversals than the three-Chron N-R-N flow magnetostratigraphy? – a palaeomagnetic evidence from the dyke-swarm near Mumbai. *Geophys J Int* 213:1503–1523
- Beane JE, Turner CA, Hooper PR, Subbarao KV, Walsh JN (1986) Stratigraphy, composition and form of the Deccan basalts, Western Ghats, India. *Bull Volcanol* 48:61–83
- Bhattacharji S, Chatterjee N, Wampler JM, Nayak PN, Deshmukh SS (1996) Indian intraplate and continental margin rifting, lithospheric extension and mantle upwelling in Deccan flood basalt volcanism near the K/T boundary: evidence from mafic dyke swarms. *J Geol* 104:379–398
- Bondre NR, Hart WK, Sheth HC (2006) Geology and geochemistry of the Sangamner mafic dyke swarm, western Deccan volcanic province, India: implications for regional stratigraphy. *J Geol* 114:155–170
- Cadman A, Tarney J, Park RG (1990) Intrusion and crystallization features in Proterozoic dyke swarms. In: Parker AJ, Rickwood PC, Tucker DH (eds) *Mafic dykes and emplacement mechanisms*. Balkema, Rotterdam, pp 13–24
- Cox KG, Hawkesworth CJ (1984) Relative contributions of crust and mantle to flood basalt magmatism, Mahabaleshwar area, Deccan Traps. *Philos Trans R Soc Lond A* 310:627–641
- Cucciniello C, Choudhary AK, Zanetti A, Sheth HC, Vichare S, Pereira R (2014) Mineralogy, geochemistry and petrogenesis of the Khopoli mafic intrusion, Deccan Traps, India. *Mineral Petrol* 108:333–351
- Cucciniello C, Demonerova EI, Sheth H, Pande K, Vijayan A (2015)  $^{40}\text{Ar}/^{39}\text{Ar}$  geochronology and geochemistry of the Central Saurashtra mafic dyke swarm: insights into magmatic evolution, magma transport, and dyke-flow relationships in the northwestern Deccan Traps. *Bull Volcanol* 77, art 45, <https://doi.org/10.1007/s00445-015-0932-0>
- Currie KL, Ferguson J (1970) The mechanism of intrusion of lamprophyre dykes indicated by “offsetting” of dykes. *Tectonophysics* 9:525–535
- Daniels KA, Kavanagh JL, Menand TJ, Sparks RSJ (2012) The shapes of dykes: evidence for the influence of cooling and inelastic deformation. *Geol Soc Am Bull* 124:1102–1112
- DeGraff JM, Aydin A (1987) Surface morphology of columnar joints and its significance to mechanics and direction of joint growth. *Geol Soc Am Bull* 99:605–617
- Deshmukh SS, Sehgal MN (1988) Mafic dyke swarms in Deccan volcanic province of Madhya Pradesh and Maharashtra. In: Subbarao KV (ed) *Deccan flood basalts*. Geol Soc Ind Mem 10:323–340
- Dessai AG (2011) The geology of the Goa Group: revisited. *J Geol Soc India* 78:233–242
- Dessai AG (2018) *Geology and mineral resources of Goa*. New Delhi Publ, Delhi
- Dessai AG, Viegas AAAA (1995) Multigeneration mafic dyke swarm related to Deccan magmatism, south of Bombay: implications on the evolution of the western continental margin. In: Devaraju TC (ed) *Dyke swarms of peninsular India*. Geol Soc Ind Mem 33:435–451
- Devey CW, Lightfoot PC (1986) Volcanological and tectonic control of stratigraphy and structure in the western Deccan traps. *Bull Volcanol* 48:195–207
- Ernst RE, Buchan KL, Palmer HC (1995) Giant dyke swarms: characteristics, distribution and geotectonic applications. In: Baer G, Heimann A (eds) *Physics and chemistry of dykes*. Balkema, Rotterdam, pp 3–21
- Fernandez OA (2009) Physiography and general geology of Goa. In: Mascarenhas A, Kalavampara G (eds) *Natural resources of Goa: a geological perspective*. Geol Soc Goa, Panjim, pp 11–24
- Fialko YA, Rubin AM (1999) Thermal and mechanical aspects of magma emplacement in giant dyke swarms. *J Geophys Res* 104(B10):23033–23049
- Gadgil R, Miranda MA, Viswanath TA (2018) Deformational features of intraformational para-conglomerate of the Palaeoproterozoic Sanvordem formation, Goa group indicates a brittle-ductile dextral shear. *Int J Geom Geosc* 8:24–40
- Galindo I, Gudmundsson A (2012) Basaltic feeder dykes in rift zones: geometry, emplacement and effusion rates. *Nat Hazards Earth Syst Sci* 12:3683–3700
- Gautneb H, Gudmundsson A, Oskarsson N (1989) Structure, petrochemistry and evolution of a sheet swarm in an Icelandic central volcano. *Geol Mag* 126:659–673
- Geshi N (2005) Structural development of dyke swarms controlled by the change of magma supply rate: the cone sheets and parallel dykes swarms of the Miocene Otoge igneous complex, central Japan. *J Volcanol Geotherm Res* 141:267–281
- Gokul AR (1985) Structure and tectonics of Goa. In: *Earth’s resources for Goa’s development*, pp 14–21
- Greenland LP, Okamura AT, Stokes JB (1988) Constraints on the mechanics of the eruption. In: Wolfe EW (ed) *The Pū‘u ‘Ō‘ō eruption of Kilauea Volcano, Hawaii: episodes 1 through 20, January 3, 1983 through June 8, 1984*. US Geol Surv prof pap 1463:155–164
- Grossenbacher KA, McDuffie SM (1995) Conductive cooling of lava: columnar joint diameter and stria width as functions of cooling rate and thermal gradient. *J Volcanol Geotherm Res* 69:95–103
- Gudmundsson A (1983) Form and dimensions of dykes in eastern Iceland. *Tectonophysics* 34(3–4):81–96
- Gudmundsson A (1984) Formation of dykes, feeder dykes and the intrusion of dykes from magma chambers. *Bull Volcanol* 47:537–550
- Gudmundsson A (1995) The geometry and growth of dykes. In: Baer G, Heimann A (eds) *Physics and chemistry of dykes*. Balkema, Rotterdam, pp 23–34
- Gudmundsson A (2011) *Rock fractures in geological processes*. Cambridge Univ Press, 578 p
- Gudmundsson A, Loetveit IF (2005) Dyke emplacement in a layered and faulted rift zone. *J Volcanol Geotherm Res* 144:311–327
- Halls HC (1982) The importance and potential of mafic dyke swarms in studies of geodynamic processes. *Geosci Can* 9:145–154
- Hansen SE, Sorlok T, Johannsson AE (1998) Mechanical properties of rocks. SINTEF report, STF22 A98034, Trondheim
- Hoek JD (1991) A classification of dyke-fracture geometry with examples from Precambrian dyke swarms in the Vestfold Hills, Antarctica. *Geol Rundsch* 80:233–248
- Hooper PR, Widdowson M, Kelley S (2010) Tectonic setting and timing of the final Deccan flood basalt eruptions. *Geology* 38:839–842

- Hou GT, Kusky TM, Wang CC, Wang YX (2010) Mechanics of the giant radiating MacKenzie dyke swarm: a palaeostress field modelling. *J Geophys Res* 115(B02402). <https://doi.org/10.1029/2007JB005475>
- Iyer SD, Wagle BG (1987) Morphometric analysis of the river basins in Goa. *Geogr Rev Ind* 49:11–18
- Iyer SD, Banerjee G, Wagle BG (1989) Statistical analysis of lineaments of Goa. *India Curr Sci* 58:1316–1319
- Iyer SD, Wagle BG, D'Cruz EE (1990) Dyke swarms along the Goa coast, India. *Nat Sem Rec Rec Geol West Ind, MS Univ, Vadodara*, p 14
- Ju W, Hou GT, Hari KR (2013) Mechanics of mafic dyke swarms in the Deccan large igneous province: palaeostress field modelling. *J Geodyn* 66:79–91
- Long PE, Wood BJ (1986) Structures, textures, and cooling histories of Columbia River basalt flows. *Geol Soc Am Bull* 97:1144–1155
- Lyle P (2000) The eruption environment of multi-tiered columnar basalt lava flows. *J Geol Soc Lond* 157:715–722
- Mahoney JJ (1988) Deccan traps. In: Macdougall JD (ed) *Continental flood basalts*. Kluwer Acad Publ, Dordrecht, pp 151–194
- Marinoni LB (2001) Crustal extension from exposed sheet intrusions: review and method proposal. *J Volcanol Geotherm Res* 107:27–46
- Marinoni LB, Gudmundsson (2000) Dykes, faults and palaeostresses in the Teno and Anaga massifs of Tenerife (Canary Islands). *J Volcanol Geotherm Res* 103:83–103
- Martha TK, Ghosh D, Vinod Kumar K, Lesslie A, Ravi Kumar MV (2013) Geospatial technologies for national geomorphology and lineament mapping project – a case study for Goa state. *J Indian Soc Remote* 41:905–920
- Martinez-Poza AI, Druguet E, Castano LM, Carreras J (2014) Dyke intrusion into a pre-existing joint network: the Aiguablava lamprophyre dyke swarm (Catalan coastal ranges). *Tectonophysics* 630:75–90
- McHone JG, Anderson DL, Beutel EK, Fialko YA (2005) Giant dykes, rifts, flood basalts, and plate tectonics: a contention of mantle models. In: Foulger GR, Natland JH, Presnall DC, Anderson DL (eds), *Plates, plumes, and paradigms*. *Geol Soc Am Spec Pap* 388: 401–420
- Mège D, Korme T (2004) Dyke swarm emplacement in the Ethiopian large igneous province: not only a matter of stress. *J Volcanol Geotherm Res* 132:283–310
- Melluso L, Sethna SF, Morra V, Khateeb A, Javeri P (1999) Petrology of the mafic dyke swarm of the Tapti River in the Nandurbar area (Deccan volcanic province). In: Subbarao KV (ed) *Deccan volcanic province*. *Geol Soc Ind Mem* 43:735–755
- Nicholson R, Pollard DD (1985) Dilation and linkage of echelon cracks. *J Struct Geol* 7:583–590
- Nogueira CR, Terrinha P, Moreira M (2009) Assessing magma flow direction in dykes from vesicle shapes and orientations. *Geophys Res Abstr (EGU)*, p13369
- Pande K, Vadakkeyakath Y, Sheth H (2017)  $^{40}\text{Ar}/^{39}\text{Ar}$  dating of the Mumbai tholeiites and Panvel flexure: intense 62.5 Ma onshore–offshore Deccan magmatism during India–Laxmi Ridge–Seychelles breakup. *Geophys J Int* 210:1160–1170
- Paquet F, Dauteuil O, Hallot E, Moreau F (2007) Tectonics and magma dynamics coupling in a dyke swarm of Iceland. *J Struct Geol* 29: 1477–1493
- Parfitt EA, Wilson L (2008) *Fundamentals of physical volcanology*. Blackwell Publ, 230 p
- Park JK, Buchan KL, Harlan SL (1995) A proposed giant radiating dyke swarm fragmented by the separation of Laurentia and Australia based on palaeomagnetism of ca. 780 Ma mafic intrusions in western North America. *Earth Planet Sci Lett* 132:129–139
- Patil SK, Rao DR (2002) Palaeomagnetic and rock magnetic studies on the dykes of Goa, west coast of Indian Precambrian shield. *Phys Earth Planet Inter* 133:111–125
- Pinel V, Jaupart C (2004) Likelihood of basaltic eruptions as a function of volatile content and volcanic edifice size. *J Volcanol Geotherm Res* (110):1–15
- Platten IM (1995) Flow and crystallization in dykes: a review of field and laboratory data in the light of recent advances in mathematical modelling. In: Devaraju TC (ed) *Dyke swarms of peninsular India*. *Geol Soc Ind Mem* 33:1–47
- Pollard DD (1973) Derivation and evaluation of a mechanical model for sheet intrusions. *Tectonophysics* 19:233–269
- Pollard DD, Segall P, Delaney PT (1982) Formation and interpretation of dilatant echelon cracks. *Geol Soc Am Bull* 93:1291–1303
- Powar KB, Vadetwar SB (1995) Mineralogy and geochemistry of basic dykes and associated plugs of the Revas–Murud sector, Konkan coastal belt, Maharashtra. In: Devaraju TC (ed) *Dyke swarms of peninsular India*. *Geol Soc Ind Mem* 33:339–363
- Prabhakar Rao P, Raju AV, Nair MM (1985) *Geomorphology of Goa. Earth's resources for Goa's development*. Panjim: Goa seminar Vol pp 583–586
- Ray R, Sheth HC, Mallik J (2007) Structure and emplacement of the Nandurbar–Dhule mafic dyke swarm, Deccan Traps, and the tectonomagmatic evolution of flood basalts. *Bull Volcanol* 69: 537–551
- Renne PR, Sprain CJ, Richards MA, Self S, Vanderkluysen L, Pande K (2015) State shift in Deccan volcanism at the Cretaceous–Palaeogene boundary, possibly induced by impact. *Science* 350: 76–78
- Samant H, Patel V, Pande K, Sheth HC, Jagadeesan KC (2019)  $^{40}\text{Ar}/^{39}\text{Ar}$  dating of tholeiitic flows and dykes of Elephanta Island, Panvel flexure zone, western Deccan Traps: A five-million-year record of magmatism preceding India–Laxmi Ridge–Seychelles breakup. *J Volcanol Geotherm Res* 379:12–22
- Schirnack C, Bogaard PV, Schmincke H-U (1999) Cone sheet formation and intrusive growth of an oceanic island — the Miocene Tejada complex on Gran Canaria (Canary Islands). *Geology* 27:207–210
- Sheth H (2018) *A photographic atlas of flood basalt volcanism*. Springer, New York, p 383
- Sheth HC, Cañón-Tapia E (2015) Are flood basalt eruptions monogenetic or polygenetic? *Int J Earth Sci (Geol Rund)* 104:2147–2162
- Sheth HC, Melluso L (2008) The Mount Pavagadh volcanic suite, Deccan traps: geochemical stratigraphy and magmatic evolution. *J Asian Earth Sci* 32:5–21
- Sheth HC, Ray JS, Ray R, Vanderkluysen L, Mahoney JJ, Kumar A, Shukla AD, Das P, Adhikari S, Jana BK (2009) Geology and geochemistry of Pachmarhi dykes and sills, Satpura Gondwana Basin, Central India: problems of dyke–sill–flow correlations in the Deccan Traps. *Contrib Mineral Petrol* 158:357–380
- Sheth HC, Zellmer GF, Kshirsagar PV, Cucciniello C (2013) Geochemistry of the Palitana flood basalt sequence and the eastern Saurashtra dykes, Deccan traps: clues to petrogenesis, dyke–flow relationships, and regional lava stratigraphy. *Bull Volcanol* 75:art 701. <https://doi.org/10.1007/s00445-013-0701-x>
- Sheth HC, Zellmer GF, Demonerova EI, Ivanov AV, Kumar R, Patel RK (2014) The Deccan tholeiite lavas and dykes of Ghatkopar–Powai area, Mumbai, Panvel flexure zone: geochemistry, stratigraphic status, and tectonic significance. *J Asian Earth Sci* 84:69–82
- Sheth HC, Meliksetian K, Gevorgyan H, Israyelyan A, Navasardyan G (2015) Intercanyon basalt lavas of the Debed River (northern Armenia), part of a Pliocene–Pleistocene continental flood basalt province in the South Caucasus. *J Volcanol Geotherm Res* 295:1–15
- Sheth HC, Vanderkluysen L, Demonerova EI, Ivanov AV, Savatenkov VM (2019) Geochemistry and  $^{40}\text{Ar}/^{39}\text{Ar}$  geochronology of the Nandurbar–Dhule mafic dyke swarm: dyke–sill–flow correlations and stratigraphic development across the Deccan flood basalt province. *Geol J* 54:157–176
- Sneddon IN, Lowengrub M (1969) Crack problems in the classical theory of elasticity. John Wiley, New York, p 221

- Song S-R, Lo H-J (2002) Lithofacies of volcanic rocks in the central coastal range, eastern Taiwan: implications for island arc evolution. *J Asian Earth Sci* 21:23–38
- Sparks RSJ (1978) The dynamics of bubble formation and growth in magmas: a review and analysis. *J Volcanol Geotherm Res* 3:1–37
- Su Y, Huber C, Bachmann O, Zajacz Z, Wright H, Vazquez J (2016) The role of crystallization-driven exsolution on the sulfur mass balance in volcanic arc magmas. *J Geophys Res* 121:5624–5640
- Swanson DA, Wright RL, Helz RT (1975) Linear vent systems and estimated rates of magma production and eruption for the Yakima basalt on the Columbia plateau. *Am J Sci* 275:877–905
- Vanderkluyzen L, Mahoney JJ, Hooper PR, Sheth HC, Ray R (2011) The feeder system of the Deccan Traps (India): insights from dyke geochemistry. *J Petrol* 52:315–343
- Varga RJ, Gee JS, Staudigel H, Tauxe L (1998) Dyke surface lineations as magma flow indicators within the sheeted dike complex of the Troodos Ophiolite, Cyprus. *J Geophys Res* 103(B3):5241–5256
- Vijayan A, Sheth H, Sharma KK (2016) Tectonic significance of dykes in the Sarnu-Dandali alkaline complex, Rajasthan, northwestern Deccan Traps. *Geosci Front* 7:783–791
- Wagle BG, Rajamanickam GV (1980) A petrographic study of Precambrian quartzites from Goa coast. *Mahasagar-Bull Nat Inst Oceano* 13:9–21
- Widdowson M, Gunnell Y (1999) Lateritization, geomorphology and geodynamics of a passive continental margin: the Konkan and Kanara coastal lowlands of western peninsular India. *Spec Publ Int Assoc Sed* 27:245–274
- Widdowson M, Pringle MS, Fernandez OA (2000) A post K-T boundary (Early Palaeocene) age for Deccan-type feeder dykes, Goa, India. *J Petrol* 41:1177–1194
- Wilson L, Head JW (1981) Ascent and eruption of basaltic magma on the Earth and Moon. *J Geophys Res* 86:2791–3001
- Yong Technology, Inc. (2014) GeoRose. Edmonton, Canada. <http://www.yongtechnology.com/download/georose>. Accessed 12 July 2016